The Use of Porous Graphitic Carbon in Liquid Chromatography Performance and Polar Retention Effect

Paul Ross

To Tracy, Christina and Grace.

Declaration

This thesis has been composed by myself and has not been submitted in any previous application for a degree. The work reported here was executed by myself unless otherwise stated.

December 1998

Acknowledgements

I would like to thank Prof. J. H. Knox for providing the opportunity to continue with research begun by previous students within his group on a quite unique material, and also for his encouragement and advice throughout the period of study.

I am very grateful to Hypersil Ltd for their financial sponsorship and to friends and colleagues within the company who offered endless encouragement, in particular to John Dolphin who never doubted the successful completion of the degree.

I am also grateful to Dr D. Barrett and Prof. M. Davies at Nottingham University for the loan of the Surface Tension Analyser and for the use a second instrument within Pharmaceutical Sciences building at Nottingham.

Finally I would like to thank my family. To my parents for their tireless support throughout, to my two daughters Christina and Grace for the patient way in which they put up with their Dad working all the time. To the Wilsons for the hot dinners and use of their spare room provided on frequent visits to Edinburgh.

Abstract

This thesis is primarily concerned with the use and development of Porous Graphitic Carbon (PGC) for High Performance Liquid Chromatography (HPLC). Chromatographic studies carried out using PGC since its introduction in 1988 have shown it to posses quite unique separating properties. In particular the media has been shown to be very selective for the separation of closely related compounds such as geometric and diastereoisomers. It has also been shown to be very retentive towards compounds of increasing polarity. The magnitude of this interaction is considerable, we define it as the retention over and above that which might have been predicted if the polar functional group was replaced with a non polar group of similar size. We have called this effect, the Polar Retention Effect on Graphite (PREG). Previous attempts to correlate retention on graphite with energies associated with those molecular interactions associated with other chromatographic media have been largely unsuccessful. This has in part been due to the fact that there has been no attempt to measure in units of energy the magnitude of PREG.

The main body of the thesis is then concerned with experiments, which provide information regarding the magnitude of PREG. We investigate a) the relative strength of analyte/graphite interactions to that of analyte/solvent interactions, b) the effect of coating discrete or polymeric molecules to the graphite surface on PREG and c) measure the energy associated with PREG for a range of analytes and correlate this energy with physical and calculated parameters associated with each analyte.

In order to gain a measure of PREG we have developed a method which allows PREG to be measured and quantified. Based on our values of PREG we have put forward a hypothesis for the mechanism responsible for this interaction. Further work still needs to be done to strengthen this hypothesis, we therefore put forward a number of ideas and suggestions for future workers to which continue to investigate the mechanism associated with PREG.

List of Contents

Chapter I

Chapter 4

Chapter 5

Chapter 1 - Introduction

1.1 Development of the Chromatographic Process

This thesis is primarily concerned with the use and development of Porous Graphitic Carbon (PGC) for high performance liquid chromatography HPLC. Its introduction to this scientific field is relatively recent, when one considers that a commercial product was only introduced in 1988, while the liquid chromatography itself was first introduced at the turn of the century, and HPLC in the mid-1970's.

The first Chapter reviews the historical development of liquid chromatography, and provides a brief theoretic background of liquid chromatography. It outlines the chromatographic supports that are currently available to HPLC and extends this discussion to include specific modes of chromatography that have also developed. The limitations associated with these modes of chromatography are discussed. These limitations show why PGC was developed, and how it may contribute to the further development of the technique in the future.

The first Chapter concludes with a review of observations made on the use of PGC since its introduction and defines the nature of the work presented later in the thesis.

1.1.1 Brief History of Chromatography

At the turn of the 20th century, both Tswett[1], who was based in Russia, and Day[2], based in America, discovered that the percolation of a liquid mixture through a bed of a porous solid could result in separation of that mixture according to the varying adsorption affinities of its constituents. Tswett's contribution was more significant than Day's, since he developed the technique in great detail and gave a good, qualitative understanding of the basis of the chromatographic process. For a variety of reasons, the discoveries of Tswett and Day lapsed into obscurity following their deaths. The value of the chromatographic method was not generally appreciated until the historic separation of carotene isomers performed by Kuhn, Lederer and Winterstein[3] in 1931.

Noticeable practical development followed, including thin layer chromatography (TLC) by Izmailov and Shraiber[4]. There are, however, several limitations with this form of

chromatography. Firstly, both paper chromatography and thin layer chromatography depend
upon surface tension to move the solvent along the bed so that its rate of movement is not controlled. Secondly, the separating chromatographic bands are not eluted from the column. Finally, the technique provides relatively poor resolution.

However, it was Martin and Synge[5] in 1941 who first cut through the apparent complexity of the chromatographic process with a brilliant theoretical analogy. By means of their hypothesis, chromatographic separation could be described quantitatively in terms of the partition of sample between bed and solvent, the bed consisting of a number of equilibrium stages or theoretical plates. The Martin and Synge model provided a foundation for the development of quantitative theories of partition, ion exchange and gas chromatography during the twenty years that followed. The thermodynamics of adsorption chromatography was treated in detail by Snyder[6] in the 1960's and now forms the basis for understanding of this mode of chromatography.

In 1941 Martin and Synge introduced liquid-liquid partition chromatography using silica gel loaded with water as a chromatographic stationary phase. The separations were in fact a mixture of adsorption and partition chromatography. At about the same time, Tiselius[7,8,9] developed frontal analysis and displacement analysis. The paper by Martin and Synge also suggested the possibilities of gas chromatography. Martin predicted that if the liquid-mobile phase was replaced by a gas phase, the increase in the transfer rate should result in highly efficient separations. Martin and Synge also suggested the use of small particles and high pressures for LC, *i. e.* HPLC or high pressure liquid chromatography.
However, during this time Martin and Synge were developing liquid partition chromatography using paper as the support material and, although it is surprising now, no other workers took up Martin's suggestion for gas chromatography.

In the 1950's James and Martin[10] turned their attention to separating substances by distribution of analytes between a gas and liquid. The technique became known as gas-liquid chromatography (GLC), or simply gas chromatography (GC). In 1952 they published papers describing the first gas chromatograph. The results were startling and attracted a great deal of attention. Within a few years of publishing their foundation work, GC had

completely replaced analytical low-temperature distillation, and was being employed by the solvent industry, the essential oil industry, and in the field of biochemistry. The tremendous ability of GC to separate and analyse complex mixtures is now widely appreciated, and compared to previous analytical methods it provided separations that were faster and better. The introduction of automated equipment took the technique into a league of its own. Following the suggestion of Martin and Synge in 1941, Giddings[11] postulated in 1965 that, if efficiencies comparable to gas chromatography were to be achieved in liquid chromatography, small particles of 2-20μm size would have to be employed. This would, however, cause very high inlet pressures. In other words, the modernisation of liquid chromatography could only be achieved by relinquishing the gravity flow system used at the time.

Despite the major successes and advances made with gas chromatography, the technique was restricted in its application range. Since GC relies on a volatilisation process to mobilise the analytes, compounds that are insufficiently volatile cannot pass through the column. Also, because of the high run temperatures, compounds that are thermally unstable can decompose during the analysis. In 1976 it was estimated[12] that only 20% of the known organic compounds could be analysed by gas chromatography without prior chemical modification of the sample. Liquid chromatography (LC) on the other hand was not limited by sample volatility or thermal stability. Thus, LC was and indeed still is ideally suited towards the separation of macromolecules and ionic products of biomedical interest, labile natural products, and a wide variety of other high molecular weight and less stable compounds, such as:

Nucleic Acids	Plant Pigments	Surfactants
Amino Acids	Polar Liquids	Pharmaceuticals
Dyes	Explosives	Plant and Animal Metabolites

Such advantages provided the impetus for the development and modernisation of the of LC technique. However, by the 1960's and early 1970's there were still many major barriers to making LC a practical reality. Modernisation of high pressure pumps, detector systems and the need for high purity solvents were among the first of the difficulties that needed to be overcome. By the mid-1970's and early 1980's, many of the initial difficulties with equipment had been overcome. This was due largely to the contributions from the pioneers

of HPLC such as Kirkland[13], Huber[14], Lipsky[15] and Horvath[16]. The use of very small particles, 3-10 μm in diameter, became the norm for the new/modernised type of liquid chromatography. Originally, the technique was termed "high pressure liquid chromatography." Later, as its most stunning attribute, high efficiency, became established, it became known as "high performance liquid chromatography" or HPLC. A good understanding of theoretical aspects of HPLC, based on experience with gas chromatography, was available. In the two decades that followed, an explosion of scientific papers on HPLC across a whole range of different industries ensued.

A significant part of the technique's success was due to the progression towards the use of chemically-bonded stationary phases. Up to the introduction of HPLC, and for the first few years after its introduction, the more traditional modes of liquid chromatography were still employed. These traditional modes of liquid chromatography had some clear limitations: a) adsorption chromatography using unmodified adsorbent surfaces was not very applicable to very polar or ionic molecules, and b) liquid-liquid partition chromatography using coated adsorbent particles proved to be troublesome in practice due to the need for a thermostated pre-column loaded with stationary phase to prevent stripping of the stationary phase from the analytical column.

Because of these limitations, HPLC using chemically-bonded stationary phases became very popular. These new stationary phases were, and still are typically prepared by bonding an organic ligand to the surface of an adsorbent (usually silica). The use of the bonded phases allowed for polar and ionic molecules to be efficiently chromatographed. They also gave much more freedom of choice in eluant selection than provided by liquid-liquid partition chromatography. Gradient elution techniques could be used with bonded phases without fear of stripping the stationary phase.

The main types of ligand used in commercial bonded phases are:

(1) Hydrophobic groups , especially octadecyl ($C_{18}H_{37}$) groups but also those with shorter chain lengths, such as C_1, C_4 and C_8.

(2) Polar groups, such as aminopropyl, cyanopropyl, ether, and glycol.

(3) Ion-exchange groups, such as sulphonic acid, amino and quarternary ammonium.

Porous graphitic carbon (PGC) offers similar benefits as silica in terms of mechanical stability, easily withstanding the pressures associated with HPLC. However PGC offers a potentially wider application range. This is in part due to PGC's compatibility with a wider

range of organic solvents and its enhanced chemical stability at high and low pH relative to silica. Its potential to be used in many specific modes of chromatography is therefore great. Before discussing these modes in detail, it is first of all necessary to define the process of liquid chromatography itself, and to become familiar with many of the terms and conditions associated with the technique. The specific modes of chromatography are discussed in more detail in Section 1.4.2.

1.1.2 The Chromatographic Process and the Different Modes of Chromatography

The aim of any chromatographic system as defined by Knox[17], is to achieve the optimum combination of analyte resolution, speed, and economical use of pressure for a given mixture. In order to achieve this aim, peaks should be made as narrow as possible. Figure 1.1 shows a typical chromatographic separation as the analytes move through the column.

The resolution of two (or more) analytes requires disengagement of peaks. This is achieved through the balance between two processes. The first process is termed the 'differential migration' of the two analytes. The migration rate of any analyte depends upon its distribution between the mobile and stationary phases. Compounds whose individual molecules spend most of their time in the stationary phase move through the column rather slowly. Conversely, compounds whose individual molecules spend most of their time in the mobile phase will move through the column rather rapidly. It is therefore the distribution coefficient (K) of the analyte between the mobile and stationary phases that determines the rate of differential migration of the analyte through the column. The separation of two analyte bands increases directly with the distance migrated.

The second process is band broadening, and it is to be minimised wherever possible. This process counteracts the separation arising from differential migration. Band broadening in chromatography arises from a number of kinetic effects that are random in nature. Their combined effect is analogous to molecular diffusion in that an initially sharp band will gradually spread out as it migrates and assume a Gaussian profile. The width or standard deviation of this profile increases with the square root of the distance moved (or the time for which it has moved). Thus, while band separation increases as the first power of the distance migrated, band width increases as the square root of the distance migrated.

Both of these conclusions were reached by Martin and Synge. In consequence, the resolution of any two analyte bands, which is defined as their separation divided by their mean width, will increase as the square root of the average distance migrated. Resolution, R_s, of two chromatographic peaks A and B, is defined by equation [1.1]:

$$R_s = \frac{t_R(B) - t_R(A)}{0.5(w_t(B) + w_t(A))} \qquad [1.1]$$

where t_R is the retention time, and w_t is the peak width at the base measured in the same units as t_R.

The process of chromatography as described above is the basis for any chromatographic system. There are five modes of liquid chromatography: adsorption or liquid-solid chromatography, liquid-liquid chromatography with coated stationary phases, liquid-liquid chromatography with covalently bound stationary phases, ion exchange chromatography, and size exclusion chromatography.

Typically, a chromatographic method may be run in either normal or reversed phase, and requires a column of more or less inert packing material that is then coated with the stationary phase. Normal phase chromatography refers to the traditional form of liquid chromatography. It is based on interactions between the polar functional groups of the analytes and polar sites on the surface of the packing, usually silica or alumina. Mobile phase systems are generally hydrocarbons, such as hexane, or chlorinated hydrocarbons, such as dichloromethane. Reversed phase liquid chromatography refers to the interaction between the hydrophobic parts of the analytes with a non-polar stationary phase, either coated or covalently bonded onto the surface of the packing. Mobile phases in reversed phase chromatography generally have a high aqueous content.

1.1.2.1 Adsorption Chromatography

The basis of separation achieved by adsorption chromatography is the selective adsorption of components in a mixture onto active sites on the surface of the adsorbent. In order to achieve this, eluant molecules already adsorbed have to be displaced. The system can be thought of as a reaction causing this displacement (See Figure 1.2a). The adsorption – desorption process is considered to be reversible and its kinetics to be so fast that thermodynamic equilibrium is readily attained[18]. The adsorption of an analyte is then determined by:

(1) the relative volumes of adsorbed and non-adsorbed phases, and

(2) the net adsorption energy of the analyte.

The volume of adsorbed phase (V_a) is the product of substrate-specific surface area (S_{BET}) and the thickness, t, of the adsorbed monolayer:

$$V_a = S_{BET} \times t \qquad [1.2]$$

The adsorption of an analyte originates from attractive forces such as London-type dispersion forces, induction forces, charge transfer, and hydrogen bonding interactions. Depending on the size and strength of the interactions, adsorption can be divided into two types: physical adsorption (physisorption) and chemical adsorption (chemisorption). Physisorption takes place through short-range intermolecular attraction and repulsion forces such as London type dispersion forces, induction forces and charge transfer between adsorbed molecule and adsorbent surface. In chemisorption, an electron transfer takes place between the surface atoms of the adsorbate and the adsorbent and a true chemical bond is formed.

Although a clear distinction between physisorption and chemisorption is not yet possible, the magnitude of the heat of adsorption has been found to be the most useful criterion. In chemisorption, the heat of adsorption usually exceeds 80KJ/mol, whereas the heat of adsorption in physisorption varies between 8 and 40 KJ/mol. Furthermore, chemisorption often requires appreciable activation energy, whereas physisorption is a non-activated process. The primary mode of interaction for chromatographic adsorbents is therefore via physisorption. Kiselev, *et al*[19] divided adsorbents into three groups, described as follows.

Type I adsorbents have no ions or active functional groups exposed at the surface. These adsorbents are represented by graphitized carbon, boron nitride, etc. They are thought to be capable only of non-specific interactions with all types of analytes.

Type II adsorbents have positively charged sites such as Brönstead and Lewis acid centres at the surface. These adsorbents are represented by oxide adsorbents such as porous silica, and are capable of non-specific interactions like Type I adsorbents. However, they are capable of additional interactions, for example with adsorbate molecules that have a) high electron density, b) positively charged groups at the periphery and c) having groups which consist of both a) and b). Hydrogen bonding between adsorbate and adsorbent is often particularly important with oxide adsorbents.

Type III adsorbents are described as those that carry centres with high electron density.

An in-depth discussion of molecular forces is given in Chapter 5 of this Thesis.

1.1.2.2 Liquid-liquid chromatography

In liquid-liquid chromatography, the process of separation of a mixture of analytes depends on the distribution coefficients of the individual compounds between a mobile phase and an immiscible stationary phase.

The adsorption forces between the support and the liquid stationary phase must be strong enough so that the stationary phase is strongly held by the support. Otherwise, it is likely to be washed out of the support by the eluting phase. It is important that the stationary phase completely fills the pores of the support.

A typical normal phase system would consist of triethylene glycol adsorbed onto wide pore silica as the stationary phase, and triethyleneglycol saturated hexane[20] as eluant (see Figure 1.2b). This system has been used to separate a wide range of phenols, steroids, and aromatic alcohols. The stability of such a stationary phase is limited, however, as the mobile phase has to be saturated with the stationary phase and accurate thermostating of the reservoir is essential. This can give rise to irreproducible retention and loss of efficiency. These difficulties are magnified for reversed phase systems, where the stationary phase is non-polar (e. g. squalane) and the mobile phase (e. g. water:alcohol mixtures) is polar. The forces holding the non-polar stationary phase to the support are very weak causing the stability of the system to be poor.

1.1.2.3 Ion Exchange Chromatography

Ion exchange chromatography requires the interaction of charged analytes with oppositely charged functional groups on the stationary phase. These stationary phases can be in the form of strong or weak, cation or anion exchangers. Elution is controlled by either increasing the ionic strength of the buffer, thus increasing the concentration of competing counter ions, or changing the pH, which can modify the charge of the analyte or the ion exchanger on the surface. The application range for ion exchangers is broad covering both organic and inorganic analytes. However, the main application range is for the separation of biopolymers, specifically proteins and nucleic acids.

1.1.2.4 Size Exclusion Chromatography

In size exclusion chromatography, separation is based on the partial exclusion of analytes from the pores of the packing, due to the size of the analyte relative to the pores. Molecules too large to enter the pores are eluted with the mobile phase in a volume V_o (interstitial volume outside the particles). Molecules small enough to permeate all the pores elute in a volume V_m (interstitial volume V_o plus particle pore volume V_p). Size exclusion

chromatography is used most often for the analysis or characterisation of industrial polymers and biopolymers.

1.1.2.5 Covalently-Bonded Stationary Phases

Covalently bonding the stationary phase to the surface of the support has to a large extent removed the stability difficulties seen with liquid-liquid partition chromatography. As a consequence, liquid partition systems are rarely used today, having been almost entirely replaced by the use of covalently-bonded silica stationary phases. Again, in the majority of cases, it is amorphous silica which is used as the support, where the surface hydroxyl groups or silanols now provide a convenient surface functionality with which to covalently bond the stationary phase (See Figure 1.2c).

1.1.2.6 Bonded Phases

The flexibility in choice of ligand type has allowed for a wide range of covalently-bonded silica stationary phases to be developed. The market size stands at approximately 80 million dollars and is now used in wide ranging industries for an even broader range of applications. Table 1a provides a breakdown of the market segments that use chromatography.[21]

Table 1.1a: Liquid Chromatography Usage: Breakdown by Industry Segment

Field of Work	% of respondents	Field of Work	% of respondents
Pharmaceuticals	26.1	Instrumental / design / development	1.6
Medical/biological/clinical	17.0	Cosmetics / Toiletries	1.2
Agriculture / food / beverage	13.4	Energy / petroleum / fuels	1.2
Environmental	11.9	Water	1.2
Biotechnology	5.9	Paints / coatings / inks	0.4
Plastics / polymers / rubbers	4.0	Other	11.9
Contract Analysis	3.2		

Information from the same survey provides an indication to the most popular bonded phase chemistries used. In this survey, three selections were invited from respondents. The results have been collated as number of mentions, and tabulated in Table 1.1b.

Table 1.1b: Commercial Preferences for Bonded Phases

Bonded Phase	No. of mentions	Bonded Phase	No. of mentions
ODS (C_{18})	199	Amino	15
Octyl ($_{C8}$)	78	Aqueous size exclusion	10
Silica	56	Alkyl (C_1/C_2)	7
Anion exchange	53	Non-aqueous size exclusion	7
Cyano	41	Butyl	5
Cation exchange	29	Diol	5
Chiral	21	Hydrophobic interaction	1
Phenyl	16		

Reversed Phase HPLC

From the data in Table 1.1b, it is clear that two of the most popular phases in use are the ODS (C_{18}) and Octyl (C_8). These phase are commonly referred to as "reversed phase" stationary phases, since the surface of the silica now has a relatively non-polar character and analytes are eluted in a polar mobile phase (alcohol:water). (The term "reversed phase" is historical, harkening to the fact that the first liquid chromatographic systems comprised a polar stationary phase and non-polar mobile phase. Hence, new systems are the "reversed" of these orginal ones.) Although the more popular hydrophobic moieties are shown to be the octadecyl (C_{18}) groups and octyl (C_8), groups with shorter chain lengths such as C_1 and C_4 also show some popularity. Selectivity is based on predominantly dispersive interactions [22] between analyte and stationary phase, with control of separation and retention achieved by variation of the solvent (mobile phase) strength/solubility. Water is used as the base solvent. The volume percent of an organic solvent, such as methanol or acetonitrile, is used to increase or decrease solvent strength. The solvent strength is relative to the dispersive interactions between the analyte and stationary phase. Retention and selectivity may also be affected by column temperature and pH. In general, the more polar analytes elute faster than the less polar analytes.

The popularity of columns packed with octadecyl silane (ODS, C_{18}) derivatized silica is due to their wide breadth of application, from neutral polar and non polar to acidic, basic and amphoteric analytes. The selectivity of a given ODS phase depends to a large extent on the type of silane used and the conditions under which the synthesis has taken place, since both

of these factors will effect the density of the bonded phase ligands on the surface. This density is important since the greater the access of an analyte to the underlying silica support, the greater the opportunity for secondary interaction (interactions other than dispersive interactions, such as hydrogen bonding). This possibility arises because there are about five silanol (OH) groups per nm^2 of surface on a silica gel, corresponding to 8-9 μmol m^{-2}. It is stereochemically impossible to react more than ~50% of the silanol groups even with ligands as small as trimethylsilyl (C_1).

Bonded Normal Phase Chromatography

When polar groups such as aminopropyl, cyanopropyl, ether or glycol, are employed as the functional group, it is more usual to use a mobile phase system which consists of an organic solvent in the absence of water. A more polar solvent such as ethyl acetate or propyl alcohol is employed to modify retention. In normal phase chromatography, the less polar analytes interact less strongly with the stationary phase and elute before the more polar analytes. Note that these phases can also be used in reversed phase solvent systems (water-based) and provide quite different selectivities than the more conventional phases for reversed phase chromatography, such as C_{18} and C_8.

Before discussing the application of the various phases in any greater detail, it is first necessary to define some of the common parameters used in chromatography.

1.1.3 Basic Definitions

The major objective of chromatography theory is to understand two processes: the process which control relative migration rates, and the process that dictates the degree of band spreading. To elucidate these processes, it is first necessary to define the relevant terms and parameters. Figure 1.3 illustrates a typical chromatogram.

1.1.3.1 Retention

The time which elapses between the injection and the elution of the peak is known as the elution time, t_R, of the analyte. The corresponding elution volume, V_R, and elution time are related via volumetric flow rate, f_v, by:

$$V_R = t_R f_v \qquad [1.3]$$

If V_m is the volume of the eluant in the column, the time to pass V_m into the column is denoted by t_m, and is equal to the retention time of an unretained analyte. The phase capacity ratio, k', is a measure of the degree of retention of an analyte and is defined by:

$$k' = \frac{t_R - t_m}{t_m} = \frac{V_R - V_m}{V_m} \qquad [1.4]$$

The relative position of one peak to another on the same chromatogram can then be expressed as the ratio of their two k' values or alpha (α) value. The term α is also called the selectivity with respect to two compounds, here, compounds 1 and 2:

$$\alpha = k'_2/k'_1 \qquad [1.5]$$

It is very difficult to determine accurately the total volume of mobile phase in the column (V_m), although an approximate value measured from the volume of a supposedly unretained peak is often used. This does not provide an accurate value for two reasons:

i. This volume also includes the volume of solvent in the tubing leading from the injector to the column and from the column to the detector.
ii. There is no simple definition of an unretained analyte, especially since some analytes can be excluded from part of the pore structure of the packing. Even components of eluant (mobile phase) generally do not elute simultaneously, nor do solvent refractive index disturbance peaks.

The accurate determination of V_m has been the subject of considerable debate. Its definition and review of methods of measurement are discussed in detail by Knox and Kaliszan[23].
The following recipes have been advocated for the determination of V_m:

(a) V_m is the elution volume of a solvent disturbance or system peak obtained by injecting an eluant (mobile phase) component.
(b) V_m is the elution volume of an unionised analyte which gives the lowest retention volume and which is small enough not to be sterically excluded from the pore structure of the packing.
(c) V_m is the elution volume of analyte or ion , usually a UV-absorbing ion.
(d) V_m is the volume of liquid which the column contains (obtained for example by weighing the column when full of liquid and then empty) less the volume of any adsorbed eluant components.

(e) V_m is the volume of liquid which, when subtracted form the elution volumes, V_R, of a series of homologues, provides a linear dependence of log $(V_{Rn} - V_m)$ against n, the number of carbon atoms in the homologues.

Knox and Kaliszan argued that none of the above statements gave an acceptable definition of V_m. Instead, they believe the only satisfactory definition is as follows:

The column dead volume, V_m, is the total volume of all components of eluant present within the packed part of the column. They conclude that the primary method for determining V_m should be to measure the retention volume, V_R, of isotopically labelled samples of all eluant components. V_m is then obtained from equation [1.6]:

$$V_m = V_{A^*}\chi_A + V_{B^*}\chi_B + V_{C^*}\chi_C + \ldots\ldots \qquad [1.6]$$

Where χ_A , χ_B , and χ_C are volume fractions of the eluant components A, B and C, and V_{A^*}, V_{B^*} and V_{C^*} are the breakthrough volume of the labelled eluant fronts. (Note, deuterated components can be detected by refractometer). The values so obtained are found to be independent of the identity of the components in the eluant. In practice, an accurate value for V_m is not of great importance but is vital always to state how the supposed value of V_m is measured. Method (b), described above, is the method widely used in practice.

Linear Velocity

Another important parameter used in describing the chromatographic process is *linear velocity*. This describes the rate of movement of eluant along the column, and is denoted by u. It is related to the retention time, t_m, and column length, L, by:

$$u = L/t_m \qquad [1.7]$$

and to volume flow rate by:

$$u = f_v/a_m$$

Where a_m is the mean cross sectional area of the eluant phase within the column. The linear velocity of an analyte band, u_{band}, is inversely proportional to its elution time:

$$u_{band}/u = t_m/t_R = 1/(1 + k') \qquad [1.8]$$

These basic definitions and terminology allow us to describe the two processes of differential migration and band spreading.

Differential Migration

During the chromatographic process, molecules move while in the mobile phase at the mean linear speed of the mobile phase, u. When in the stationary phase, they do not move at all. Therefore, it follows that the speed of a band of analyte molecules relative to the mobile phase is given by:

$$\frac{u_{band}}{u} = \frac{q_m}{q_m + qs} = \frac{1}{1 + q_s/q_m} = \frac{1}{1 + k'} \qquad [1.9]$$

$$\text{then: } k' = q_s/q = \frac{C_s V_s}{C_m V_m} = D\,(V_s/V_m) \qquad [1.10]$$

where q_m and q_s are the quantities of analyte in the mobile or stationary phases, V_s/V_m is the phase ratio, and D is the distribution coefficient of the analyte between two phases, i.e. $D = C_s/C_m$.

Band Spreading

By band spreading, we mean the degree to which the chromatographic peak becomes dispersed as it traverses the length of the column. When discussing the factors that cause band spreading, it is usual to use terminology that describes the chromatographic system in terms of zones, since we are no longer considering equilibria. The mobile zone is not necessarily identical to the eluant phase, since part of the eluant may be held within the pores of the packing material. Similarly, the stationary zone, being the partitioning material inside the pores, does not always correspond to the stationary phase, as this may be a bonded phase, an adsorbent surface phase, or a discrete liquid phase depending on the type of chromatography employed. The mean rate of eluant movement, is now given by:

$$u_{band}/u_o = \text{fraction of analyte in the mobile zone at equilibrium} \qquad [1.11]$$

$$= \frac{q_{mz}}{q_{mz} + q_{sz}} = \frac{1}{1 + (q_{sz}/q_{mz})} = \frac{1}{(1 + k'')} \qquad [1.12]$$

In the above equations, u_o is the linear velocity of the mobile zone, and q_{mz} and q_{sz} are the quantities of analyte in the mobile and stationary zones, respectively. The times t_o and V_o are the elution times of an excluded analyte, such as high molecular weight polymer, or an

ionised analyte. The ratio $q_{s'}/q_{m'}$, denoted by k'' in Equation [1.12], is referred to as the zone capacity ratio.

1.1.3.2 Band Dispersion

The main contributors towards band broadening arise from the flow dynamics of the column. The flow dynamics of the column causes an initially sharp band profile to spread out as it migrates along the column. Ideally the band profile of a chromatographic peak should migrate as a Gaussian distribution resulting in a completely symmetrical peak. Gaussian profiles (Y) can be described mathematically by the equation:

$$Y = Y_0 \, \epsilon^{-\Delta z^2 / 2\sigma^2} \qquad [1.13]$$

where Y_o is maximum peak height, σ is the standard deviation of the peak, and σ^2 its variance, both measured in length units, z is the distance migrated, and Δz is the distance from the peak apex.

Statistical arguments can be employed for the discussion of the concentration profile within the band. For example, if we consider a small element of an analyte placed in a vessel containing stationary solvent, the space occupied by the analyte increases as time passes due to diffusion of the analyte into the surrounding liquid. The standard deviation of this distribution will increase with time, more specifically with the square root of time. In other words, the variance of the distribution increases with direct proportion to time:

$$\sigma^2 = 2Dt \qquad [1.14]$$

We can relate this to band dispersion in a column as follows:

If: $\sigma^2 = 2Dt$ and $t_z = z/u$

then: $\sigma^2 = 2Dz/u$

and thus: $H = \sigma^2/z = 2D/u$

Thus, the band width in a column, σ, will increase as the square root of the distance travelled, z.

The proportionality factor, D, is called the diffusion coefficient. The equation to define D was developed first by Albert Einstein and is called the Einstein Equation. Exactly the same phenomenon occurs when we position a narrow slice of analyte inside a packed bed.

However, in the presence of solid particles, diffusion is obstructed and its rate is smaller than in neat solvent:

$$\sigma^2 = 2\gamma Dt \qquad [1.15]$$

The factor γ is called the "obstructive factor" and its value depends on the amount and the nature of the obstruction that is in the way of the free diffusion of the molecule between phases. The two factors, which hinder diffusion in this way, are:

1. Tortuosity of the pores, which results in an increased diffusion path length
2. Constriction of the pores, which gives rise to non-uniform concentration gradients

1.1.3.3 Flow Properties in the Column

Although there are other processes which cause peaks to spread, they all behave like diffusion in producing variance, σ^2, which increases with the distance migrated. In other words the variance of the peak, σ^2, therefore increases linearly with the distance, z, that it has travelled. A plot of the variance against length is a straight line. The slope of this relationship is the height equivalent to a theoretical plate (HETP, sometimes simply called H):

$$H = d\sigma^2/dZ \qquad [1.16]$$

and for a uniform column:

$$H = \sigma^2/L \qquad [1.17]$$

In this concept, the height equivalent to a theoretical plate, H or HETP, can be thought of as the thickness of a slice of the column. Dividing the total column length by this length (H), gives the number of theoretical plates in the column, hence the plate count N, now more frequently described as the column efficiency:

$$N = L/H = L^2/\sigma^2 \qquad [1.18]$$

The plate count is conveniently determined from a chromatogram. Since plate count is a dimensionless parameter, it can be obtained from the peak width, w, and retention time, t_R, provided the migration velocity of the peak has been constant during the recording of the chromatogram:

$$N = L^2/\sigma^2 = f\, t_R^2/w^2 \qquad [1.19]$$

The peak width is measured in the same time units as retention time, while factor *f* depends on how the peak width is measured (see Table 1.2).

Table 1.2[24]

Factor f of equation [1.19] as a Function of Peak Width (w_p) Measurement Technique.

Method	Position of Peak Width	Factor f
Inflection Point	60.3.% of peak height	4.00
Half-height	50% of peak height	5.54
4σ method	13.4% of peak height	16.00
5σ method	4.4 of peak height	25.00
Tangent method (equivalent to 4σ)	Intersection of tangents with baseline	16.00

The details of the measurement are shown in Figure 1.4 (baseline drift is included to clarify how the baseline should be measured in the case of a drifting baseline). Note that the lines drawn represent the position at which the width should be measured, and are shown to be parallel to the baseline although the actual width measurement has to be made horizontally. It therefore follows from Table 1.2 above, that by employing the 4σ method for peak width:

$$H = L/16 \frac{(w)^2}{(t_R)^2} \qquad [1.20]$$

and that:

$$N = 16 \frac{(t_R^2)}{(w)^2} \qquad [1.21]$$

1.2 Differential Migration - Thermodynamics of Chromatography

A prerequisite for any successful chromatographic system is that the two processes of differential migration and band spreading are optimised in such a way that separation of two analyte band profiles can be achieved. In general, the sharper the band profiles the easier this becomes. We now therefore discuss in greater detail the factors that influence these two quite separate processes.

1.2.1 Distribution Equilibria

Experimental factors which influence the rate of differential migration of the analyte are those which affect the distribution coefficient (D), and are:

1. The composition of the moving (mobile) phase
2. The composition of the stationary phase

3. The separation temperature
4. The separation pressure

Since these factors are *thermodynamic quantities* they all affect the equilibrium coefficient, D, and hence the chromatographic process. The equilibrium coefficient itself can be described in terms of the phases within a column, between which an analyte is equilibrated. Giddings showed that the distribution of any analyte between phases during the chromatographic process is negligibly different from that which would be achieved at complete equilibrium[25]. Furthermore, this means that the relative distribution of an analyte (A) between two immiscible phases averaged over the chromatographic band is described precisely by the thermodynamic distribution coefficient, D:

$$D_A = C_{s(A)}/C_{m(A)} \qquad [1.22]$$

where $C_{s(A)}$ and $C_{m(A)}$ are the concentration of the analyte in the stationary and mobile phase.

The classical thermodynamic expression relating the distribution coefficient to standard free energy difference can then be employed to describe the extent of retention:

$$RT \ln D = -\Delta G^{\circ} \qquad [1.23a]$$

where ΔG° is the standard free energy of transfer from the mobile phase (m) to the stationary phase (s), R is the gas constant and T the temperature.

The column capacity ratio, k', is then related to D through the phase ratio:

$$\varnothing = V_s/V_m \qquad [1.23b]$$

Then:
$$k' = q_s/q_m = C_s V_s / C_m V_m \qquad [1.23c]$$

$$k' = \varnothing D \qquad [1.24]$$

or:
$$\Delta G^{\circ} = -RT \ln k'/\varnothing \qquad [1.25]$$

ΔG° is the change in free energy when an analyte is transferred from its standard state (e.g. 1mol/l conc^{n}) in the eluant to its standard state in the stationary phase (e.g. 1 mol/l conc^{n}).

Because:
$$\Delta G^{\circ} = \Delta H^{\circ} - T\Delta S^{\circ} \qquad [1.26]$$

Substituting ΔG° from the Equation 1.26, we get:

$$\ln D = -(\Delta H^{\circ}/RT - \Delta S^{\circ}/R) \qquad [1.27]$$

The effect of pressure on distribution coefficient is given by:

$$d \ln D/dp = +\Delta V/RT$$

where ΔV is the difference in the partial molar volume of the analyte in the two phases. Since ΔV is normally negligible for pressures up to 1000bar, the pressure effect can be disregarded in HPLC.

The effect of temperature on the distribution coefficient, which in chromatography is related to the heat of transfer of the analyte molecules between the two phases, is given by the Van't Hoff equation:

$$d \ln D/dT = + \Delta H / RT^2 \qquad [1.28]$$

whence,

$$d \ln k'/dT = \Delta H / RT^2 \qquad [1.29]$$

provided that $\varnothing$ constant. This is approximately true if the coefficient of expansion of the bulk phases is small.

Enthalpies of transfer are relatively small in liquid chromatography (LC), whereas they are large in gas chromatography (GC). Thus, variations in temperature are generally much more important in GC. Nevertheless, thermostatting of columns in LC is highly advisable if truly reproducible values of k' are required.

In order to calculate ΔH values for a chromatographic system, values of D at different temperatures need to be acquired. Since D can be defined as $k'/\varnothing$ from Equation [1.24] above, its value is determined accordingly from the chromatographic retention of the an analytes at two or more different temperatures from a plot of log k' *vs.* 1/T where the gradient is $-\Delta H/R$.

Thermodynamics Adsorption chromatography

When dealing with adsorption chromatography, the volume of the stationary phase is not a useful concept. The amount of stationary phase is more appropriately described by the weight of the adsorbent in the column, W, or by the surface area of the adsorbent in the column, A. The appropriate equations corresponding to [1.23] are then:

$$k' = \frac{C_s' W}{C_m V_m} = D_{ads} (W/V_m) \qquad [1.30]$$

and:

$$k' = \frac{C_s'' A}{C_m V_m} = \frac{D_a A}{V_m} \qquad [1.31]$$

where D_{ads} is generally called the adsorption coefficient (units cm^3g^{-1}) and C_s' is the concentration of adsorbate in moles per unit weight, or, alternatively, where D_a is the superficial adsorption coefficient (measured in cm^3m^{-2}) and C_s" is the adsorbate concentration in moles per unit area adsorbent surface. The equations corresponding to [1.26] are then:

$$V_R = V_m + D_{ads} W \qquad [1.32]$$

$$V_R = V_m + D_a A \qquad [1.33]$$

1.3 Kinetics of Chromatography, Fundamental Relationships, Plate Height, etc.

The factors that control HETP are to a large extent controlled by molecular diffusion within the column. The HETP provides a useful measure of the extent to which band width increases as it travels down the column. Its value generally depends on the linear velocity, u. When H is plotted against u, we obtain a curved relationship with a minimum and a nearly linear increase of HETP with linear velocity at the higher linear velocity range.

1.3.1 van Deemter Equations

According to van Deemter, *et al*[26] the quantity H is composed of four terms, all of which contribute towards band broadening in an additive fashion:

$$H = H_{Eddy} + H_{Longitudinal} + H_{Mass\ transfer\ (m)} + H_{Mass\ transfer(s)} \qquad [1.34]$$

(Note: Giddings later showed that this assumption was not correct. His formulation, now widely accepted, shows that eddy diffusion and mobile phase mass transfer must be combined harmonically. The Giddings formulation is discussed in more detail later in this Chapter. First we will discuss the contributors to band broadening.)

Eddy Diffusion - H_{Eddy}

Van Deemter, *et al*, postulated that this contribution to band broadening was independent of flow, they called it "Eddy Diffusion." When a sample migrates through the packed column, the individual flow paths around the packing particles are of different lengths. These

variations in the flow rate and flow direction, lead to band broadening that should only depend on how well the column is packed. According to the van Deemter treatment, H_{Eddy} is proportional to particle size and is usually given by:

$$H_{Eddy} = 2\lambda d_p \qquad [1.35]$$

where λ is a geometrical factor pertaining to the packing structure and d_p is particle diameter.

Longitudinal diffusion - $H_{Longitudinal}$

Longitudinal diffusion results from molecular diffusion in the direction of the mobile phase flow. This diffusion effect can be described as:

$$H_{Longitudinal} = \frac{2\gamma D_m}{u} \qquad \text{for gas chromatography} \qquad [1.36]$$

and:

$$H_{Longitudinal} = \frac{2(\gamma_m D_m + k'\gamma_s D_s)}{u} \qquad \text{for liquid chromatography} \qquad [1.37]$$

where γ_m and γ_s are constants that take into account the restricted diffusion path in the packed column, D_m is the diffusion coefficient in mobile phase, and D_s is the diffusion coefficient in the stationary phase. Equation [1.37] is true for both GC and LC. However, in GC, D_s is negligible.

Mobile Phase Mass Transfer - $H_{Mobile\ Phase\ Mass\ Transfer}$

In principle, there are two contributions to the resistance to mass transfer in the moving mobile phase[17]:

1. The differences in mobile phase velocity within a single stream of eluant will arise from analyte and solvent molecules midstream moving faster than those closer to the particle surface. In this instance, the term 'mobile phase mass transfer' is used to describe the dispersion effects that the differences in mobile phase velocity (Δu) would otherwise cause.
2. Stagnant mobile phase or mobile phase in the interparticle void volume causes analyte molecules to take different diffusion paths to reach the stationary phase. Those which have to diffuse a longer distance will lag behind the ones that diffuse only a short distance.

We can write the mobile phase mass transfer equation as follows:

$$H_{Mobile\ Phase\ Mass\ Transfer} = (\phi\, d_p^2/D_m)\, u \qquad [1.38]$$

where ϕ is a function of the capacity factor k`.

Stationary Phase Mass Transfer - $H_{Stationary\ Phase\ Mass\ Transfer}$

The stationary phase mass transfer describes the band dispersion caused by analyte molecules in the same migratory band, each molecule having a slightly different residence time in the stationary phase. Analyte molecules in a single analyte band diffuse randomly within the stationary phase, so that the residence periods differ before returning to the mobile zone. Those analyte molecules that remain longer in the stationary phase are thus temporarily left behind the main band of molecules which have continued down the column. Those analyte molecules that remain a short time migrate temporarily ahead. The mass transfer term, C_s, in the stationary phase is given by the equation:

$$H_{Stationary\ Phase\ Mass\ Transfer} = \text{Const.}\ \{f(k')\ (d_f^2/D_s)\ u\} \qquad [1.39]$$

The fraction d_f^2/D_s has the dimensions of seconds and represents a measure of residence time in the stationary phase. In GC literature, d_f is designated as the average film thickness of the stationary phase, and D_s is the diffusion coefficient of the sample in the stationary phase. Equation [1.39] applies to GC where film thickness was a valid concept. It does not apply in LC. In LC, it is better to think of particles as a homogeneous unit with a composite diffusion coefficient D_{sz} (sz = the stationary zone). We then do not need to consider the stagnant mobile phase in the first instance, and:

$$H_{sz} = \text{Const.}\ \{f(k')\ (d_p^2 / D_{sz})\ u\} \qquad [1.40]$$

The relationship first outlined by van Deemter, Klinkenberg and Zinderweg in Equation [1.34] has been examined and revised over the years by several workers in order to allow prediction of chromatographic behaviour from theoretical considerations of band broadening. Key contributors in this field were van Deemter, Giddings, and Knox. The revised equations are discussed in more detail in the following paragraphs.

The original treatment of band spreading by van Deemter, *et al* was developed for GC, but, as discussed above, is readily adapted to LC. When appropriate mathematical expressions for the terms in Equation [1.34] are inserted we obtain the classic form, Equation [1.41]:

$$H = 2\lambda d_p + 2(\gamma_m D_m + k'\gamma_s D_s)/u + \phi\, d_p^2\, u / D_m + \{\text{Const.}\ f(k')\ (df^2/D)\ u\} \qquad [1.41]$$

Equation [1.39] can be more easily represented as follows:

$$H = A + B/u + C_m u + C_s u \qquad [1.42]$$

The van Deemter equation as written above provided a useful description of the basic phenomena in a packed bed. However, it had two basic shortcomings. The first was the fact that the 'A' term, which describes the non-uniformity of the bed, did not withstand theoretical or practical examination. The second was that a negative deviation from linearity was generally observed at the right hand branch of the HETP that could not be accounted for by the van Deemter theory.

Giddings argued that the origin of the problem rested with the assumption in the van Deemter theory that the different contributions to the HETP are independent of each other, and that the variances of these different contributions consequently are additive.

$$\sigma_T^2 = \sum \sigma_i^2 \qquad [1.43]$$

1.3.2 Giddings Equations

Giddings[27] pointed out that the terms for eddy diffusion and resistance to mass transfer in the mobile zone are not independent. The two processes co-operate to reduce dispersion, rather than combining to increase it. According to Giddings, they are coupled to each other. The variances therefore have to be combined harmonically not simply added.

$$\sigma_T^2 = (1/\sigma_1^2 + 1/\sigma_2^2)^{-1} \qquad [1.44]$$

Justification for this can be derived from the "random walk concept." In this concept, a molecule takes random steps of length *l* relative to the average position of all molecules. The variance of the distribution is related to the step length and the number of steps, *n*, as follows:

$$\sigma^2 = l^2 n \qquad [1.45]$$

If we assume that there is a section of length S in the packed bed in which the velocity of a molecule is preserved, then the step length is related to the velocity difference as follows:

$$l = \frac{\Delta u}{u} S = wS \qquad [1.46]$$

where S is called the persistence-of-velocity span, and w is the relative velocity difference (or velocity fluctuation) between an individual molecule and the average molecule.

The number of steps taken during the chromatographic process is simply the column length L divided by the persistence-of-velocity span:

$$n = L/S \qquad [1.47]$$

The variance of the peak and consequently the HETP can now be expressed in terms of the persistence-of-velocity span and the velocity fluctuation:

$$\sigma^2 = w^2SL \qquad [1.48]$$

$$H = \sigma^2 / L = w^2S \qquad [1.49]$$

Both flow and diffusion act together to reduce the persistence-of-velocity span. For example, a molecule may diffuse into a neighbouring flow path that proceeds at a different velocity than the molecule. Thus, each mechanism independently terminates a random-walk-step. After each terminated step, a new step begins. Therefore, the only way in which diffusion and flow are additive is in the number of random steps that they initiate:

$$n = n_F + n_D \qquad [1.50]$$

where the subscripts indicate the origin of the termination of the step by either a change in flow velocity or diffusion. Consequently, the segment length is:

$$S = \frac{L}{n_F + n_D} \qquad [1.51]$$

The HETP of these coupled mechanisms becomes:

$$Hc = \frac{w^2L}{n_F + n_D} = \frac{1}{\frac{n_F}{w^2L} + \frac{n_D}{w^2L}} \qquad [1.52]$$

Since the persistence-of-velocity span for both the flow and the diffusion mechanism is defined as the column length divided by the number of steps attributable to the respective mechanism:

$$S_F = L / n_F \qquad [1.53]$$

and:

$$SD = L / n_D \qquad [1.54]$$

we can write the equation for HETP in the following form, where contributions to the HETP from flow mechanism and the contribution to the HETP originating in diffusion mechanism add harmonically:

$$H_C = \frac{1}{(1/ w^2S_F + 1/ w^2S_D)} = \frac{1}{(1 /H_F + 1 / H_D)} \qquad [1.55][1.56]$$

Since only flow and diffusion effects couple, while longitudinal diffusion and stationary phase mass transfer do not, the complete equation for the dependence of HETP on linear velocity is written:

$$H = B/u + C_s u + \frac{1}{(1/A \times 1/C_m u)} \qquad [1.57]$$

Subsequently, Giddings identified a range of five processes, each of which was "coupled," and proposed that the single coupled term in Equation [1.57] should be replaced by a sum of five similar terms. The effect of this was to widen the range of velocity over which coupling occurred bringing it more into line with experiment. At about the same time, Giddings[28] introduced the concept of dimensionless or *reduced* parameters for describing band spreading. By using reduced parameters, the performance of columns with different particle sizes and in different eluants (gases and liquids) could be compared on a common basis. A performance measure of chromatographic column, which is independent of length, is HETP. The HETP itself depends on the linear velocity of the mobile phase as it moves through the column. If we divide H by the particle size we can now express H in dimensionless or reduced parameters. Similarly, if we multiply the linear velocity by particle diameter and divide the product by the diffusion coefficient of the sample in the mobile phase, we get the dimensionless *reduced linear velocity*. This is a measure of the rate of flow over a particle relative to the rate of diffusion within a particle.

The reduced parameters, popularised by Knox, *et al*[29,30,31] offer a simplified method for optimising chromatographic performance. The reduced parameters are defined by the following equations:

reduced plate height $$h = H/d_p \qquad [1.58]$$

reduced fluid velocity $$\nu = \frac{u\, d_p}{D_m} \qquad [1.59]$$

The dependence of the reduced plate height on reduced velocity can then be expressed using the simple, semi-empirical formula:

$$h = B/\nu + Af(\nu) + C\nu \qquad [1.60]$$

where A, B, and C are dimensionless constants.

1.3.3 Kinetic Optimisation

Knox's contribution to kinetic optimisation was to introduce the third root of velocity, which gives an empirical representation of the Giddings coupling term:

$$h = B/\nu + A\nu^{0.33} + C\nu \qquad [1.61]$$

Usually, with well packed columns the constant, A, will have a value of about unity. The B factor can be estimated from the obstruction factors (particle shape and porosity) for diffusion in two phases, the k' value, and the diffusion coefficients. It is typically between 1.5 and 2.0. The C factor, which is a measure of the dispersion in the stationary phase and stagnant mobile phase, has a theoretical value of about 10^{-2} for columns packed with uniformly porous particles. In practice, the best fit for Equation [1.61] to experimental data gives $C \sim 0.1$.

The general relationship of reduced plate height versus reduced velocity, known as the Knox plot, is illustrated in Figure 1.5a. Experimental verification of the equation was obtained when it was shown that the plots of the reduced plate height, h, against reduced linear velocity gave identical curves for columns containing particles of different d_p (Figure 1.5b). The minimum value for h for a well packed column is in the range of 2 to 3, and occurs when the reduced velocity is in the range of 3 to 5. This minimum corresponds to the optimum flow conditions for the column, i.e. those conditions, which will contribute the least to band broadening. Using this knowledge it is then possible to optimise any chromatographic system.

In order to describe how the Knox equation can be used to optimise a chromatographic system, it is necessary to first define a further reduced parameter, the reduced length of the column:

$$\lambda = L/d_p \qquad [1.62]$$

It is then possible to predict and optimise the flow, particle size, and column efficiency (number of theoretical plates). For optimum conditions in packed column, the reduced linear velocity has a value of approximately 3, and since $\nu = \lambda\, d_p^2/t_m\, D_m$, it is possible to calculate the dp for any specified values of λ, t_m and D_m. For example, in a typical chromatographic system where $\lambda = 20{,}000$ (e.g. L = 100mm), $t_m = 100$s, and D_m 10^{-9} m^2s^{-1} (small molecule in water).

$$d_p = (\nu\, t_m\, D_m / \lambda)^{1/2} = 4 \times 10^{-6}\ m = 4\mu m \qquad [1.63]$$

Using these conditions, it should be possible to get an efficiency, N, of 8,000 plates (*i.e.* h = 2.5) for the column in this example.

The resolution, R_s, of two compounds, A and B, is defined as the peak separation divided by the main peak width, *i.e.*:

$$R_s = \frac{t_R(B) - t_R(A)}{1/2(w_t(B) + w_t(A)} = \frac{V_R(B) - V_R(A)}{1/2(w_v(B) + w_v(A))} \qquad [1.64]$$

We can now define resolution in terms of column efficiency and capacity factors:

Since: $V_R = V_m(1+ k')$ [1.65]

and, rearranging in units of z:

$$w_b = 4\sigma = 4\sqrt{HL} = 4L\sqrt{N} \qquad [1.66]$$

and in V_R units:

$$w_{b(v)} = 4(V_m/\sqrt{N}).(1+k') \qquad [1.67]$$

$$R_s = \frac{V_m(k'_B - k'_A)\sqrt{N}}{2V_m(1+k'_A + 1 + k'_B)} \qquad [1.68]$$

$$= \frac{(k'_B - k'_A).}{(k'_A + k'_B).} \frac{k'_A + k'_B}{(2 + k'_A + k'_B)} \cdot \frac{\sqrt{N}}{2} \qquad [1.69]$$

If $k = (k'_A + k'_B)/2$ and $k'_B/k'_A = \alpha$, then:

$$R_s = \frac{\sqrt{N}}{2} \cdot \frac{\alpha - 1}{\alpha + 1} \frac{k'}{k' + 1} \qquad [1.70]$$

1.4 Liquid Chromatographic Methods

1.4.1 Packing Materials (Manufacture, Physical Properties, *etc.*)

The 'Ideal Support for HPLC' was described by Knox and Kaur[32] in their review of Carbon in Liquid Chromatography. According to their view, such a support should possess the following properties and characteristics:

1. Particles should be spherical and available in particle diameters of 3 - 10μm.

2. Particles should be strong enough to withstand pressure gradients up to 3000 bar/m. They should not swell or shrink.
3. Particles should have a porosity in the range of 50 – 70%, extending to 80% for size exclusion chromatography applications.
4. Particles should contain no pores smaller than ~ 60Å in diameter and have a uniform pore size distribution.
5. Particles should be available with a range of mean pore diameters of 60 – 1000Å.
6. The internal surface of the material should be energetically homogeneous.
7. The internal surface should be capable of chemical modification by bonding, adsorption, or coating, or by a combination of these methods, to provide a variety of surface functionalities. It should be possible to mask both the modified surface functionalities and the original character of the surface completely.
8. Packing materials should be chemically stable under all conditions of pH and eluant composition that would be encountered in chromatographic applications.
9. The physicochemical characteristics of the material should be reproducible from batch to batch and from manufacturer to manufacturer.

It was because of the fit of carbon to this definition that considerable effort was dedicated towards its use as a chromatographic support. Carbon has none of the drawbacks associated with cleavage of bonded phase or dissolution of silica, and is ideally suited towards chromatographic analysis across the whole pH range 1 - 14. This freedom in eluant pH allows analyte ionisation or ion suppression not normally achievable with silica-based stationary phases. A porous graphitic carbon also eliminates the secondary interactions normally associated with silanols (Si-OH) found in silica, thereby yielding a much more reproducible and improved chromatographic system. In this Chapter, we discuss the packing materials most commonly used for HPLC and compare them to PGC the material developed by Knox and Gilbert[33]. The discussion is limited to physical properties of silica gel, bonded silica gels, and graphite. It describes how their properties influence the mode of chromatography and application of the chromatographic system.

Considerable coverage is given to the properties, preparation and role of bonded silica in this Chapter, since they have become the media of choice for a wide range of applications. It is the properties and limitations of such bonded phase media that provide the yardstick by which porous graphitic carbon must be measured.

1.4.1.1 Silica Gels

Amorphous silica is now the most commonly used support employed for adsorption chromatography. The surface of most silica forms is covered with hydroxylated silanols (Si-OH)[34] (hereafter called "hydroxyls"). Unlike crystalline silica, amorphous silica does not have an ordered arrangement of the hydroxyl groups. Instead, it has a heterogeneous surface consisting of sites with different adsorption strengths[23,35] (see Figures 1.6a and 1.6b). In particular, hydrogen-bonded groups are present. The number of these groups depends on the silica's pore diameter. The strength of interaction between these hydroxyl groups and an analyte is thought to be dependent on whether or not hydrogen-bonding interactions occur between neighbouring hydroxyl. In 1964 Kiselev suggested that the isolated hydroxyls were those at which selective adsorption and reaction can occur, *i.e.* they represent the strongest binding sites.[36,37] In 1966 Snyder and Ward[35] suggested that it was the paired hydroxyl groups were more reactive and consequently play the dominant role in adsorption and reaction processes on silica.

Whichever of the two theories is correct, hydroxyl groups capable of hydrogen-bonding play an influential role in retention on silica. They are considered to be the strongest sites for anything other than monofunctional analytes. It is also agreed that the hydroxyl groups have a wide range of adsorptive activity or energy. Accordingly, deactivation of adsorbents by the addition of small amounts of water or other polar compounds is generally required. The purpose of these additives is to deactivate the most active sites leaving less active, but more uniform sites for chromatographic adsorption of analytes. Without polar additives, strong silanophiles may become irreversibly bound to the silica.

1.4.1.2 Bonded Silica Gels

The majority of the most popular packing materials are prepared by covalently bonding organosilanes to the silica surface. The choice of silane chemistry now open to silica manufacturers has increased significantly since the mid-1970's when there was only a small number of organosilanes (hereafter called "silanes") commercially available. The most common silanes used for bonding silica are the chloro-, methoxy- and ethoxysilanes. Within this range there is the possibility to use silanes which have mono-, di- or trifunctionality. When used appropriately, such silanes can be employed to produce a vast range of surface chemistries with varying degrees of polarity. In the following examples silanes with monofunctionality are employed:

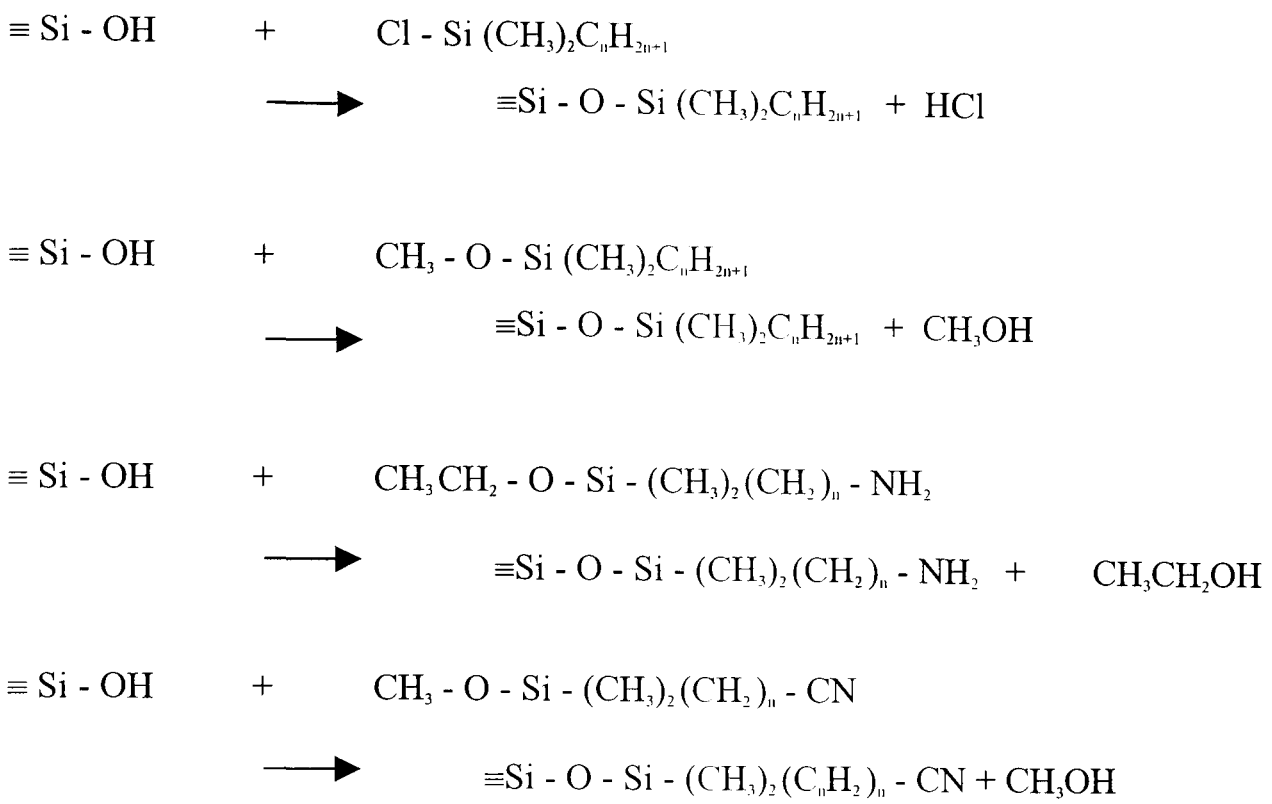

In the examples shown above, one molecule of silane reacts with one hydroxyl group. As a measure of the stoichiometry of the reaction, a factor *f* may be employed and is defined as:

$$f = \frac{\text{Moles of hydroxyl groups reacted}}{\text{Moles of silane reagent reacted}} \qquad [1.71]$$

In the examples given for monofunctional silane reagents, the value for *f* must be exactly 1. For di- and tri-functional silanes, one molecule of silane can react with more than one surface hydroxyl (silanol) group, yielding a maximum *f* value of 2 for a difunctional silane and 3 for a trifunctional silane. However, it is more likely that some silane reagent molecules will bond to only one hydroxyl leaving its remaining functional group free. Therefore, typically, the value of *f* will fall between 1 and 2. Similar arguments can be made for the trifunctional silanes where the value of *f* may fall between 1 and 3.

In order to determine the amount of silane required for a silanization reaction, it is important to be able to estimate the number hydroxyl groups available to react. A wide range of methods have been employed to obtain this number. Of the chemical methods, the reaction of surface hydroxyl groups with methyl lithium (CH_3Li) is thought to provide the most accurate data[39]. Other methods include infrared spectroscopy, isotopic exchange with deuterated water[40] (D_2O) or with tritium labelled water[38] (HTO). It is now generally accepted that the total number of hydroxyl groups per unit area of silica surface is 4.8/nm^2, corresponding to a surface concentration of 8.0 μmol/m^2. From this quantity, the mean cross sectional area (A_m) occupied by a single hydroxyl group is calculated to be:

$$A_m(OH) = 0.21 nm^2 \qquad [1.72]$$

Consequently, conversion in a 1:1 reaction will never exceed 8μmol/m². The ratio of the number of hydroxyl groups that undergo reaction, $\eta_{OH(react)}$, to the total number of hydroxyl groups present before, $\eta_{OH(total)}$, is termed the "effectiveness factor" or η:

$$\eta = \frac{\eta_{OH(react)}}{\eta_{OH(total)}} = \frac{\alpha_{OH(react)}}{\alpha_{OH(total)}} \quad \text{so that } \eta = 1 \qquad [1.73]$$

where α_{OH} represents the surface concentration of hydroxyl groups in units of μmol/m². The $\alpha_{OH(react)}$ value can be obtained by either direct measurement after reaction or by indirect calculation from carbon content. It follows that if the A_m value for a reacting silane exceeds that of the hydroxyl groups, the effectiveness parameter becomes smaller than unity and maximum coverage is less than 8μmol/m². The most common determination of A_m is made from the density of adsorbed molecules. Allowing for the shape and packing density for spherical molecules in a plane hexagonal close packing arrangement the following arrangements result:

$$A_m(nm^2/molecule) = 1.092\ (M/N_\rho)^{2/3} \cdot 10^{14} \qquad [1.74]$$

where 1.092 is a packing factor that considers the six nearest neighbour molecules in the plane, M the molecular weight, N is Avagadros number, and P is the density of the adsorbate in the ordering liquid solid form. For example, using nitrogen (N_2) as the adsorbed molecule, the above equation yields an A_m value as follows:

$$A_m\ (N_2) = 0.162\ nm^2/molecule \qquad [1.75]$$

For the smallest hydrocarbon, methane, which is spherical in shape, A_m ranges from 0.15 to 0.2 nm²/molecule. When covalently bonding organosilanes which react in a 1:1 ratio with the surface, such as trimethylchlorosilane (TMCS), the value of A_m is 0.37nm².
For larger alkyldimethyl silanes the A_m values are even higher. Using the A_m value of a chemisorbed species, the maximum conversion expressed in moles per unit surface area can be estimated as follows:

$$\alpha_{max}(mol/m^2) = 10^{18}/A_m N \qquad [1.76]$$

Some examples of the most commonly used silanes are provided in Table 1.3.[41]

Table 1.3

Some Examples of the Most Commonly Used Silanes

	A_m	$\alpha_{n\text{-alkyl}}$	η_{max}
Trimethylchlorosilane	0.49	3.37	0.42
n-Butyldimethylchlorosilane	0.56	2.97	0.37
n-Octyldimethylchlorosilane	0.61	2.71	0.34
n-Dodecyldimethylchlorosilane	0.76	2.20	0.28
n-Hexadecyldimethylchlorosilane	0.7	2.36	0.30

Alternatively, the conversion obtained experimentally under optimum conditions can be calculated from analytical data, such as carbon content:

$$\alpha_{expt}(mol/m^2) = w / MS_{BET} \qquad [1.77]$$

where M is the molecular weight and S_{BET} is the specific surface area and w is the weight of chemisorbed species in grams of adsorbent.

Bonded Phase Synthesis Methods

The experimental conditions employed to covalently bond organosilanes to the surface of silica (bonded phase synthesis) are outlined below.

The solvents normally used in bonded phase synthesis are aromatic hydrocarbons, *e.g.* toluene or mixed xylenes. These have boiling points of 110°C and 138-140°C, respectively. The synthesis procedure varies somewhat depending on the size of the batch that is to be produced and the type of silanizing reagent that is being used. Scott[42] provides a typical set-up for bonding reaction (see Figure 1.7). The procedure can be summarised as follows:

1. The silica is dried at 250°C for at least two hours to remove surface water.
2. The silica is dispersed in a flask containing toluene. Stringent precautions are taken to remove water from the reaction, especially when dichlorosilanes and trichlorosilanes are employed. These organosilanes are significantly more reactive than the monochlorosilanes (and the alkoxysilanes) and can give rise to polymer formation by the following mechanism:

   $$2Me_3Si.Cl + H_2O \rightarrow Me_3Si.O.SiMe_3$$

   This polymerization can prevent the silane reagent from bonding to the silica surface. The unbonded, polymerized silanes are removed later in the wash process.

3. A slight excess of the silane reagent is added to the silica dispersion. When chlorosilanes are employed, a small amount of pyridine is added to act as a scavenger for the hydrochloric acid released during the reaction. Pyridine is not required when alkoxysilanes are employed, as only the corresponding alcohol is liberated during the reaction. Thus, for reactions using methoxy- or ethoxysilanes the mixture is simply heated under reflux. The alcohol produced is removed by distillation.
4. The mixture is then heated under reflux conditions for a defined period which will ensure that all silanols which are sterically able to react with the silane do so. The reaction time is generally about five hours.
5. The bonded silica is then filtered on a sintered glass funnel, washed sequentially with toluene, tetrahydrofuran (THF), methanol, methanol:water (50:50 v/v) and finally with methanol and dried under vacuum.
6. It is common practice when a bonded phase with reduced silanol interaction is required, to "endcap" the remaining, unreacted silanols with a small molecular weight silanizing reagent. Typically, this might be achieved by reaction with hexamethyldisilazane or trimethylchlorosilane. Both of these silanes result in a C-1 (methyl) group bonded to the surface.
7. The endcapped product is then filtered, washed and dried as in 5. above.

Limitations of Bonded Silica Based Stationary Phases

Covalently-bonded silica stationary phases offered many advantages over the more traditional adsorption and liquid-liquid partition chromatography systems. Adsorption chromatography was not generally applicable to the analysis of polar or organic molecules and equilibration times were often lengthy with peaks tailing due to the presence of active sites at the surface. Covalently-bonded silica stationary phases allowed for a much wider application range, rapid equilibration times, and significantly improved mass transfer characteristics which in turn resulted in improved chromatographic performance. Even with these improvements, covalently-bonded silica stationary phases are not without their limitations.

We first consider the properties of the porous silica used as the support. Most chemical properties of silica are due to the surface silanols (hydroxyls). It is the silanol groups, which are responsible for the acid - base properties of the silica and contribute to the overall polarity of the surface, even when the surface is derivatized. The type and acidity of the silanol groups remaining after surface derivatization can play an important role in

determining the quality of chromatography, causing peak tailing and low efficiencies for both basic and acidic compounds. The effect is most apparent with some of the earlier silicas developed for HPLC. The observed effect on peak shape necessitated the inclusion of either a competing base or acid, such as triethyamine or acetic acid, to the mobile phase. Whether an acid or a base, the additive must be present in sufficient quantities to effectively compete with the silanol-analyte interaction. Consequently, peak shape and performance is improved dramatically when an appropriate competing agent is used.

The following silanol interactions can give rise to peak tailing:

$\equiv Si - OH \bullet\bullet\bullet\bullet\bullet\bullet\bullet NH_2\text{-}R$	Hydrogen bonding with base
$\equiv Si - OH \bullet\bullet\bullet\bullet\bullet\bullet\bullet O{=}RCOH$	Hydrogen bonding with acid
$\equiv Si - O^{-}\ {}^{+}NH_3\text{-}R$	Ion Exchange with base

In recent years, significant improvements have been made to the homogeneity of the surface silanol population of the silica support. In many cases this has resulted in the elimination for the need of a competing acid or base in the mobile phase. A homogenous silica surface is described as one whose surface silanol groups are:

a) Relatively non acidic. This is important since in their non-dissociated form (Si-OH) they will not undergo ion exchange with basic compounds.
b) All of the same type. Neighbouring silanols can then hydrogen bond with their nearest neighbours. The advantage with this type of silanol is that it is believed to be unable to hydrogen bond with the analyte.
c) Free of metallic contaminants.

The improvement to the silica substrate has been gradual. First, there was the introduction of silicas specially treated with strong acids to increase surface hydroxylation (conversion of siloxanes, Si-O-Si to Si-OH). These silicas were known as "base deactivated" silicas and have now been followed by "pure" silicas, free of contaminants such as metal ions. The introduction of pure silicas reflected the fact that the acidity or pK_a of a silanol is strongly influenced by its environment[43]. The presence metals, even at trace levels, can increase the apparent acidity of the silanol groups. Despite these improvements, very basic compounds often still have tailing peaks due to silanol interactions.

An important advantage of covalently-bonded silica stationary phases over liquid-liquid chromatography (coated silicas) was that they could the used over a much wider range of solvent systems. Additionally, they did not require saturation of the mobile phase with

stationary phase. The chromatographic system was therefore much more robust and reproducible. Gradient elution techniques could also be used without concern over stripping the coated stationary phase from the underlying silica.

Despite these advantages, covalently-bonded silica stationary phases are limited to a working pH range of 2 to 8. Below pH 2, the bonded stationary phase can be cleaved by hydrolysis of the Si-O bond. Above pH 8, dissolution of silica can occur, taking with it surface-bound ligand[44]. Both processes result in loss of the stationary phase from the silica surface, with corresponding loss in chromatographic retention and exposure of surface-active sites.

1.4.1.3 Graphites

It is now generally accepted that the structure of true, three dimensional (3D) graphite is that proposed by Hull[45] and confirmed by Bernal[46]. It consists of plain layers of carbon atoms covalently bonded in a regular open structured array, stacked in ABABABAB sequence with weak Van der Waals bonding between layers. At room temperature, the interlayer distance is 3.35Å and the interatomic distance within the layers is about 1.42Å. This is shown schematically in Figure 1.8a.

The graphite developed by Knox and Gilbert has been shown to be two dimensional (2D) graphite. The schematic model for 2D graphite is shown in Figure 1.8b. Its properties are outlined in the following paragraphs.

Two dimensional graphite is often known as disordered or turbostratic carbon and consists of near perfect graphitic layer plain segments arranged in stacks of parallel layers, but with no correlation within stacks. Layers within a stack may be displaced from their neighbours either by small translations parallel to the plane or rotations about the C-axis. The increased mean interlayer spacing (3.40 to 3.43Å) in such carbons is attributed primarily to the stacking disorder and the resultant alterations of the weak Van der Waals bonding between layers. The interatomic distance within the layers is then slightly reduced to 1.40Å. The structure may also be characterised by the apparent mean diameter and height, L_c, of the parallel layer stacks and the probabilities of ordered stacking arrangements between layers separated by n layers in the stack. These quantities are determined from the (*101*) and (*hk*) or (*hkl*) x-ray diffraction profiles. Figure 1.9a shows the x-ray diffraction pattern calculated for perfectly random polycrystalline hexagonal graphite (3D-shows). Figure 1.9b shows the

x-ray diffraction pattern for a number of carbons, which were originally thought to have potential as chromatographic supports.

Using the analogy that the strong peak at (*101*) normally observed for well-ordered 3D graphite was completely absent from turbostratic graphite, Kaur[47] demonstrated that the PGC prepared by the Knox and Gilbert method was in fact a 2D graphite. This fact is highlighted by the absence of (*101*) lines on the x-ray diffraction profile for PGC (see Figures 1.9c and 1.9d).

1.4.2 Specific Modes of Liquid Chromatography

The various modes of chromatography were referred to briefly earlier in this Chapter. Here they will be discussed in greater detail. Each depends upon quite different modes of interaction between the analytes and the stationary phase to achieve a chromatographic separation. It may furthermore be noted that within the umbrella of covalently-bonded silica stationary phases, there are a number of distinguishable subsidiary or secondary retention mechanisms. Each mode of retention is determined by the nature of the covalently-bonded ligand, as, for example, in reversed phase chromatography, ion exchange, size exclusion.

1.4.2.1 Adsorption Chromatography – Silica *vs.* Graphite

According to Snyder, adsorption chromatography is considered to be a competition for the adsorption sites on the surface between analyte and solvent molecules. Before the introduction of the analyte, these sites are covered with solvent molecules. In the presence of analyte X, the following displacement reaction occurs:

$$X + nS_{ad} = X_{ad} + nS \qquad [1.78]$$

where X and S are in solution, while X_{ad} and S_{ad} indicate adsorbed species (analytes or solvent molecules). This equation applies generally to all adsorbates (the stationary support). However, for oxide adsorbents Snyder assumed that the variation in energies of adsorption of species in general (analytes or solvent molecules) was much greater than the variation in their energies of solvation. With this major assumption, an approximate equation relating the analyte adsorption coefficient, K_{ads}, to properties of the adsorbent, the analyte, and the eluant, was derived:

$$\log_{10} D_{ads} = \log_{10} V_a + \beta(S^\circ - A_s \in^\circ) \qquad [1.79]$$

where D_{ads} is the adsorption coefficient, or the ratio of the number of moles of analyte adsorbed per gram of adsorbent to the number of moles of analyte per cm^3 in the eluant. V_a is the volume of an adsorbed monolayer of solvent molecules per gram of adsorbent. This monolayer is estimated to have a thickness of 0.35nm. For typical oxide adsorbents (like silica), where retention arises mainly from hydrogen bonding interactions between surface and analyte, V_a is reduced when water or some other polar "deactivator" is present in the eluant. Essentially, V_a measures the specific area of the adsorbent available to the analyte, which is assumed to be able to displace any molecules of the deactivator. The factor in brackets $(S^\circ - A_s \in^\circ)$ contains the properties of the eluant and analyte:

$$S^\circ = \frac{\Delta G^\circ}{2.303RT} \qquad [1.80]$$

where ΔG° is the standard free energy change for adsorption of an analyte from the solvent onto the surface of the adsorbent. S° is a dimensionless free energy of adsorption of analyte to the surface. A_s is the contact area of the analyte in units of $0.085nm^2$ which is $1/6^{th}$ the area of adsorbed benzene molecule and so corresponds to the effective area of one aromatic carbon atom. $\in^\circ$ is the energy of adsorption of the quantity of eluant required to cover the same area as the analyte molecule. $\in^\circ$ is called the eluotropic strength parameter and is taken as 0 for pentane. For a strong eluant, such as methanol, $\in^\circ$ is around 1. β is a measure of the surface activity and changes with the degree of deactivation by polar modifier, e.g. water.

A more convenient form of equation [1.79] can be derived, noting that:

$$k' = D_{ads} \frac{W}{V_m} \qquad [1.81]$$

$$\log_{10} k' = \log_{10} \frac{(V_a W)}{V_m} + \beta(S^\circ - A_s \in^\circ) \qquad [1.82]$$

The term $V_a W$ is the volume of the solvent that forms a monolayer coverage on the total active adsorbent surface within the column. $V_a W$ can be formally equated to V_s, the volume of the stationary phase in the column. We thus arrive at:

$$\log_{10} k' = \log_{10} \frac{(V_s)}{V_m} + \beta(S^\circ - A_s \in^\circ) \qquad [1.83]$$

so that the distribution coefficient between eluant and stationary phase now becomes:

$$\log_{10} D = \beta(S^{\circ} - A_s \in^{\circ}) \qquad [1.84]$$

Snyder's adsorption theory gives useful explanation of analyte retention on both silica and alumina. Weak solvents (eluants), such as hydrocarbons, have $\in^{\circ}$ values near zero, whereas strong solvents, such as methanol, have $\in^{\circ}$ values around unity.

The main assumption of the theory is that adsorption is considered as a competition for the substrate adsorption sites by different molecules based on hydrogen bonding interactions for analyte molecules and solvent molecules alike. As soon as this theory is applied to a non-polar adsorbent such as an octadecyl-modified silica gel, a polymeric phase, or graphite, the concept that solvents can organise in order of their hydrogen bonding power is lost. Thus, with graphite, for example, the apparent range of $\in^{\circ}$ is only about 0.2 units and the eluotropic series depends upon the analyte.

1.4.2.2 Liquid –Liquid Partition Chromatography

The theoretical aspects associated with liquid partition chromatography are also relevant to covalently-bonded silica stationary phases. Snyder[48], *et al* developed the following equation to describes the distribution D of an analyte , between mobile and stationary phase.

$$\text{Log } D = \frac{V_i}{RT}[(\delta_i - \delta_m)^2 - (\delta_i - \delta_s)^2] \qquad [1.85]$$

Where V_i is the molar volume of analyte I and δ_I, δ_S and δ_m are the solubility parameters for analyte, mobile and stationary phase. Solubility parameters were first introduced by Hilderbrand, *et al*[49,50]. They are defined by:

$$\delta_i = (\Delta H_{vap}/V_i)^{1/2} \qquad [1.86]$$

and, by convention, are listed in units of (calories $cm^{-3})^{1/2}$. ΔH_{vap} is the molar heat of vaporisation of the substance.

Equation [1.85] is based upon the assumption that the components of the solutions show regular solution behaviour. In regular solution behaviour, the heat of mixing is non-zero but the entropy of mixing is ideal. This assumption will not hold accurately for liquids that are so immiscible that they form two phase mixtures. This requires the difference $\delta_s - \delta_m$ to be greater than seven. Thus, the approach can only be used for semi-quantitative predictions.

The distribution coefficient is related to the capacity factor, k', by:

$$k' = \frac{D(V_s)}{(V_m)} \qquad [1.87]$$

where V_s is the volume of stationary phase and V_m is the volume of mobile phase.
Combining the equations [1.85]and [1,87] we then get:

$$\ln k' = \ln (V_s/V_m) + (V_i/RT) [(\delta_i - \delta_m)^2 - (\delta_i - \delta_s)^2] \qquad [1.88]$$

Thus control of k' can be achieved by careful choice of δ_m and δ_s in a liquid system, but any two phase mixture will only have a limited range of analyte polarities or δ_i values. Further adjustment to k' can then be made by either changing the phase ratio (V_s/V_m) or by using different phase systems with the same solubility parameters. The latter method exploits the fact that, although liquids or mixtures of liquids can have the same overall solubility parameters, the parameters can arise from different physical-chemical properties of the liquids. For example a proton donating stationary phase and a proton accepting stationary phase might have the same solubility parameter but slightly different solubility for weakly basic analytes. A paper by Keller, *et al*[51] deals with this effect in more detail.
For the reasons discussed above, liquid partition chromatography is rarely used today, having been almost entirely replaced by covalently-bonded silica stationary phase LC. Consequently its application and practicalities are not discussed further here.

1.4.2.3 Ion Exchange Chromatography

High performance ion exchange chromatography is generally carried out on chemically derivatized silica. This, however, limits the range of usefulness to between pH 2 and 8. Consequently, to operate outside this pH range it is necessary to use polymer-based rather than silica-based supports. The separation mechanism is the same, but the pH application range is much wider. Polymers were, in fact, the supports for the first ion exchange chromatography materials. However, they were limited by their poor mechanical stability. This prevented the use of smaller particles such as those used by silica-based ion exchangers, which give rise to the increased efficiencies associated with high performance separations. Improvements made to modern polymer technology have yielded ion exchange materials with considerably higher efficiency and stability than the earlier technology. Ion exchange often provides considerably better chromatography of polar, ionisable compounds than reversed phase, where they are typically not retained. Most ion exchange materials fall into two groups: those which contain acid groups, such as sulphonic acid or carboxylic acid, for the separation of cationic compounds, and those which contain a basic group, such as an

amine or quaternary amine, for the separation of anionic compounds. It is important to buffer the mobile phase in this mode of chromatography, to control the ionisation of the analyte and the position of the acid - base equilibria of the ion-exchange properties of the media. However, this is not essential for strong ion exchange.

The exchange process may be represented as follows[12]:

$$\sim N^+ C^- + X^- = \sim N^+ X^- + C^- \qquad [1.89]$$

where C^- is the counter ion to the fixed ion exchange site $\sim N^+$ and will be present in the eluant. Analyte X^- can then displace C^- to give the ion pair N^+X^-. For effective chromatography this displacement reaction must be at equilibrium, retention is therefore controlled by the equilibrium [1.89] for which the equilibrium constant K_{IE} is:

$$K_{IE} = \frac{[C^-][\sim N^+ X^-]}{[X^-][\sim N^+ C^-]} \qquad [1.90]$$

The capacity factor, k', being proportional to the distribution coefficient, D_{IE}, is given by:

$$k' \alpha K_{IE} = \frac{[\sim N^+ X^-]}{[X^-]} = K_{IE} \cdot \frac{[\sim N^+ X^-]}{[X^-]} \qquad [1.91]$$

Since the concentration of the ion exchange sites, $[\sim N^+X^-]$, is constant and fixed by the rigid structure of the matrix, k' is inversely proportional to the concentration the counter ion (ionic strength) in the eluant:

$$k' \alpha [X^-]^{-1} \qquad [1.92]$$

The pH of the eluant may also affect k', although only indirectly through the fraction of analyte ionised and the fraction of ion exchange groups ionised. If we consider a solvent system that is buffered to control pH and the position of the acid base equilibria:

$$R.COOH + H_2O \rightleftharpoons R.COO^- + H_3O^+$$

then the fraction of ionised molecules for either the stationary phase ion exchanger, the analyte (if it is a an acid) or the eluant is given by:

$$\text{Fraction ionised} = \frac{[R.COO^-]}{[R.COO^-] + [RCOOH]} \qquad [1.93]$$

$$= \frac{K_a}{[H_3O^+] + K_a} \qquad [1.94]$$

When the pH is significantly less than the pK_a, the fraction ionised is inversely proportional to $[H_3O^+]$, and so is k', provided that the unionised form is not adsorbed by the matrix. The k' will therefore be reduced if the pH is lowered to reduce the ion exchange capacity of the stationary phase or ionisation of the analyte.

1.4.2.4 Bonded Phase Chromatography

The theoretical aspects associated with mechanism of retention in bonded phase chromatography are still debated. However, the Solvophobic Theory proposed by Horvath, *et al*[53] has been generally accepted by the practitioner.

The Solvophobic Theory is based on the analysis of the equilibrium between an isolated solvated molecule of analyte A, an isolated solvated ligand L and their solvated combination AL. A is in the eluant phase, whereas the underlined species L and AL are in the stationary phase. The distribution equilibrium is represented by:

$$\underline{L} + A \Leftrightarrow \underline{LA} \qquad [1.95]$$

The analyte molecule is imagined to consist of a hydrophobic part and a hydrophilic part, whereas the surface of the bonded phase ligand is hydrophobic. The eluant is said to consist of a mixture of hydrophilic and hydrophobic components, although both components may be combined in the same eluant molecule. The hydrophobic parts of the analyte and the ligand are solvated by the hydrophobic component of the eluant. The hydrophilic parts of the analyte are solvated by the hydrophilic component of the eluant. Horvath, *et al* focused on the decrease in the area of contact with the solvent when the ligand, L, and analyte, A combine to form LA. It is noted that the new contact surface is made by joining the hydrophobic part of the analyte with the hydrophobic part of the ligand, with the elimination of some of the hydrophobic component of the eluant. The association process is analysed with the help of a thermodynamic bridge (see below), where the subscript "solv" indicates a solvated species, and subscript "gas" indicates a species in the gas phase.

Gas Phase

$$\begin{array}{ccc} A_{gas} + L_{gas} \Rightarrow gas & Al_{gas} & \qquad [1.96] \\ \Uparrow & \Downarrow & \\ \text{Desolvation} & \text{Solvation} & \end{array}$$

Solution/Stationary Phase $A_{solv} + \underline{L}_{solv} \Rightarrow_{soln} \underline{AL}_{solv}$ [1.97]

The thermodynamic bridge illustrates the transfer of analyte A from solution to association with ligand, L, via evaporation into the gas phase. Underlined species are in the stationary phase.

According to this theory, the overall transfer represented by the lower process labelled $\Rightarrow_{soln}$ can be achieved by desolvating 'A' and $\underline{L}$ by transfer into the gas phase (process $\Uparrow$), linking them together in the gas phase (process $\Rightarrow_{gas}$) , and then resolvating AL (process $\Downarrow$). The free energy change for the linking is not discussed in detail but it seems to be assumed that the bonding between A and $\underline{L}$ is entirely by London dispersion interactions. The solvation and desolvation processes can be explained as follows:

Taking the solvation of AL, a cavity must first be created in the solvent of appropriate size to take the molecule AL. AL is then placed in the cavity and solvative bonds are formed between AL and the solvent molecules at the wall of the cavity. The free energy required to form the cavity is determined primarily by the surface tension of the solvent and the wall area of the cavity, although a correction factor is required to take account of entropy, reorganisation energy and cavity size:

$$\Delta F_{cavity} = CA_{cavity}\,\gamma \qquad [1.98]$$

where A_{cavity} is the surface area of the cavity, γ is the surface tension of the solvent and C is the correction factor.

1.4.2.5 Ion Pair Chromatography

The technique of ion pair extraction has long been used for the extraction of drugs from body fluids into organic phases. In its simplest form the partition equilibrium is represented by:

$$B^+_{aq} + P^-_{aq} = (B^+P^-)_{org} \qquad [1.99]$$

where B^+ may be the protonated form of the base to be extracted, and P^- is the anion of an acid that is to be used as the pairing ion. (B^+P^-), the ion pair, will behave like a very polar organic molecule and will therefore preferentially dissolve in a polar organic phase, leaving the ionic forms in the aqueous phase. By choosing a suitable pairing ion and adjusting its concentration the base can be very effectively extracted into the organic phase. The role of

the anion and cation can be reversed so that either cationic or anionic species can be extracted by the ion pairing agents.

The extraction equilibrium constant for such a system is given by:[54]

$$E_{BP} = \frac{[B^+ P^-]_{org}}{[B^+]_{aq}[P^-]_{aq}} \qquad [1.100]$$

Equation [1.100] is only true if (P^-C^+) is weakly adsorbed, where C^+ is the solvent counter ion. If (P^-C^+) is strongly adsorbed, then:

$$k' \alpha \frac{1}{[C^+]} \qquad [1.101]$$

It is assumed that the pairing ion, P^-, is present in relatively high concentrations in the liquid phase and is associated with a counter ion C^+, whereas the analyte ion, B^+, is only present at very low concentration compared to P^-. The distribution coefficient is then given by:

$$D_{B+} = \frac{[B^+ P^-]_{org}}{[B^+]_{aq}} = E_{BP}[P^-]_{aq} \qquad [1.102][1.103]$$

Since k' is proportional to D_{B+} in reversed phase chromatography or $1/D_{B+}$ in normal phase chromatography, k' is observed to be proportional to the pairing ion concentration in the former and to its reciprocal in the latter. Control of the pairing ion concentration is therefore a simple way of controlling retention. Graphite can undoubtedly be used as a support for ion pair chromatography, since ion pairing agents are likely to be strongly adsorbed.

1.4.2.6 Chromatography of Chiral Compounds

Chiral compounds are those that possess an asymmetric carbon, which is called the chiral centre. Often, the two (or more) enantiomers exhibit very different activity in biological systems. Chiral chromatography allows the separation of the enantiomers via a chiral selector. Chiral recognition requires a very close interaction between the chiral centre in the selector and the chiral centre in the enantiomers to be separated. In order to achieve separation, diastereoisomeric pairs must be formed which have different binding and/or

partitioning properties. Wainer[55] outlined the basic types of interactions that may take place in a chromatographic system and form the basis by which chiral resolution is achieved:

1. Covalent bonding to form diastereoisomers which are subsequently separated by chromatography.
2. Transient formation of diastereoisomeric complexes based on non-bonding interactions. These non-bonding interactions will normally be a combination of attractive interactions such as hydrogen bonding, π - π, and dipole stacking, coupled with steric repulsion. Pirkle[56] elegantly exploited such interactions.
3. Formation of diastereoisomeric inclusion complexes or complexes with highly structured molecules, such as proteins. The most common examples of the former are the cyclodextrins.
4. Formation of diastereoisomeric ion pairs.
5. Formation of covalent organometallic analyte/selector complexes.

In chromatographic terms, separation of the enantiomers can be achieved on chiral stationary phases by formation of diastereoisomers via derivatizing agents or by employing mobile phase additives on achiral stationary phases. Typical chiral stationary phases include silica gel coated with cellulose derivatized phenyl carbamate, ester, and amylose derivatives.[57] These can be covalently-bound to the silica or simply adsorbed to it. Derivatization of the cellulose gives rise to a range of different phases (see Figure 1.10). Generally, these phases are used in normal phase mode, *i.e.* the eluants are organic solvents without water.

PGC is an achiral phase, that is, it has no specific chiral selectors. Nonetheless PGC has been used very successfully to give impressive separations of enantiomeric compounds by a number of workers[58]. This has been achieved using chiral mobile phase additives in both aqueous and non-aqueous mobile phase systems. PGC has also been used as a chiral stationary phase when its surface has been coated with polymeric chiral selectors. These selectors comprise such molecules as dimethylphenylcarbamate cellulose,[59] polyphenylalanine,[60] or discrete molecules such as enantiomerically-pure amino acids derivatized with naphthylsulphonylchloride, as shown by Wan[61].

When biological activity of the analyte (enantiomer) is required, predominantly aqueous phase systems are used. In such cases, protein-bound stationary phases are preferred as the separation media. Typically, mobile phases containing up to 30% organic solvent can be

used to control of retention before irreversible damage (denaturation) to the protein occurs. Protein-bound chiral phases also allow for chromatography without need for derivatization, and a high degree of specificity is obtained. Typical proteins that may be employed in this way include α_1-acid glycoprotein (AGP), ovamucoid (OV) and serum albumins, where human and bovine are the most common. Covalently-bound cyclodextrin phases are also popular and operate on the principle of occlusion.

1.4.2.7 Exclusion Chromatography

Exclusion chromatography is also known as gel permeation, or gel filtration chromatography. It is uniquely useful for separating high-molecular weight species (molecular weight > 2000 daltons), particularly those which are non-ionic. Besides the resolution of individual macromolecules, such as proteins and nucleic acids, gel permeation chromatography is often used to obtain the molecular weight distribution of synthetic polymers. Separation is based on the molecular size or hydrodynamic volume of the analytes to be separated. The analytes passing through the column take part in a distribution process between the moving mobile phase and the solvent held stationary in the pores of the packing. At equilibrium, the distribution of an analyte can be defined in terms of a distribution coefficient, D_{SEC}:

$$D_{SEC} = C_{sz}/C_{mz} \qquad [1.104]$$

where C_{sz} and C_{mz} are the concentrations of the analyte per unit volume of stationary and mobile phase, respectively. The quantity being measured chromatographically is the elution volume, V_E, which is related to D_{SEC}:

$$V_E = V_o + D_{SEC} \times V_s \qquad [1.105]$$

where V_o is the void or interstitial volume of the column and V_s is the volume of solvent held in the stationary in the pores of the packing material, provided that no chemical interactions contribute to retention.

When molecules are too large to enter the pores of the packing material they elute first from the column and $D_{SEC} = 0$. Smaller molecules, which can fully access the pores, elute last with $D_{SEC} = 1$. The elution rate of the polymers with intermediate molecular weight depends on their relative sizes (see Figure 1.11a). Between the molecular size limits, a selective permeation takes place. The analytes of intermediate size are eluted in order of decreasing size (molecular weight), with elution volumes between $V_t = V_o$ and $V_E = V_o + V_s$.

The molecular weight selectivity is dependent on both the hydraulic radius of the media and the root mean square of radius of gyration of an analyte polymer. This is represented graphically in Figure 1.11b. Here, the molecular weight selectivity is expressed by the reciprocal of the slope of the calibration curve in the linear working range, as:

$$S = \frac{V_E(j) - V_E(i)}{\log[MW(i)/MW(j)]} \qquad [1.106]$$

The smaller the slope, the greater the selectivity (S) to size differences.

The ability of gel filtration to separate macromolecules on the basis of size makes it an essential fractionation tool for applications such as peptide or protein separation. In such an application area the support matrix is usually non-silica based due to silica's high absorptive properties associated with retention of biological compounds and subsequently poor recoveries. Instead, typical supports used for this type of chromatography include Sephadex (cross-linked dextran-polycarbohydrate), BioGel P, (cross-linked polyacrylamide), and Sepharose (agarose). The essential attribute of the eluants, which are typically aqueous buffers, is that they maintain the biological activity of the analytes. For non-biological applications, support matrices comprising organic polymers, such as divinylbenzene, are common. In this case, eluants are usually organic solvents to ensure solubility of the analytes.

1.4.2.8 Affinity Chromatography

Affinity chromatography is now one of the most desirable protein purification methods devised to date[62]. The technique recognises that most proteins bind to other compounds in a specific and reversible manner. Bio-selective adsorption is based upon complementary interaction of two molecules (affinants), and is dependent on structure and functionality of those molecules. For example if an enzyme inhibitor, *e.g.* Soya bean trypsin inhibitor, is immobilised onto a support matrix, then, given the right conditions, the matrix could selectively adsorb the enzyme trypsin from a matrix of proteins and other substances in solutions.

The principle of affinity and pseudoaffinity chromatography is illustrated in Figure 1.12. The selectively-adsorbed protein may be desorbed by using different conditions (*e.g.* ionic strength or pH). The change in conditions alters the configuration of the binding site so that it no longer retains the analyte. The analyte is then released into the mobile phase and

eluted from the column. Alternatively, a similar effect would be observed if the conditions altered the configuration of the analyte.

Apart from the general demands of a chromatographic media for biomolecules of hydrophillicity, macroporosity, and rigidity, media used for affinity separations must also by necessity be easy to derivatise and insoluble, so that no leakage of matrix or ligand takes place. It must also have very little non-specific adsorption characteristics. In practice, the majority of affinity separations have been carried out using agarose as the support matrix because it is readily available and fulfils most of the above criteria. Irreversible adsorption and dissolution due to in-place cleaning procedures at high pH, are the main reasons for silica being rarely used as the matrix support for affinity chromatography.

1.5 Review of Chromatography on Carbon

1.5.1 Historical Survey

Three substantial reviews have been written over the last twenty years, each following the progress of the use of carbon as a chromatographic support.[63 64 65] Following is a short review distilled from information in these articles.

Carbons have been considered for chromatographic supports going back to the early 1940's. At around this time carbon adsorbents had for many years played an important role in industrial purification and refinement processes[66]. Carbon was therefore thought to be an obvious choice for the early fundamental studies in column liquid chromatography.

The carbons used at this time were made from industrial products and not specifically designed for chromatography. In the 1940s and 1950's charcoal was used extensively and very successfully by Tiselius, *et al*[67 68 69] for frontal analysis and displacement chromatography of amino acids, peptides, and acids. In order to prevent irreversible adsorption, carbons were pre-treated with modifiers such as stearic acid or n-octadecane. In this way it was thought that carbon would then provide a completely homogeneous surface onto which model chromatographic studies could take place. At this time advances were continually being made in the production of carbon materials, for example:

- carbon blacks were produced in various grades for the rubber industry
- the high temperature treatments of carbon materials, including graphitization, were examined.

These materials were used for investigative studies for the host of chromatographic techniques that were developing at that time.

In 1951, gas chromatography was developed as a potential separation technique.[70] [71] Using this technique, columns packed with active carbon as the adsorbent allowed for the separation of hydrocarbons.[72] Using this same technique Kiselev, *et al*[73] [74] used graphitized carbon black as the model adsorbent for examining gas-solid interactions. Graphitized Carbon black (GCB) was also used in studies for gas liquid chromatography, where once again the homogeneous surface was thought to provide the ideal support for the stationary phase. GCB was found to be highly reproducible even when obtained from a number of different manufacturing sources. With these advantages, Kiselev described GCB as the ultimate stationary phase for gas chromatography. Research continued through the 1960's and into the early 1970's and resulted in a much better understanding of the mechanism and excellent separations of volatile hydrocarbons. However, although Kiselev proved GCB to be highly suited towards GC, its success did not yet transfer to LC.

In 1946, Claessons[75] obtained excellent separation using frontal analysis chromatography on 5-40μm activated carbon charcoal. Detection was via refractometer. Because charcoal exhibits non-linear isotherm behaviour, it is ideally suited for frontal analysis, but not for the elution chromatography used today. Adsorption isotherm theory is discussed in detail in Chapter 2.

In 1967 and latter in 1970 experiments were carried out using active carbons for thin layer chromatography (TLC).[76] [77] However, the black colour of the plates made simple visualisation of the compounds very difficult. This drawback could be avoided by using radio-labelled analytes, or by subsequent elution on to a silica layer. However, at that time the only active carbons available had poor chromatographic properties. Thus, active carbons in TLC soon gave way to silica gels and alumina. Both gave acceptable chromatographic resolution and colourless bands, which could be visualised with a colour reagent spray.

The early 1970's saw a new era in chromatography with the development of high performance liquid chromatography (HPLC). Microparticulate silicas and their surface modified derivatives rapidly become the preferred column packings for HPLC. However these silica-based material are limited to a pH 2-8 range. Carbon still offered the potential

to utilise the entire pH range. This became the impetus for continued investigation of new carbons for HPLC.

In 1975, Guichon *et al* recognised the potential for carbon black as a chromatographic support for liquid chromatography. However, the carbon material they studied was too mechanically weak to withstand HPLC pressures. Colin, Eon, and Guichon[78] [79] [80] found they could strengthen carbon black by deposition of pyrolytic carbon from benzene vapour at 900°C. The resulting "graphitized" product showed some improvement in performance and HETP (efficiency), but its overall performance did not make it a viable alternative to covalently-bonded reversed phase silica.

In 1980 Unger[81] tried to develop and produce HPLC graphite from purified active carbons and cokes. Although the carbons they produced were very strong and readily withstood HPLC pressures, they had very low surface areas, limited adsorptive properties and gave poor chromatographic performance. Activity in carbon refers to the presence of micropores (pores less than 20Å in diameter). Micropores give rise to a very high specific surface area, typically 900 m^2g^{-1} for charcoal. Micropores lead to poor mobile phase mass transfer of an analyte from the stagnant mobile phase within the pores of the particle to the mobile phase on the outside of the particle. Also, isotherms are strongly non-linear at low surface coverages due to a wide range of surface activity. This leads to significant band broadening and a carbon product that is of little use for chromatography. It was therefore necessary to remove such micropores from the carbon structure if it was to be used as a chromatographic support for HPLC. This was achieved by heating the carbon to a high temperature. Unger heated the carbons in his study to 1800°C. This reduced the surface area from 900m^2g^{-1} to 9 m^2g^{-1}. Although the microporosity had been removed, the surface area was too low to be useful for HPLC. Comparable silica phases have a surface area of between 30m^2g^{-1} and 400m^2g^{-1} which allows for useful retention of analytes.[35]

Another attempt to produce carbon for HPLC was made by Plzak, *et al.*[82] Their material was produced by electrochemical reduction of polytetrafluoroethylene at an alkali metal / mercury amalgam electrode. Again, the material was mechanically strong but gave poor chromatographic properties, (the surface area reduced to 20 m^2g^{-1} from 2000 m^2g^{-1} after heating to graphitization).

A major breakthrough was made in 1981by Liberti, *et al*[83] who confirmed that graphitized carbon black (GCB) could indeed provide satisfactory peaks, not only in gas chromatography, but also in liquid chromatography. However, the main difficulties with the fragility of non graphitized carbon black had still not been resolved.

In 1982, Knox and Gilbert[84] published a paper which described a novel method for making mesoporous glassy carbon using silica gel as a template. This procedure, discussed in detail in the next section, gave the required physical properties in terms of surface area (adsorptive properties) and mechanical stability. However, the chromatographic properties were still poor. It was well known that glassy carbon produced from phenol formaldehyde resin contained micropores. In order to remove the micropores, the glassy carbon was graphitized (heated to temperatures > 2000°C). Removal of micropores reduced the surface area from 400 m^2g^{-1} to 100 m^2g^{-1}. Now, the surface area arose entirely from the mesoporous structure. With the micropores removed, the porous graphitic carbon (PGC) produced now gave the long sought after breakthrough in column performance[85] (see Figure 1.13).

In 1988, the PGC manufacturing process developed by Knox, Kaur and Gilbert at the Wolfson Unit in Edinburgh University was transferred to Hypersil (formally Shandon), where further optimisation of the media's performance took place. The trade name Hypercarb™ was given to the porous graphitic carbon produced by Shandon/Hypersil. The material is now commercially available.

1.5.2 Gas Chromatography and Adsorption

Dias[86] demonstrated that heats of adsorption for a range of small molecules, typically those solvents used for HPLC, were related to retention on PGC by the molecular area of the molecule in contact with the surface, the "molecular footprint". The heats of adsorption were determined from the dependence of log k' on temperature using the van't Hoff equation. The major interactions of molecules with PGC when adsorbed from the gas phase were therefore considered to be non-specific dispersive interactions. These dispersive interactions arise from the interaction of instantaneous dipoles present in the graphite and the analyte molecules. Instantaneous dipoles in turn arise from the non-uniform distribution of the electrons in any atom at any particular instant. Molecular interactions are discussed in greater detail in Chapter 5.

Kiselev and Isirikyan[87] observed that heats of adsorption for both hexane and benzene on graphite are 20-50% larger than their heats of condensation. In a later review,[34] Knox points out that at first sight this may have been unexpected since one might have predicted lower heats of adsorption due to the inability of PGC to totally surround the analyte molecule. Knox states however that detailed calculations are in agreement with theory, and that the expected higher heat of adsorption can be explained by:

a) The high electron density in graphite also plays a part. The density of graphite is 2.2g/mL while density of a typical organic liquid 0.9g/mL.
b) The increased dispersive forces associated with the very small amplitude of thermal vibration of the carbon atoms in the surface of the graphite. This allows an adsorbate molecule to be closer to the carbon atoms in the graphite surface than it would be to neighbouring molecules in a liquid consisting of the same molecules.

The prime point of importance here is that the dispersive interactions of adsorbate molecules with graphite are very strong and that even with polar molecules, such as HCl, dispersive interactions are far more important than dipole-induced-dipole interactions.
A further important feature of Kiselev's and Isirikyan work is the qualitative difference between the ΔH versus surface coverage plots for benzene and hexane. The curve for benzene is flat up to near monolayer coverage, whereas that for hexane rises to a maximum just before this point. Kiselev concluded that adsorbed benzene molecules were localised and immobile, while adsorbed hexane molecules were mobile and could mutually interact. Their interaction augmented the energy of adsorption as the surface coverage increased.
In terms of selectivity, Kiselev and Yashin[88] point out that graphite can provide a unique stereochemical selectivity and that this can, on occasion, be predicted. As an example they site the xylene isomer molecules as separated on GCB. When one xylene molecule is adsorbed onto graphite, the two large methyl groups must always be in close contact with the surface, and these prevent many of the ring CH groups from touching the surface. Thus, with m-xylene, only the single ring CH group at position 5 on the ring can lie on the surface. Accordingly, m-xylene is eluted before o- and p-xylenes where two CH groups are touching the surface. This simple model was also used by Belyakova, *et al*[89] to explain the separation of the more complex terpene isomers. Graphite has also been shown to have unusual selectivity towards structural (geometric) isomers. This was ascribed to the favoured

adsorption of these isomers, which can most easily be accommodated to the surface of the graphite.

The work done in gas chromatography therefore suggested that the primary mode of interaction between analyte and graphite was via dispersive interaction. There was no reason to suppose that this type of interaction would be any different for liquid chromatography. The dispersion forces were observed to be very strong for analytes on graphite. It was believed that analyte retention in liquid chromatography would be stronger on graphite than dispersive forces experienced for silica-based reversed phase C18 media. Experience with gas chromatography had also suggested that because of the flat surface, had the potential to separate structurally related substances, such as geometric isomers. The fluid, brush-like surface of silica-based C18 media would not possess such selective power. At this stage, it appeared that graphite in LC would behave as a perfect reversed phase material showing particularly strong retention properties, rather like a "exceptionally strong " C18 silica.

1.5.3 Liquid Chromatography on PGC

When porous graphite (PGC) was first introduced as a commercially available chromatographic support for liquid chromatography, its mechanism of retention was expected to be much the same as had been described previously for gas chromatography. Interactions were via dispersive forces between analyte and graphite surface. PGC was therefore expected to behave like a very strong silica-based C18 in terms of its retention behaviour towards analytes, with the additional advantages that it may show improved selectivity for closely related compounds such as geometric isomers. It would also be stable across the entire pH range. The pore size, particle size, surface area, and mechanical stability were similar to commercially available silica-based C18 media. PGC therefore met all the requirements described Knox and Kaur[90] for the Ideal HPLC support. Initial studies by Kaur[91] supported this view.

However, when graphite became commercially available in 1988 in packed columns, a much wider study into the chromatographic potential of PGC was possible. Before long, several workers had observed that, while in many instances PGC did behave rather like a stronger C18-bonded silica, other observations suggested that it behaved quite differently.

A substantial review covering these investigations and the observations has been carried out[92]. Some of the key points to come out of the review were as follows:

Relative to other supports, graphite shows:

1. A lack of any eluotropic series. The eluotropic series for oxide supports, such as silica and alumina is based on the ability of the solvent to hydrogen bond with the surface. No such interactions can take place at the surface of graphite.
2. Increased retention of non-polar compounds based on dispersive interaction compared to reversed phase silica.
3. Increase selectivity towards structurally-related compounds.
4. A polar retention effect , whereby analytes of increasing polar functionality show an unexpected high affinity towards the graphite surface.

Retention of polar analytes in reversed phase systems

In any reversed phase system, as the hydrophobic properties of the analyte increase, so do the dispersive interactions between stationary phase and the analyte. Retention increases. Conversely, as the polarity of the analyte increases or hydrophobicity decreases, the dispersive interactions between analyte and stationary phase decrease and so does retention. This simple observation holds true for all reversed phase systems with the exception of PGC, where it has been observed that retention in a number of cases increases as the polarity of the analyte increases. We have called this effect "the polar retention effect on graphite" or PREG.

Each of the points raised above are now reviewed in more detail in the following paragraphs.

Solvent Strength Properties

Kaur[93] investigated a range of solvents typically used in HPLC. Although she was able to arrange these solvents in order of eluting power for a particular functional group, the lack of any universal eluotropic series became clearly apparent. This is a feature of graphite and makes it quite distinct from oxide adsorbents. It was noted that in the absence of any universal eluotropic series, the range of eluotropic strength (using the Snyder scale[94]) for any given compound or functional group, was very small. Typically, this was around 0.2 units on PGC (omitting water) compared to about 1 unit for oxide adsorbents, such as silica and alumina. This major difference is explained by Snyder's own theory, whereby adsorption of an analyte from solution is thought of as a molecule of analyte replacing one or more

molecules of eluant at the adsorbent surface. With oxide adsorbents, the eluotropic strength of a solvent is related to its heat of adsorption per unit area. For oxide sorbents the solvent's eluotropic strength is highly dependent on its ability to hydrogen-bond with the surface groups (*i.e.* Si-OH on the silica). Therefore, a wide-range of strengths is possible as one moves from non-hydrogen bonding solvents, such as hydrocarbons, to alcohols, acids, and ultimately water, which forms strong hydrogen bonds with surface Si-OH groups. These hydrogen bonds are so dominant that differences in the solution interaction energies of the analyte with solvent, and solvent with solvent can be ignored. With PGC, no such hydrogen-bonding can take place at the surface. The dominant contribution to the heat of adsorption associated with oxide sorbents is absent in PGC.

Solution interaction between analyte and solvent were therefore expected to be of significant importance in determining retention and selectivity on graphite. Because the heats of adsorption of solvents per unit area from the gas phase are, in fact, very similar, it was thought that graphite should be relatively unselective with regard to analyte functionality. To a first approximation, adsorption onto graphite appeared to be dominated by non-specific dispersive forces.

Retention behaviour for non polar compounds

Möckel and co-workers[95] studied the retention of a range of simple aliphatic and aromatic compounds on PGC. In each case, plots of log k' *vs.* carbon number, n, were linear with good correlation. The equation for this relationship is:

$$\mathrm{Log}_{10}\, k' = \alpha + \beta n \qquad [1.107]$$

The gradients, β, of the plots for the different homologous series $CH_3(CH_2)_{(n-1)}X$ were similar irrespective of X, and gave a measure of the selectivity of the materials with respect to addition of the CH_2 group. For Inertsil™ C18, β [$=\log(k'_{n+1}/k'_n)$] had a value of 0.08 whereas for PGC the value was 0.26 , showing that PGC has much greater discrimination for the methylene group than does C18.

Kriz, *et al*[96] made a similar observation when comparing plots of different homologous series, $CH_3(CH_2)_{(n-1)}Ar$ with a series of polymethylbenzenes, $Ar(CH_3)_{n+1}$. The value of β was found to give a value of 0.42 for PGC compared to 0.22 for Hypersil™ ODS. A tabulated summary of Kriz's results is given in Table 1.4 below:

Table 1.4

Comparison of α(CH3) and α(CH2) selectivity on different stationary phases

Support	$\alpha(CH_3)$	$\alpha(CH_2)$	Eluant
PGC	0.46	0.22	Methanol
C18-Silica	0.17	0.17	Methanol:Water (80:20w/w)
Silica	0.046	0.1	Pentane
Alumina	0.195	0.00	Pentane

The results from both sets of workers show that as the value of n is increased, the relative retention on PGC increases at a much faster rate than that of C18 or oxide supports. Therefore, whereas the retention of a monosubstituted benzene may be similar for both C18 and PGC, a di- or tri-substitution will cause a significantly greater increase in retention on PGC.

1.5.4 Liquid Chromatography - Polar Retention Effects

Kalizan and co workers[97 98] and Lim and co-workers[99] were among the first to realise that PGC had quite different retention behaviour for polar analytes than the more commonly used reversed phase materials, *i.e.* C18-silica. Kalizan, *et al*, using heptane as the eluant studied a wide range of simple aromatic compounds where one hydrogen was substituted with a wide range of more polar functional groups. They observed that substitution with a polar group increased retention. This was in stark contrast to their observations on C18-silica reversed phase materials where typically the retention is observed to decrease. Kaliszan correlates his results with a polarity parameter,[100] Δ, and concluded that a localised segment of the molecule was responsible for retention rather than the π electrons of the localised ring. He also pointed out that graphite behaved somewhat like a metal and that this was not unexpected in view of the electrical conductivity of the layer planes of the graphite.

Lim[101] and co-workers made similar observations with the separation of pertechnetate and perrhennate ions in a predominantly aqueous eluant where separations could not be explained solely on the basis of dispersive interaction. Indeed a very strong interaction

between the charged ion and the graphite surface was required to counter the hydration energy in solution.

Möckel, *et al*[102] in a comprehensive study, showed the value of the y-intercept, α, in Equation [1.107], provided a further confirmation of this peculiar retention behaviour on graphite. The substitution of X (where X is hydrogen) with any group, polar or non-polar, had a positive effect on retention. Retention either increased, or at least balanced the increased attraction for the analyte with the polar mobile phase. The results were in qualitative agreement with Kaliszan, where once again retention of polar compounds on graphite was in stark contrast to the results observed for C18-silica where the increased affinity of the polar substituent for the mobile phase resulted in each case with a reduction in retention. The adsorption energy for polar groups onto PGC must therefore contain terms additional to those of purely dispersive interactions.

Tanaka, *et al*[103] investigated the retention properties of PGC using a series of alkanols. Their results complement those of Möckel and Kaliszan. Once again, retention of polar compounds was seen to increase with increasing polarity. In Tanaka's study, it was observed that if the contribution to the retention from the alkanes was removed and (-H) replaced by a more hydrophilic group,-X, the retention reduced considerably for a C18-silica. For PGC, it increased. Thus, the increased solubility when substituting -H by a more polar group is more than compensated for by the additional affinity for graphite. Substitutions, relatively speaking, have a positive effect on retention for PGC and in a number of cases (halogen substitution) the additional affinity of graphite for the substituent group exceeds its additional affinity for solvent (in others -CN, $-COCH_3$, and -OH the two effects more-or-less cancel out).

Coquaert and Hennion[104] [105] [106] demonstrated how differently PGC retains polar compounds compared to C18-silica and Hamilton PRP-1™, a polymer-based reversed phase material. This was done by comparing extrapolated log k'_w values for a range of compounds in their mono-, di- and tri-substituted forms. An example from their paper is given in Table 1.5 below. The log k'_w values refer to log k' values of an analyte in 100% water. Often, because of solubility limitations, these values can be obtained by extrapolation of the plot log k' v C_{org}:

$$\log k' = \log k'_w + AC_{org} \qquad [1.108]$$

where C_{org} is the percent organic solvent in a water:organic solvent mixture and A is the slope of the line, and k'_w is the intercept at the y axis (log k' at 100% water).

Table 1.5

Values of log k'_w for Polyhydroxy Benzenes on Reversed Phase Media

	C18-Silica	PRP-1	PGC
Phenol	1.55	2.40	1.80
1,3-dihydroxybenzene	- NR	1.35	2.35
1,3,5-trihydroxbenzene	- NR	0.5	2.70

(- NR, analyte is not retained)

The results show that while the retention of monosubstituted benzenes may be similar for C18-silica, PRP-1, and PGC, a di- or tri-substitution to the benzene ring, (increasing polarity) will cause a significant increase in retention on PGC and a decrease in retention on C18-silica and PRP-1. In the case of C18-silica, the di- and tri-hydroxyphenols are not retained.

As part of the same study on the use of PGC for the removal of contaminants from water samples, Coquart and Hennion[107 108 109] correlated log k' and log P for a number of stationary phases, including PGC. The correlation with C18-silica and C8-silica was very good. The correlation with PRP-1 was less clear (the data points were more scattered). With PGC, data points for polar compounds lay well above the lines for alkyl benzenes or alkanes, suggesting a different mechanism of retention for PGC to that of purely dispersive interactions.

Clearly, evidence was growing for a quite different mode of retention on PGC than on the more common reversed phase stationary phases. None of the existing theories for retention allow for such a difference, including:

(1) The Horvath theory[110] emphasises surface interactions of analyte with solvent, but assumes that interactions of analyte with stationary phase involve only dispersive interactions. The observed polar retention effect on graphite [PREG] means that forces other than dispersion forces play a large part in determining analyte retention. The theory cannot therefore be applied to graphite.

(2) Similarly Snyder's theory of adsorption chromatography cannot be applied to graphite as it is based upon the ability of the analyte molecule to displace solvent molecules from the surface of the adsorbent based on hydrogen bonding interactions with

the surface. There are no such interactions possible at the surface of graphite. However, if an alternative polar retention force could be identified, Snyder's theory might be applicable if this alternative interaction replaced hydrogen bonding.

1.5.5 Applications Demonstrating Unique Chromatographic Properties of PREG

The polar retention effect on graphite therefore gives rise to applications not possible on silica-based or polymer-based reversed phase materials. Outlined below are a few examples where PREG has been put to good use. In 1997, Knox and Ross[111] produced a more detailed review of applications on PGC since its introduction to the market.

Separations of sugars, carbohydrates, and glucuronides

Carbohydrates are widely found in nature, and their separation poses a huge challenge to the chromatographer, because of their great diversity of structure and composition.

Carbohydrates are often highly water soluble, and therefore difficult to retain using silica-based or polymeric reversed phases. The polar retentive effect allows PGC to retain these compounds, even from highly aqueous eluants.

Three examples have appeared recently which demonstrate the potential for PGC for carbohydrate separation: Davies, Smith, Harbin and Hounsell[112] demonstrated the separation of a range of alditols containing from two to five monosaccharides. A gradient elution of increasing acetonitrile concentration in water was used with trifluoroacetic acid constant at 0.05%. Generally, retention increased with the size of the oligosaccharide. The order of elution of similar oligosaccharides depended upon the nature of the linkages between units, with 1-3 linked compounds eluting before 1-4 linked compounds. The use of PGC enabled facile separation and identification of the chosen oligosaccharides, and could be applied to identify glycopeptides from a tryptic digest. The authors conclude that PGC is a new and uniquely selective packing material for oligosaccharide analysis

Steffansson and Hoffmann[113] required a method for determining the four diastereometric glucuronides which arise from the metabolism of a new antiarrhythmic drug, Almokalant. The glucuronides were first isolated from urine by adsorption on to a terbium-loaded cation exchanger (the precolumn), and then desorbed by an acidic mobile phase. The desorbed glucuronides could not be retained by a C18-silica material, but were retained by PGC

(Hypercarb™). They could then be eluted with an acidic eluant such as 0.1% acetic acid in methanol:water (30:70), which provided an excellent separation of the R- and S- pairs (α values were typically 1.5). While the precolumn had to be replaced daily, the Hypercarb column proved very robust, with no change in retention parameters over hundreds of injections. When the eluant was changed to 0.01 M H_2SO_4, significant improvement in performance was obtained. Efficiencies were as high as 4000 theoretical plates for the 100 mm long column. All four glucuronides could then be separated after prior isolation using the original system in a small-scale preparative mode.

Stefansson and Lu[114] studied the separation of a range of mono- and disaccharides, sugar acids and sugar amines up to pH 13. Generally, sugars are unionised except at very high pH (12 to 14). Under these conditions they can be retained in LC as ion pairs. Silica-based reversed phase materials cannot be used at high pH but polymer-based materials, such as PRP-1, PLRP-S™ (Polymer Labs) and PGC, are tolerant. Disaccharides were much more strongly retained than monosaccharides, sugar acids were somewhat more retained, and amino sugars similarly retained.

These examples provide excellent illustrations of the strong retentive power of PGC for highly water-soluble carbohydrate-containing compounds. An important potential use of is the separation of water-soluble metabolites, such as glucuronide- and sulphates-metabolites of drugs[114b]. The use of PGC in this area is far from fully explored. However it is clearly a promising material for carbohydrate analysis.

Environmental applications

C18-silicas and polystyrene resins are satisfactory materials for compounds of environmental interest that are not too hydrophilic and have log P values above about 2 (P is the octanol/water partition ratio). However, many of these compounds, including polyhydric phenols, atrazines and their degradation products, which are often very water soluble, have log P values below 2. With C18-silica and polymer-based materials, the breakthrough volumes associated with solid phase extraction (SPE) techniques are far too small to allow for adequate trace enrichment. PGC (Hypercarb), with its retentive properties for polar compounds, has proved to be the only material so far developed which provides adequate retention.

Hennion and her co-workers were among the first to exploit this characteristic, having studied this area in depth. Major problems had been experienced with the extraction and chromatography of the triazine-based herbicides since these are highly polar and have log P values ranging from 2.7 for atrazine to negative values for cyanuric acid, ammelidine and ammeline[115]. Since retention by C18-silicas and polymer-based materials more or less follows the log P values as seen from plots for a range of benzene derivatives given by Hennion and Cocquart,[116] such compounds cannot be extracted by the conventional materials. PGC (Hypercarb) was thus the choice for SPE. However, subsequent chromatography was carried out on an C18-silica column.

Further work[117] confirmed that Hypercarb was highly effective for a wide range of polar pesticides having log P values above -0.5 when used as an SPE material, especially if reverse flushing was used to desorb the materials. Reverse flushing was found to be essential if high recoveries were to be achieved. By using reverse flushing, a minimal amount of methanol could be used, which could subsequently be evaporated and the residues taken up in eluant for chromatography.

Clinical Applications

Lim and co-workers[118,119] were early pioneers in the use of PGC, and they achieved some remarkable separations of inorganic ions and complex ions using it. The TcO_4^- and RhO_4^- ions (pertechnetate and perrhenate ions) are highly hydrophobic anions, but would be expected to be unretained on most reversed phase materials. Graphite, however, can apparently interact by electron transfer mechanism (the likely source of PREG) with molecules containing a lone pair of electrons or aromatic ring electrons. Lim showed that these ions could be retained and separated by PGC using aqueous trifluoroacetic acid (TFA) as the eluant.

In another paper, Emery and Lim[120] showed that various organo-metallic charged complexes of technetium and rhenium could also be separated on PGC using TFA solutions containing 2% to 10% acetonitrile. Work on further complexes of technetium showed that cationic and anionic complexes could be separated in the same chromatogram. The sign of ionic charge was not an important factor for retention by graphite. Graphite can evidently behave equally as an electron donor or electron acceptor. They coined the term "Electronic Interaction Chromatography" for this type of separation.

Gu and Lim[121] were the first to study the retention highly water soluble substances by PGC. They found that oxalic acid could not be retained without ion-pairing when using the standard reversed phase supports, but was totally retained by PGC unless a competing acid was added to the eluant. They claimed this as a further example of Electronic Interaction Chromatography.

Krause[122] applied PGC to the determination of ethylene thiourea (ETU), which is a metabolite of ethylenebisthiocarbamate fungicides. ETU is extremely polar and water soluble. Electrochemical detection was preferred over UV, but its use required the presence of phosphoric acid. With bonded-silica columns the phosphoric acid had to be added following chromatography to avoid damaging the column. With polymer and PGC columns it could be incorporated in the eluant which simplified the procedure. Five different bonded silica columns, polymer columns, and PGC were investigated. The polymer columns seemed to cause decomposition of the ETU with use, but PGC provided long-term stability and good quantitation. ETU was eluted as a sharp, symmetrical peak with $k' = 1.7$. The eluant was 5% acetonitrile in water containing 8 mM phosphoric acid.

These examples reviewed above are amongst the most remarkable that have been obtained using PGC since the analytes are normally unretained on reversed phase materials. They illustrate the remarkable ability of graphite to interact with molecules having a lone-pair or aromatic-ring electrons which can apparently interact with graphite by some kind of electron transfer. The nature of this process requires further investigation in order that a physicochemical explanation can be achieved which can then form the basis of quantitative prediction of retention phenomena on PGC.

1.6 Aim of Thesis

Two critical, recent reviews[92,123] provide a good platform on which to base the research for this thesis. In summary, the two reviews provide up-to-date information on the structure and performance of PGC. They also provide a view of the current situation regarding the theories associated with PGC's mechanism of retention. The reviews also give an in-depth

view of the fields of application for which PGC is now being used, and where it might be applied in the future.

From the review we find that the four main areas of work which still require further investigation. These are as follows:

1. Continued development of PGC manufacturing process in order to improve the chromatographic performance.

2. Investigations into understanding eluant-analyte interactions (dispersive, dipole-dipole, and hydrogen-bonding interactions) and how they compare with retention on graphite.

3. Coating PGC to give selectivity more like that of a silica-based reversed phase material.

4. Determination of the energy associated with retention onto graphite from a liquid mobile phase.

5. Further analysis and description of PREG, its quantitation and explanation.

We therefore investigate each one of these areas in the Chapters which follow.

Chapter 1 References

[1] M. S. Tswett, Proceedings of the Warsaw Society of Natural Science, Biological Section, 6, 14 (1903)
[2] Day, D. T., Science 17 (1903) 1007.
[3] R. Kuhn, E. Lederer, A. Winterstein, S., Hoppe Seyler's Z. Physiol. Chem., 197, 141 (1931)
[4] Izmailov, N. A. and Shraiber, M. S., Farm. Farmakol., 4, 8 (1938).
[5] A. J. P. Martin and R. L. M. Synge, Biochem. J., 35, 1358 (1941)
[6] L. R Snyder, *Principles of Adsorption Chromatography*, Chromatographic Science Series , Edward Arnold Publishers (1968)
[7] Tiselius A., Advances in Colloid Sci., 1, 81 (1941)
[8] Tiselius A., Kolloid-Z., 105, 101 (1943)
[9] Tiselius A., Adv. Protein Chem., 3, 67 (1947)
[10] James, A. T. and Martin, A. J. P., Analyst, 77, 915 (1952)
[11] Giddings, J. C., *Dynamics of Chromatography*, Marcel Dekker, New York, (1965)
[12] Snyder, L. R. and Kirkland, J. J., *Introduction to Modern Liquid Chromatography*, Second Edition, John Wiley and Sons, New York, 1979
[13] Kirkland, J. J., editor, *Modern Practice of Liquid Chromatography*, Wiley-Interscience (1971)
[14] Huber, J. F. K and Hulsman, J.A.R.J., Anal. Chim. Acta, 38, 305 (1967)
[15] Lipsky, S.R., Harvath, C., Preiss, B., Anal. Chem. 32 (1960) 1782.
[16] Horváth, C., Melander, W. and Molnár, I., J.Chromatogr., 125,129 (1976)
[17] Knox, J. H., *High-Performance Liquid chromatography*, Edinburgh University Press, 1980.
[18] Unger, K. K., *Porous silica*, J.Chromatogr. Library, vol, 16, Elsevier Scientific Publishing Company, (1979)
[19] Kiselev, A.V., Discuss. Faraday Soc., 40, 205 (1965)
[20] Knox J. H., *High Performance Liquid Chromatography*, Edinburgh University Press (1978)
[21] LC/GC International survey, 1995-96
[22] Scott R. P. W., *Silica Gel and Bonded Phases , Their Production , Properties and Use in LC*, John Wiley & Sons 1993
[23] Knox J. H. and Kaliszan,R., J.Chromatogr., 349, 211 (1985)
[24] De Neue, U., *HPLC Columns: Theory, Technology and Practice*, Wiley-VCH (year?)
[25] See reference 11
[26] van Deemter, J. J., Zuiderweg, F. J. and Klinkenberg, A., Chem. Eng. Sci., 5, 271 (1956)
[27] See reference 11
[28] See reference 11
[29] Laird, G. L., Jurand, J., Knox, J. H., Proc. Soc. Anal. Chem., 11, 310 (1974)
[30] Done, J. N. and Knox, J. H., J. Chromatogr. Sci., 10, 606 (1972)
[31] Kennedy, G. J. and Knox, J. H, J.Chromatogr. Sci., 10, 549 (1972)
[32] Knox.J.H and Kaur.B., Euro. Chromatogr., News, 1(1987)12
[33] Knox, J. K. and Gilbert, M. T., U.K. patent 7939449,1979
[34] Berthod, A., J.Chromatogr., 549,1 (1991)
[35] Iler, R. K., *Colloidal Chemistry of Silica and Silicate*, Cornell University Press, New York, (1955)
[36] See reference 18
[37] Davydov, V. Ya., Kiselev, A. V. and Zhuravlev, L. T., Russ. J. Phys. Chem., 38, 1108 (1964)
[38] Snyder, L.R. and Ward, J. W., J. Phys. Chem., 70(1966) 3941
[39] Knox, J. H., *High Performance Liquid Chromatography*, Edinburgh University Press, (1978)
[40] Stahlin,W., Ph.D. Thesis, Universitat Munchen, Munchen, (1976)
[41] See reference 39
[42] Scott R. P. W., *Silica Gel and Bonded Phases , Their Production , Properties and Use in LC*, John Wiley & Sons, 1993.
[43] Cox, G. B. and Stout, R.W., J.Chromatogr., 384, 315 (1987)
[44] Kirkland, J. J., van Straten, M. A. and Claessens, H. A., J. Chromatogr., 691, 3 (1995)
[45] Hull, A. W., Phys. Rev., 10, 66 (1917)

46 Bernal, J. D., Proc. Royal Soc. (London), A106, 749 (1924)
47 Knox, J, K., Kaur, B., Millward, G.R., J. Chromatogr., 352: 3 (1986)
48 Karger, B. L., Snyder, L. R. and Horváth, C., *An Introduction to Separation Science*, Wiley Interscience, New York, 1973
49 Hilderbrand, J. H and Scott, R. L., *Regular Solutions*, Prentice-Hall, Englewood Cliffs, New Jersey, (1962)
50 Hilderbrand, J. H. and Scott, R. L., *Solubility of Non-Electrolytes*, 3rd ed., Reinhold Publishing Corp., New York, (1949)
51 Keller, R. A., Karger, B. L. and Snyder, L. R., *Gas Chromatography*, p.125, Institute of Petroleum, London (1971).
52 See reference 39
53 Horváth, C., Melander, W. and Molnár, I., J.Chromatogr., 125,129 (1976)
54 See reference 39
55 Wainer, I,W, *Clin. Pharmacol.*, 18: 139 (1993)
56 Pirkle, W. H. and Pockapsky, T. C., *Chem. Rev.*, 89(1989) 347.
57 *Chiral HPLC Columns*, Daicel Chemical Industries, Ltd.
58 Ross, P. and Knox, J. H., "Carbon-Based Packing Materials for Liquid Chromatography, Applications" in *Advances in Chromatography*, vol. 37, pp. 120, Marcel Dekker, Inc., New York, (1996)
59 Greib, S., Ph.D Thesis, Warwick University, (1992)
60 Kelly, E., Ph.D Thesis, Warwick University, (1996)
61 Wan, Qiann-Hong, Ph.D. Thesis, Edinburgh University (1992)
62 Caughlin, R. T. and Thomson, A. R., *Biosep, State of the Art Report, Proteins , Recovery and Purification,* AERE Harwell, 1983
63 Knox, J. H., Unger, K. K. and Mueller, H., "Prospects for Carbon as Packing Material in HPLC," J. Liq. Chromatogr., 6(S-1), 1 (1983)
64 Knox, J. H. and Kaur, B., "Carbon in Liquid Chromatography," in *High Performance Liquid Chromatography*, P. Brown and R. Hartwick, Eds., John Wiley & Sons, London, (1989)
65 Knox, J. H. and Ross, P., "Carbon-Based Packing Materials for Liquid Chromatography, Structure, Performance and Retention Mechanism" in *Advances in Chromatography*, vol. 37, pp. 73, Marcel Dekker, Inc., New York, (1996)
66 Cheremisinoff, P. N. and Ellerbusch, F. (editors), *Carbon Adsorption Handbook*, University of Michigan Press, Ann Arbor, Michigan, (1978) make sure this is the right publisher, I added it.
67 Tiselius A. and Hahn, L., Kolloid-Z., 105, 177 (1943)
68 Williams, R. J. P., Hagdahl, L. and Tiselius, A., Arkiv. Kemi., 7, 1 (1954)
69 Waksmundzki, A. and Oscik, J., Ann. Univ. Marie Curie-Sklodwska, Lublin, Poland, Sect. A6, 87, (1951)
70 Cremer, E. and Prior, F., Z. Elektrochem., 55, 66 (1951)
71 Cremer, E. and Muller, R., Z. Elektrochem., 55, 217 (1951)
72 Kiselev, A. V and Yashin, Ya. I., Zh. Fiz. Khim., 40, 603 (1966)
73 Kiselev, A. V and Yashin, Ya. I., Abh. Deut. Akad. Wiss. Berlin, kl. Chem. Geol. Biol., 2, 103, (1966)
74 Kiselev, A. V., Kuzntesov, A. V., Filatova, I. Yu. and Shcherbakova, K., Zh. Fiz. Khim., 44, 1272, (1970)
75 Oscik, J., Ann. Univ. Marie Curie-Sklodowska, Lublin, Poland, Sect. AA, 1, (1952)
76 Perron, R. and Madelmont, C., Bull. Soc. Chim. Fr., 3443, (1967)
77 Prochazka, Z., J. Chromatogr., 48, 113, (1970)
78 Colin, H., Eon, C. and Guichon, G., J. Chromatogr., 16, 138 (1982)
79 See reference 78
80 Colin, H. and Guichon, G., J. Chromatogr., 137, 19 (1977)
81 Unger .K. K., Roumeliotis, P., Mueller, H. and Goetz, H. J., Chromatographia 202 (1983)
82 Halász, I. and Horváth, C., Nature, 197, 71, (1963)
83 Ciccioli, P., Tappa, R., Di Corcia, A., and Liberti, A., J.Chromatogr., 206, 35 (1981)

[84] Knox, J. H. and Gilbert, M. T. U.K patent 7939449 (1979), U.S. patent 4263268 (1979), F.R.G. patent P2946688-4 (1979)
[85] See reference 47
[86] Dias, H., *Ph.d thesis*, University of Edinburgh, (1990)
[87] Isirikyan, A. and Kiselev, A. V., Russ. J. Phys. Chem.,36, 618.
[88] Kiselev, A. V. and Yashin, Y. I., *Gas Adsorption Chromatography*, J.E.S Bradley Transl., Plenum Press, London, (1969)
[89] Belyakova, L. D., Kiselev, A. V. and Kovaleva, N. V., Russ. J. Phys. Chem., 42, 1204 (1968)
[90] Knox.J.H and Kaur.B., Euro. Chromatogr., News, 1(1987)12
[91] See reference 47
[92] Knox, J. H. and Ross, P., "Carbon-Based Packing Materials for Liquid Chromatography, Structure, Performance and Retention Mechanism" in *Advances in Chromatography*, vol. 37, pp. 73, Marcel Dekker, Inc., New York, (1996)
[93] Kaur, B., LC-GC Int., 3:41 (1989).
[94] Snyder, L. R., *Principles of Adsorption Chromatography*, Marcel Dekker, Inc., New York, (1968)
[95] Möckel, H. J., Braedikow, A., Melzer, H. and Aced, G., J. Liq. Chromatogr., 461, 139 (1989)
[96] Kríz, J., Adamcovà, E., Knox, J. H. and Hora, J., J. Chromatogr., 663 151 (1995)
[97] Kaliszan, R., Osmialowski, K., Bassler, B.J. and Hartwick, R. A., J. Chromatogr., 461, 139 (1989)
[98] Kaliszan, R., Osmialowski, K., Bassler, B.J. and Hartwick, R. A., J. Chromatogr., 461, 139 (1989)
[99] Lim , C. K., Biomed. Chromatogr., 3: 92 (1989)
[100] Kaliszan, R., *Quantitative Structure-Chromatographic Activity Relationships*, John Wiley & Sons, New York, (1987)
[101] Lim, C. K., Biomed. Chromatogr., 479, 212 (1989)
[102] Mockel, H. J., Braedicow, A., Melzer, H, and G.Aced, J.Liq.Chromatgr., 14:2477 (1991)
[103] Tanaka, N., Tanigawa, T., Kimata, K., Hosaya, K. and Araki, T, J. Liq.Chromatogr., 549: 29 (1191).
[104] Coquart, V. F., Ph.D. thesis, University of Paris, (1993)
[105] Coquart, V. F., and Hennion, M.-C., J. Chromatogr., 600, 195 (1992)
[106] Hennion, M.-C. and Coquart, V. F., J. Chromatogr., 642, 211 (1993)
[107] Coquart, V. F., Ph.D. thesis, University of Paris, (1993)
[108] See reference 105
[109] See reference 106
[110] See reference 52
[111] Knox, J. H. and Ross, P., "Carbon-Based Packing Materials for Liquid Chromatography, Structure, Performance , and Retention Mechanism" in *Advances in Chromatography*, vol. 37, pp. 121-162, Marcel Dekker, Inc., New York, (1996)
[112] Davies, M., Smith, K. D., Harbin, A. M. and Hounsell, E. F., J. Chromatogr., 609, 125 (1992)
[113] Steffanson. M. and Hoffman, J., Chirality, 4, 509 (1992)
[114] Steffanson, M. and Lu, B., Chromatographia, 35, 61 (1993)
[114b] Ayrton, J. Evans, M.B., Harris, A.J and Plumb, R.S., J.Chromoatogr., B 667 173-178 (1995)
[115] See reference 105
[116] See reference 106
[117] Hennion, M.-C, Pichon, V., Chen, L., and Guenu, S., Environ. Sci. Technol., 28, 576A (1994)
[118] Emery, M. F. and Lim, C. K., J. Chromatogr., 479, 212 (1989)
[119] Gu, G. and Lim, C. K., J. Chromatogr., 515, 183 (1990)
[120] Lim, C. K., Biomed. Chromatogr., 3, 92 (1989)
[121] Gu, G. and Lim, C. K., J. Chromatogr., 515, 183 (1990)
[122] Krause, R. T., J. Liq. Chromatogr., 12, 1635 (1989)
[123] Ross, P. and Knox, J. H., "Carbon-Based Packing Materials for Liquid Chromatography, Applications" in *Advances in Chromatography*, vol. 37, pp. 121-162, Marcel Dekker, Inc., New York, (1996)

Fig 1.1
Schematic of Band Migration and Dispersion Along a Column

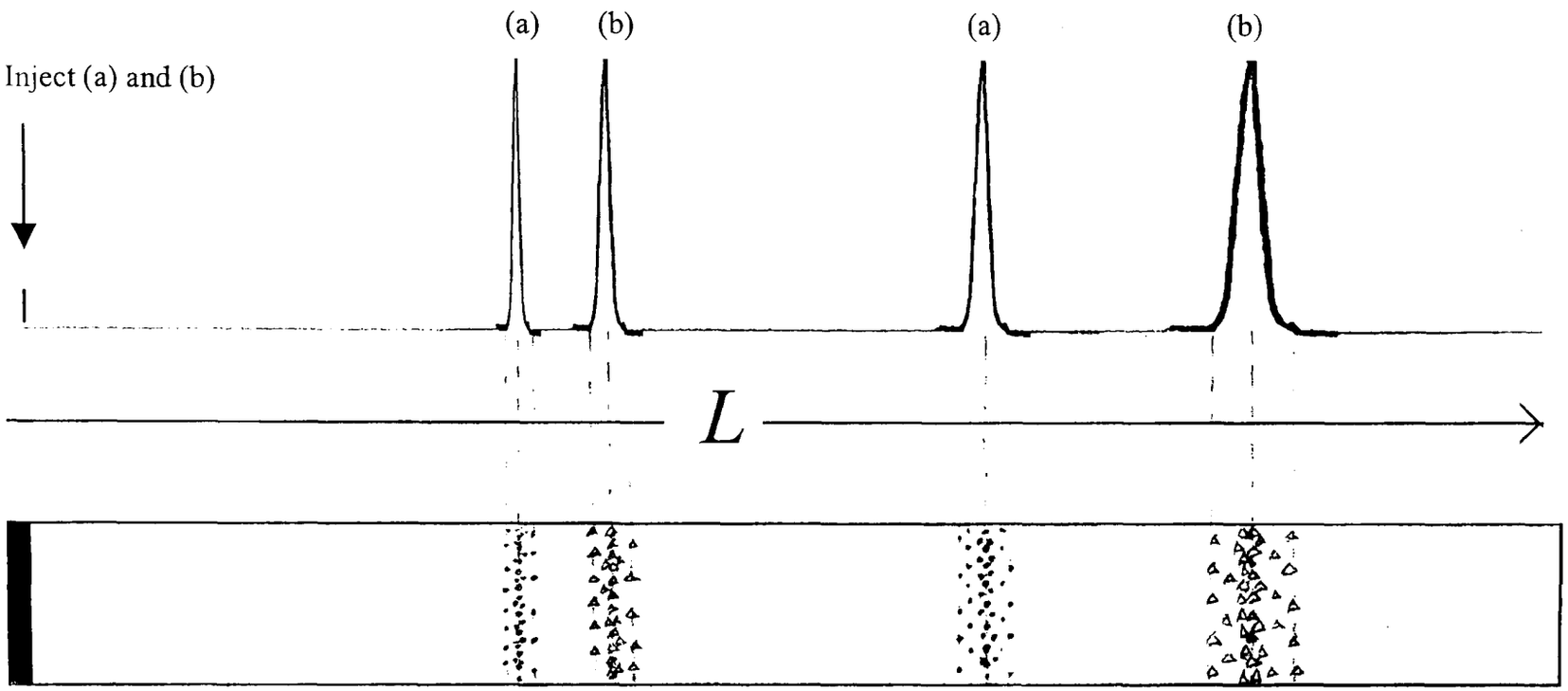

In a uniform bed the width of the bands of two analytes (a) and (b) increases with the square root of the distance they have migrated, while the distance between the centres of the bands increases proportionally to the distance that the bands have migrated.

Figure 1.2, Modes of Chromatography

Figure 1.2(a) *Adsorption Chromatography* *(A = Analyte Molecule)*

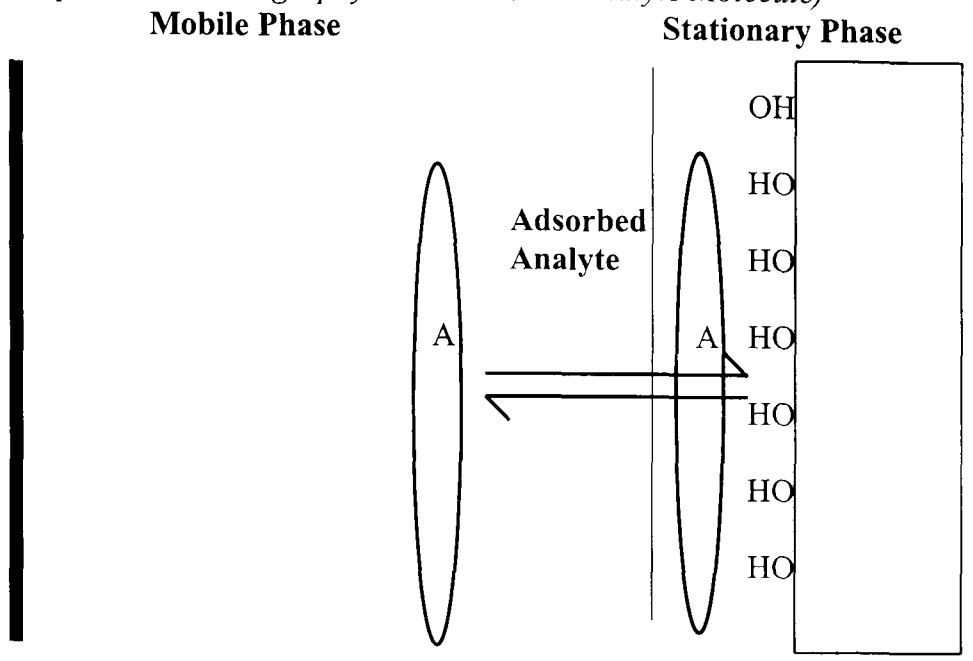

Figure 1.2(b) *Liquid Liquid chromatography* *(A = Analyte Molecule)*

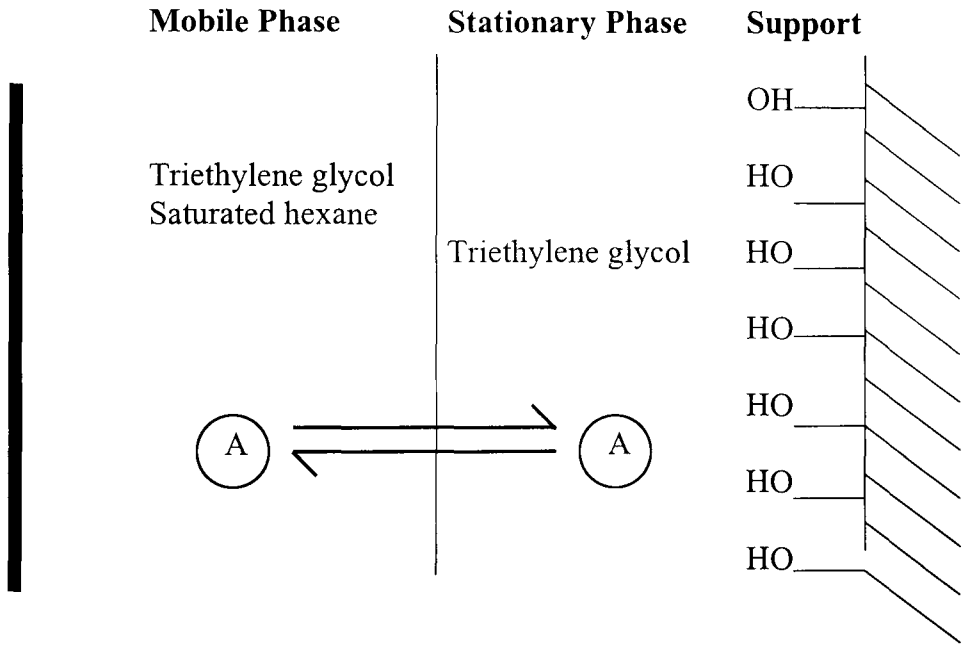

Figure 1.2(c) *Bonded Phase Partition Chromatography* *(A = Analyte Molecule)*

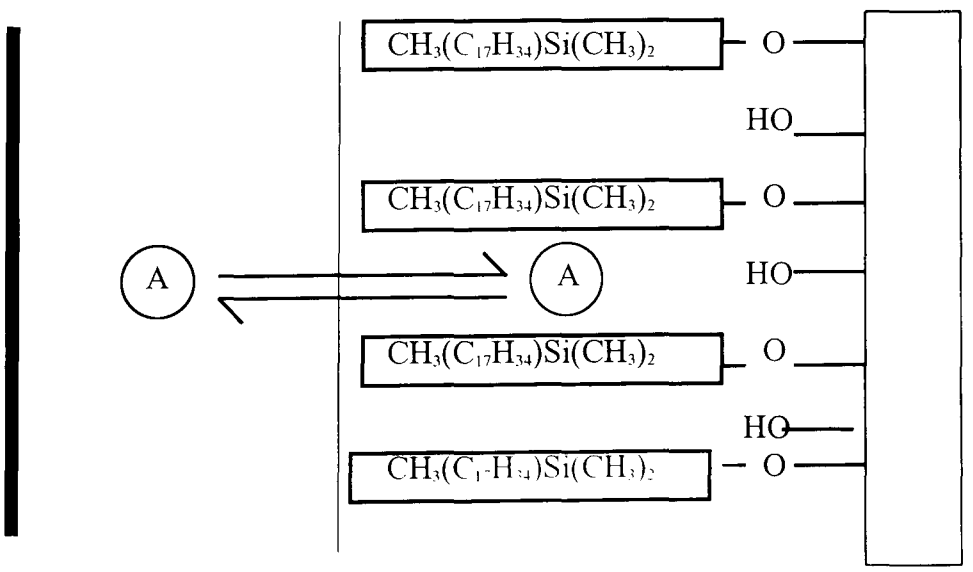

Fig 1.3
Parameters for Defining Retention and Peak Width

Fig 1.3a

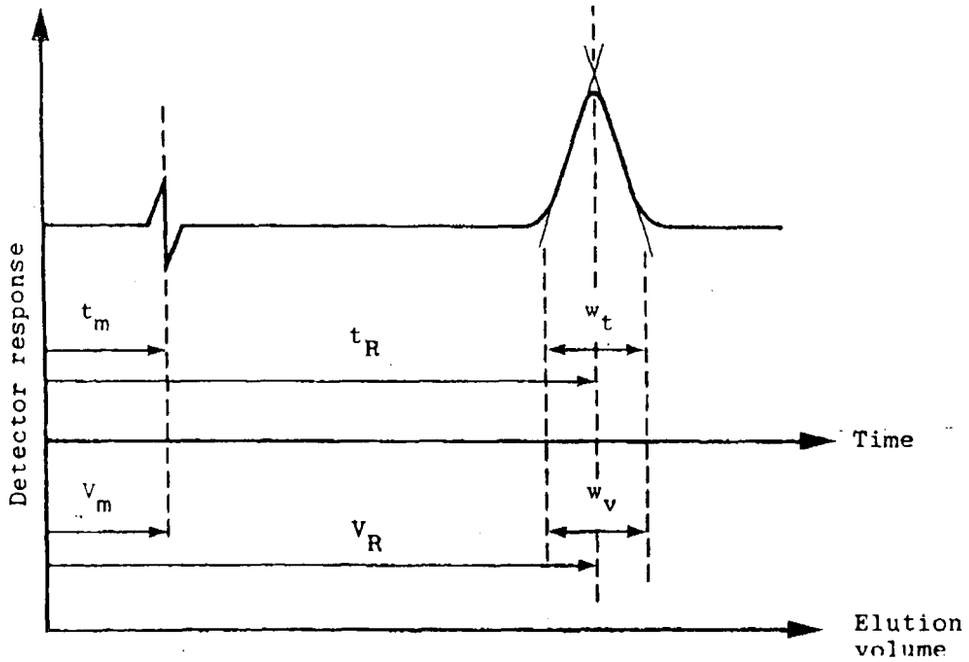

Fig 1.3b

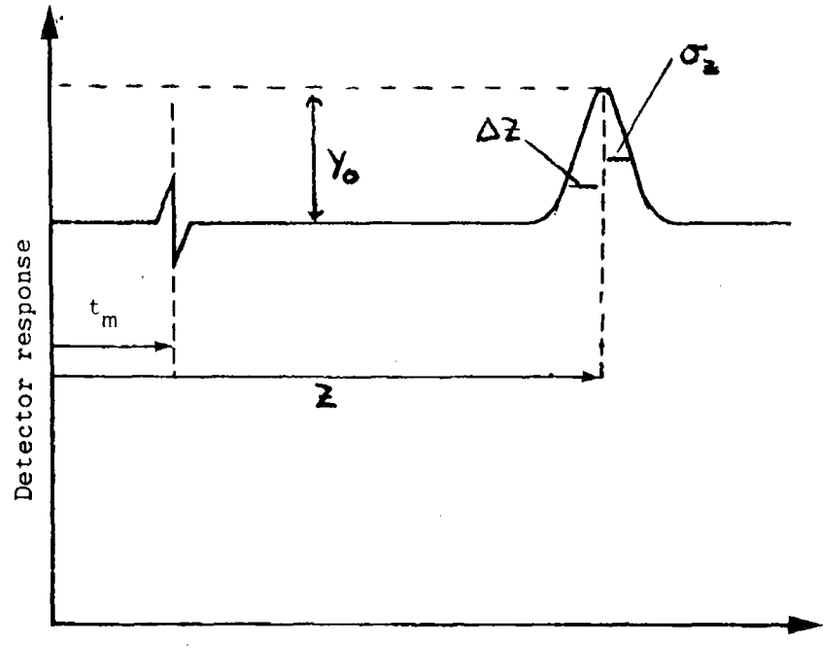

Fig 1.4

Procedures to Measure the Variance of a Peak

(a)

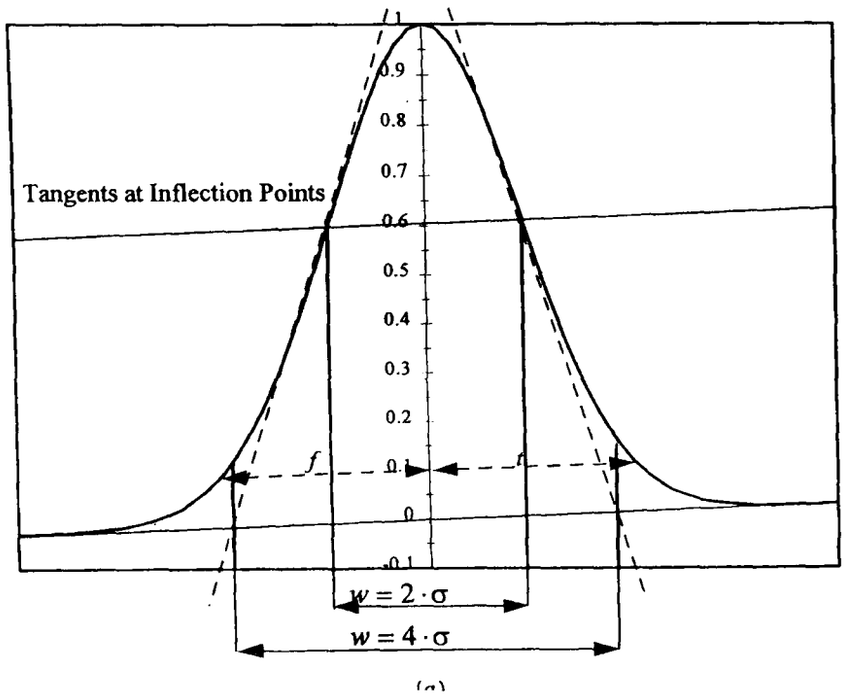

(a - continued)

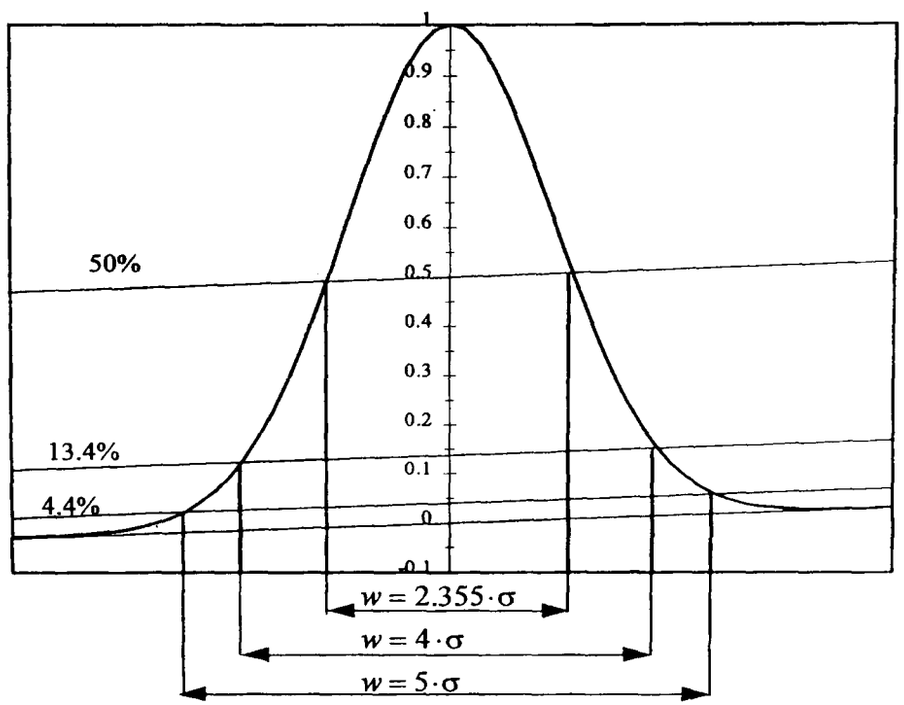

(*b*)

Figure 2.3 (Continued)

For a truly Gaussian Peak these procedures are accurate. The axis in the middle shows the the percentage of the peak height at which the variance is measured. The bottom of the graph shows the width measured in various units of standard deviation. In the tangent methods tangents are drawn to the inflection points of the peak , and the peak width is determined from the intersection points of the tangents with the baseline.. Also illustarted is the determination of the asymmetry factor , in this case measured at 10% peak height.

Data copied from : HPLC Columns, theory, Technology, and Practice by Uwe D. Neue

Fig 1.5(a) & (b)
Knox Plot

Schematic copied form J.H.Knox , High Performance Liquid Chromatography, Edinburgh University Press

Fig 1.5(a)Knox Plot

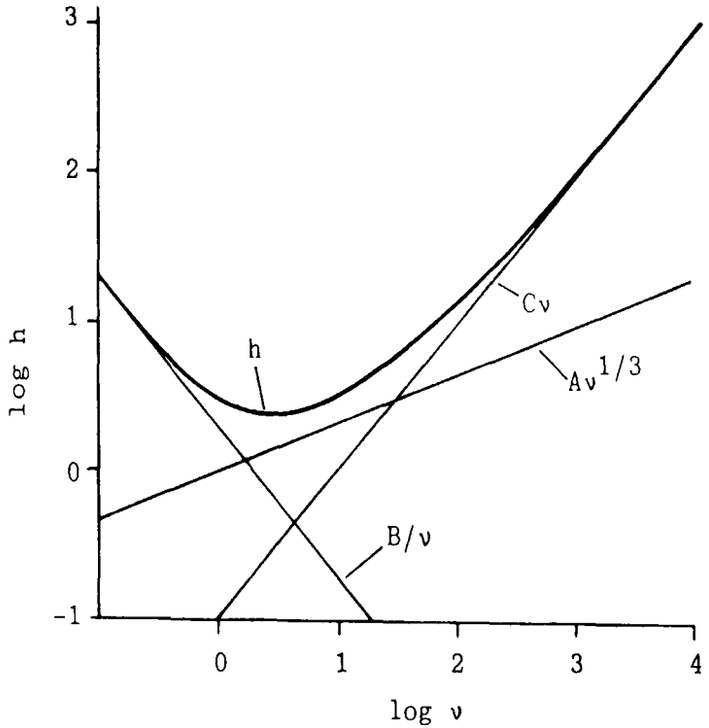

Dependence of h upon v according to equation [1.56] showing individual contributions from each of the three terms used.

Fig 1.5(b)
Experimental Kox Plot

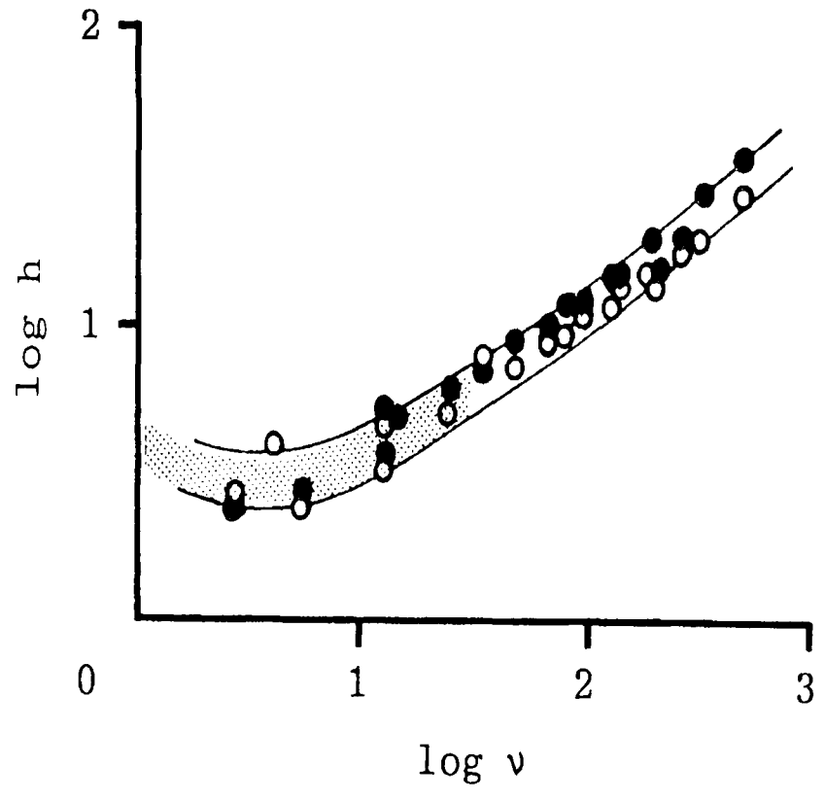

Superposition of (h,v) curves for materials of different particle size. Shaded band refers to 6-10um Spherisorb Alumina, points refer to 50um Porasil.

Fig 1.6(a) &(b)
Silica Surfaces

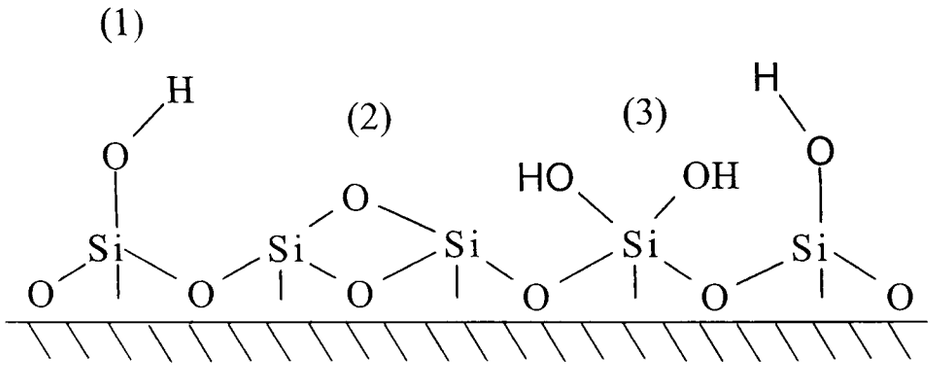

1. Lone Silanol
2. Siloxane
3. Geminal Silanol
4. Vicinal Silanols

Fig 1.6a Hydroxylated Hetrogeneous Surface

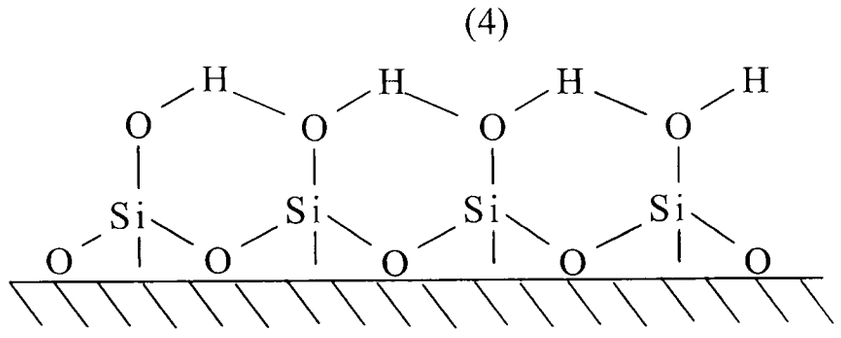

Fig 1.6b Hydroxylated Homogeneous Surface

Fig 1.7

Silica Bonding Apparatus

Fig 1.7

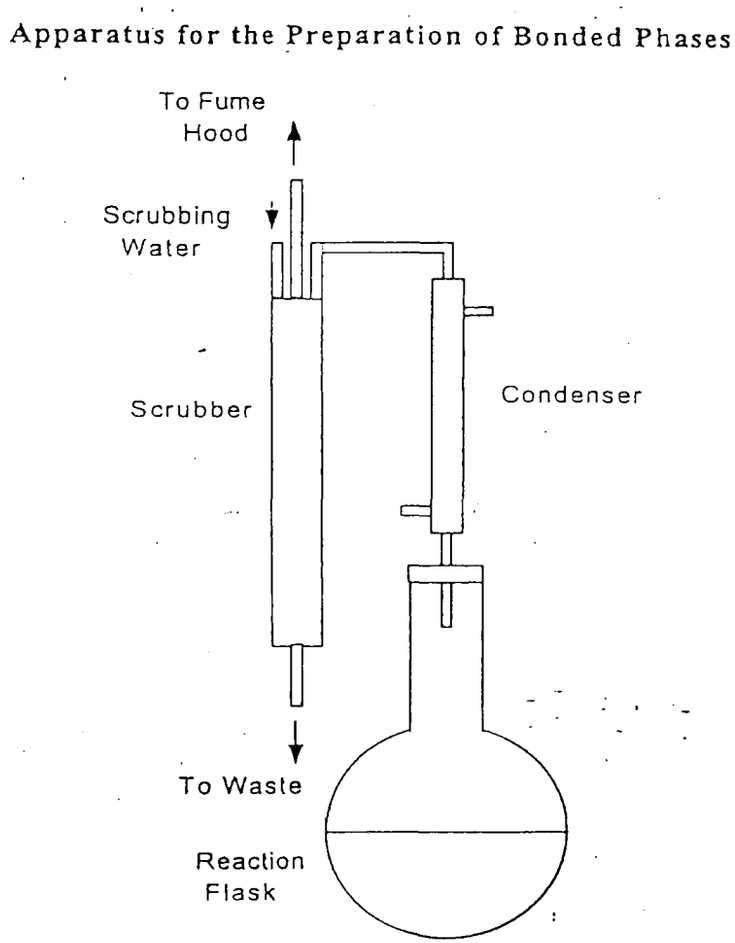

Fig 1.8(a) & (b)

Schematic Representations of the Structure of Graphitized Carbons

Fig 1.8(a)
Stable Bernal Structure of True 3D-Graphite

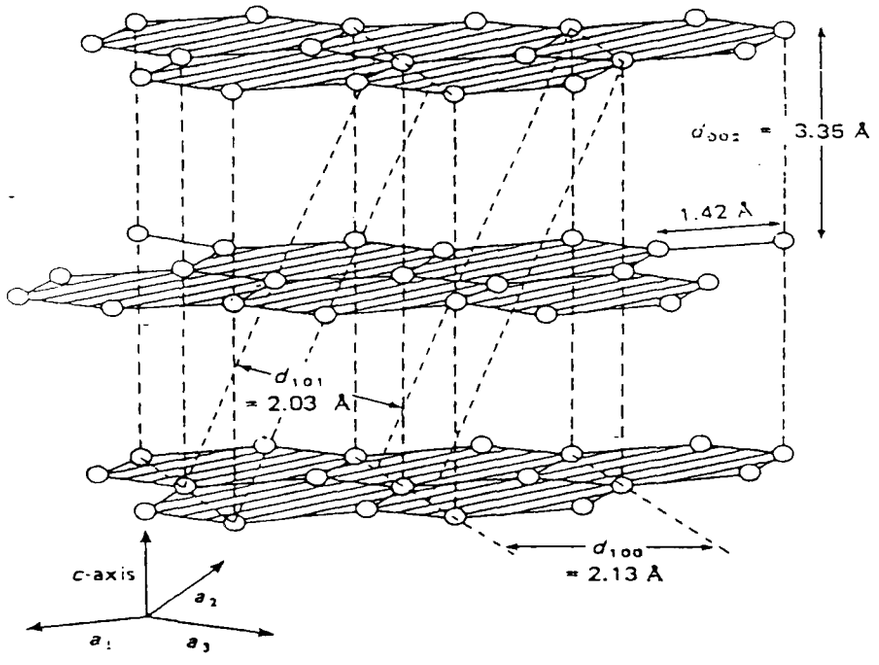

Fig. 1. Atomic structure of a perfect graphite crystal.

Fig 1.8(b)
Schamatic Structure of 2D-Graphite

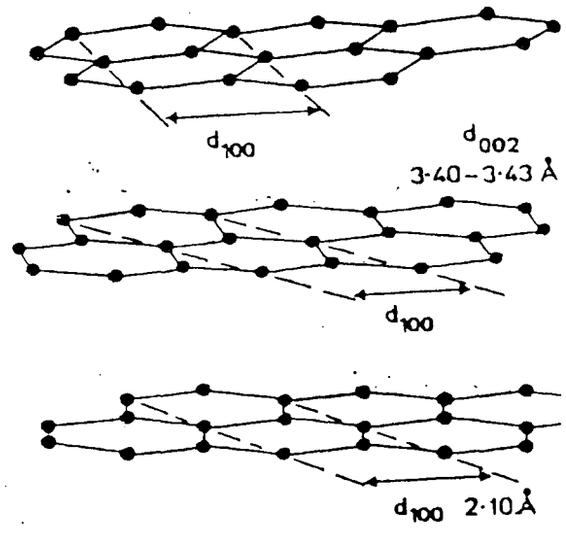

2D - GRAPHITE (b)

Fig1.9
X-Ray Diffractograms of (a) Perfect, (b) Potential Chromatographic Carbons and (c)PGC

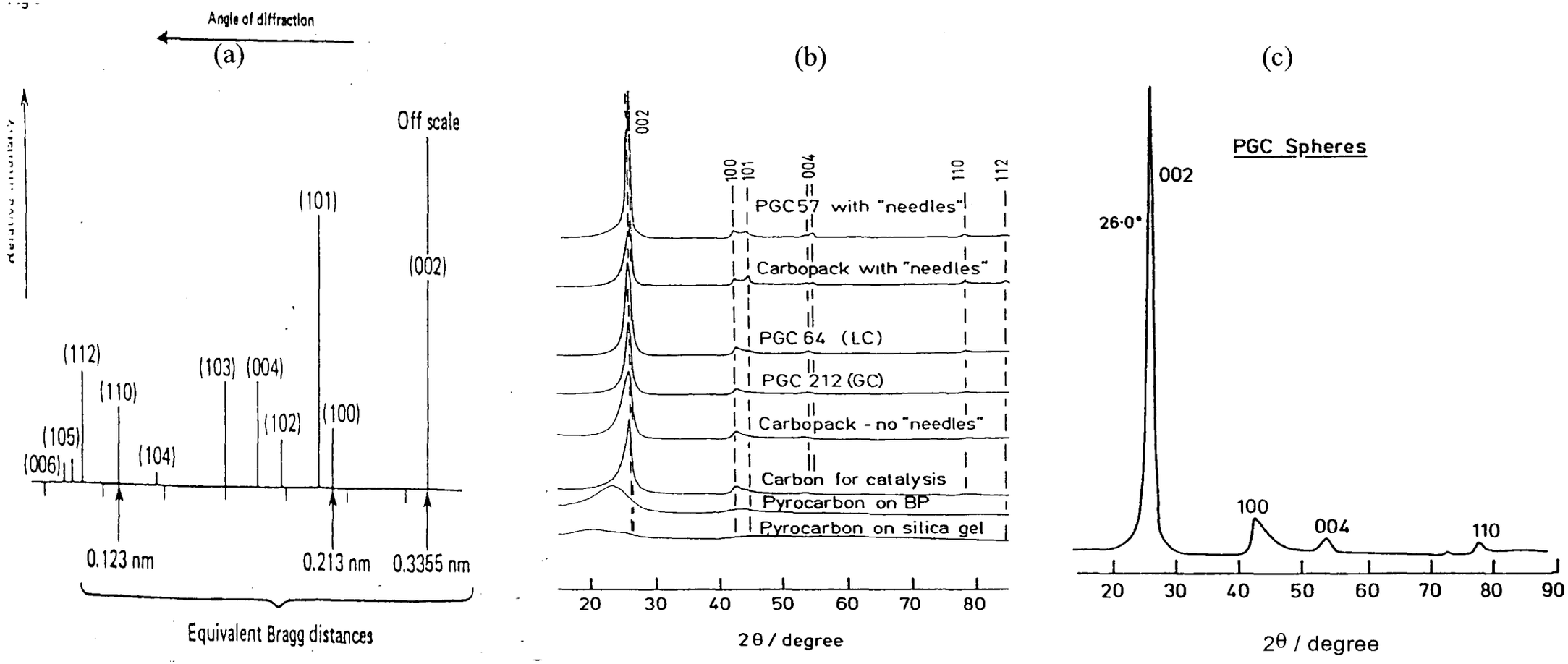

Ref:J.H.Knox and B.Kaur and G.R Milward, JChromatography., 352, 3 - 25 (1986)

Fig 1.10

Chiral Stationary Phases

Fig 1.10

Type of adsorbent	Separation	Eluent
Cellulose ester derivative 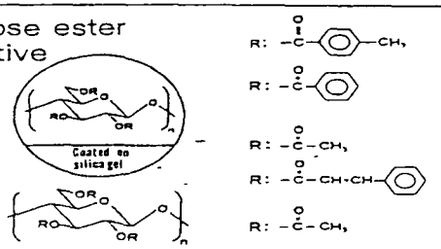	Compounds possessing amide group, aromatic group, carbonyl group, nitro group, sulfonyl group, cyano group, hydroxyl group, amine, and carboxylic acid	● Hexane/IPA ● Hexane/Ethanol
Cellulose carbamate derivative 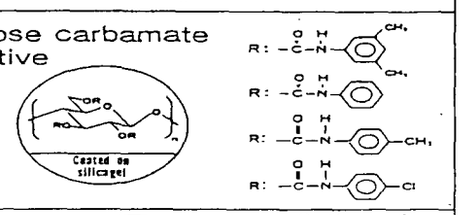		● Hexane/IPA
Amylose derivative 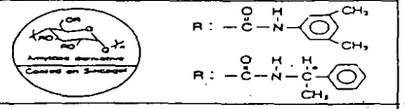		● Hexane/Ethanol ● Hexane/IPA
10μm, reversed-phase type of CHIRALCEL OD 5μm, reversed-phase type of CHIRALCEL OJ	(in addition to the above, amino acid derivative)	● Buffer/ACN ● Buffer/Methanol
Polymetha-crylate 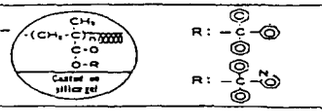	Compounds possessing aromatic group	● Methanol ● Hexane/IPA
Ligand exchange  WH / WM - WE	Amino acids, their derivatives	● aq. $CuSO_4$
Ligand exchange (coating type)	hydroxy carboxylic acids	
Crown ether	$-NH_2$ group	● aq. $HClO_4$

Fig 1.11(a) &1.11(b)
Size Exclusion Chromatography

Fig 1.11(a)

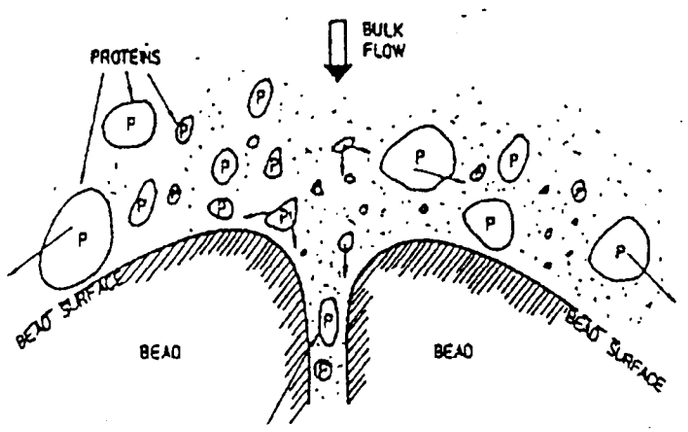

Molecules (P) with size < Pore diameter may pass into the pore of the particle.Those > Pore diameter remain in the bulk of the mobile phase and do not enter the pores.

Fig 1.11(b)

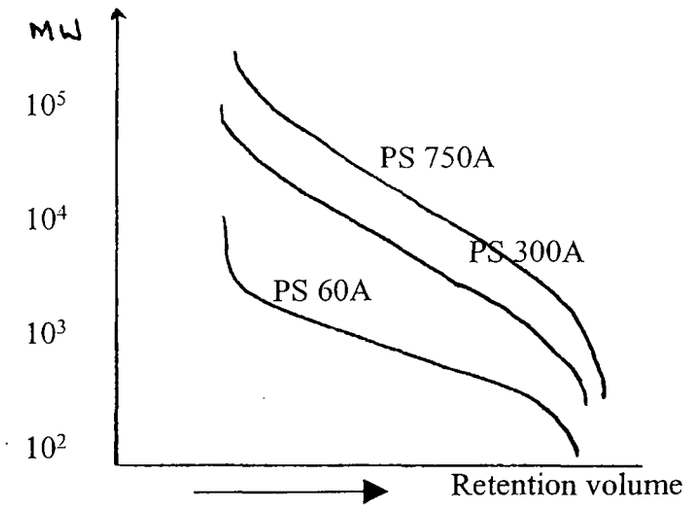

Schematic representation of Log - linear calibration curve for polystyrenes dissolved in a solvent on silica packings of graduated pore sizes.the nominal pore sizes are indicated on the curves

Fig 1.12
Principles of Affinity Chromatography

Fig 1.12

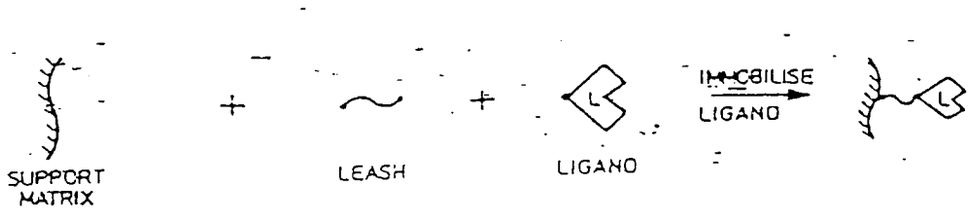

THEN SELECTIVELY ADSORB THE REQUIRED PROTEIN (P) ONTO THE LIGAND (L)

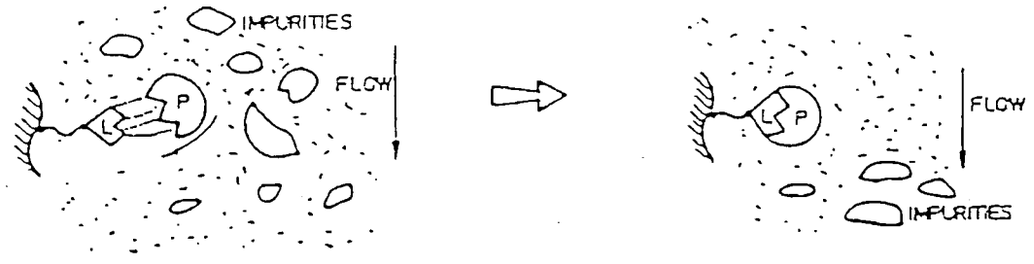

Fig 1.13
Breakthrough in Chromatographic Performance of PGC

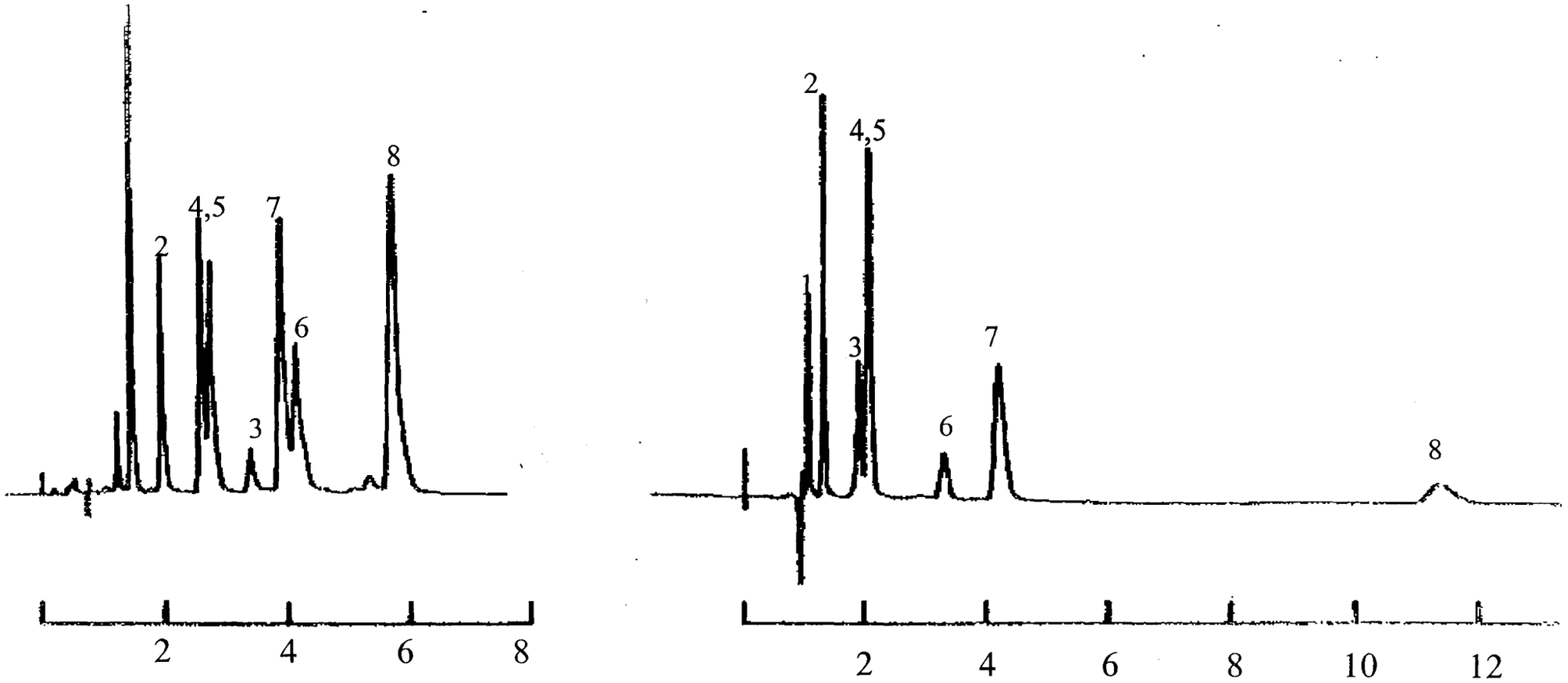

Separations of methylbenzenes on ODS Hypersil and PGC64
Eluent: methanol:water (95:5 for PGC and 70:30 for ODS)
Peaks: (1)Benzene , (2) toluene, (3) m-xylene, (4) p-xylene, (5) o-xylene,
(6) 1,3,5-trimethylbenzene , (7) 1,2,4-trimethylbenzene, (8) 1,2,4,5-tetramethylbenzene

Chapter 2 – Performance Studies

2.1 Review of Recent Developments Related to the Structural Properties and Chromatographic Performance of PGC

During the development of porous graphitic carbon (PGC) the chromatographic performance has been shown to vary quite considerably from batch to batch. This has been most apparent in batches that gave poor column efficiency and exhibited peaks that tailed badly for all types of solutes. The difference in batch performance was attributed initially to residue oxides left behind during the graphitization process[1].

Poor peak shape and chromatographic performance (as measured by column efficiency) are often associated with adsorbents whose surface sites are not homogenous. Ideally when all surface sites have identical properties, a situation exists where, between given limits and at low concentration, the peak due to any solute will be Gaussian (a statistically normal distribution centred around a mean value). Its width will be independent of the quantity of solute injected and its height will increase linearly with amount injected. Such linear behaviour is not seen if the surface is heterogeneous, e.g. containing sites of different activity. Such heterogeneity results in peak shapes that are broad and often tail significantly.

In an attempt to improve the chromatographic performance of PGC, Wan[2] investigated the possibility of masking the secondary sites by selective adsorption of discrete molecules onto the PGC surface. Dibenzofluorene (DBF) and dibenzanthraquinone (DBAQ) were chosen as the adsorbate molecules because of their flat structure. Flat or planar molecules are expected to exhibit strong adsorptive properties when placed in contact with PGC. They were applied in low concentrations to the surface of PGC so that only the active sites, the PGC surface, would be covered. Coverage of the active site was assumed to be as a result of purely dispersive interactions between the adsorbate and PGC surface. Wan termed this as "deactivation" of the graphitic carbon and found that the performance of the PGC could be improved significantly. Furthermore subsequent washing of the coated carbon with toluene (known to be a strong solvent for hydrocarbons on PGC), did not appear to remove the adsorbed DBAQ and consequently the improved performance of PGC was retained. This raised the possibility of coating the whole surface of PGC with molecules that may directly influence the chromatographic performance and application of PGC. Wan, for

example explored coating the surface of PGC with discrete chiral molecules in order to separate enantiomeric compounds. Also, in 1994 Grieb[3] coated the PGC surface with derivatized cellulose to separate enantiomeric compounds. Our own research into the coating of the PGC to influence its retention properties is discussed in Chapter 4 of this Thesis.

An alternative to deactivation is to improve the crystallographic properties of PGC during its manufacture. Several workers have shown that carbons, which can form large, flat plate-like structures during a liquid stage of the polymerisation process, go on to form well-ordered 3d-graphite. It is thought that graphites prepared in this way also possess a more homogeneous surface. Such carbons are described as "Soft Carbons" while those, which do not go through a liquid phase, are described as "Hard Carbons." The carbon formed from the polymerisation of phenol and formaldehyde (the components of the polymer used to manufacture PGC) is a "Hard Carbon" since it derives from a polymerisation of a cross-linked polymer that cannot melt. Improvements in crystallographic properties of hard carbons have also been reported by following several routes. These include methods such as the use of high pressure during the graphitization process and the introduction of metal catalysts to the initial polymer synthesis prior to carbonisation and graphitization.

The aim of this Chapter is therefore to review the whole process by which PGC is made and where possible improve the surface homogeneity, either by, "deactivation," improvement in crystallographic structure , or simply removing deposits left on the surface during the graphitization process.

2.2 Improvements in PGC Surface Homogeneity

Before discussing our experimental approach and results, we first look in greater detail at the significance of active sites on the surface of an adsorbent. Also, we consider how their presence can influence chromatographic performance in terms of the type of adsorption isotherm and peak shape produced. The synthetic route according to Knox and Kaur[4] is then reviewed followed by a short review of the different methods used by previous workers to achieve improvement to the crystallographic properties of the graphite structure.

2.2.1 Adsorption Isotherms

When an adsorbent and a vapour are brought into contact, at equilibrium the concentration of the vapour is greater at the interface than in the bulk phase. This phenomenon is called adsorption.[5]

Adsorption can be subdivided according to the type and strength of interaction:

(a) Physical adsorption (physisorption), which takes place through short-range intermolecular attraction and repulsion forces,

(b) Chemical adsorption (chemisorption), which takes place through electron transfer between surface atoms of the adsorbent and adsorbate.

The rate at which a surface is covered with adsorbate depends on a number of factors:

(a) The activation energy. This is generally very small and rarely plays a dominant role.

(b) The frequency of collisions. This is usually quite high.

(c) The sticking factor, s, which is the proportion of collisions with the surface that leads to adsorption. This is usually the dominant factor.

$$s = \frac{\text{rate of adsorption of molecules by surface}}{\text{rate of collision of molecules with surface}} \qquad [2.1]$$

The sticking factor depends on how much of the surface is uncovered. As the surface sites become filled, the sticking probability becomes smaller. The extent of surface coverage plays an important role in adsorption studies and is normally expressed in terms of the fractional coverage (θ).

$$\theta = \frac{\text{number of adsorption sites filled}}{\text{number of adsorption sites available}} \qquad [2.2]$$

The fraction of coverage depends on the equilibrium between the molecules on the surface and the molecules in the gas phase. The position of this equilibrium will depend on the pressure of the system. The dependence of the fractional coverage on the pressure, at a set temperature is called the "adsorption isotherm of the system." At equilibrium the adsorption of molecules is balanced by their desorption. The rate of desorption is proportional to the surface concentration. The surface concentration is dependent upon the

activation energy of desorption, or the enthalpy of desorption. When a surface contains a variety of sites the activation energy for desorption is likely to vary from one site to another. The simplest type of isotherm assumes that every adsorption site is equivalent, and the ability of molecules to bind there is independent of whether or not the neighbouring sites are occupied. This is the principle assumption of the underlying derivation of the Langmuir isotherm:

$$\text{Langmuir Isotherm:} \quad \theta = K(A) / (1 + K(A)) \qquad [2.3]$$

where $K = k_a/k_d$, and k_a is the rate coefficient for adsorption for molecule A, and k_d is the rate coefficient for desorption for molecule A.

The system described translates to liquid chromatography in the following way. The gas phase is now simply replaced by a liquid. Adsorption of solvent molecules to the surface then occurs in a similar way to that described in the gas phase. However in the liquid phase the number of solvent molecules present dictates that the surface of the adsorbent will always be saturated. In this medium we therefore discuss the adsorption of solutes suspended in the solvent where a competition for adsorption to the adsorbent surface occurs with the solvent molecule, *i.e.* displacement of solvent molecules by analytes molecules and then of the analyte molecules by solvent molecules. The equilibrium that exists between an analyte suspended in the mobile phase and an analyte adsorbed at the surface, represents the migration velocity of the solute through the system. The position of the equilibrium will depend on the concentration of the analyte in the liquid phase, C_m (concentration in the mobile phase). The Langmuir Equation can then be written as:

$$q_s/C^* = K q_m / [1 + K q_m] \qquad [2.4]$$

where q_s is the quantity of the analyte in the stationary phase (adsorbent), q_m is the quantity of the analyte in the mobile liquid phase, C^* is the saturation capacity of the adsorbent.

$$K C^* = k_a/k_d \qquad [2.5a]$$

When there is a linear relationship between the concentration of the analyte in the stationary phase and the concentration in the mobile phase, basic chromatography theory assumes Gaussian peak shape. Thus for sufficiently small samples:

$$Kq_m << 1 \text{ and } q_s/q_m = K/C^* = \text{constant} \qquad [2.5b]$$

Peak height then increases linearly with sample size, while peak width and retention time remain the same. Snyder[6] referred to this as the "linear adsorption isotherm sorption." The total concentration of the analyte in the system is given by:

$$C = C_s + C_m \qquad [2.6]$$

At some critical sample size, the concentration of the analyte in the mobile phase increases to such an extent that C_s/C_m starts to deviate from the constant relationship and a concentration profile emerges in the form of a non-gaussian peak shape. Note the retention time is measured at the apex of the peak where the concentration is greatest. For a small injection of gaussian peak shape, the apex of the peak is at the centre of the concentration profile. As the concentration of solute is increased in the non-linear region of the isotherm, the concentration of the solute in the mobile phase relative to the stationary phase increases. Now a larger part of the concentration band profile, travelling through the column, spends more time in the mobile phase relative to that spent in the stationary phase. Thus the apex of the peak is seen to move forwards, while the tail remains in its original position. Further increase in sample size causes further decrease retention time.

$$k'_{(front)} = C_s / C_m \qquad [2.7a]$$

While the k' value for a specific concentration in the tail of the peak is given by:

$$k'_{(tail)} = dC_s/dC_m \qquad [2.7b]$$

For analytical separations it is almost always preferable to work within a sample size range where peak widths and k' values are constant; that is, sample sizes should be within the linear capacity of the column.

The slope of the initial gradient gives a clear indication as to the strength of adsorption onto the stationary phase. The steeper the slope, the greater the adsorption and the lower the concentration in the eluent at which monolayer coverage is reached, *i.e.* as the isotherm approaches its plateau. Further, by plotting $1/C_s$ *vs.* $1/C_m$ (where $1/C_s$ is proportional to the fraction of the surface covered), confirmation that the isotherm does in fact show true Langmuir behaviour can be obtained, provided a straight line graph is obtained. If the straight-line plot is extrapolated to intercept on the $1/C_s$ axis, the concentration of the analyte in the stationary phase at monolayer coverage can be obtained. Wan[7] showed examples of this behaviour.

The Langmuir isotherm however demonstrates the ideal adsorption characteristics of an adsorbent where all sites are perfectly homogeneous. For adsorbents that do no meet this requirement, different isotherm behaviour is observed. Here analytes are preferentially adsorbed to a small number of sites on the adsorbent surface. These sites, because of their small number, are easily overloaded and consequently give rise to peak tailing. This is most obvious in chromatograms where one particular analyte appears to have poor peak shape while others show gaussian behaviour. This type of adsorption isotherm is known as the Freundlich isotherm and is used to describe surfaces, that have more than one type of adsorption site.

A third type of isotherm also exists and can give rise to very strange behaviour. It arises due to the increased adsorption properties of the support once an analyte has been adsorbed to the surface. It is known as the S-type isotherm and can result in peak fronting with the main concentration profile of the peak actually increasing in retention. Such isotherms result from associations of adsorbate molecules on the surface or from condensation into micropores.

Clearly peak shape and chromatographic behaviour can give a good indication of the type of isotherm and consequently the homogeneity of the adsorbent surface (see Figure 2.1(a) and Figure 2.1(b)). Kieselev[8] showed how the isotherm could be derived directly from the peak shape, provided kinetic dispersion is minimised.

2.2.2 Preparation of PGC

2.2.2.1 Preparation of PGC Following the Knox and Gilbert Process

The following text summarises the Knox and Gilbert method for PGC preparation.

A silica gel template is impregnated with phenol-formaldehyde resin. The resulting silica-resin is then carbonised at 1000°C to give a silica-carbon composite. The silica from this composite is finally dissolved leaving a porous glassy carbon. In order to make this material useful for a chromatographic support, it is heated to above 2000°C to induce graphitization. This eliminates microporosity leaving the mesoporous structure of the original silica gel intact. The final porous graphitic carbon (PGC) has a specific surface area of 100-150 m^2/g. The physical properties are therefore comparable to current silica-based chromatographic supports. A full comparison of physical properties is given below.

Physical Properties of Silica Gels and Graphitic Carbons

Material	Specific Surface Area m^2/g	Specific Pore Volume mL/g	Porosity %	Mean Pore Diameter (Å)
Hypersil - Silica	170	0.68	60	100
Wide pore silica gel and template for making PGC	50	1.4	75	300
PGC 1000°C	350	1.4	75	300+micro pores
PGC 2500°C	120	1.4	75	300

2.2.2.2 Preparation of PGC Using the Current Modified Process

The PGC manufacturing process used during our study followed essentially the same procedure as the original Knox and Gilbert method, with only a few modifications. These modifications are described in the following sections.

2.2.2.3 Silica Preparation

Manufacture of PGC requires the preparation of a highly porous 5μm spherical silica particle having a pore size of approximately 500Å and pore volume of approximately 1.2mL/g. An overview of the process is shown in Figure 2.2(a), and described in greater detail in the following paragraphs.

For this precursor silica, the starting material is silica sol consisting of particles (primary particles) of solid silica approximately 15nm diameter. The sol is charge-stabilised in a ~1% solution of sodium hydroxide. The charge is stabilised at basic pH because between pH 7 and 10.5, the silica particles are negatively charged and repel each other and consequently do not collide. Inter-particle bonds occur below pH 7 where the silica surface is not ionised. Polymerisation of the silanol groups then occurs via the condensation reaction:

$$\equiv Si\text{-}OH + HO\text{-}Si\equiv \longleftrightarrow \equiv Si\text{-}O\text{-}Si\equiv + H_2O$$

Accordingly the sol is first acidified with hydrochloric acid to pH6 to initiate coagulation of the primary particles into larger secondary particles. Once the reaction is initiated, the sol is emulsified in petroleum spirit using a high speed mixer in the presence of an emulsifier. The size of the globules (secondary particles) thus formed have a mean particle size between 1μm and 30μm depending on the speed of the emulsification. The slower the speed the larger the secondary particle produced. Each secondary particle is made up of the original primary particles which continue to polymerise, increasing inter-particle bonds and

hardening the structure and framework of the secondary particle. The emulsifying agent stabilises the secondary particles during their formation and initial hardening. It is then removed along with the petroleum spirit by mixing with a suitable aqueous salt solution to destabilise the emulsion. This results in a suspension of silica gel particles in water.
The aqueous suspension is then hydrothermally treated in water at 200°C in an autoclave. Prior to hydrothermal treatment the pore size of the particles is approximately 100Å. Hydrothermal treatment is a process that allows the size of the pores to be increased to approximately 500Å or larger. The process relies on the variation in solubility of silica with radius of curvature of surface. Iler[9] describes the process as follows:

1. When very small individual silica particles are brought into the same solution as larger particles, especially at pH 9-10 where hydroxyl ions catalyse dissolution and deposition of silica, the smaller ones dissolve and the larger ones grow.

2. If there has been an aggregation or flocculation of colloidal silica particles so that two or more particles are brought together, then at the point of contact the radius of curvature is negative and extremely small. The solubility of the silica in this region is very low, and silica dissolves from the particle surfaces and is deposited around the point of contact to minimise the negative radius of curvature, thus forming a coalescence or neck between particles.

Both 1 and 2 above are very relevant to the hydrothermal treatment of the silica prepared as the template to our PGC process, since the size and the way in which the primary particles fit or link together will influence their solubility in the way described.
After removal of water and drying from acetone the silica is fractionated by air classification to tighten the particle size distribution. Typically, an acceptable distribution *i.e.* one which will provide acceptable column packing of the media, is one that has 90% of the particles within ±1.5μm of the mean. The silica is then ready for impregnation with polymer.

2.2.2.4 First Polymerisation

The objective is to fill the pores to about 95% with phenol formaldehyde polymer. Only sufficient polymer melt is used to fill all the pores, as excess use of the polymer will cause the individual particles to stick together. It is important that this does not happen and that only discrete 5μm particles with their surface and pores filled with polymer are obtained.

The formation of conglomerates will ultimately effect the performance of the particles when used in their chromatographic mode. This necessitates prior knowledge (measurement) of the specific pore volume, which is obtained by titration with water or mercury posorimetry. A 6:1 phenol:hexamine (w/w) mixture is prepared and ground in a pestle and mortar. This is then mixed with the porous silica, which is then rotated in a 20L flask held horizontally inside the polymerisation oven, as in Figure 2.2(b). This is heated to 80°C. The phenol: hexamine mixture melts at 80°C, allowing the mixture to be drawn into the pores by capillary action. The pores are then filled with the polymer melt. Polymerisation takes place at 120°C over a period of 18 hours. The temperature is then raised to 145°C for a period of 6 hours during which time the final stages of polymerisation occur.

2.2.2.5 Carbonisation

A nickel chromium inconel tube is charged with the silica/polymer and placed into position on the carbonisation furnace. The system is then flushed with nitrogen gas while the inconel tube is rotated in order to keep the particles from fusing together during the heat process where the temperature is raised over a period of several hours to 1000°C. The apparatus and temperature profile are shown in Figure 2.2(c).

During this heating process a considerable quantity of phenolic residues are produced, and are carried away with the flow of nitrogen gas and trapped further down the line in an aqueous sodium hydroxide scrubber unit. At 1000°C the polymer contained within the pores of the silica becomes carbonised but the carbon/silica particles still remain discrete. During the process of carbonisation some 50% shrinkage of the polymer occurs although the outer particle diameter remains unchanged. Thus some porosity is created within the carbonised particle. This is filled by a second polymerisation procedure, once again employing phenol:hexamine. The carbonisation step is then repeated.

2.2.2.6 Dissolution of Silica

Dissolution of silica is achieved by boiling the silica / carbon in 5M KOH for a period of sixteen hours. The carbon is then washed copiously with warm water before drying. Removing the silica template leaves a highly amorphous carbon which contains both micropores (pores less than 20Å) and mesopores (pores between 20Å and 500Å), which are formed from the primary structure of the original 5μm silica particles.

2.2.2.7 Final Heat Treatment Prior to Graphitization

A further heating of the carbon to 1000°C for a period of 6 hours is now carried out. The aim is to remove excess water held in the micropores and any hydrocarbons from the material, since the latter give rise to the formation of graphitic needles in the final graphitization process. Graphite needles are small, pin-like structures of 3D graphite formed during the graphitization process[10] and are thought to arise from the pyrolysis of hydrocarbons, usually methane, at approximately 1800 - 2300°C.

2.2.2.8 Graphitization

The amorphous carbon is place in a graphite crucible, which is placed inside the heating chamber of the graphitization furnace. The amorphous carbon is gradually heated to 1800°C under vacuum, and then to 2500°C in an inert atmosphere (argon). See Figure 2.2(d) for the heating profile.

The graphitization process involves the complete restructuring of the carbon from an amorphous structure with micropores and high surface area, to a well-ordered 2D crystalline mesoporous (250Å) graphitic carbon structure with a much-reduced surface area (approximately $100 m^2 g^{-1}$).

2.2.2.9 Slurry-Packing PGC into HPLC Columns

The packing of PGC into HPLC columns is done using a Shandon Column Packer, a device specifically designed for the packing of HPLC columns. The technique involves:

preparing the PGC as a slurry (usually using methanol as the solvent, 1.2g PGC in 30 mL methanol)

filling the column and column reservoir (attached in series) with PGC slurry

connecting the column and column reservoir to a high pressure solvent pump

forcing the particles into the column with a packing solvent (methanol) at 8000psi solvent pressure

after 150mL of packing solvent is passed through the column the high pressure solvent pump is switched off and after a short period of time the column is disconnected from the reservoir. Column end-fittings are then attached to the column.

2.3 Factors Affecting the Crystallographic Properties of Graphite

2.3.1 Definition of the Graphitization Process

Bernal[11] defined the process of graphitization as follows: "The development of carbon to form the stable Bernal structure or as the development of three dimensional order in an initially two dimensional ordered carbon." This definition can be applied equally well to three quite different processes:

1) The first process involves the graphitization from one relatively well-ordered phase to another. This process refers to the substantial or complete graphitization of soft carbons to form 3D graphite. Examples of soft carbons include conventional petroleum and pitch cokes.

2) The second process refers to the graphitization of highly ordered carbon, *e.g.* diamond, and pyrolytic carbons which when graphitized form 3D-graphite.

3) The third process involves the development of an ordered crystallographic structure from an initially distorted or defective solid. It is the ordered stacked arrangement of the layers that are noticeably absent from these carbons. This process refers to graphitizing of hard carbons (non-graphitizing carbons). These include glassy or vitreous carbon fibres and chars.

Based on these definitions, the following paragraphs outline the factors which can influence the degree to which each type (2D or 3D) of graphite is produced.

According to the Bernal definition, the formation of 2D-graphite from amorphous carbon would not be graphitic carbon. In this then we have perhaps incorrectly used the term graphitizable for the conversion of any disordered carbon into 2D- or 3D-graphite.

2.3.2 Hard and Soft Carbons

Franklin, *et al*[12] considered the graphitization process in terms of progressive improvement of the initially highly defective structure that exists in carbon. For this reason geometric aspects of the microstructure are important. Furthermore they suggest that a carbon's graphitization behaviour is largely determined very early in the history of the carbon, when its basic structure is established. The existence of an extensive layer plane structure with near parallel stacking is said to be the pre-requisite for good graphitization. The nature, concentration, and distribution of the defects in the structure were also thought to play an important role.

Fitzer, Mueller, and Schaefer[13] expanded on this view, stating that all pyrolysis processes of organic compounds that take place in the non-fluid state result in disordered carbon (hard

carbons) while the thermal decomposition of molten organic substances leads to well-ordered residues (soft carbons). A condition for the latter is the maintenance of a fluid phase over as broad a temperature range as possible. The fluid phase range is maintained by various means such as removal of solid components or of compounds tending towards condensation.

Kipling and Shooter[14] were able to show that the main temperature range of thermal decomposition (usually between 400°C and 500°C) coincides with the fluid range of the material being pyrolysed.

The fluid range and the range of coke formation have been found to coincide for aromatic hydrocarbons and thus seem to satisfy the requirements for the formation of well-ordered cokes.

Only the fluid phase offers sufficient mobility to the reacting molecules during thermal decomposition to permit preferred orientation. Pyrolysing molecules must exhibit a planar structure. This is because such molecules exhibit free mobility, the dispersion effect then offers the possibility of overlaying in the sense of a build-up and registration of layers. This dispersion effect is more pronounced the greater the area of the interacting planar molecules. Only aromatic compounds satisfy the requirement of planar molecular structure. The formation of aromatics has been proven by X-ray analysis.[15] Only the aromatic molecules yield two-dimensional *hk* reflections.

According to de Boer[16] neighbouring molecules bonded by dispersion forces tend to touch in as large an area as possible. This dispersing effect is more pronounced the greater the area of the interacting planar molecules. Bradburn *et al*[17], based on theoretical calculations have shown that as the number of carbon atoms in the planar molecules increases, the mean mobile binding energy per carbon atom also increases. These calculations have led to the conclusion that it is not until a crystallite has built up to at least 20 or 30 atoms that it possesses the power of attracting further atoms with increasing facility. In the case of aromatics, this molecular size corresponds to coronene, (a polyaromatic hydrocarbon consisting of six benzene rings all directly attached to a centrally positioned seventh benzene ring).

By the combination of findings based on polarisation microscopy with chemical and X-ray analysis, it is possible to draw the following sequence for the formation of well ordered cokes, from which well ordered graphite is obtained:[18]

First step:	Formation of planar molecules by way of building reactions within the fluid phase.
Second step:	Parallel arrangement of these planar molecules due to dispersion effect.
Third step:	Preferential growth of planar molecules having molecular diameters greater than 25Å.
Fourth step:	Agglomeration of such molecular structures leading to molecular weights on the order of 500d.
Fifth step:	Agglomeration of these mesophase spherulites leading to a uniform mesophase.

However even the cokes produced from fluid phase pyrolysis can lead to the formation of both well-ordered and relatively disordered graphitic carbon. It is therefore necessary to understand the crystalline pre-order as it materialises during pyrolysis of aromatic hydrocarbons.

According to Milliken[19] and Kenney[20] the crystalline pre-order depends upon the way in which the aromatic fractions agglomerate. In the case of primary pyrolysis, products exhibiting biphenyl bonds, will allow ease of rotation which in turn prevents a pre-order from being established, *i.e.* a parallel arrangement of the aromatic system. On the other hand, if larger planar aromatics are being built by ring addition reactions, the requirements for a parallel arrangement are satisfied. See Figure 2.3 for aromatic hydrocarbons yielding pyrolysis residues of good and poor pre-order.

Mueller[21] found that graphitization of cokes from acenaphthylene produced highly-ordered graphitic materials. The pyrolysis mechanism of acenaphthylene in the liquid phase is given in Figure 2.4(a).

Decacyclene has been shown to be a principle intermediate product in the formation of coke from acenaphthylene. Although starting with decacyclene as the original material might produce less weight loss during pyrolysis, it also leads to a coke of somewhat inferior pre-order. Mueller has explained this as being due to the smaller temperature range in which this material is in the fluid phase (Figure2.4(b)). This means that the longer the temperature range which a material spends in the fluid phase, the more ordered the graphitic carbon produced from it. Pyrolysis of anthracene is also found to produce a well ordered coke giving rise to the formation of well ordered graphitic carbon.

Polymers containing oxygen.

In almost all cases the pyrolysis mechanism for strongly cross-linked polymers containing oxygen take place in the solid state.

i.e. pyrolysis of: Phenol-formaldehyde polymers (as in the case of PGC)

Polyfurfuryl alcohol[22]

Phenylene oxide polymers[23]

Cellulose[24]

The mechanism for pyrolysis of phenol-formaldehyde is given in Figure 2.5. This mechanism is particularly relevant since it is the mechanism for phenol/formaldehyde polymer by which PGC is currently prepared. The mechanism of solid state pyrolysis pertaining to highly cross-linked polymers distinguishes itself fundamentally from the liquid state pyrolysis leading to planar sheets of polycyclic aromatics. The resulting aromatic systems will be turbostratic (two dimensional) and angularly displaced, in a similar way to how they existed previously in the cross-linked polymers. The molecules are not sufficiently mobile for ordered rearrangement. Limited rotation becomes possible only in biphenyl structure, but even it is not sufficient to result in good graphitizability. PGC as prepared by the Knox and Gilbert method would be described as a having been prepared from a hard carbon.

2.3.3 Factors Affecting the Rate of Graphitization

High Pressure

Noda and co-workers[25] found that high pressures in the range 10 Kbar using only moderate temperatures produced a remarkable acceleration in the rate of graphitization for a wide variety of carbon types. Substantial graphitization of glassy carbon occurred in as little as 3 minutes at temperatures, 2600°C under 10 Kbar. Under similar conditions polyvinyl chloride coke graphitized at 1600°C[26]. Kinetic studies in the range 1-5Kbar showed that in glassy carbon[27] and in calcined cokes[28] graphitization occurs by a heterogeneous two phase mechanism. The use of such pressures does not, however, seem feasible for the production of PGC, which must retain its porosity throughout the graphitization process.

Pre-treatment

Pre-treatment of cokes at 1500 - 2000°C progressively decreased the amount of two-phase graphitization, but an enhanced homogeneous graphitization was observed under pressure when the temperature exceeded the pre-treatment value.

Plastic deformed pyrolitic carbon[29,30,31] has also been shown to give enhanced graphitization. It is thought that the externally applied pressure tends to augment the intrinsic internal differential thermal expansion stresses to induce the sudden transformation of localised volumes of the disordered carbon into graphite or graphitizable carbon. Again such a method would not be applicable to the production of PGC.

Metal Catalysts

In studies aimed at elucidating the mechanism of formations of natural graphite, alumina and various calcium minerals were shown to catalyse graphitization at moderate temperatures under pressure. A number of trace metals have also been shown to increase graphitizability.

Banerjee, Hirt and Walker[32] reported the formation of well graphitized film by pyrolysis of carbon dioxide on a nickel substrate at 713°C, and Mo, W, and Pt substrates on carbon films at 1000°C.

Evidence for a liquid phase solution/precipitation mechanism includes the use of cobalt and hard carbons and iron and hard carbons [33,34]. The use of boron also has a history of claims as a graphitization catalyst[35,36,37].

Gillot *et al*[38] have shown that similar phenomena can occur entirely in the solid state. Fine carbide particles burrow randomly through the glassy carbon matrix, ingesting disordered carbon on the leading surface of the particle and depositing it as graphite at the trailing surface, as illustrated schematically in Figure 2.6. In this way they report that 2-5 wt% of vanadium carbide can completely graphitize furfury alcohol coke in 20 hours at 2200°C. Similar results were obtained with titanium carbide at 2600°C. Two possible mechanisms for the carbide particle migration were proposed: Preferential dissolution of disordered carbon and precipitation of graphite, or decomposition of the carbide at the trailing surface of the carbide particle to react with disordered carbon on the leading interface.

According to Yokokawa, Hosakawa and Takegami[39] substantial graphitization of a number of hard carbons occurred at temperatures as low as 1400 - 1500°C, in the presence of a few weight percent of oxides or halides of copper. Kinetic studies using CuO as the additive indicated that the growth of the graphitic phase (d=3.36 - 3.37Å) was a first order rate process with an activation energy of 100 - 150Kcal mol^{-1}. And the rate of graphitization is said to increase linearly with additive concentration. The authors attributed the effect of cleavage of cross-linked bonds by the copper through some undefined mechanism.

It is perhaps significant that the catalysts were introduced into the resins prior to carbonisation. This raises the possibility that purely mechanical effects, such as deformation associated with shrinkage of the resin around the additive particles or increased thermal expansion stresses, may have played an important role in the observed catalytic effect.

For all the above the effectiveness of the graphitization aid depends on its ability to promote a substantial reorganisation of the structure - solution-precipitation types of catalysis are very effective because of the free energy of the disordered structure. (Improvement is thus much more significant in the highly disordered non-graphitizing carbon.)

The use of metallic catalyst can clearly be applied in the production of PGC, but there would then be the question of whether the impurity itself would introduce undesirable heterogeneous sites and whether the metallic catalyst could be completely removed.

2.4 Experimental Approach

Following the observations made by previous workers a broad range of experiments were undertaken in order to improve the chromatographic performance of PGC.

These may be summarised under the following headings:

1. Surface deactivation of PGC using anthracene at fractional monolayer coverages following graphitization.
2. Incorporation of soft carbons (acenaphthene and acenaphthylene) in the porous glassy carbon prior to graphitization.
3. The post-graphitization removal (cleaning) of surface impurities which might have been deposited during the cooling process after the graphitization.
4. The introduction of copper oxide into the phenol formaldehyde mixture prior to polymerisation as outlined by Yokokawa, *et al*[40].

2.5 Results and Discussion

2.5.1 Chromatographic Characterisation

In order that improvements to the chromatographic performance of PGC could be assessed for the various experiments, it was decided to focus on a single test mixture. Previous workers had developed a test mixture which had proven to be sensitive to what might be classed "very poor" or "poor" or "good" graphite. The composition of the test mixture and its sensitivity towards chromatographic performance of various PGC batches is demonstrated in Figure 2.7.

Although the batch of PGC shown in Figure 2.7c is described as having "good" chromatographic performance, it can be seen that good peak shape and plate height is achieved for the phenols, while significantly poorer peak shape is observed for the aromatic ethers, anisole and phenetole. This observation is significantly exaggerated for Figures 2.7(a) and 2.7(b), with the result that poorer resolution is observed for the anisole and p-cresol peaks. Measurement of alpha 4/3,

i.e. $k'_{phenetol}/k'_{p\text{-}cresol}$, provides a simple assessment of the chromatographic properties for a given batch of PGC. An alpha value >1.2 is considered acceptable whereas a value of <1.2 is considered unacceptable, since it results in the co-elution of the anisole and p-cresol (Figure 2.7(b)) or, even worse, co-elution of phenetole and 3,5-xylenol (Figure 2.7(c)).

The test solution is clearly sensitive to the quality of the PGC surface and has been employed throughout this study, with particular emphasis placed on the alpha 4/3 value.

2.5.2 Deactivation of PGC Using Anthracene

This experiment involved the deposition of vaporised anthracene onto the surface of the PGC at both 5% and 50% monolayer coverage.

Significant improvement in chromatographic performance was observed. This supported the earlier observations by Wan who had made similar observations using gas chromatography (GC) grade PGC (particles > 60μm). Interestingly, as seen in Figure 2.8, there appears to be very little loss in retention of 3,5-xylenol for the 5% coated PGC when compared to the bare PGC. Retention values are significantly reduced for the 50% coated PGC, with a loss in resolution despite an overall improvement in peak shape and alpha (α) 4/3 value. The α 4/3 values are observed to increase for both experiments, consistent with an improvement in the overall chromatographic performance. The 5% monolayer coated PGC appears to give the best results in that it maintains resolution and improves peak shape.

2.5.3 Incorporation of Soft Carbons to the Polymer Mix - Acenaphthene and Acenaphthylene

These experiments involved the impregnation of the starting polymer with either acenaphthene or acenaphthylene. In each case the temperature was adjusted to allow maximum melt time. Polymer/silica particles were then carbonised and silica removed by dissolution. The subsequent chromatography as shown in Figures 2.9(a), 2.9(b), and 2.9(c), was very disappointing. It showed no improvement over PGC manufactured by previous workers and less than the quality associated with the surface deactivation of the graphite with anthracene as described in Section 2.5.2. The chromatography for the acenaphthene experiment gave the poorest results with complete loss of resolution for peaks 3 and 4 and significant loss in resolution of peaks 5 and 6. The chromatographic performance of the acenaphthylene is better than the acenaphthene, but it is still not as good as the untreated PGC material.

2.5.4 Evidence for Surface Deposits on PGC and its Subsequent Removal

During the development and refining of the PGC process, poor chromatographic performance was often attributed to the graphitization process. This was the one part of the process which had to be carried out by external contractors (Centorr Inc, USA). As a consequence, allowable observations by those developing the process were limited to the final chromatography. This made refining the graphitization process difficult. The graphitization process, along with the rest of the manufacturing process, is now carried out at Hypersil, Runcorn, UK. Hypersil allowed us direct access to this equipment in order to investigate this part of the process further.

Following the observations by Kaur[41] the poor quality for some batches of PGC could be attributed to:

1. Deposition of elements / compounds on the surface of PGC during the graphitization process. These contaminants may possibly arise from:

   a) impurities already in the furnace left over from previous contractor samples. With the dedicated furnace now situated at Hypersil this possibility is removed.

   b) by-products given off during the graphitization of the carbon which deposit on the surface of the graphite during the cooling process. Some

evidence for by-product precipitation was already shown by Kaur with the formation of pyrolitic carbon termed "Graphite Needles."

2. Oxidation of the carbon surface caused by insufficient purging of the furnace chamber, or a slight leak in the system. All precautions were taken to ensure complete purging and absence of leaks. Consequently little improvement could be made to this area of the process. Oxygen is admitted when the furnace is opened to the air when its temperature is below 200°C. Oxidation of free radical sites can undoubtedly occur at this stage and consequently the furnace is allowed to cool to room temperature before the furnace is opened.

It was therefore decided to investigate the improvement of the chromatographic performance by looking for signs of impurity deposition on the surface.

Because PGC is "black" at all wavelengths, it is difficult to see surface impurities by spectroscopic techniques. However it was possible that deposits on the PGC surface would be similar to those on the graphite heat chamber of the furnace. The latter is also made from graphite. It, too, is black and so gives no indication of surface deposition. However, the end-plates of the heating chamber are stainless steel-coated copper. It was here that the first important observation was made.

Immediately after a graphitization process (approximately 40g carbon), the furnace was allowed to cool in an inert atmosphere of argon after which the end plate was removed.

Two types of deposits on the internal surface of the end plate were seen:

1. The first was a black deposit, which resembled soot.
2. The second deposit was a dry fine powder, blue-green in colour.

After only a few minutes it became clear that the blue-green deposit was hygroscopic and began to form droplets which then ran down the face of the endplate. Several samples of the fluid were collected. Examination of this liquid revealed:

(a) that it was insoluble in organic solvents such as acetone and methanol

(b) that it was soluble in water, suggesting that the deposit was an inorganic compound.

(c) that it was not retained on PGC and was eluted with the solvent front even when using 100% water as eluent.

(d) that it comprised sulphur and potassium along with other inorganic ions, the most significant being potassium, as measured by scanning electron microscopy (SEM) (Figure 2.10(a)).

The principle operation of SEM is that a finely pointed beam of electrons (of diameter <10nm) scans the sample, point by point. The incidence of the electron beam at the point on the sample gives rise to emitted electrons, which are of two types: secondary electrons and back-scattered electrons. Points on the sample which give rise to large quantities of electrons therefore give bright points on the display tube and points on the sample where the quantity of emitted electrons is low show up as dark points. Intermediate values give finely divided shades of grey on the display tube. The secondary electrons produce photons when they strike a scintillator and are subsequently transformed into electrical impulses in a photomultiplier. The image of the sample surface so formed has an almost three-dimensional appearance. In SEM the specimen area on which the electron beam is incident emits x-rays which are used for the analysis of the elements contained in the sample. There are two types of detector systems, which can detect and indicate the relative intensities of the characteristic radiation emitted: energy dispersive systems and wave-length dispersive systems.

The principle component of the energy dispersive system is a solid state detector, which produces an electrical pulse proportional to the energy of each incident x-ray quantum. The series of amplified pulses are sorted according to their energy in a multi-channel analyser. In only a few minutes all elements between sodium and uranium can be detected simultaneously. No elements are omitted. It is this mode of operation which was most useful to us in our study of the deposit on the surface of the furnace end-plate and washed extracts from the PGC itself. Unfortunately no quantitative information was obtained.

It was possible that if these compounds were deposited on the furnace end-plate they might also be deposited on the PGC itself. Over a period of time the impurity, if hygroscopic, would become hydrated. In this state it was thought possible that it may simply be removed from the surface of PGC by heat treatment under vacuum. In retrospect this was unlikely since potassium would not be volatile, only the adsorbed water. However, a sample of PGC which had shown poor chromatographic performance (alpha 4/3 <1.2) was left overnight in the open atmosphere (air), and then heated under a vacuum at 100°C for 18 hours. The resulting chromatography for this dried PGC material was significantly better for both the phenols and aromatic ethers than prior to drying (see Figures 2.11(a) and (b), and Table 2.1(a)). This observation further implicated the hydration hypothesis.

Further studies were made using other PGC batches. All batches showed significant improvement to the chromatographic performance upon drying. For some batches the vacuum oven temperature appeared to play a more important role than for others, as we see in Figure 2.12. Here, PGC117 shows significant improvement as we move from 100°C to 135°C drying temperatures. With batch PGC117R2 the temperature had to be increased to 200°C in order to get the same performance. It was thought likely that the differences between various batches toward the applied temperature may have been due to the degree of hydration of the surface impurity or its quantity. The more fully hydrated the more easily removed. The maximum temperature for the vacuum oven was set at 210°C, therefore limiting our studies. Each batch investigated showed significant improvement in chromatographic performance upon heating, with the best performance observed for batch 116R3. Table 2.1(b) summarises these observations.

In order to confirm that the improvement in chromatographic performance was not a result of adsorbed oil fumes from the rotary vacuum pump, Professor Knox treated a sample independently at Edinburgh University. This was done using a mercury vapour diffusion pump backed up by liquid nitrogen diffusion traps before the pump. The results as shown in Table 2.1(b) confirmed those obtained previously by showing an improvement in the alpha 4/3 value from 1.22 to 1.27.

In order to facilitate the hydration of the surface impurity the graphite was suspended in a surfactant soap solution (sodium dodecylsulphate or SDS). Note that because of the hydrophobic nature of PGC it requires a surfactant to wet the surface and enable suspension in water. A minimum of 7% SDS was found to be necessary to wet the surface and allow for suspension of the PGC particles. The suspension was left overnight, filtered, and washed in acetone to remove water and then dichloromethane to remove all traces of SDS. The PGC was then dried in the vacuum oven at 200°C in the normal way. The improvement in performance is shown for batch 121R4 in Figure 2.13 and Table 2.1(c).

Clearly a significant breakthrough had been made. In order to determine the nature of the deposit which had been removed from the surface of the carbon, the SDS solution used for the washing process was kept and evaporated to dryness using a rotary evaporator. The addition of methanol to the solution prevented bubble formation and loss of product during rotary evaporation. The resulting powder samples were sent for SEM analysis, along with a control sample of the SDS powder that had not been used to wash the PGC. The results are shown in Figure 2.10(b) and 2.10(c). Once again significant quantities of potassium and smaller quantities of sulphur and inorganic impurities were observed in the carbon sample

while none appeared in the control. We therefore concluded that these elements have come from the surface of the graphite during its contact with the SDS solution.

In order to establish if the surface contamination had occurred during the graphitization process, samples of PGC pre- and post-graphitization were analysed by inductively coupled plasma analysis (ICP) to determine levels of potassium and sulphur. The potassium levels prior to furnace treatment were high (1757μg/mL). They were reduced significantly during the graphitization process (88.5μg/mL). The high figure for potassium is most likely as a consequence of residual potassium hydroxide remaining adsorbed to the graphite surface after the silica dissolution procedure. The level of sulphur was found to have altered very little before (30.7μg/mL) and after (21.3μg/mL) graphitization. We therefore see no contamination from the graphitization step. An explanation for the presence of sulphur is not clear. Further investigation into the purity of the chemicals employed during the polymerisation or carbonisation processes may yield the answer.

2.5.5 Improvements to the Particle Size Distribution

During the manufacturing process of PGC, the silica template is prepared so that it has a very narrow particle size distribution. This is in keeping with the view that the columns packed with particles that have a narrow particle size distribution give highest column efficiencies and lowest pressure drop. The modern, high performance columns generally employ distributions no wider than 25% around the mean.[42] (Early studies[43] had found that a 40% around the mean was the norm.) The particle size distribution of the final PGC product was observed to be considerably broader than the starting 5μ silica i.e > 25% around the mean. This is likely to have been due to the presence of graphitized polymer, i.e. polymer that had not entered into the silica particle porous cavities leading to either coagulation of particles or the generation irregular particles that did not exists as part of any silica particle. The washing process with SDS provided the ideal opportunity to improve the particle size distribution via a settling process (sedimentation). Sedimentation had several attractions as a fractionation process:

a) The apparatus required was simple (Pyper[44]), see Figure 2.14.
b) Those particles which lay outside the original silica template particle size distribution were thought likely to show different settling velocities compared to discrete particles of PGC due to differing densities and size.

The 7% SDS solution described earlier proved to be the ideal suspension for fractionation by sedimentation. An important consideration when choosing a solvent for fractionation by sedimentation is whether the particles will flocculate or deflocculate when suspended in the solvent. If the particle-particle interaction is stronger than the particle solvent interaction, the particles will flocculate and particle aggregates will form and settle rapidly. If there is no attraction and instead repulsion between particles, the particles settle as individuals and the suspension is more stable. The SDS solution offered a deflocculating system which allowed the PGC particles to settle discretely without aggregation. Pyper had observed that the concentration of slurry (weight of particles per volume of solvent) effected the yield of fractionalised product. This was also found to be the case with our studies, and consequently the fractionation process became one of partial shaving of the distribution with a number of sedimentation steps.

The sedimentation velocity of a porous particle in a solvent can be estimated by Stokes equation:

$$u_s = \frac{1}{18} \cdot \frac{d_p^2}{\eta} \cdot e_{sk}(\rho_{sk} - \rho_l) \qquad [2.9]$$

where d_p is the particle diameter, η is the viscosity, e_{sk} is the fraction of the particle occupied by the particle skeleton, ρ_{sk} is the density of the skeleton and ρ_l is the density of the liquid.

Figure 2.15(a) shows the distribution of particles prior to sedimentation. A 6.5μm cut-off point for heavy particles was required since particles above this size had not been present in the original silica particle size distribution. Stokes equation was therefore used to determine the settling time required to obtain a particle size cut of 6.5μm. Particles that take longer to settle would remain in suspension and can be removed, while heavy particles would have settled and formed a thick slurry at the base of the container. A settling time of 114 minutes was measured. The improved particle size distribution obtained by sedimentation is shown in Figure 2.15(b). The number of sedimentation steps is outlined schematically in Figure 2.16.

Significant improvement in column efficiency was observed for the fractionated material with improved particle size distribution. The column efficiency was seen to increase from typically 35,000 plates per meter to 60,000 plates per meter, and up to 70,000 plates per

meter when optimum flow rate conditions were employed. See the plot of Reduced Plate Height *vs*. Linear Velocity in Figure 2.17.

Subsequent batches of PGC were then given the same treatments: SDS fractionation followed by vacuum oven drying at 200°C. They all showed the same chromatographic improvement (see Figure 2.18, Table 2.2). Calculated RSD values for variation in batch selectivity (alpha values), are extremely low, typically < 0.04.

We conclude that it is not only the mean particle size of a media but also its particle size distribution which plays an important role in the degree to which band spreading occurs. We also conclude that much of the poor performance associated with PGC up to this point has been related to the fact that the particle size distribution has been too broad.

2.5.6 Copper Experiments

Following the work of Yokakawa *et al*[45] copper, in the form of copper oxide, was introduced to the phenol hexamine mixture prior to polymerisation. The quantity copper oxide employed was (a) 5% and (b) 20% by weight based on silica, or 3% and 12% of the total weight of phenol hexamine used. In relation to the final carbon this would correspond to roughly 6% and 24%.

The process was then followed as for the current PGC process, with copper again being introduced during the second polymerisation. The initial graphitization was made at 1500°C in argon. Above this temperature copper vaporises and would consequently have been deposited somewhere on the internal walls of the furnace system. This was not an acceptable proposition, so the carbon was removed from the furnace after graphititization at 1500°C. The carbon was then boiled in dilute nitric acid to remove residual copper. It was then packed into a column and the chromatographic performance observed. It was observed that although the performance was poor, graphitization had already started to occur i.e several of the analytes in the phenols test mixture were retained whereas in the pre graphitized material no such retention is observed.

The same material was then reintroduced to the furnace and graphitization at 2500°C was made in the usual way. The chromatography from this material was found to be similar to the best batches produced following the vacuum oven/heat treatment described above (see Table 2.3 and Figure 2.19). However no further improvement in performance or change in selectivity was observed over that already seen for PGC having had the surface SDS wash procedure and vacuum oven treatment. Consequently no further experiments employing copper were investigated

2.6 Conclusions

Following Wan, the deactivation of PGC proved a successful way of improving the chromatographic properties of PGC. However our attempts to improve the chromatographic performance by improving the crystallographic structure of PGC by application of soft carbons prior to graphitization proved to be unsuccessful.

However, a significant breakthrough in the chromatographic performance of PGC was made by the implementation of a surface clean-up procedure followed by a fractionation process to remove agglomerated or non-porous particles. The clean-up procedure was shown to reduce levels of primarily potassium, and sulphur. The presumed source of the potassium is residual from the KOH employed is the silica dissolution step. The source of the sulfur is uncertain at this point.

The use of a metal catalyst in the form of copper oxide also proved to be highly successful in improving chromatographic performance, but offered no improvement over the clean-up procedure with sodium dodecylsulphate (SDS).

2.7 Experimental Detail

2.7.1 Anthracene Deactivation Experiments

Two experiments were undertaken:

a) Anthracene 50% monolayer

b) Anthracene 5% monolayer

The experiment took place at Edinburgh University.

a) 1mg weighed accurately was mixed with 1.2828g of PGC batch PGC106/R1

b) 9mg weighed accurately was mixed with 1.1995g of PGC batch PGC106/R1

The same wash procedure given to both samples is outlined below.

The PGC and anthracene powder samples were placed together in a glass ampoule containing a glass frit. The ampoule was then placed vertically into a vacuum system where it was evacuated to 1mmHg. The ampoule was then sealed and placed into a bench-top heating device and heated 430°C. It was kept at this temperature for approximately 18 hours after which time the temperature was increased to 510°C. It was kept at this

temperature for a further seven hours and then allowed to cool. The coated PGC was then packed into an HPLC column and tested chromatographically.

2.7.2 Incorporation of Soft Carbons to the Polymer Mix - Acenaphthylene and Acenaphthene

2.7.2.1 Acenaphthylene Impregnation - Soft Carbon Investigation

The purpose of the experiment was to modify the surface of the PGC by improving the crystallographic properties of the graphite produced. Acenaphthylene was introduced by mixing a known quantity with carbon prior to graphitization. The determined quantity was calculated to initially fill the pores during the fluid phase carbonisation but during this process it was known that 80% weight loss occurs which would leave 20% spread across the carbon surface. Graphitization of the product was carried out in the normal manner.
The quantity of acenaphthylene required was calculated as follows:

100g(carbon) x 1.0042g/mL(density of melt) x 0.4mL/g(total volume of pores) = 41.68g

100g of carbon (PR 2/36/CI) was then mixed with 41.68g of acenaphthylene (pore volume of carbon 0.4mL/g). The mixture was heated to 100°C for 4 hours in a rotary oven and the acenaphthylene melt allowed to fill the pores by capillary action. The material was next transferred to Edinburgh University for final carbonisation, the temperature profile and observations are given in Figure 2.20. Dissolution of silica and graphitization were carried out as described for PGC (Section 2.2.2). A full breakdown of experimental data is given in Table 2.4. The material was then tested chromatographically.

2.7.2.2 Acenaphthene Impregnation - Soft Carbon Investigation

PR2/55-Acenaphthene

A 100g larger scale experiment had to be abandoned due to difficulties with the carbonisation step. A thick liquid by-product condensed and blocked the nitrogen outlet pipe so that there was a potential pressure build up in the inconel tube. A small scale experiment was therefore undertaken.
The quantity of acenaphthene required was calculated as follows:

20g(carbon) x 1.00g/mL(density of melt) x 0.4mL/g(total volume of pores) = 8g

20g of carbon /silica was mixed with 8g of acenaphthene. The density of the acenaphthene melt was determined to be 1.0g/mL. The mix was rotated for 2 hours at 95-100°C. Dissolution of silica and graphitization of the carbon product was carried out as for PGC.

2.7.3 Surface Contamination Investigations

Experimental data for the preparation of PGC batches used in this section and the next is given in Table 2.5.

Vacuum Oven Treatment

Thownson and Mercer Vac ovens were employed. Maximum temperature was 210°C. Typical vacuum employed was 0.02mHg. The samples were treated at various temperatures for 18 hours. The glass container was covered with a light piece of filter paper with a number of pin pricks placed in it. This prevented the fine carbon particles becoming mobile as liquid is removed from their surface.

SDS Suspension

PGC does not wet in water unless there is a detergent (surfactant) present. Complete wetting, *i.e.* when all the particles were observed to go into suspension, occurred only when a 7% SDS solution was employed.

2.7.4 Particle Fractionation - Sedimentation

A set-up resembling that described by Pyper and shown in Figure 2.14 was employed. The Stokes equation was used to calculate the settling time for particles equal to or larger than 6.5μm. Particles smaller than this would stay in suspension.

$$dp = \frac{(18\,\eta\,h)^{1/2}}{(\rho_s - \rho_g)g.t)^{1/2}}$$

$$\text{so that } t = \frac{18\,\eta\,h}{(\rho_s - \rho_g)g.\,dp^2}$$

then, if h = 15cm or 0.15m

$\rho s = 2.2 \times 103$ kg/m^3

$\rho g = 1.0 \times 103$ kg/m^3

$g = 9.81$ m/sec^{-1}

dp = 6.5μm settling time (t) = 8494 seconds or 141 minutes

Time (t) was employed between settling and supernatant removal. Particle size analysis of the supernatant is carried out using a Particle Data, Size Analyser. The supernatant product

"B" was then re-suspended and allowed to settle for a further 2.25 hours. The supernatant "C" was removed and allowed to settle for a period of 24 hours. The supernatant was then discarded along with unwanted fine particles.

The sediment from fractions "A", "B" and "C" are all re-suspended and the process repeated until no product was observed in the supernatant solution after the 2.25 hours settling time. Finally the product from each beaker containing "D" was combined to give the final product. An overview of the complete process is given in Figure 2.16. In total, twenty-four fractionation steps are required for a PGC batch size of 80g.

2.7.5 Incorporation of Copper into the Polymer Mix

These experiments involved adding a known quantity of copper oxide to the initial polymer mix-phenol:hexamine. The remainder of the procedure up to the graphitization step was identical to that described for PGC. Following dissolution of silica in 5M KOH, the material was graphitized at 1500°C for 6 hours. After cooling a sample was tested chromatographically while the remainder of the material was boiled with dilute nitric acid to remove the copper. The process is described as follows: approximately 50g carbon was slurried in 160mL methanol, to this was added 300mL 0.1M HNO_3 (methanol was included to facilitate wetting the carbon. The methanol vapour was allowed to escape until the temperature reached 90°C at which point the distillation apparatus was converted to the reflux mode and the slurry was allowed to reflux for a further 18 hours. The filtrate was observed to be pale blue indicating the presence of copper. The material was then graphitized as described for PGC. Experimental details are given in Table 2.6. Chromatographic results are shown in Table 2.3.

Chapter 2 References

[1] Kaur, B., Ph.d Thesis, *Porous Graphitic Carbon , A New Material for HPLC*, University of Edinburgh (1986)
[2] Wan, Qian Hong, Ph.d Thesis, University of Edinburgh, (1992)
[3] Greib, S., Ph.D Thesis, Warwick University, (1992)
[4] Knox, J. H. and Kaur, B., in *High Performance Liquid Chromatography*, P. Brown and R. Hartwick, Eds., John Wiley & Sons, London, (1989)
[5] Unger, K. K., *Porous Silica*, J.Chromatogr. Library, vol, 16, Elsevier Scientific Publishing Company, (1979)
[6] Snyder, L.R and Kirkland, J. J., *Introduction to Modern Liquid Chromatography*, 2nd Ed., John Wiley & Sons, New York, (1979)
[7] See reference 2
[8] Kiselev, A. V and Yashin, Y.I., *Gas Adsorption Chromatography*, J. E. S. Bradley, Trans. Plenum Press London, (1969)
[9] Iler, R. K., *The Chemistry of Silica,* A Wiley-Interscience Publication, (1979)
[10] See reference 1
[11] Bernal, J. D., Proc. Royal Soc. (London), A106, 749 (1924)
[12] Franklin. R. E, Acta Cryst, 3 107 (1950)
[13] Fitzer, E., Mueller, K., Schaefer, W., *The Chemistry of the Pyrolytic Conversion of Organic Compounds to Carbon* in Chemistry & Physics of Carbon, vol. 7, Ed Walker, Marcel Dekker (1971)
[14] Kippling, J. J. and Shooter, P. V, *2nd Conference on Industrial Carbon and Graphite*, Society of Chemical Industry, p. 15.
[15] Fitzer, E., Mueller, K., Schaefer, W., *The Chemistry of the Pyrolytic Conversion of Organic Compounds to Carbon* in Chemistry & Physics of Carbon, vol. 7, Ed Walker, Marcel Dekker (1971)
[16] de Boer, W., Trans, Faraday Soc, 32, 10, (1936)
[17] Bradburn, M., Coulson, C. A., Rushbrooke, G. S., *Proc. Roy. Soc.*, Edinburgh, 62A, 336 (1936)
[18] Milliken, S. R., Ph.D Thesis Pennsylvania State University (1954)
[19] See reference 18
[20] Kinney, C. R, Proc Conf. Carbon, 1st & 2nd Buffalo 1953, 1955 University of Buffalo Press 1956, P83.
[21] See reference 15
[22] Schafer, W.and Fitzer, E., Carbon , 8, 353 (1970)
[23] Kalka, J.,Ph.D Thesis, Karlsuhe University, West Germany (1970)
[24] Overhoff, D., Ph.D Thesis, Karlsuhe University, West Germany, P118 (1966)
[25] Noda, T.and Inagaki, M., *Bull. Chem. Soc Japan*, 37, 1534 (1964)
[26] Noda, T.and Kato, H., Carbon, 3, 289 (1965)
[27] Kamya, K., Inagaki M., Miztani, M.and Noda, T., Bull. Chem . Soc Japan, 41, 2169 (1968)
[28] Noda, T., Kamya, and Inagaki, M., Bull. Chem . Soc Japan, 41, 485 (1968)
[29] Blackman and Ubbelolide, Proc .Soc (Lond), A266, 20 (1962)
[30] Kotlensy and Markers, Proc.Conf Carbon 5th, Penn State (1961)
[31] Bragg, *et al*, Carbon, 1, 171 (1964)
[32] Banerjee, B. C., Hirt, T. J., and Walker, Jr. P .L., Nature, 192, 450 (1961)
[33] Hivert, A., Mathieu, and Tacvorian, S., Compt Rand., 252, 1771 (1961)
[34] Albert, P., *Paper 36, Paris Conf*, June 1968, J. Chim Phys. Special Issue, Apr., p.171 (1969)
[35] Albert, P. and Parisot, J., *Proc. Conf. Carbon* , Buffalo June 1967
[36] Maillard, P. and Maire, J., *Compt. Rend.*, 267C, 436, (1968)
[37] Trask, R. B., *Paper P86, 8th Conference on Carbon*, Buffalo, June 1967
[38] Gillot, Blux, Cornuault, P. and Chaffaut, F., *Ber. Deut. Keram. Ges.*, 45, 224 (1998)
[39] Yokokawa, Hosakawa and Takegami, Carbon, 4, 459 (1966)
[40] See reference 39
[41] See reference 1

[42] Uwe D. Neue, *HPLC Columns Theory, Technology, and Practice,* Wiley-VCH, (1997)
[43] Strubert, W., Chromatographia, 6, 50 (1972)
[44] Pyper, H. M. and Knox, J. H., Ph.D. Thesis, University of Edinburgh (1984)
[45] See reference 39

Table 2.1
Chromatographic Data for Surface Improvements to PGC

2.1a

PGC Batch	PGC 116R3	PGC 116R3 Vac 100°C
k' ACETONE	0	0
k' PHENOL	0.29	0.26
k' ANISOLE	0.76	0.6
k' PARACRESOL	0.86	0.8
k' PHENETOLE	1.49	1.21
3,5 XYLENOL	1.95	1.92
ALPHA 3/2	2.61	2.29
ALPHA 4/3	1.13	1.34
ALPHA 5/4	1.72	1.5
ALPHA 6/5	1.31	1.59
PHENETOLE (N)	11457	38482
XYLENOL (N)	39320	43463
XYLENOL (As)	1.85	1.34

2.1b

PGC 117R2	KNOX VAC. 135c	117R2 VAC200°C
20	135	200
0	0	0
0.32	0.28	0.3
0.79	0.72	0.72
0.96	0.91	0.91
1.58	1.43	1.42
2.25	2.4	2.09
2.49	2.54	2.28
1.22	1.27	1.26
1.64	1.57	1.56
1.43	1.49	1.48
20081	16542	25236
35537	28586	37030

2.1c

PGC121R 4 not treated	PGC121R 4 Vac 200°C	SDS + Vac 200°C
0	0	0
0.28	0.27	0.28
0.69	0.63	0.63
0.85	0.83	0.86
1.37	1.26	1.27
1.96	1.93	2.04
2.43	2.31	2.24
1.23	1.31	1.37
1.61	1.52	1.47
1.43	1.54	1.61
25201	38337	41210
39377	42371	41219
1.67	1.8	1.5

N = plate number per meter
A = peak asymmetry
Mobile Phase conditions: 95% Methanol: Water , flow rate 1 ml/min ,254nm

Table 2.2
Chromatographic Data for Surface Improvements to PGC

2.2a

SOLUTE	PGC121 Not treated	PGC121 VAC 200	PGC121 SDS Vac 200	PGC 121 Fractionated Vac 200
k' ACETONE	0	0	0	0
k' PHENOL	0.28	0.27	0.28	0.27
k' ANISOLE	0.69	0.63	0.63	0.65
k' PARACRESOL	0.85	0.83	0.86	0.91
k' PHENETOLE	1.37	1.26	1.27	1.33
k' 3,5 XYLENOL	1.96	1.93	2.04	2.15
k' ALPHA 3/2	2.43	2.31	2.24	2.44
k' ALPHA 4/3	1.23	1.31	1.37	1.4
k' ALPHA 5/4	1.61	1.52	1.47	1.47
k' ALPHA 6/5	1.43	1.54	1.61	1.62
N PHENETOLE	25201	38337	41210	55913
N XYLENOL	39377	42371	41219	53200
A XYLENOL	1.67	1.8	1.5	1.68

2.2b

SOLUTE	PGC 122R3 Fractionated Vac 200C	PGC 123R1 Fractionated Vac 200C	PGC 125R3 Fractionated Vac 200C	PGC 127R3 Fractionated Vac 200C
k' ACETONE	0	0	0	0
k' PHENOL	0.32	0.33	0.38	0.34
k' ANISOLE	0.74	0.72	0.9	0.77
k' PARACRESOL	1	1	1.18	1.04
k' PHENETOLE	1.47	1.44	1.78	1.51
k' 3,5 XYLENOL	2.33	2.33	2.72	2.39
k' ALPHA 3/2	2.28	2.21	2.37	2.24
k' ALPHA 4/3	1.35	1.39	1.32	1.36
k' ALPHA 5/4	1.47	1.43	1.51	1.45
k' ALPHA 6/5	1.58	1.62	1.53	1.58
N PHENETOLE	53755	53055	46542	50033
N XYLENOL	54337	62984	57714	56709
A XYLENOL	1.93	1.64	1.42	1.38

Mobile Phase conditions: 95% Methanol: Water , flow rate 1 ml/min ,254nm

Table 2.3 Experimental Data for Copper Experiments

Copper levels for PR 3/62

PR 3/62	g(Cu)/g(total	% total
1st polymerisation	0.6	5.94
1st carbonization	0.8	7.81
2nd polymerisation	0.15	14.6
2nd carbonisation	0.16	15.8
Dissolution of silica	0.26	26.2
Heat treatment	0.26	26.4
Graphitization at 1500C	0.26	26.6
Dissolution of copper	0.24	24.1
Graphitization at 2500C		1.2

Chromatographic Data

PGC-BATCH	PR 3/33	PR 3/53	PR 3/53 VAC 200	PR 3/54	PR 3/54 VAC 200	PR 3/56 VAC 200	PR3/62	PR3/62 VAC 200
ACETONE	0	0	0	0	0	0	0	0
PHENOL	0.32	0.39	0.34	0.37	0.34	0.35	0.29	0.27
ANISOLE	0.71	0.98	0.79	0.84	0.77	0.78	0.71	0.63
PARACRESOL	0.98	1.17	1.05	1.09	1.03	1.05	0.87	0.83
PHENETOLE	1.41	1.94	1.57	1.64	1.53	1.56	1.41	1.25
3,5 XYLENOL	2.3	2.69	2.46	2.5	2.4	2.45	2.04	1.95
ALPHA 3/2	2.22	2.53	2.29	2.29	2.28	2.26	2.44	2.31
ALPHA 4/3	1.37	1.2	1.34	1.3	1.34	1.34	1.23	1.33
ALPHA 5/4	1.44	1.65	1.49	1.5	1.49	1.48	1.62	1.5
ALPHA 6/5	1.62	1.39	1.57	1.53	1.57	1.58	1.44	1.56
PHENETOLE (N)	31277	16918	34218	23158	29253	26626	18139	28909
XYLENOL (N)	33207	32593	40072	30864	27078	26779	26148	30424
XYLENOL (A)	1.63		1.56		1.86	1.22	2.17	1.78

Mobile Phase Test Conditions: 95 % Methanol:Water

Table 2.4

Acenaphthylene Experimental Data

Carbonisation Temperature Profile

Hold Temperature	**Heating Rate**	**Duration**
300°C	200 °C/hour	30 minutes
600°C	50 °C/hour	1 min
1000°C	50 °C/hour	120 min

Weight of carbon/acenaphthylene pre-carbonisation	119.9 grams
Weight of carbon/acenaphthylene post-carbonisation	73.76 grams
Weight Loss	46.14 grams
% Weight Loss	38.4%

Calculation for weight loss of acenaphthylene:

Initial quantities of acenaphthylene: carbon had been 41.6g: 100g or 29.4% acenaphthylene

Starting weight for carbonisation total was	120 grams
Starting weight of carbon	84.72 grams
Starting weight for carbonisation acenaphthylene	35.28 grams
Final weight total	73.76 grams
If we assume 20% weight loss for PGC	68 grams expected
Final weight acenaphthylene	7.056 grams expected
% Weight loss for acenaphthylene	80%

Observations during carbonisation

1. Pink/Red brown product in trap flask, also present were very small yellow crystals - these could not be collected. The pink product was sticky and soluble in xylene.
2. Crystals/deposited in the plastic tubing immediately after the nitrogen metal tube outlet. Colours very brown/red /yellow green. Pencil type crystals plus some wet residue.
3. Crystals deposited in metal N_2 outlet tubing next to 2. plastic tubing (sample taken from at least 8 inches into the metal tube). Pencil shaped crystals under the microscope.
4. Crystals taken from the middle of the metal N_2 outlet tubing. Mostly red and quite abundant. Black particles also present but these were thought to have fallen through from lower down the metal tube. Pencil shaped crystals plus aggregates crystals plus carbon particles.
5. Black particulate material collected from the end of N_2 metal tube inside the furnace.
6. Brown crystals formed on plate next to seal.

Table 2.5

Experimental Data for PGC Experiments

	PGC	PGC	PGC	PGC	PGC
Experiment Batch	**121**	**122**	**123**	**125**	**127**
Wt of silica used (PR 723) (grams)	393.8	339.3	325	350	360
Pore volume (mL/g)	1.49	1.51	1.47	1.57	1.52
Wt of phenol = 0.925 x wt sil x pore vol	542.8	476	442	508.3	5506
Wt of hexamine = 0.154 x wt sil x 1.49 (grams)	90.4	79.3	73.6	84.6	84.3
Start weight for Polymerisation (grams)	1025	894	839.6	941.2	946.6
Final weight (grams)	973	848	795.7	892.8	896.7
% yield	94.9	94.8	94.8	94.8	94.7
1st Carbonisation					
Start weight (grams)	971	846	794	881	895
Final weight (grams)	585	508	496.7	540.7	526.3
% yield	60.2	60.1	62.6	61.37	58.8
2nd Polymerisation					
Weight sil/carb (grams)	545	464.3	468.2	515	526.2
Pore volume (mL/g)	0.35	0.39	0.38	0.46	0.43
Phenol = 0.925 x wt sil/carb x pore vol	176.4	167.5	164.6	219	209
Hexamine = 0.154 x sil/carb x pore vol	29.4	27.7	27.4	36.5	34.8
Start weight, 2nd Polymerization (grams)	750.1	658.8		769	768
Final weight (grams)	710	634.3	632	740.5	746.7
% yield	94.65	96.3	95.8	96.3	97.25
2nd Carbonisation					
Start weight (grams)	706	634	630	736	620
Final weight (grams)	580	522	529.9	609	289.7
% yield	82.15	82.3	84.1	82.8	46.7
Dissolution of Silica					
Start weight (grams)	556	520	529	607	620
Final weight (grams)	252.5	243	250	298	289.7
% yield	45.4	46.8	47.2	49.2	46.7
Final Heat Treatment					
Start weight (grams)	253	241	248	295.7	288
Final weight (grams)	212	230	243	283	260.6
% yield	83	95.4	98	95.7	90.4
Graphitization					
Start weight (grams)	82	60	80	90.3	90
Final weight (grams)	66.6	53.5	73.1	84.6	85
% yield	81.2	89.2	91.3	93.4	94.4

Table 2.6

Experimental Data for Copper Experiments

Experiment Batch	PR3/33	PR3/53	PR3/62
Weight of silica used (PR 723) (grams)	100	180	100
Pore volume (mL/g)	1.49	1.49	1.49
Weight of phenol = 0.925 x wt sil x pore vol (grams)	137.8	248.1	137.8
Weight of hexamine = 0.154 x wt sil x 1.49 (grams)	22.9	41.3	22.9
Weight of copper oxide = 0.05 x 180 (grams)	5	9	20
Start weight of Polymerisation (grams)	265	478	280.
Final weight (grams)	249	450	266
% yield	94%	94.1%	95%
Start weight of Carbonisation (grams)	240	444	266
Final weight (grams)	162	291 65%	176
% yield	65%		66%
2nd Polymerisation wt sil/carb (grams)	160	295	143
Pore volume (mL/g)	0.3	0.23	0.4
phenol = 0.925 x wt sil/carb x pore vol (grams)	44.4	62.8	53
hexamine = 0.154 x sil/carb x pore vol (grams)	7.4	10.5	8.8
Cu in phen/hex(P1) x phen+hex (grams)	6.4	1.26	7.7
Start weight 2nd Polymerization (grams)	218	368	212
Final weight (grams)	207	358	198
% yield	95%	97.2%	93.4%
2nd Carbonisation			
Start weight (grams)	205	356.5	208.5
Final weight (grams)	161.9	287	167
% yield	79%	80.6%	80.1%
Dissolution of Silica			
Start weight (grams)	155	286	161
Final weight (grams)	74.4	141.5	94.3
% yield	48%	49.5%	58%
Final Heat treatment			
Start weight (grams)	******	*****	92.3
Final weight (grams)			84.6
% yield			91.6%
Graphitization			
Start weight (grams)	40	30	45.5
Final weight (grams)	34	25.8	39.3
% yield	85	86	86.3

***** final heat treatment part of graphitization

See separate section for graphitization process to 1500°C

Fig 2.1
Adsorption Isotherms

a) Adsorption Isotherms

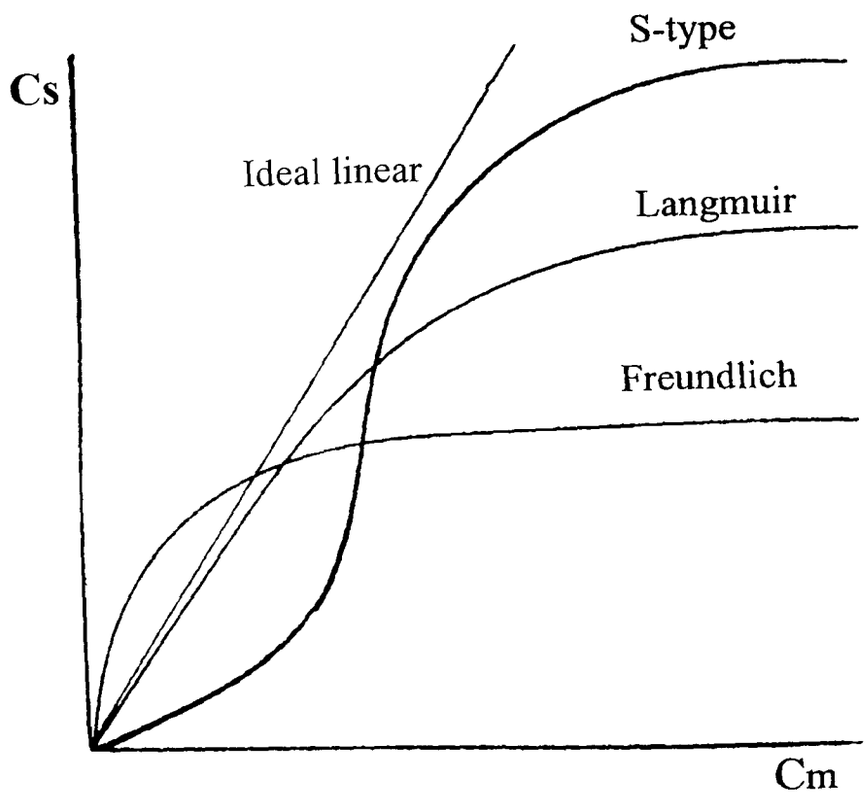

b) Schematic representation of the effect
of increasing sample concentration on analyte elution profile

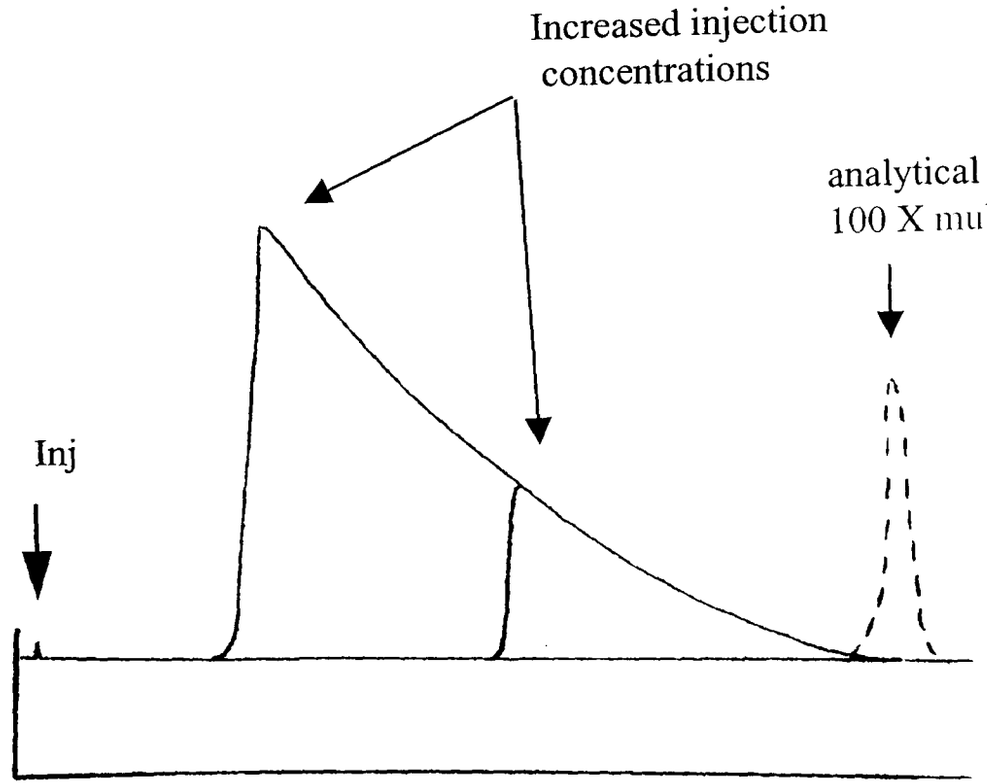

Fig 2.2a
Wide Pore Silica Particle Formation Schematic

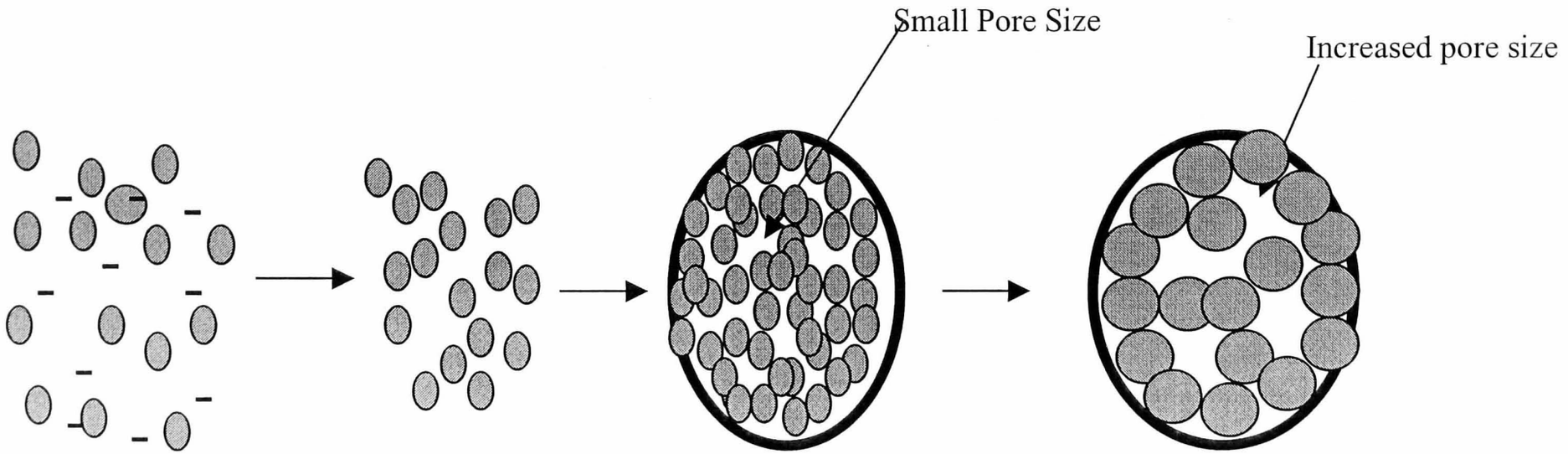

Primary Sol Particles 15nm particle size

Charge stabilised

No collision

Charge Stabilisation

pH Adjustment

Removal of Stabilisation

Collisions

Interparticle bonds

Emulsification

Secondary Particles

Controlled hardening

Removal of emulsifier

Silica particles hydrothermally treated

to increase pore size as microspheres increase in size. Also hardens the original secondary particles.

Fig 2.2(b) & 2.2(c)
Polymerisation and Carbonisation Equipment Setup

(b) Polymerisation Experimental Apparatus

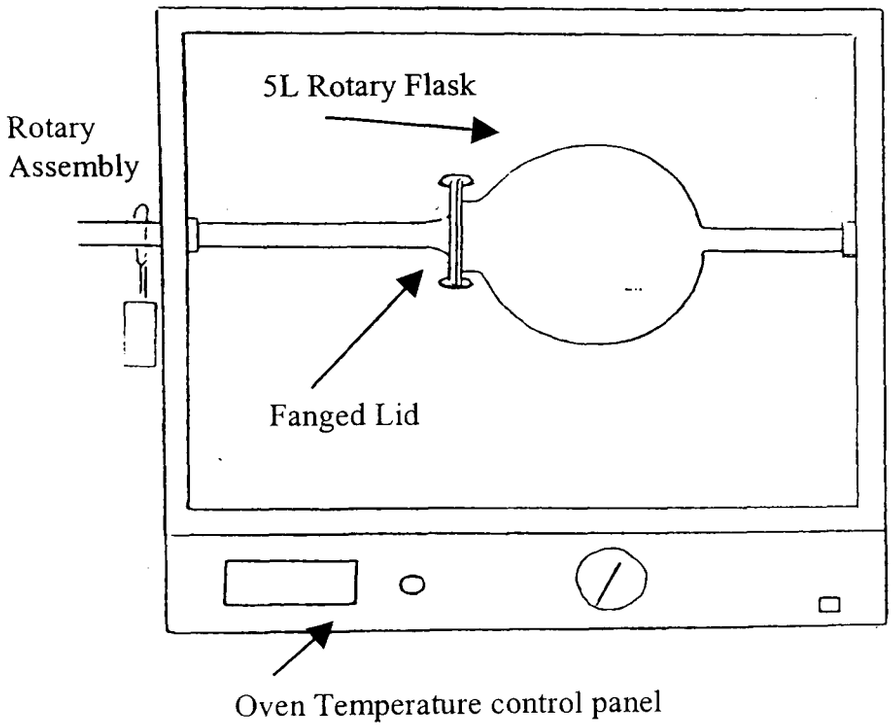

(c) Carbonisation Experimental Apparatus

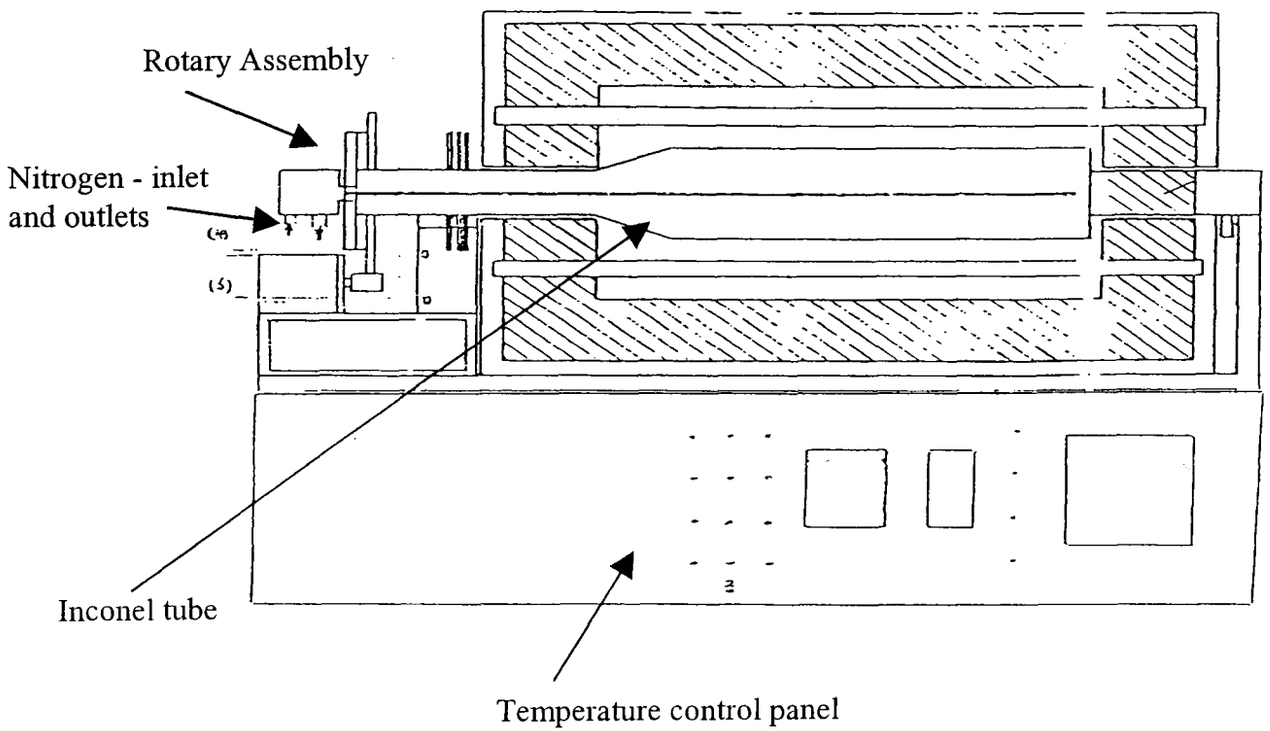

Polymerisation Temperature Programme for Rotary Oven

Ambient	to	80 deg C at 120 deg C/hr	16hrs
		80 deg C overnight	
80 deg C	to	120 deg C at 120 deg C/hr	16hrs
		120 deg C overnight	
120 deg C	to	147 deg C/hr	
		147 deg C for 5hrs	

Carbonisation Temperature Programme for Carbonisation Pro

1	Delay 4 hours while purging the system	
2	Ambient to 150 deg C	200 deg C/hr
3	150 deg C to 600 deg C	50 deg C/hr
4	600 deg C to 1000 deg C	70 deg C/hr
5	1000 deg C	

Fig 2.2(d)
Graphitization Furnace and Temperature Program

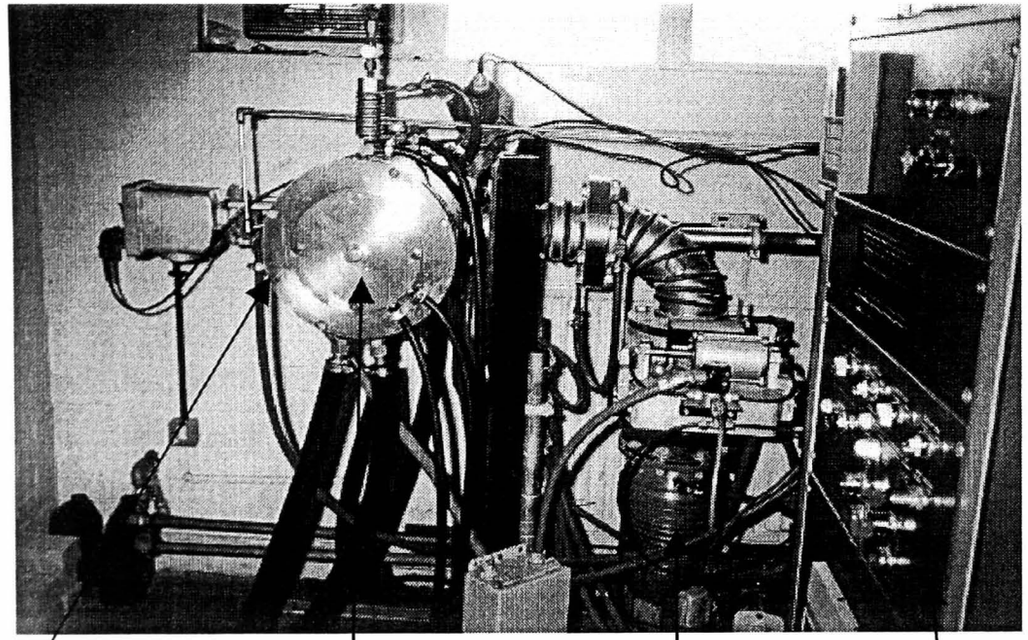

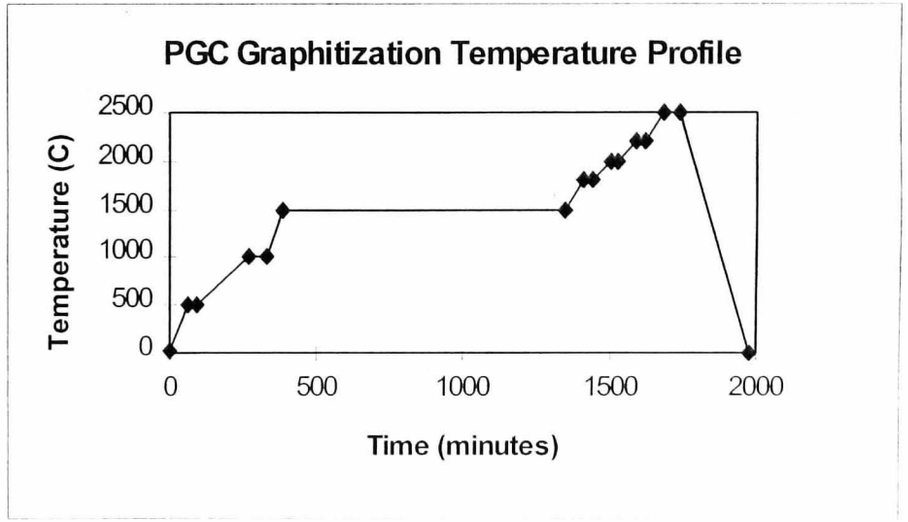

Commutative Time (mins)	Temp (C)	Time(mins)
0	20	0
60	500	60
90	500	30
270	1000	180
330	1000	60
390	1500	60
1350	1500	960
1410	1800	60
1440	1800	30
1500	2000	60
1530	2000	30
1590	2200	60
1620	2200	30
1680	2500	60
1740	2500	60
1980	0	240

Fig 2.3

Aromatic Hydrocarbons Yielding Pyrolysis of Good and Poor Pre-order

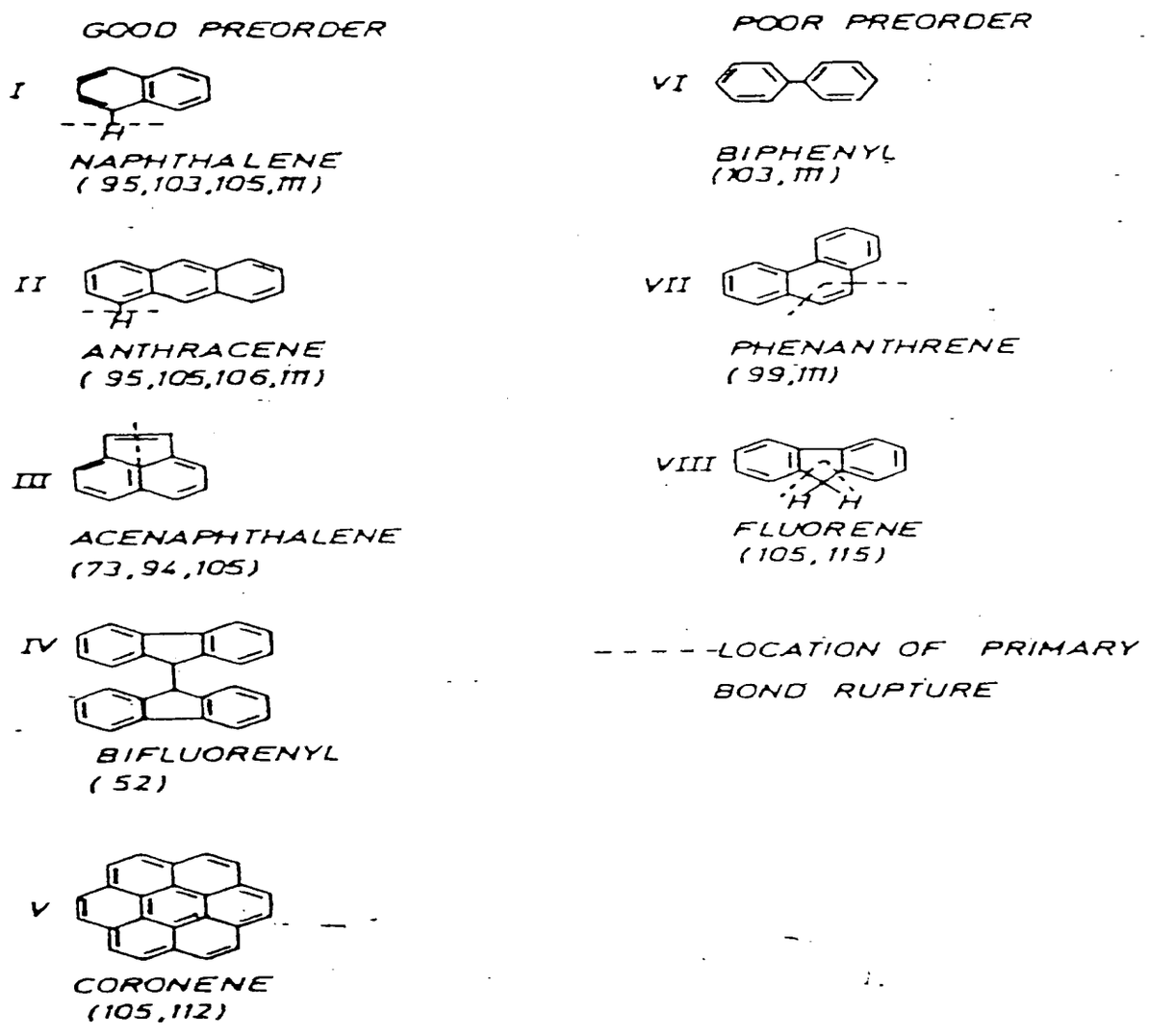

Aromatic hydrocarbons yielding pyrolysis residues of good and poor preorder.

Fig 2.4(a) and 2.4(b)

(a)

Mechanism of Liquid Pyrolysis of Acenaphthylene

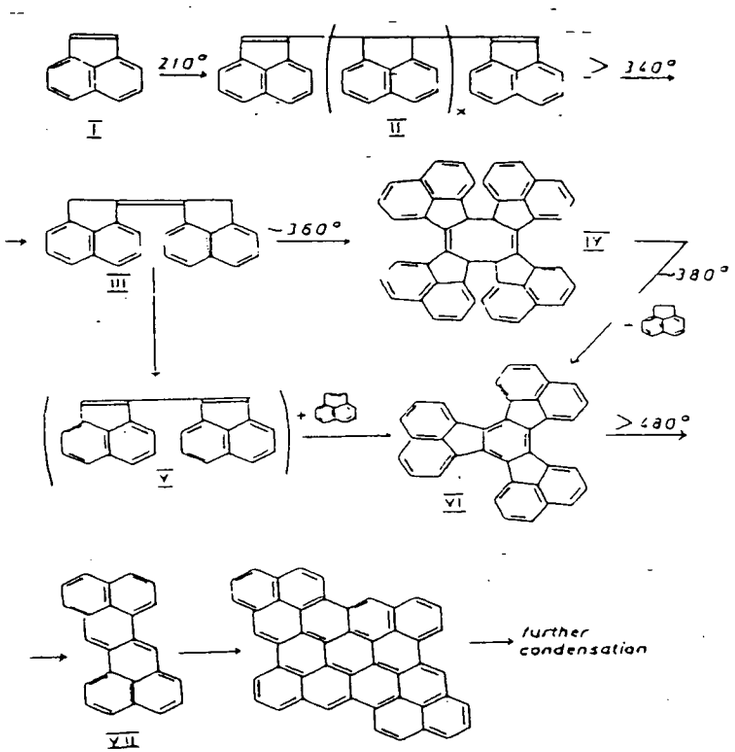

Fig. 32. Mechanism of liquid-phase pyrolysis of acenaphthylene (*94,121*).

(b)

TGA of acenaphthylene and decacyclene.

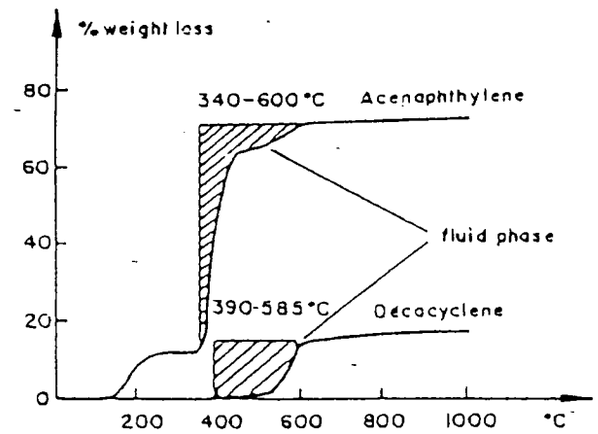

TGA of acenaphthylene and decacyclene. Decomposition maximum of decacylene: ~590°C.

Fig 2.5
Schematic of the Pyrolysis of Phenol-Formaldehyde

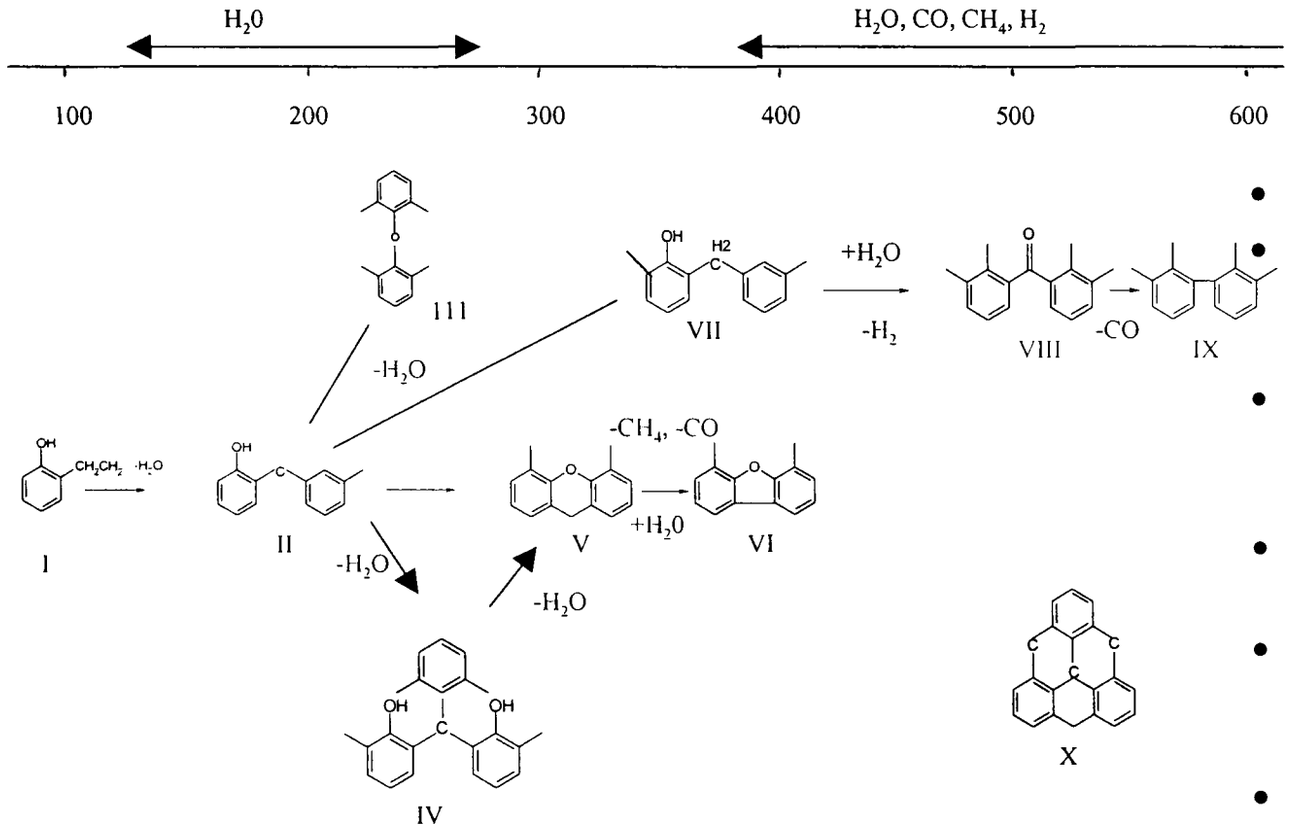

- Catalytic hardening
  - chemical condensation accopanied by formation of methylene bridges and release of water (I & II)
- formation of ether bonds (III)
- condensation of a phenolic group witha methylene bridge occurs to yield a triphenylmethane structure. (IV)
- the cyclic ether diphenylpyran is produced above 400C occurs due to condensation of two phenolic groups accompanied by cyclization (V)
- At around 400C the pyran ring releases methane and yiels the more stable furan ring. (VI)
- At 450C the remaining methylene bridges are oxidized by the water of pyrolisis to form keto groups (VIII)
- >460C the keto groups release carbon monoxide thus yielding the biphenyl structures (XI)
- > 600C dibenzofUran is formed. (VI)

Schematic and data copied from E.Fitzer Mueller and Schaefer , Conversion of Orgganic compounds to carbon Chemistry of Physics of carbon , vol 7 , ed Walker, Marcel Dekker 1971

Fig 2.6

Migration of Carbide Particle through Vitreous Carbon Matrix consuming Disordered Carbon and Depositing Graphite

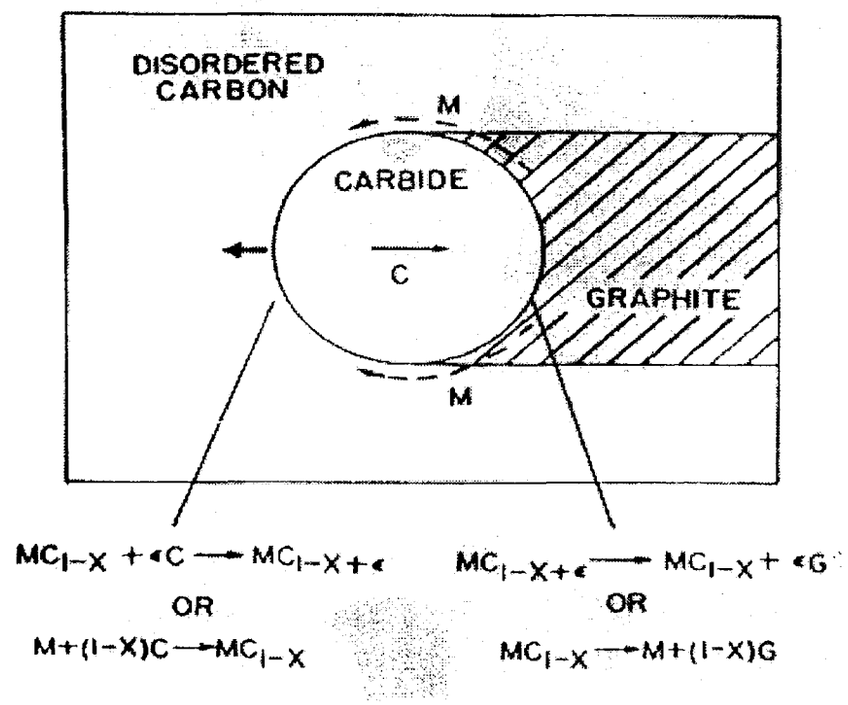

- Carbide particles burrow randomly through the glassy carbon,
- ingesting disordered carbon on the leading surface,
- depositing it as graphite at the trailing surface.

- Two possible mechanisms are given
  - Preferential solution of disordered carbon and precipitation of graphite,
  - decomposition of carbide at the trailing surface to form graphite and free metal which diffuses along the surface of the carbide particle to react with disordered carbon on the leading interface.

Copied from D.B Fischbach, The kinetics and Mechanism of Graphitization.

Fig 2.7
PGC Chromatographic Performance

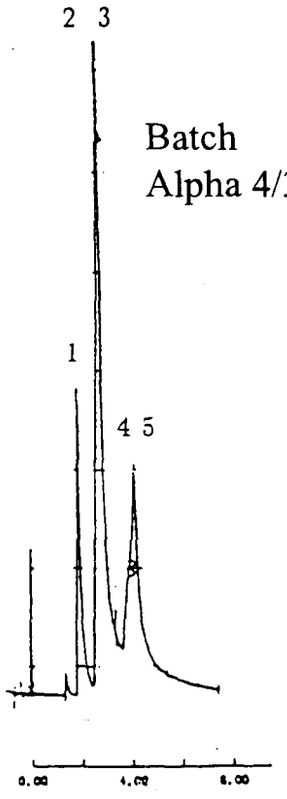

Batch
Alpha 4/3 = 1

(a) Very Poor

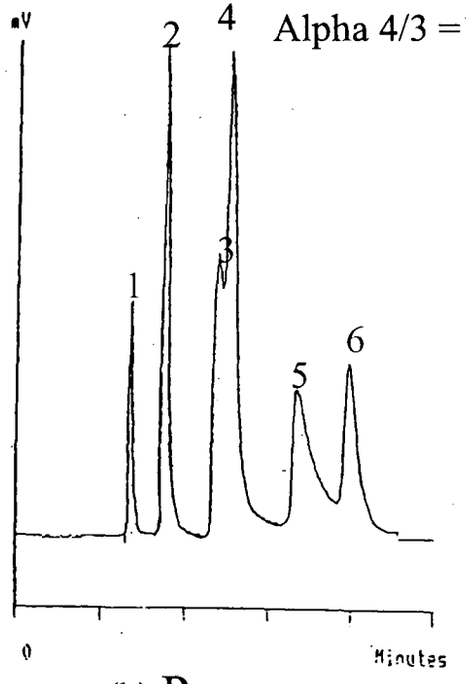

Batch : 116/R3
Alpha 4/3 =1.13

(b) Poor

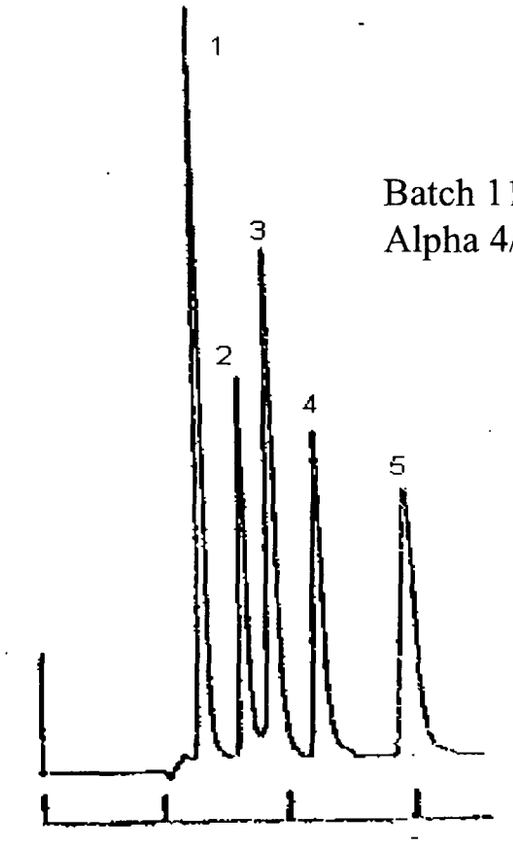

Batch 117/R2
Alpha 4/3 =1.22

(c) Good

Mobile Phase Conditions:	95% Methanol:Water
Columns:	100 x 4.6mm
Solutes:	1. Acetone, 2. Phenol, 3. Anisole, 4. P-Cresol, 5. Phenetole, 6. 3,5-Xylenol

Fig 2.8
Anthracene Deactivation Experiments

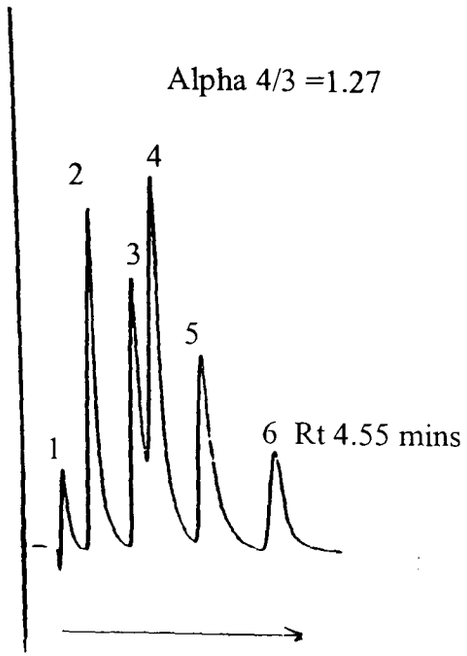

PGC 106/R1
Control - no anthracene

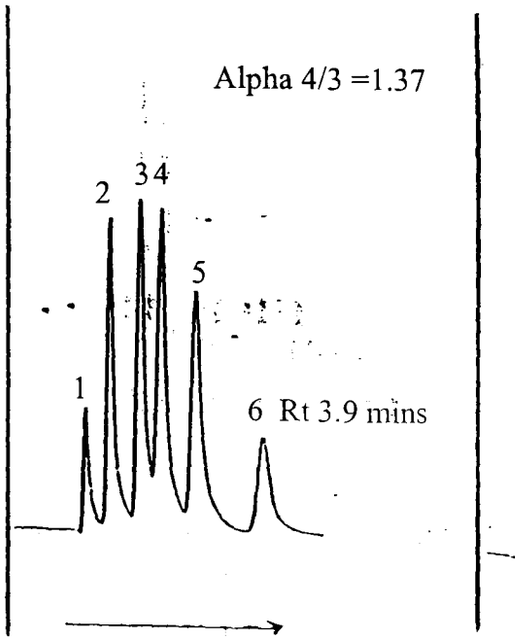

Anthracene PGC 106/R1
5% Partial Monolayer

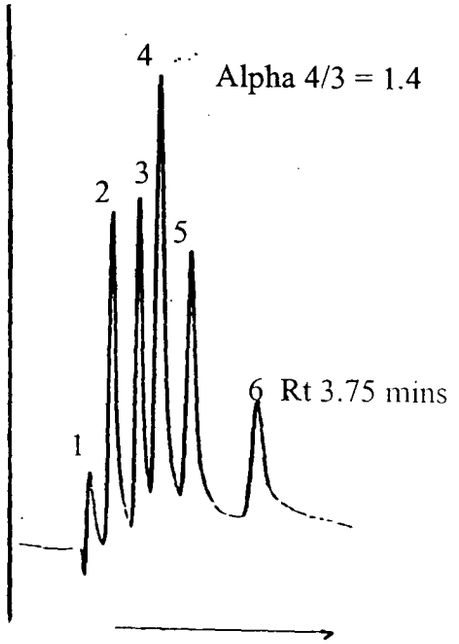

Anthracene PGC 106/R1
50% Monalayer coverage

Column: 50mm x 4.6mm
Mobile Phase Conditions : 95 % Methanol:Water
Test Solutes : 1. Acetone , 2.Phenol , 3. Anisole , 4. P-Cresol , 5.Phenetole , 6. 3,5-Xylenol

Fig 2.9
Soft Carbon Pyrolysis Experiments Chromatographic Results

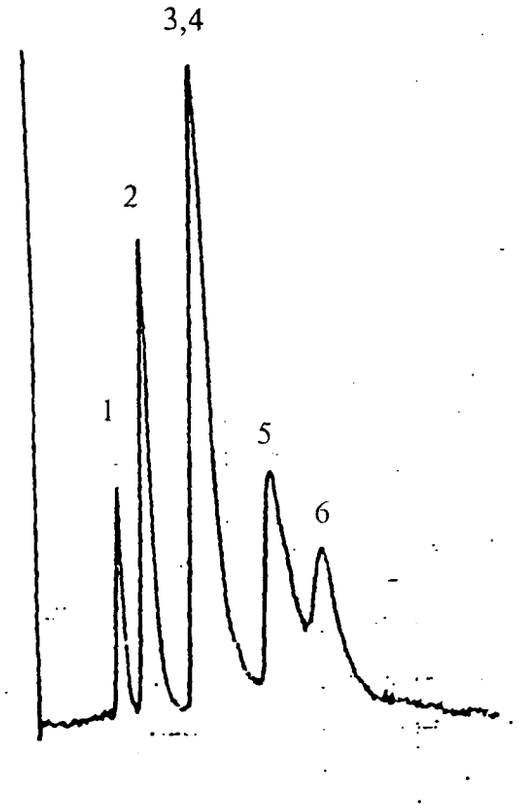

PGC + Acenaphthene expt

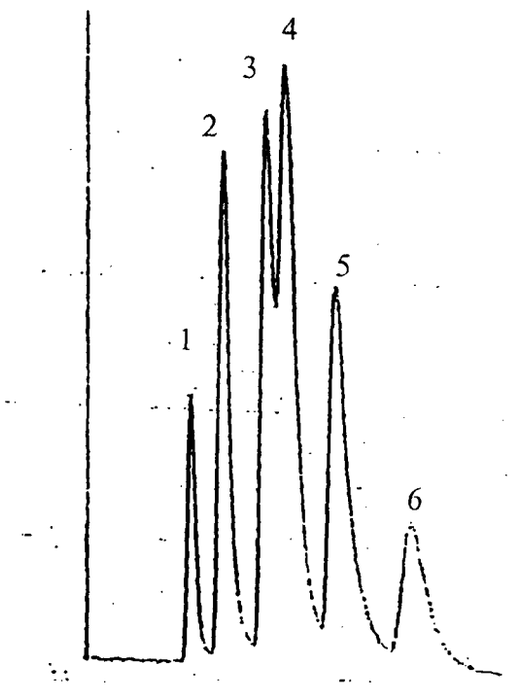

PGC +Acenaphthylene

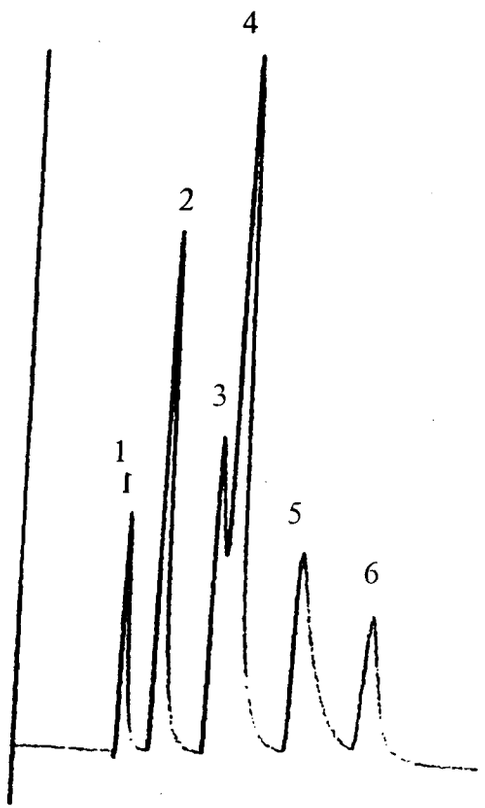

PGC 114/r6 - Control Expt

Column: 50mm x 4.6mm
Mobile Phase Conditions : 95 % Methanol:Water
Test Solutes : 1. Acetone , 2.Phenol , 3. Anisole , 4.P-Cresol , 5.Phenetole , 6. .3,5-Xylenol

Fig 2.10

SEM of Surface Impurities

(a)

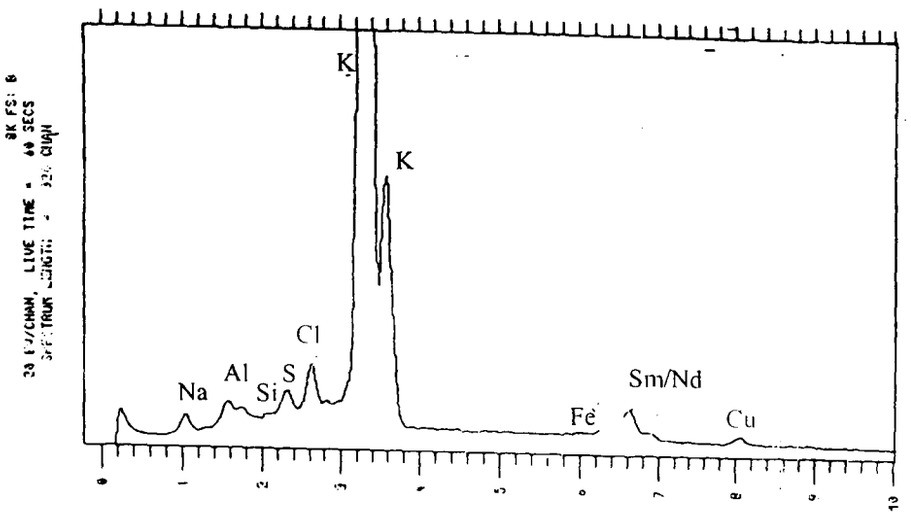

(b)

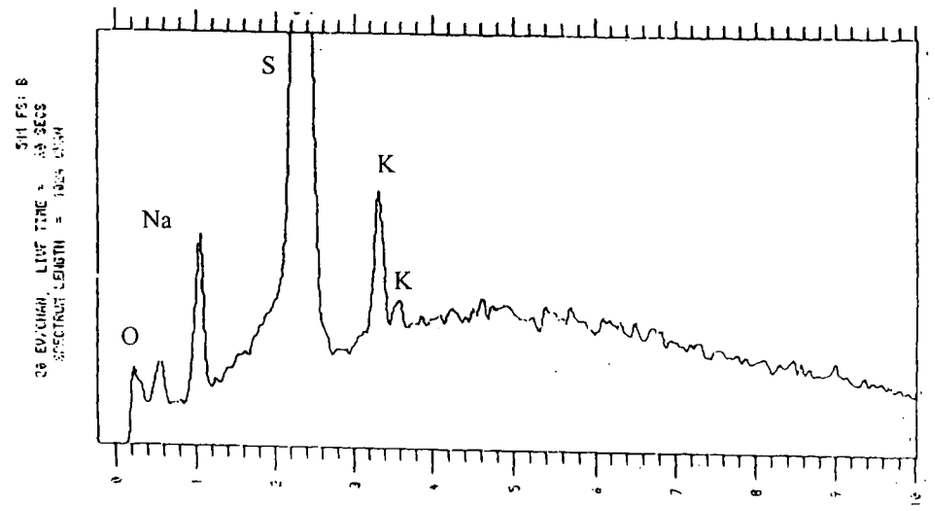

(c)

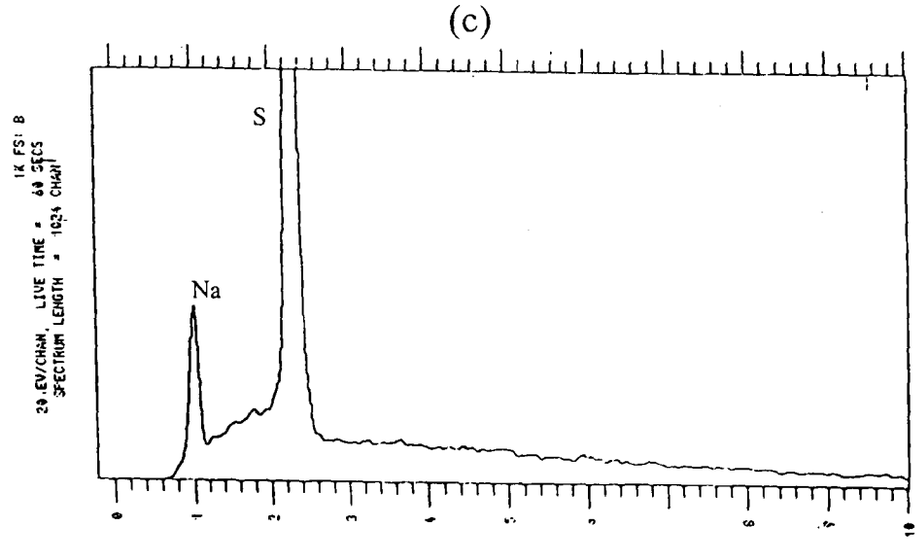

(a) Top Left: SEM of Furnace end-plate deposit

(b) Top Right: SEM of SDS +PGC surface deposit

(c) Bottom Right: SEM of SDS

Fig 2.11

Improvement in chromatographic Performance after Vacuum Oven treatment at 100C

Before treatment

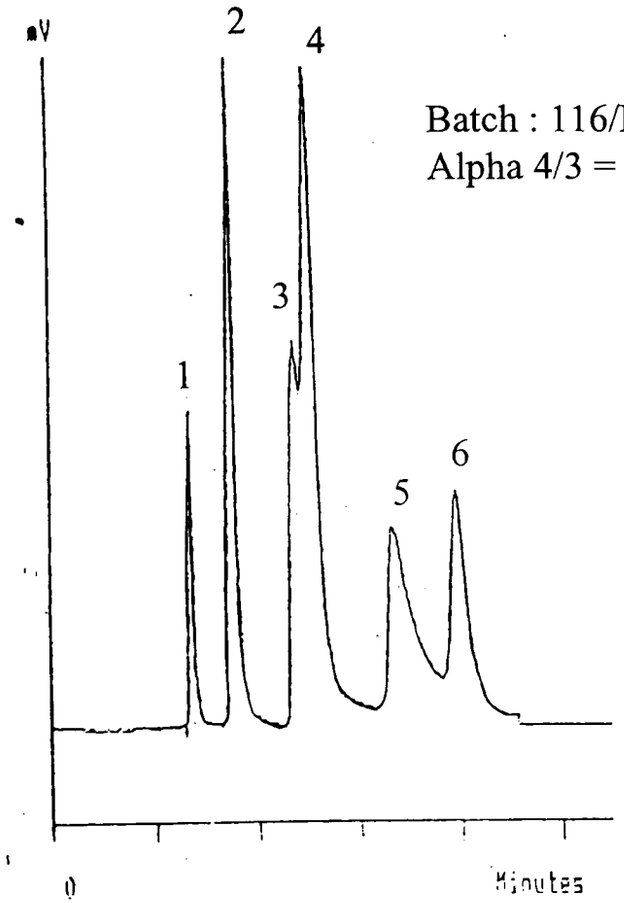

Batch : 116/R3
Alpha 4/3 = 1.13

After treatment

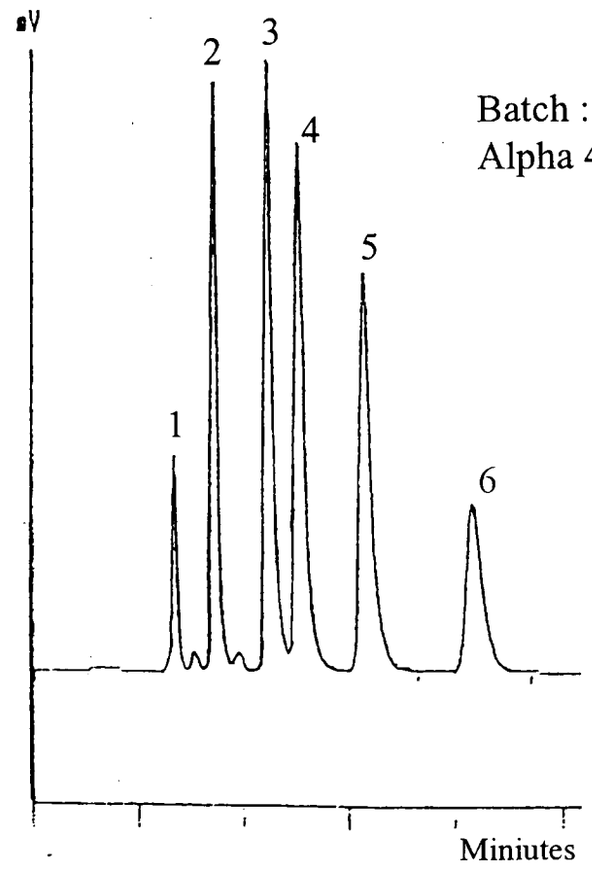

Batch : 116/R3
Alpha 4/3 = 1.34

Mobile Phase Conditions: 95% Methanol:Water

Columns: 100 x 4.6mm

Solutes: 1. Acetone, 2. Phenol, 3.Anisole, 4. P-Cresol, 5.Phenetole, 6. 3,5-Xylenol

Fig 2.12 & 2.13
Improvement in Chromatographic Performance with Surface Treatment

No treatment

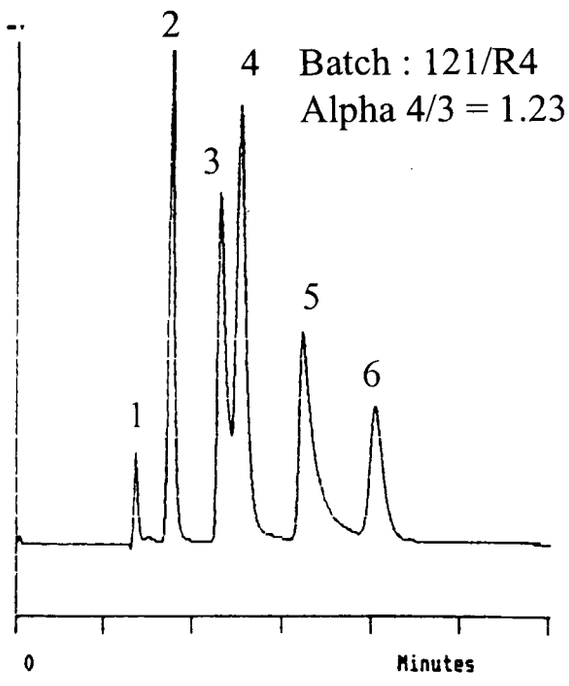

Batch : 121/R4
Alpha 4/3 = 1.23

Fig 2.12 Vac treatment 200C

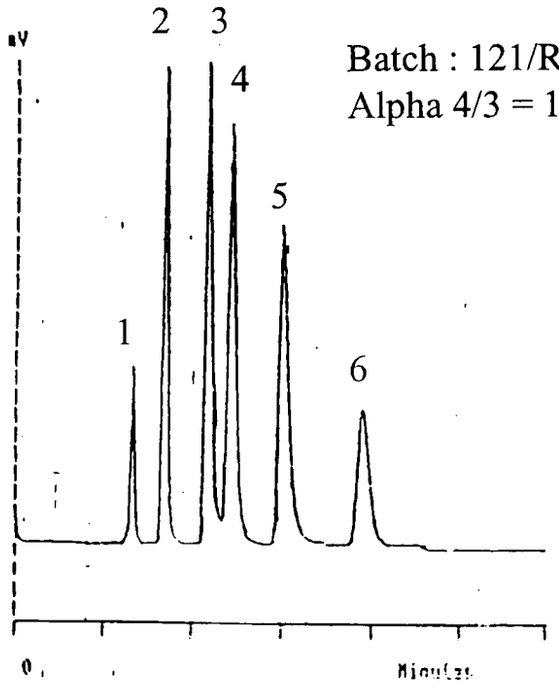

Batch : 121/R4
Alpha 4/3 = 1.31

Fig 2.13 SDS Wash + Vac 200C

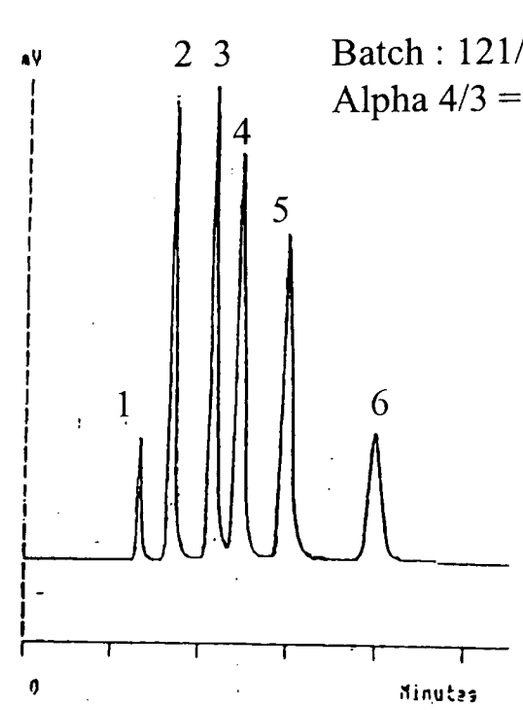

Batch : 121/R4
Alpha 4/3 = 1.37

Mobile Phase Conditions: 95% Methanol:Water
Columns: 100 x 4.6mm
Solutes: 1. Acetone, 2. Phenol, 3.Anisole, 4. P-Cresol, 5.Phenetole, 6. 3-5 Xylenol

Fig 2.14
Sedimentation/Fractionation Apparatus

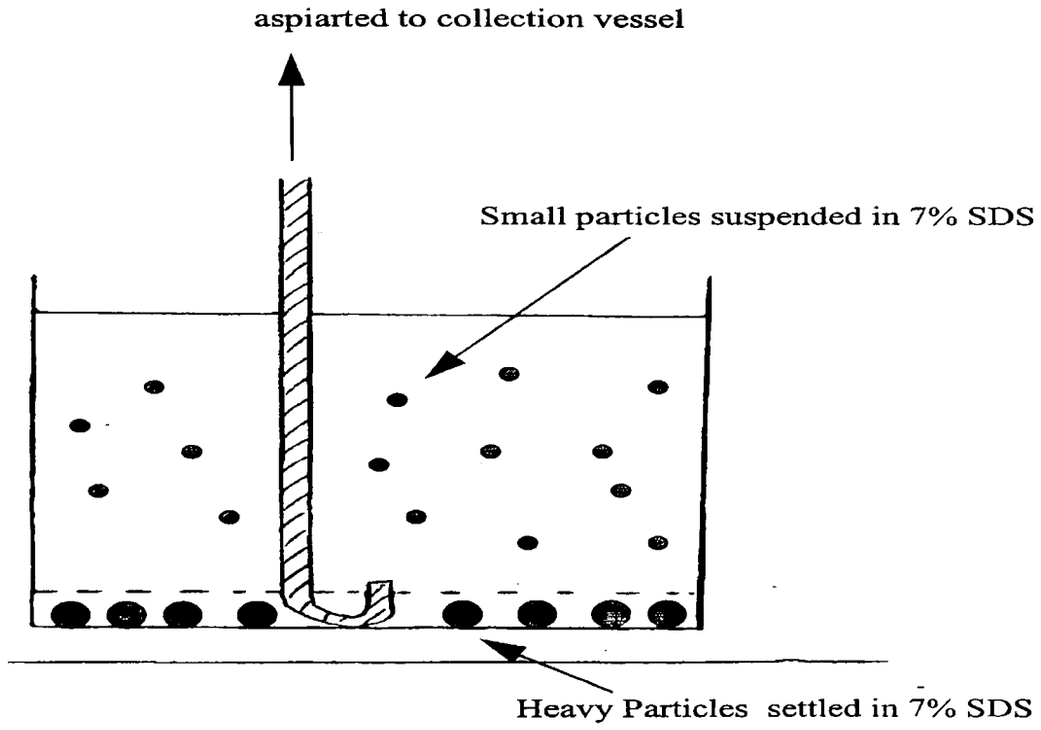

The apparatus consists of :
- a tall 1.5L beaker
- a stop clock to measure settling time
- 7% SDS solution
- a pipe with bend to remove suspended particles
- an aspirator + collection vessel

Fig 2.15
Improvement to PGC Particle Size Distribution by Sedimentation

(a) Pre Sedimentation Process

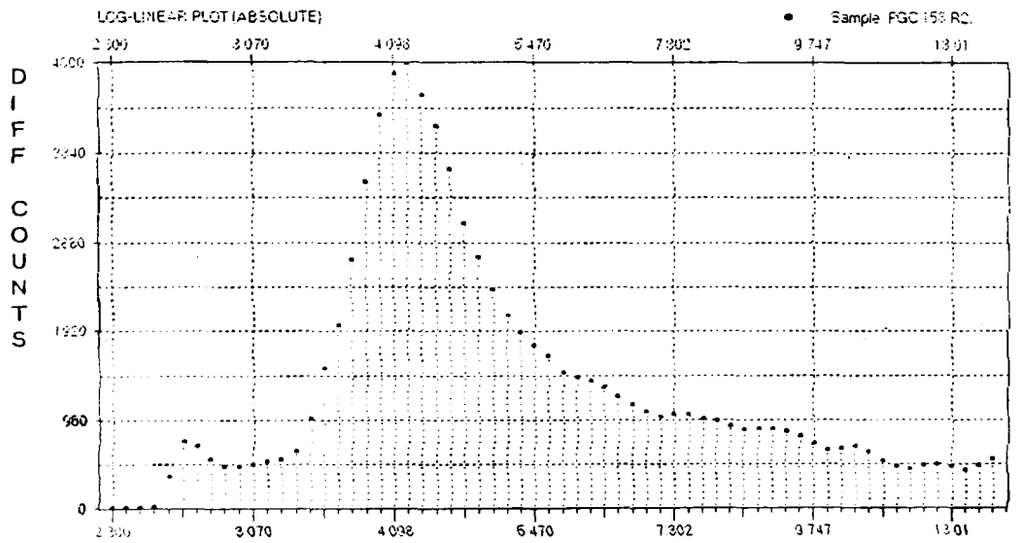

Geometric Mean Size:	5.240 um	Arithmetic Mean Size:	5.646 um
Geom. Std Deviation:	1.446 um	Median Size:	4.641 um
Geom. Skewness:	0.717	Mode Size:	4.203 um
Geom. Coeff Variation:	27.60	Kurtosis:	4.244
Arith Std Deviation	2.471 um		

(b) Post Sedimentation Process

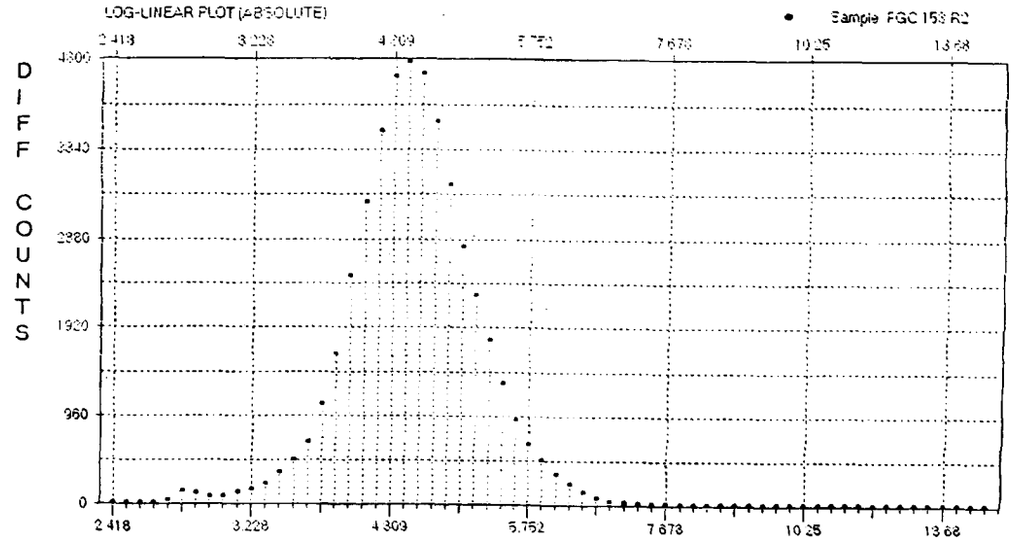

Geometric Mean Size:	4.535 um	-- PERCENTILES --
Geom. Std Deviation:	1.143 um	99.24% Counts above 2.999 um
Geom. Skewness:	0.044	0.271% Counts above 6.998 um
Geom. Coeff Variation:	25.20	99.09% Counts above 3.074 um
		1.896% Counts above 6.076 um
Arithmetic Mean Size:	4.576 um	
Median Size:	4.474 um	
Mode Size:	4.485 um	
Kurtosis:	28.278	
Arith Std Deviation	0.620 um	

Fig 2.16
PGC Fractionation / Sedimentation Process

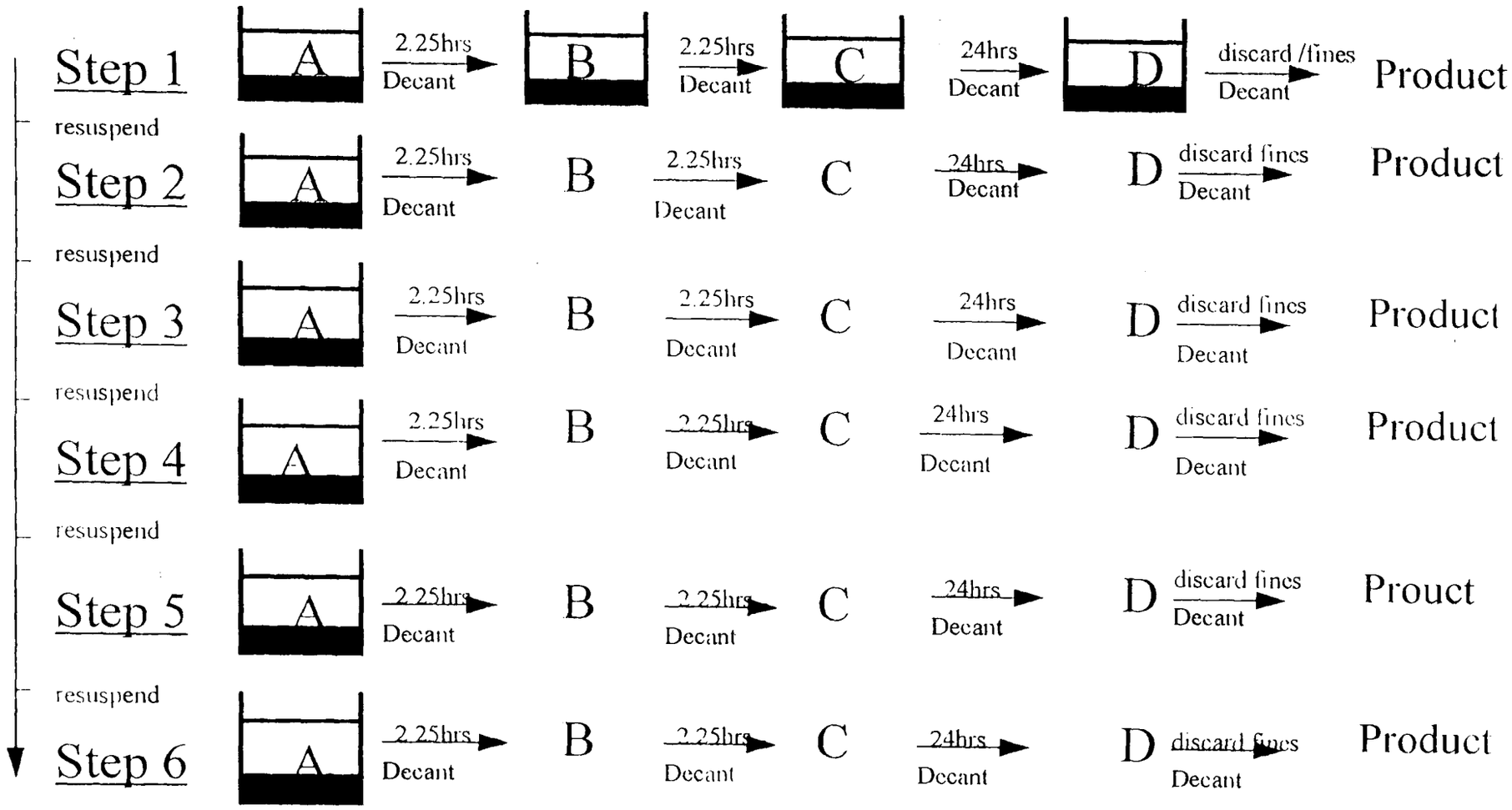

Fig 2.17
Chromatographic Performance of Fractionated PGC

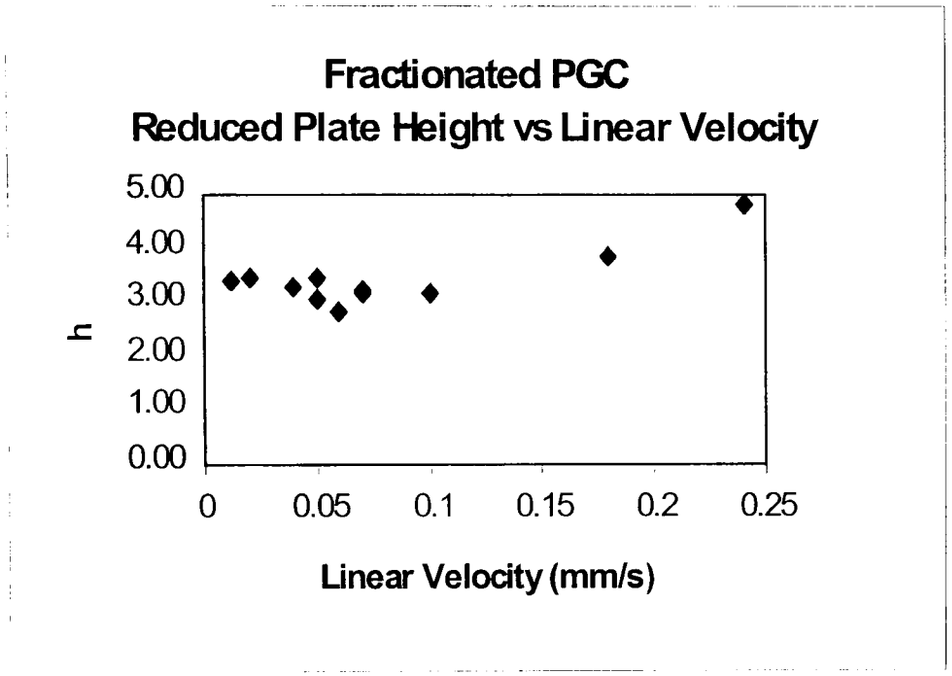

Flow mls/min	Linear Velocity (v)	Column Efficiency (N)	Reduced plate height (h)
0.2	0.02	57767	3.46
0.3	0.04	60385	3.31
0.44	0.05	57514	3.48
0.45	0.05	64671	3.09
0.5	0.06	70697	2.83
0.55	0.07	62596	3.20
0.6	0.07	61427	3.26
0.8	0.1	62966	3.18
1	0.012	58409	3.42
1.5	0.18	51522	3.88
2	0.24	41471	4.82

Fig 2.18

Reproducibility of PGC Surface Treatment

(a)

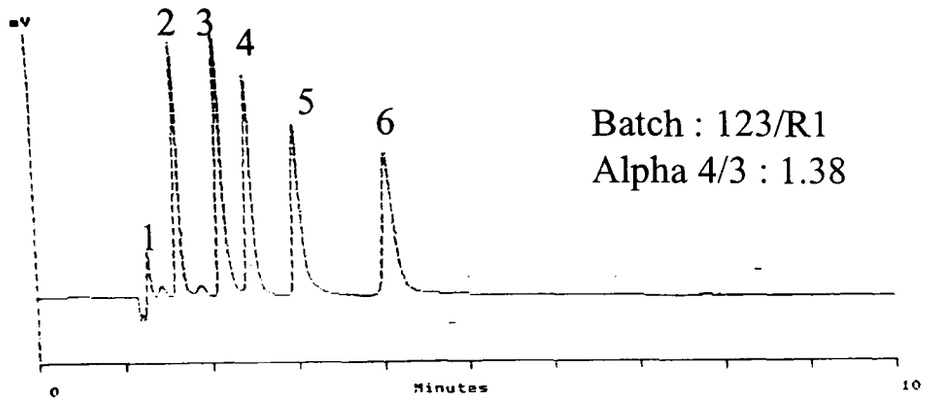

(b)

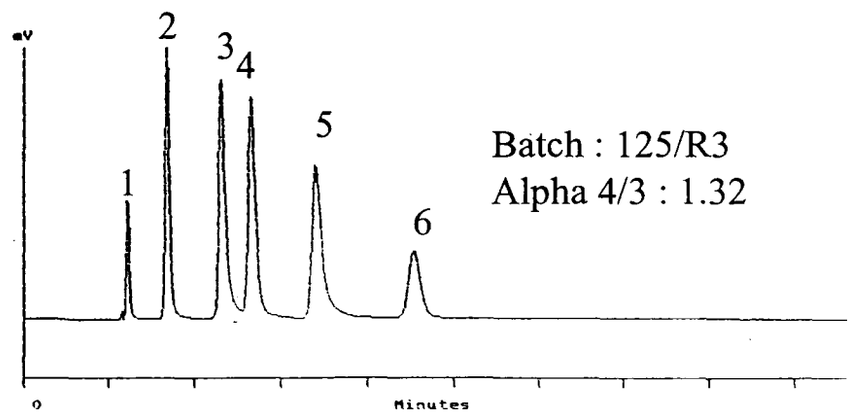

(c)

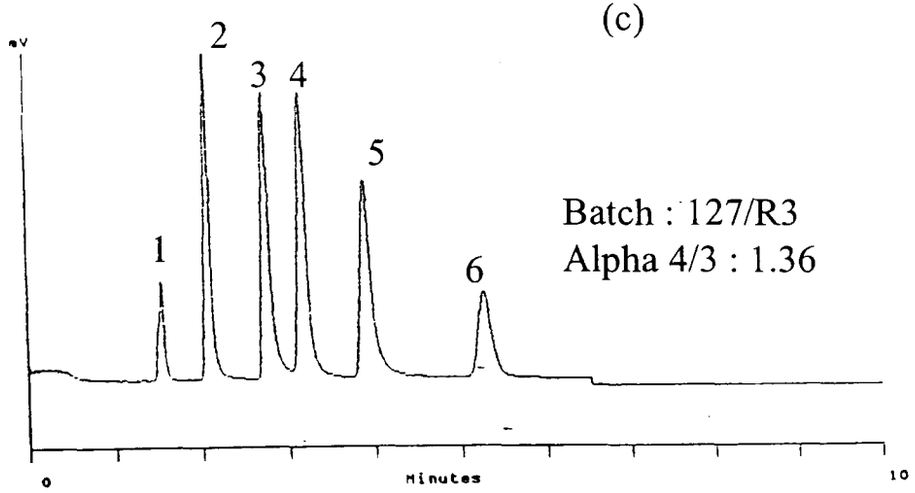

(d)

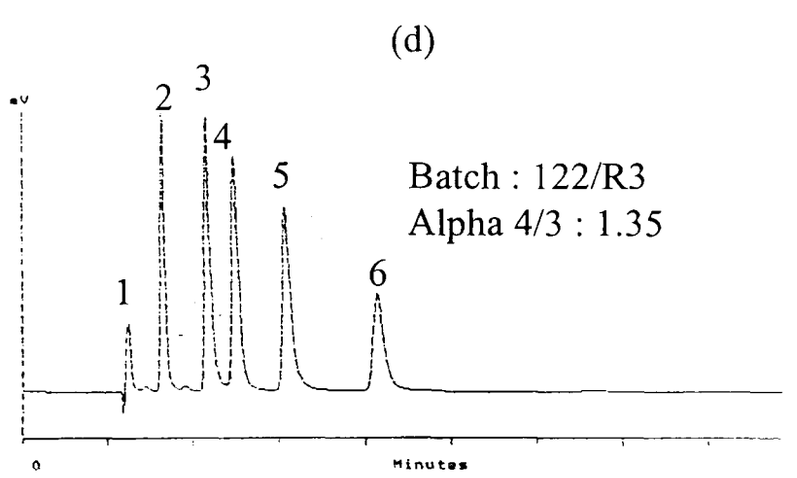

Mobile Phase Conditions: 95% Methanol:Water
Columns: 100 x 4.6mm
Solutes: 1. Acetone, 2. Phenol, 3.Anisole, 4. P-Cresol, 5. Phenetole, 6. 3,5-Xylenol

Fig 2.19
Copper Impregnation/Graphitization Experiments

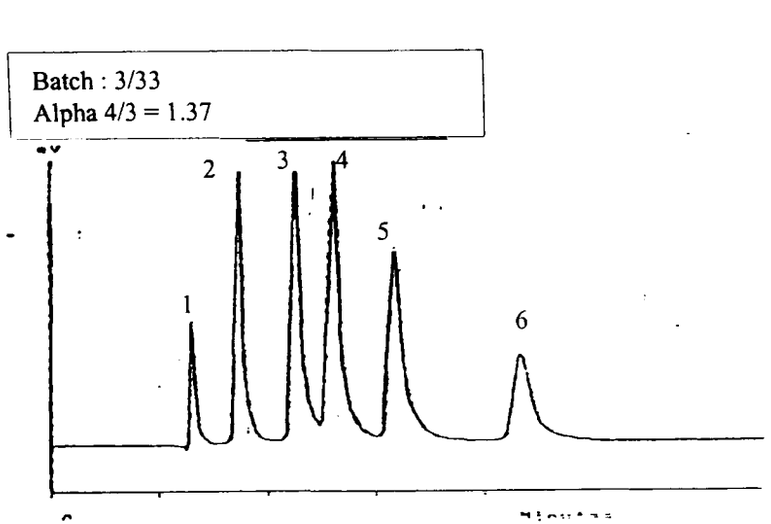

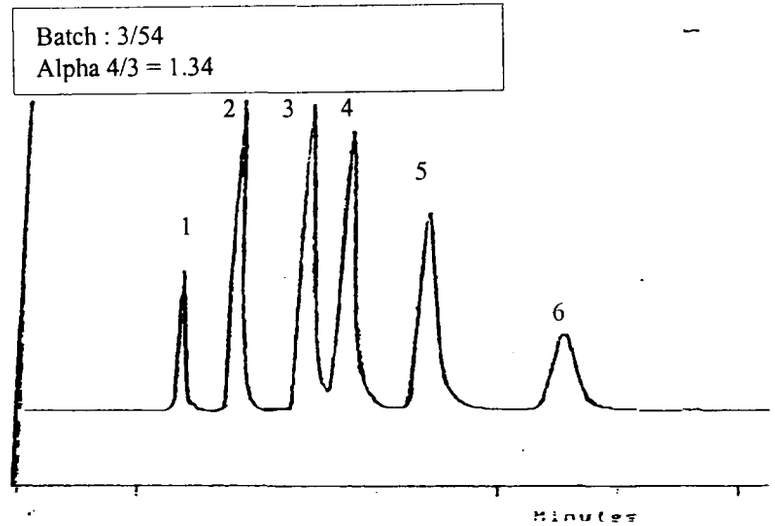

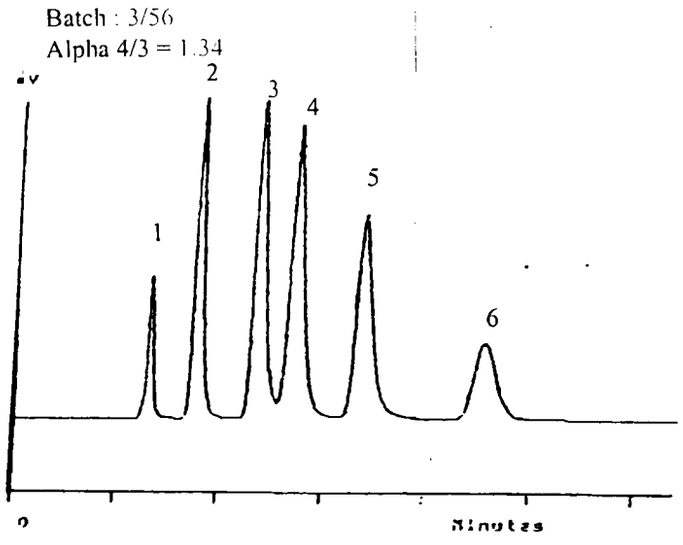

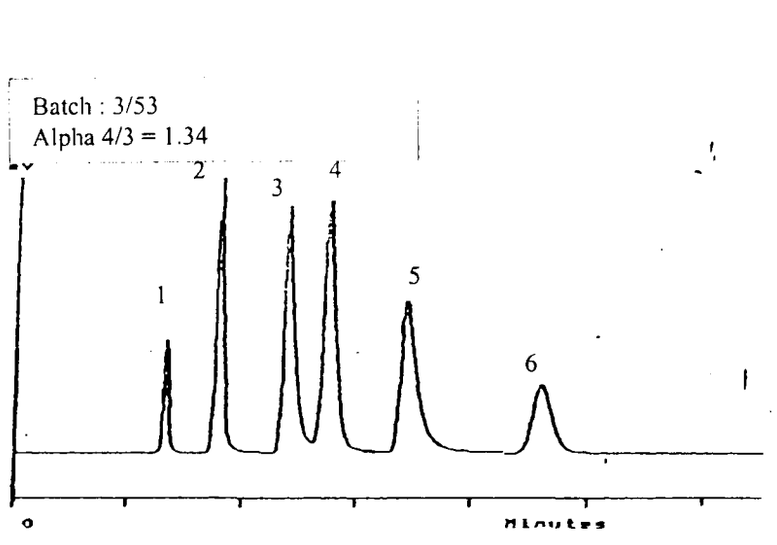

Mobile Phase Conditions: 95% Methanol:Water
Columns: 100 x 4.6mm
Solutes: 1. Acetone, 2. Phenol, 3.Anisole, 4. P-Cresol, 5. Phenetole, 6. 3,5-Xylenol

PAGE

NUMBERING

AS ORIGINAL

Chapter 3 – Surface Tension Studies

3.1 Introduction

If graphite was an unselective adsorbent, then when in contact with a solution, the composition of the layer of molecules in the solution in immediate contact with the graphite surface should be similar to that at the corresponding gas/liquid interface. Adsorption at the gas /liquid interface will accordingly provide a true reflection of adsorbence at such a non-selective adsorbent.

PGC has, however, been shown to show selective adsorption towards certain types of analyte functional groups (as in the case of the polar retention effect (PREG) which was discussed in Chapter 1). A study that compares the adsorption of analytes at both the PGC/liquid interface and the gas/liquid interface will provide a relative measure of PREG.

3.1.1 Graphite as an Unselective Adsorbent

Previous workers[1] have shown that heats of adsorption from the gas phase onto graphite are very similar for a variety of common substances when computed per unit area of the adsorbate. On the basis of such observations it has been claimed that graphite might indeed be expected to be relatively unselective as an adsorbent. Consequently it was expected that it would show no special affinity for polar groups, such as

-OH, =O, Cl, NH_2, *etc.*

The Gibbs Adsorption Isotherm covers adsorption at the gas/liquid interface for a two component mixture (e.g. solvent and solute) and is given as:

$$\Gamma = -(1/RT)\{d\gamma/d(\ln C_{bulk})\} \qquad [3.1]$$

where C_{bulk} is the bulk concentration of the adsorbate and Γ is the excess of solute per unit area at the surface over and above the amount which would be present if the normal bulk distribution of solute and solvent was constant up to the interface. Thus, if a very thin layer at the interface was sliced off, as in the McBain and Humphreys[2] surface microtome experiment, the solution collected would be expected to have a larger concentration of the solute than the bulk phase if the solute were positively adsorbed at the surface. Measurement of the excess concentration of the solute in this solution (*i.e.* the concentration in the interface sample minus the concentration in the bulk phase) would then enable the

excess quantity of solute to be determined. This, divided by the area of surface sliced off, would give a measure of Γ.

Equation [3.1] may be rearranged to give:

$$K_{ads} = \Gamma/C_{bulk} = -(1/RT)\{d\gamma/dC_{bulk}\} \qquad [3.2]$$

where K_{ads} is the distribution coefficient for the solute between surface and bulk phases, and γ is the surface tension.

3.1.2 Surface Tension Hypothesis for Retention on an Unselective Adsorbent(1)

In a chromatographic system, an analyte is partitioned between a stationary phase and a mobile phase. The concentration of the analyte in both the mobile phase and stationary phase is assumed to be close to zero. Typical modern packing materials consist of a stationary phase, usually a chemical group such as octadecyl, bonded to a high surface area substrate, such as silica. The stationary phase is thus very thin, typically 1 to 2 nm thick. The packing materials, comprising the stationary phase bonded to the substrate, are packed into cylindrical "columns." The mobile phase comprises the eluent fed to the column. The mobile phase permeates the pores within the packing material and the space between the particles of the packing material. Supposing that the interface between a solvent and its vapour could be made stationary while the underlying solvent could be made to move, we would then simulate a chromatographic system. If graphite was indeed a totally unselective adsorbent toward a specific analyte, we would assume that the composition (analyte concentration) at the graphite-liquid interface was the same as that at the liquid-vapour interface. Graphite would then simply act as a "surface area extender". The area of the surface would then be of the order of 50 m^2/mL, which, given the volume of eluent in the pores of the material, translates into a total phase thickness of about 20 nm. The interface layer comprises about 1/20th of this depth. In this way, the interface would be effectively fixed while the bulk liquid could be moved, and we would, in effect, have achieved the chromatographic system just proposed

Retention on graphite, if it was totally unselective, could then be correlated with the surface tension of the solvent and the concentration of solute via the Gibbs Adsorption isotherm. In chromatographic terms the capacity factor (k') for an adsorbent can be written:

$$k'_{ST} \equiv q_{surf}/q_{bulk} = (C_{surf} \times A_{surf})/(C_{bulk} \times V_{bulk}) \quad [3.3]$$

In the context of adsorption to a liquid interface, the surface concentration, C_{surf}, is not simply Γ as given by Equation [3.1], but Γ plus the amount of analyte per unit area which would have been present if the surface excess was zero. This may be written:

$$C_{surf} = \Gamma + C_{bulk} \times t_{surf} \quad [3.4]$$

where t_{surf} is the thickness of the surface layer. The term, t_{surf}, is an arbitrary quantity which might be taken as the thickness of one or two molecular layers at the surface, say 1 or 2 nm. We then obtain for the capacity factor:

$$k'_{ST} = (C_{surf} \times A_{sur})/(C_{bulk} \times V_{bulk}) \quad [3.5]$$

$$= (\{\Gamma + C_{bulk} \times t_{surf}\} A_{surf})/(C_{bulk} \times V_{bulk}) \quad [3.6a]$$

$$= (\{-d\gamma/RT(dC_{bulk}/C_{bulk})^{-1} + C_{bulk} \times t_{surf}\} A_{surf})/(C_{bulk} \times V_{bulk}) \quad [3.6b]$$

$$= \{-1/RT \times d\gamma/dC_{bulk} + t_{surf}\} A_{surf}/V_{bulk} \quad [3.7]$$

$$k'_{ST} = \phi \times \{t_{surf} - (1/RT)(d\gamma/dC_{bulk})\} \quad [3.8]$$

where ϕ is the phase ratio and equals A_{surf}/V_{bulk}.

A chromatographic system is represented in the following diagram, where t_{surf} is the thickness of the surface layer, t_{pore} is the nominal thickness of the pore liquid, and t_{ext} the nominal thickness of the extra-particle mobile phase. The terms t_{pore} and t_{ext} equal V_{pore}/A_{surf} and V_o/A_{surf}, respectively.

Diagram Representing a Chromatographic System

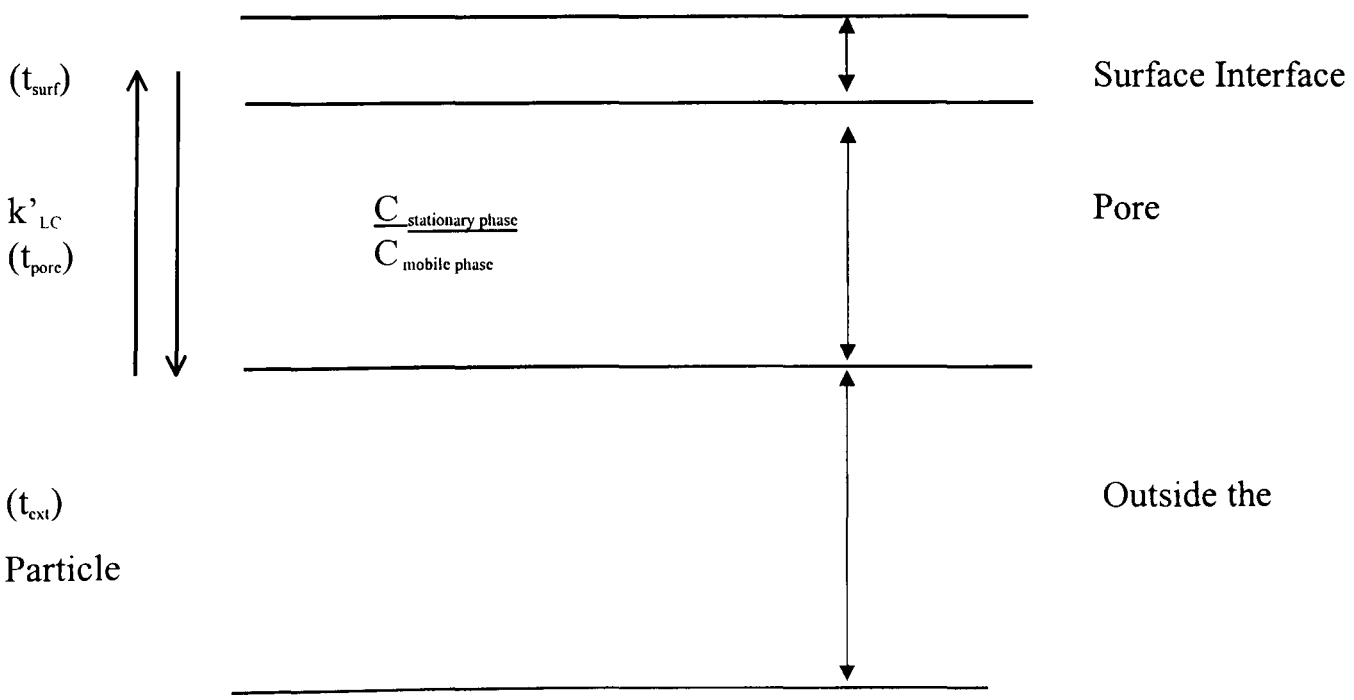

3.1.3 Surface Tension Hypothesis for Retention on Graphite(II)

In reality, graphite is unlikely to be totally unselective. However, the Surface Tension Hypothesis enables us to split the overall retention by graphite into two factors The first factor, k'_{ST}, encompasses the adsorption of the analyte at the vapour-liquid interface. The second factor, k'_{GR}, encompasses the specific effect of graphite. It is the factor by which graphite changes the concentration which the analyte would possess at the liquid-vapour interface.

$$k'_{LC} = k'_{ST} \times k'_{GR} \qquad \text{or} \qquad k'_{GR} = k'_{LC}/k'_{ST} \qquad [3.9]$$

where k'_{LC} is the k' value obtained experimentally by HPLC, k'_{ST} is the value calculated from surface tension measurements. Note that Equation [3.9] arises because ΔG values are additive:

$$\Delta G^{\circ}_{LC} = \Delta G^{\circ}_{ST} + \Delta G^{\circ}_{GR} \qquad [3.10]$$

3.1.4 Objectives of Work

Therefore, the objective of this work is to investigate the relationship between k'_{LC} and k'_{ST} in order to evaluate the real role of graphite in HPLC separations by separating the contributions of the solvent-related and the graphite-related factors. However, before proceeding with the experimental approach, the historical development and theoretical aspects of surface tension and its measurement will be reviewed.

3.2 Surface Tension Theory

The term surface tension was first applied to the early idea that the surface of a liquid had some kind of contractile skin. More subtly, it can convey the erroneous impression that extending a liquid surface somehow stretches the molecules in the surface. Mathematically, surface tension, γ, is defined as a cohesive force acting at right angles to any line of unit length on the liquid surface (see Figure 3.1). It is more common to define surface tension and surface energy as the work required to increase the area of a surface isothermally by a unit amount:

$$\text{Work} = \int \gamma \, dA \qquad [3.11]$$

where dA equals the change in area.

As a consequence of surface tension, there is a balancing pressure difference across any curved surface, the pressure being greatest on the concave side. An example of where γ is thought of in terms of energy per unit area and where the pressure exerted is clearly apparent is the soap bubble. In the absence of fields, such as gravitational, a soap bubble is spherical, being the shape of minimum surface area for a given enclosed volume. If we consider a soap bubble of radius r, its total surface free energy is $2 \times 4\pi r^2\gamma$ (the 2 arises because a soap bubble has two surfaces). If the radius were decreased by dr, then the change in surface free energy would be $16\pi r\gamma dr$. Since shrinking decreases the surface energy, the tendency to do so must be balanced by work against the pressure difference across the film: $dw = \Delta p\, 4\pi r^2 dr$. Equating this to the decrease in surface free energy gives:

$$dw = \Delta p 4\pi r^2 dr = 16\pi r\gamma dr \qquad [3.12]$$

which reduces to:

$$\Delta p = 4\gamma/r \qquad [3.13]$$

For a droplet of liquid with only one surface the appropriate equation for the excess pressure is

$$\Delta p = 2\gamma/r \qquad [3.14]$$

Equation [3.14] is known as the Laplace equation for a spherical surface. For a surface with two principal radii of curvature, r_1 and r_2, the appropriate equation, known as the Young Laplace equation, reads:

$$\Delta p = \gamma(1/r_1 + 1/r_2) \qquad [3.15]$$

We therefore arrive at the conclusion that the smaller the bubble the greater the pressure of the air on the inside as compared to the outside.

If dn moles of liquid is transferred from a plane surface with a vapour pressure p_o to the droplet with a vapour pressure p_r, the free energy increase is equal to dn RT ln p_o/p_r, assuming ideal gaseous behaviour. Equating this with the free energy change produced by the change in surface area gives:

$$dn\ RT \ln p_r/p_o = 8\pi r\gamma dr \qquad [3.16]$$

However:

$$dn = dV \times \rho/M = 4\pi r^2 dr\, \rho/M \qquad [3.17]$$

Rearranging, we obtain:

$$RT \ln p_o/p_r = 2\gamma M/\rho r = 2\gamma V_m/r \qquad [3.18]$$

where ρ is the density of the liquid, V_m is the molar volume of the liquid, and M is the molar mass. Equation [3.18] is known as the Kelvin equation. It can also be applied to a concave capillary meniscus, in which case the curvature is negative and vapour pressure lowering is predicted.

The above equations are fundamental to the various techniques now employed for the measurement of surface tension, such as Capillary Rise, Pendant Drop, Wilhelmy Plate, Ring, and Oscillating Jet methods. The Wilhelmy Plate method, which we have used in this work, is discussed in greater detail in the experimental Section.

3.2.1 Thermodynamics of Adsorption - Gibbs Adsorption Equation

In order to understand adsorption at an interface between two bulk phases, α and β, it is necessary to define a "surface zone" and a "surface phase". The "surface zone" is bound by two imaginary planes, which are parallel to the region of changing composition between the two bulk phases (see Figure 3.2). One surface, AA', lies within the bulk phase, α, and the other, BB', lies within the bulk phase, β. The transition zone between two bulk phases is only a few molecules thick. This means that these two boundary planes can be very close together, so that the composition at AA' is essentially that of phase α and at BB' is essentially that of phase β. The "surface phase" is a plane, SS', that lies between AA' and BB' and is within the region of changing composition. It is strictly two dimensional, having no thickness and no volume. The real system is now compared with an imaginary model system in which the compositions of the bulk phase α and β are maintained constant up to the plane SS'. Because of the variation of composition within the transition region, the actual amounts of each component within the surface region will be different from the amounts in the model system. The differences will depend upon where the plane SS' is drawn. The surface excess, Γ, of any component is defined as the amount of that component which is present in the real system less the amount that would be present in the model system. The Gibbs theory evaluates these surface excesses. Thus, if n_i^σ is the amount of

component i in the surface zone, σ, in excess of that which would be present in the model system, the surface excess concentration of component i is given by:

$$\Gamma_i = n_i\sigma/A \qquad [3.19]$$

where A is the interfacial area. This excess may be regarded as being located in the "surface phase", that is within the plane SS'. The value of Γ may be positive or negative. Its magnitude for any component i depends upon the location of SS within the interface region. The Gibbs adsorption isotherm may be derived by the follows series of equations. The total thermodynamic energy of a bulk phase is given by the expression:

$$U = TS - pV + \sum\mu_i n_i \qquad [3.20]$$

The corresponding expression for the thermodynamic energy of a two dimensional surface phase, σ, as just described is:

$$U = TS + \gamma A + \sum\mu_i n_i\sigma \qquad [3.21]$$

The pV and γA terms in Equations [3.20] and [3.21] have opposite signs since pressure is an expanding force and surface tension is a contracting force. Differentiating Equations [3.20] and [3.21] gives:

$$dU = TdS + SdT - pdV - Vdp + \sum\mu_i dn_i + \sum n_i d\mu_i \qquad [3.22]$$

$$dU\sigma = TdS\sigma + S\sigma dT + \gamma dA + Ad\gamma + \sum\mu_i dn_i\sigma + \sum n_i\sigma d\mu_i \qquad [3.23]$$

From the laws of thermodynamics for bulk and surface phases, we have:

$$dU = TdS - pdV + \sum\mu_i dn_i \qquad [3.24]$$

and:

$$dU\sigma = TdS\sigma + \gamma dA + \sum\mu_i dn_i\sigma \qquad [3.25]$$

Subtracting Equation [3.24] from Equation [3.22], we obtain:

$$SdT - Vdp + \sum\mu_i dn_i = 0 \qquad [3.26]$$

and:

$$S\sigma dT + Ad\gamma + \sum\mu_i dn_i\sigma = 0 \qquad [3.27]$$

At constant temperature for a surface phase, we obtain:

$$d\gamma = -\sum(n_i\sigma/A)d\mu_i = -\sum\Gamma_i d\mu_i \qquad [3.27b]$$

Supposing that our system contains three components 1, 2 and 3, and supposing that 2 and 3 are solvent components in significant concentration, while 1 is a solute component present in very small concentration, approaching zero concentration. Equation [3.22] then takes the form:

$$d\gamma = -(\Gamma_1 d\mu_1 + \Gamma_2 d\mu_2 + \Gamma_3 d\mu_3) \qquad [3.28]$$

There also exists the relationships for the chemical potentials:

$$\mu_1 = \mu_1^\circ + RT\ln \alpha_1 \qquad [3.29]$$

and:

$$d\mu_1 = RTd \ln \alpha_1 = RTd \alpha_1/\alpha_1 \quad etc.$$

so:

$$d\gamma = -RT(\Gamma_1 d \alpha_1/\alpha_1 + \Gamma_2 d \alpha_2/\alpha_2 + \Gamma_3 d \alpha_3/\alpha_3) \qquad [3.30]$$

Since component 1 is present in very small concentrations compared to components 2 and 3, it follows that the first term dominates the RHS (right hand side) of Equation [3.23]. We can therefore write, to a good approximation:

$$d\gamma/RT = -\Gamma_1 d \alpha_1/\alpha_1 \qquad [3.31]$$

Since the solution of component 1 is dilute, we can also write: $\alpha_1 = c_1$, to give the normal form of the Gibbs Equation:

$$\Gamma_1 = -RT(d\gamma/d \ln c_1) \qquad [3.32]$$

or, rearranging:

$$\Gamma_1/c_1 = -RT (d\gamma/dc_1) \qquad [3.33]$$

This derivation does not require any special positioning of the surface SS'. Such special pleading is required only when dealing with components present in finite amounts. Thus, for a system containing two major components, Equation [3.21] takes the form:

$$d\gamma = -(\Gamma_1 d\mu_1 + \Gamma_2 d\mu_2) \qquad [3.34]$$

Introducing chemical activities we obtain:

$$d\gamma = -RT(\Gamma_1 d \ln \alpha_1 + \Gamma_2 d \ln \alpha_2) \qquad [3.35]$$

$$= RT(\Gamma_1 d\alpha_1/ \alpha_1 + \Gamma_2 d\alpha_2/ \alpha_2) \qquad [3.36a]$$

If we cannot make the assumption that one of the components is present in trace quantity, then we are forced to make an arbitrary assumption about the placing of the surface SS'. If, for example, our model contains methanol-water solutions and we want to determine whether or not methanol (component 1) is adsorbed preferentially at the surface, it is convenient to consider that the surface excess of water (component 2) is zero. This is readily achieved by positioning SS' so that $\Gamma_2 = 0$. Equation [3.27] then reverts to Equation [3.25], and we once again obtain the usual form of the Gibbs equation, namely Equation [3.26]. We could, however, equally well have considered that methanol was the solvent and that water was rejected from the surface. We would then have made the assumption that $\Gamma_2 = 0$, noting in passing that the sign of $d\gamma/dc_1$ is the opposite to that of $d\gamma/dc_2$ at any composition of the solution.

Therefore, the final conclusion is that, irrespective of the number of components in the solution, the Gibbs equation correctly gives the amount of a trace solute adsorbed at any interface. We also note that this applies equally to any number of trace components in a multicomponent solution.

Returning now to chromatography, if we wish to define k'_{ST} for a model system consisting of an interface which is stationary and a mobile phase flowing over it, then we have to make a non-thermodynamic assumption. This is because the chromatographic theory requires that we know the total amount of material in the stationary phase, not just the excess. We can only do this by assigning a thickness to the surface layer, which enables the underlying concentration of solute to be included with the surface excess, and so gives the total amount of material in the stationary phase. The inclusion also allows for the possibility that Γ_1 is negative. Clearly the real concentration of solute i at the interface cannot be negative, and so the absolute magnitude of a negative Γ_1 is limited. However, the actual concentration of the solute in the surface zone can be less than the concentration in the bulk of the solution. In such a case, the degree of retention of the solute will actually be less than that of a so-called "unretained" solute. Such a solute would be partially excluded from the stationary phase.

3.2.2 Determination of k'_{ST}

In order to calculate k'_{ST} for a particular analyte, $\delta\gamma/\delta C_{bulk}$ must be obtained. In general, surface tension varies linearly with the concentration of analyte at sufficiently low

concentrations so that k'_{ST} can be calculated from the gradient of such a plot (see Equation [3.5]. The molecular forces between solvent and analyte are those which are responsible for the solubility of an analyte. It is anticipated that analytes that are less soluble in a given solvent will be expelled from the bulk of the solvent and be adsorbed at the surface. This causes a reduction in the surface tension. Conversely, solutes which are solvophilic and highly soluble (for example sugars) will be desorbed from the surface so causing an increase in the surface tension as their concentration is increased. Both situations have been observed in the present study and are allowable based on our definition of k'_{ST} given in the theoretical section. An example of the typical plots of surface tension *vs.* % analyte concentration is shown in Figure 3.3.

3.2.3 Surface Tension Measurement

In order to obtain values of $\delta\gamma/\delta C$ for various analytes, a method for measuring the surface tension is required. There are many methods employed for measuring surface tension. A review of the different methods is given in the following paragraphs. From this review, we concluded that the Wilhelmy Plate method would be most suitable for our purposes.

3.2.3.1 Capillary Rise Method

The capillary rise method is generally accepted as one of the most accurate of all methods, partly because the theory has been worked out with considerable exactitude and partly because the experimental variables can be closely controlled. To some extent this is a historical accident, and other methods now rival or surpass the capillary rise method in perceived value.

The primary attribute of the capillary rise method is that it is still considered to be one of the most accurate, providing precision (reproducibility of measurement) on the order of a few hundredths of a percent.[3] On the other hand, for practical reasons a zero contact angle is required as are fairly large volumes of solution. Additionally, with glass capillaries there are limitations to the alkalinity of the solution to be measured. The basic geometry of the capillary rise experiment is shown in Figure 3.4. In the simplest treatment, where the meniscus is assumed to be part of a sphere and the liquid above the level h (the height x) is ignored, we may write, using the Laplace equation [3.12]:

$$\Delta P = h\rho g = 2\gamma/R = (2\gamma \cos\theta)/r \qquad [3.36b]$$

or, rearranging:

$$\gamma = (rh\rho g)/(2\cos\theta) \qquad [3.37]$$

which, by applying the definition of the capillary constant:

$$a^2 = 2\gamma/\rho g \qquad [3.38]$$

becomes:

$$a^2 = rh/\cos\theta \qquad [3.39]$$

3.2.3.2 Methods Based on Shape of Static Drops or Bubbles

Small drops or bubbles will tend to be spherical because surface forces depend on the area which decreases as the square of the linear dimension whereas distortions due to gravitational effects depend on the volume which decreases as the cube of the linear dimension. Likewise, a drop of liquid in a second liquid of equal density will be spherical. When gravitational and surface tension effects are comparable, it is possible, in principle, to determine the surface tension from measurements of shape of the drop bubble. Shapes of sessile and hanging drops and bubbles are shown in Figure 3.5. The method's general procedure is to first form the drop or bubble under conditions where it is free from disturbances, and then measure certain key dimensions. Measurements are typically taken from a photograph.

An accuracy of several tenths of γ is attainable, and the method is well suited to long term changes in the surface tension.

To obtain worthwhile results by this method requires careful experimentation, followed by lengthy, tedious calculations which, at best, still possess an error of as much as 0.1% or more. The calculation procedure is essentially one of fitting the experimental profile to each theoretical profile derived by Bashforth and Adams' tables first compiled by Sugden[4]. To make such comparisons, all theoretical curves have to be scaled to a common maximum diameter, that of the drop, and the best fit value of β determined by the best apparent fit, after which the surface tension can be calculated from the equation:

$$\beta = b^2\rho g/\gamma \qquad [3.40]$$

where β is the parameter which defines the shape of meniscus and can have positive or negative values, and ρ is the relative density difference. A more detailed account may be

found in the paper written by Padday[5]. Each of the static drop methods is discussed in greater detail below.

Pendant drop method

A drop hanging from a tip (or clinging bubble) elongates as it grows larger because the hydrostatic pressure, ΔP, eventually becomes appreciable relative to the curvature of the apex. The surface tension may be calculated using the formula:

$$\gamma = \rho g b^2/\beta = \rho g d_e^2/\beta(d_e/b)^2 = \rho g d_e^2/H \qquad [3.41]$$

where ρ is the density of the liquid, b is the radius at the drop's apex, β is the dimensionless parameter which is related to the shape of the drop, d_e is the equatorial diameter of the drop, and $H = \beta(d_e/b)^2$.

The optical problems associated with measuring the drop with sufficient accuracy are significant, and a photographic image is normally used. However, this measurement technique brings with it a new set of difficulties because of the extremely small distances between the objective, the camera, and the drop. The shape of the drop recorded on the camera film or plate is essentially that recorded by tangents drawn from the optical centre of the lens to the sides of the drop. Because allowances for measurement errors must be made, the accuracy of γ is at best about 0.1% using this technique.

An alternative method[6] also employing a pendant drop to measure surface and interfacial tension is based upon the measurement of height of the drop at the point of instability. This is the point at which further increase in the drop results in detachment. No empirical corrections are required, but the limitation to accuracy is the actual measurement of the height. The accuracy would normally be of the order of $\pm 0.01 Nm^{-1}$ or 10%.

3.2.3.3 The Ring Method

This method involves the determination of the force required to detach a ring or loop of wire from the surface of a liquid. It belongs to the family of detachment methods to which the 'Drop Weight method' and 'Wilhelmy Slide method' also belong. The Ring method is generally attributed to du Nouy[7] and, as with all detachment methods, the first approximation of the detachment force is given by the surface tension multiplied by the periphery of the surface detached. Thus, for a ring as illustrated in Figure 3.6a:

$$W_{tot} = W_{ring} + 4\pi R\gamma \qquad [3.42]$$

The horizontal ring is dipped into the liquid and surface and then slowly raised. The point of instability corresponds to the point of maximum force. Thus, as the ring is pulled from the surface, the force exerted on the ring, as measured by a balance, increases steadily until the point is reached when the ring detaches itself from the surface. Equation [3.42] assumes that R>>r and that the inner and outer radii of the ring may be taken as equal. It also assumes that the inner and outer menisci approach verticality together (*i.e.* the contact angle, θ, is zero), corresponding to the point of rupture or instability.

Harkins and Jordon[8] found the above equation to be in serious error since many of the above assumptions required reconsideration, including:

1. The inner and outer radii are not equal.
2. The inner and outer menisci do not approach verticality together. Thus, at the rupture point neither surface is likely to be vertical and the radii of curvature are not likely to equal R.
3. When the rupture occurs, some liquid remains on the ring and can be seen there as small drops.

Harkins and Jordon therefore worked out an empirical correction factor so that Equation [3.42] now becomes:

$$f = (\gamma/p) = f(R^3/V' \times R/r) \qquad [3.43]$$

where f is the force required to detach the ring, p denotes the ideal surface tension, and V is the meniscus volume.

Experimentally, Harkins and Jordan used a chainomatic balance to determine the maximum pull. However, a popular simplified version of the tensiometer, as it is sometimes called, makes use of a torsion wire ring, which is usually constructed of platinum. The ring should

be kept horizontal (a departure of 1° was found to introduce an error of 0.5%, whereas one of 2.1° introduced an error of 1.6%). Also, care must be taken to avoid any disturbance to the surface as the critical point of detachment is reached. The ring is usually flamed before use to remove surface contaminants such as grease, and it is desirable to use a container for the liquid that can be overflowed so as to ensure the presence of a clean liquid surface.
A zero or near zero contact angle is necessary otherwise results will be falsely low. This was found to be the case for surfactant solutions where adsorption of surfactant molecules on the ring changed its wetting characteristics, and where liquid-liquid interfacial tensions were measured. In such cases, a polyethylene ring may be used.

3.2.3.4 The Wilhelmy Slide Method

Unlike other detachment methods such as the "Ring method'' generally attributed to du Nouy or ''drop weight method'' Tate (1964), the Wilhelmy Slide method , first developed in 1863 , does not require correction factors and accurate values can be determined experimentally.
The basic observation of the Wilhelmy method is that a thin plate such as a microscope cover glass, will support a meniscus whose weight both as measured statically or by detachment is given very accurately by the general equation:

$$W_{tot} = W_{plate} + \gamma Cos\theta p \qquad [3.44]$$

where p is the perimeter of the plate in contact with the surface, θ is the contact angle, W_{tot} is the total weight of the slide in contact with the surface and W_{plate} is the dry weight of the slide. When used as a detachment method, the procedure is essentially the same as with the ring method but the above equation holds to 0.1% so that no corrections are needed.
It should be noted that as with capillary rise, there is an adsorbed film of vapour with which the meniscus merges smoothly. The meniscus is not hanging but rather forms a liquid like film (see Figure 3.6b). The correction for the weight of such film should be negligible, however. The most widely used experimental procedure is to raise the liquid level gradually until it just touches the hanging plate suspended from a balance (a recording electro-balance). The increase in weight is then noted. A general equation is:

$$\gamma \cos\theta / g = \Delta W / p \qquad [3.45]$$

where p is the perimeter, ΔW is the change in weight, *i.e.*, force exerted by the plate when it is brought into contact with the liquid, and g is the acceleration due to gravity. The contact angle, if finite, may be measured in the same experiment.

A brief review of the other methods of surface tension measurement is given in Table 3.1.

3.3 Experimental Approach - Overview

Our approach was to calculate values of $d\gamma/dC$ based on experimental results in order to determine k'_{ST}.

In order to do this we first measured surface tension values for a range of analytes at different concentrations. The plot of γ *vs.* % concentrations allows $d\gamma/dC$ to be calculated and, consequently, values of k'_{ST}.

(Note : $d\gamma/dC$ is the gradient of the surface tension v % concentration plot and is given in units of dyne/(cm^2 % concentration).)

$$K_{ads} \equiv C_{surface}/C_{bulk} = -(1/RT)\{d\gamma/dC_{bulk}\} \qquad [3.46]$$

$$k_{ST}' = K_{ads} \times \phi \equiv K_{ads} \times \{A_{interf}/V_{surface}\} \qquad [3.47]$$

We then compare these values of k'_{ST} with values for the same analytes determined chromatographically, k'_{LC}. Finally, the role of graphite, k'_{GR}, on retention of the analytes is calculated from the ratio k'_{LC}/k'_{ST}.

3.3.1 Surface tension measurement

Two different instruments were employed to make surface tension measurements:

a) A CAHN Dynamic Contact Angle Analyser (model DCA-322) made available for a two week period at Nottingham University. This apparatus was used to determine the results used as part of the feasibility study, Figures 3.7 and 3.8.

b) A Surface Tension Analyser built at Nottingham University by Dr Martin Davies. This analyser was used to determine surface tension measurement for the expanded analyte investigations, Figure 3.9.

Both analysers employ the Wilhelmy Plate method of analysis but required different modes of use. The experimental set-up for each system and the precautions taken to ensure accurate results are outlined in the next section. Assessment of the accuracy and reproducibility for each set of apparatus was carried out before commencement of the feasibility study or expanded surface tension study. The results are presented in Tables 3.2 and 3.3, and discussed in Sections 3.4.2 and 3.4.3.

3.3.2 Feasibility Study

The following list gives a summary of the experiments undertaken as the feasibility study. These experiments all employed the use of a limited range of simple analytes: phenol, aniline, anisole, 3,5-xylenol, 2,6-xylenol, and benzylalcohol.

i. The accuracy of the surface tension apparatus was determined, Tables 3.2, Figures 3.7, 3.8
ii. The effect of increasing organic content (methanol) on the surface tension of water was measured. The results are presented in Table 3.4 and Figure 3.10.
iii. Surface tension measurements for each analyte were made at increasing analyte concentrations. The change in $\delta\gamma/\delta C$ for increasing organic content was also measured, see Table 3.5 and Figures 3.11-16). $\delta\gamma/\delta C$ was calculated for a range of analytes for a number of methanol-water mixtures which were then extrapolated to zero.
iv. k'_{ST} values were calculated from the $d\gamma/dC$, and presented in Table 3.6a. A breakdown of the calculations is provided in Table 3.6b. The $\log_{10} k'_{ST}$ and $\log_{10} k'_{LC}$ data was then plotted to compare the predicted effect on retention from the various methanol water concentrations (Table 3.7 and 3.8, Figure 3.17-21) and extrapolated to allow comparison of retention data in pure water.
v. A direct plot of $\log_{10} k'_{ST}$ values versus to $\log_{10} k'_{LC}$ was then made to determine the role of graphite in retention of these preliminary compounds from the solvent (Figure 3.22).

3.3.3 Expanded Experimental Study

Reproducibility and accuracy of surface tension measurements determined using the modified surface tension equipment (Table 3.3) were established before proceeding with the general surface tension study. The feasibility study was then extended to include compounds which were more likely to provide information concerning PREG. In general, these compounds were made up from families of polysubstituted benzenes and offered a wide range of polarity. Once again, a range of surface tension measurements were made for increasing analyte concentrations to give $\delta\gamma/\delta C$, this time in 100% water. A summary of the

types of compounds used in the experiments along with the $\delta\gamma/\delta C$ values and k'_{ST} obtained is given in Table 3.9.

The calculated values for $\delta\gamma/\delta c$ and corresponding values of k'_{ST} are presented along with summary tables for each set of analytes in Tables 3.10-3.17 and Figures 3.23-27. This data was then used to calculate values for k'_{ST}. This data is presented in Table 3.18. The method of calculation is the same as that used in the feasibility study where a worked example and breakdown of each calculation is given (Table 3.6b). The k'_{LC} for the same range of analytes was determined in pure water (Table 3.19). The method by which capacity factors were determined in pure water is discussed in Section 3.4.1.

Within the discussion for the phenyl-alkanols the selectivity of k'_{ST} values were then compared to that of k'_{LC}, (Table 3.20 and Figure 3.24). The determination of k'_{LC} values in pure water are discussed in section 3.4.1. Plots of $\log_{10} k'_{LC}$ *vs.* % methanol-water composition are given in Table 3.19 and Figures 3.28-31.

Finally, $\log_{10} k'_{ST}$ values which incorporate all the compounds investigated in the expanded study were plotted versus $\log_{10} k'_{LC}$ values (Table 3.18 and Figure 3.32) to determine the role of graphite in retention, *i.e.* k'_{GR}.

3.4 Experimental Detail

3.4.1 k'_{LC} Determination in 100% Water

Determination of k'_{LC} in 100% water (k'_{W}) can be difficult due to either extremely long retention times or poor peak shape. Therefore, it has been necessary to measure retention values at different methanol-water concentrations and extrapolate the data according to Equation [3.48]. The equation holds true for any given analyte where the organic content of eluent is changed:

$$\log_{10} k' = \log_{10} k'_{w} + AC \qquad [3.48]$$

where C is the volume fraction of organic component, e.g. methanol, acetonitrile and 'A' is the gradient. The equation is discussed in greater detail in Chapter 5 of the thesis. Plots of $\log_{10} k'_{LC}$ *vs.* % methanol-water composition are given in Table 3.19 and Figures 3.28-31.

3.4.2 Surface Tension Experimental (1)

Analysis was carried out at Nottingham University using the CAHN Dynamic Contact Angle analyser (Model DCA322). The experimental set up is given in Figure 3.7a. The

schematic of the rise and fall of the glass plate slide is seen in Figure 3.7b. The equipment itself consists of an electro-balance, which on the lower side carries an arrangement for a slide attachment (microscope cover glass slides). The balance or slide does not move throughout the analysis and records only the change in force acting upon the slide as the solution is raised and lowered across it by an automatic jack positioned beneath the solution of interest. The measuring area is contained within a case to avoid contamination from dust particles. Temperature of the sample is controlled using a water circulator. The apparatus and its use are described in greater detail in the following paragraphs.

Method of analysis and precautions taken to maximise accuracy

Before commencing with experimental investigations, the balance was calibrated each day with Standard weights following the user guide manual. The surface tension of a clean sample of water was determined and compared to literature values. The dish containing the sample solution is itself contained in a double-walled vessel, and connected via an inlet and outlet to a thermostated water circulator, thus ensuring temperature control of the sample to be analysed. The sample and holder are then further enclosed, preventing the possibility of dust, particulate, or drafts from disturbing the surface of the solution and interfering with the accuracy of the results. The sample solution is raised slowly so that the slide becomes immersed in the solution to a predetermined depth. At this point, the sample solution is slowly lowered again at a controlled rate until the slide leaves the surface of the liquid. The mass of the plate is monitored continuously with respect its position within the liquid (see Figure 3.9b).

The plot in Figure 3.8a shows force exerted on the slide at a particular immersion depth. It can be observed that as the liquid touches the slide, there is an increase in force, which decreases as the slide becomes more deeply immersed in the liquid. This is due to the buoyancy effect, which causes an apparent loss in weight of the slide. As the sample solution is lowered and the slide reduces its immersion depth the force is again observed to increase linearly until it finally detaches from the liquid surface and the force drops back to zero. If a perpendicular line is drawn upwards from the point at which the liquid first touched the slide, the force at this point can be determined from the linear line drawn for the receding sample. Measuring the point of contact in this way allows for the errors associated with buoyancy to be considerably reduced so that they no longer form part of the equation used to calculate the surface tension.

The change in weight of the slide at any particular immersion depth represents the force exerted by the plate when in contact with the liquid. The relationship between the applied force and surface tension is given by Equation [3.45].

Initial experiments revealed that extreme cleanliness of the glass slide used for the analysis was essential to obtain accurate results. What happens with a dirty slide is shown quite clearly in Figure 3.8b. It can be seen that the receding line of force versus position does not retrace the same line as when it was advancing and as a consequence the measured value for the surface tension of water is much reduced. It was therefore found necessary to clean the slide prior to analysis by passing it through a blue bunson flame to ensure removal of any organic impurities. Once this was done, the plot for Figure 3.8a was re-established and a more accurate determination of surface tension achieved. Apparently, the main difficulty with unclean slides is that they do not wet evenly or reproducibly.

It should also be noted that, in general, before accurate results could be obtained on each cleaned slide, the slide itself had to be immersed in the solution at least five times. This was thought to be due to the removal of dust particles from the surface of the liquid as they clung to the plate due to surface tension forces. The particles were subsequently burned off as the slide was cleaned between each immersion.

Sample concentration changes

Typically, sample concentration changes were varied over a range of 0-0.8% (w/v) for any one analyte in any one solvent mixture. The chosen procedure was to weigh out the required material into the first solvent mixture and then to make four dilutions from this mixture with the solvent mixture taken from the parent solution. A fresh sample was weighed out separately for each solvent mixture and diluted in the same way. A 25mL aliquot of each sample solution was pipetted into the sample container readied for analysis. This container was then placed into the double-walled container to ensure consistent temperature during analysis. In general, samples were left for five minutes to thermally equilibrate.

The errors associated with the CAHN instrument and the method of analysis were monitored primarily by:

a) Measuring a pure water sample prior to each run (see Table 3.2a).

b) Running the phenol sample over the same concentrations in a 5% methanol water solvent mixture three times (see Table 3.2b).

Clearly, to make any worthwhile statistical evaluation of the errors involved, requires substantially more results. However, the equipment was only available for a two week period and most of the first week was spent learning how to use the equipment and establish the need for clean slides and a reasonably reproducible measurement of water on its own.

3.4.3 Surface Tension Experimental (2)

Analysis was carried out on a Surface Tension Analyser built at Nottingham University by Dr. Martin Davies.

Method of analysis and precautions taken to maximise accuracy

A schematic of the apparatus is in given in Figure 3.9a. The set up consists of a flat surface, which supports an electro-balance. A specially manufactured slide is suspended from the balance. The output from the balance is recorded via a digital voltmeter, which is calibrated daily such that 1mv = 1mg using standard weights. The position of the electro-balance, and hence the slide suspended from it, can be moved gradually with fine adjustment via a small handle situated at the top of the support stand. This allows the slide to be moved vertically downwards until it just touches the surface of the liquid. This is the point at which the measurement needs to be made so that buoyancy errors are minimised. By using the fine adjustment and observing the shadow cast by the edge of the slide about to be immersed into the solution, it was found that the point contact could be finely judged. Once the slide is just touching the surface, a trip switch on the balance is activated manually. This allows the slide to drop to a pre-determined depth (approximately 3mm) and effectively wets the slide. Reactivation of the balance returns the slide back to its original position at the surface of the liquid. At this point, the mV reading on the digital voltmeter is recorded (see Figure 3.9b). In general, a given solution would need to be tested in this way from six to ten times before reproducible data could be obtained. After each measurement, the slide was cleaned. The surface tension values measured each time were found to increase until no further change was noted over several more measurements of the same solution. This observation of increasing surface tension was thought to have been due to particles contaminating the liquid air interface. These particles were deposited on the slide during each measurement, similar to that observed for the CAHN instrument. To reduce such contamination, the slide was cleaned with chromic acid prior to each measurement. In general, seven to ten measure-wash cycles were required per solution to effectively remove the surface particulate contamination and enable a reproducible surface tension measurement. The

weight of the freshly cleaned slide is recorded on the electro-balance prior to each analysis so that its weight can be subtracted from the final reading to give the true weight/force associated with the surface tension at the liquid surface.

Concentration changes

Two approaches were utilised:

1) 25mL of pure water was added to the container and the surface tension measured following the method described above. 25mL of a 1% solution was then added by burette to the 25mL to give a 0.5% solution. Subsequent volumes of the solution were then added in the same way and surface tension measurements determined.

2) 25mL of pure water was added to the container and the surface tension measured as described above. This was then discarded and 25mL of the concentrated solution added. The surface tension was measured before 25mL of pure water was added via dispenser. The diluted sample was then once again measured. This process was repeated at least three more times in order to obtain a range of surface tension values at different concentrations (the volume of the container allowed for 125mL only).

Accuracy of results

A number of precautions were taken to ensure reproducible surface tension measurements and consequently k'_{ST}. These precautions included:

1) The dish containing the sample solution was itself contained in a double walled vessel which was connected via an inlet and outlet to a thermostated circulating water bath. This ensured constant temperature control of the sample to within plus or minus 1°C.

2) The sample and holder were further enclosed within a purpose-built Perspex housing. This minimised the presence of dust particles or drafts from disturbing the surface of the solution and interfering with the accuracy of the results.

3) Temperature control of the atmospheric environment within the Perspex housing was achieved by employing a light bulb as a heat source. This was rigged so that the light was turned on if the temperature dropped 1°C below 20°C, and was turned off at 1°C above 20°C. The thermocouple controlling the light bulb arrangement was fixed to the arm suspending the slide so that it was very close to the environment of the sample to be measured. A thermometer was placed near the sample to be analysed so that the atmospheric temperature could be observed within the chamber.

4) Prior to any measurement, the slide balance was always calibrated using standard weights. Calibration of the voltmeter allowed mV = mg conversion so that surfaces tension values could be calculated.

Initial experiments revealed that the cleanliness of the glass slide to be paramount if accurate and reproducible results were to be obtained. Prior to each analysis, the slide was this time dipped into a solution of chromic acid followed by three separate washes with HPLC-grade water.

Observed Accuracy

Using this method, the surface tension of water was found to be within 0.6% to literature values (72.8 dynes/cm). The surface tension value obtained was reproducible for a number of repeat samples on the same day and on different days and was in good agreement with the CAHN surface tension analyser used at Nottingham (see Table 3.3a). The mV readings taken from the voltmeter could only be made to an accuracy of plus or minus 0.1mV, which equates to plus or minus 0.2 dynes per cm.

The error in k'_{ST} was determined by measuring $d\gamma/dC$ for phenol in pure water for three separate experiments (see Table 3.3b). The k'_{ST} error was found to be approximately 7%.

3.5 Results and Discussion

3.5.1 Results and Discussion - Feasibility Study

The initial aim of this study was to determine how the surface tension of water changed with increasing quantities of methanol. The results are shown in Table 3.4 and Figure 3.10. It was observed that as the percentage of methanol is increased the surface tension value for the mixture decreases from 72.75 dynes/cm for pure water to 22.61 dynes/cm for pure methanol at 20°C.

For the range of simple aromatic compounds, a near linear relationship was observed for each plot of γ *vs.* % concentration at low analyte concentrations (see Table 3.5 and Figures 3.11 –16). The results are in keeping with the literature sources[9]. These sources also illustrate that beyond a certain analyte concentration, linearity is lost as the drop in surface tension becomes less apparent. The linear slope of $\delta\gamma/\delta C$ was found to become increasingly negative as the organic content of the solvent was reduced. This indicates that the analyte surface excess was greatest under these conditions. In some instances, for example, anisol in 50:50 methanol water (Figure 3.13) and 2,6-xylenol in 80:20 methanol:water (Figure 3.15), the value of $\delta\gamma/\delta C$ was found to be positive. This indicates that the surface excess of the analyte is negative under these conditions. In such cases where $\delta\gamma/\delta C$ was found to be positive, a linear relationship between $d\gamma$ and dC still was observed. The slope of this relationship can only be marginally positive and is dependant on the thickness of the surface layer as described in the theoretical section of this Chapter. We recall from Equation [3.2] that the surface excess, Γ, refers to the excess of analyte at the surface over and above that which would normally be at the surface, C_{surf} if $\Gamma = 0$. In order to take account of positive values of $d\gamma/dC_{bulk}$ we must take account of the surface thickness:

$$C_{surf} = \Gamma + t_{surf}C_{bulk} \qquad [3.4]$$

Accordingly we use Equation [3.7] to calculate values for k'_{ST}, *i.e.*:

$$k'_{ST} = \{ - (1/RT)\{d\gamma dC_{bulk}) + t_{surf} \} A_{surf} / V_{bulk} \qquad [3.7]$$

or:

$$k'_{ST} = \{k_{ads} + t_{surf} \} \phi$$

Thus, in order to make allowance for positive values of $d\gamma/dC_{bulk}$, the thickness of the surface t_{surf} must be sufficient to allow for a positive value of $(K_{ads} + t_{surf})$.

Values of $(K_{ads} + t_{surf})$ have been calculated using surface thickness (t_{surf}) of 1Å, 3Å, and 10Å. Each were sufficient to give positive values of $(k'_{ads} + t_{surf})$. However, in order to calculate values for k'_{ST} a surface thickness of 10Å has been employed since this value most closely resembles the molecular thickness of a solvent monolayer. The k'_{ST} values are given in Table 3.6 and the method of calculation is given in Table 3.6b. Where $\delta\gamma/\delta C$ is positive, the calculated values for k'_{ST} are very small. In such cases, it might be expected that the analyte would elute along with the solvent front and show no retention by the surface.
When values of k'_{ST} values were compared to the actual chromatographic values (k'_{LC}) and plotted as their $\log_{10}$ *vs.* the percent of methanol, nearly linear relationships were observed for all analytes. Both k'_{ST} and k'_{LC} show an increase in retention with a decrease in methanol concentration (Table 3.7 and Figures 3.17-21). It is also noteworthy that, although the values of k'_{ST} and k'_{LC} are similar at high concentrations of methanol, the values for k'_{LC} are much greater than k'_{ST} when the percentage of methanol is small.
Both sets of data are in accordance with the following equations:

$$\log_{10} k'_{LC} = AC + \log_{10} k'_{w} \qquad [3.49]$$

$$\log_{10} k'_{ST} = AC + \log_{10} k'_{wST} \qquad [3.50]$$

where k'_{w} refers to k'_{LC} in 100% water and k'_{wST} refers to k'_{ST} in 100% water.

A summary of the data is given in Table 3.8. Gradient values (A_{ST}) are approximately five- to ten-fold greater than both the gradient values determined by chromatography of graphite (A_{LC}) and $\log_{10} k'_{w}$ values. Despite similar elution orders, differences clearly exist between the two systems suggesting that there is a contribution to retention and selectivity from the graphite other than that reflected in the analyte solvent interaction.

Typically, the order of elution for most analytes predicted by k'_{ST} followed the same order as that of k'_{LC}. The plot of $\log_{10} k'_{ST}$ *vs.* $\log_{10} k'_{LC}$ given in Figure 3.22 further supports this observation. However, the gradient for this plot is approximately six, not one as would have been expected if graphite had behaved as a purely unselective adsorbent. The k'_{ST} values in table 3.6 were observed to be very much less than k'_{LC} for all of the analytes tested. It must

be concluded, therefore, that the surface tension hypothesis may not hold. PGC does not behave as a totally unselective adsorbent for polar molecules.

3.5.2 **Results and Discussion – The Expanded Study**

The results presented and discussed in this section refer to the broader range of analytes outlined in Table 3.9. The k'_{LC} values in pure water were determined by the extrapolation method described in Section 4.2.1.

Phenyl alkanols

The $\delta\gamma/\delta C$ values for the homologous series of Phenyl alkanols (Table 3.10 and Figure 3.23) were found to become increasingly negative as the alkane chain length was increased. Traube's rule states that in dilute solutions the surface tension is lowered by a factor of three for each additional CH_2 group for a homologous series of surfactants. The summary in Table 3.11 shows how the gradient changes as the number of $-CH_2-$ is increased, the change in surface tension ($d\gamma_{n+1}/d\gamma_n$) approaching a value of three as the number of $-CH_2-$ groups reaches six. The results are similar to those obtained for LC, *i.e.* $k'_{(n)/(n+1)}$, where adsorption at the graphite/liquid interface increases by a factor of three for each subsequent addition of a $-CH_2-$ group.

The plot of $\log_{10} k'_{ST}$ *vs.* number of carbon atoms in the aliphatic side chain(n) shows a linear relationship and is in agreement with Equation [3.51].

$$\log_{10} k' = \alpha n + \beta \qquad [3.51]$$

where α is the gradient, n is the number of $-CH_2-$ groups present in the phenyl alkanol side chain, and β is the intercept which corresponds to the $\log_{10} k'_{ST}$ for benzene. $\text{Log}_{10} k'$ in this case refers to $\log_{10} k'_{ST}$ for values determined by surface tension. The equation also holds true for retention on graphite. The $\log_{10} k'_{LC}$ for values determined by HPLC are given in Table 3.12a. The use and the history of the equation [3.51] is discussed in greater detail in Chapter 5 of the thesis. At this point, however, we simply use the equation to compare the behaviour of these compounds at the water/air interface compared to that at the water/graphite interface. In order to compare directly, k'_{LC} values have been calculated for pure water, the data in Table 3.12 has been extrapolated to give values of $\log_{10} k'_{w}$.

The slope (α, 0.43) for the $\log_{10} k'_{ST}$ data is similar to that observed for the $\log_{10} k'_{LC}$ when plotted against n, (α, 0.4) (see Figure 3.24). The results indicate that the selectivity of the

two systems is similar, with slightly greater selectivity observed for the values calculated from the PGC.

Values for k'_{LC}/k'_{ST} *i.e.* k'_{GR} are small (Table 3.12b) suggesting that these analytes arrange themselves at the graphite-liquid interface in a similar way as they do at the gas-liquid interface. It also suggests that solvent interaction with the analyte controls the retention behaviour of these compounds to a large extent.

Hydroxybenzenes

The surface tension data and calculations of $\delta\gamma/\delta C$ are given in Table 3.13 The plot of γ *vs.* analyte concentration is given in Figure 3.25. Good linearity was observed. The $\delta\gamma/\delta C$ values corresponding k'_{ST} values for the hydroxybenzenes (see Table 3.13) were found to become progressively <u>less</u> negative as the polarity of the molecule increased, *i.e.* tri-hydroxy < di-hydroxy < phenol. The k'_{ST} values therefore show the reverse order to that obtained for k'_{LC} on PGC. A summary of the data is given Table 3.14, where a large difference between k'_{ST} and k'_{LC} values is observed. Consequently, for these more polar compounds, k'_{GR} is large and graphite can be said to make a major contribution towards the retention of these compounds, completely overcoming any analyte-solvent interactions (hydrogen bonding) which exist.

Polysubstituted phenylcarboxylic acids

The surface tension data and calculated values of $\delta\gamma/\delta C$ are given in Table 3.15. The plots of γ *vs.* analyte concentration are shown in Figure 3.26. The plots show good linearity across the range of concentrations investigated. The slope was observed to become less negative as the number of

–COOH groups increased, the slope being steepest for benzoic acid. Consequently when k'_{ST} is calculated the retention order is completely the reverse to that of k'_{LC}, (see Table 3.16). In this respect, these analytes behave in a similar manner to the hydroxybenzenes where k'_{GR} is large and increases as the polarity of the analyte increases.

Once again, $\log_{10} k'_{GR}$ values are <u>very</u> high suggesting a mechanism of interaction which greatly exceeds the energy associated with analyte solvent interactions. We will discuss this in greater detail in Chapter 5 of the thesis.

Polysubstituted nitrobenzenes

The $\delta\gamma/\delta C$ plots for the nitro substituted benzenes (Table 3.17 and Figure 3.27), gave disappointingly poor linearity. Poor solubility in water for these compounds meant that very low concentrations had to be employed. This resulted in very small changes in γ being observed and hence inaccuracy in $d\gamma/dC$. Further difficulties were experienced with the determination of k'_{LC} where retention of the 1,3- and 1,4-dinitrobenzene was so strong that k'_{LC} could not be determined. Hence, values of k'_{GR} were very large, *i.e.* > 500.

Extrapolated data for k'_{LC} in pure water

The chromatographic results for each set of compounds measured at different methanol water concentrations in order to extrapolate is presented in Table 3.19. Extrapolation of the data allowed log k'_{LC} to be determined in pure water. Good linearity was observed for each set of analytes (see Figures 3.28-31).

Overview for the expanded study

When the $\log_{10} k'_{ST}$ data is plotted against $\log_{10} k'_{LC}$ data (see Table 3.20, Figure 3.32) the points can be seen to be split in two groups. The first group, containing those which represent non-polar compounds (phenyl alkanols), lie along a straight line. The second group shows no consistency, having points scattered over a small range of k'_{ST}, but wide range of k'_{LC}. The ΔG_{GR} values show that there is only a small contribution towards the retention of these compounds on graphite over and above that which would be predicted from adsorption of the analyte at the gas liquid interface (water in this case). Conversely, the contribution of graphite to the retention of polar compounds appears to be so large that the analyte retention is almost completely independent of analyte-solvent interactions. *i.e.* ΔG_{GR} is large.

Thus, the data clearly illustrates that graphite cannot be considered to be an unselective adsorbent. Instead, it suggests that there <u>is</u> a polar retention effect on graphite. This effect represents a mechanism of retention of strength that <u>far</u> exceeds any analyte-solvent interactions that may take place.

3.6 Conclusions

This study has compared the adsorption of a range of analytes at both the PGC/liquid interface and the gas/liquid interface in order to provide a relative measure of PREG. In order to do this, the relationship between k'_{LC} and k'_{ST} has been investigated. The k'_{ST} values have been calculated from surface tension measurements made either in pure water or in methanol:water mixtures for analytes at different concentrations according to the Gibbs Adsorption Isotherm. The k'_{ST} is therefore calculated on the basis that PGC behaves as an unselective adsorbent. Our results confirm that this statement is far from the truth.

In general, it was found that adsorption to the gas/liquid interface was less than adsorption to the graphite/liquid interface. Graphite in the LC context is thus much more selective towards dissolved analytes compared to the solvent itself. The exception is the phenyl alkanols, where the selectivity on graphite was seen to be very similar to the solvent. Polar molecules demonstrated an additional effect where, despite only very slight adsorption to the liquid/gas interface, analyte molecules were strongly adsorbed at the graphite/liquid interface even when pure water was used as the solvent. In water, hydrophilic interaction between the polar groups of the analyte and the water molecules are strong, effectively counteracting the hydrophobic interactions of the non-polar part of the analyte molecule. With graphite the overall interaction energy at the graphite/liquid interface is more than enough to counteract any hydrophilic analyte solvent interactions which occur, and actually appears to increase with the increasing polarity of the analyte. This is the effect which we have called PREG.

The energies associated with PREG are therefore significantly higher than those associated with analyte-solvent interactions, as demonstrated by the very high values determined for $\Delta G_{graphite}$ for the hydroxybenzenes. The role of the solvent appears to be only in the way in which it orientates analytes to the flat surface of the graphite.

We will return in Chapter 5, Section 5.5.8 to discuss the energies that are associated with PREG relative to those energies associated with analyte-solvent interactions.

Chapter 3 References

[1] Dias, H., Ph.D. thesis, University of Edinburgh (1990)
[2] McBain, J. W., and Humphreys C. W., J. Phys. Chem., 36, 300 (1932)
[3] Jaycock, M. J., *Chemistry of Interfaces,* published by Ellis Harwood Limited (1981)
[4] Bashforth, F., and Adams J. C., *An attempt to test the theory of capillary action*, Cambridge University Press (1883)

[5] Padday, J. F., in *Surface and Colloidal Science*, Ed. E. Matijevic, Wiley Science, New York, Vol. 1, p39 (1969)
[6] Levin, P. F., Pitts E., and Terry G. C., J. Chem. Soc., Faraday Trans. I, 72, 1519 (1976)
[7] du Nouy, L., J. Gen. Physiol., 1, 521 (1919)
[8] Harkins W. D. and H. F. Jordon., J. Am. Chem. Soc., 41, 499 (1919)
[9] Padday, J. F., in *Surface and Colloidal Science*, Ed. E. Matijevic, Wiley Science, New York, Vol. 1, p39 (1969)

Table 3.1

Comparison of Surface Tension Experimental Techniques

Method	Suitability	
	Pure Liquids	Solutions
Capillary height	Very satisfactory when the capillary wets reproducibly	Difficult when the contact angle is not 0°
Sessile Drop	Very satisfactory	Very useful for studying surface ageing.
Pendant Drop	Very satisfactory but has experimental difficulties.	Very useful for studying surface ageing
Wilhelmy plate	With a good experimental set up, very accurate and convenient.	Provides accurate data on surface ageing.
Maximum Pull on a cylinder	Very satisfactory. Easy to operate with simple apparatus.	Satisfactory if used with care and small displacements used with maximum pull.
Maximum Pull on a cone	Similar to cylinder method , but since the cone constant is universal , the results are easier to calculate	
Du Nouy ring	Satisfactory	Unsatisfactory
Drop weight or drop volume	Very satisfactory	Poor when ageing effects suspected
Maximum bubble pressure	Has experimental problems but useful where other methods are difficult to use.	Gives problems with ageing solutions.

[a] **Table reference: M. J. Jaycock, *The Chemistry of Interfaces*, page 64, published by Ellis Harwood Limited (1981)**

Table 3.2a.b

Reproducibility of SurfaceTension Measurement using the Nottingham CAHN Instrument

Table 3.2a
Pure Water at 20°C
Surface Tension of Water values given in dynes per cm
'Same Day Measurements'

	run (1) dynes/cm	run (2) dynes/cm	run (3) dynes/cm	Mean	Stdev	%Covar
day 1	72.32	72.34	72.29	72.32	0.03	0.03
day 2	72.33	72.31	72.31	72.32	0.01	0.02
day 3	72.35	72.32	72.32	72.33	0.02	0.02
day 4	72.33	72.34	72.31	72.33	0.02	0.02
day 5	72.29	72.33	72.34	72.32	0.03	0.04
day 6	72.31	72.32	72.35	72.33	0.02	0.03
day 7	72.32	72.33	72.32	72.32	0.01	0.01
day 8	72.33	72.33	72.35	72.34	0.01	0.02
day 9	72.32	72.34	72.29	72.32	0.03	0.03
day10	72.32	72.32	72.35	72.33	0.02	0.02

Next Day Measurements

mean	72.32	72.33	72.32	
Stdev	0.02	0.01	0.02	
%cov	0.02	0.01	0.03	

Table 3.2b
Phenol in 5% Methanol:Water) data given in units of dynes per cm at 20°C

% Conc	run (1) dynes/cm	run (2) dynes/cm	run (3) dynes/cm
0	64.95	64.90	64.89
0.1	64.34	64.38	64.35
0.2	63.70	63.71	62.69
0.3	62.91	62.91	62.91
0.5	61.43	61.43	61.43
0.8	59.28	59.28	59.28
1.2	55.61	55.61	55.61
Gradient	**-7.23**	**-7.29**	**-7.24**

Mean	-7.25
Average gradient deviation	0.02
Error in k'_{ST} approx 1.2%	

Temperature for all experiments 20C

Table 3.3

Reproducibility of Surface Tension Measurement using the Surface Tension Instrument (2)

Table 3.3a

Pure Water
Surface Tension of Water at 20°C

Same Day Measurements

	run (1) dynes/cm	run (2) dynes/cm	run (3) dynes/cm
day 1	72.5	72.3	72.7
day 2	72.5	72.5	72.5
day 3	72.7	72.5	72.3
day 4	72.5	72.5	72.3
day 5	72.5	72.5	72.5
day 6	72.5	72.5	72.5
day 7	72.7	72.5	72.5
day 8	72.5	72.5	72.5
day 9	72.5	72.5	72.3
day10	72.5	72.5	72.5

Next Day Measurements

mean	72.5	72.5	72.5
Stdev	0.1	0.1	0.1
%cov	0.1	0.1	0.2

Table 3.3b

Phenol in Pure Water at 20°C

% Conc	run (1) dynes/cm	run (2) dynes/cm	run (3) dynes/cm
0	72.5	72.5	72.5
0.2	70.3	70.1	70.3
0.4	66.8	66.6	66.7
0.5	64.9	64.7	64.9
0.6	63.9	63.9	63.7
0.8	61.2	61	61.2
Gradient	-14.1	-14.0	-13.8
Mean		-14.0	
Average gradient deviation		0.1	
Error in k'st approx. 7%			

(mv readings could only be made to plus or minus 0.1 mv -this equates to plus or minus 0.2 dynes per cm)

Temperature for all experiments 20C

Table 3.4
Surface Tension of different methanol:water compositions

% Methanol/Water	Surface Tension (γ)
0	72.60
5	62.84
10	57.02
20	51.63
30	45.91
40	40.56
50	36.80
60	33.56
70	30.70
80	28.34
90	25.93
100	23.19

Surface tension values are given in dynes per cm
Temperature 20C

Table 3.5
Surface Tension values at different analyte concentrations and different methanol water compositions

Temperature for all data is 20C

Phenol				**Aniline**			
%Conc'n	5% MeOH	20%MeOH (dynes/cm)	50%MeOH (dynes/cm)	Conc'n 100*g/ml	5%MeOH (dynes/cm)	40%MeOH (dynes/cm)	50%MeOH (dynes/cm)
100*g/ml	(dynes/cm)						
0	64.95	51.63	36.80	0	64.95	40.56	36.80
0.1	64.34			0.2	64.56	39.63	37.33
0.2	63.70	50.00	37.36	0.3		41.21	
0.3	62.91			0.4	63.23	40.58	37.46
0.4		49.41	37.13	0.6	62.41	39.74	37.58
0.5	61.43			0.8		39.88	37.77
0.6		48.53	36.77				
0.8	59.28						
1		47.61	36.79				
1.2	55.61						
Gradient	-7.2	-3.64	-1.16	Gradient	-5.25	-0.42	-0.6

Anisol			**3,5Xylenol**			
Conc'n 100*g/ml	40%MeOH (dynes/cm)	80%Meoh (dynes/cm)	Conc'n 100*g/ml	20%MeOH (dynes/cm)	40%MeOH (dynes/cm)	80%MeOH (dynes/cm)
0	40.56	28.34	0	51.63	40.56	28.34
0.1	40.21		0.2	47.01	39.71	28.97
0.2	40.27	28.73	0.4	44.16	39.28	28.85
0.3	39.78	29.84	0.6	41.17	37.79	28.98
0.4	39.66	29.00	0.8	39.28	38.96	28.94
0.6	39.39	28.81				
0.8	39.20	28.89				
Gradient	-1.34	0.34	Gradient	-13.75	-1.11	0

Table 3.5 - continued

Surface Tension values at different analyte concentrations and different methanol water compositions

2,6 Xylenole				**Benzyl Acohol**		
Conc'n 100*g/ml	20%MeOH (dynes/cm)	40%MeOH (dynes/cm)	80%MeOH (dynes/cm)	Conc'n 100*g/ml	20%MeOH (dynes/cm)	10%MeOH (dynes/cm)
0	51.63	40.56	28.34	0	51.63	57.02
0.2	48.5	39.7	28.6	0.2	49.68	56.14
0.4	46.06	39.6	28.73	0.4	48.77	55.2
0.6	44.41	39.24	28.77	0.6	48.03	54.09
0.8	46.13	38.76	28.82	0.8	47.73	53.02
Gradient	-10	-2.21	0.23	Gradient	-5.13	-4.16

Table 3.6
Surface Tension Calculation of k'_{ST} and k'_{GR} and comparison with k'_{LC} for the feasibility study (Series 1)

Analyte	Solvent	Grad 1* dg/dC	density g/ml	Mw wt	conc 1% mol/l	Grad 2 dγ/dC	K_{ads}	ti + K_{ads} 10Å	ti + K_{ads} 3Å	ti+K_{ads} 1Å	k'_{ST} 10Å	k'_{ST}'' 3Å	k'_{ST}''' 1Å	k'_{LC}	k'_{GR}
Phenol	5% MeOH	-7.20	0.93	94.00	0.10	-72.42	0.03	0.08	0.04	0.03	3.99	2.24	1.74	45.7	11.5
	20%MeOH	-3.64	0.93	94.00	0.10	-36.61	0.02	0.07	0.03	0.02	3.25	1.50	1.00	17.0	5.2
	40%MeOH	-1.16	0.93	94.00	0.10	-11.67	0.00	0.05	0.02	0.01	2.74	0.99	0.49	3.0	1.1
Aniline	5%MeOH	-5.25	0.98	93.00	0.11	-49.88	0.02	0.07	0.04	0.03	3.53	1.78	1.28	17.7	5.0
	40%MeOH	-0.42	0.98	93.00	0.11	-3.99	0.00	0.05	0.02	0.01	2.58	0.83	0.33	2.0	0.8
	50%MeOH	-0.60	0.98	93.00	0.11	-5.70	0.00	0.05	0.02	0.01	2.62	0.87	0.37	1.2	0.4
Anisol	40%MeOH	-1.34	1.00	108.00	0.09	-14.42	0.01	0.06	0.02	0.01	2.80	1.05	0.55	20.3	7.3
	80%MeOH	0.34	1.00	108.00	0.09	3.66	0.00	0.05	0.01	0.00	2.42	0.67	0.17	1.5	0.6
3,5Xylenol	20%MeOH	-13.75	1.03	122.00	0.08	-162.38	0.07	0.12	0.08	0.07	5.84	4.09	3.59	214.0	36.7
	40%MeOH	-1.11	1.03	122.00	0.08	-13.11	0.01	0.06	0.02	0.01	2.77	1.02	0.52	41.1	14.8
	80%MeOH	0.00	1.03	122.00	0.08	0.00	0.00	0.05	0.02	0.01	2.50	0.75	0.25	4.4	1.8
2,6 Xylenol	20%MeOH	-10.00	1.02	122.00	0.08	-119.93	0.05	0.10	0.06	0.05	4.97	3.22	2.72	181.0	
	40%MeOH	-2.21	1.02	122.00	0.08	-26.50	0.01	0.06	0.03	0.02	3.04	1.29	0.79	32.3	10.6
	80%MeOH	0.23	1.02	122.00	0.08	2.76	0.00	0.05	0.01	0.00	2.44	0.69	0.19	4.3	1.8
Benzyl Alcohol	10%MeOH	-5.13	0.96	106.00	0.09	-56.66	0.02	0.07	0.04	0.03	3.66	1.91	1.41	37.0	10.1
	20%MeOH	-4.16	0.96	106.00	0.09	-45.94	0.02	0.07	0.03	0.02	3.44	1.69	1.19	20.8	6.0

* Grad 1 is the gradient of the surface tension vs % Conc'n plot in units of dynes/(cm%) = 0.001 N/(m%)

** Grad 2 is the Grad 1 but in units of dyn/(cm mol/l) = 0.001 N/(m mol/l)

Table 3.6b

Explanation of Terms and Calculations for k'_{ST} in Tables 3.6a and 3.9

Analyte	14 k'_{GR} Solvent k'_{LC}/k'_{ST}'	1 Grad1 dγ/dC	2 g/ml density	3 Mw wt	4 conc 1% mol/l	5 Grad 2 dγ/dC	6 K_{ads}	7 ti + K_{ads} 10Å	8 ti + K_{ads} 3Å	9 ti+K_{ads} 1Å	10 k'_{ST}' 10 Å	11 k'_{ST}'' 3 Å	12 k'_{ST}''' 1 Å	13 k'_{LC}
Benzyl Alcohol	WATER 1.18	-15.08	0.96	106	0.09	-166.5	0.07	0.12	0.08	0.07	5.92	4.17	3.67	6.98

Columns **Column Description**

1 This is the gradient of the Surface tension vs % Concentration plot in units of dynes/(cm %) = 0.001 N/ (m %)

2 This is the density of the analyte in units of g/ml

3 This is the molecular weight of the analyte

4 This is the concentration for 1% analyte in units of mol/l, calculated by dividing the density(2) by the molecular weight

5 This is the gradient (1) now in units of dyn/(cm mol/l) = 0,001 N/ (m mol/l)

6 K_{ads} = -(1/(8.3*293)*Grad2 (5)

7, 8, 9 ti + K_{ads}, allows us to take into account the surface interface thickness necessary for a chromatographic system
ti is calculated as follows

ti = 50,000 x thickness of surface layer (10Å , 3Å , 1Å) values must be positive if the Gibbs adsorption isotherm is to be complied with.

where the specific surface area of the mobile phase interface is 50 sq m per ml = 50,000 sq m/litre

10, 11, 12 $k'_{ST} = (K_{ads} + ts_{urf})(A_{surf}/V_{bulk})$

$k'_{ST}' = (Kads + 0.05) \times (50,000/1000)$

$k'_{ST}'' = (Kads + 0.015) \times (50,000/1000)$

$k'_{ST}''' = (Kads + 0.005) \times (50,000/1000)$

13 $k'_{LC} = k'_{w}$ (100% water) chromatographic capacity factor

$k'_{GR} = k'_{LC}/k'_{ST}' = (13)/(10)$

Table 3.7
Extrapolated data for k'_{ST} and k'_{LC} to Give Values in Pure Water

	% methanol	log k'_{ST}	A	log k'_{STw}	log k'_{LC}	A	log k'_{w}
Phenol	5	0.60	-0.005	0.62	1.66	-0.03	1.83
	20	0.51			1.23		
	40	0.44			0.48		
Aniline	5	0.55	-0.003	0.56	1.25	-0.03	1.38
	40	0.41			0.30		
	50	0.42			0.07		
Anisol	40	0.45	0.008	0.13	1.31	-0.03	2.44
	80	0.38			0.18		
3,5Xylenol	20	0.77	-0.006	0.89	2.33	-0.03	2.89
	40	0.44			1.61		
	80	0.40			0.64		
2,6 Xylenol	20	0.70	-0.005	0.80	2.26	-0.03	2.80
	40	0.48			1.51		
	80	0.39			0.64		
Benzyl Alcohol	10	0.56	-0.003	0.59	1.57	-0.03	1.82
	20	0.54			1.32		

Table 3.8

Summary Table for plots of $\log_{10} k'_{ST}$ and $\log_{10}{}'_{LC}$ vs % Methanol:Water

Analyte	A_{ST}	$\log_{10} k'_{STw}$	A_{LC}	$\log_{10} k'_{w}$
Phenol	-0.005	0.62	-0.03	1.83
Aniline	-0.003	0.56	-0.03	1.38
Anisol	0.008	0.13	-0.03	2.44
3,5Xylenol	-0.006	0.89	-0.03	2.89
2,6 Xylenol	-0.005	0.80	-0.03	2.80
Benzyl Alcohol	-0.003	0.59	-0.03	1.82

Table 3.9

Calculated values for k'_{ST} and k'_{GR} for Compounds used in the Expanded Study

Analyte	[1]Grad 1 dγ/dC	[2]density g/ml	[3]Mw wt	[4]conc 1% mol/l	[5]Grad 2 dγ/dC	[6]K_{ads}	[7]ti + K_{ads} 10Å	[8]ti + K_{ads} 3Å	[9]ti+K_{ads} 1Å	[10]k'_{ST}' 10Å	[11]k'_{ST}'' 3Å	[12]k'_{ST}''' 1Å	[13]k'_{LC}	[14]k'_{GR}
Benzyl alcohol	-15.08	0.960	106.0	0.091	-166.54	0.068	0.12	0.08	0.07	5.92	4.17	3.67	76	12.8
Phenethyl alcohol	-36.14	0.980	122.2	0.080	-450.46	0.185	0.24	0.20	0.19	11.76	10.01	9.51	398	33.8
Phenyl propanol	-86.86	0.992	139.2	0.071	-1218.76	0.501	0.55	0.52	0.51	27.56	25.81	25.31	851	30.9
4-Phenyl-1-butanol	-209.16	1.042	150.2	0.069	-3015.92	1.240	1.29	1.26	1.25	64.51	62.76	62.26	1949	30.2
Phenyl pentanol	-534.12	1.060	164.3	0.065	-8275.38	3.403	3.45	3.42	3.41	172.64	170.89	170.39	9549	55.3
6-phenyl –1- hexanol	-1435.4	1.053	178.3	0.059	-24312.85	9.997	10.05	10.01	10.00	502.37	500.62	500.12	46773	93.1
Phenol	-14.11	0.935	94.0	0.099	-141.85	0.058	0.11	0.07	0.06	5.42	3.67	3.17	68	12.5
1,2 dihydroxybenzene	-6.05	1.149	110.1	0.104	-57.97	0.024	0.07	0.04	0.03	3.69	1.94	1.44	87	23.6
1,2 dihydroxybenzene	-6.05	1.149	110.1	0.091	-66.40	0.027	0.08	0.04	0.03	3.87	2.12	1.62	87	22.5
1,3 dihydroxybenzene	-3.36	1.272	110.1	0.116	-29.08	0.012	0.06	0.03	0.02	3.10	1.35	0.85	118	37.9
1,4 dihydroxybenzene	-2.35	1.320	110.1	0.120	-19.60	0.008	0.06	0.02	0.01	2.90	1.15	0.65	78	26.7
1,2,3 trihydroxybenzene	-0.68	0.863	126.1	0.068	-9.94	0.004	0.05	0.02	0.01	2.70	0.95	0.45	39	14.4
1,3,5 trihydroxybenzene	0.00	1.460	126.1	0.116	0.00	0.000	0.05	0.02	0.01	2.50	0.75	0.25	741	296.5
Benzoic Acid	-2.29	1.204	122	0.099	-23.21	0.010	0.06	0.02	0.01	2.98	1.23	0.73	53	17.6
1,2,4 Benzene carboxylic acid	-1.07	1.546	210	0.074	-14.53	0.006	0.06	0.02	0.01	2.80	1.05	0.55	36	13.0
Phthalic acid	-1.80	1.593	166	0.096	-18.76	0.008	0.06	0.02	0.01	2.89	1.14	0.64	1174	406.8
Nitrobenzene	-9.43	1.266	123	0.103	-91.70	0.038	0.09	0.05	0.04	4.39	2.64	2.14	2	0.5
1,3 Dintrobenzene	-43.08	1.575	161	0.098	-440.65	0.181	0.23	0.20	0.19	11.56	9.81	9.31		0.0
1,4 Dinitrobenzene	-10.16	1.625	161	0.101	-100.72	0.041	0.09	0.06	0.05	4.57	2.82	2.32		0.0

For a full explanation of all calculations and column headings ([1-14]) see table 3.6b

Table 3.10 n- Phenyl Alkohols

Surface Tension Experimental Data and Corresponding Gradient for the Rate of Change of Surface Tension with Analyte Concentration

	weight (g)	vol (ml)	Response [1] mv	% conc [2]	slide [3] (cm)	P [4]	[5] γ (dynes per cm)	[6] conc1%	[7] dγ/dC
Benzyl Alcohol		0	269.2	0.00	3.64	0.98	72.48	0.096	-15
	0.13	25	240.7	0.50	3.64	0.98	64.80		
	12.55	50	255.7	0.25	3.64	0.98	68.84		
	12.60	75	260.6	0.17	3.64	0.98	70.16		
	12.60	100	262.7	0.13	3.64	0.98	70.73		
Phenethyl alcohol		0	269.3	0.00	3.64	0.98	72.50	0.084	-36
	0.07	25	234	0.30	3.64	0.98	63.00		
	7.45	50	252	0.15	3.64	0.98	67.85		
	7.45	75	259	0.10	3.64	0.98	69.73		
	7.45	100	262	0.07	3.64	0.98	70.54		
Phenyl propanol		0	269.3	0.00	3.64	0.98	72.50	0.072	-87
	0.07	25	192.5	0.30	3.64	0.98	51.83		
	7.47	50	219.4	0.15	3.64	0.98	59.07		
	7.47	75	235.3	0.10	3.64	0.98	63.35		
	7.47	100	243.5	0.07	3.64	0.98	65.56		
4-Phenyl-1-butanol	0.00	0	269.3	0.00	3.64	0.98	72.50	0.064	-209
	0.05	75	225.7	0.07	3.64	0.98	60.77		
	1.68	50	246.9	0.03	3.64	0.98	66.47		
	1.68	75	255.3	0.02	3.64	0.98	68.73		
	1.68	100	259.9	0.02	3.64	0.98	69.97		
5-Phenyl-1- pentanol	0.00	0	269.3	0.00	3.64	0.98	72.50	0.059	-534
	0.07	150	195.2	0.05	3.64	0.98	52.55		
	1.25	50	218.9	0.02	3.64	0.98	58.93		
	1.25	75	235.9	0.02	3.64	0.98	63.51		
	1.25	100	243.5	0.01	3.64	0.98	65.56		

[1] Response (mv)
[2] % conc of the analyte in the solution tested in units of %
[3] Glass Slide perimeter (P) measured in centimetre's
[4] g , acceleration due to gravity
[5] Surface tension data in units of dynes per cm
[6] This is the concentration for 1% analyte in units of mol/l, calculated by dividing the density(2) by the molecular weight
[7] gradient – rate of change in surface tension with analyte concentration

Table 3.10 n- Phenyl Alcohol's - continued

Surface Tension Experimental Data and Corresponding Gradient for the Rate of Change of Surface Tension with Analyte Concentration

	Weight (g)	vol (ml)	Response mv	% conc	slide (cm)	P	γ (dynes per cm)	conc 1%	dγ/dC
6 Pheny-1-hexanol	0.00	0	269.3	0.00	3.64	0.98	72.50	0.053	-1435
	0.05	375	212	0.01	3.64	0.98	57.08		
	0.33	50	235.6	0.01	3.64	0.98	63.43		
	0.33	75	246.2	0.00	3.64	0.98	66.28		
	0.33	100	253.3	0.00	3.64	0.98	68.20		

Table 3.11

Change in Surface Tension with Respect to $-CH_2-$ number

Analyte	Solvent	dγ/dC	$d\gamma_{n+1}/d\gamma_n$	$k'_{ST(n+1)/K'st(n)}$
Benzyl Alcohol	WATER	-15		
Phenethyl alcohol	WATER	-36	2.4	2.0
Phenyl propanol	WATER	-86	2.4	2.3
4-Phenyl-1-butanol	WATER	-209	2.4	2.3
Phenyl pentanol	WATER	-534	2.6	2.7
5-Phenyl –1- hexanol	WATER	-1435	2.7	2.9

Table 3.12a

Log k'_{LC} Data for Retention on PGC

Alkanols	log k'	log k'	log k'	log k'	log k'		Slope A	log k'_w
% Methanol	50	60	70	80	90			
benzyl alcohol	0.73	0.36	0.10	-0.15	-0.23		-0.03	1.88
phenyl propanol	1.53	0.83	0.51	0.21	-0.22		-0.04	3.29
phenyl butanol	1.86	1.16	0.80	0.45	-0.03		-0.04	3.29
phenyl pentanol	1.99	1.57	1.16	0.77	0.07		-0.04	3.99
phenyl hexanol		1.97	1.51	1.07	0.59		-0.05	4.67
Hydroxybenzenes								
	log k'	log k'	log k'	log k'	log k'	log k'	Slope A	log k'_w
% Methanol	20	30	35	40	50	60		
Phenol	1.42	1.01	0.85	0.69	0.45	0.18	-0.03	1.83
1,2 dihydroxybenzene		1.08	0.93	0.74	0.51	0.23	-0.03	1.94
1,3 dihydroxybenzene	1.80	1.20		0.88	0.64	0.34	-0.03	2.07
1,4 dihydroxybenzene		1.04	0.86	0.64	0.49	0.19	-0.03	1.89
1,2,4 trihydroxybenzene		0.90	0.81	0.67	0.48	0.21	-0.02	1.59
1,3,5 trihydroxybenzene	2.35	1.93		1.66	1.34	0.99	-0.03	2.87
Benzoic acids								
	log k'	log k'	log k'	log k'			Slope A	log k'_w
% Methanol	60	70	80	90				
Benzoic acid	0.52	0.33	0.12	0.05			-0.02	1.72
Phthalic acid	0.60	0.43	0.28	1.22			-0.02	1.56
1,2,4-Carboxybenzene	1.94	1.73	1.57	1.51			-0.02	3.07
Nitrobenzenes								
	log k'	log k'	log k'	log k'	log k'		Slope A	log k'_w
% Methanol	80	85	90	95	100			
Nitrobenzene	0.50	0.41	0.29	0.21	0.11		-0.02	1.99

Table 3.12b

Summary Table for $\log_{10}$ k' values for the Phenyl Alkanols

Analyte	$\log_{10} k'_{ST}$	$\log_{10} k'_{LC}$	$\log k'_{GR}$
Benzyl Alcohol	0.77	1.88	1.11
phenethyl alcohol	1.07	2.60	1.53
phenyl propanol	1.44	2.93	1.49
4-Phenyl-1-Butanol	1.81	3.29	1.48
phenyl pentanol	2.24	3.98	1.74
6 phenyl 1 hexanol	2.70	4.67	1.97

(NB. Values of log k'_{LC} are calculated using t_{surf} = 10Å)

Table 3.13 Hydroxybenzenes

Surface Tension Experimental Data and Corresponding Gradient for the Rate of Change of Surface Tension with Analyte Concentration

	weight (g)	vol (ml)	[1]Response mv	[2]% conc	[3]slide (cm)	[4]P	[5]γ (dynes per cm)	[6]conc 1%	[7]dγ/dC
Phenol	0.05	25	261.5	0.20	3.6	0.98	70.33	94	-14.08
	0.10	25	248.5	0.40	3.6	0.98	66.83		
	0.12	25	241.5	0.50	3.6	0.98	64.95		
	0.15	25	237.5	0.60	3.6	0.98	63.87		
	0.20	25	227.5	0.80	3.6	0.98	61.18		
water			269.5	0.00	3.6	0.98	72.48		
Resorcinol	0.05	25	266.5	0.20	3.6	0.98	71.67	110.1	-3.58
	0.10	25	262.5	0.40	3.6	0.98	70.60		
	0.13	25	265.5	0.50	3.6	0.98	71.40		
	0.15	25	261.5	0.60	3.6	0.98	70.33		
	0.20	25	259.5	0.80	3.6	0.98	69.79		
water			269.5	0.00	3.6	0.98	72.48		
Phloroglucinol	0.05	25	268.5	0.20	3.6	0.98	72.21	126.1	-0.45
	0.10	25	268.5	0.40	3.6	0.98	72.21		
	0.12	25	268.5	0.50	3.6	0.98	72.21		
	0.15	25	268.5	0.60	3.6	0.98	72.21		
	0.20	25	266.5	0.80	3.6	0.98	71.67		
water			269.5	0.00	3.6	0.98	72.48		
Hydroquinone	0.05	25	267.5	0.20	3.6	0.98	71.94	110.1	-2.24
	0.10	25	266.5	0.40	3.6	0.98	71.67		
	0.12	25	265.5	0.49	3.6	0.98	71.40		
	0.15	25	264.5	0.60	3.6	0.98	71.13		
	0.20	25	262.5	0.80	3.6	0.98	70.60		
water			269.5	0.00	3.6	0.98	72.48		

[1]Response (mv)
[2] % conc of the analyte in the solution tested in units of %
[3] Glass Slide perimeter (P) measured in centimetre's
[4] g , acceleration due to gravity
[5] Surface tension data in units of dynes per cm
[6] This is the concentration for 1% analyte in units of mol/l, calculated by dividing the density(2) by the molecular weight
[7] gradient – rate of change in surface tension with analyte concentration

Table 3.13 Hydroxybenzenes - continued

Surface Tension Experimental Data and Corresponding Gradient for the Rate of Change of Surface Tension with Analyte Concentration

	weight (g)	vol (ml)	[1]Response mv	[2]% conc	[3]slide (cm)	[4]P	[5]γ (dynes per cm)	[6]conc 1%	[7]dγ/dC
Brenzkatechin	0.05	25	265.5	0.20	3.6	0.98	71.48	110.1	-6.05
	0.10	25	260.5	0.40	3.6	0.98	70.13		
	0.13	25	258.5	0.50	3.6	0.98	69.60		
	0.15	25	254.5	0.60	3.6	0.98	68.52		
	0.20	25	251.5	0.80	3.6	0.98	67.71		
water			269.5	0.00	3.6	0.98	72.48		
Pyrogallol	0.05	25	268.5	0.20	3.6	0.98	72.29	126.1	-0.57
	0.10	25	268.5	0.40	3.6	0.98	72.29		
	0.12	25	268.5	0.50	3.6	0.98	72.29		
	0.15	25	268.5	0.60	3.6	0.98	72.29		
	0.20	25	267.5	0.80	3.6	0.98	72.02		
water			269.5	0.00	3.6	0.98	72.48		

[1]Response (mv)
[2] % conc of the analyte in the solution tested in units of %
[3] Glass Slide perimeter (P) measured in centimetre's
[4] g , acceleration due to gravity
[5] Surface tension data in units of dynes per cm
[6] This is the concentration for 1% analyte in units of mol/l, calculated by dividing the density(2) by the molecular weight
[7] gradient – rate of change in surface tension with analyte concentration

Table 3.14
Summary table - Comparative k' and dγ/dC values for the Hydroxybenzenes

	dγ/dC	$\log_{10} k'_{ST}$	$\log_{10} k'_{LC}$	$\log_{10} k'_{GR}$
Phenol	-14.11	0.73	1.83	1.1
1,2-dihydroxybenzene	-6.05	0.56	1.94	1.33
1,3-dihydroxybenzene	-3.36	0.49	2.07	1.58
1,4-dihydroxybenzene	-2.35	0.46	1.89	1.43
1,2,4-trihydroxybenzene	-0.68	0.43	1.59	1.16
1,3,5-trihydroxybenzene	0	0.40	2.87	2.47

(NB. Values of log k'_{LC} are calculated using t_{surf} = 10Å

Table 3.15
Polysubstituted Carboxybenzenes
Data for Surface Tension and Gradient for the Plot of Surface Tension vs % Concentration

	weight (g)	vol (ml)	[1]Response mv	[2]% conc	[3]slide (cm)	[4]P	[5]γ (dynes per cm)	[6]conc 1%	[7]dγ/dC
1,2,4-Carboxybenzene	0.00		269.3	0.00	3.64	0.98	72.50	210.1	-0.71
	0.15	50	268.5	0.30	3.64	0.98	72.29	210.1	
	7.54	50	268.9	0.15	3.64	0.98	72.40	210.1	
	7.54	75	269.1	0.10	3.64	0.98	72.45	210.1	
	7.54	100	269.2	0.08	3.64	0.98	72.48	210.1	
benzoic acid	0.00	0	269.3	0.00	3.64	0.98	72.50	122.1	-1.83
	0.31	25	261.3	1.24	3.64	0.98	70.35	122.1	
	30.90	50	265.1	0.62	3.64	0.98	71.37	122.1	
	30.09	75	266.8	0.40	3.64	0.98	71.83	122.1	
	30.09	100	267.8	0.30	3.64	0.98	72.10	122.1	
Phthalic acid	0.00	0	269.3	0.00	3.64	0.98	72.50	166.1	-2.86
	0.15	100	267.7	0.15	3.64	0.98	72.07	166.1	
	3.76	50	268.7	0.08	3.64	0.98	72.34	166.1	
	0.04	75	268.7	0.00	3.64	0.98	72.34	166.1	
	0.04	100	269.2	0.00	3.64	0.98	72.48	166.1	

[1] Response (mv)
[2] % conc of the analyte in the solution tested in units of %
[3] Glass Slide perimeter (P) measured in centimetre's
[4] g , acceleration due to gravity
[5] Surface tension data in units of dynes per cm
[6] This is the concentration for 1% analyte in units of mol/l, calculated by dividing the density(2) by the molecular weight
[7] gradient – rate of change in surface tension with analyte concentration

Table 3.16

Summary Table for Comparative k' values for the Polysubstituted Phenyl Carboxylic Acids

Analyte	$\log_{10} k'_{ST}$	$\log_{10} k'_{LC}$	$\log_{10} k'_{GR}$
Benzoic Acid	0.47	1.72	1.25
1,2,4 Benzene carboxylic acid	0.45	1.56	1.11
Phthalic acid	0.46	3.07	2.61

(NB. Values of log k'_{LC} are calculated using t_{surf} = 10Å)

Table 3.17

Polysubstituted Nitrobenzene

Data for Surface Tension and Gradient for the Plot of Surface Tension vs % Concentration

	weight (g)	vol (ml)	[1]Response mv	[2]% conc	[3]slide (cm)	[4]P	[5]γ (dynes per cm)	[6]conc 1%	[7]dγ/dC
Nitrobenzene	0.00		269.3	0.00	3.64	0.98	72.50	123.1	-9.43
	0.10	175	267	0.06	3.64	0.98	71.88	123.1	
	1.43	50	268.3	0.03	3.64	0.98	72.23	123.1	
	1.43	75	268.8	0.02	3.64	0.98	72.37	123.1	
	1.43	100	268.8	0.01	3.64	0.98	72.37	123.1	
1,3 Dinitrobenzene			269.3	0.00	3.64	0.98	72.50	168.1	-43.08
	0.01	50	268.4	0.01	3.64	0.98	72.26	168.1	
	0.25	50	268.7	0.01	3.64	0.98	72.34	168.1	
	0.25	75	268.9	0.00	3.64	0.98	72.40	168.1	
	0.25	100	269.1	0.00	3.64	0.98	72.45	168.1	
1,4 Dinitrobenzene			269.3	0.00	3.64	0.98	72.50	168.1	-10.16
	0.01	50	268.2	0.01	3.64	0.98	72.21	168.1	
	0.27	50	268.6	0.01	3.64	0.98	72.32	168.1	
	0.27	75	268.6	0.00	3.64	0.98	72.32	168.1	
	0.27	100	268.7	0.00	3.64	0.98	72.34	168.1	

[1]Response (mv)
[2] % conc of the analyte in the solution tested in units of %
[3] Glass Slide perimeter (P) measured in centimetre's
[4] g , acceleration due to gravity
[5] Surface tension data in units of dynes per cm
[6] This is the concentration for 1% analyte in units of mol/l, calculated by dividing the density(2) by the molecular weight
[7] gradient – rate of change in surface tension with analyte concentration

Table 3.18

log k'_{ST} and Log k'_{LC} Data for fig 3.31

Analyte	log k'_{ST}	log k'_{LC}
Benzyl Alcohol	0.77	1.88
phenethyl alcohol	1.07	2.60
phenyl propanol	1.44	2.93
4-phenyl-1-butanol	1.81	3.29
phenyl pentanol	2.24	3.98
6 phenyl 1 hexanol	2.70	4.67
Phenol	0.73	1.83
1,2-dihydroxybenzene	0.57	1.94
1,3-dihydroxybenzene	0.49	2.07
1,4-dihydroxybenzene	0.46	1.89
1,2,3-trihydroxybenzene	0.43	1.59
1,3,5-trihydroxybenzene	0.40	2.87
Benzoic Acid	0.47	1.72
1,2,4 Benzene carboxylic acid	0.45	1.56
Phthalic acid	0.46	3.07
Nitrobenzene	0.64	0.30
1,3-dintrobenzene	1.06	
1,4-dinitrobenzene	0.66	

k'_{LC} date for 1,3 and 1,4 nitrobenzene not completed.

Fig 3.1

Attractive Forces Between Molecules at the Surface and the Interior of a Liquid

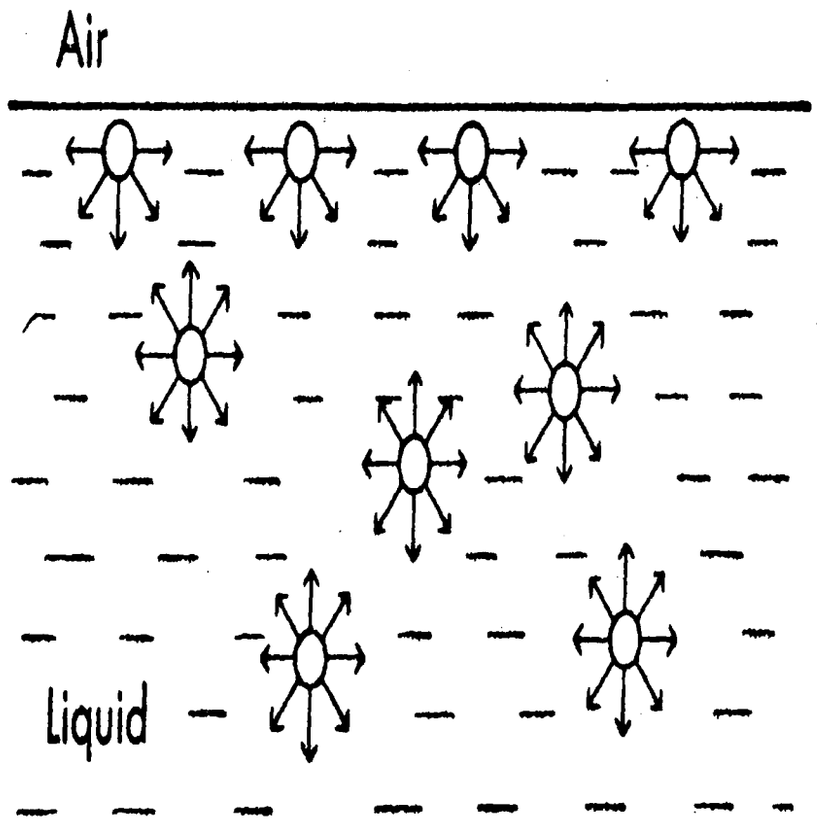

- Molecules which are located at the centre of a liquid are subjected to equal forces of attraction in all directions, whereas those located at the surface experienceunbalanced attractive forces resulting in a net downward pull.

Fig 3.2
Representations of a Surface Interface Between
Two Immiscible Liquids

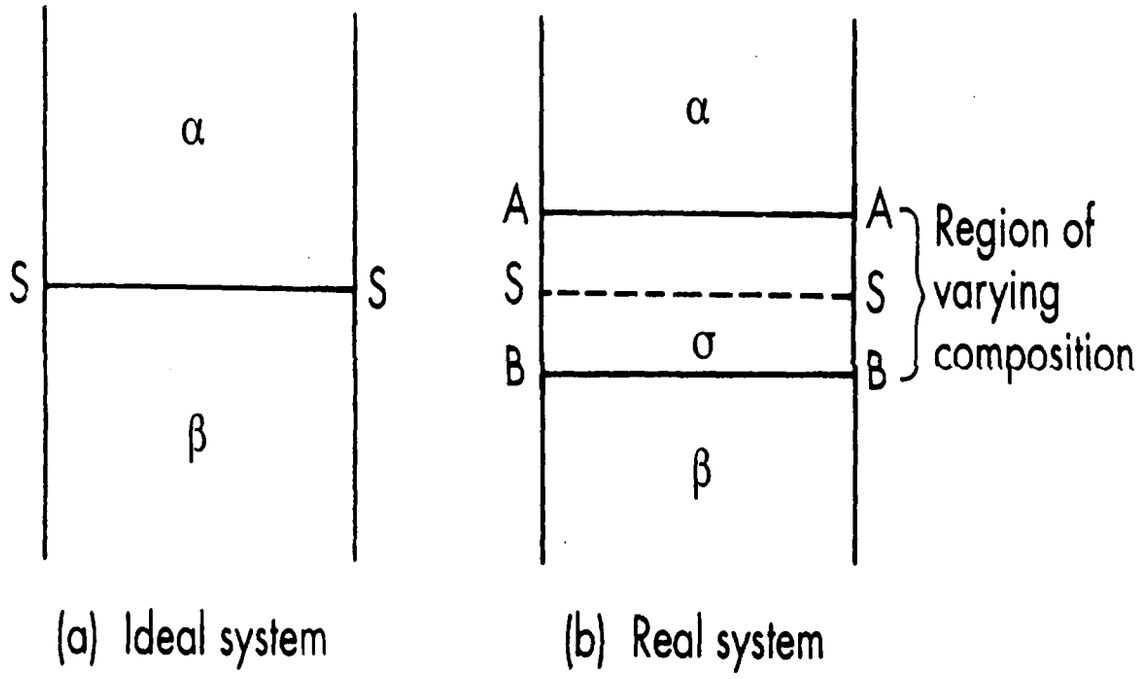

Representation of an interface between bulk phases α and β

Fig 3.3
Schematic Representation for Typical Surface Tension
Behaviour with Change in Concentration of the Analyte

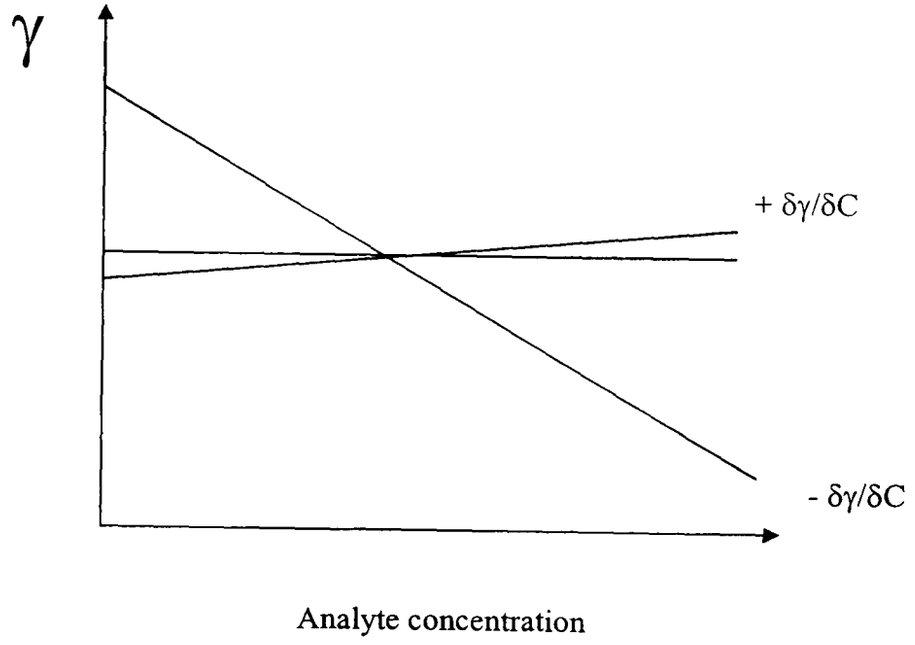

Fig 3.4, 3.5
Methods for Surface Tension Measurement

Fig 3.4

Axially Symmetric Menisci

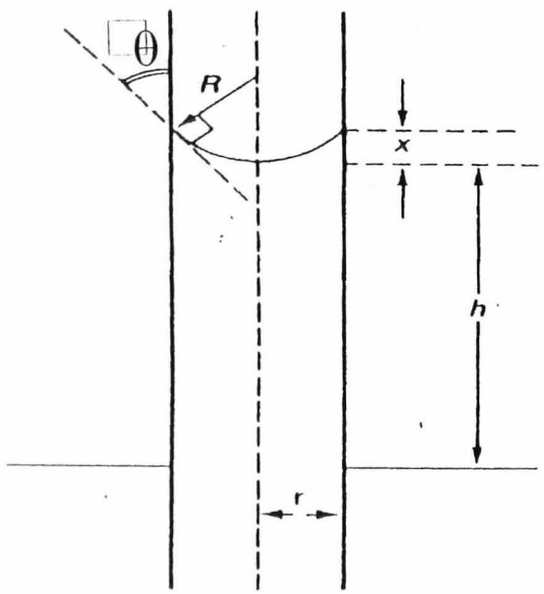

– A liquid meniscus in a capillary tube.

Fig 3.5

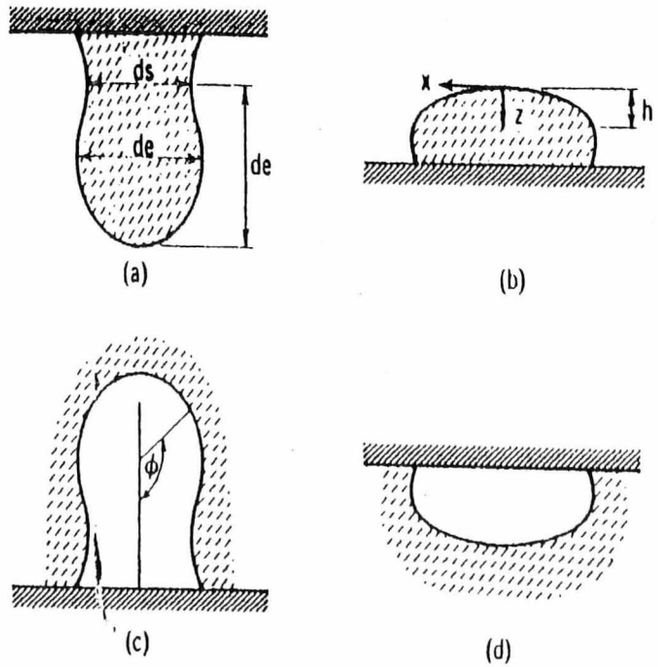

Shapes of sessile and hanging drops and bubbles: (*a*) hanging drop, (*b*) sessile drop, (*c*) hanging bubble, (*d*) sessile bubble.

Figs 3.6a and 3.6b
Methods for Surface Tension Measurement

- Fig 3.6a
- Ring Method

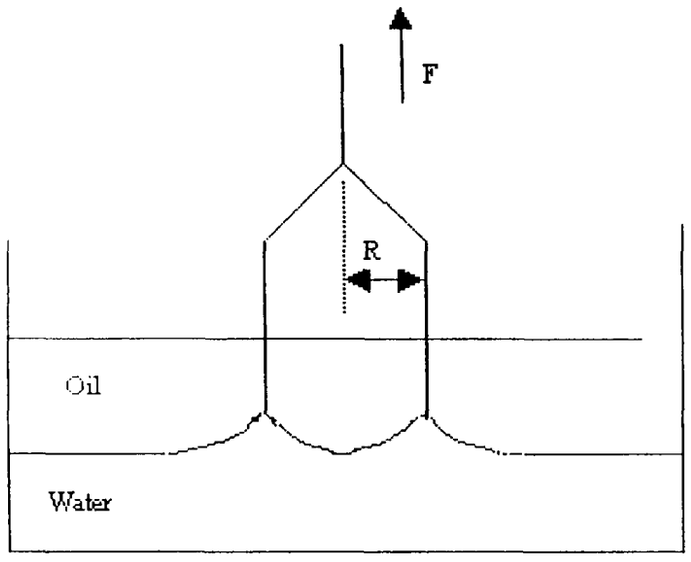

Measurement of interfacial tension

- Fig 3.6b
- Wilhelmy Plate Method

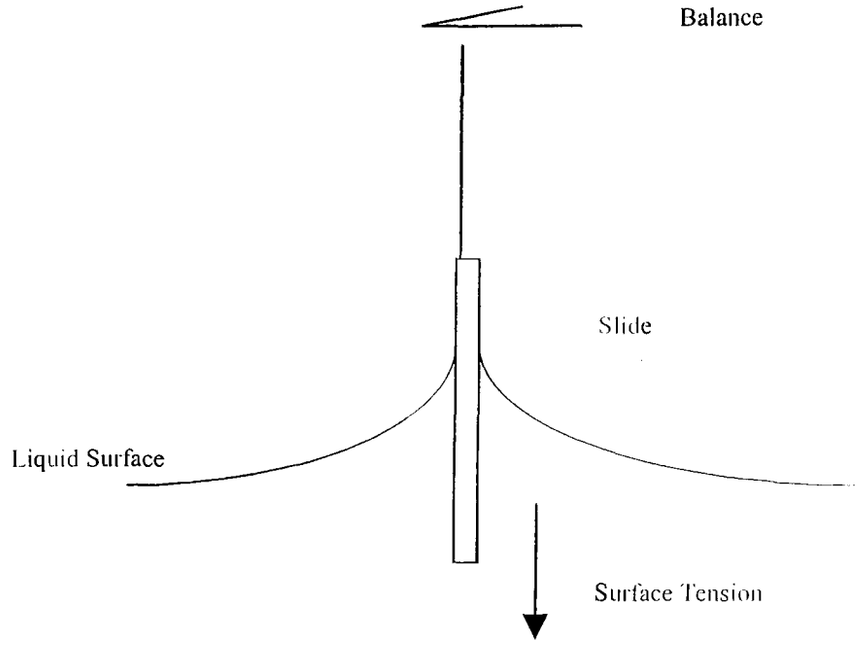

Fig 3.7

Experimental Set-Up for the CAHN Surface Tension Analyser

Fig 3.7a

a) A CAHN Dynamic Contact Angle Analyzer (model DCA-322) at Nottingham University.

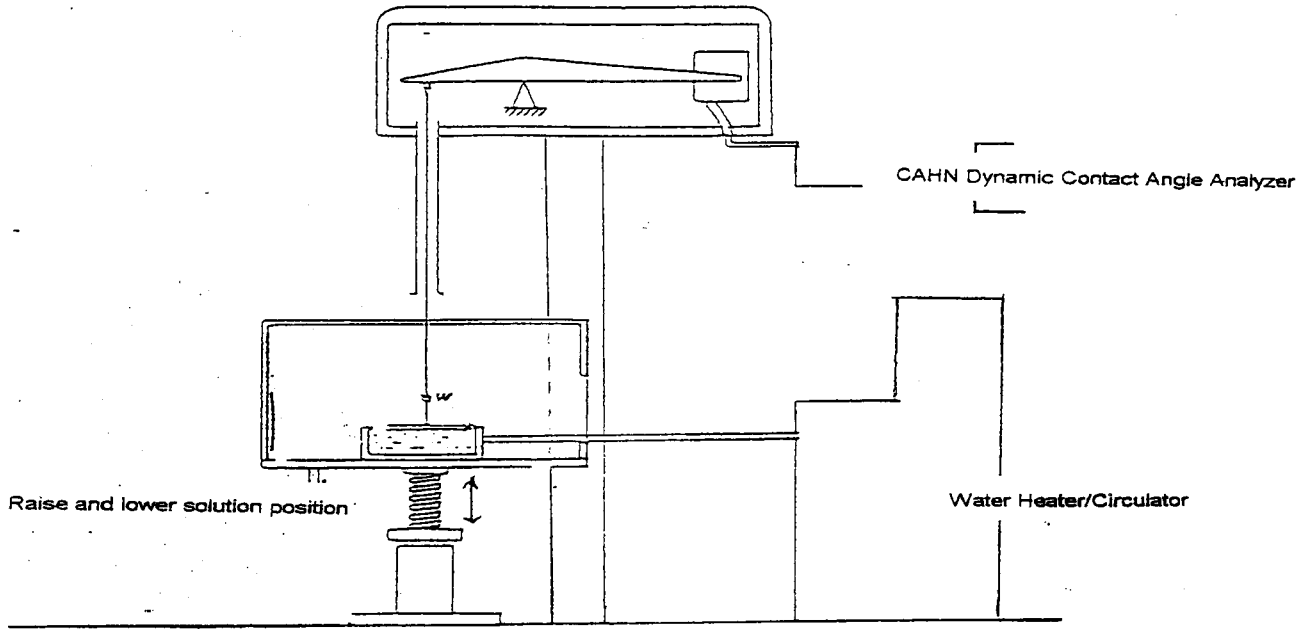

Fig 3.7b Schematic rise and fall of the slide.

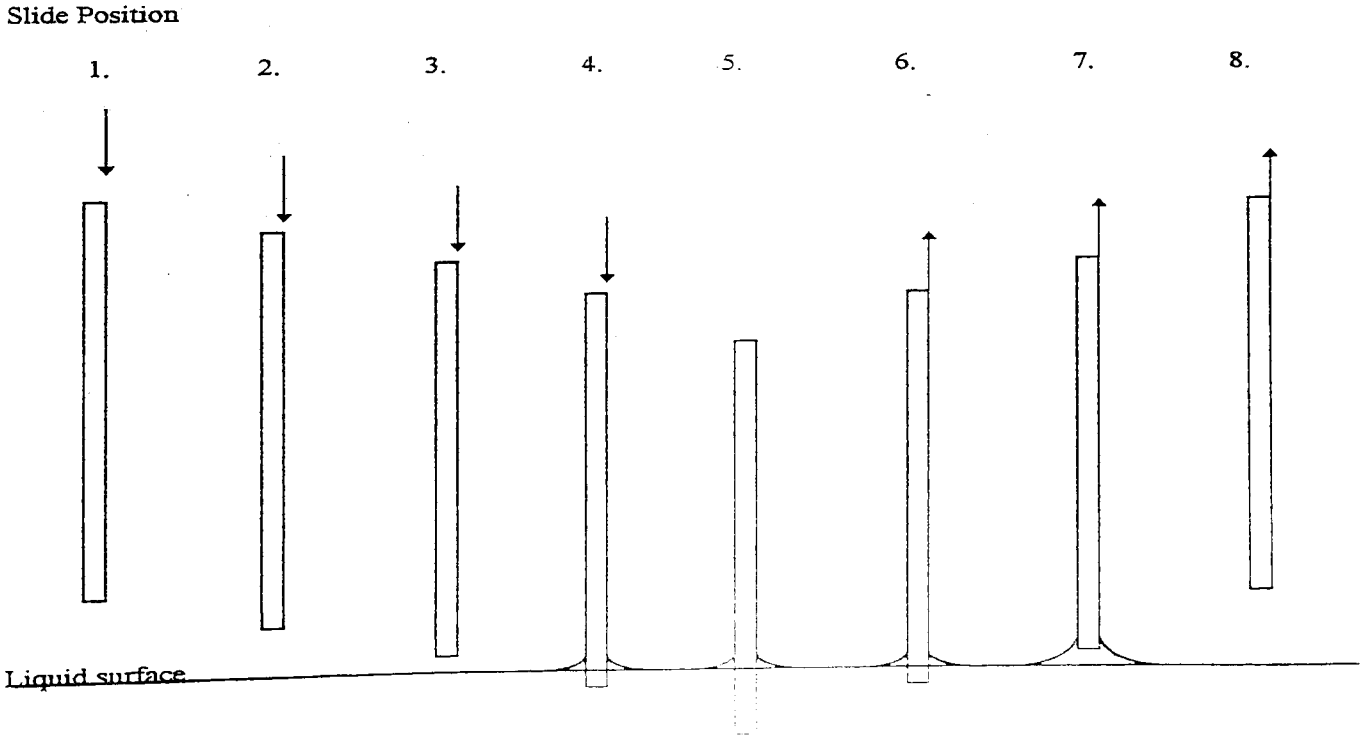

Fig 3.8

Example of How Cleanliness of the Slide Affects the Accuracy of the Surface Tension Measurement

Fig 3.8a Clean Slide

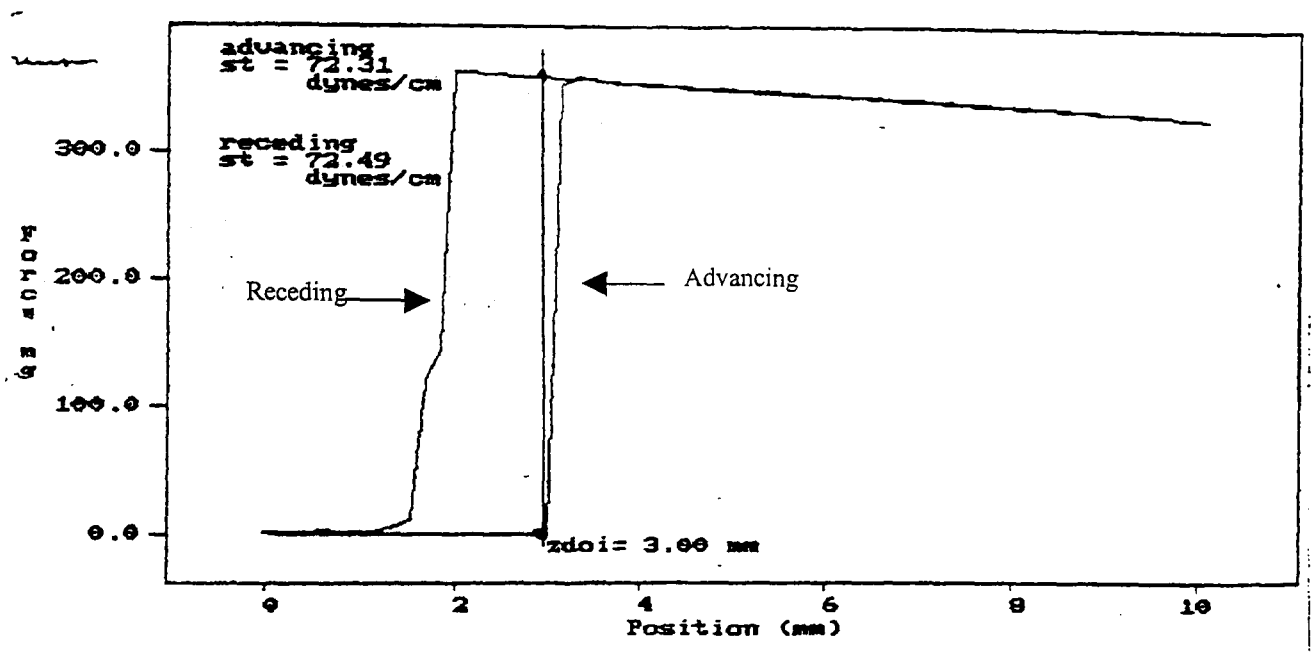

Fig 3.8b Dirty Slide

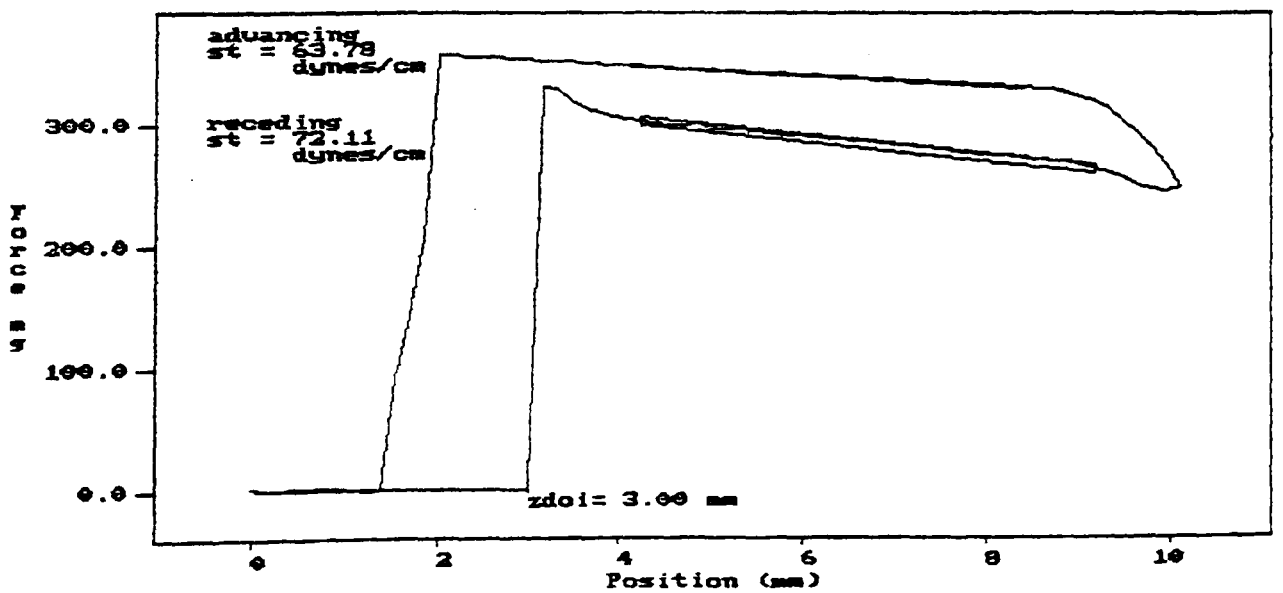

Fig 3.9

Experimental Set-Up for the Modified Surface Tension Analyser

Fig 3.9a

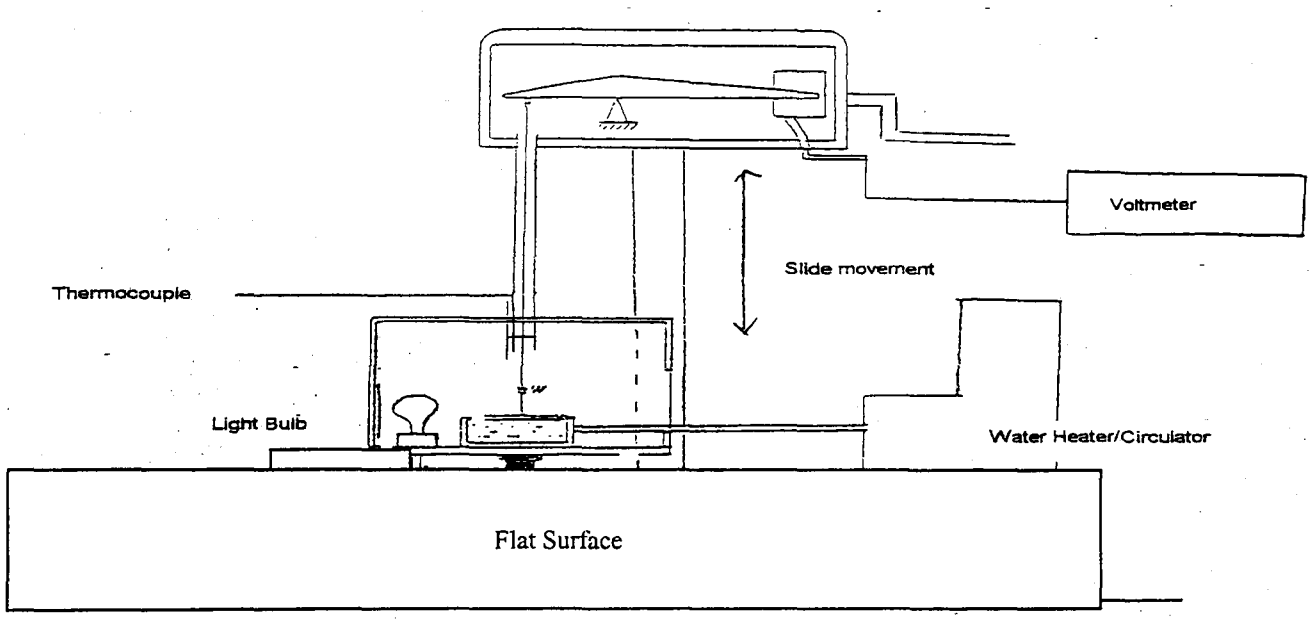

Fig 3.9b

Schematic of the rise and fall of the slide

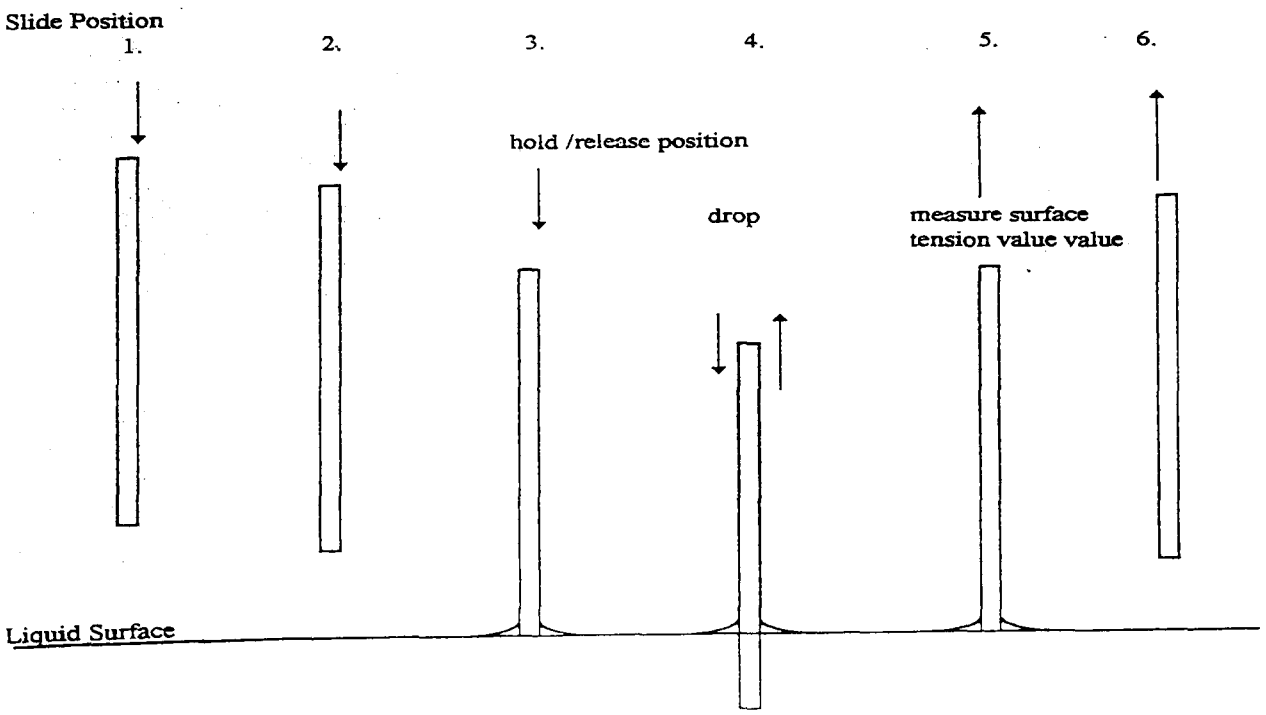

Fig 3.10

Variation in Surface Tension of Water with % Methanol

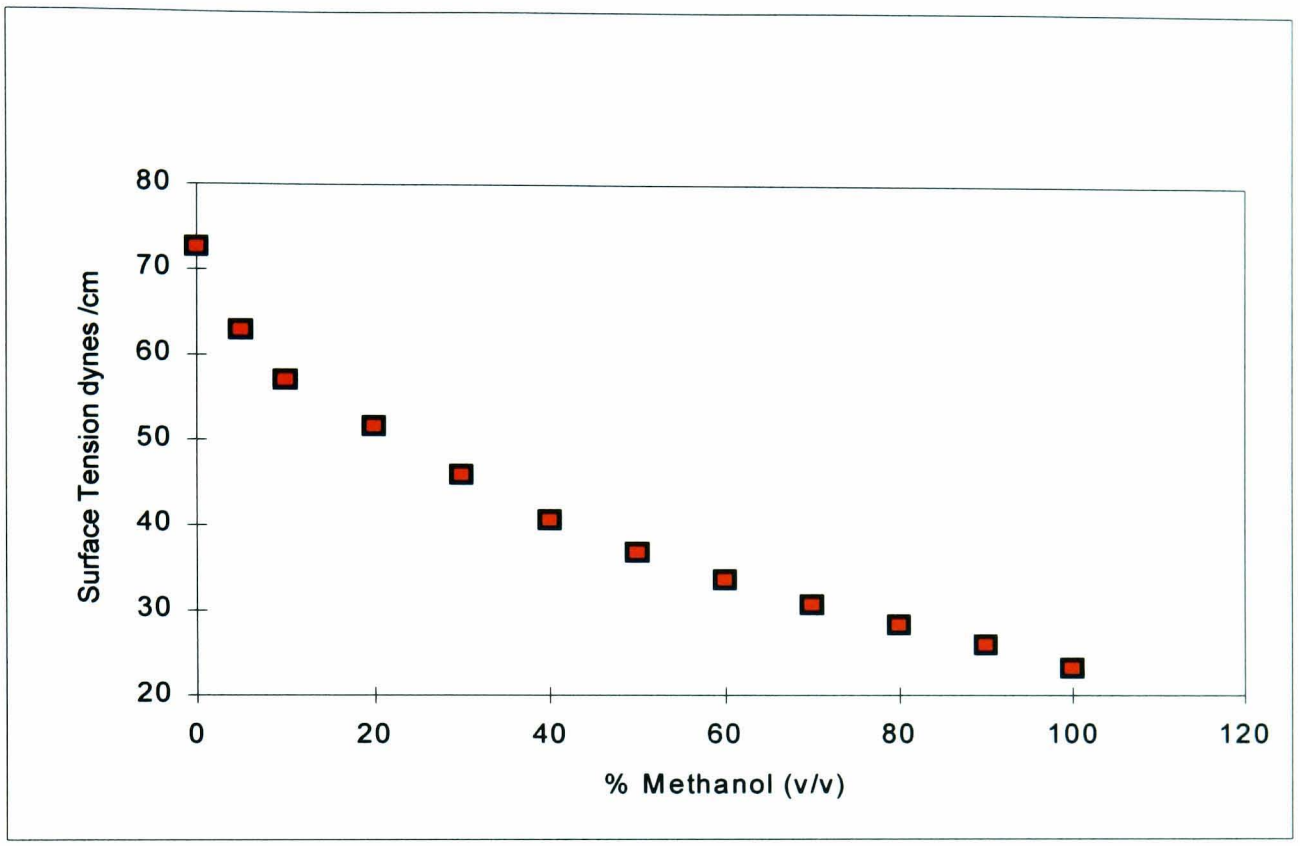

Fig 3.11

Variation in Surface Tension Measuremnt for Increasing Concentrations of Phenol in Methanol :Water

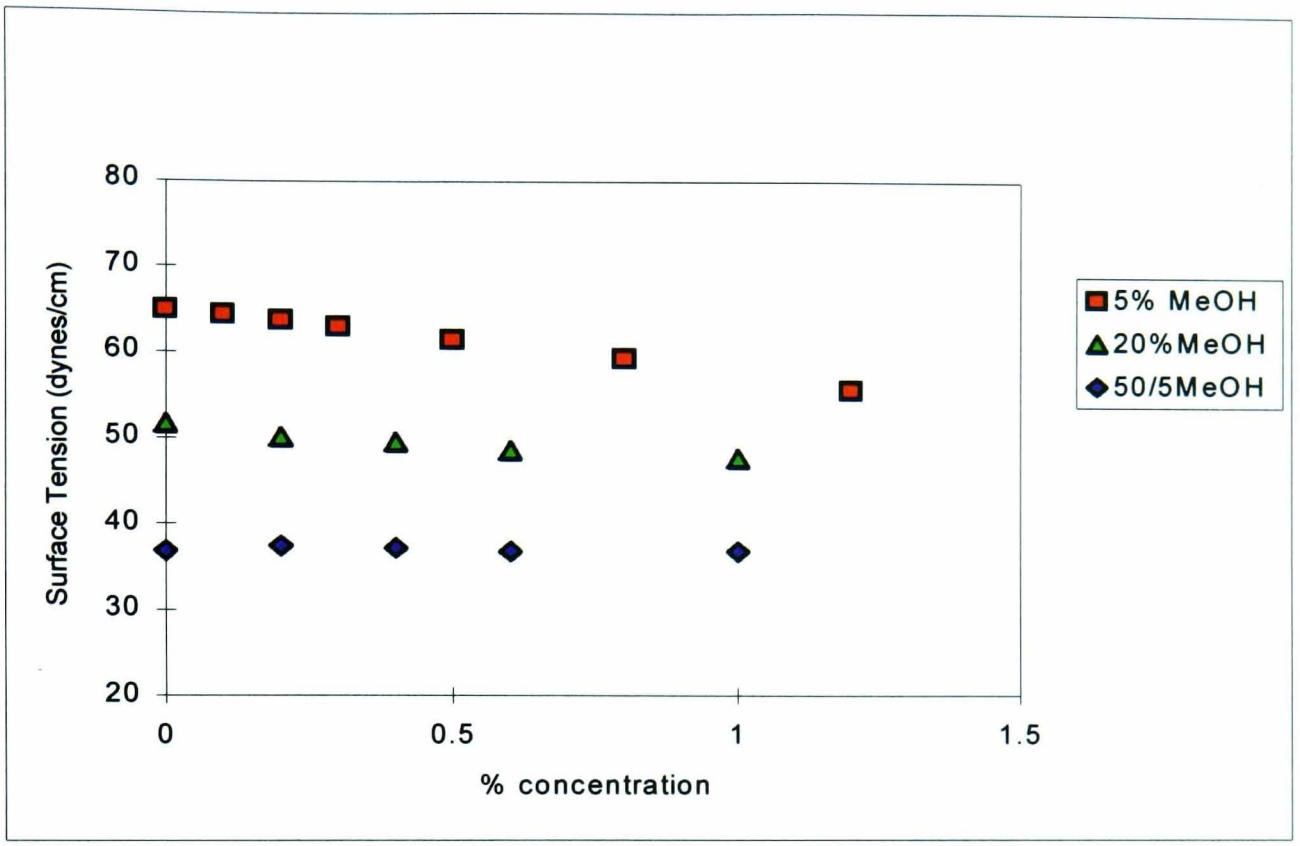

Fig 3.12

Variation in Surface Tension Measurements for Increasing Concentrations of Aniline in Methanol :Water

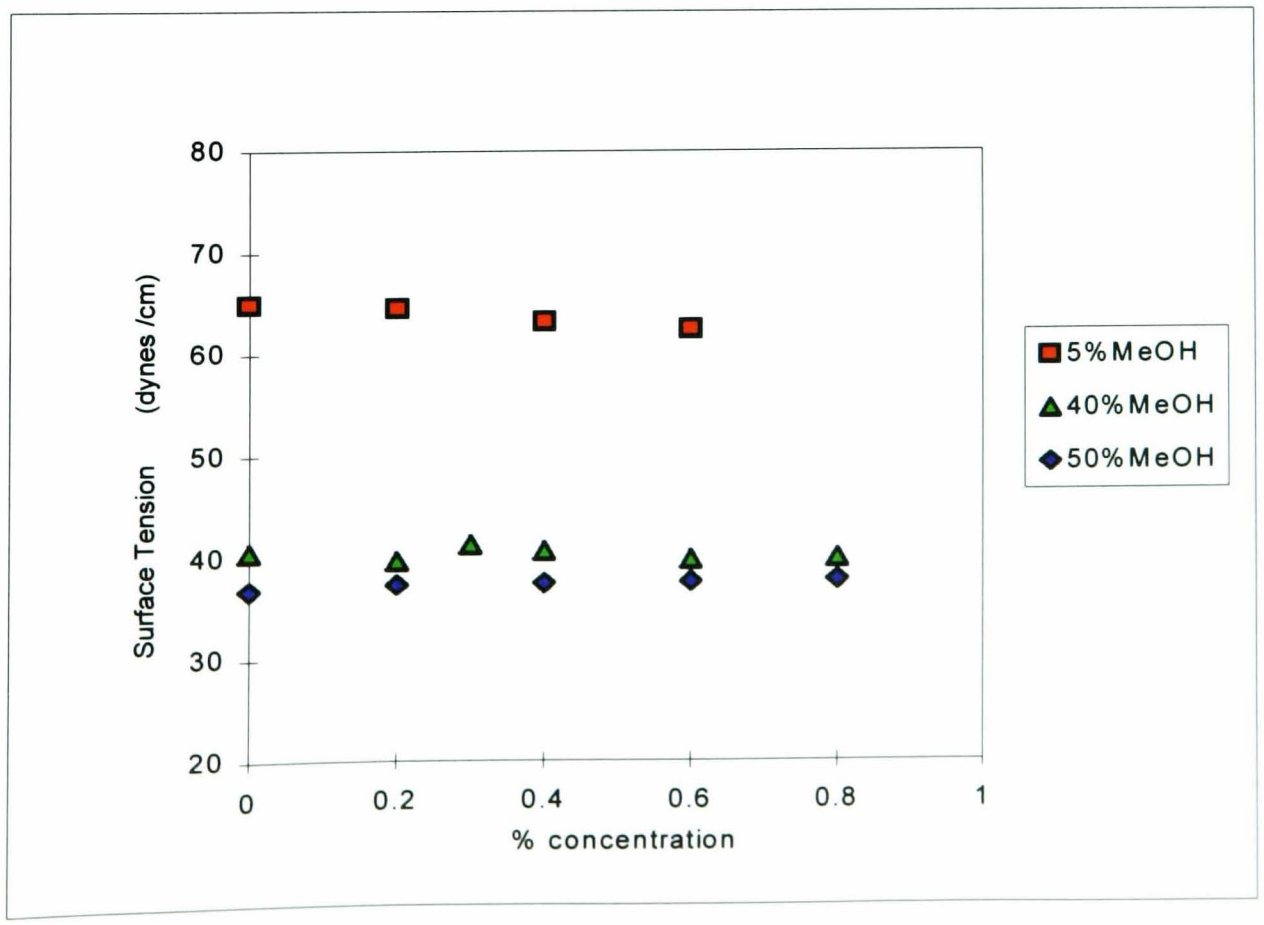

Fig 3.13

Variation in Surface Tension Measurements for Increasing Concentrations of Anisol in Methanol :Water

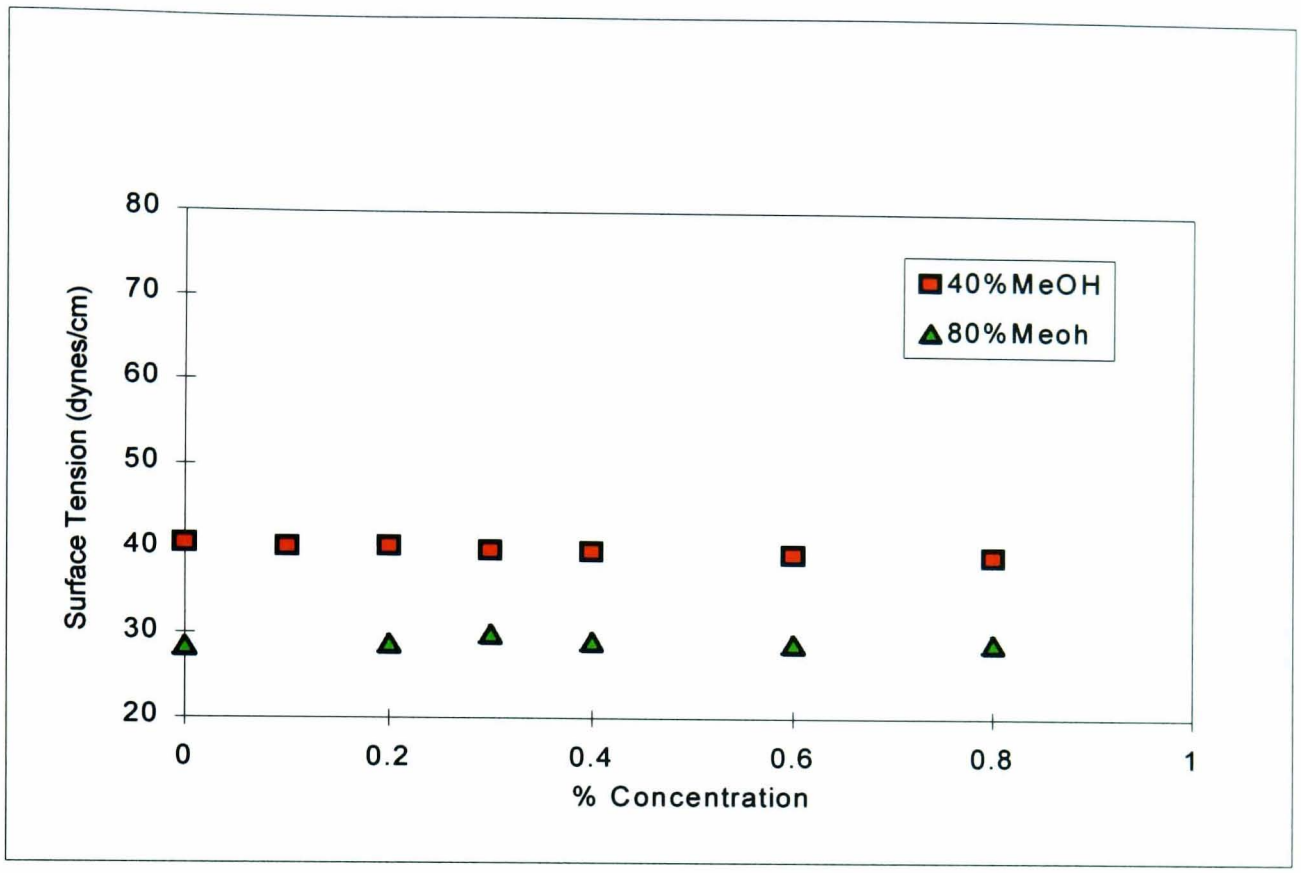

Fig 3.14

Variation in Surface Tension Measurements for Increasing Concentrations of 3,5 Xylenol in Methanol :Water

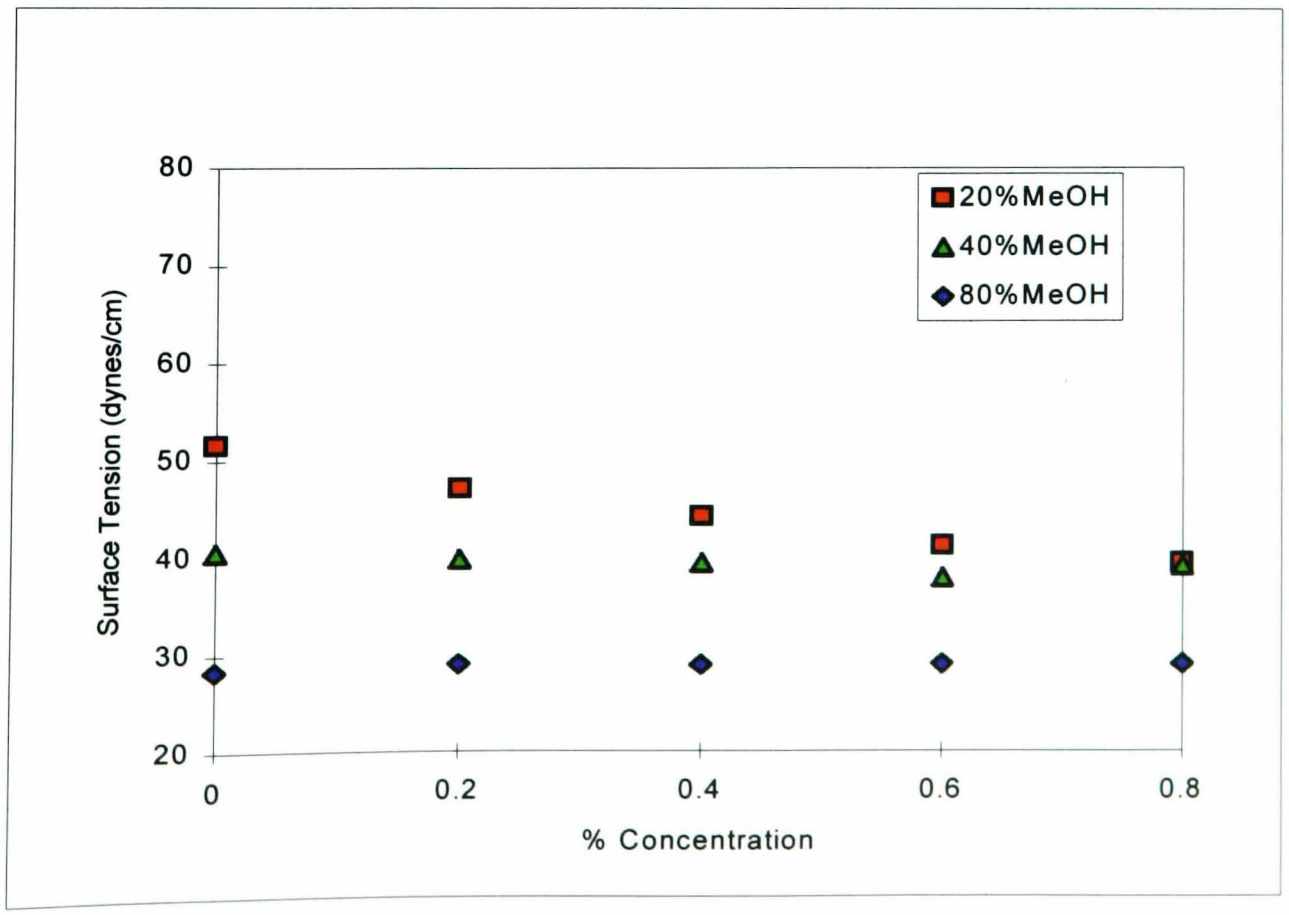

Fig 3.15

Variation in Surface Tension Measurement for Increasing Concentrations of 2,6 Xylenol in Methanol :Water

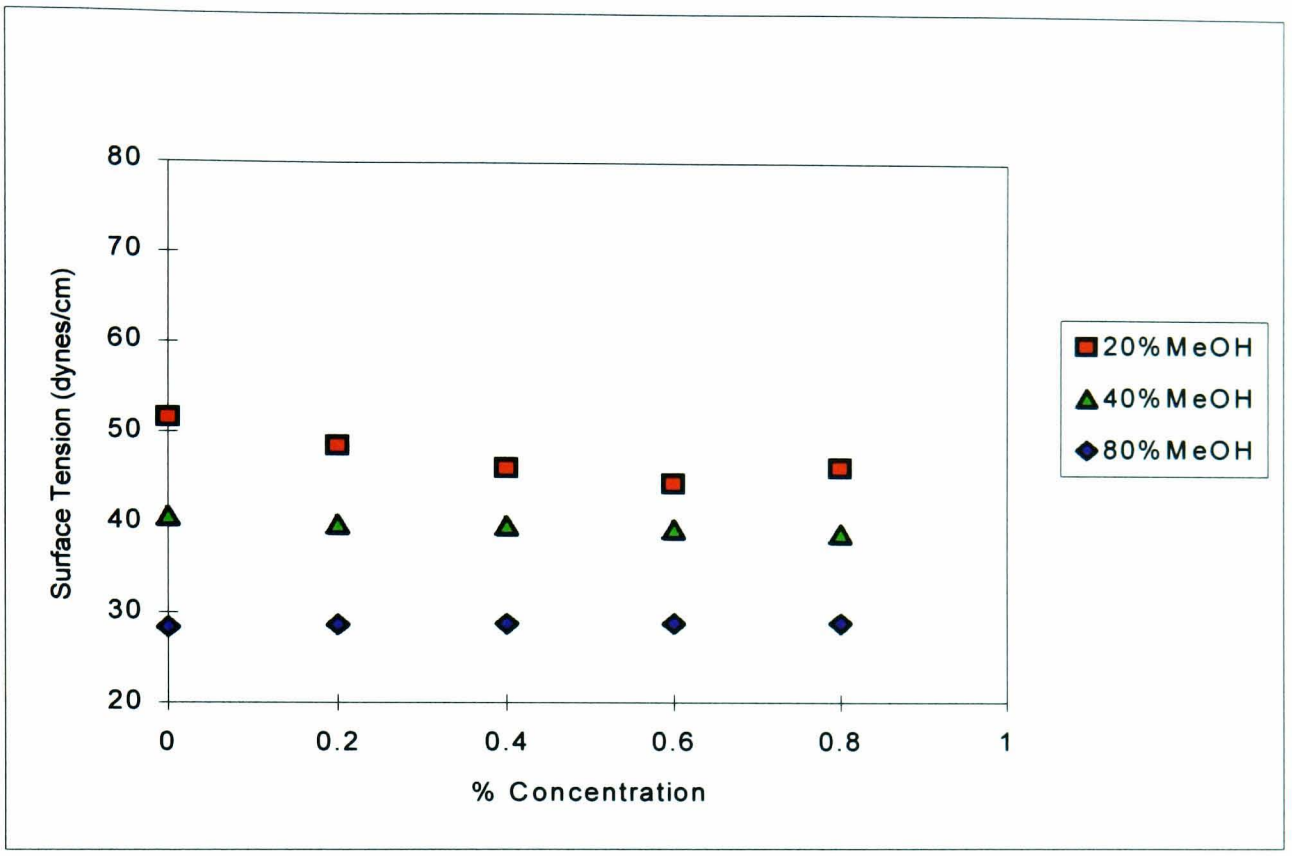

Fig 3.16

Variation in Surface Tension Measurment for Increasing Concentrations of Benzyl Alcohol in Methanol :Water

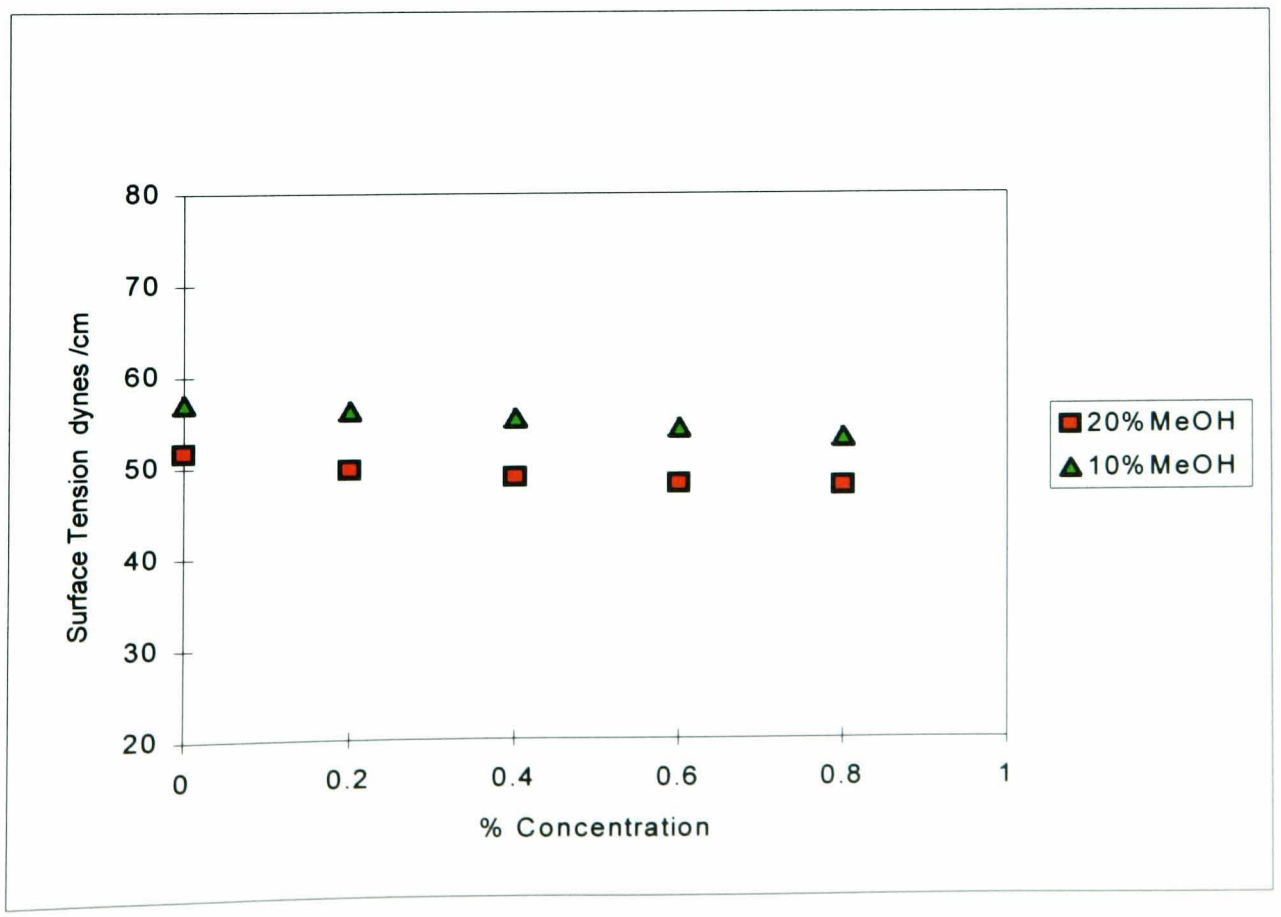

Fig 3.17

Comparative Plots for Phenol log k'_{LC} and k'_{ST} vs % Methanol

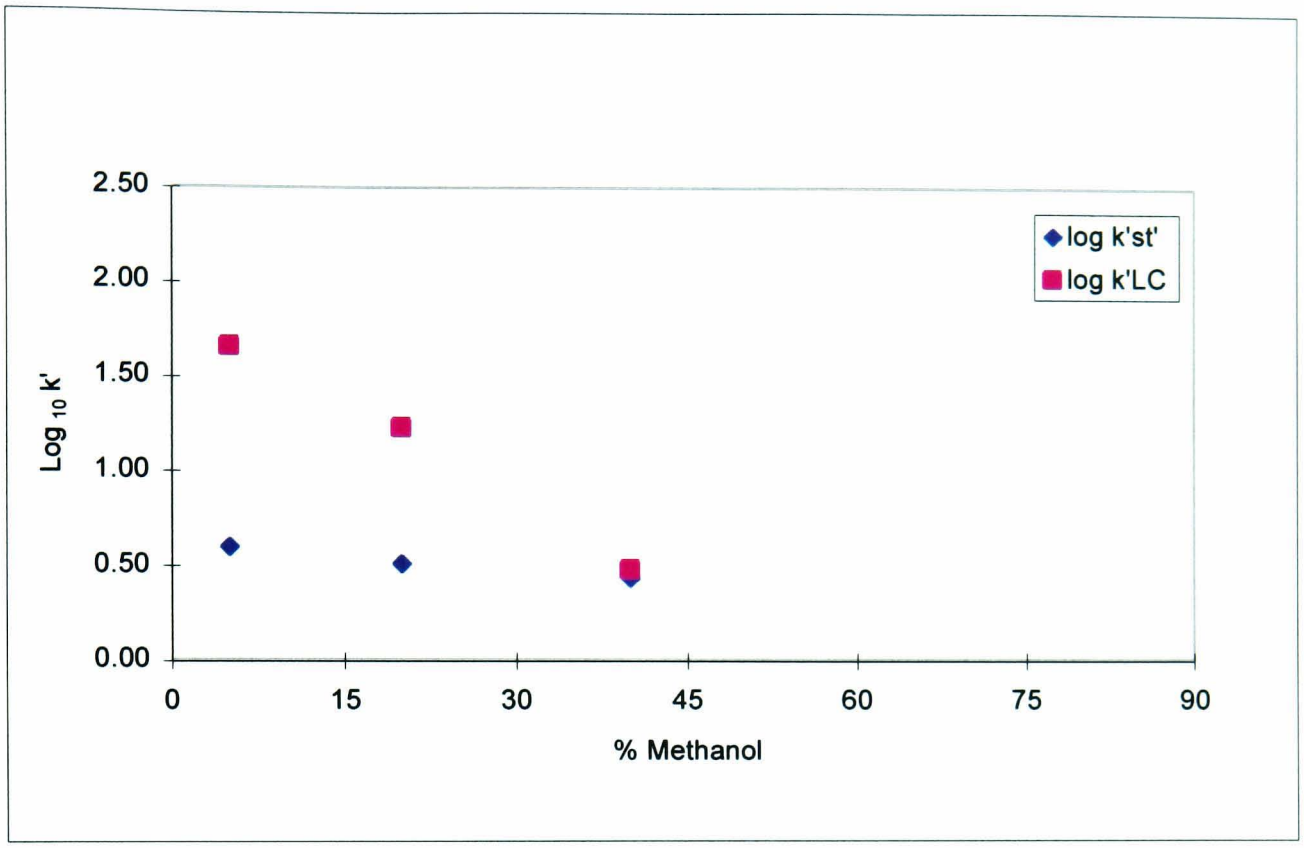

Fig 3.18

Comparative Plots for Aniline log k'_{LC} and k'_{ST} vs % Methanol

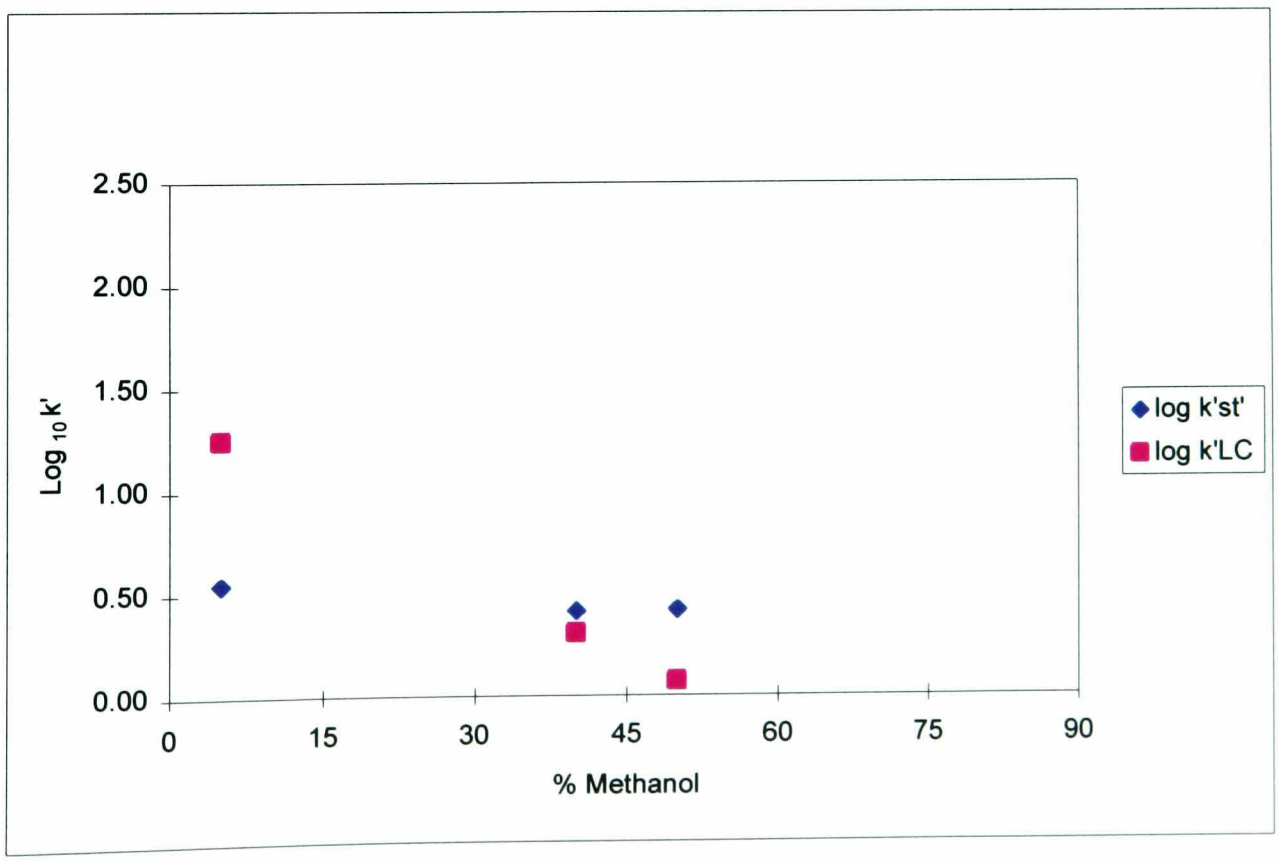

Fig 3.19a

Comparative Plots for Anisol log k'_{LC} and k'_{ST} vs % Methanol

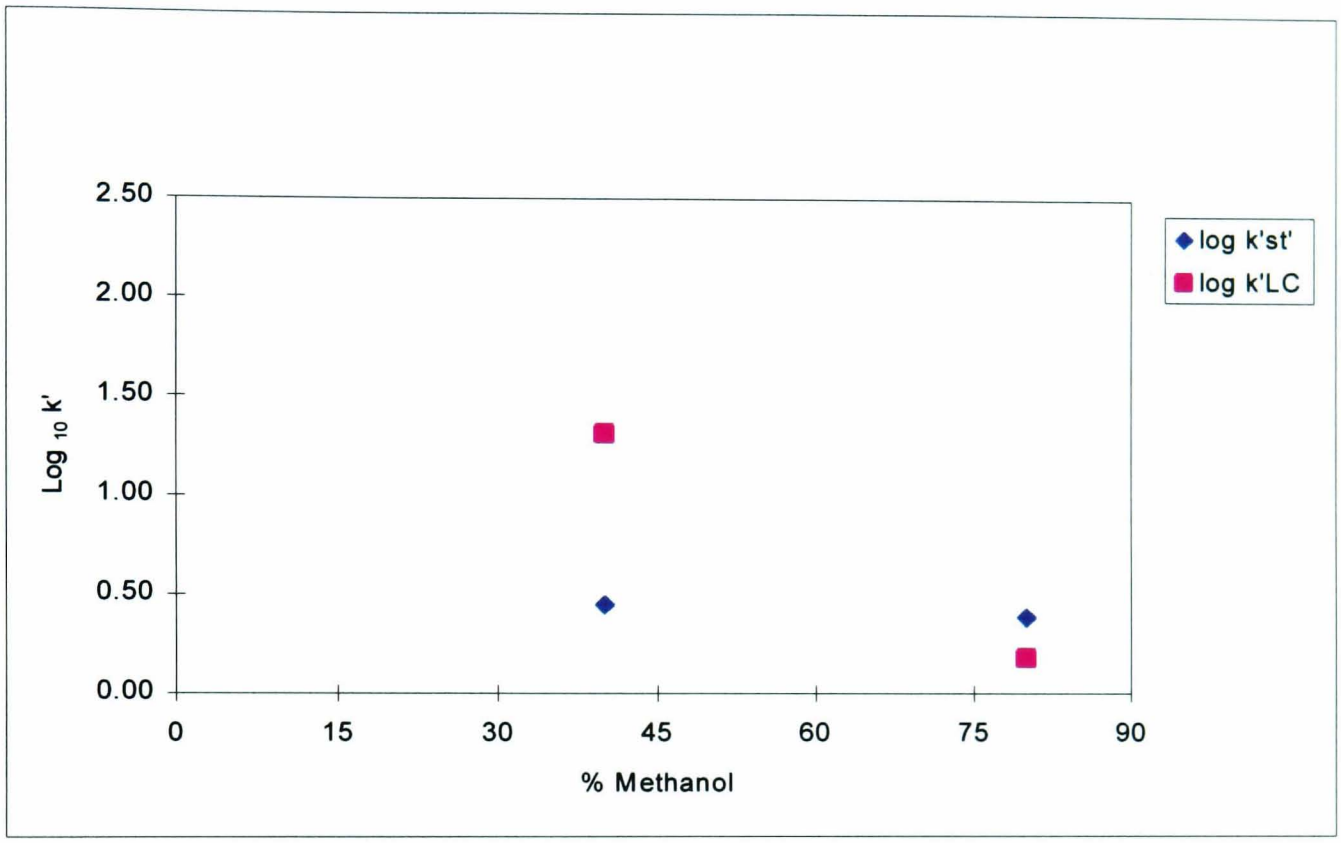

Fig 3.19b

Comparative Plots for 3,5 Xylenol log k'_{LC} and k'_{ST} vs % Methanol

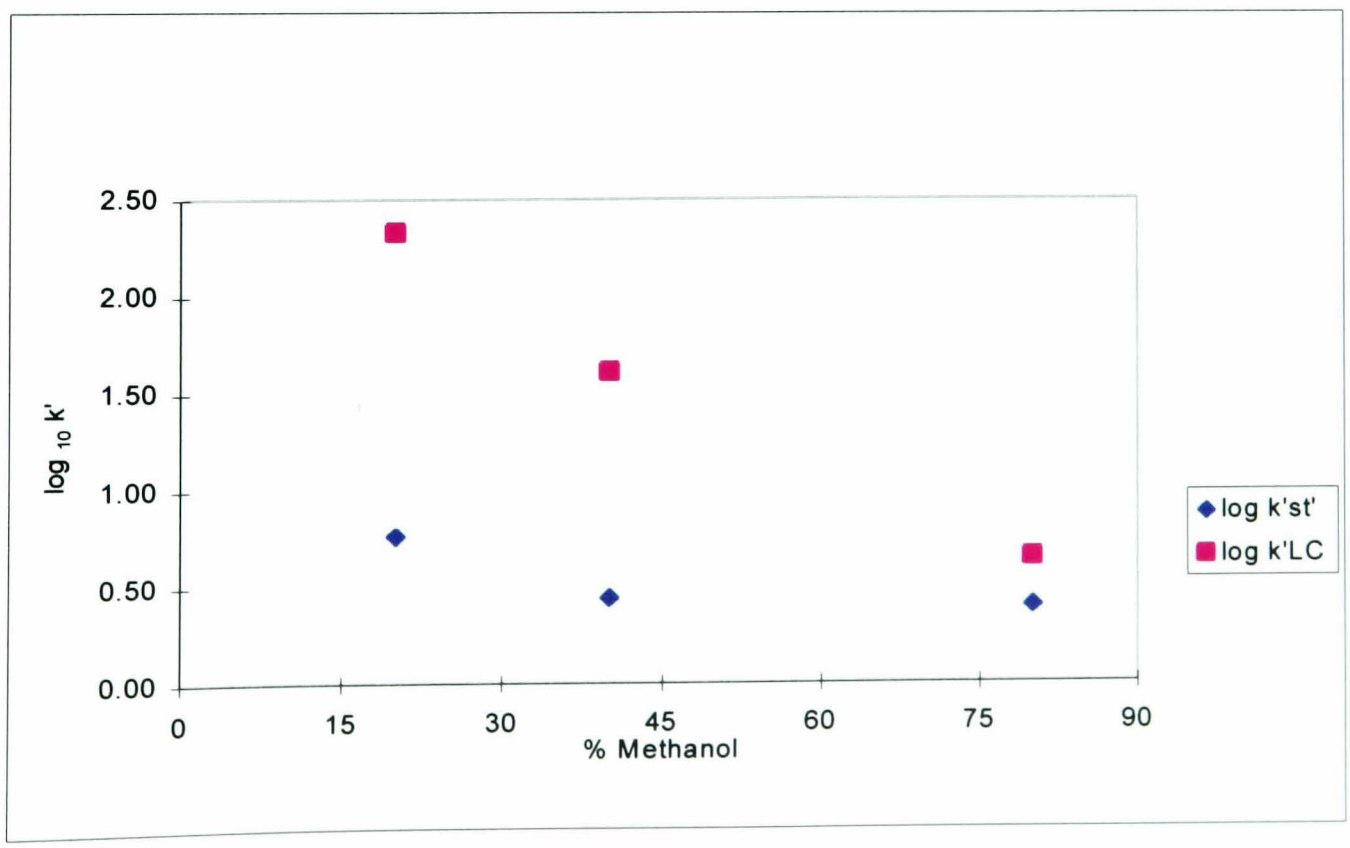

Fig 3.20
Comparative Plots for Benzyl Alcohol log k'_{LC} and k'_{ST} vs % Methanol

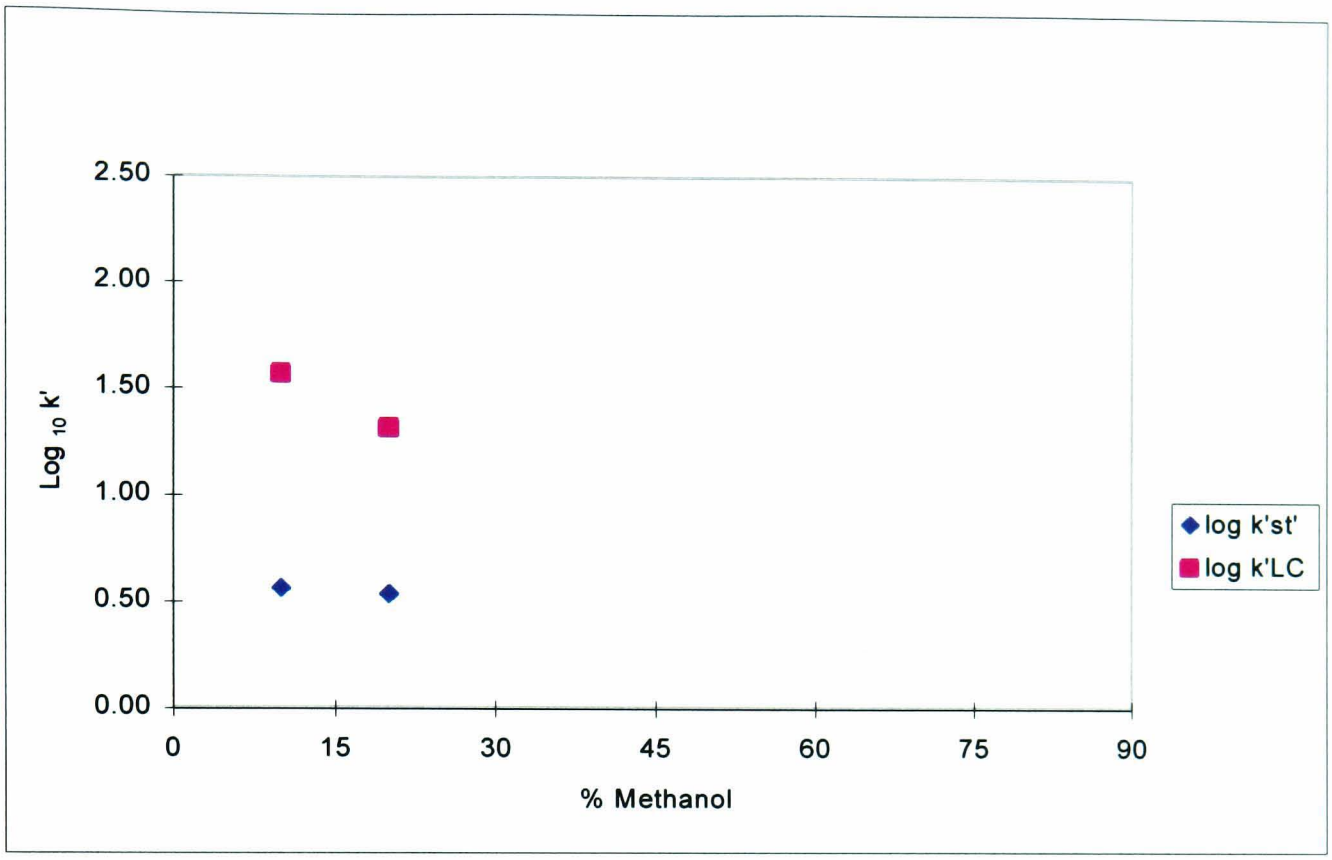

Fig 3.21
Comparative Plots for 2,6 Xylenol log k'_{LC} and k'_{ST} vs % Methanol

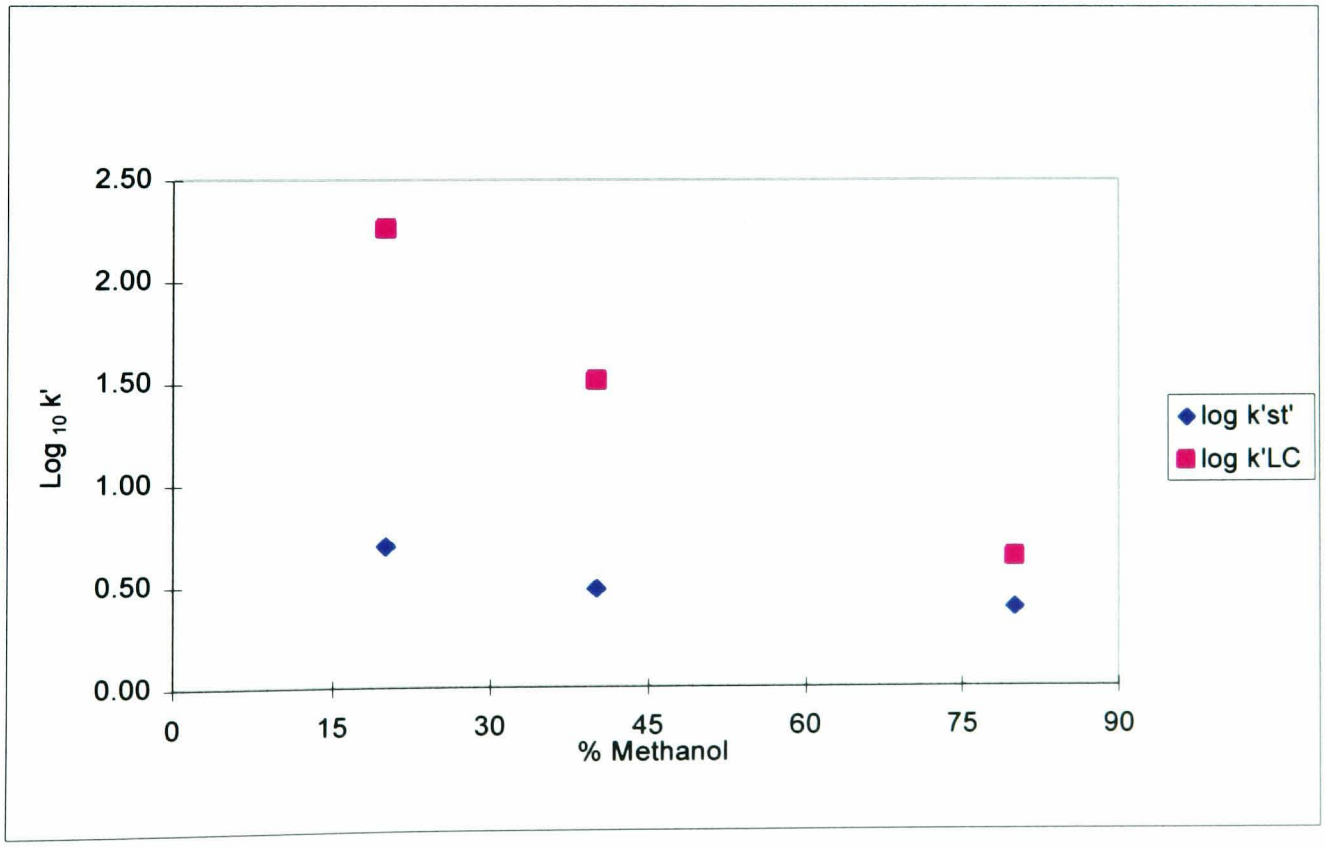

Fig 3.22
Plot of log k'_{LC} vs k'_{ST} data Feasibility study

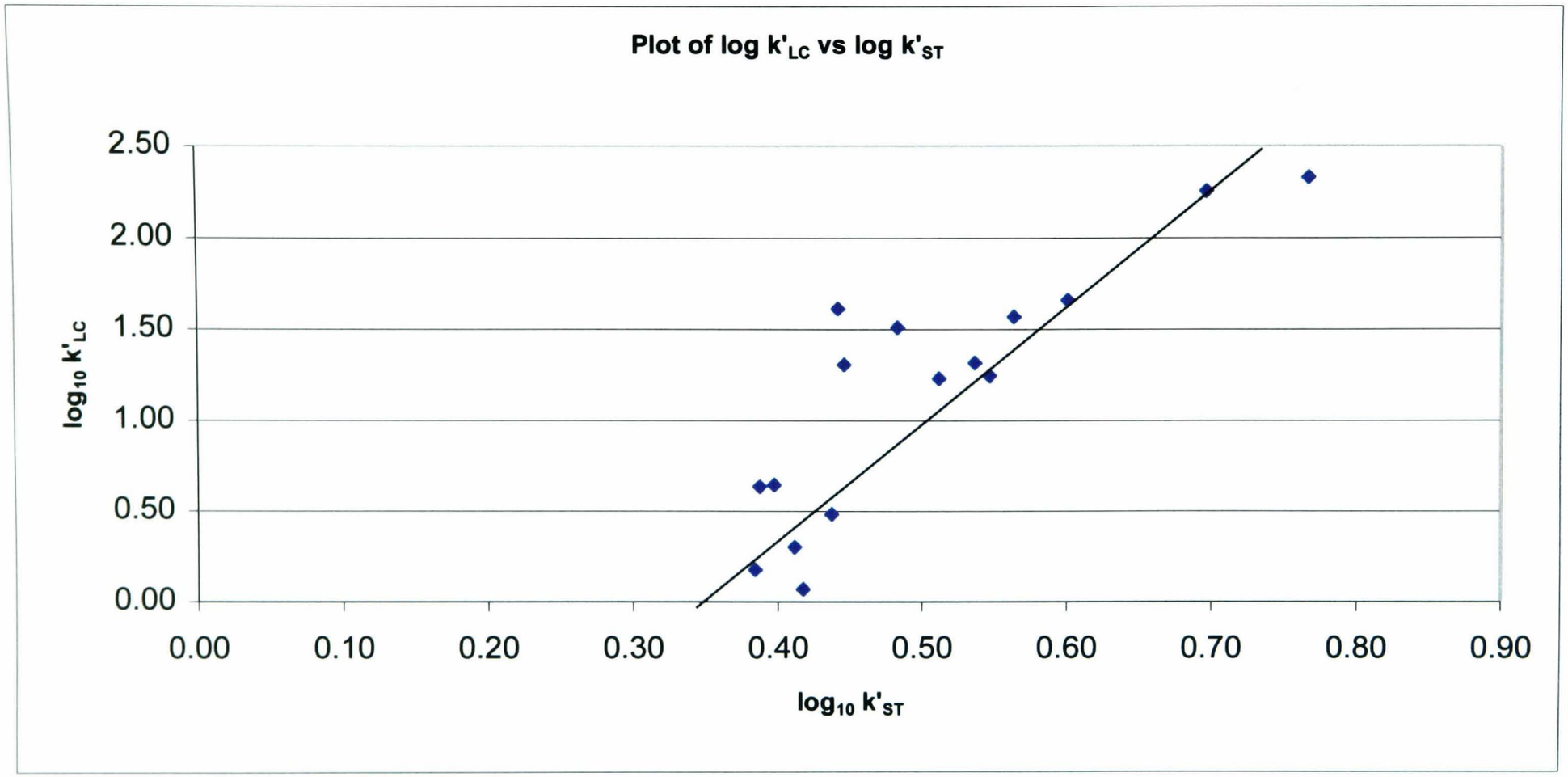

Gradient Approximately = 6

Fig 3.23

Variation in Surface Tension Measurement for Alkanol Concentration in Pure Water

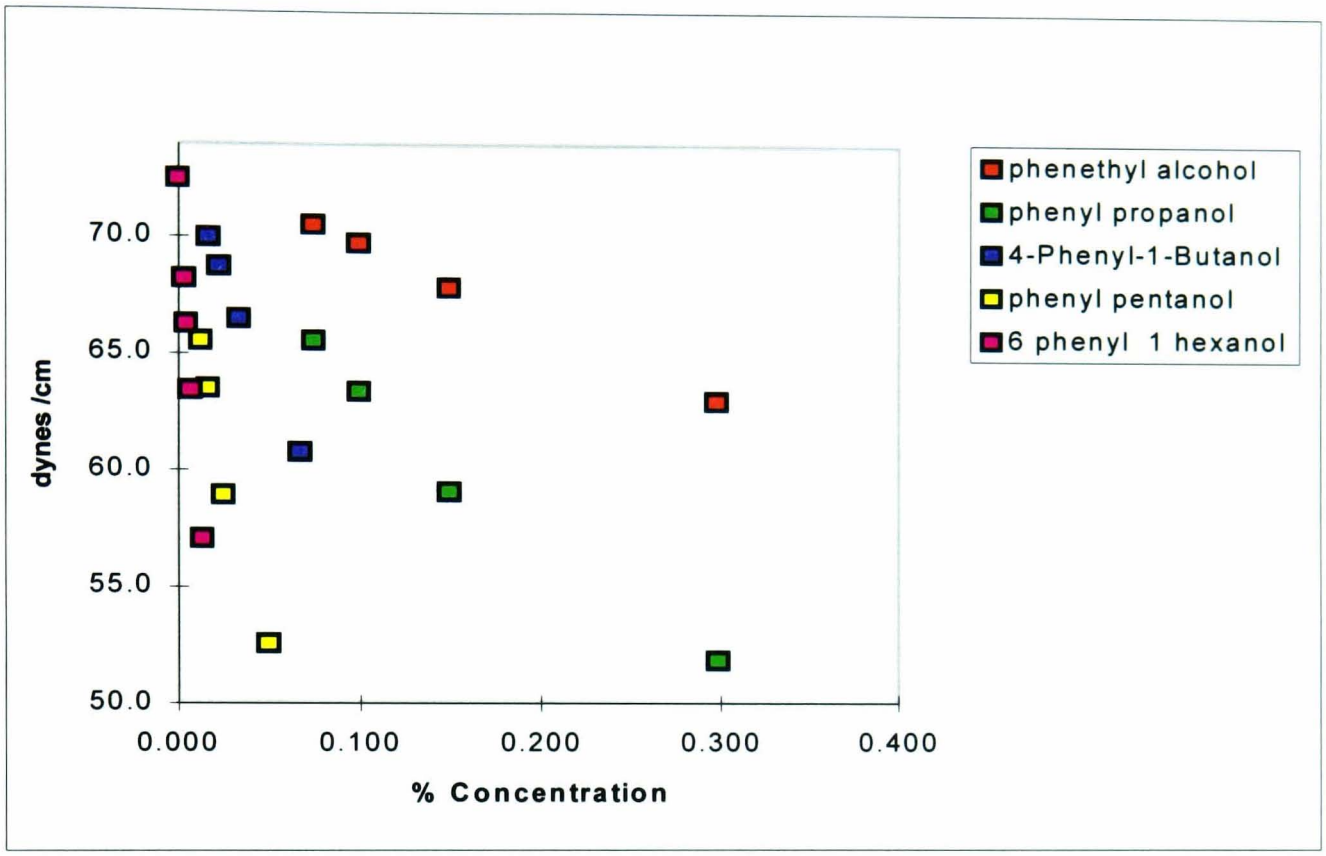

Fig 3.24

Comparative Plot of log k'_{LC} and k'_{ST} vs -CH_2- number in the Phenyl-Alkanol Side Chain.

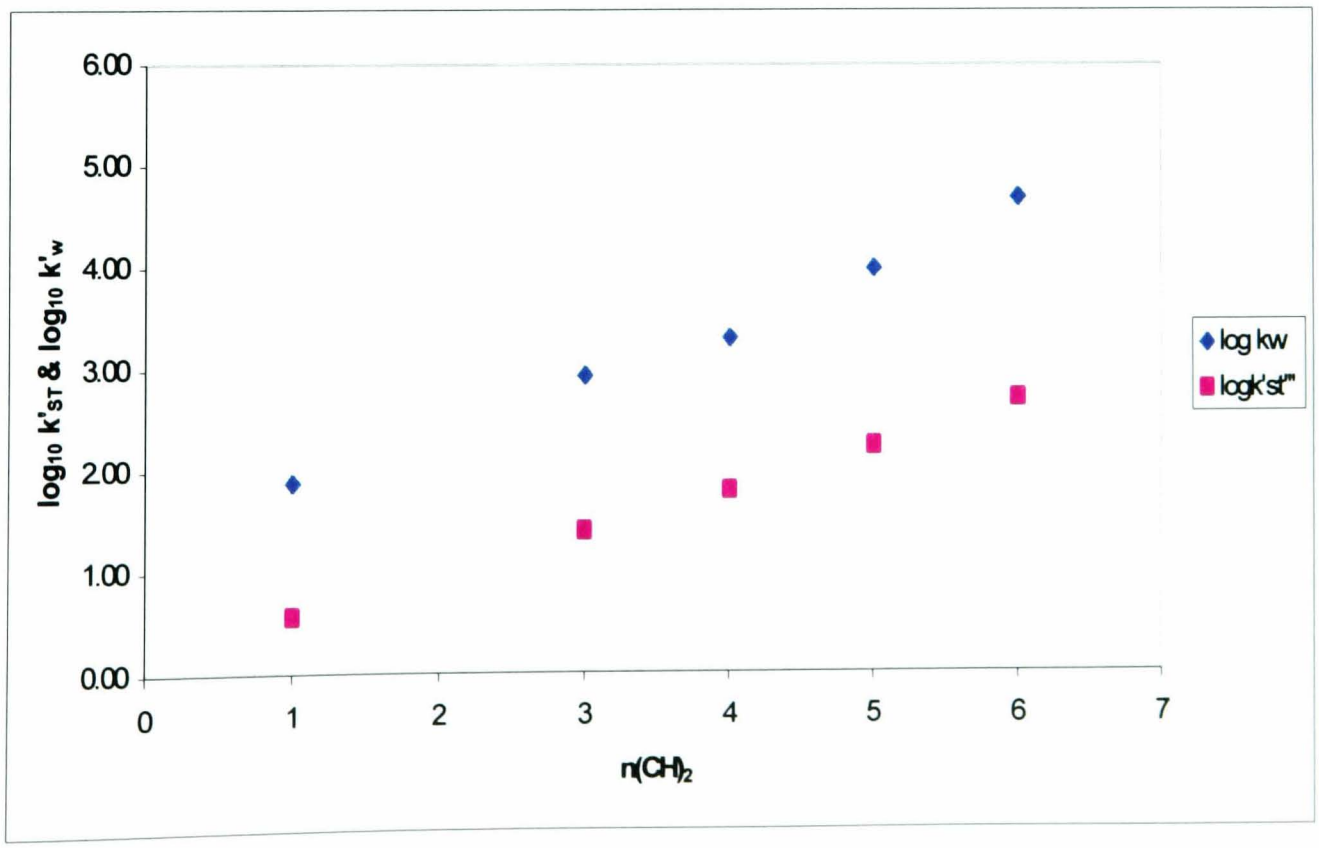

Fig 3.25

Variation in Surface Tension Measurement for Increasing Concentrations of Hydroxybenzenes in Pure Water

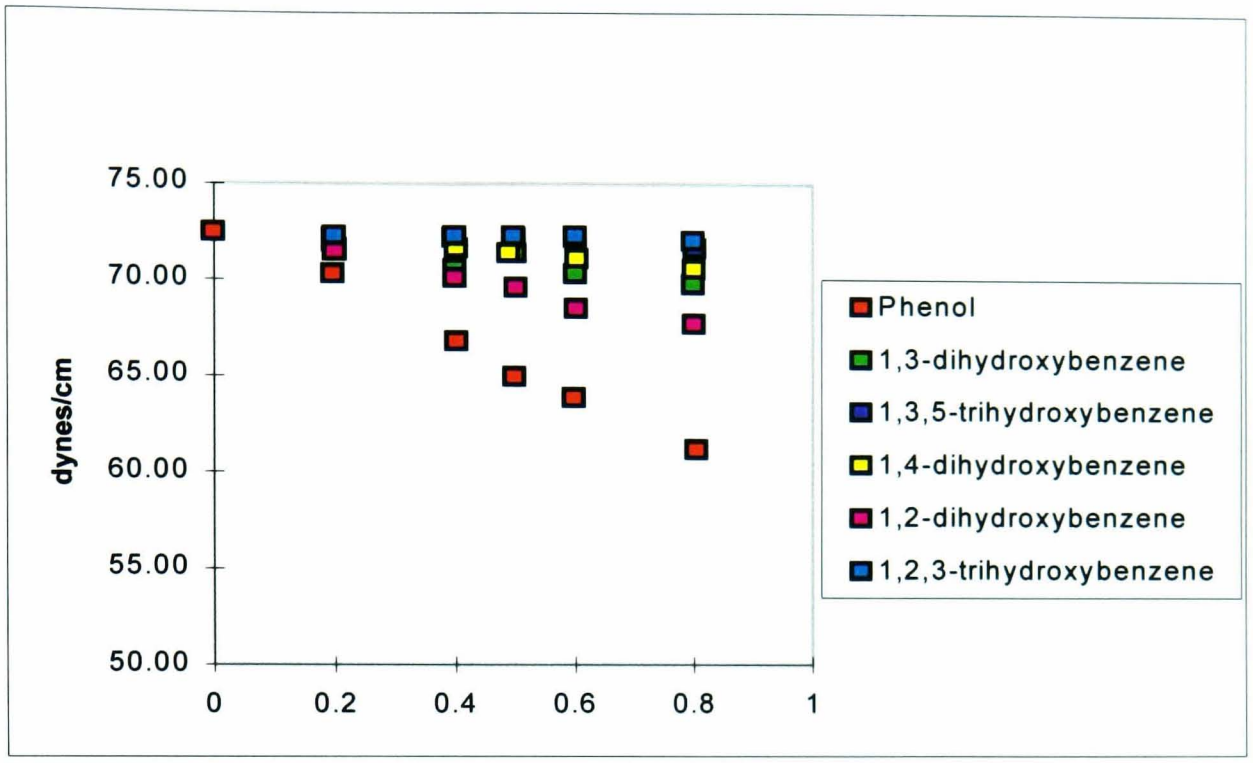

Fig 3.26

Variation in Surface Tension Measurement for Increasing Concentrations of Polysubstituted Carboxybenzenes in Pure Water

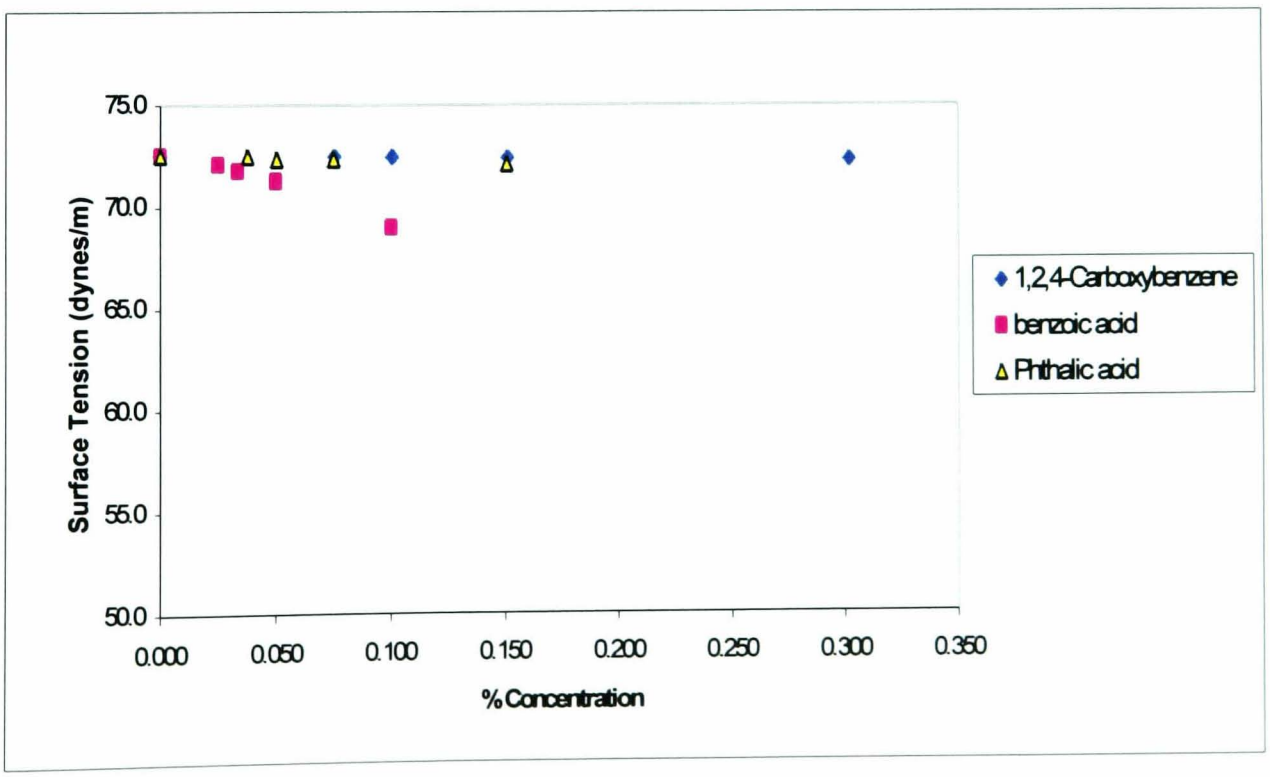

Fig 3.27
Variation in Surface Tension for Increasing Concentrations of Poly Substituted Nitrobenzenes in Pure Water

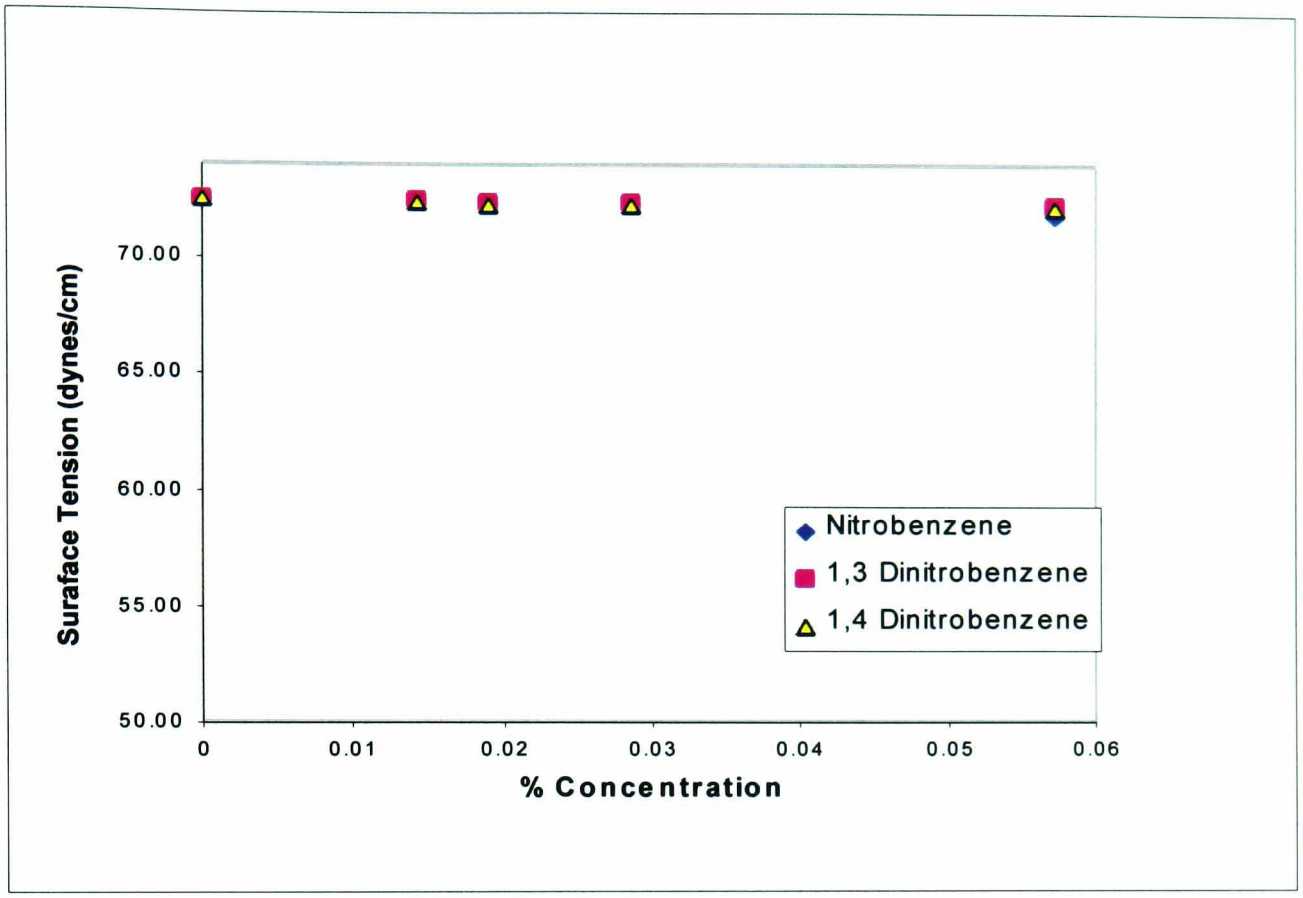

Fig 3.28

log k'_{LC} Phenylalkanols versus % Methanol

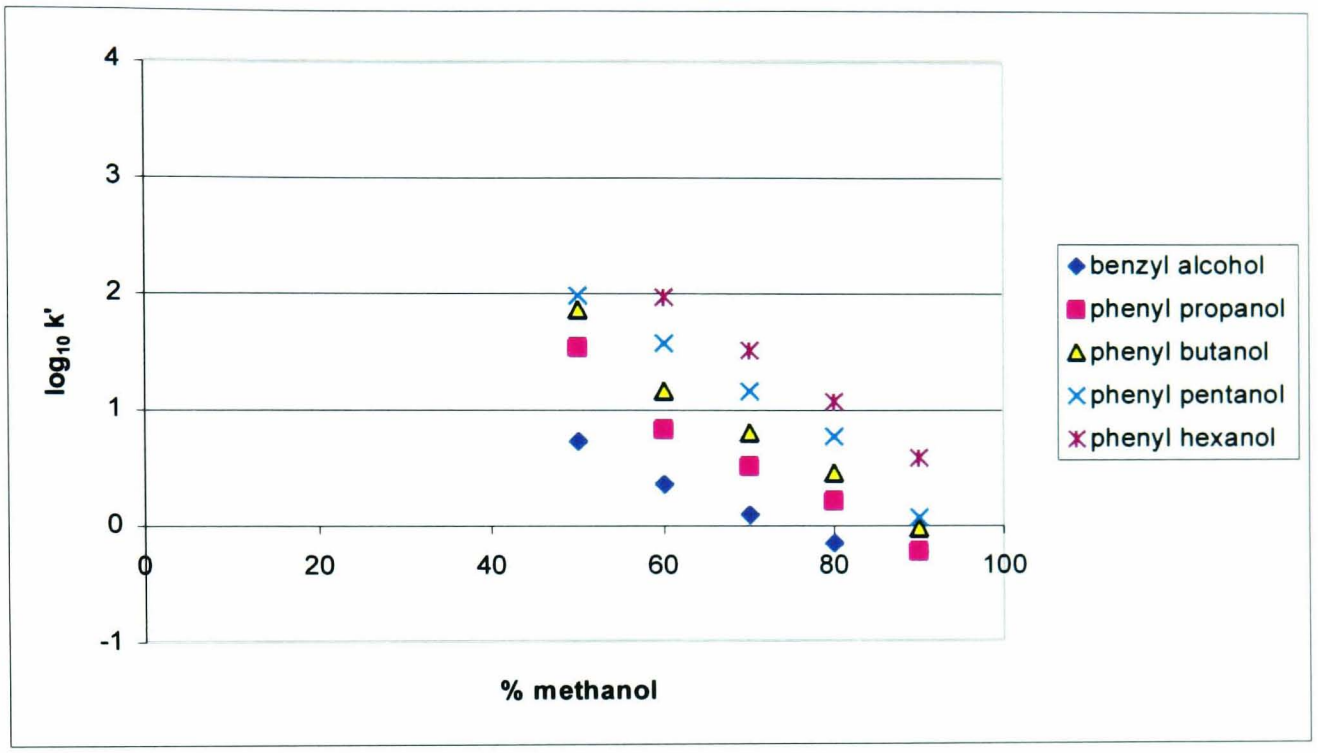

Fig 3.29

log k'_{LC} Hydroxybenzenes versus % Methanol

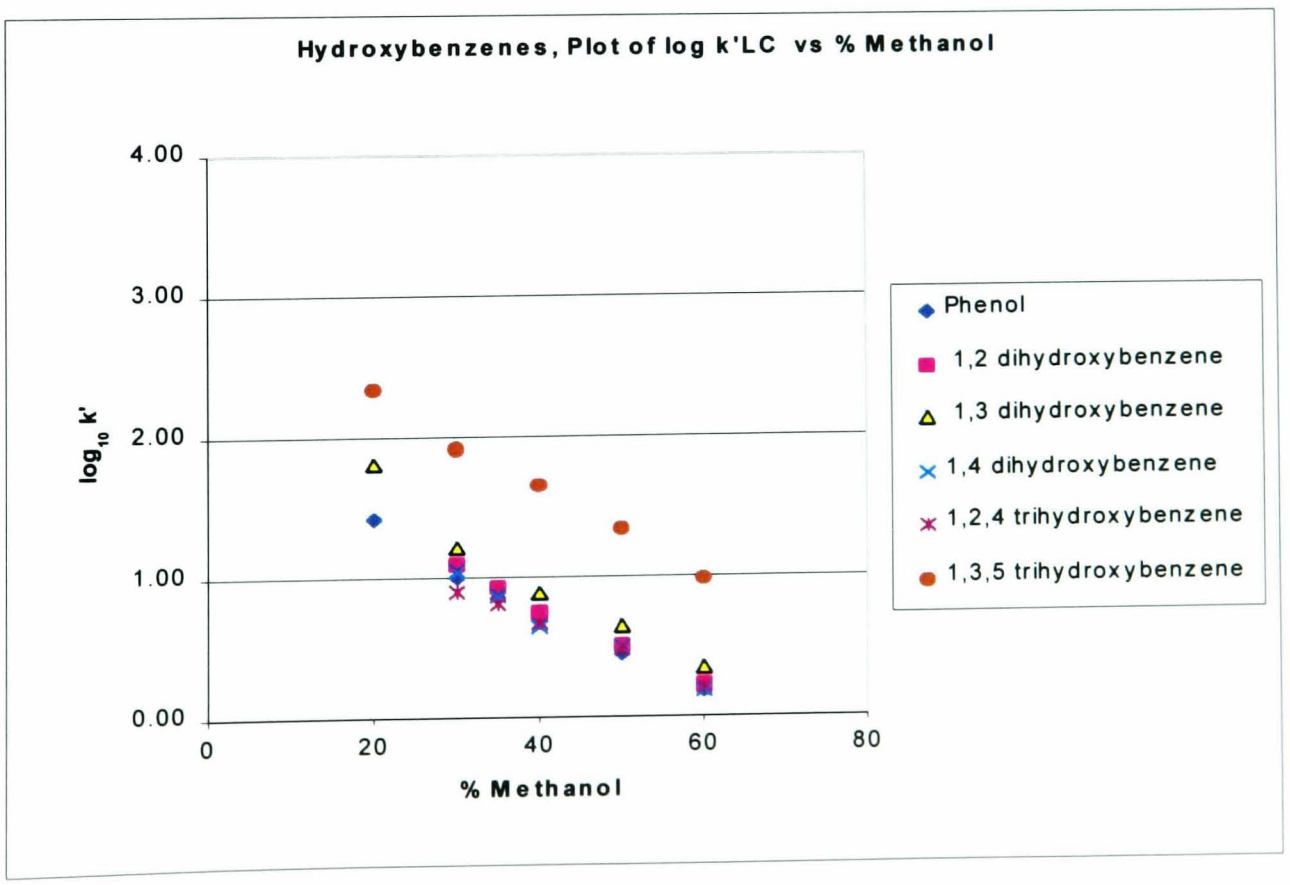

Fig 3.30

log k'_{LC} Carboxybenzenes versus % Methanol

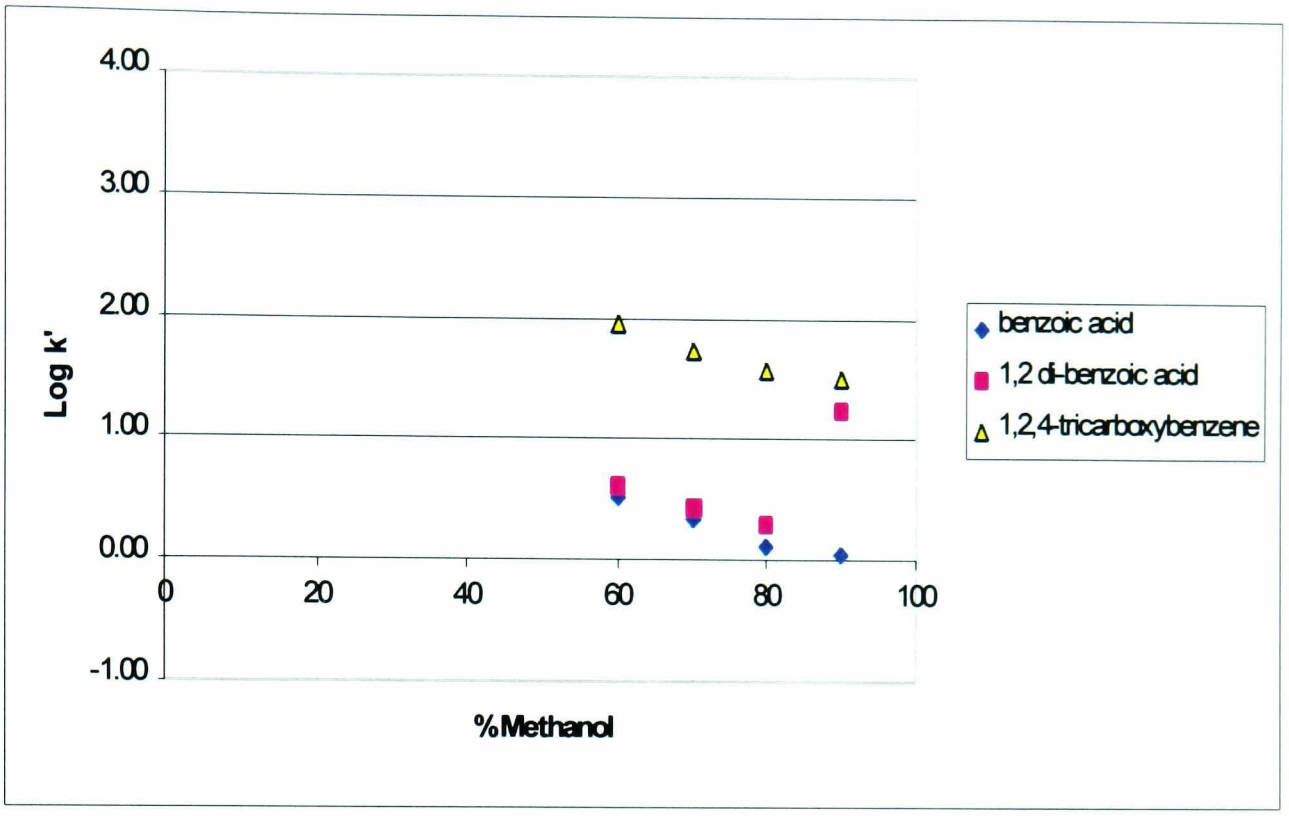

Fig 3.31

log k'_{LC} Nitrobenzenes versus % Methanol

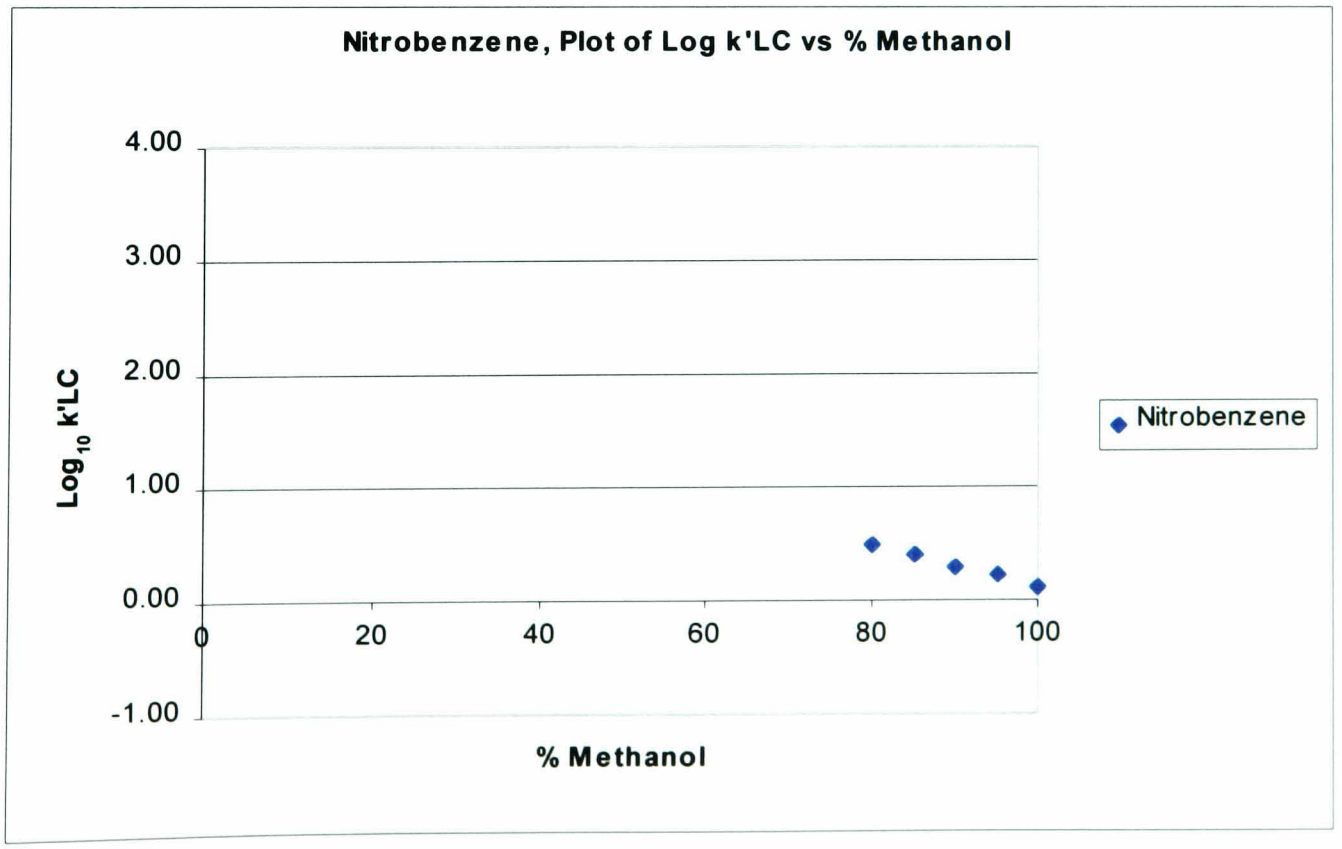

Fig 3.32

Plot of log k'_{LC} vs k'_{ST} for all Analytes in the Extended Study

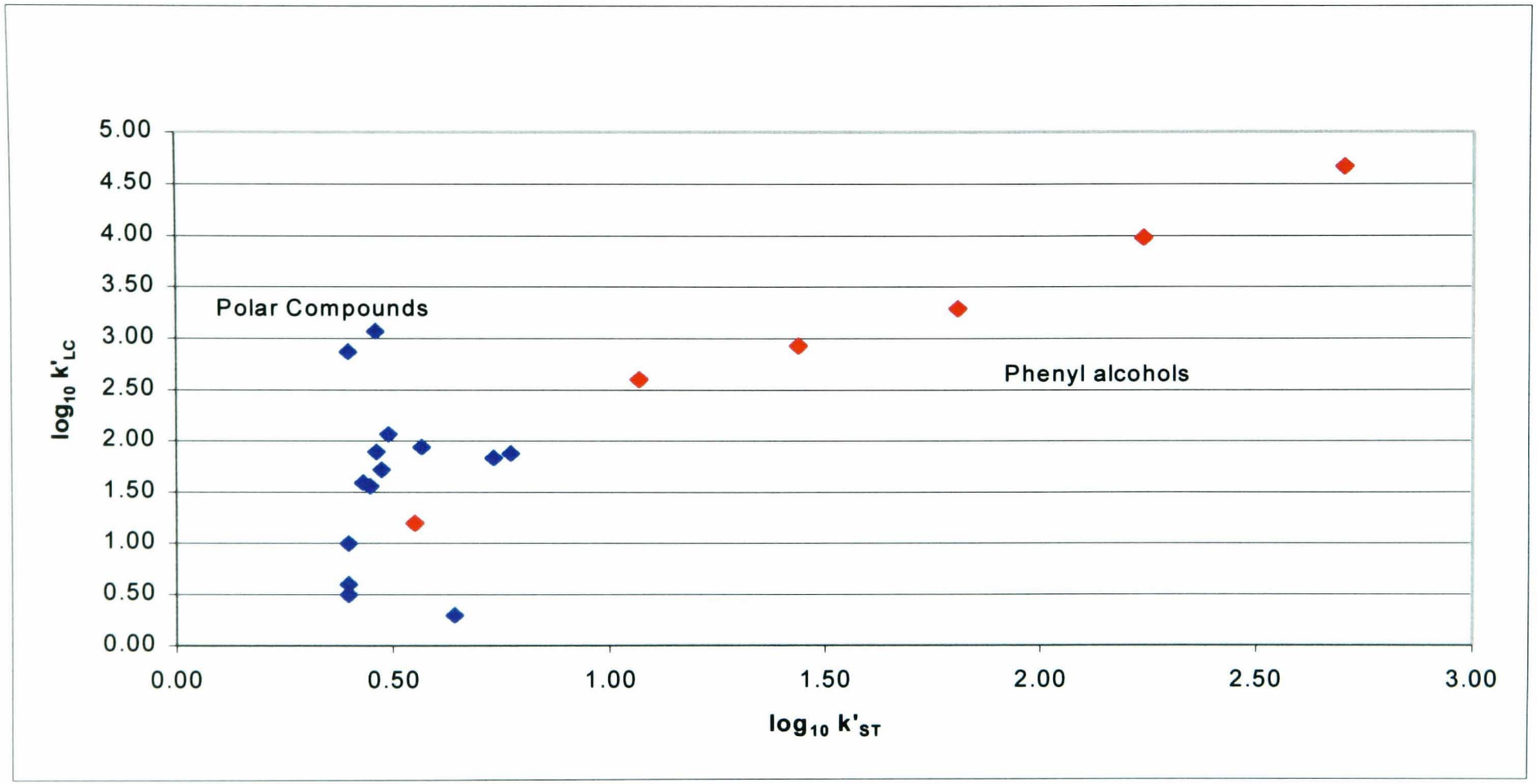

Chapter 4 – Coated PGC

4.1 Aim of the Chapter

The aim of this Chapter is to investigate the effect of coating the surface of PGC with various discrete molecules or polymeric molecules in order to determine what effect, if any, such molecules have on the strong hydrophobic effect or the unexplained polar retention effect of graphite (PREG). It may also prove possible to prepare a coated PGC, which will give similar selectivity and performance as a silica-based C18.

In order to do this it was necessary to determine which molecules would be most suitable for coating the surface of the PGC, and to establish an efficient technique for coating. Our initial objective was to coat the surface sufficient to mask the PREG, but insufficient to alter the porosity of the PGC to any great extent. For this reason, monolayer coverage of the surface was required. Adsorption isotherms provide a particularly sensitive and useful way of observing monolayer formation and adsorbate behaviour at the substrate surface. These isotherms therefore provide us with a useful technique to identify adsorbate molecules which might ultimately be used for our coating experiments.

Adsorption isotherm behaviour was discussed in Chapter 2 of the Thesis. For the benefit of this Chapter we now extend the discussion of isotherms and the information that they provide.

4.2 Adsorption Isotherm Theory (Continued from Chapter 2)

We recall that the basic theory of chromatography assumes Gaussian peak shape for a given analyte, provided there is a linear relationship between the concentration of the analyte in the stationary phase and concentration in the mobile phase. When the concentration is increased beyond this linear region, the peak shape usually shows a sharp front and extended tail. This behaviour is directly related to the adsorption isotherm where the plot of C_s *vs.* C_m, is concave to the C_m axis.

Adsorption isotherms take into account that the quantity adsorbed onto the adsorbent, q_s, is a product of the capacity ratio k' and the quantity of analyte in the mobile phase, q_m.

When the chromatographic peaks are Gaussian:

$$k' = q_s / q_m \qquad [4.1]$$

When the isotherm is concave to the q_m axis, the chromatographic peak is tailed. For any part of the tail, the k' value is given by:

$$k'_{tail} = dq_s/dq_m \qquad [4.2]$$

For any part of the front, the k' value is given by Equation [4.1] *i.e.*:

$$k'_{front} = q_s/q_m \quad = C_sA_s/C_mV_m \qquad [4.3]$$

Equations [4.2] and [4.3] are illustrated in Figures 4.1 and 4.2. If a series of elution profiles are measured for different analyte concentrations it is possible to build up a picture of the complete isotherm, Figure 4.2. Isotherms built up in this way normally follow what is called the "breakthrough method."

The procedure involves passing a mobile phase that contains a known concentration of analyte C_m through the column containing the support media. The retention volume is measured at the midpoint of the front of the analyte breakthrough elution profile as it passes through the detection system $V_{breakthrough}$. The term q_s is then calculated from:

$$q_s = (V_{breakthrough} - V_m).\ C_m$$

q_m is given by C_mV_m hence k' is calculated for any value of C_m. The plot of q_s *vs.* q_m is then the described isotherm.

It is critical that the system is completely flushed and all traces of analyte removed from the media surface before a new analyte concentration is passed through the column. The breakthrough volume is then measured in the same way. The process is repeated for approximately ten different concentrations, which will cover the breadth of the adsorption isotherm. Correction factors must of course be made for the volume of solvent between the end of the column and the detector system. For our experiments this volume was found to be 0.014mL.

The initial gradient (slope) of the isotherm gives a clear indication of the strength of adsorption onto the stationary phase. The steeper the slope the greater the adsorption and the lower the concentration at which monolayer coverage is reached, *i.e.* the point at which no further change of q_s occurs for increasing q_m. This is useful information since our

purpose is to identify molecules that may be suited towards forming stable coatings on the surface of PGC.

Furthermore, if Langmuir behaviour is observed, a linear plot of $1/q_s$ *vs.* $1/q_m$ will allow us to determine the surface concentration of analyte for monolayer coverage. We recall from Chapter 2 that Langmuir behaviour occurs where every surface adsorption site is equivalent, and the ability of molecules to bind there is independent of whether or not the neighbouring sites are occupied. In theory C_m must be infinite to get monolayer coverage. In practice, this represents about 90 - 99% coverage. The intercept gives us q_s, the surface concentration for monolayer coverage. The quantity of an adsorbed molecule required to give monolayer coverage provides us with further information concerning the orientation of analyte molecules at the surface interface. For example, the quantity may be lower for a molecule that lies flatly against the PGC surface compared to one which approaches the surface end-on. These are all-important parameters that need to be determined before starting our coating experiments. We therefore now discuss a series of preliminary experiments designed to investigate the adsorption of different types of adsorbate molecule on the PGC surface. We then use the information gained from these experiments to choose a range of coating compounds which will help to achieve our real aim, which is to investigate and compare the chromatographic retention properties of the coated PGC to that of uncoated PGC.

4.2.1 Adsorption Isotherms on PGC

Two types of molecule were investigated, flat molecules, such as the polyaromatic hydrocarbons, and those that contain a high degree of aliphatic character, such as cetylpyridinium bromide. Dias[1] has shown that adsorption onto graphite in gas chromatography (GC) was determined largely by the molecular area of the analyte ("footprint") in contact with the PGC surface. The greater the molecular area the greater the adsorption to the surface. Bassler, *et al*[2] has shown similar correlation of molecular size for analytes retained on PGC. We therefore investigate molecules that (a) have a rigid, flat structure or (b) have a three-dimensional structure, but can still spread out along the surface. In order to observe the retention behaviour by UV detection, we have chosen molecules that possess some aromatic character (UV-absorbing). We also assume that this will not interfere with the general behaviour of these molecules at the surface of the PGC.

The analytes chosen for our adsorption isotherm studies are listed in Table 4.1, along with their abbreviated descriptor which is used throughout the remainder of this Chapter. The structures for these compounds are given in Figures 4.3 and 4.4 along with the relevant molecular weights.

4.2.2 Experimental Detail

4.2.2.1 Breakthrough Adsorption Isotherms

"Breakthrough adsorption isotherms" refers to a chromatographic method for the determination of an adsorption isotherm of an adsorbate onto a chromatographic support. The procedure involves pumping a solution of the adsorbate through the column until it breaks through the bed. That is, until the adsorbate is observed eluting from the column by the detector. The column is then washed with pure eluent to remove all adsorbate. The procedure is then repeated with a higher concentration of adsorbate. The full experimental procedure is given below.

1. The pump, column and detector are primed with HPLC grade solvent (dichloromethane) and the detector zeroed at a wavelength of 254nm.
2. The column is disconnected at its pump end, and the system, pump and tubing are flushed with the first mobile phase containing the initial concentration of adsorbate. The pump and tubing are then reconnected to the top of the column. The system from

column to the detector is still primed at this stage with clean dichloromethane and has not yet received the adsorbate.

3. The pump is started, simultaneously starting the chart recorder.
4. When the breakthrough of the adsorbate is observed and the plateau reached, that is, no further increase in concentration is observed, the pump and recorder are stopped. The column inlet is disconnected and the pump system flushed with clean dichloromethane. The pump is then reconnected with the column and the column is flushed with dichloromethane until the detector zero base line has been reached. At this point, all of the adsorbate has been washed from the column.
5. The above procedure is then repeated with each new mobile phase concentration.

4.2.2.2 Calculations for Breakthrough Experiments

Each breakthrough experiment has a series of calculations carried out on the experimental data. The data is presented in Table 4.2. A full breakdown of the calculations used to describe the degree of coverage is given in Table 4.2b. These calculations provide the data with which the adsorption isotherms in their linear and non-linear forms can be plotted. Column 6 in each Table refers to the 'pump correction factor.' This is described in greater detail in the following paragraphs.

Once the column is primed with each new mobile phase concentration, it is then reconnected and the pump switched on, and the recording of the elution profile commences. However when the pump is started it takes several minutes to reach the required flow rate, *i.e.* as the pressure required to force the solvent through the column system builds up. During this first few minutes the pump is therefore not delivering its full 1mL/min flow rate.

4.2.2.3 Correction Factors for Measuring the Adsorbate Retention Volume During the Breakthrough Experiments

In order to correct the retention volume recorded for each elution profile, the solvent flow profile was measured over the first 10 minutes after start up. This involved weighing the solvent collected at the detector outlet as it emerged and then recording the weight of solvent collected at one minute intervals. The weights were converted to volumes by taking into account the density of the solvents used (0.6872g/mL for hexane and 1.3266g/mL for dichloromethane).

These figures were then plotted as volume collected *vs.* time (see Figure 4.5). The data for each elution profile were then corrected accordingly. The retention volume figures given in column 9 of Table 4.2 include this correction.

4.2.3 Results and Discussion of Results for Adsorption Isotherms on PGC

Tabulated data for all adsorption isotherms data can be found in Table 4.2. Plots for the adsorption isotherm data can be found in Figures 4.6 a-e.

The isotherms observed for naphthalene, anthracene and pyrene (Figures 4.6a, and 4.6b and4.6c) are in good agreement with Langmuir-type behaviour. This is confirmed by the linearity of the plot of $1/q_s$ *vs.* $1/q_m$ in Figures 4.7 a-c. At high values of $1/q_m$ however, some deviation from linearity was observed perhaps suggesting a small number of secondary adsorption sites (Fig 4.7 d). These points were not used when the data was extrapolated to give the value at the intercept.

In most cases the isotherm data for the polyaromatic hydrocarbons is in good agreement with predicted values of surface coverage based on calculations using the molecular area (calculated from the molecular volume). The data is shown in Table 4.3. However, the surface coverage for cetylpyridinium bromide and dodecylbenzene sulphonate sodium salt are more than twice the expected values. Pyrene shows the most significant degree of adsorption, having the steepest gradient for the plot of q_s *vs.* q_m, and reaching monolayer coverage at the lowest concentration. The results are in good agreement with Dias[3] and Mockel[4] who reported that adsorption increased with molecular area. The q_s for monolayer coverage is 3.0, 2.0 and 1.42 μmol/m^2 for napthalene, anthracene and pyrene, respectively. The predicted values for coverage give 2.08, 1.48 and 1.23μmol/m^2 based on analyte molecular areas. The observed surface coverages are therefore somewhat higher than the predicted values. However if we allow for the error involved with the extrapolated $1/q_s$ value, the results are in fairly good agreement with predicted quantities required for monolayer coverage.

The results with these flat molecules therefore suggest that a large molecule like decacyclene would be very strongly adsorbed to the PGC, and would offer increased coating stability over a two-, three- or four-membered ring molecules. Such a molecule may also prove useful as an anchor for future coated PGC supports.

The dodecylbenzene sulphonate and cetylpyridinium bromide isotherms (Figures 4.6 e-f) show similar type behaviour to one another in that both isotherms are much flatter in appearance than the polyaromatic hydrocarbons. Consequently, the constant value for q_s becomes much more difficult to determine. The concentration required to reach monolayer coverage is also surprisingly high. The q_s for monolayer coverage is 2.0μmol/m² for both dodecylbenzene sulphonate and cetylpyridinium bromide, while calculated values give 0.83 and 0.76μmol/m². Plots of $1/q_s$ *vs.* $1/q_m$ are given in Figures 4.7d and 4.7e. These results suggest that this type of molecule:

a) starts to form secondary and tertiary layers at the PGC surface, and
b) does not lie flatly on the PGC surface.

For example, the pyridine group in cetylpyridinium bromide is preferentially adsorbed causing the alkyl chain to stand up in a brush-like formation. At low concentrations the alkyl chain may lie flatly on the surface initially but that as the concentration of the analyte is increased it becomes displaced by the pyridine. A similar argument can be made for benzene sulphonic acid functionality of the dodecylbenzene sulphonate.
Linear plots were obtained for $1/C_s$ *vs.* $1/C_m$ for each of the adsorbates (Figures 4.7 a-e), confirming Langmuir-type behaviour.

The values of $1/q_s$ were determined from the plots of $1/q_s$ *vs.* $1/q_m$ by extrapolation of the data to the $1/q_s$ axis. The error involved with this value is approximately 0.15, which gives rise to an overall error for q_s of $\pm$20μmol/g.

The calculated values for surface coverage assumes that the molecules lie in a closely packed, well-ordered arrangement without gaps between the molecules. Molecular areas are calculated from the molecular volume of each adsorbate. An example of the calculation is given in Table 4.3b.

In reality, the actual organisation of the molecules deviates from this ordered arrangement, and agreement between experimental and predicted values for surface coverage suffers as a result. For example there are likely to be gaps between the molecules on the surface and so we might have expected our experimental results for $1/q_s$ to be slightly lower than those predicted. Experimental values might be higher than predicted values when preferential adsorption of different parts of the adsorbed molecule occurs, or where there is overlap of

these molecules. This may explain why we see a considerable difference between predicted and experimental coverage for both cetylpyridinium bromide and dodecylbenzene sulphonate.

4.3 Coating Experiments on PGC

The experimental work can be divided into three sections:

1) Coating methods
2) Chromatographic characterisation of coated PGC
3) Physical characterisation of the coated PGC

Before discussing each of these areas in detail, we first give an overview of the experimental approach and give reference to the data Tables and corresponding Figures which were obtained.

4.3.1 Overview

While Wan's work[5] was directed at the modification of PGC by coating to provide alternative modes of chromatography, such as ion exchange or chiral chromatography, our objective is to determine the extent to which the strongly hydrophobic properties and charge-dependent properties associated with PREG could be modified by coating. In so doing it was hoped that information regarding the mechanism of retention could also be obtained. In addition it was considered possible that a phase with similar chromatographic selectivity to that of a C18-silica, which is the most commonly used in liquid chromatography packing material, might be developed. This would be advantageous since retention behaviour would be predictable and such a phase would also be alkali-resistant, as aspect where the C18-silica is deficient.

However it was thought useful to begin our coating experiments by repeating some of the experiments carried out earlier by Wan. We first coated the PGC with the derivatized amino acid naphthylsulphonyl L-phenylalanine, for the separation of chiral amino acids. Secondly we coated the PGC with polyethyleneimine to act as a weak anion exchanger. Both experiments were successful, yielding coated PGC that functioned for the designed chromatographic modes.

The following molecules were chosen to begin a more detailed study of coating larger molecules onto the surface of graphite:

Pyrene, Squalane, Polystyrene, Polyphenylglycidylether, Decacyclene

The structural information and molecular weights associated with each molecule are given in Figure 4.8. The range of molecules selected includes both discrete and polymeric molecules. Discrete molecules, such as pyrene and decacyclene, will lie very flatly against the surface of PGC and are strongly adsorbed. Squalane, because it contains no functionality that might give rise to anything other than dispersive interactions, was expected to mimic typical C18-silica behaviour. The polymeric molecules polystyrene and polyphenylglycidylether offer progressively more polar character and three dimensional structure increasing the likelihood of a different analyte interaction to that of the same analyte with the PGC surface.

Coating Methods

Several methods of coating the PGC surface were investigated. They are discussed in detail in the next sections, but generally fall into two categories: Dynamic (sequential and breakthrough) and Evaporative.

Dynamic coating method – In this method, a column packed with uncoated PGC is coated either by pumping a mobile phase containing the adsorbate molecule through the column (dynamic-breakthrough), or by sequentially injecting fixed volumes of adsorbate onto the column (dynamic-sequential). The adsorbate loading is monitored by the selectivity and retention changes for a given test mixture. Once consistency (no change in selectivity or retention upon injection) is observed, breakthrough or maximum load of the adsorbate molecule has been reached.

Evaporative coating method – In this method, the surface of the PGC is coated with the adsorbate by mixing a known weight of PGC with a solution containing a known weight of adsorbate. The solution is evaporated by rotary evaporation, depositing the adsorbate on the surface of the PGC. The coated PGC is then packed into the column following the method set out in Chapter 2.

The dynamic breakthrough coating method was the initial method of choice since it offered a relatively simple method of coating onto efficiently packed columns. It was felt that the packing of previously coated PGC might prove difficult due to the effect of the coating on

the particle's dispersion and suspension properties in the slurry solvents. Determination of the correct packing procedure for a new material can often be time consuming and laborious with the added possibility that with a coated material some of the coating might be washed from the column.
A summary of the quantities coated onto the PGC columns using the dynamic breakthrough coating method is given in Table 4.4.

With the exception of polyphenylglycidylether (PPGE), the coating compounds behaved similarly to the compounds used in our isotherm studies, giving rise to monolayer coverage at approximately 25-30mg coating compound per gram of PGC. The reason why PPGE behaved quite differently is likely to be because it maintains its three-dimensional structure at the surface and does not spread out flatly. Consequently, only a small proportion of the molecular structure comes in contact with the PGC surface. We discuss this in greater detail later in this Chapter.

Chromatographic Characterisation

The chromatographic characterisation of coated PGC is divided in to two parts. The first is concerned with the overall retention change associated with the coated PGC. This was investigated using:

a) a non polar analyte (phenylhexane)
b) a polar analyte (1,3 dihydroxybenzene)

The data for this study is presented in Table 4.5, and the graphical representations are given in Figures 4.9a and 4.9b. In order to provide a useful reference point we have extended the chromatographic characterisation to include a comparison with C18- and C8-silica (using Hypersil silica). Each of the columns packed with coated PGC particles showed a significant drop in retention relative to columns packed with uncoated PGC particles. This confirmed the presence of the adsorbate on the coated PGC particles. Relative to uncoated PGC, the most significant drop in retention for the non-polar analyte was seen in the polyphenylglycidylether-coated PGC column. For the polar analyte, the decacyclene-coated PGC column showed the greatest drop in retention.

The second part of the chromatographic study investigates the retention behaviour of a wide range of analyte types and polarities on the coated PGC columns. A full breakdown of the

chromatographic tests and probes employed is listed in Table 4.6. Initial studies were made using the phenols test mixture referred to in Chapter 2. This was followed by a more detailed study involving compounds with a wide range of polarity.

The chromatographic characterisation using test mixture 1 (phenols) gave a rapid indication as to whether or not the surface of the PGC had actually been coated since considerable changes in overall retention time and elution order were observed (see Table 4.7 and Table 4.8). These results suggested that the PGC had been successfully coated.

Test mixtures 2-6 were evaluated by plotting log k' *vs.* n or C in accordance with equations [4.4] or [4.5],

$$\log k' = \log k'_w + AC \qquad [4.4]$$

$$\log k' = \alpha n + \beta \qquad [4.5]$$

where n is either the number of $-CH_2-$ plus terminal CH_3 groups for an alkylbenzene or the number of $-CH_3$ groups present for the polymethylbenzene, β is the extrapolated value at the y-intercept, which corresponds to the theoretical retention of benzene, C is the volume fraction of organic component (*e.g.* methanol), and $\log k'_w$ is the k' value for the analyte retention in pure water.

Log k' data for each analyte test mixture on coated PGC columns is given in Table 4.9 to Table 4.14. The graphs which plot this data, are shown in Figure 4.10 to Figure 4.16. The Figures are divided further to provide information for each individual coated column. Accordingly each column is labelled as a, b, c, d, e or f:

Test mixture	**Table**	**Summary Table**	**Figure**
Phenols	4.7,8		4.10,a,b,c,d,e
Alkylbenzenes	4.9	4.10	4.11 a,b,c,d,e,f
Polymethyl substituted benzenes	4.11	4.12	4.12 a,b,c,d,e,f
Hydroxy-phenols	4.13	4.14	4.13 a,b,c,d,e,f
Anilines	4.15	-	4.14 a,b,c,d,e,f
Halo-benzenes	4.16	4.17	4.15 a,b,c,d,e,f
Other mono-substituted benzenes	4.18	4.19	4.16 a,b,c,d,e,f

where,

a = Uncoated PGC

b = Squalane-Coated PGC

c = Polystyrene-Coated PGC

d = Polyphenylglycidylether-Coated PGC

e = Decacyclene -Coated PGC

f = C18-silica (Hypersil C18)

Following the chromatographic characterisation, the polyphenylglycidylether (PPGE) coated column proved to be the one which most consistently showed different behaviour to that of the uncoated PGC. Consequently it was decided to investigate this compound further by coating a second series of PGC columns but with only fractional monolayer coverage. In order to gain more accurate control of the coverage, the evaporative adsorption method of coating was employed. (The evaporative method is more accurate because the weight of both adsorbate and PGC can be precisely measured. Also, the yield is nearly 100%, that is, nearly 100% of the adsorbate molecules are deposited on the PGC surface, with the exception of some unavoidable losses due to deposition on the walls of the reaction vessel.) Chromatographic behaviour was monitored using test mix 1 (phenols). A clear change in chromatographic selectivity and improvements to peak shape was observed as the amount of coated material was increased (see Table 4.20 for data and Figure 4.17a for the plot of $\log_{10}$ k' *vs.* loading). The log k' value for the longest retained peak (phenetole) was found to be 0.19 and gave similar retention behaviour to that of the column coated using the breakthrough method which gave a $\log_{10}$ k' value for phenetole of 0.25 (see Figure 4.17b). The two coated PPGE columns also gave similar elution order to one another, differing markedly from the uncoated PGC. The coated PPGE columns behave similarly to the Hypersil C18-silica material, where the phenols show less retention relative to the aromatic ethers, the reverse to that shown for uncoated PGC (see Figures 4.18a-d). Significant improvement in peak shape is observed for the PGC coated using the evaporative adsorption method when compared to either the PGC or the PPGE coated PGC using the dynamic breakthrough method.

Once the chromatographic measurements were made, surface characterisation techniques were employed to establish that the adsorbate molecule was actually on the PGC surface. Techniques such as static secondary ion mass spectrometry (SSIMS), X-Ray photoelectron

spectroscopy and thermogravimetric analysis, were all employed to this end. X-Ray photoelectron spectroscopy proved to be the most useful of these techniques.

4.3.2 Initial Coating Experiments on PGC

Previous coating experiments on PGC have already been carried out by Wan[6] employing either discrete molecules or polymeric type molecules. As a lead into this area of our work we decided to start by repeating their work, firstly in the preparation of the anion exchanger, polyethyleneimine (PEI), and secondly in the preparation of chiral phases made with naphthylsulphonyl chloride derivatized enantiometically pure amino acids. Both types of coatings had been prepared previously by Wan[7]. We refer to these phases only briefly in this Thesis as they have been prepared only to gain experience in the coating of PGC. Examples of chromatographic behaviour of the phases are given in Figures 4.19a and 4.19b. In both cases separation was achieved based on either the ion exchange mode or chiral modes of chromatography discussed in detail in Chapter 1 of this Thesis and were consequently in good agreement with the work carried out by Wan. Details referring to the experimental preparation of the PEI coated PGC are given in a poster prepared for the Chiral Symposium in Stockholm, 1994. This work was a combined effort and co-workers are listed in the same reference[8].

4.3.3 Coating Methods

Three methods of coating were investigated: Dynamic-Sequential, Dynamic-Breakthrough, and Evaporative Adsorption.

4.3.3.1 Dynamic Coating – Sequential Injection Methods

Pyrene as Coating Adsorbate Molecule

Sequential injections of fixed quantities of pyrene were made. Between injections, the degree of coating was monitored by observing the change in retention behaviour. This was achieved by injection of two solutes whose retention was expected to reduce until monolayer coverage was observed. Aliquots of 100μL ethanol containing 0.5mg pyrene were injected. The eluent or mobile phase was HPLC grade ethanol. The column was 100 x 4.6mm, flow rate was 1.0mL/min, and detection wavelength 254nm. Between each injection of pyrene a test mixture consisting of dimethylphalate and phenyloctane was injected. The data is given in Table 4.21. The change in retention *vs.* the quantity of pyrene injected was plotted in Figure 4.20a. Decrease in retention was observed only up to a point

where 5mg of pyrene had been loaded onto the column. This was a significantly lower amount than had been expected, since the isotherm data had suggested that a quantity of 38mg was required to give monolayer coverage. Pyrene was clearly not retained as strongly as expected when using ethanol as the mobile phase solvent. Because of this limitation, we feared that the pyrene once deposited might bleed slowly from the PGC surface over a period of time making chromatographic results inconsistent. Work with the pyrene coated PGC was therefore discontinued.

Squalane (1) as Coating Adsorbate Molecule

Fixed quantities of squalane (8mg/mL, 100μL =0.8mg in ethanol/methanol 1:1) were injected at regular intervals onto the PGC column. Between each injection, a test mixture of comprising dimethylphalate and phenylheptane was injected and the retention of each analyte measured. The mobile phase eluent employed was HPLC Grade Ethanol/Methanol (1:1). Column dimensions were 100 x 4.6mm, the flow rate was 1.0mL/min, and detection wavelength 254nm. The injections were repeated until no further change in the retention of either analyte was observed. The data is presented in Table 4.22 and then graphically in Figure 4.20b. No change in retention occurs after 9mg of squalane has been injected onto the column. As found in the pyrene experiments, this is much smaller quantity than that required to give monolayer coverage and suggests that squalane is not retained sufficiently on PGC when ethanol:methanol (1:1) is used as the mobile phase.

Squalane (2) as Coating Adsorbate Molecule

Fixed quantities of a concentrated squalane solution (125mg/mL, 10μL = 1.25mg) were injected until breakthrough of squalane was observed. Between each injection a test mix comprising acetone (t_m or void time marker), toluene, ethyl benzene, ortho-xylene, 4-phenylbutan-1-ol, and 1,2,3-trimethylbenzene was injected to monitor the surface coverage. Methanol was used as the mobile phase solvent. As with the previous squalane experiment, the loading required before breakthrough occurred was 9mg of squalane (see Figure 5.20c).

In each experiment (squalane (1) and (2)) a decrease in retention of each test analyte was observed upon injection of the squalane solution. A point was reached where further injection had no effect on the retention of the analytes injected even although breakthrough of squalane was not observed. The quantity of squalane injected at this point suggested that considerably less than a monolayer coating had been achieved. It was assumed that

incomplete monolayer coverage was a direct consequence of the solubility of squalane in ethanol:methanol mixture used as the mobile phase. It was therefore decided that future squalane-coated PGC columns would be run with mobile phases comprising water:methanol mixtures, in which the squalane is completely insoluble.

4.3.3.2 Dynamic Coating –Breakthrough Methods

Pyrene, Squalane, Polystyrene, Polyphenylglycidylether (PPGE), Decacyclene as Coating Adsorbate Molecules

The solubility of each coating compound was determined by dissolving each to its saturation point in a solvent at slightly elevated temperatures. The saturation point was taken as the maximum concentration at which the compound remained in solution upon cooling of the solvent. The solution at that point is then "saturated" with the coating compound.

Saturated solutions of each coating compound were pumped through columns (100mm x 4.6mmID) containing uncoated PGC. The solution concentration and volume were calculated to provide a sufficient mass of coating compound to establish a monolayer on the surface of the PGC in the columns. Monolayer formation was defined by the point of breakthrough of the coating compound. The point of breakthrough was measured by allowing the column eluate to drip into a solution in which the coating compound was insoluble and formed a milky precipitate. This was a visual observation. Classic HPLC detectors (UV or refractive index) were not used in order to avoid fouling the detector cell windows with the coating compound. Such fouling is difficult and time consuming to clean adequately and one runs the risk of permanently damaging the delicate optics.
The quantities of coating compound required to give monolayer coverage have already been discussed and are presented in Table 4.4. The large amount of PPGE required for monolayer coating is supported by two separate sets of analyses: (1) data obtained using the "evaporative adsorption method" where fractional monolayer coverage of PPGE was investigated, and (2) when the quantity of fractional monolayers of PPGE coated on PGC was confirmed by thermogravimetric (TGA) analysis after a chromatographic study. We discuss this in greater detail later in Section 4.3.4.3.

Confirmation of the quantity of polystyrene loaded onto the PGC during this process was obtained by unpacking the column and analysing the material by TGA analysis. A mass of

28mg polystyrene per gram of coated PGC particles was found to be present. This is in reasonable agreement with the amount thought to have been loaded (28.8mg/g of PGC).

4.3.3.3 Evaporative Adsorption Method

This method involved suspending the PGC particles in a solution with the adsorbate and evaporating the solvent thereby depositing the adsorbate (coating compound) on the surface of the PGC. The coated PGC particles were then packed into an HPLC column. This method was employed to prepare a series of PPGE-coated PGC columns with fractional monolayer coverage. The procedure is described as follows.

Fractional Monolayer Coating of PGC with Polyphenylglycidylether (PPGE)

HPLC grade dichloromethane (DCM) was used to dissolve measured quantities of PPGE. Each solution was added to 1.1g of dry PGC powder and stirred thoroughly to allow wetting of the PGC surface. PPGE solutions containing 95.5, 47.8, and 28mg in 50mL DCM, and 9.6 and 0.96mg in 20mL DCM were employed. The solvent from each suspension was removed by rotary evaporation at reduced pressure at 45°C. The coated PGC powder was re-suspended in methanol, in which PPGE is insoluble, and packed into an HPLC column as described in Chapter 2.

4.3.3.4 Summary Discussion of Coating Methods

The dynamic breakthrough method was chosen to coat the columns. The reasons for this were firstly that it allowed an efficient column to be packed with PGC before the coating experiment began. Secondly the method was facile and required only knowledge of the coating compound's solubility and saturation limits in a given solvent to be able to coat the column. Additionally, the breakthrough end point was easily observed. Results using this method were in good agreement with those of the evaporation technique for polystyrene and PPGE.

The dynamic injection method also showed good agreement with the dynamic breakthrough method for squalane. In both methods, 10 mg of squalane were required to give monolayer coverage. However, the dynamic injection method was time consuming and appeared to offer no real advantage over the breakthrough method.

4.3.4 Characterisation by Chromatographic Analysis

4.3.4.1 Accuracy of Results

In order to confirm the accuracy of the analyte k' values for analytes that show low retention, benzyl alcohol was included in the test mixture as internal standard. Repeat injections confirm the value of t_m used to calculate analyte k'. Retention data for benzyl alcohol is not given in the result tables as it was used only as a reference when required. The t_m was found to vary very little when measured in this way, confirming the accuracy of the k' values observed for some of the analyte mixtures. In mixtures where the presence of benzyl alcohol would interfere with the measurement of the retention time for the analyte of interest it was not included.

4.3.4.2 Chromatographic Results and Discussion

Mix 1 Phenols

This test mixture is the same as the one that was used in Chapter 2. There it was observed that changes in the PGC surface, *e.g.* impurities, caused significant changes in retention and peak shape for the two aromatic ethers, anisole and phenetole. It was thought that the phenol test might also prove to be sensitive to monolayer or near monolayer coverage of PGC for the coating compounds chosen. This was in fact found to be the case. The retention and selectivity data for each of the coated PGC columns is given in Tables 4.7 and 4. We also compared the retention behaviour for these coated PGC columns to that of Hypersil C18-silica. The results are considered in terms of (1) the overall retention capacity and (2) the elution order for each of the analytes.

(1) Overall retention capacity

The overall retention capacity for each of the coated PGC columns tested is summarised in Table 4.7. There is an observed drop in retention capacity of approximately 80% on the coated PGC when compared to that of the uncoated PGC. The retention capacity therefore resembles Hypersil C18-silica. The PPGE column showed the lowest retention capacity, in agreement with earlier results discussed in Section 4.3.1 for the retention of phenylhexane.

(2) Order of elution

Each of the coated PGC columns showed a different elution order compared to that of uncoated PGC. In general, there appeared to be a shift away from the selectivity shown by the uncoated PGC towards the selectivity observed for the Hypersil C18-silica material.

The change in selectivity is most pronounced for the aromatic alcohols, which are now less retained than the aromatic ethers, anisole and phenetole. The shift in selectivity is illustrated Table 4.8 and in Figures 4.10a-e where the chromatograms are presented for each of the coated PGC columns. In these Figures, phenetole is represented in yellow, anisole in orange, and 3,5-xylenol in pink. In all cases the elution order of phenetole and 3,5-xylenol are reversed relative to the uncoated PGC. The same observation is also made for anisole and p-cresol.

The selectivity changes are considerable and give us our first indication that it might be possible to mask the polar retention effect (PREG) observed on the uncoated PGC.

Mix 2 n-Alkylbenzenes

The log k' data for the retention of alkylbenzenes on the coated and uncoated PGC columns is presented in Table 4.9. Plots of log k' *vs.* n, where n is the number of -CH_2- groups in the aliphatic side chain are presented in Figure 4.11. Linear relationships are observed for all columns and are therefore in agreement with Equation [4.5]:

$$\log k' = \alpha n + \beta \qquad [4.5]$$

where α s the gradient (slope) and β the y-intercept,.which is the theoretical log k' for benzene (zero -CH_2- groups).

The αCH_2 values obtained for the plot of log k' *vs.* n were still found to be significantly greater than those of Hypersil C18- or C8-silica. In this respect the coated PGC columns were observed to behave in a similar manner to the uncoated PGC column.

Table 4.10 provides a summary of the data relating to Equation [4.5] for each column. The decrease in the value of β is consistent with the observations seen for test mix one, with the polyphenylglycidylether (PPGE) coated PGC showing the lowest retention. The β values for C8-silica and C18-silica are -0.72 and -0.63 respectively, and are higher than for coated and uncoated PGC columns.

Mix 3 Polymethyl Benzenes

The log k' data for the retention of polymethyl benzenes on the coated and uncoated PGC columns are presented in Table 4.11. Plots of log k' *vs.* n, where n is the number of -CH_3 groups directly attached to the aromatic ring are presented in Figure 4.12.

Reduced retention was again observed for each of the coated PGC columns. Also, the gradient for the plot of log k' *vs.* n on the coated PGC was found to be very close to that of the uncoated PGC. In this respect the retention behaviour is similar to that observed for the alkylbenzenes, where significantly higher αCH_3 values were observed for all coated and uncoated PGC columns compared to that of C18-silica. Table 4.12 provides a summary of the data relating to Equation [4.5].

Difficulties with column back-pressure arose with the decacyclene-coated PGC column. Consequently it was not tested with this test mixture. In general, it was observed that:

$$0.45 < \alpha CH_3 < 0.52 \text{ for coated and uncoated PGC}$$

$$\alpha CH_3 < 0.2 \text{ for Hypersil C18- and C8-silica.}$$

The gradient values (α in Equation [4.5]) for coated and uncoated PGC are very similar, and are consistently higher than C18- or C8-silica. The results for uncoated PGC and C18-silica are in good agreement with those of previous workers[9].

The results indicate that by coating the PGC surface it is possible to reduce the overall retention of both the n-alkylbenzenes and polymethylbenzenes, *i.e.* the overall hydrophobic interactions associated with PGC. Retention, however, is still likely to be due to adsorption of the analytes onto the PGC surface. Reduction in retention is because the coating compounds compete with the analytes for the adsorptive sites on the PGC. The mechanism by which the analytes are retained is therefore not due to interaction with the coated molecules but with the graphite and consequently although overall retention is reduced we observe the same αCH_2 and αCH_3 values to those observed for uncoated PGC.

Mix 4 Hydroxy-Phenols

The log k' data for the retention of hydroxy-phenols on the coated and uncoated PGC columns are presented in Table 4.13. Plots of log k' *vs.* % methanol in water showed good linearity and are in keeping with Equation [4.4] (see Figures 4.13a-e).

$$\log k' = \log k_w + AC \qquad [4.4]$$

For each of the coated PGC columns (except PPGE) the retention order of the hydroxybenzenes was reversed relative to that observed for uncoated PGC at 30% methanol

in water. At this methanol:water composition, the retention order for the coated PGC was found to be similar to that of Hypersil C18-silica:

Uncoated PGC elution order:	1,3,5-trihydroxybenzene >> 1,3-dihydroxybenzene > phenol
Coated PGC elution order:	phenol > 1,3-dihydroxybenzene > 1,3,5-trihydroxybenzene
C18-silica elution order:	phenol > 1,3-dihydroxybenzene > 1,3,5-trihydroxybenzene

However this observation was only true when the composition of the mobile phase contained significant levels of methanol. Extrapolation of the data to give values of log k'_w showed similar elution order to that of the uncoated PGC. This change in elution order comes about due to much steeper gradients observed for analytes which show increasing polarity. The clearest example for this is 1,3,5-trihydroxybenzene. Gradient values 'A' for phenol, 1,3-dihydroxybenzene and 1,3,5-trihydroxybenzene are summarised for each column in Table 4.14. However the PPGE-coated column behaved quite differently. In this case the gradient values are all once again consistent from analyte to analyte (-0.02) irrespective of polarity. Although the elution order is the same when the data is extrapolated to pure wayer, the coated PGC retains 1,3,5-trihydroxybenzene while Hypersil C18-silica does not.

The gradients (slopes) are constant only for the uncoated PGC, the PPGE-coated PGC and Hypersil C18-silica, irrespective of analyte polarity. The way in which the coating compound molecules mask the surface of PGC is clearly affected by the mobile phase composition.

Polyphenylglycidylether (PPGE) was the only coating compound that had any significant polar character to its structure. Our experimental results suggest that in order to have a strong influence on the polar retention effect on graphite (PREG) a polar coating molecule needs to be employed. The polar portion of the coating molecule interacts with the surface of the PGC in such a way as to reduce PREG interactions.

Mix 5 Anilines

The log k' data for the retention of aniline and phenylenediamine isomers on the coated and uncoated PGC columns is presented in Table 4.15. Plots of log k' *vs.* % methanol in water shown in Figures 4.14a-e show good linearity. This is in keeping with Equation [4.6]. However, discrimination between these compounds on most of the columns proved to be very difficult since, with the exception of aniline, on squalane- and decacyclene-coated PGC, and C18- and C8-silica, the solutes were essentially unretained. Consequently log k'_w and gradient values of α have not been calculated.

Retention was observed for the PPGE- and polystyrene-coated PGC. On both of these, the retention order was the same as uncoated PGC, although retention for the latter was found to be significantly greater.

The order of retention was found to be:

Aniline > 1,2-phenylenediamine > 1,4-phenylenediamine > 1,3-phenylenediamine

Mix 6 Halobenzenes

The log k' data for the retention of the halobenzenes on the coated and uncoated PGC columns are presented in Table 4.16. Plots of log k' *vs.* % methanol in water are shown in Figures 4.15a-e. In general they show good linearity in keeping with Equation [4.4]. All columns show the same retention order: bromobenzene > chlorobenzene > fluorobenzene. The coated columns do however show quite different degree of retention. On the PPGE-coated PGC column, 55% methanol in water gives the same retention of fluorobenzene as 80% methanol in water on uncoated PGC.

Very little difference is observed for gradient, α, values. The log k'_w values are similar for all columns with the exception of the PPGE-coated PGC column, which shows significantly lower values. A summary of these values is given in Table 4.17.

Mix 7 Other Mono-Substituted Benzenes

(acetophenone, nitrobenzene, anisole, methylbenzoate)

The log k' data for the retention of the halobenzenes on the coated and uncoated PGC columns are presented in Table 4.18. Plots of log k' *vs.* % methanol in water are shown in Figures 4.16a-d. In general they show good linearity, in keeping with Equation [4.4]. Retention order is observed to be:

methylbenzoate > anisole > nitrobenzene > acetophenone

The primary observation from this test is that anisole and nitrobenzene are significantly more retained on the PGC relative to Hypersil C18-silica. Polystyrene- and decacyclene-coated PGC show similar elution order to uncoated PGC when the data is extrapolated to give log k'_w values. The PPGE-coated PGC once again gave the same retention order as Hypersil C18-silica. Summary of the chromatographic data is given in Table 4.19.
We can conclude that the type of interaction that causes the increased retention of nitrobenzene relative to the other compounds has been masked in the case of the PPGE-coated PGC column but not with the other coated PGC columns. In the case of the Hypersil C18-silica, the interaction is absent altogether.

4.3.5 Fractional Monolayer Coating with Polyphenylglycidylether (PPGE)

Polyphenylglycidylether coated PGC columns were further investigated in order to determine what fraction of a monolayer was required to mask the polar retention effect. From our earlier experiments, it was determined that 198mg of PPGE were sufficient to provide monolayer coverage. The chromatographic performance for each partially coated column was monitored by observing the change in retention and selectivity of the analytes in test mix 1, phenols. The data is presented in Table 4.20. Figure 4.17a illustrates how k' values change for each of the analytes as the amount of PPGE loaded increases. Only once 95.5mg PPGE were loaded did the selectivity resemble our initial experiments. The observed drop in retention and change in selectivity are in good agreement with the PPGE-coated PGC from the earlier experiment coated using the breakthrough method. This suggests that full monolayer coverage (which required 198mg PPGE) is not required to mask the PREG. Figure 4.17b shows how the trends of retention behaviour shown by fractional monolayer coated are extended to include the extra data from the breakthrough method, confirming that approximately 180mg had been loaded onto the column. A chromatographic comparison of uncoated PGC and Hypersil C18-silica with PPGE-coated PGC columns (at fractional coverages) is given in Figures 4.18a-d. Even small quantities of PPGE are observed to improve the peak shape of the analytes in test mix 1 (Figure 4.18b), in particular the aromatic ethers. The retention order is quite different to that shown for the uncoated PGC where the phenols are retained more strongly. The coated PGC columns therefore behave much more like the Hypersil C18-silica column, in terms of both overall retention and selectivity.

A critical aspect of the physical characterisation of the PGC coating is to measure the mass of the coating compound deposited on the PGC surface. Our initial approach was to wash the coating from the surface with a strong wash solvent, then evaporate the wash solvent and weigh the remaining residue. However it was found that the polymeric compounds could not be removed from the surface by washing with solvents that are considered to be strong solvents on PGC *i.e.* toluene, dichloromethane or THF. In a final attempt to determine accurately the quantity of PPGE and polystyrene on the PGC surface, the columns were unpacked and the coated PGC material sent for thermogravimetric analysis. The results are discussed in Section 4.3.4.3.

4.3.6 Physical Characterisation of Coated PGC Using Surface Techniques

The aim was to confirm that the coating compounds employed had in fact been adsorbed to the PGC surface. In order to do this the columns were unpacked, the material dried from methanol in a vacuum oven at 40°C.

The methods employed were:

Static Secondary Ion Mass Spectrometry (SSIMS)

X-Ray Photoelectron Spectroscopy (XPS)

Thermogravimetric analysis (TGA)

A short review for each of the above methods is given in Appendix 4.1 at the end of this Chapter.

The data for the SSIMS and XPS analyses was gathered using equipment at Nottingham University. The data is discussed in the following paragraphs.

4.3.6.1 Static Secondary Ion Mass Spectrometry (SSIMS) Data

Secondary ion mass spectrometry, SIMS, is the mass spectrometry of atomic molecular particles emitted when a surface is bombarded by energetic primary particles. Usually the surface is a solid, although it can be a liquid. The emission process is known as sputtering. The primary particles can be electrons, ions, neutrals, or photons. The secondary ions which are detected may be emitted from the surface in the ionised state or they may be initially emitted as neutrals to be post-ionised before analysis.

Benninghoven introduced static SIMS (SSIMS) in 1969 for the investigation of monolayers on solids and chemical reactions on solid surfaces. In contrast to the more widely known

technique of dynamic SIMS (high sensitivity elemental analysis, depth profiling), static SIMS has remained relatively unexploited[10].

Overall the SSIMS data for the coated PGC samples were all very similar. Charging problems meant that the ion intensities were low and poor negative ion spectra were obtained. Unfortunately, it was impossible from the SSIMS data to determine conclusively whether the polymers were present on the surface or not.

4.3.6.2 X-Ray Photoelectron Spectroscopy (XPS)

X-Ray Photoelectron Spectrometers (XPS) became commercially available in 1969 and XPS was used to study polymers shortly thereafter. It is a relatively benign technique in terms of radiation damage to the surface and sample preparation is generally minimal. The information is inherently quantitative, all elements except for hydrogen are analysed and core level chemical shifts provide a reasonable degree of organic structure information. XPS can be used to obtain elemental analysis, relative concentrations of the element present and information on their chemical connectivity from a sample's surface.

XPS was far more conducive to characterisation of the coated PGC samples than SSIMS, although difficulties for some of the coated PGC did still arise. The XPS results for each of the coated PGC materials are discussed below.

Squalane, Decacyclene coated PGC and Uncoated PGC

Squalane and decacyclene were extremely difficult to discriminate from the PGC surface since, like carbon, they comprise a single element type, carbon. These samples however did show charging effects. The fact that differential charging occurs suggests that the PGC surface is heterogeneous, which may indicate the presence of the coating compounds. The uncoated PGC may show heterogeneity due to hydrocarbon contamination.

Polystyrene on PGC

The C:O ratios on polystyrene-coated PGC are much higher than for squalane-coated PGC. The oxygen signal is likely due to trapped solvent, *i.e.* methanol or water, in the sample. As we probe deeper into the sample, from 70Å to 20Å below the surface, the O1s content increases. This is consistent with the theory of trapped solvent where one would expect less solvent near the surface because of evaporation. The lack of double peaks in the polystyrene-coated PGC sample suggests that the surface is homogeneous, *i.e.* there is a substantial coating of polystyrene on the PGC surface. Also noticeable is the high binding

energy side of the C1s peak, the π - π^* transition from the phenyl groups. This peak, 6 to 7eV shifted from the main peak with typical intensity 5-10% of the main peak, is common for aromatic polymers. This also suggests the presence of polystyrene on the surface.

Polyphenylglycidylether (PPGE) on PGC

Both the Cls and O1s spectra show differential charging effects (double peaks). Comparing these spectra to those of a spin-cast PPGE film on a silicon wafer, shows that, although the C1s should have a double peak, the O1s does not, confirming that the PPGE on PGC exhibits charging effects. The presence of double peaks in the XPS spectra indicates charging effects. Because there can be no surface carbon signal on the spin-cast silicon wafer, you do not see the C1s double peaks. However, one does see the doubling on the PPGE-coated PGC, suggesting charging effects and the activity of surface carbon.
The relative surface C:O ratio of 14:1, indicates the presence of the PPGE polymer. In the other coated PGC samples where oxygen is not present in the coating compound's molecular structure the C:O ratio is much higher.

PPGE on Silicone Wafer

The surface C:O ratio of 4.18:1 was in good agreement with the polymer structure. The C1s spectrum showed two peaks due to C1s in a high hydrocarbon environment. The C1s spectrum gives peak areas for the two peaks of:

C1s HC – 1198 = 2.83

C1s O-C 846 = 2.00

The expected ratio from the structure is 3:2 and is in good agreement with the calculated data (2.83:2.0).

4.3.6.3 Thermogravimetric Analysis

Thermogravimetric analysis (TGA) was employed to confirm the presence and quantify the amount of the polymer on the surface of PGC. In this technique the temperature of the sample is raised at a constant rate while the sample weight is continually monitored. During this process the temperature of the polymer or any molecule shows a characteristic combustion profile. The graph of weight loss against temperature can be plotted. However, more useful information can be obtained from the Derivative Thermogravimetric Analysis plot, which shows the rate of weight loss per degree temperature rise.

TGA is used to measure the thermal stability of polymers, diffusion characteristics and desorption characteristics such as uptake of water. Considerable care is required from the analyst as slight variations in parameters such as rate of temperature change, sample size, sample particle size (pellets or powder) and atmosphere, can alter the resultant plot [2]. Other applications to which TGA can be used are: determination of additives, characterisation of blends and copolymers, flame retardant capability, extent cross-linking, and thermal life. Figures 4.21a-c show the TGA analysis for (a) the uncoated PGC, (b) polystyrene, and (c) polyphenylglycidylether. Figure 4.22 shows the TGA analysis for polystyrene-coated PGC. Figure 4.23 shows the TGA for PPGE-coated PGC at fractional monolayer coverage.

The results for polystyrene-coated PGC are higher than expected. The predicted loading by the breakthrough coating experiment is 28mg/g PGC, while TGA analysis gives 92mg/g PGC. The TGA data and plot of TG % *vs.* temperature is typical of plots normally obtained for the exothermic reaction concerning the combustion of a polymer, *i.e.* a gradual weight loss with temperature increase is observed.

One of the PPGE columns coated with fractional monolayer quantities (25.5mgPPGE/g of PGC) was also analysed by TGA. This sample was found to be in good agreement with the loading predicted by the evaporative method, *i.e.* TGA gave 32mg PPGE/g of PGC. This further supports the observed higher than expected loading of the PPGE by both the evaporative and the breakthrough loading techniques.

The results therefore confirm the presence of the two polymers on each of the two coated PGC samples.

4.4 Conclusion

Several methods for coating PGC have been investigated. Of these, the dynamic breakthrough method offered the simplest approach. It also had the added benefit that an efficiently packed column of uncoated PGC was readily available from a commercial source. This eliminated the lengthy packing optimisation studies. In practice, however, the evaporative coating method was preferred because it allowed for better control of the loading of the coating compound. The main concern with the evaporative method was that the coated PGC would require developing a complicated column packing procedure. In fact, a relatively simple packing method was developed for the PPGE-coated PGC columns where methanol was employed as both the slurry and packing solvent.

The presence of the coating compounds at the PGC surface was confirmed:

a) by physical techniques such as TGA and XPS
b) by the observed significant drop in chromatographic retention and changes in selectivity for the phenols test mixture.

The chromatographic characterisation, especially the retention of polar compounds such as the hydroxybenzenes, of the coated PGC columns allowed several interesting observations to be made. Using a mobile phase with moderately high organic content, the hydroxybenzenes, without exception, showed the same or very similar retention order to a C18-silica, and the reverse of that shown by uncoated PGC. On the coated PGC and C18-silica, the more polar compounds eluted first while on uncoated PGC, they eluted last. With one exception, as the aqueous content of the mobile phase increased, the retention order on each column is observed to become more like the uncoated PGC, with the most polar analytes eluting last. This effect was particularly noticeable for the 1,3,5-trihydroxybenzene, the most polar of the analytes.

The PPGE-coated PGC column was the exception to this observation. It did not show any indication of returning to PGC type retention behaviour at high aqueous content. In fact the gradient (slope) remained constant for each of the analytes.

Relative to uncoated PGC, the coated PGC showed lower retention but similar selectivity for non-polar compounds such as the n-alkylbenzenes and the polymethylbenzenes.

This suggests that very strong interactions still exist between the analyte and the underlying graphite, even for the PPGE-coated PGC.

When the analyte molecules are sufficiently polar or a better fit (alignment to the surface) they interact preferentially with the graphite surface, displacing the coated molecule in the process. The exception is PPGE. For polar compounds the observation becomes most pronounced when the composition of the mobile phase is highly aqueous. We will discuss in greater detail the influence of solvent composition on the polar retention effect (PREG) in Chapter 5, Section 5.5.4.

No such dependence on solvent composition is observed for the PPGE-coated PGC for the retention of the polar compounds (hydroxybenzenes). Consequently, it can be concluded that displacement of the PPGE by the analyte at the PGC interface does not take place. This suggests that the polar nature of PPGE plays a significant role in its retention mechanism at

the PGC surface, effectively masking the polar retention effect for analytes in the mobile phase. We discuss this further in Chapter 5, Section 5.5.4.

The PPGE coating created a PGC with selectivity very similar to C18-silica, where the more polar compounds elute first. A 100mg PPGE coating was found to be sufficient to achieve this change in selectivity and at the same time provide a column with good chromatographic performance (efficiency and peak symmetry).

Appendix 4.1

Static Secondary Ion Mass Spectrometry (SSIMS)

Secondary ion mass spectrometry, SIMS, is the mass spectrometry of atomic molecular particles that are emitted (a process known as sputtering) when a surface, usually a solid although it may be a liquid, is bombarded by energetic primary particles. The primary particles may be electrons ions, neutrals, or photons. The secondary ions which are detected may be emitted from the surface in the ionised state or they may be initially emitted as neutrals to be post-ionised before analysis.

Benninghoven introduced static SIMS in 1969, for the investigation of monolayers on solids and chemical reactions on solid surfaces. In contrast to the more widely known technique of dynamic SIMS (high sensitivity elemental analysis, depth profiling), static SIMS has remained relatively unexploited[11].

Static SIMS, SSMIS, relies primarily on slow collision sputtering which occurs due to the internal flux of moving target atoms intersecting the surface in the time scale $10\text{-}14 < t < 10\text{-}12$s. This type of process refers to a situation when the primary flux density is not large. The treatment is known as the collision cascade theory of sputtering and the general outline of the process is widely accepted.

The primary particle of energy E_o collides with the surface atoms. Symmetry considerations suggest that at least three surface atoms may be involved. Some energy may be lost by electronic excitation, but most is transferred by a nuclear stopping mechanism during hard sphere or billiard ball-type collisions. Knock-on collision cascades between atoms in the near surface region are initiated.

The energy transferred, Et, in a nuclear stopping collision from atom M_1 to atom M_2 varies from 0 to a maximum of $[4M_1M_2)/M_1+M_2)^2]E_0$. Some energy will be dissipated into the bulk by displacement cascades. Here the incident ion can remove bulk atoms out of their regular lattice sites, creating defects. After displacement, however, a very efficient process of recombination occurs such that the number of defects remaining per ion is 1 to 10^{-3}. Some cascades will return to the surface causing the emission of secondary particles or sputtering. This sputtering occurs within 1 to 2nm of the surface whereas displacement or lattice damage can occur down to 10 to 25nm. The atomic sputter yields and secondary particle energy terms predicted by Sigmunds treatment are generally in good agreement with experimental values.

Other types of sputtering can also occur but these are generally not utilised by static SSIMS. For example, prompt collision sputtering is a direct impact process between the incident particle and the sputtered particle involving only surface atoms. Thermal sputtering occurs at high primary beam densities and is due to transient vaporisation from the impact region.

A proportion of the particles released from the surface are ionised and can be analysed. Static SIMS is primarily concerned with molecular ions rather than fragment ions.

X-Ray Photoelectron Spectroscopy (XPS)

X-Ray Photoelectron spectrometers (XPS) became commercially available in 1969 and XPS was used to study polymers shortly thereafter. It is a relatively benign technique in terms of radiation damage to the surface and sample preparation is generally minimal. The information is inherently quantitative, all elements except for hydrogen are analysed and core level chemical shifts provide a reasonable degree of organic structure information.
In XPS the sample of interest is placed in a high vacuum system (pressure -10 to -8 torr) and irradiated with soft x-rays, usually Mg Kα or AlKα with energies of 1253.6 eV and 1486.6 eV respectively. When the soft x-rays interact with the sample atoms, various processes can occur, including photo-emission of core, valence and Auger electrons and x-ray fluorescence. The principle event is the photo-emission of core electrons, which is accompanied by a relaxation process, which returns the ionised atom to a lower energy state. This can be achieved via x-ray fluorescence or by the emission of an Auger electron. The emitted electrons are collected, passed through a lens system and slowed using a retard voltage. Next the photoelectrons enter into a Concentric Hemispherical Analyser (CHA). If they possess the correct energy they can then exit into a channeltron detector. The spectrum is scanned by varying the retard voltage.
The binding energies, Eb, of the photoelectrons are obtained using Einstein's Equation:

$$Eb = h\upsilon - Ek - \phi$$

where hυ is the x-ray photon energy (constant for a given source), ϕ is the sample work function (constant for a given spectrometer) and Ek is the measured kinetic energy, of the photoelectron. An XPS spectrum is a plot of photoelectron intensity *vs.* the kinetic or binding energy of the photoelectrons. Only electrons that escape without undergoing inelastic collisions contribute to the main photoelectron peak. Hence, XPS is highly surface sensitive and probes the top 5nm of the sample surface.

The core level binding energy, Eb is unique for a given element thus allowing elemental identification except for hydrogen and helium, which cannot be detected. These unique binding energies of core levels of atoms are sufficiently affected by their chemical environment to cause a detectable shift, ranging from 0.1-10 eV or more in magnitude, in the measured photoelectron energy. This effect is termed as the chemical shift. In basic terms chemical shifts are a result of variation of electrostatic screening experienced by core electrons as valence electrons are drawn towards or away from the atoms of interest. Careful measurement of an element's binding energy can therefore tell us something about the chemical environment of the element. Peak intensities are proportional to the number of atoms sampled. After using the appropriate sensitivity factors, relative atomic compositions can be calculated with detection limits of approximately 0.2 atom %. Thus, XPS can be used to obtain elemental analysis, relative concentrations of the element present, and information on their chemical connectivity from a sample's surface.

Thermogravimetry (TGA)/Derivative Thermogravimetric Analysis (DTG)

In this analytical technique, the temperature of the sample is raised at a constant rate while sample weight is continually monitored. The atmosphere under which the analysis is performed should also be documented. The graph of weight loss against temperature can be plotted, but more useful information can be obtained by taking the first derivative the results providing a DTG (Derivative Thermogravimetric Analysis) plot which shows the rate of weight loss against temperature.

The technique is used to measure the thermal stability of polymers, diffusion characteristics, desorption characteristics such as uptake of water. Considerable care is required from the analyst as slight variations in parameters such as rate of temperature change, sample size, sample particle size (pellets or powder) and atmosphere, can alter the resultant plot[2]. Other applications to which TG can be used are, determination of additives, characterisation of blends and copolymers, flame retardant capability, extent cross-linking, resistance and thermal life. As with most thermal methods TG is not an absolute identification tool, but is a study of sample behaviour, thus it needs to be presented with other analytical test results for conclusive information about a sample[2]. Data can be reported as "simultaneous," which means more than one technique has been used on the same sample at the same time. This

occurs with coupled instrumentation, or if the analysis is described as "combined" then other data from separate experiments have been quoted to support the conclusions.

References for Chapter 4

[1] Dias, H., Ph.D Thesis, University of Edinburgh (1990)
[2] Bassler, B. J., Kaliszan, R. and Hartwick, R. J. Chromatogr., 461, 139 (1989)
[3] See reference 1
[4] Mockel, H. J., Braedikow, A, Melzer, H., and Aced, G., J.Liq. Chromatogr., 14, 2477 (1991)
[5] Qian Hon Wan, Ph.D Thesis , Edinburgh University
[6] See reference 5
[7] See reference 5
[8] McGann, A., Ross, P. and Roycroft, E., Poster presentation at Chiral Symposium, Stockholm (1994)
[9] Kriz, J., Adamcova, E., Knox J. H., and Hora J., J.Chromatogr., 663, 151 (1995)
[10] Briggs, D., Brown, A. and Vickerman, J. C, *Handbook of Static Secondary Ion Mass Spectrometry.*
[11] See reference 10.

Table 4.1

Molecules Used to Study Isotherm Behaviour on PGC

Coating Compound and solvent	Abbreviated form
Pyrene run in CH_2Cl_2	Pyrene
Anthracene run in CH_2Cl_2	Anthracene
Naphthalene run in CH_2Cl_2	Napthalene
Cetyl pyridinium bromide run in CH_2Cl_2	Cety-Pyr-Br
Dodecylbenzene sulphonate run in CH_2Cl_2	DDSA

Table 4.2
Adsorption Isotherm Data on PGC

(For full explanation of terms used in this table see table 4.2b)

[1]Cm mg/ml	[2]Cm µmol/ml	[3]Vm ml	[4]t_A ml	[5]V_A ml	[6]cor	[7]V_{cor} ml	[8]k'	[9]Mwt	[10]mg q/ (column)	[11]mg q/g(PGC)	[12]umol/g (PGC)	[13]Cs µmol/sqm	[14]1/Cm 1/(µmol/ml)	[15]1/Cs 1/(µmol/sqm)
Naphthalene														
0.01	0.08	0.67	3.90	3.90	1.18	2.72	3.07	130	0.02	0.05	1.00	0.01	12.80	87.82
0.02	0.16	0.67	4.00	4.00	1.20	2.80	3.19	130	0.04	0.11	2.08	0.02	6.40	42.26
0.04	0.31	0.67	3.80	3.80	1.15	2.65	2.97	130	0.08	0.20	3.87	0.04	3.20	22.73
0.1	0.78	0.67	3.80	3.80	1.15	2.65	2.97	130	0.20	0.50	9.68	0.11	1.28	9.09
0.3	2.34	0.67	3.75	3.75	1.18	2.58	2.85	130	0.57	1.44	27.94	0.32	0.43	3.15
0.5	3.91	0.67	3.70	3.70	1.17	2.53	2.79	130	0.93	2.35	45.46	0.52	0.26	1.94
Anthracene														
0.01	0.06	0.67	11.60	11.60	2.00	9.60	13.37	178	0.09	0.23	3.19	0.04	17.80	27.63
0.025	0.14	0.67	10.60	10.60	2.00	8.60	11.87	178	0.20	0.50	7.07	0.08	7.12	12.44
0.05	0.28	0.67	9.35	9.35	1.95	7.40	10.08	178	0.34	0.85	12.00	0.14	3.56	7.33
0.1	0.56	0.67	8.20	8.20	1.90	6.30	8.43	178	0.56	1.42	20.09	0.23	1.78	4.38
0.2	1.12	0.67	7.00	7.00	1.80	5.20	6.78	178	0.91	2.28	32.32	0.37	0.89	2.72
0.4	2.25	0.67	6.10	6.10	1.75	4.35	5.51	178	1.47	3.71	52.52	0.60	0.45	1.68
1	5.62	0.67	4.95	4.95	1.65	3.30	3.94	178	2.63	6.63	93.87	1.07	0.18	0.94
3	16.85	0.67	3.55	3.55	1.55	2.00	1.99	178	4.00	10.07	142.51	1.62	0.06	0.62
5	28.09	0.67	2.95	2.95	1.45	1.50	1.25	178	4.16	10.48	148.36	1.69	0.04	0.59
10	56.18	0.67	2.30	2.30	1.20	1.10	0.65	178	4.32	10.88	154.06	1.75	0.02	0.57
Pyrene														
0.02	0.10	0.67	20.00	40.00	2.00	38.00	55.89	202	0.75	1.88	23.46	0.27	10.10	3.75
0.04	0.20	0.67	16.00	32.00	2.00	30.00	43.91	202	1.17	2.96	36.87	0.42	5.05	2.39
0.1	0.50	0.67	11.10	22.20	2.00	20.20	29.24	202	1.95	4.92	61.38	0.70	2.02	1.43
0.3	1.49	0.67	6.00	12.00	2.00	10.00	13.97	202	2.80	7.05	87.98	1.00	0.67	1.00
0.5	2.48	0.67	4.55	9.10	1.90	7.20	9.78	202	3.27	8.23	102.64	1.17	0.40	0.86
0.7	3.47	0.67	3.90	7.80	2.05	5.75	7.61	202	3.56	8.96	111.79	1.27	0.29	0.79
1	4.95	0.67	3.00	6.00	1.75	4.25	5.36	202	3.58	9.02	112.57	1.28	0.20	0.78

Table 4.2 continued

Adsorption Isotherm Data on PGC

[1]Cm mg/ml	[2]Cm µmol/ml	[3]Vm ml	[4]t_A ml	[5]V_A ml	[6]cor	[7]V_{cor} ml	[8]k'_{front}	[9]Mwt	[10]mg q	[11]mg q/g(PGC)	[12]umol/g (PGC)	[13]Cs µmol/sqm	[14]1/Cm 1/(µmol/ml)	[15]1/Cs 1/(µmol/sqm)
Dodecylbenzene sulphonate														
0.1	0.23	0.67	14.10	14.10	2.00	12.10	17.11	438	1.14	2.88	16.57	0.19	4.38	5.31
0.2	0.46	0.67	8.30	8.30	1.90	6.40	8.58	438	1.15	2.89	16.61	0.19	2.19	5.30
0.4	0.91	0.67	7.20	7.20	1.80	5.40	7.08	438	1.89	4.77	27.43	0.31	1.10	3.21
1	2.28	0.67	5.40	5.40	1.70	3.70	4.54	438	3.03	7.64	43.94	0.50	0.44	2.00
3	6.85	0.67	5.70	5.70	1.70	4.00	4.99	438	10.00	25.19	144.87	1.65	0.15	0.61
5	11.42	0.67	4.20	4.20	1.55	2.65	2.97	438	9.91	24.97	143.63	1.63	0.09	0.61
7	15.98	0.67	3.60	3.60	1.35	2.25	2.37	438	11.07	27.90	160.50	1.82	0.06	0.55
10	22.83	0.67	3.30	3.30	1.50	1.80	1.69	438	11.32	28.52	164.06	1.86	0.04	0.54
Cetyl pyridinium bromide														
0.2	0.50	0.67	5.10	2.55	1.35	1.20	0.80	404	0.11	0.27	1.67	0.02	2.02	52.64
1	2.48	0.67	4.70	2.35	1.30	1.05	0.57	404	0.38	0.96	6.00	0.07	0.40	14.66
5	12.38	0.67	4.60	2.30	1.30	1.00	0.50	404	1.66	4.18	26.08	0.30	0.08	3.37
10	24.75	0.67	4.50	2.25	1.30	0.95	0.42	404	2.82	7.11	44.31	0.50	0.04	1.99
20	49.50	0.67	4.30	2.15	1.25	0.90	0.35	404	4.64	11.69	72.91	0.83	0.02	1.21
30	74.26	0.67	4.20	2.10	1.25	0.85	0.27	404	5.46	13.76	85.79	0.97	0.01	1.03
50	123.76	0.67	4.10	2.05	1.22	0.83	0.24	404	8.10	20.41	127.27	1.45	0.01	0.69
Naphthalene sulphonyl chloride														
1	4.41	0.67	13.80	3.45	0.15	3.30	3.94	226	2.63	6.63	73.93	0.84	0.23	1.19
2	8.82	0.67	11.00	2.75	0.20	2.55	2.82	226	3.76	9.48	105.73	1.20	0.11	0.83
5	22.06	0.67	9.50	2.38	0.20	2.18	2.26	226	7.54	18.98	211.65	2.41	0.05	0.42
10	44.12	0.67	7.25	1.81	0.18	1.64	1.45	226	9.70	24.43	272.32	3.09	0.02	0.32
15	66.17	0.67	6.50	1.63	0.20	1.43	1.13	226	11.36	28.61	318.95	3.62	0.02	0.28
20	88.23	0.67	6.30	1.58	0.20	1.38	1.06	226	14.14	35.63	397.17	4.51	0.01	0.22

For full explanation of terms used in this table see table 4.2b

Table 4.2b

Breakdown and Explanation of Calculations Given in Table 4.2

Column 1, C_m (mg/ml) C_m represents the concentration of the adsorbate in the mobile phase. The concentration of adsorbate is given in milligrams per millilitre.

Column 2, Cm (μmol/ml) Here the concentration in the mobile phase is given in micromoles per millilitre.

Column 3, V_m(ml)V_m, represents the dead volume of the system. This refers to the solvent already in the system i.e. from the top of the column through to the detector cell. This can be measured directly from the chromatogram if a solvent front profile can be observed. During these experiments no solvent front profile was observed and the dead volume had to be calculated.

The column dimensions for each experiment were 50 x 4.6mm. The volume of the empty column volume is then;

$V = \pi r^2.L = 0.83ml$

Where r is the radius of the column and L is the column length.
The volume of PGC in the column is given by,

0.3969(g)/2.25(g/ml) = 0.1764ml

Where 0.3969 is the weight of PGC in a column, and 2.25g/ml is the density of graphite at 20C.
Therefore the total pore volume + the volume from interparticle space is:

0.83ml less 0.1764ml = 0.6536ml

The volume occupied by the tubing between column and detector is:

$\pi r^2 L = 0.014ml$

Where 0.254mm is the diameter of the tubing (0.010'') of length L, 27.5cm
The total dead volume V_o = 0.6536ml + 0.014ml = 0.66ml

Column 4, t_A , t_P etc t gives the retention of adsorbate A(anthracene) or P (pyrene) etc as measured from the elution profile.

Column 5, V_A, V_P (ml) V is the retention volume of A (anthracene) or P (pyrene) etc measured in mls. In this case all volumes have been calculated from column 4 and therefore also takes into account the chart speed of the recorder.

Column 6, is the pump correction volume

Column 7, V_A corrected This is the retention volume as measured in column 5 but corrected for pump start-up time.

Table 4.2b continued

Breakdown and Explanation of Calculations Given in Table 4.2

Column 8, k'_{front} this is the adsorbate retention capacity factor for the front slope of the elution profile. It is calculated as follows.

$$k'_{front} = (V(corrected) - V_m)/V_m$$

Column 9, Molecular weight

Column 10, Amount absorbed (q) in mg by the entire column $= (V_{cor} - V_m).C_m$
$= C_m.\ k'.\ V_m$

Column 11 Amount absorbed (q)in mg per gm of packing $= C_m.k'.V_m / W_{packing}$

Column 12 Amount absorbed (μmol/gm) $= C_m.k'.V_m / (W_{packing}.Mw)$
Where 0.3969g is the weight of PGC in the column

*Column 13,,*Amount adsorbed (μmol/m^2) $= C_m.k'.V_m /(W_{packing}.Mw\ .\ A)$

Where the surface area 'A' in units of m^2/g, for 1g of PGGC is $88m^2/g$ as measured by Coulter Omnisorb surface area analyser (single point B.E.T)

Column 14 is the reciprocal of column 2

Column 15 is the reciprocal of column 13

Table 4.3a
Monolayer Coverage Values

		'Experimental Data'				'Calculated Data'			
Adsorbent Molecule	$1/q_s$	q_s $\mu mol\ m^{-2}$	q_s $\mu mol\ g^{-1}$	*Molecular area calculated	Mole wt	q_s $\mu mol\ m^{-2}$	q_s $\mu mol\ g^{-1}$	Ratio $q_{s(obs)}/q_{s(calc)}$	loading mg/g
Naphthalene	0.20	3.0	264	80	130	2.08	183	1.44	34.3
Anthracene	0.5	2.0	176	112	178	1.48	130.0	1.35	31.3
Pyrene	0.7	1.42	125	136	202	1.23	108.0	1.16	25.3
Cetyl-Pyr-Br	0.5	2.0	176	218	404	0.76	66.9	2.63	71.1
DDS	0.5	2.0	176	198	438	0.83	73.0	2.41	77.1

Table 4.3b
Worked Example for the Calculation of Molecular Area

Example Dodecylbenzene Sulphonate

Determination of molecular area for a -CH_2 - group

Mwt = 14
Molar Volume = 14ml
Molecular volume in cubic angstroms = $\frac{14 \times 10^{-6} \times 10^{30}}{6.022 \times 10^{23}} = 25Å^3$

where 6.022×10^{23} is Avagadros number.

Cube side length = 3Å
Area = $9Å^2$

For an aromatic carbon we get $8\ Å^2$
For oxygen and sulphur we get $9\ Å^2$

Therefore for sodium dodecylbenzene sulphonate we get a total molecular area of

CH_2	$12 \times 9Å^2$	=	$108Å^2$	(12 methylene groups)
Aromatic Carbon	$6 \times 8Å$	=	$48Å^2$	(6 aromatic carbon atoms)
Oxygen and sulphur	$4 \times 9Å$	=	$36Å^2$	(3 oxygen and 1 sulphur atoms)

Total molecular area for DDSA = $192Å^2$

Table 4.4
Summary of Quantities Loaded on to PGC by the Dynamic Method

Coating Compound	Solvent	Wash con'c (mg/ml)	Total Volume (ml)	Vm (ml)	V (ml)	loading (mg)	Wt of PGC (g)	Loading mg/g	Mwt	Loading (umol/g)
Pyrene	CH_2Cl_2	20	2	1	1	20	0.8	25	202	124
Squalane	CH_2CL_2/MEOH (1:1)	10	3.5	1	2.5	25	0.8	31.3	422	74
Polystyrene	CH_2Cl_2	10	3.3	1	2.3	23	0.8	28.8	13,000	2
Polyphenylglycidylether (PPGE)	CH_2Cl_2	9	18	1	17	159	0.8	198	605	328
Decacyclene	CH_2Cl_2	5	5.3	1	4.3	21.5	0.8	26.9	450	60

Table 4.5
Data Showing the Overall Hydrophobic and Polar Retention for Coated PGC Experiments

Column	log k' Phenylhexane	Column	log k' 1,3-Dihydroxybenzene
PPGE	-0.03	C18 HYPERSIL	-0.47
C8 HYPERSIL	0.03	PPGE	-0.26
DECACYCLENE	0.3	DECACYCLENE	0.27
C18 HYPERSIL	0.45	POLYSTYRENE	0.29
SQUALANE	0.62	SQUALANE	0.35
POLYSTYRENE	0.75	PGC	1.2
PGC	1.21		

Columns given in order of increasing retention capacity

Table 4.6
Test Probes Employed for Chromatographic Characterisation

Mix 1 Phenols;
Acetone, Phenol, Anisole, Paracresol, Phenetole, 3,5 Xylenol

Mix 2 Alkylbenzenes;
Toluene, Ethylbenzene, n-Propylbenzene, n-Butylbenzene,
n-Pentylbenzene, n-Hexylbenzene

Mix 3 O-substituted benzenes
Toluene, 1,2 dimethylbenzene, 1,2,3 trimethylbenzene,
1,2,3,4 tetramethylbenzene, 1,2,3,4,5,6 hexamethylbenzene

Mix 4 Hydroxybenzenes;
Phenol, 1,2-dihydroxybenzene, 1,3-dihydroxybenzene,
1,4 -drihydroxybenzene, 1,3,4-trihydroxybenzene

Mix 5 Anilines
Aniline, 1,2 Phenylendiamine, 1,3 Phenylendiamine, 1, Phenylendiamine

Mix 6 Halobenzenes
Fluorobenzene, Clorobenzene, Bromobenzene

Mix 7 Monsubstituted benzenes
Acetophenone, Methylbenzoate, Nitrobenzene, Anisole

Table 4.7
Retention Data for the Longest Retained Peak Employing the Test Mixture 1 on Coated and Uncoated Columns

Column 100 x 4.6mm	Mobile Phase Methanol:Water	Last Peak k'
PGC	95:5	5.08
C18 Hypersil	60:40	1.50
Squalane	60:40	1.23
Polystyrene	60:40	1.91
Polyphenylglycidylether	60:40	1.24
Decacyclene	60:40	1.31

Table 4.8
Selectivity Data for Test Mix 1 for Coated PGC Experiments

Column	k' Acetone	k' Phenol	k' Anisole	k' p-Cresol	k' Phenetole	k' 3,5-Xylenol
PGC	0	0.59	1.65	1.98	3.65	5.08
SQUALANE	0	0.26	1.50	0.57	3.48	1.23
POLYSTYRENE	0	0.28	1.68	0.77	3.27	1.91
PPGE	0	0.26	1.01	0.70	1.77	1.24
DECACYCLENE	0	0.45	1.04	0.82	2.15	1.31
C18 HYPERSIL	0	0.40	1.81	0.80	3.26	1.50

Table 4.9
Chromatographic Retention Data for Alkylbenzenes

	*C1	C2	C3	C4	C5	C6	C7	C8	C9	Alpha	Beta
PGC	-0.37	x	x	x	0.60	0.87	1.14	1.43	1.70	0.28	-1.05
SQUALANE	-0.23	x	x	x	0.35	0.62	0.86	1.13	1.41	0.27	-1.24
POLYSTYRENE	-0.48	-0.17	-0.02	0.14	0.52	0.75	1.00	1.26	1.52	0.25	-0.97
PPGE	-0.51	x	x	x	-0.23	-0.03	0.12	0.37	0.63	0.22	-1.53
DECACYCLENE	x	x	x	x	0.04	0.30	0.56	0.81	1.06	0.26	-1.49
C18	0.02	-0.37	-0.19	-0.02	0.29	0.45	0.61	0.76	0.91	0.15	-0.63
C8	-0.15	-0.62	-0.47	-0.33	-0.08	0.03	0.15	0.25	0.35	0.11	-0.72

Mobile phase : 80% methanol water for all but PGC where 95 5 methanol:water was used
* C1 , C2 etc refer to the number of -CH2- groups present in the aliphatic chain
x' represents points not measured

Table 4.10
Summary of Data Relating to Equation [4.5] for the Retention of Alkylbenzenes

Column 100 x 4.6mm	Mobile Phase	Gradient α	Intercept β
PGC	95%	0.28	-1.05
Squalane	80%	0.27	-1.25
Polystyrene	80%	0.25	-0.97
Polyphenylglycidylether	80%	0.22	-1.53
Decacyclene	80%	0.26	-1.49
C8 Hypersil	80%	0.11	-0.72
C18 Hypersil	80%	0.15	-0.63

Table 4.11
Chromatographic Retention Data for the Polymethylbenzenes

	C1	C2	C3	C5	C6	α	β
PGC	-0.37	0.06	0.57	1.52	2.13	0.52	-0.98
SQUALANE	-0.23	0.15	0.61	1.45	2.06	0.48	-0.81
POLYSTYRENE	-0.48	-0.13	0.34	1.25	1.77	0.48	-1.09
PPGE	-0.51	-0.27	0.16	1.08	1.56	0.46	-1.18
DECACYCLENE	x	x	x	x	x	x	x
C18	0.02	0.19	0.38	0.76	0.88	0.17	-0.16
C8	-0.15	-0.02	0.11	0.39	0.51	0.13	-0.28

Mobile phase : 80% methanol water for all but PGC where 95 5 methanol: water was used
* C1 , C2 etc refer to the number of -CH3-- groups attached directly to the benzene ring
x' represents points not measured

Table 4.12
Summary of Data Relating to Equation [4.5] for the Retention of the Polymethylbenzenes

Column 100 x 4.6mm	Mobile Phase	Gradient α	Intercept β
PGC	95%	0.52	0.98
Squalane	80%	0.48	1.09
Polystyrene	80%	0.48	0.81
Polyphenylglycidylether	80%	0.46	1.18
Decacyclene*	.	-	-
C8 Hypersil	80%	0.13	0.28
C18 Hypersil	80%	0.17	-0.16

Table 4.13
Chromatographic Retention data for Hydroxybenzenes

PGC		log k'	log k'	log k'	log k'	log k'	Gradient A	log k'$_w$
% Methanol	20	30	35	40	50	60		
Phenol	1.42	1.01	0.85	0.69	0.45	0.18	-0.03	1.83
1,2-dihydroxybenzene		1.08	0.93	0.74	0.51	0.23	-0.03	1.94
1,3-dihydroxybenzene	1.80	1.20		0.88	0.64	0.34	-0.03	2.07
1,4-dihydroxybenzene		1.04	0.86	0.64	0.49	0.19	-0.03	1.89
1,2,4-trihysroxybenzene		0.90	0.81	0.67	0.48	0.21	-0.02	1.59
1,3,5-trihydroxybenzene	2.35	1.93		1.66	1.34	0.99	-0.03	2.87
Squalane	log k'	log k'	log k'	log k'	log k'		Gradient A	log k'w
% Methanol	5	10	15	20	30			
Phenol	0.86	0.79	0.67	0.54	0.24		-0.03	1.07
1,2-dihydroxybenzene	0.69	0.44	0.28	-0.03	-0.29		-0.04	0.81
1,3-dihydroxybenzene	1.05	0.78	0.56	0.35	-0.07		-0.04	1.20
1,4-dihydroxybenzene	0.85	0.62	0.33	0.10	-0.30		-0.05	1.08
1,2,4-trihydroxybenzene	0.73	0.59	0.44	0.24	-0.07		-0.03	0.92
1,3,5-trihydroxybenzene	1.43	1.13	0.83	0.56	-0.15		-0.06	1.77
Polystyrene	log k'	log k'	log k'	log k'	log k'		Gradient A	log k'w
% Methanol	10	15	20	25	30			
Phenol	0.87	0.73	0.64	0.48	0.45		-0.02	1.02
1,2-dihydroxybenzene	0.75	0.60	0.42	0.30	0.17		-0.03	1.02
1,3-dihydroxybenzene	0.89	0.75	0.56	0.43	0.29		-0.03	1.21
1,4-dihydroxybenzene	0.79	0.62	0.41	0.31	0.15		-0.03	1.08
1,2,4-trihydroxybenzene	0.75	0.62	0.47	0.38	0.26		-0.02	0.98
1,3,5-trihydroxybenzene	1.32	0.83	0.67	0.57	0.37		-0.03	1.29

Table 4.13 ...continued

Table 4.13 ...continued

Polyphenylglycidylether	log k'	log k'	log k'	log k'	log k'	Gradient A	log k'w
% Methanol	5	10	15	20	30		
Phenol	0.47	0.38	0.28	0.20	-0.06	-0.02	0.60
1,2-dihydroxybenzene	0.19	0.02	-0.10	-0.21	-0.42	-0.02	0.24
1,3-dihydroxybenzene	0.42	0.24	0.12	-0.03	-0.26	-0.02	0.49
1,4-dihydroxybenzene	0.10	0.02	-0.16	-0.32	-0.49	-0.03	0.27
1,2,4-trihydroxybenzene	0.20	0.21	0.06	-0.05	-0.46	-0.03	0.54
1,3,5-trihydroxybenzene	0.30	0.21	0.11	0.02	-0.19	-0.02	0.40
Decacyclene	log k'	log k'	log k'	log k'	log k'	Gradient A	log k'w
% Methanol	5	10	15	20	30		
Phenol	0.77	0.67	0.62	0.57	0.41	-0.01	0.81
1,2-dihydroxybenzene	0.50	0.37	0.28	0.15	-0.06	-0.02	0.58
1,3-dihydroxybenzene	0.83	0.68	0.58	0.48	0.27	-0.02	0.89
1,4-dihydroxybenzene	0.73	0.57	0.41	0.32	0.07	-0.03	0.83
1,2,4-trihydroxybenzene	0.65	0.54	0.48	0.41	0.22	-0.02	0.69
1,3,5-trihydroxybenzene	0.78	0.60	0.30	0.12	-0.32	-0.05	1.07
Hypersil C18	log k'	log k'	log k'	log k'	log k'	Gradient A	log k'w
% Methanol	5	10	15	20	30		
Phenol	0.79	0.72	0.61	0.53	0.33	-0.02	0.92
1,2-dihydroxybenzene	-0.72	-0.68	-0.72	-0.84	-1.46	x	x
1,3-dihydroxybenzene	0.21	0.07	-0.10	-0.20	-0.46	-0.03	0.34
1,4-dihydroxybenzene	x	x	x	x	x	x	x
1,2,4-trihydroxybenzene	0.32	0.31	0.18	0.07	-0.13	-0.02	0.53
1,3,5-trihydroxybenzene	x	x	x	x	x	x	x

x = analyte not retained

Table 4.14
Summary of Gradient (A) Values for the Hydroxybenzenes on Coated and uncoated PGC

Column 100 x 4.6mm	(A) Phenol	(A) 1,3-Dihydroxybenzene	(A) 1,3,5-Trihydroxybenzene
PGC	-0.03	-0.03	-0.03
Squalane	-0.03	-0.04	-0.06
Polystyrene	-0.02	-0.03	-0.03
Polyphenylglycidylether *	-0.02	-0.02	-0.02
Decacyclene	-0.01	-0.02	-0.05
C18 Hypersil	-0.02	-0.04	-

Table 4.15

Chromatographic Retention Data for Anilines

PGC	log k'	lok k'	log k'	log k'		Gradient A	log k'_w
% Methanol	40	50	60	70			
Aniline	0.35	0.14	-0.09	-0.27		-0.02	1.19
1,2Phenylenediamine	0.26	0.07	-0.10	-0.25		-0.02	0.94
1,3Phenylenediamine	-0.13	-0.32	-0.48	-0.59		-0.02	0.49
1,4Phenylenediamine	-0.08	-0.27	-0.38	-0.50		-0.01	0.48
Squalane	log k'	log k'	log k'	log k'	log k'	Gradient A	log k'_w
% Methanol	5	10	20	30	50		
Aniline	1.00	0.81	0.28	0.12	-0.61	-0.04	1.17
1,2Phenylenediamine	0.84	0.63	0.09	-0.18	-1.15	-0.04	1.04
1,3Phenylenediamine	0.57	0.44	-0.28	-0.51	-2.10	-0.04	0.79
1,4Phenylenediamine	0.50	0.45	-0.03	-0.32	-0.71	-0.03	0.67
Polystyrene	log k'	log k'	log k'	log k'		Gradient A	log k'_w
% Methanol	40	50	60	70			
Aniline	0.09	-0.09	-0.32	-0.54		-0.02	0.94
1,2Phenylenediamine	0.17	-0.10	-0.33	-0.51		-0.02	1.07
1,3Phenylenediamine	x	x	x	x		x	x
1,4Phenylenediamine	-0.13	-0.24	-0.34	-0.42		-0.01	0.25

Table 4.15.....continued

Table 4.15.....continued

Polyphenylglycidylether	log k'	log k'	log k'	log k'	Gradient A	log k'_w
% Methanol	20	30	40	45		
Aniline	0.05	-0.12	-0.28	-0.34	-0.02	0.37
1,2Phenylenediamine		-0.25	-0.51	-0.62	-0.02	0.50
1,3Phenylenediamine	-0.44	-0.61	-0.80	-0.87	-0.02	-0.10
1,4Phenylenediamine	x	x	x	-0.62		

Decacyclene	log k'	log k'	log k'	log k'	Gradient A	log k'_w
% Methanol	20	40	50	60		
Aniline	0.57	0.06	-0.23	-0.55	-0.03	1.13
1,2Phenylenediamine	0.41	-0.13	-0.39	-0.66	-0.03	0.95
1,3Phenylenediamine	0.15	-0.46	-0.83	-1.20	-0.03	0.83
1,4Phenylenediamine	-0.06	-0.60	-1.20	-0.80	-0.02	0.32

C18 Hypersil	log k'	log k'	log k'	log k'	Gradient A	log k'_w
% Methanol	0.3	0.35	0.4	0.45		
Aniline	0.11	0.01	-0.11	-0.20	-0.02	0.71
1,2Phenylenediamine	x	x	-0.76	-0.75	x	x
1,3Phenylenediamine	x	x	-0.83	x	x	x
1,4Phenylenediamine	-0.61	-0.67	-0.70	x	x	x

x = analyte not retained

Table 4.16
Chromatographic Retention Data for Halobenzenes on Coated and Uncoated PGC

PGC	log k'	log k'	log k'	log k'		Gradient A	log k_w
% Methanol	80	85	90	95			
Fluorobenzene	-0.27	-0.40	-0.55	-0.67		-0.03	1.89
Chlorobenzene	0.20	0.06	-0.09	-0.22		-0.03	2.48
Bromobenzene	0.36	0.21	0.07	-0.08		-0.03	2.70
Polystyrene	log k'	log k'	log k'	log k'	log k'	Gradient A	log k_w
% Methanol% Methanol	75	80	85	90	95		
Fluorobenzene	-0.16	-0.27	-0.43	-0.62	-0.80	-0.03	2.1
Chlorobenzene	0.33	0.19	0.01	-0.15	-0.33	-0.03	2.7
Bromobenzene	0.49	0.36	0.19	0.02	-0.15	-0.03	2.8
Polyphenylglycidylether	log k'	log k'	log k'	log k'		Gradient A	log k_w
% Methanol	40	45	50	55			
Fluorobenzene	0.21	0.08	-0.06	-0.27		-0.02	0.98
Chlorobenzene	0.72	0.56	0.39	0.19		-0.02	1.57
Bromobenzene	0.94	0.77	0.60	0.38		-0.02	1.84
C18 Hypersil	log k'	log k'	log k'	log k'	log k'	Gradient A	log k_w
% Methanol	60	65	70	75	80		
Fluorobenzene	0.29	0.15	-0.03	-0.19	-0.34	-0.03	2.18
Chlorobenzene	0.58	0.42	0.23	0.06	-0.18	-0.03	2.67
Bromobenzene	0.67	0.50	0.31	0.14	-0.04	-0.04	2.79

Table 4.17
Summary of Chromatographic Parameters Observed for Halobenzenes on PGC and Coated PGC

Column 100 x 4.6mm	F-Benzene A	Cl-Benzene A	Br-Benzene A	F-Benzene log k'_w	Cl-Benzene log k'_w	Br-Benzene log k'_w
PGC	-0.03	-0.03	-0.03	1.89	2.48	2.70
Polystyrene	-0.03	-0.03	-0.03	2.1	2.7	2.8
Polyphenylglycidylether	-0.02	-0.02	-0.02	0.98	1.57	1.84
C18 Hypersil	-0.03	-0.03	-0.04	2.18	2.67	2.79

Squalane and decacyclene columns were not investigated with this test mixture.

Table 4.18
Chromatographic Retention Data for Other Mono Substituted Benzenes on PGC and Coated PGC

PGC	log k'	log k'	log k'	log k'	log k'	Gradient A	log k'_w
% Methanol	80	85	90	95	100		
acetophenone	0.23	0.14	-0.01	-0.10	-0.23	-0.02	1.98
nitrobenzene	0.50	0.41	0.29	0.21	0.11	-0.02	1.99
anisole	0.56	0.48	0.33	0.24	0.11	-0.02	2.29
methyl benzoate	0.79	0.68	0.54	0.45	0.34	-0.02	2.62
Polystyrene	log k'	log k'	log k'	log k'		Gradient A	log k'_w
% Methanol	70	75	80	90			
acetophenone	0.32	0.24	0.05	-0.18		-0.03	2.69
nitrobenzene	0.32	0.24	0.05	-0.18		-0.03	2.69
anisole	0.52	0.38	0.20	-0.10		-0.04	3.44
methyl benzoate	0.79	0.68	0.49	0.22		-0.04	3.48
Polyphenylglycidylether	log k'	log k'	log k'	log k'	log k'	Gradient A	log k'_w
% Methanol	40	45	50	55	60		
acetophenone	0.44	0.33	0.23	-0.02	-0.17	-0.03	1.68
nitrobenzene	0.44	0.33	0.23	0.07	-0.05	-0.02	1.42
anisole	0.81	0.65	0.53	0.34	0.19	-0.03	2.07
methyl benzoate	0.81	0.69	0.58	0.41	0.28	-0.03	1.87
Decacyclene	log k'	log k'	log k'			Gradient A	log k'_w
% Methanol	30	35	40				
acetophenone	0.79	0.64	0.51			-0.03	1.64
nitrobenzene	0.85	0.70	0.55			-0.03	1.78
anisole	1.14	0.94	0.76			-0.04	2.26
methyl benzoate	1.14	0.98	0.84			-0.03	2.02

Table 4.18 .....continued

Table 4.18 .....continued

C18 Hypersil	log k'	log k'	log k'	log k'	Gradient A	log k'_w
% Methanol	35	40	45	50		
acetophenone	0.76	0.58	0.42	0.26	-0.03	1.94
nitrobenzene	0.82	0.67	0.54	0.40	-0.03	1.79
anisole	1.07	0.93	0.79	0.66	-0.03	2.05
methyl benzoate	1.20	1.02	0.84	0.66	-0.04	2.47

Table 4.19
Summary of Chromatographic Data for Other Monosubstituted Benzenes on PGC and Coated PGC

Column 100 x 4.6mm	Acetophenone		Nitrobenzene		Anisol		Mehtylbenzoate	
	A	log k'_w	A	log k'_w	A	log k'_w	A	log k'_w
PGC	-0.02	1.98	-0.02	1.99	-0.02	2.29	-0.02	2.62
Polystyrene	-0.03	2.69	-0.03	2.69	-0.04	3.44	-0.04	3.48
Polyphenylglycidylether	-0.03	1.68	-0.02	1.42	-0.03	2.07	-0.03	1.87
Decacyclene	-0.03	1.64	-0.03	1.78	-0.04	2.26	-0.03	2.02
C18 Hypersil	-0.03	1.94	-0.03	1.79	-0.03	2.05	-0.04	2.47

Table 4.20

Effect on Chromatographic Retention of Test Mix 1 for Fractional PPGE Coated PGC

log k' analyte	Loading 0 mg	Loading 1.0 mg	Loading 1.9 mg	Loading 4.8 mg	Loading 9.6 mg	Loading 28.7 mg	Loading 47.8 mg	Loading 95.5 mg	Loading 180 mg
Phenol	-0.25	-0.24	-0.25	-0.24	-0.30	-0.48	-0.62	-0.64	-0.58
Anisole	0.18	0.09	0.07	0.05	0.02	-0.16	-0.22	-0.07	0.003
p-Cresol	0.25	0.25	0.23	0.24	0.18	-0.03	-0.17	-0.30	-0.22
Phenetole	0.49	0.39	0.37	0.34	0.32	0.11	0.04	0.19	0.25
3,5-Xylenol	0.63	0.62	0.61	0.62	0.56	0.35	0.19	0.05	0.093

Table 4.21

Dynamic Coating of PGC with Pyrene

Analytes: Dimethylphthalate (DMP) and Phenyl-heptane

loading (mg)	k' DMP	k' Phenyl-heptane
0.5	0.91	2.04
1	0.86	1.96
1.5	0.90	-
2	0.85	1.89
2.5	0.82	1.84
3	0.79	1.76
3.5	0.78	1.79
4	0.83	1.74
4.5	0.80	1.76
5	0.79	1.79
5.5	0.75	1.67
6	0.74	1.68
6.5	0.74	1.68
7	0.76	1.72
7.5	0.74	1.72
8	0.73	1.69
8.5	0.72	1.69
9	0.72	1.66
9.5	0.72	-1.00
10	0.73	1.69

Table 4.22
Dynamic Coating of PGC with Squalane

Analytes: Dimethylphthalate (DMP) and Phenyl-heptane

Load (mg)	k' DMP	k' Phenyl-heptane
0	1.52	3.01
0.8	1.46	2.89
1.6	1.41	2.82
2.4	1.34	2.74
3.2	1.29	2.65
4	1.22	2.57
4.8	1.16	2.47
5.6	1.09	2.40
6.4	1.03	2.33
7.2	0.97	2.25
8	0.91	2.17
8.8	0.84	2.09
9.6	0.78	2.00
10.4	0.81	2.02
11.2	0.81	2.07
12	0.80	1.98
12.8	0.81	2.02
13.6	0.82	2.02
14.4	0.83	2.03

Fig 4.1 & Fig 4.2
Relationship Between Capacity Factors and Partition Isotherm

Fig 4.1
Measurement of Capacity factors from a Chromatogram

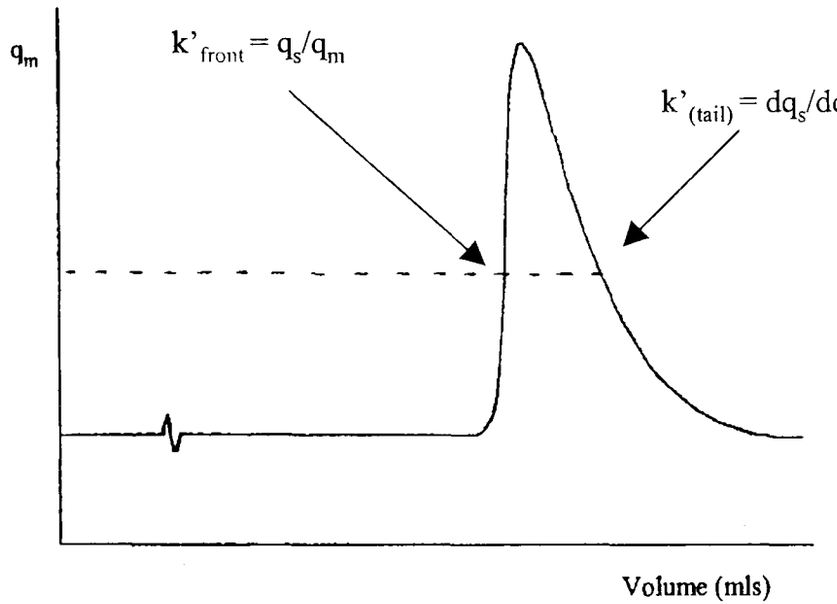

Fig 4.2
Capacity Factors as part of the Partition Isotherm

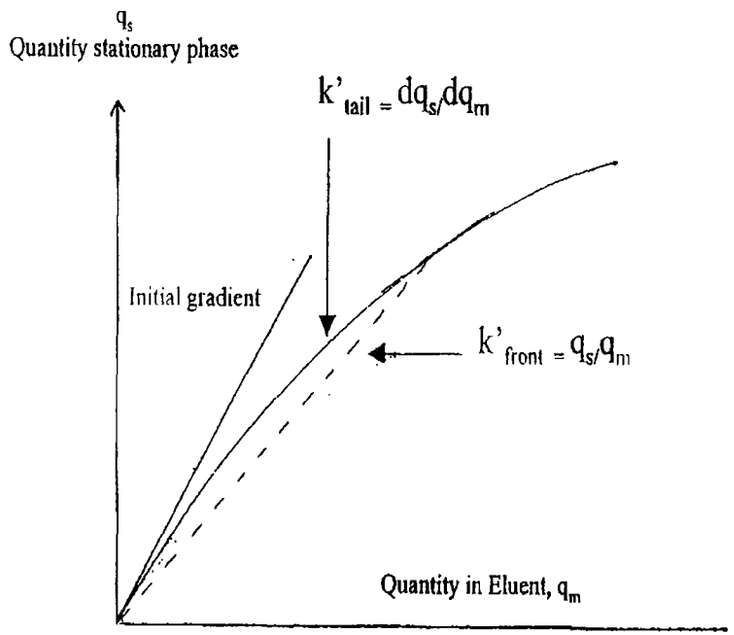

Fig 4.3

Molecular Structures for Polyaromatic Compounds used in PGC Isotherm Studies

Naphthalene

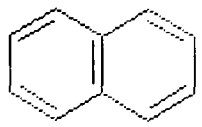

N2380

MW = 130
Molecular area = $80A^2$

Anthracene

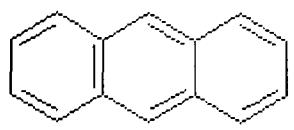

10590

MW = 178
Molecular area = $112A^2$

Pyrene

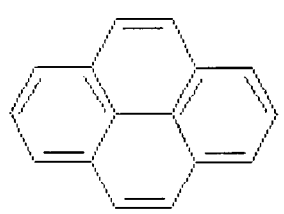

13,159-8

MW = 202
Molecular Area = $136A^2$

Fig 4.4

Molecular Structures for other Compounds used in the Isotherm studies

Benzenedodecyl Sulphonate , Sodium salt

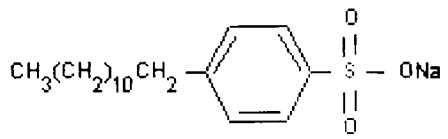

28,995-7

MW = 438
Molecular Area = $198A^2$

Cetylpyridinium bromide

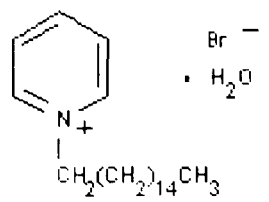

C5881

MW = 404
Molecular Area = $218A^2$

All chemicals were purchased from Aldrich Chemical Company. The number beneath the structures are the Aldrich catalogue numbers.

Fig 4.5
Pump Calibration Check

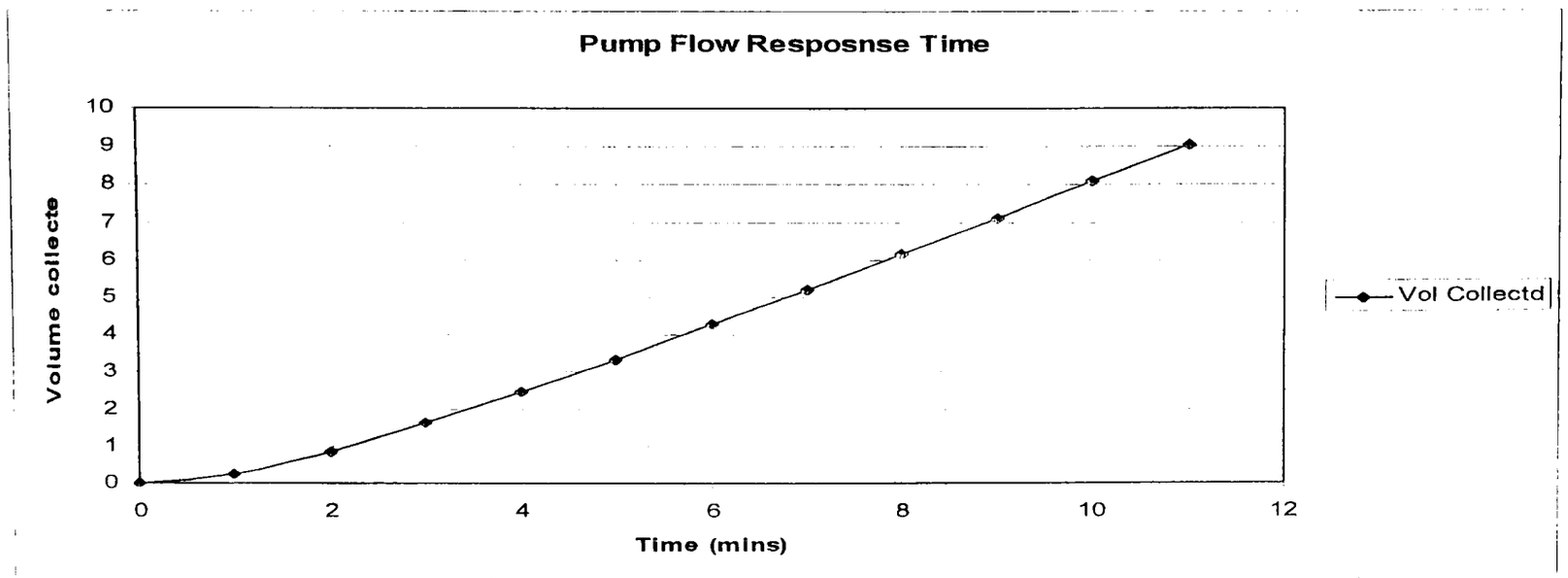

Time	Wt CH2Cl2	Vol Collectd	Change in vol
0	0	0	0
1	0.34	0.25	0.25
2	1.13	0.85	0.6
3	2.14	1.61	0.76
4	3.26	2.45	0.84
5	4.45	3.35	0.9
6	5.68	4.28	0.93
7	6.92	5.21	0.93
8	8.17	6.16	0.95
9	9.45	7.12	0.96
10	10.72	8.08	0.96
11	12.01	9.05	0.97

Fig 4.6

Adsorption Isotherms for Polyaromatic Hydrocarbons on PGC

Fig 4.6a

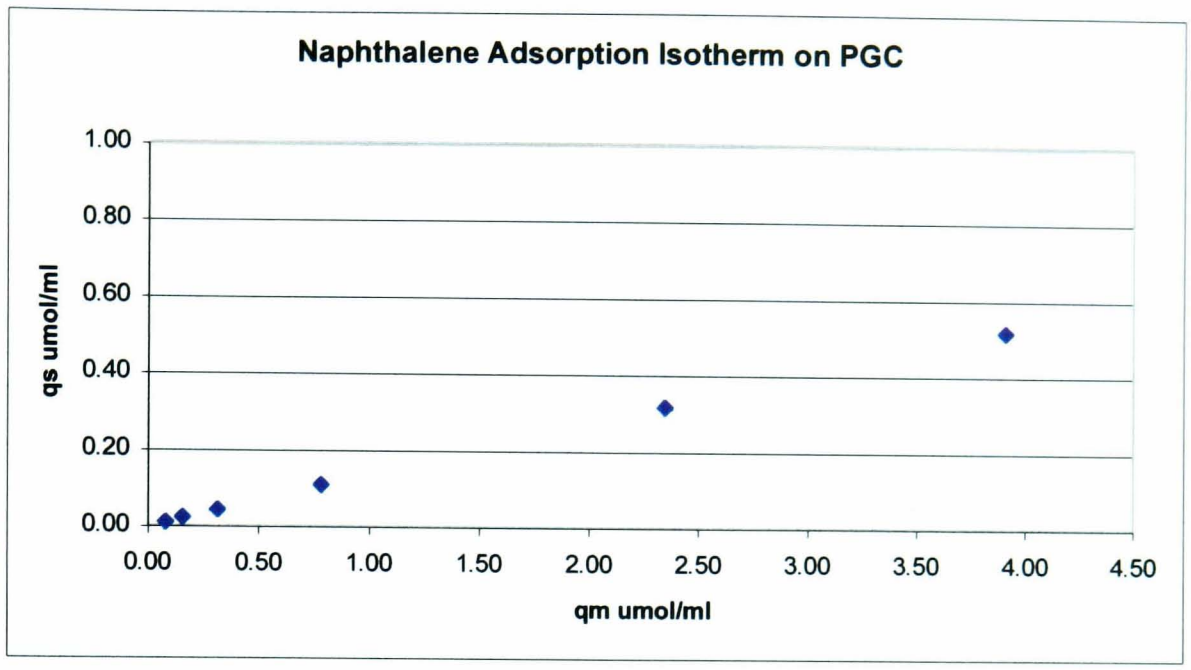

Fig 4.6b

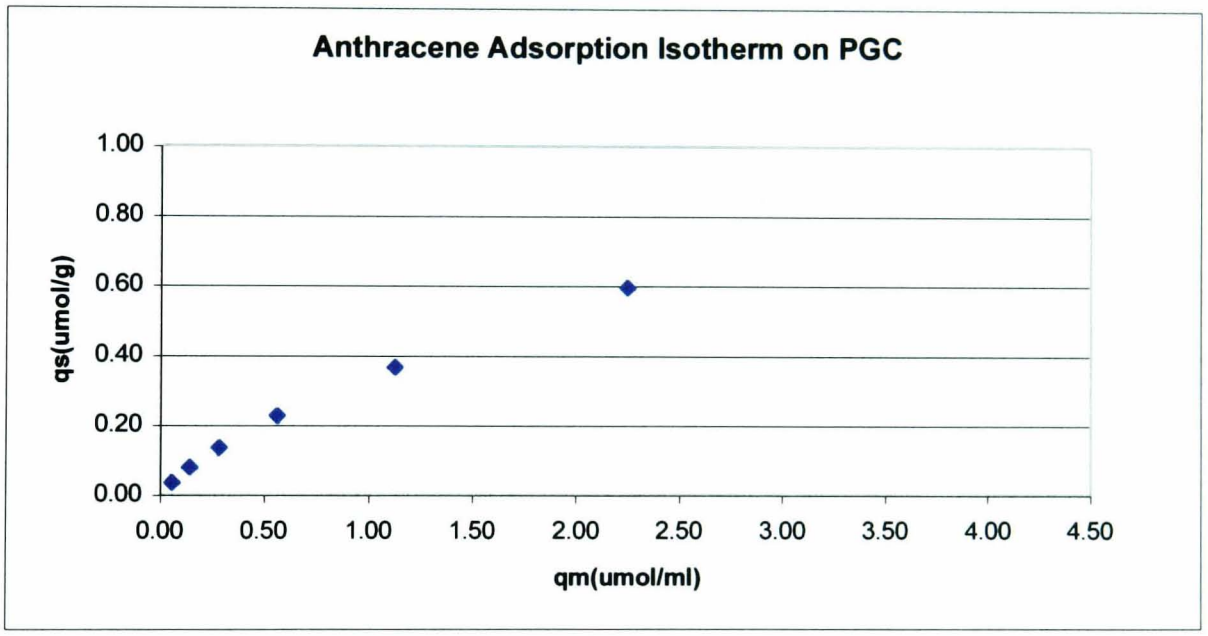

Fig 4.6c

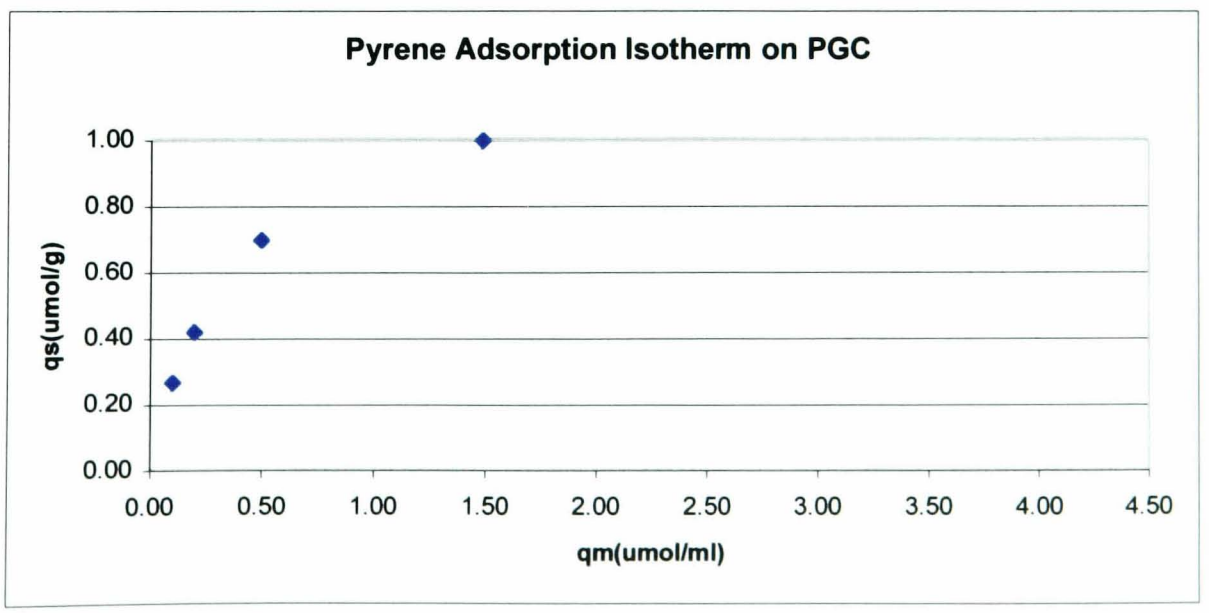

Fig 4.6 Continued

Adsorption Isotherms for Linear Surfactant Type Molecules on PGC

Fig 4.6d

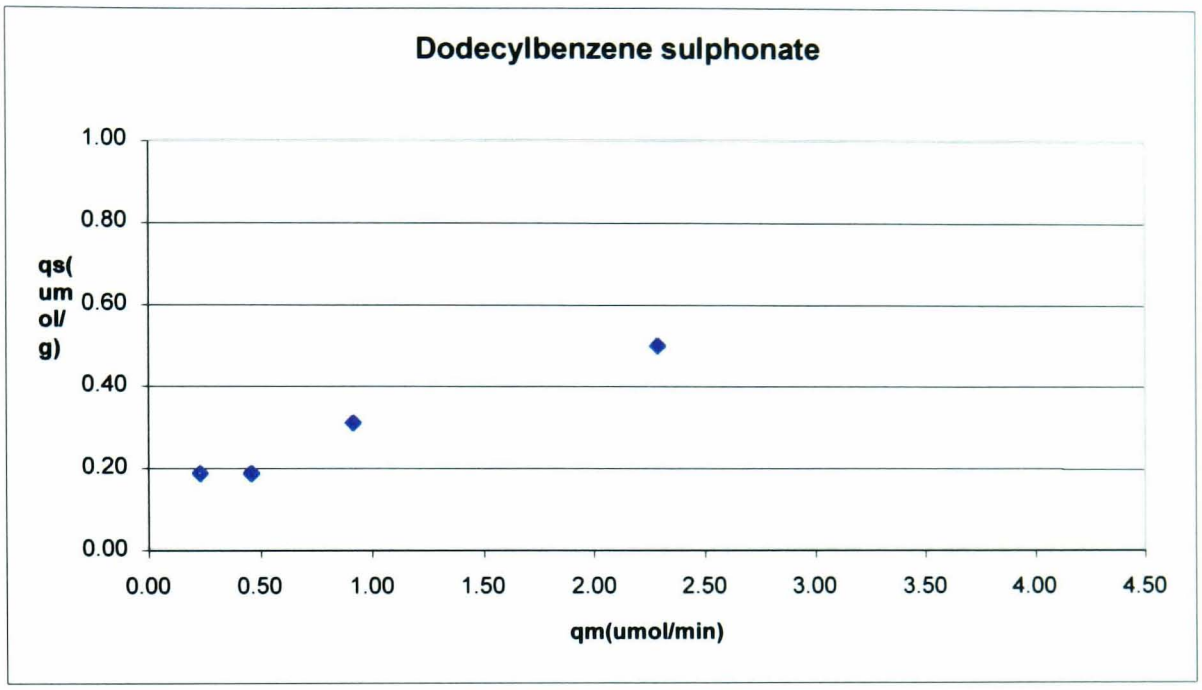

Fig 4.6e

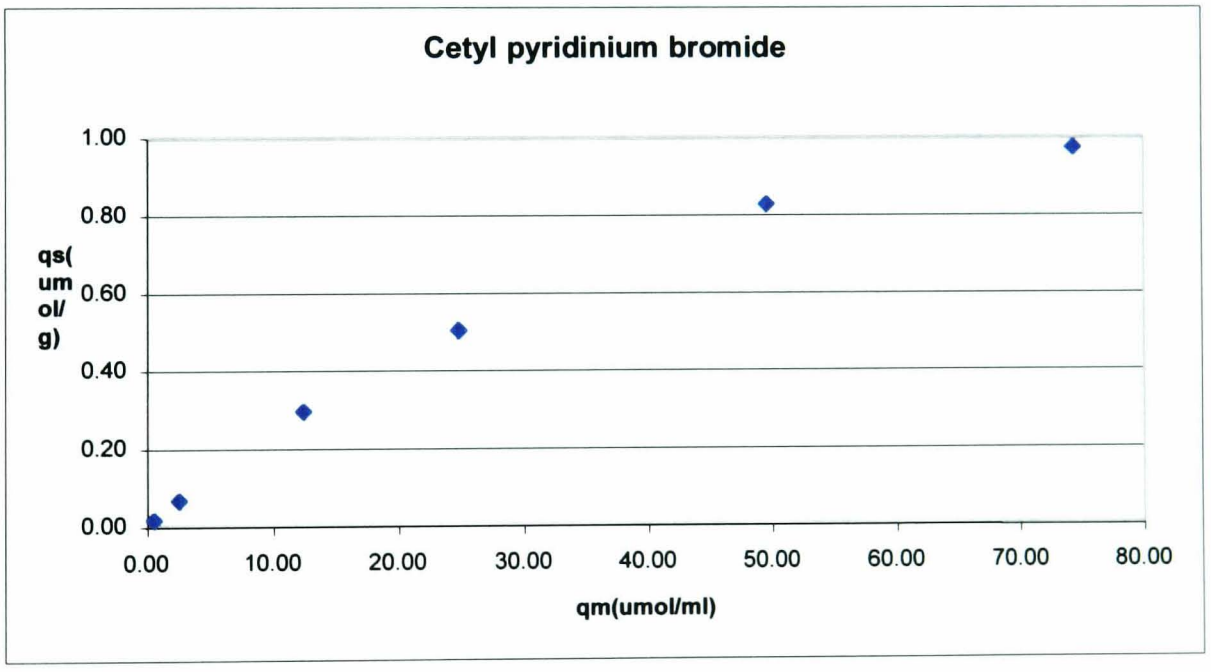

Fig 4.7

Linear plot for 1/qs vs 1/qm

Fig 4.7a

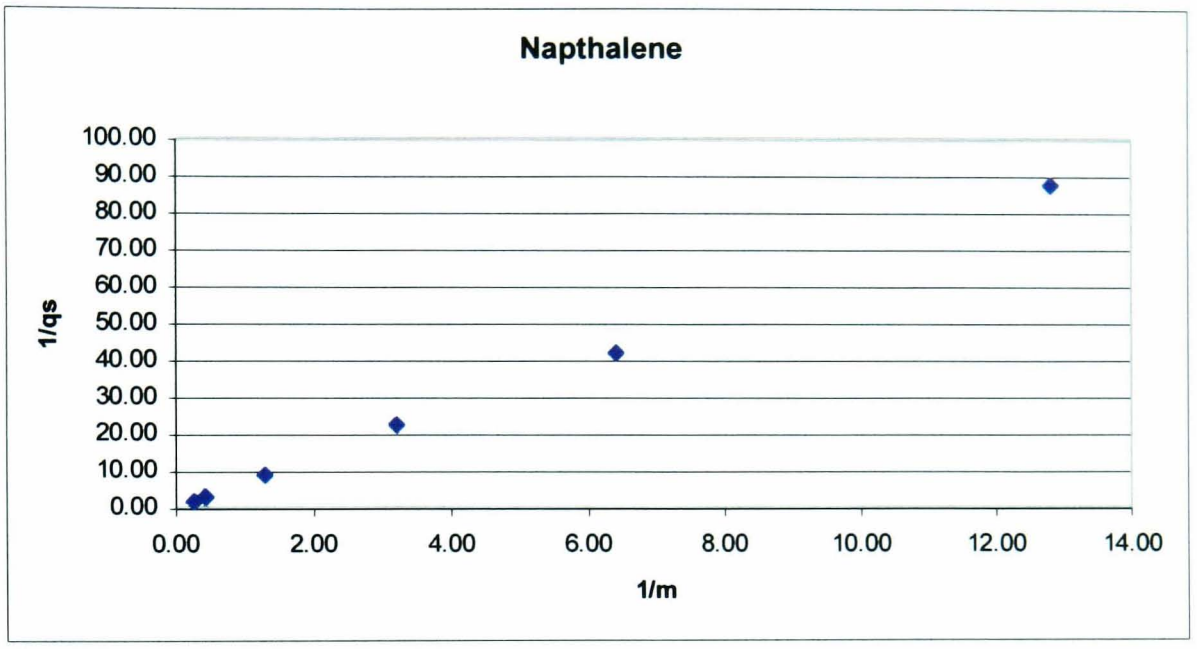

Fig 4.7b

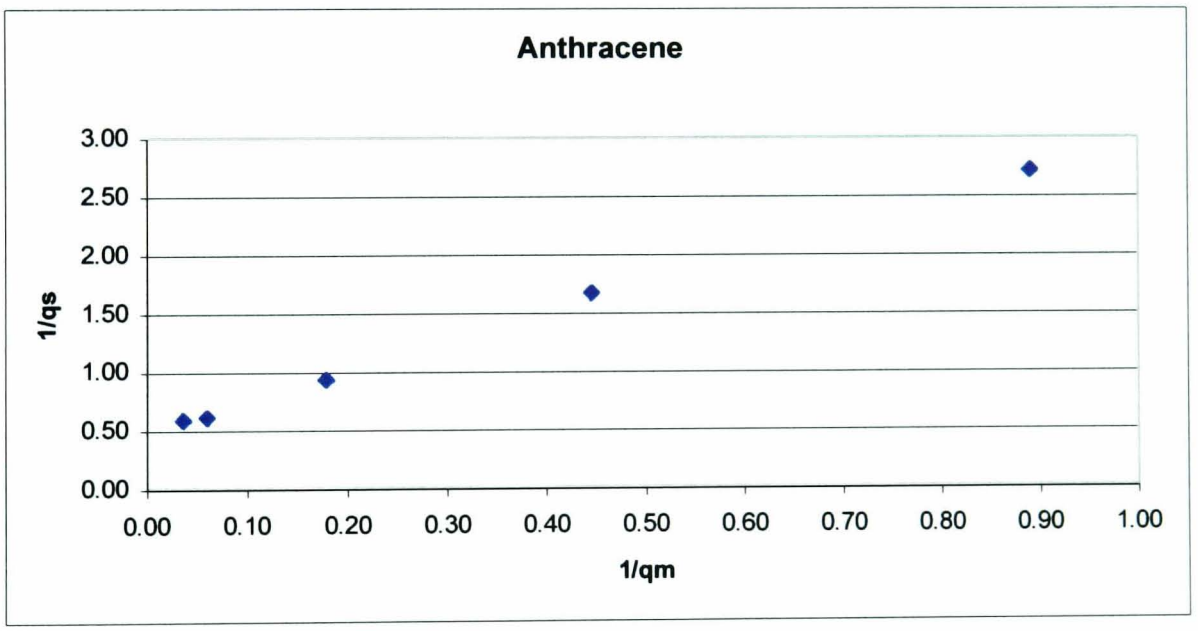

Fig 4.7c

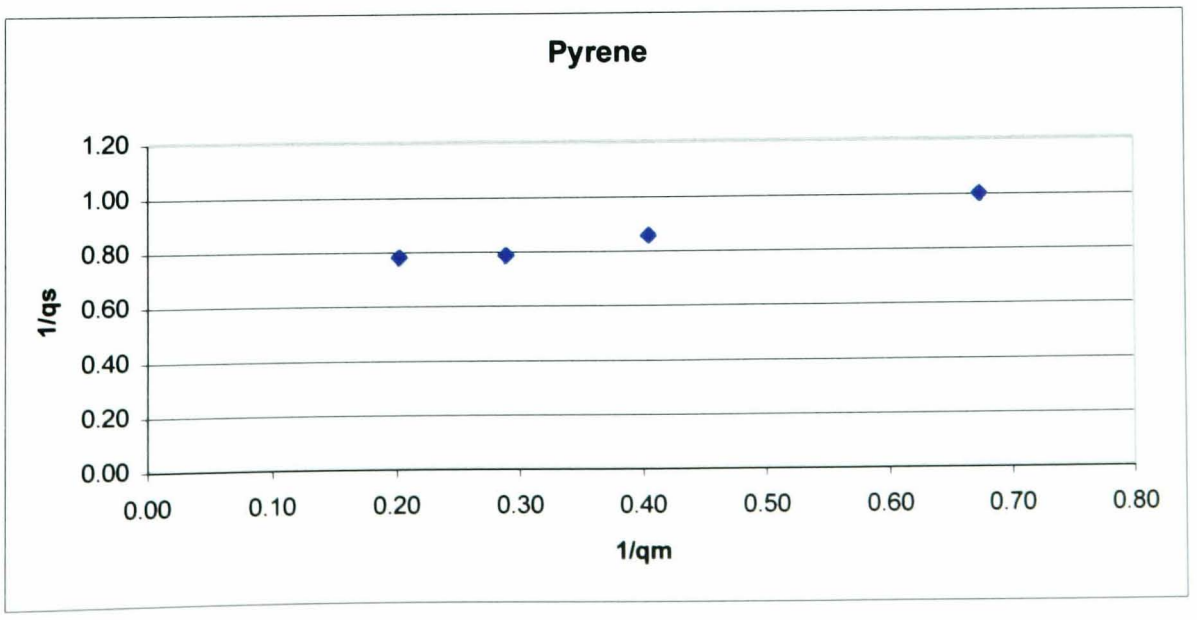

Fig 4.7 Continued

Linear plot for 1/qs vs 1//qm

Fig 4.7d

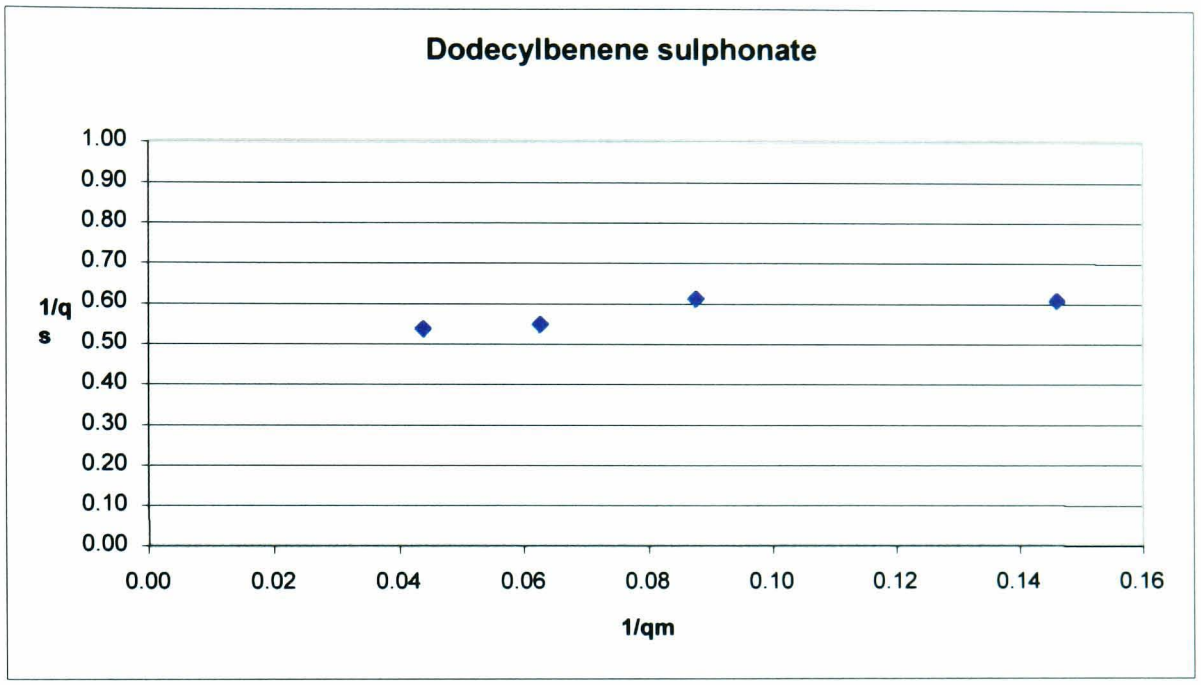

Fig 4.7e

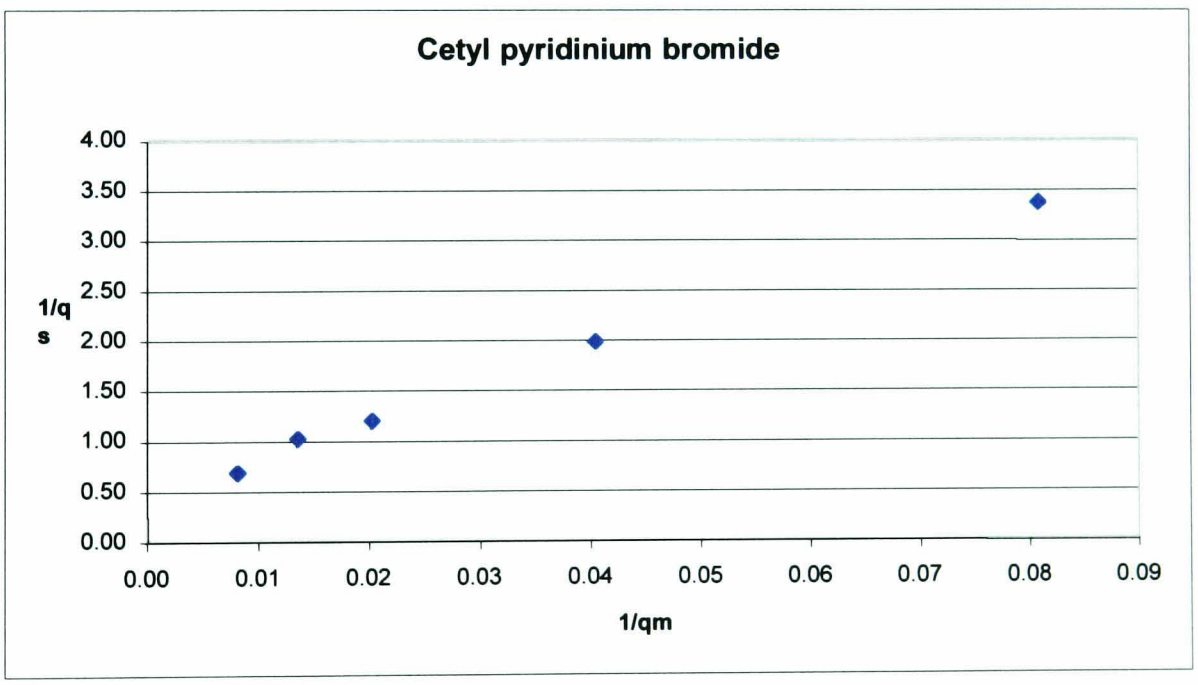

Fig 4.8

Structures for Compounds used in the PGC Coating Experiments

Pyrene

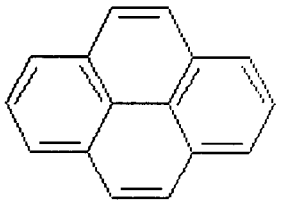

13,159-8

MW = 202.3

Squalane

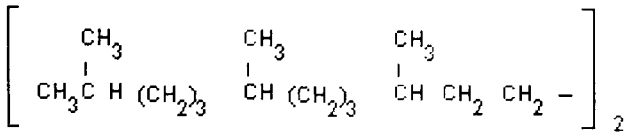

S4510

MW = 422.8

Polystyrene

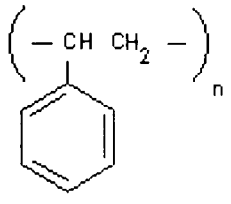

37,951-4

MW =13,000

Polyphenylglycidylether

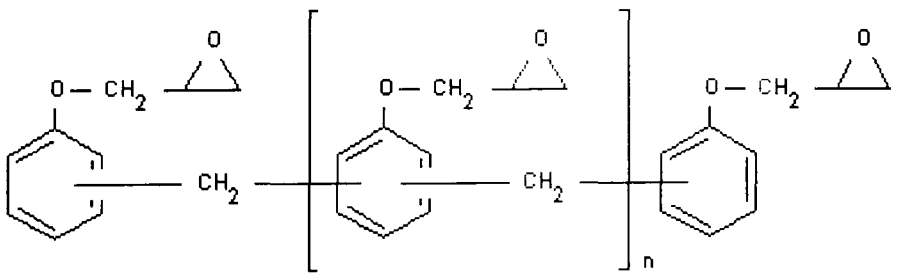

40,675-9

MW = 605

Decacyclene

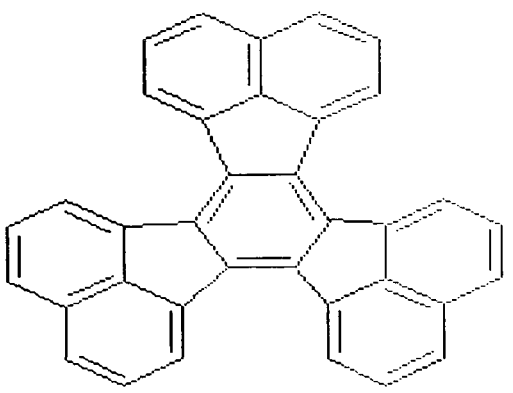

D20-0

MW = 450.5

All chemicals were purchased from Aldrich Chemical Company. The number beneath the structures are the Aldrich catalogue numbers.

Fig 4.9a
Comparison of Hydrophobic Retention of Phenylhexane for PGC Coating Experiments

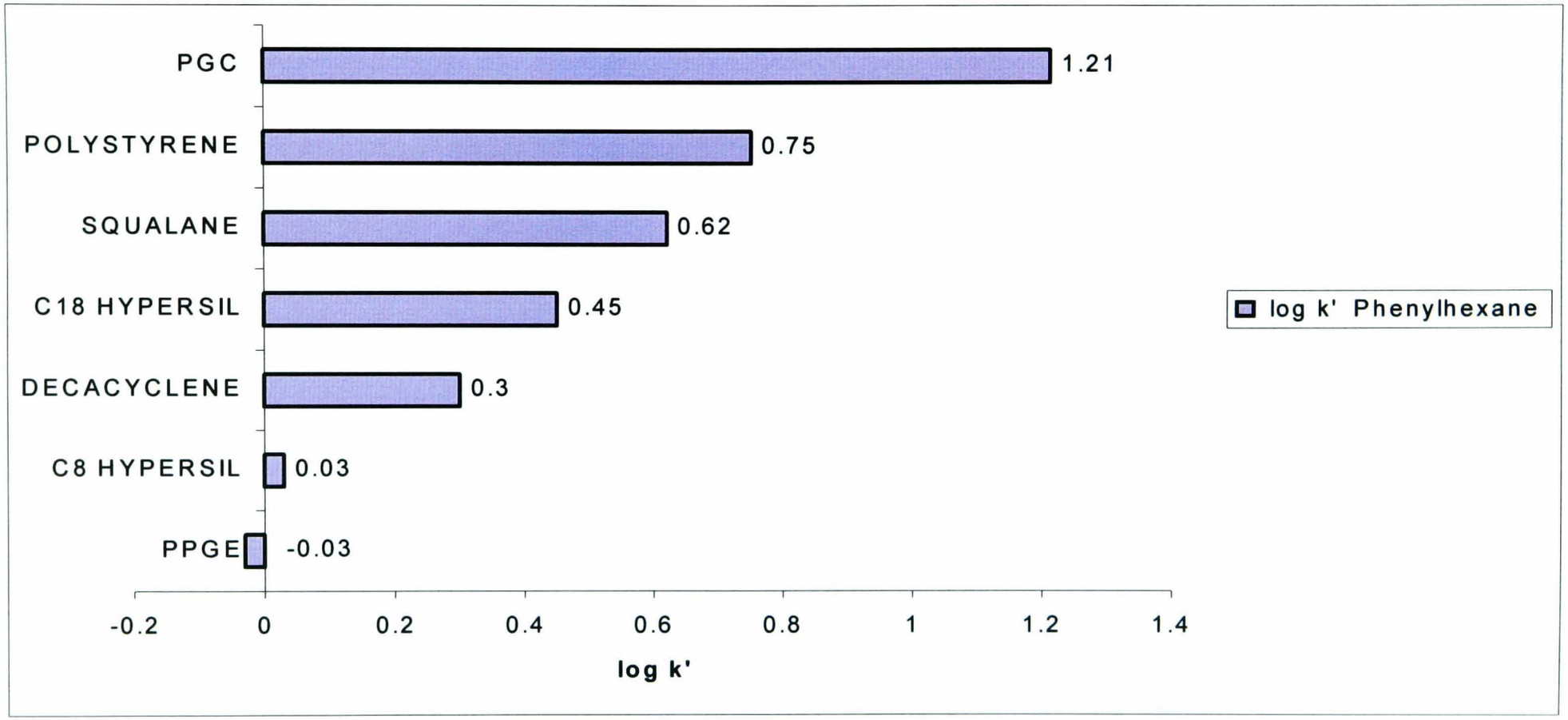

All columns: 100 x 4.6mm Flow: 1.0ml/min
Mobile Phase: 80% Methanol:Water Absorbence: 254nm

Fig 4.9b

Comparison for Polar Retention of 1,3 Dihydroxyphenol for PGC Coating Experiments

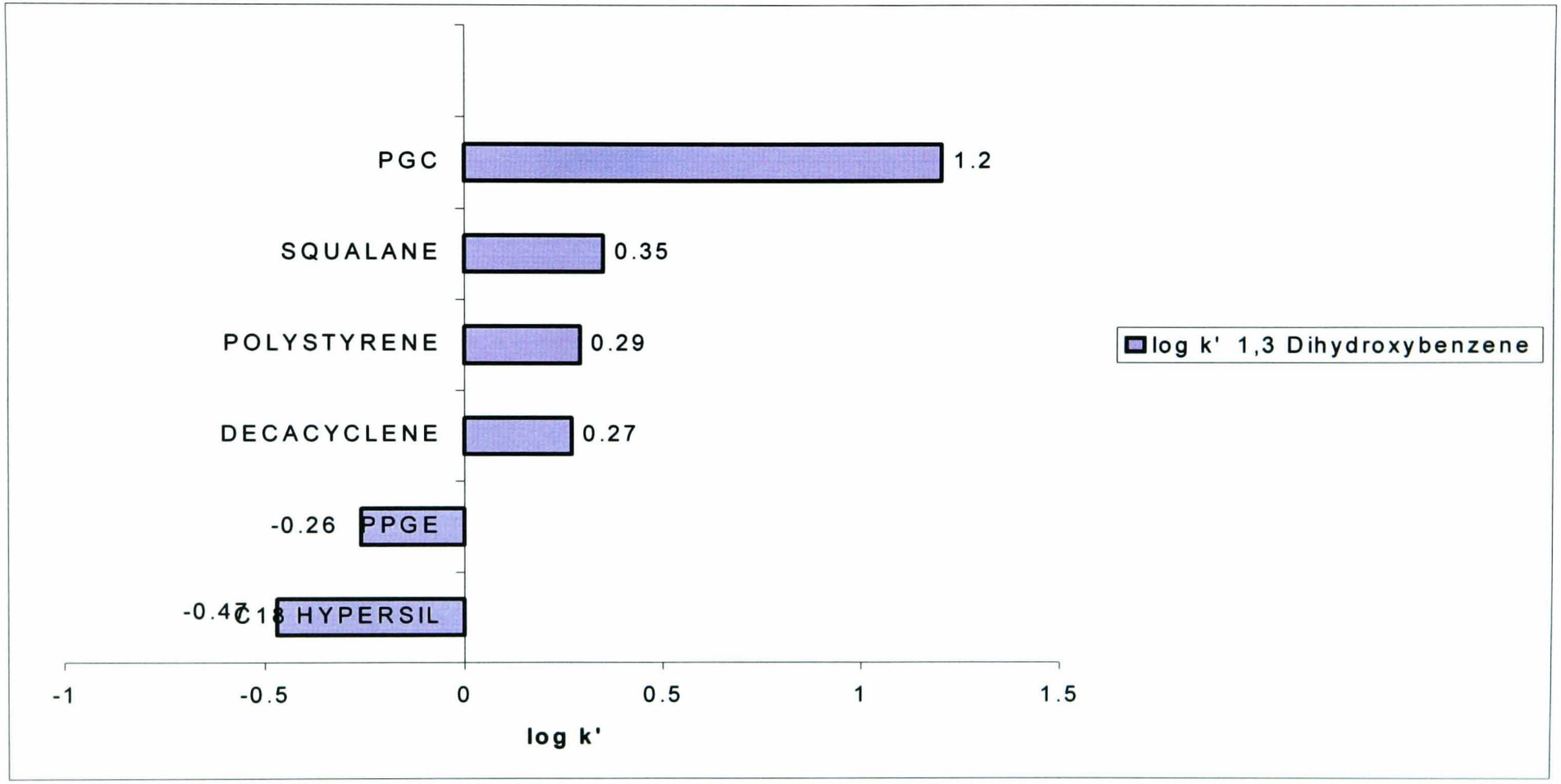

All columns: 100 x 4.6mm
Mobile Phase: 30% Methanol:Water

Fow: 1.0ml/min
Absorbance: 254nm

Fig 4.10
Chromatographic selectivity of Coated PGC with Test Mix 1

Fig 4.10a

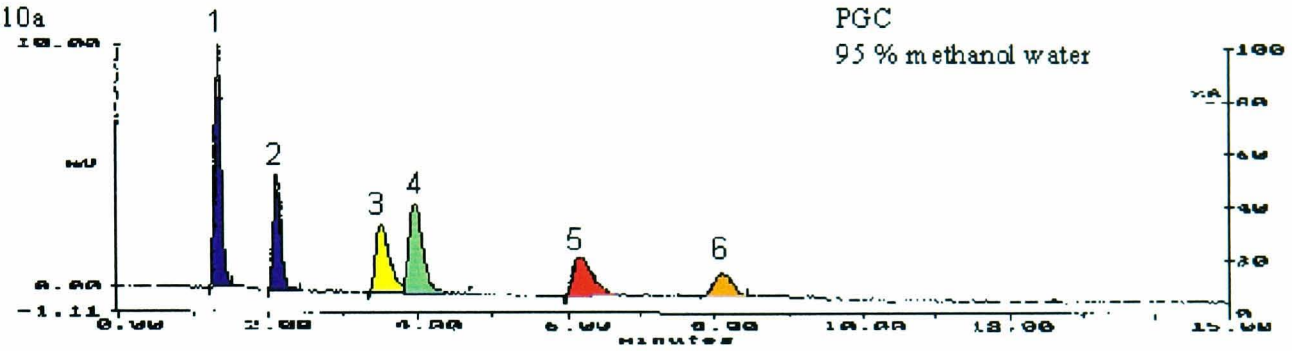

Fig 4.10b

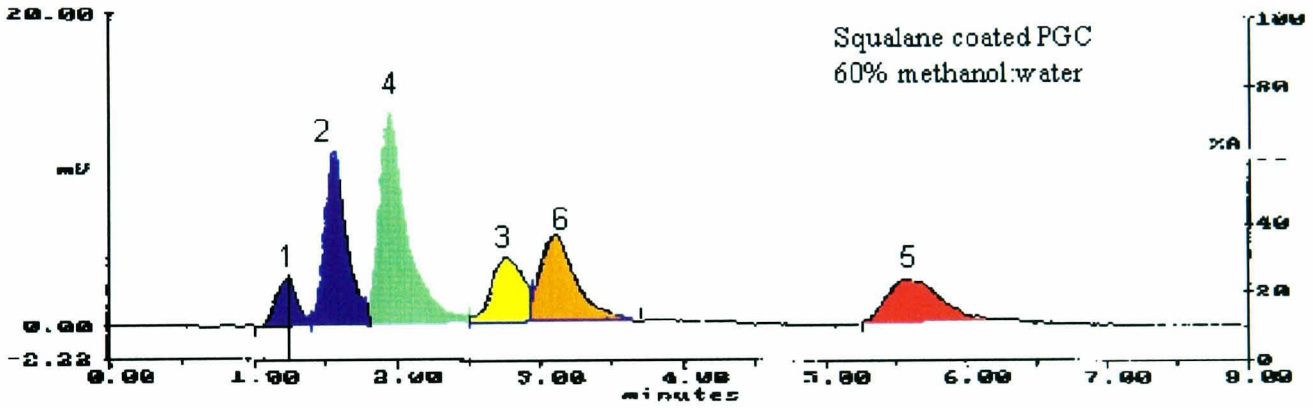

Fig 4.10c

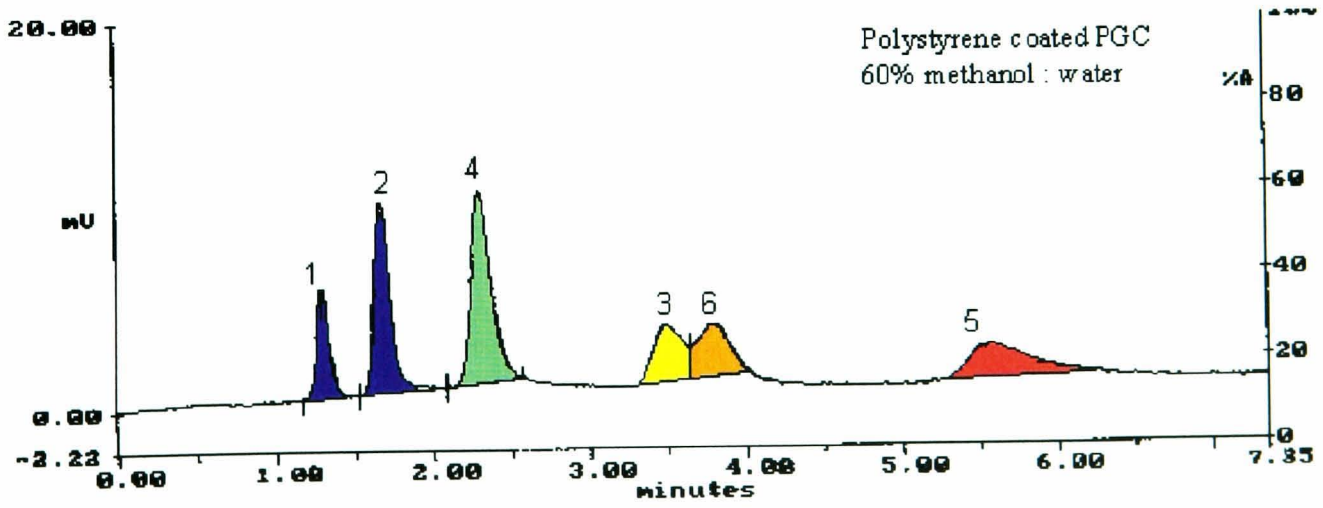

Column: 100mm x 4.6mm
Test Solutes : 1. Acetone , 2.Phenol , 3. Anisol , 4.Para Cresol , 5.Phenetol , 6. .3.5Xylenol

Fig 4.10
Chromatographic selectivity of Coated PGC with Test Mix 1

Fig 4.10c

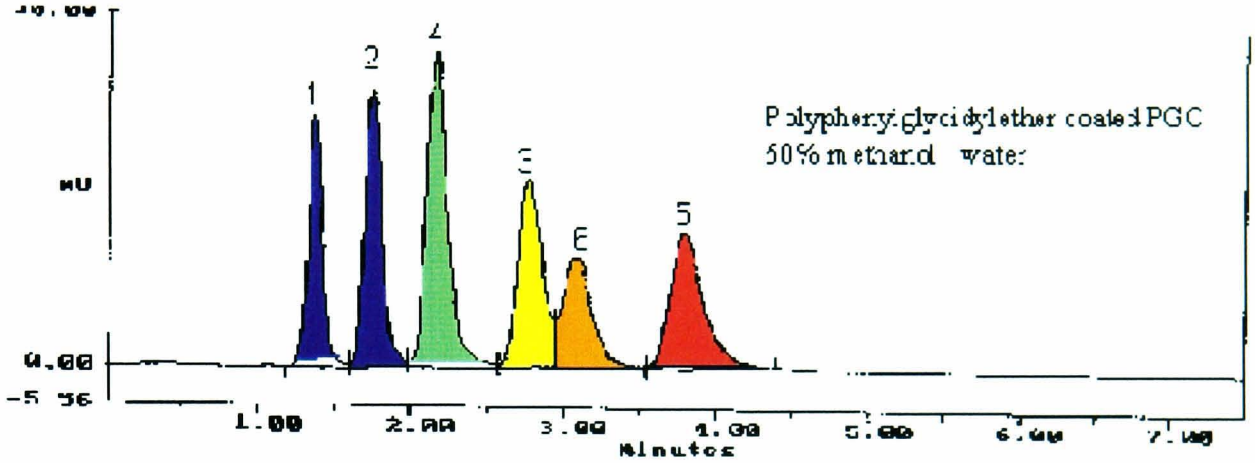

Fig 4.10d

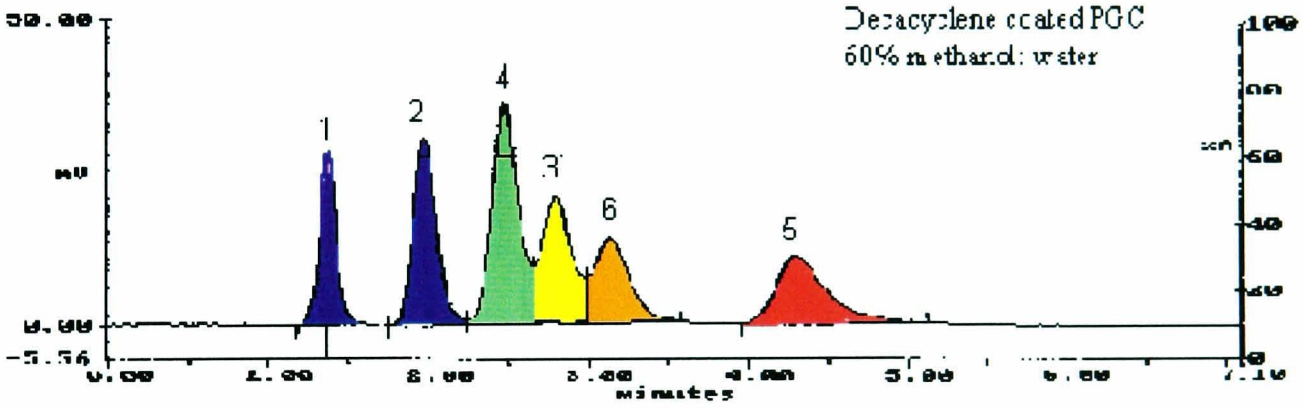

Fig 4.10e

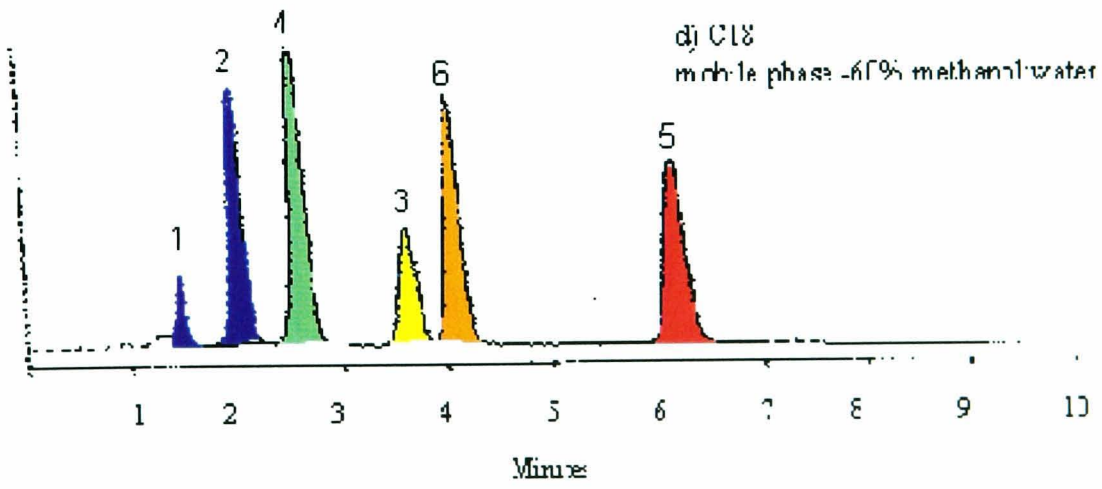

Column: 100mm x 4.6mm
Test Solutes : 1. Acetone , 2.Phenol , 3. Anisol , 4.Para Cresol , 5.Phenetol , 6. .3.5Xylenol

Fig 4.11

Retention of Alkylbenzenes for PGC Coating Experiments

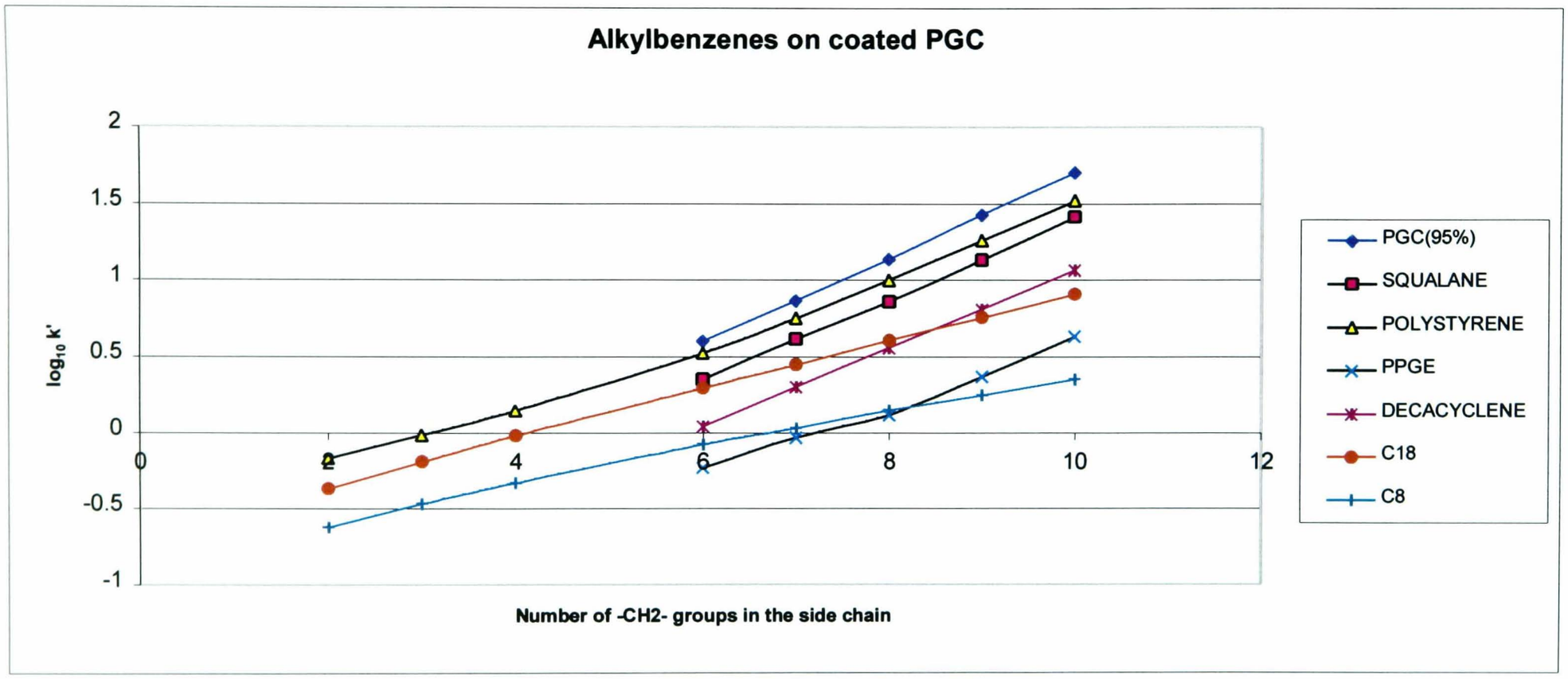

Mobile Phase : 80% Methanol:water for all but bare PGC where 95% was employed.

Absorbance 254nm

Flow 1.0ml/min

PPGE is the abbreviated chosen for Polyphenylglycidylether

Fig 4.12

Retention of Ortho Methyl Substituted Benzenes for PGC coating Experiments

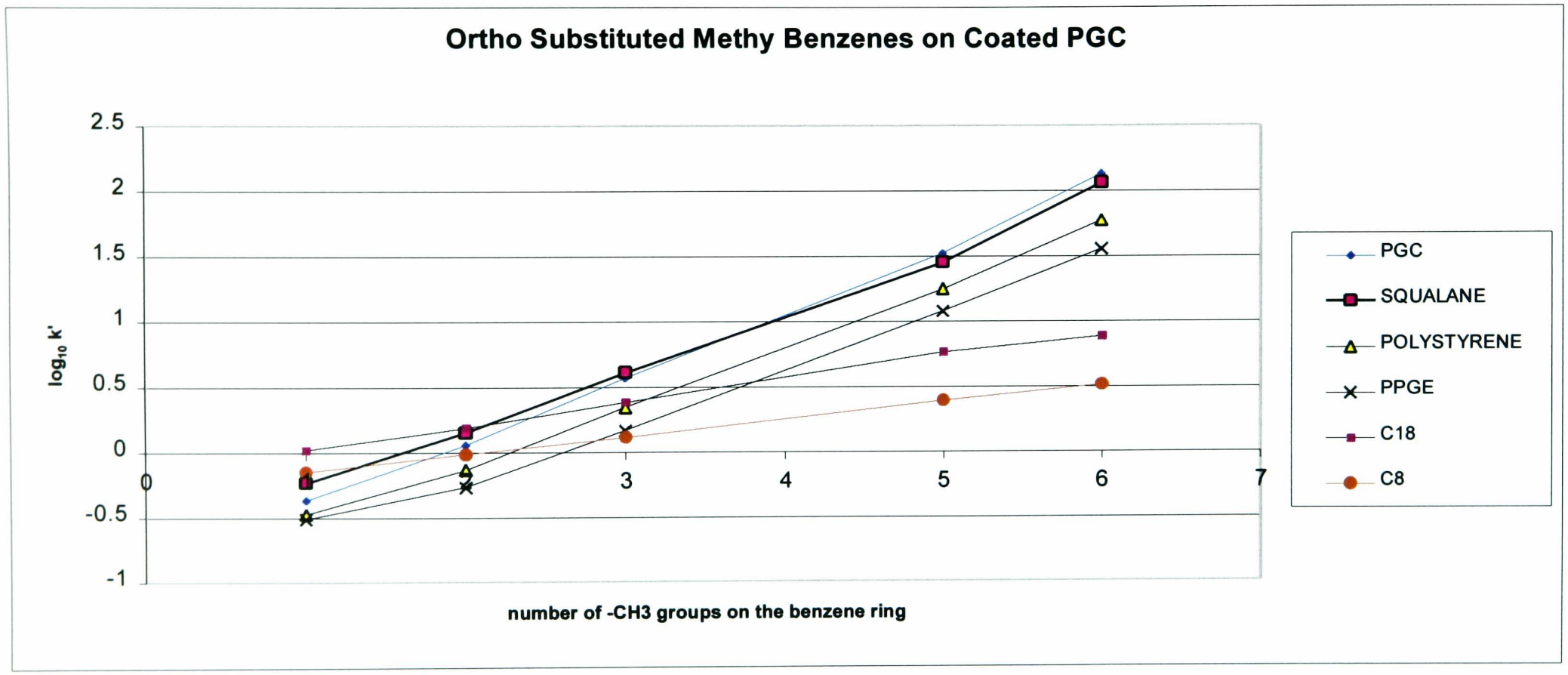

Mobile Phase : 80% Methanol:water for all but bare PGC where 95% was employed.

Absorbance 254nm

Flow 1.0ml/min

Decacyclene coated PGC column not run - see main text

PPGE is the abreviated chosen for Polyphenylglycidylether

Fig 4.13

Retention of Hydroxybenzenes in various Methanol:Water Compositions for PGC Coating Experiments

Fig 4.13a

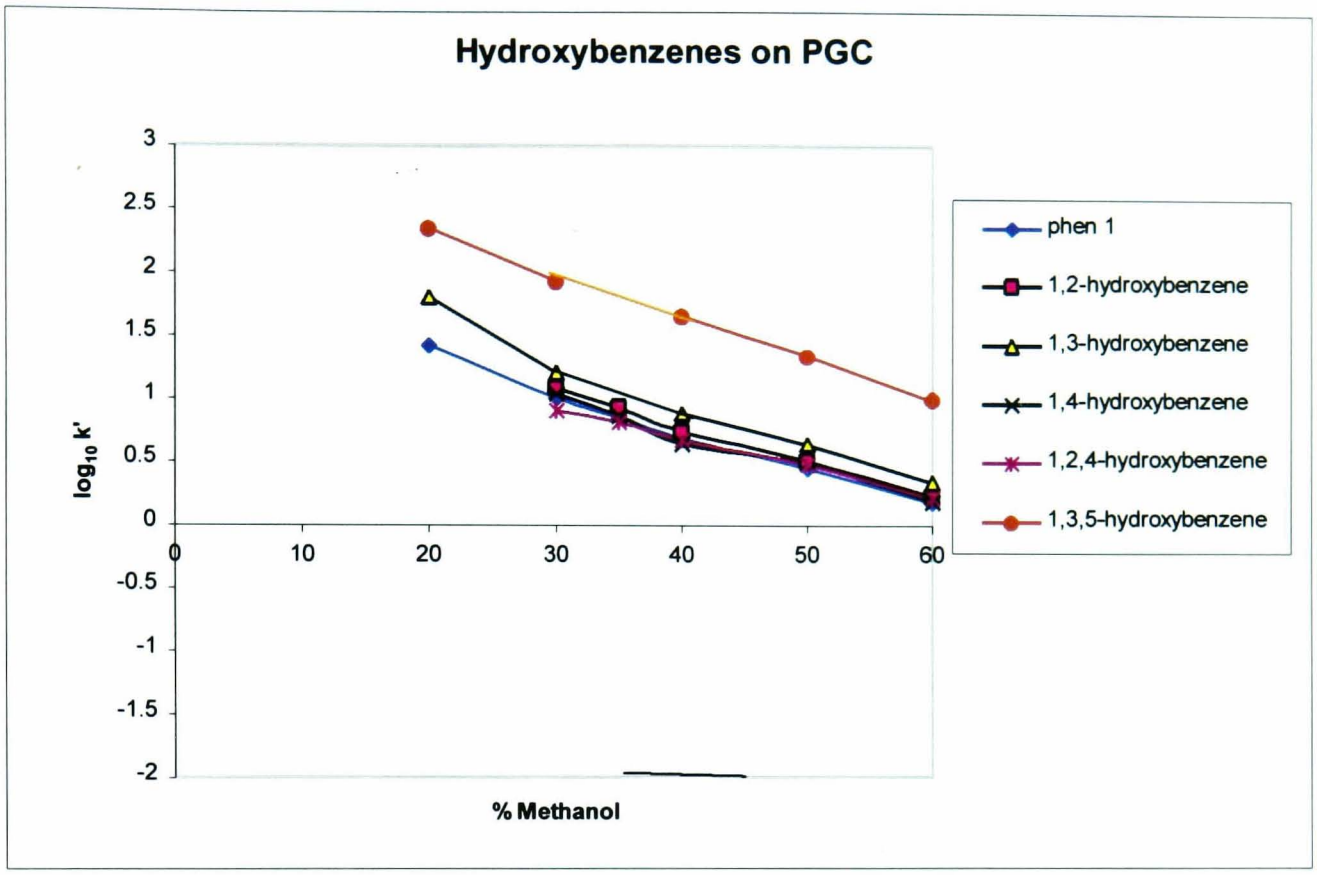

Fig 4.13b

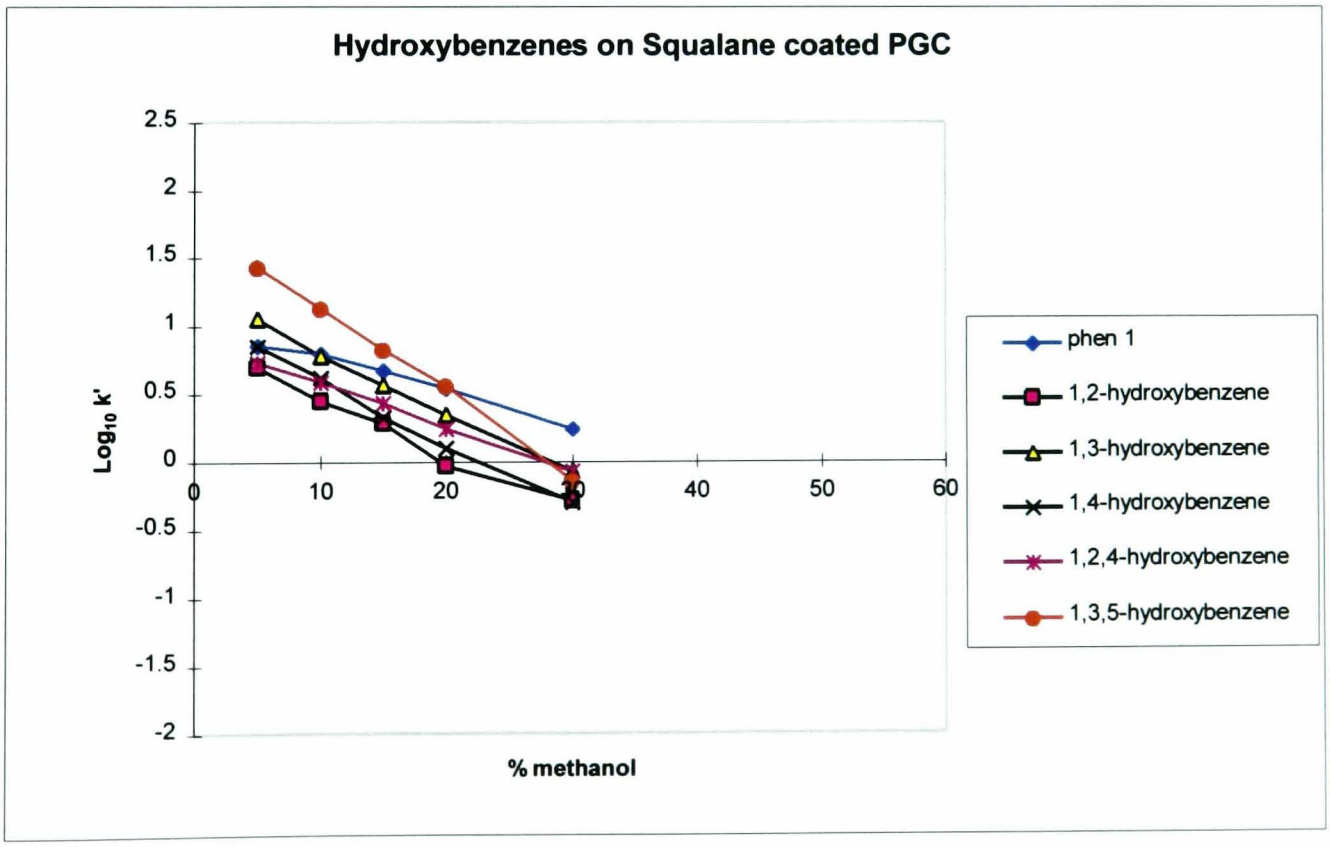

Figure 4.13

Retention of Hydroxybenzenes in various Methanol:Water Compositions for PGC Coating Experiments

Fig 4.13c

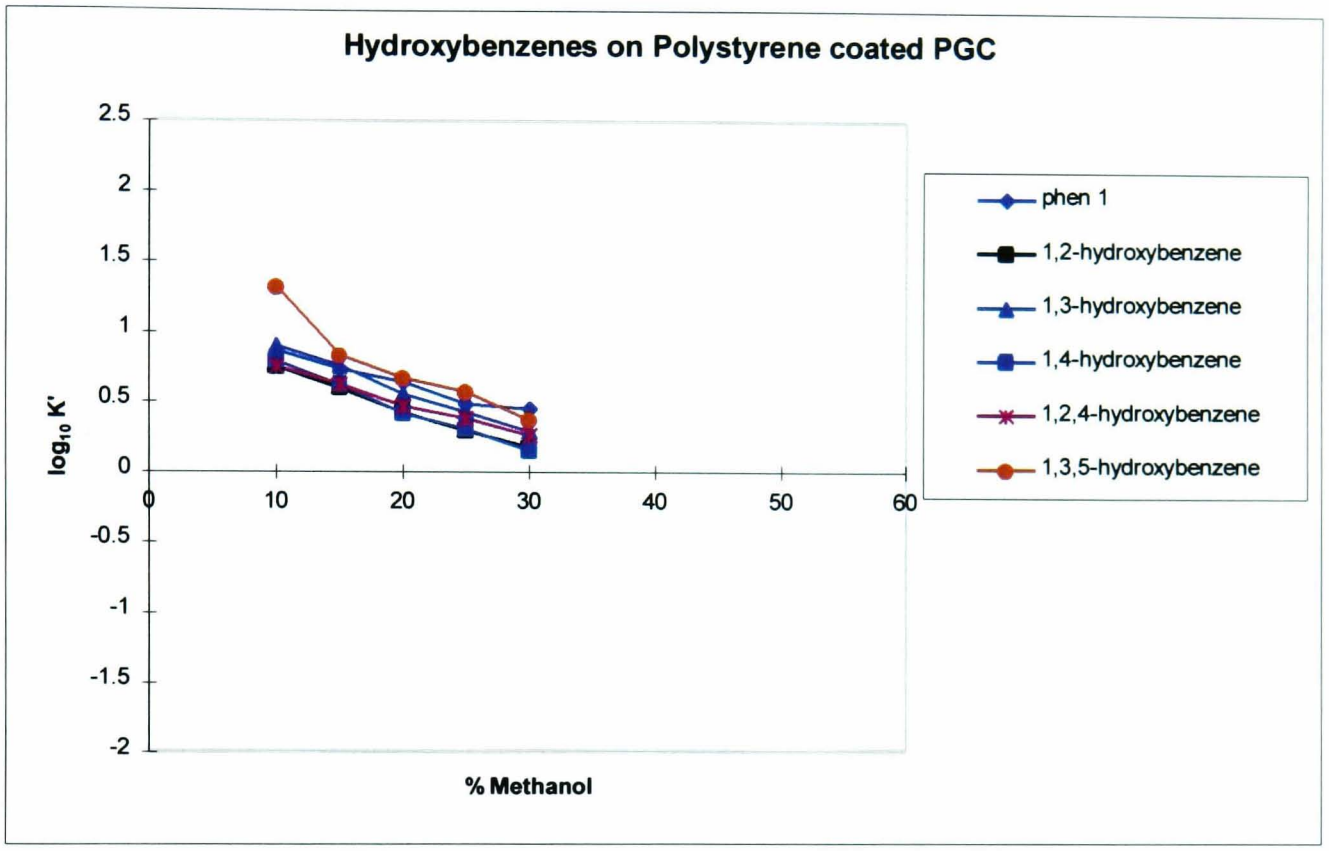

Fig 4.13d

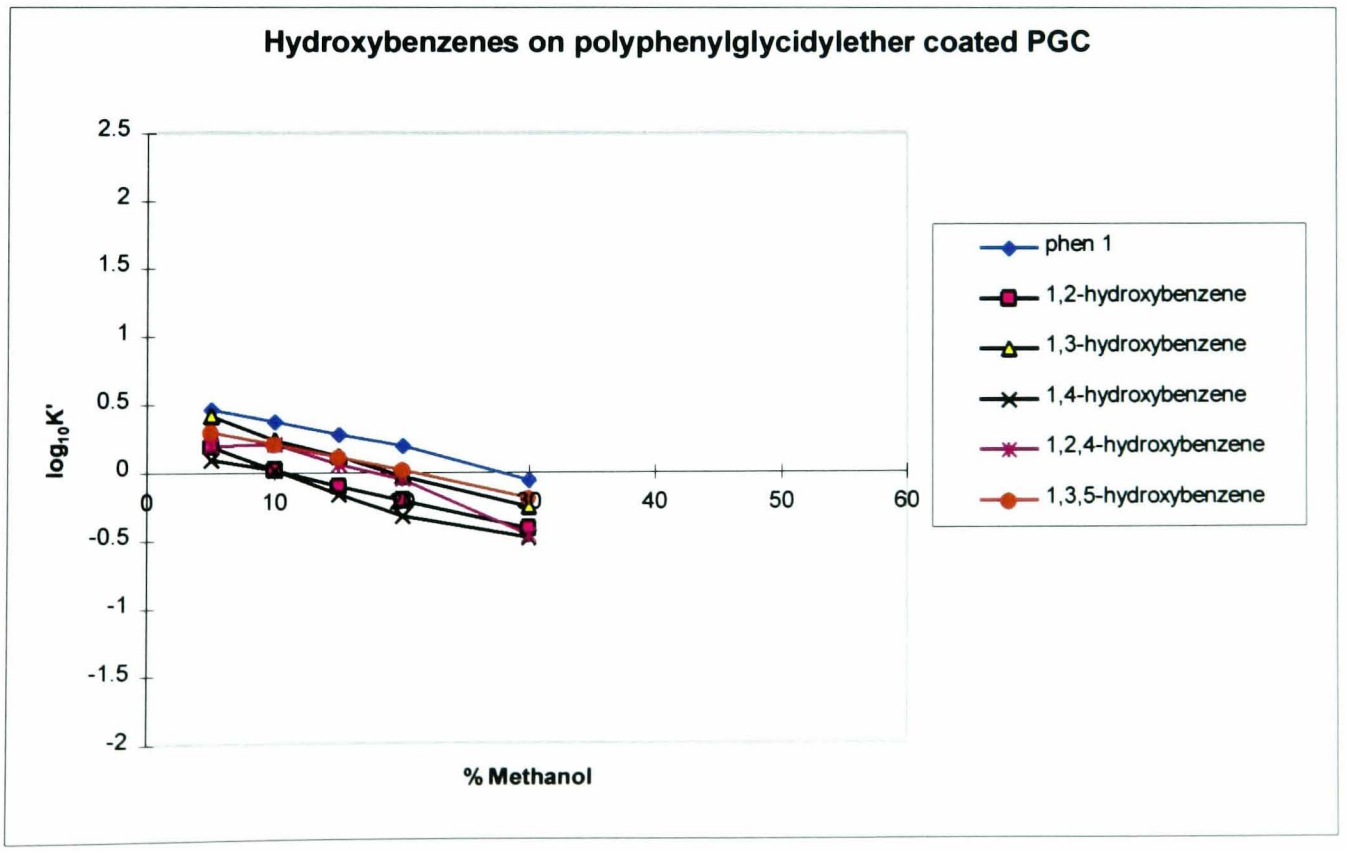

Fig 4.13 continued

Retention of Hydroxybenzenes in various Methanol:Water Compositions for PGC Coating Experiments

Fig 4.13e

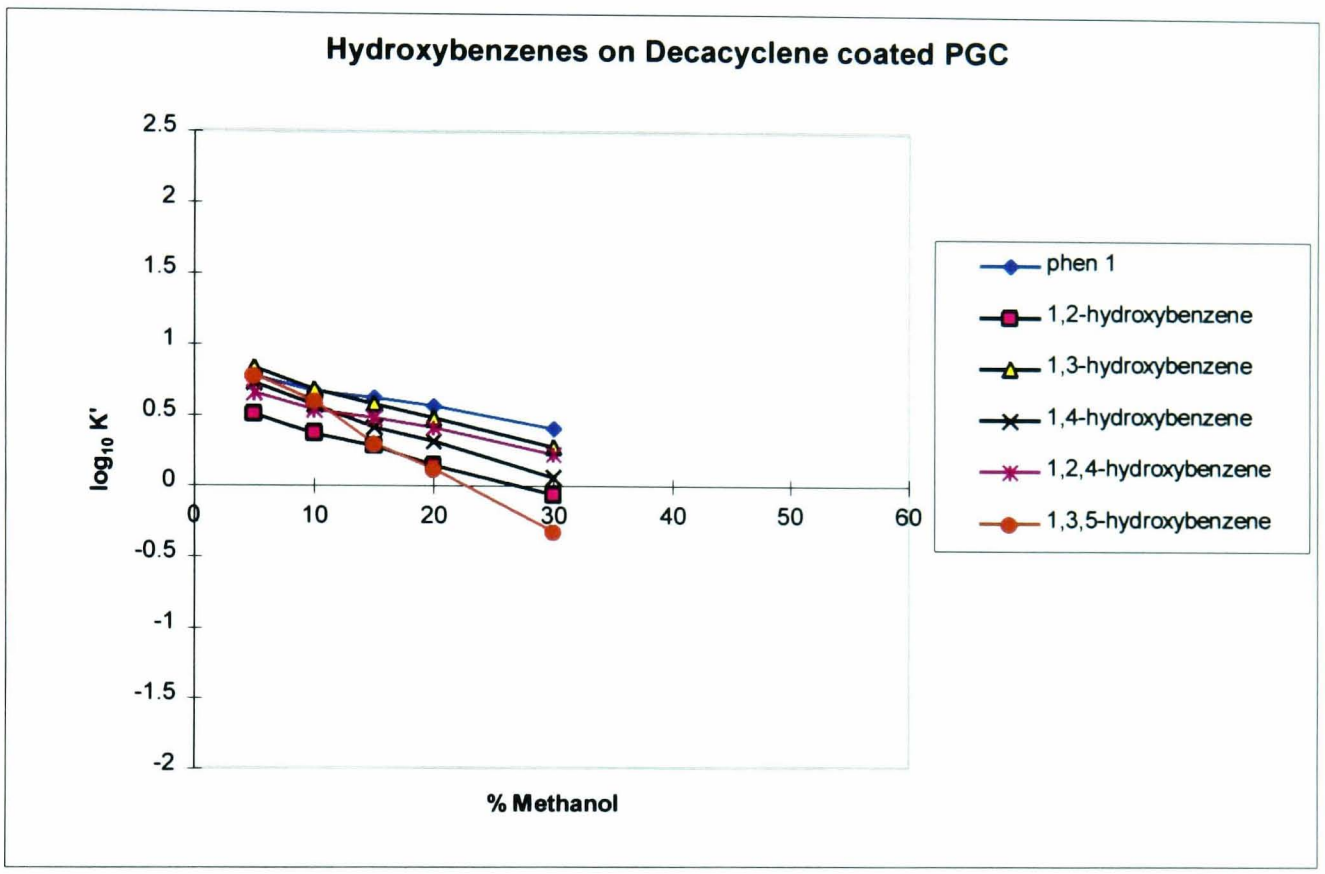

Fig 4.13f

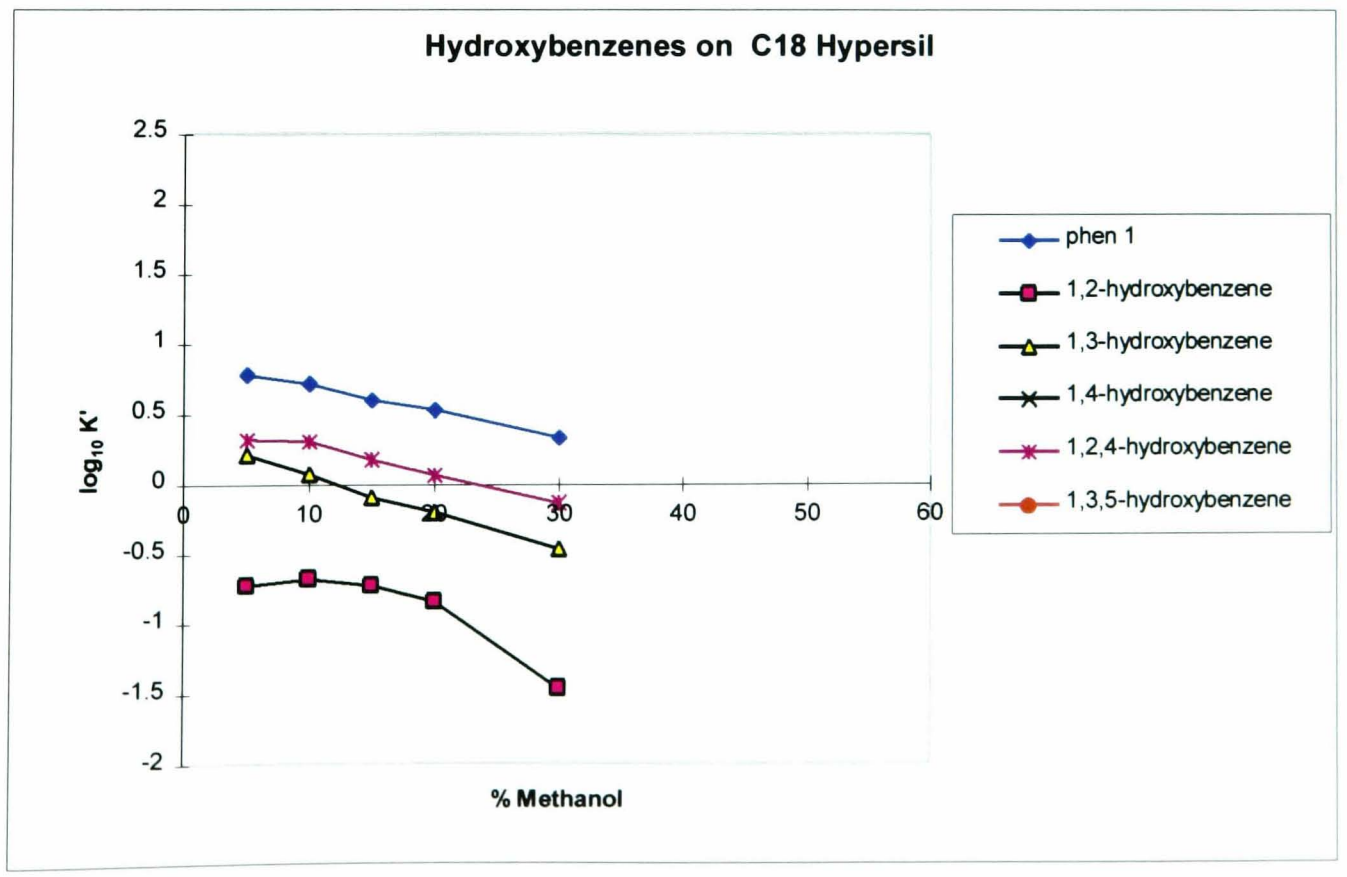

Fig 4.14

Retention of Anilines in various Methanol:Water Compositions for PGC Coating Experiments

Fig 4.14a

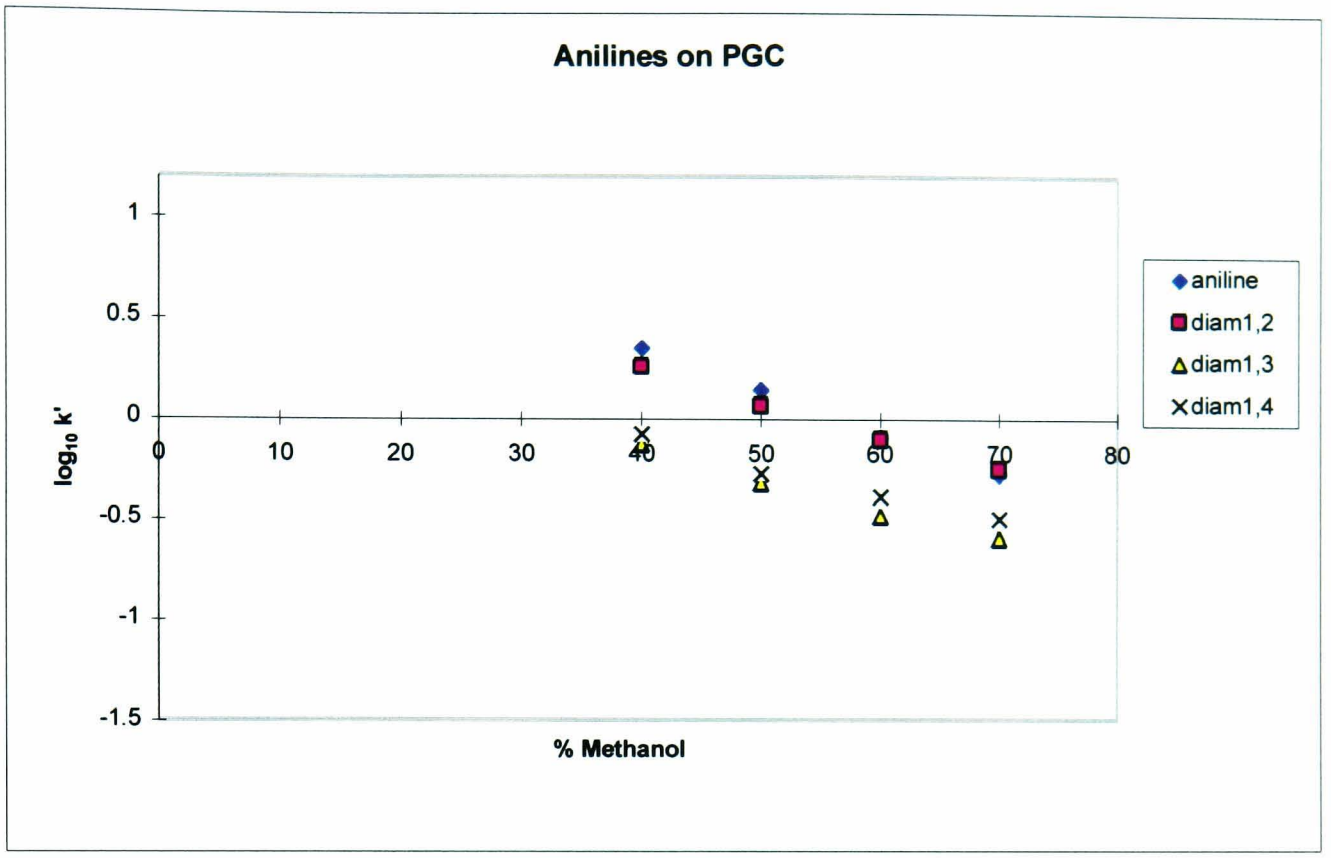

Fig 4.14b

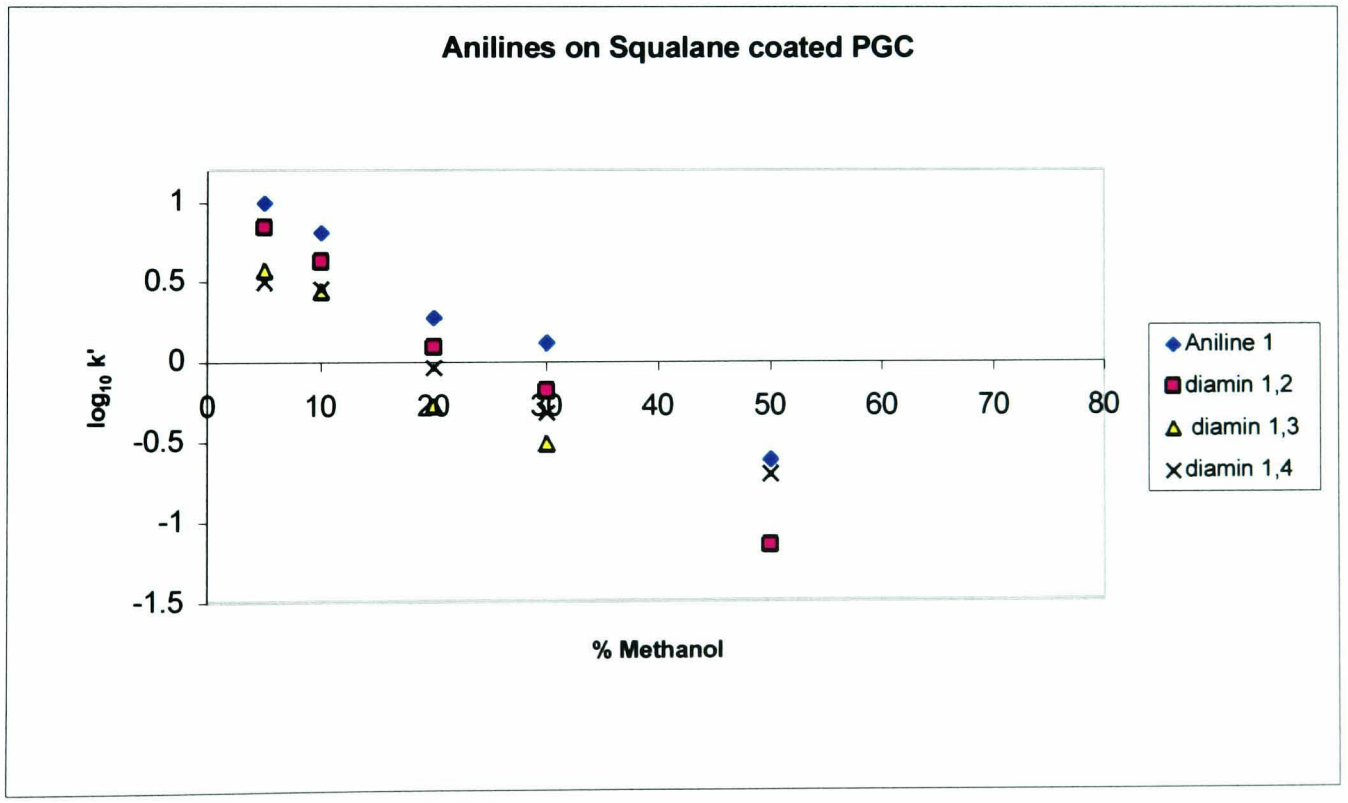

diamin - is the abbreviation we have chosen to use for Phenylenediamine

Fig 4.14 continued

Retention of Anilines in Various Methanol:Water Compositions for PGC Coating Experiments

Fig 4.14e

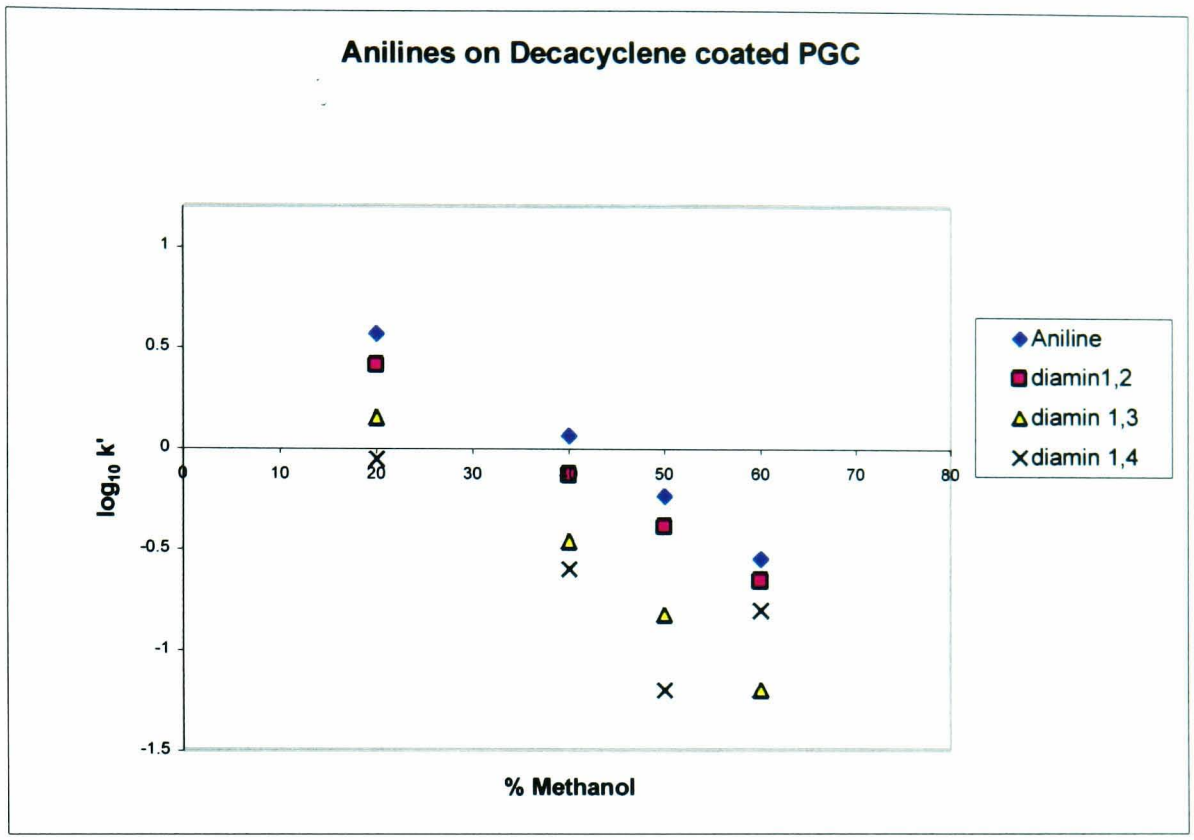

Fig 4.14f

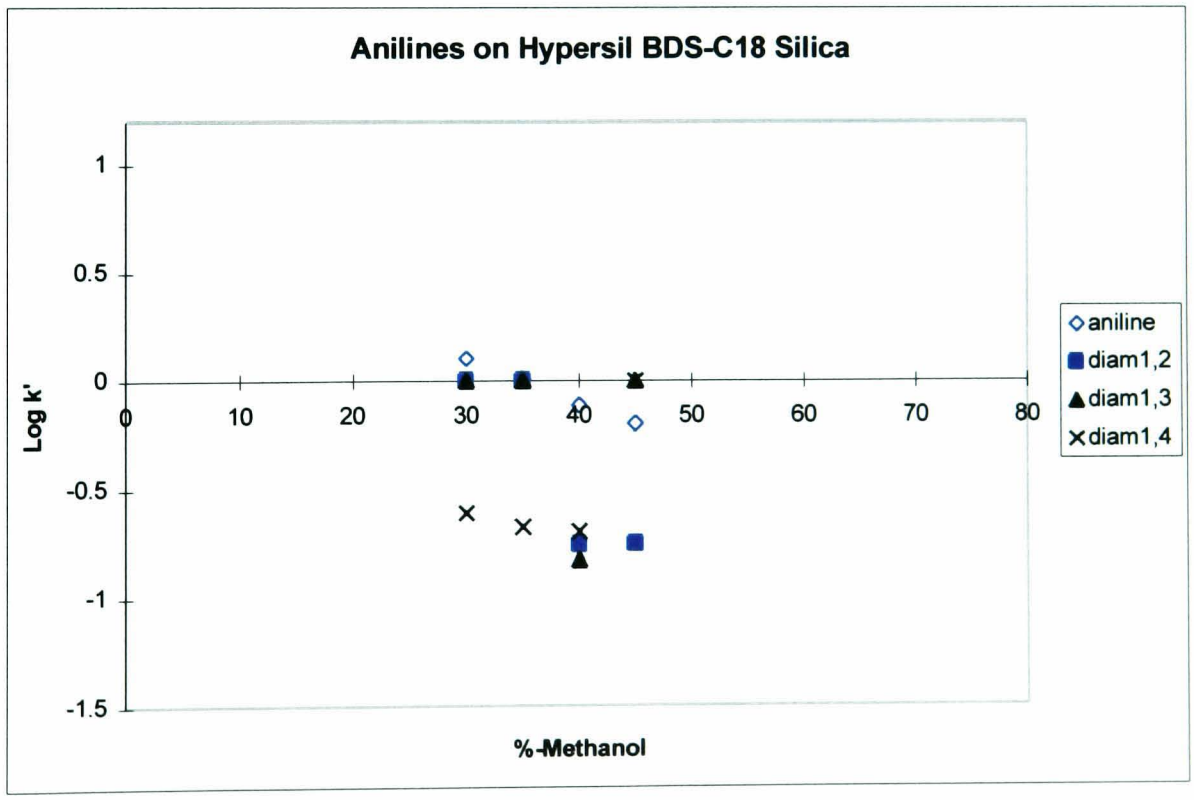

diamin - is the abbreviation we have chosen to use for Phenylenediamine

*Fig 4.14f 1,2 Phenylene diamine not retained - data not plotted

*Fig 4.14f 1,3 Phenylene diamine not retained - data not plotted

Retention of Anilines in various Methanol:Water Compositions for PGC Coating Experiments

Fig 4.14c

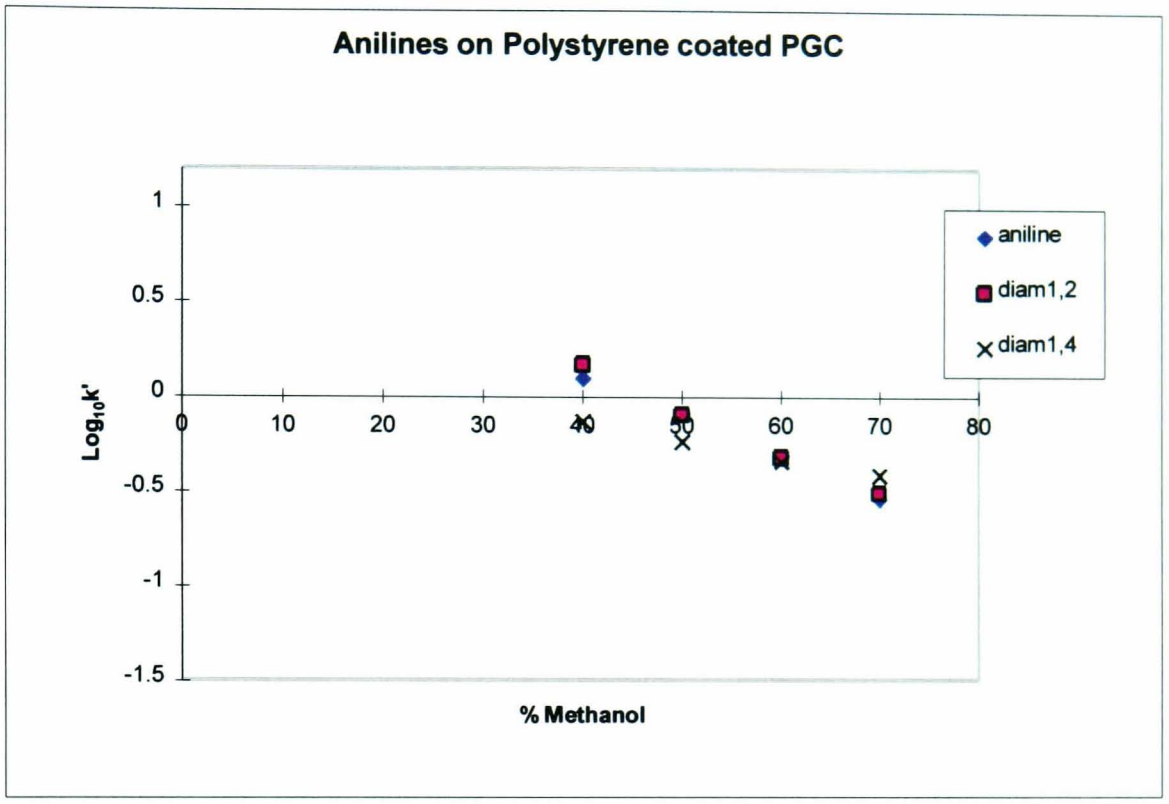

Fig 4.14d

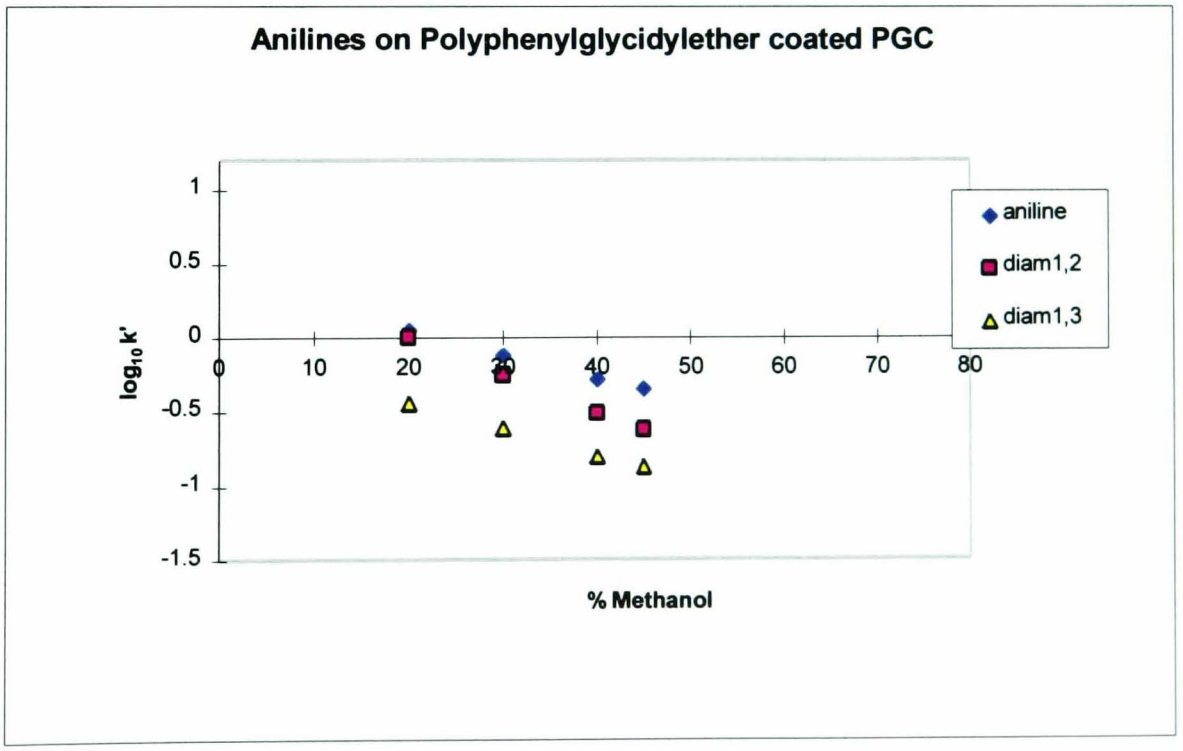

*Fig 4.14c 1,4 Phenylene diamine not retained - data not plotted

*Fig 4.14d 1,3 Phenylene diamine not retained - data not plotted

diamin - is the abbreviation we have chosen to use for Phenylenediamine

Retention of Halobenzenes in various Methanol:Water Compositions for PGC Coating Experiments

Fig 4.15a

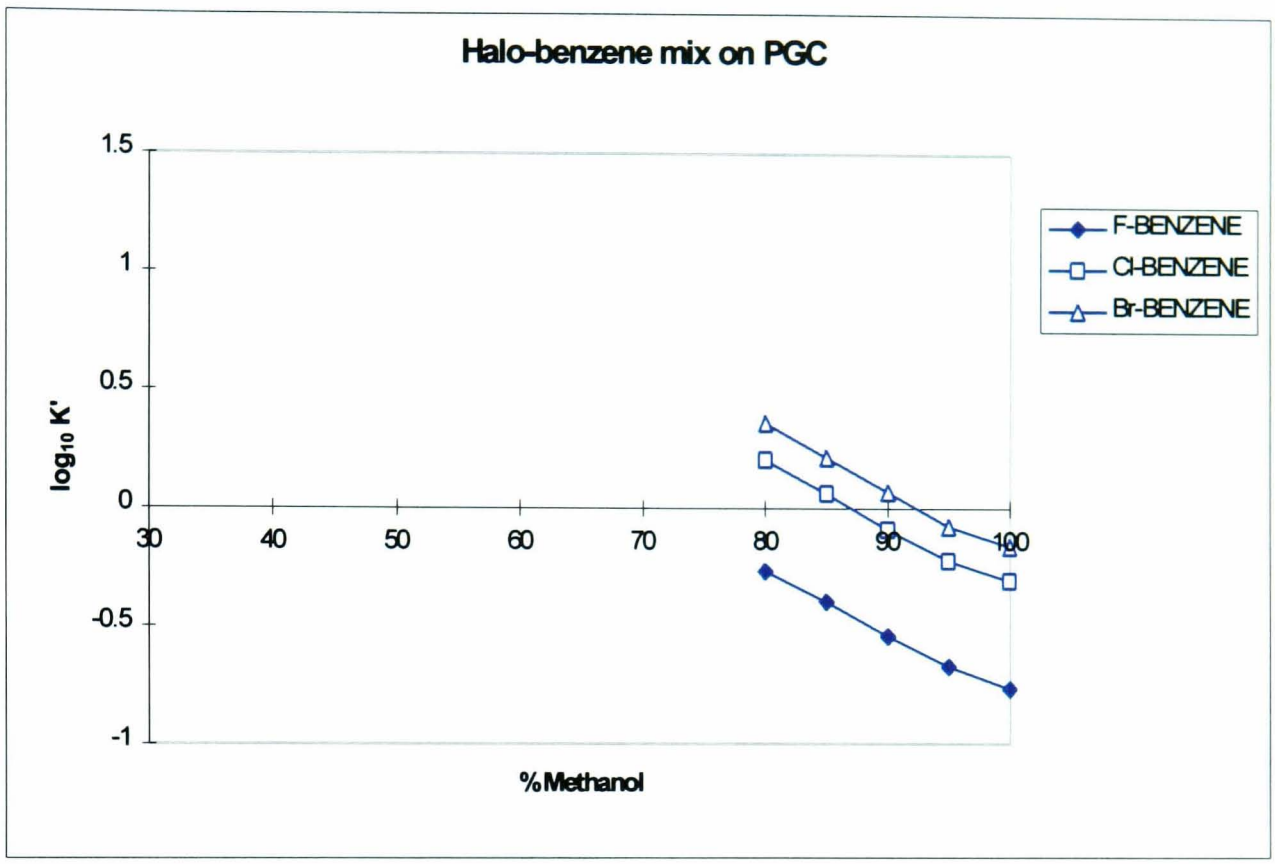

Fig 4.15b Squalane coated PGC not tested

Fig 4.15c

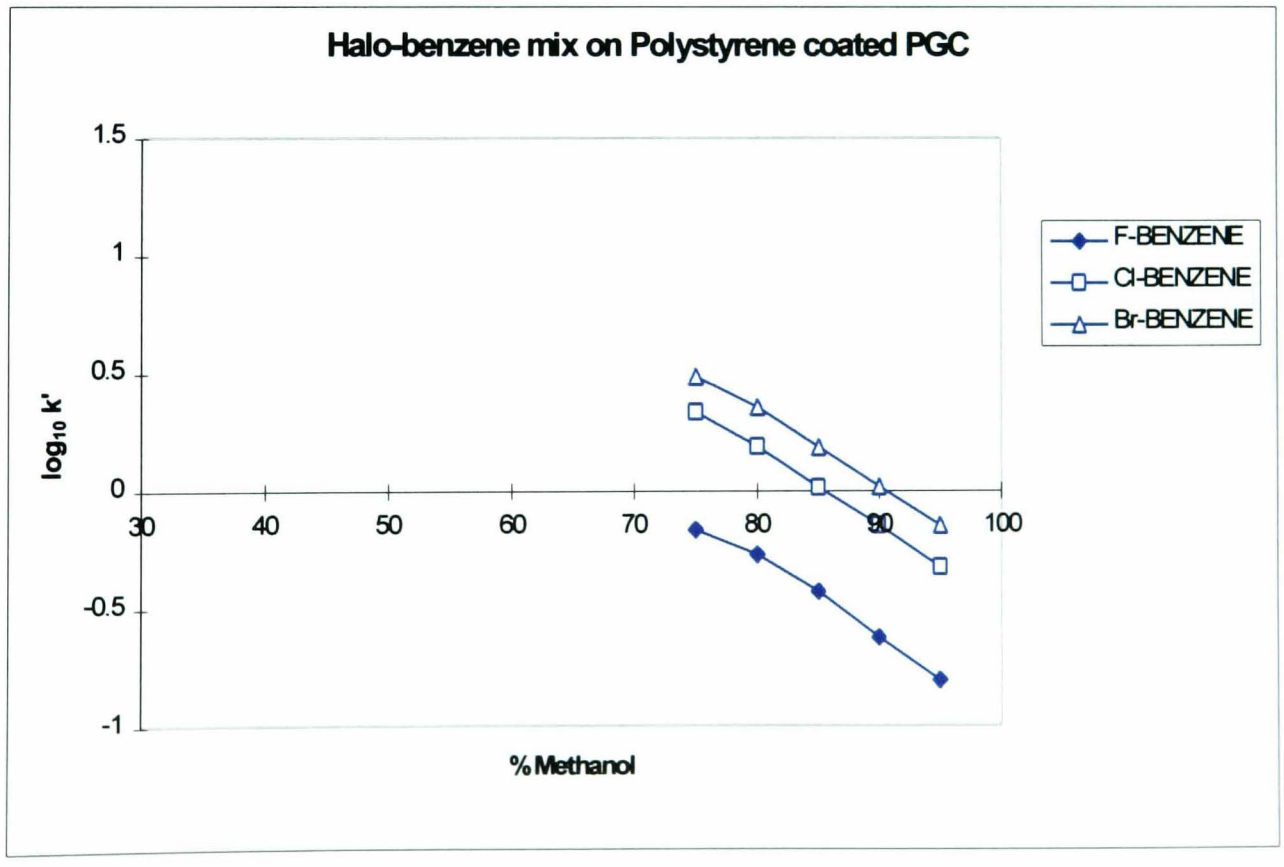

Fig 4.15 continued

Retention of Halobenzenes in various Methanol:Water Compositions for PGC Coating Experiments

Fig 4.15d

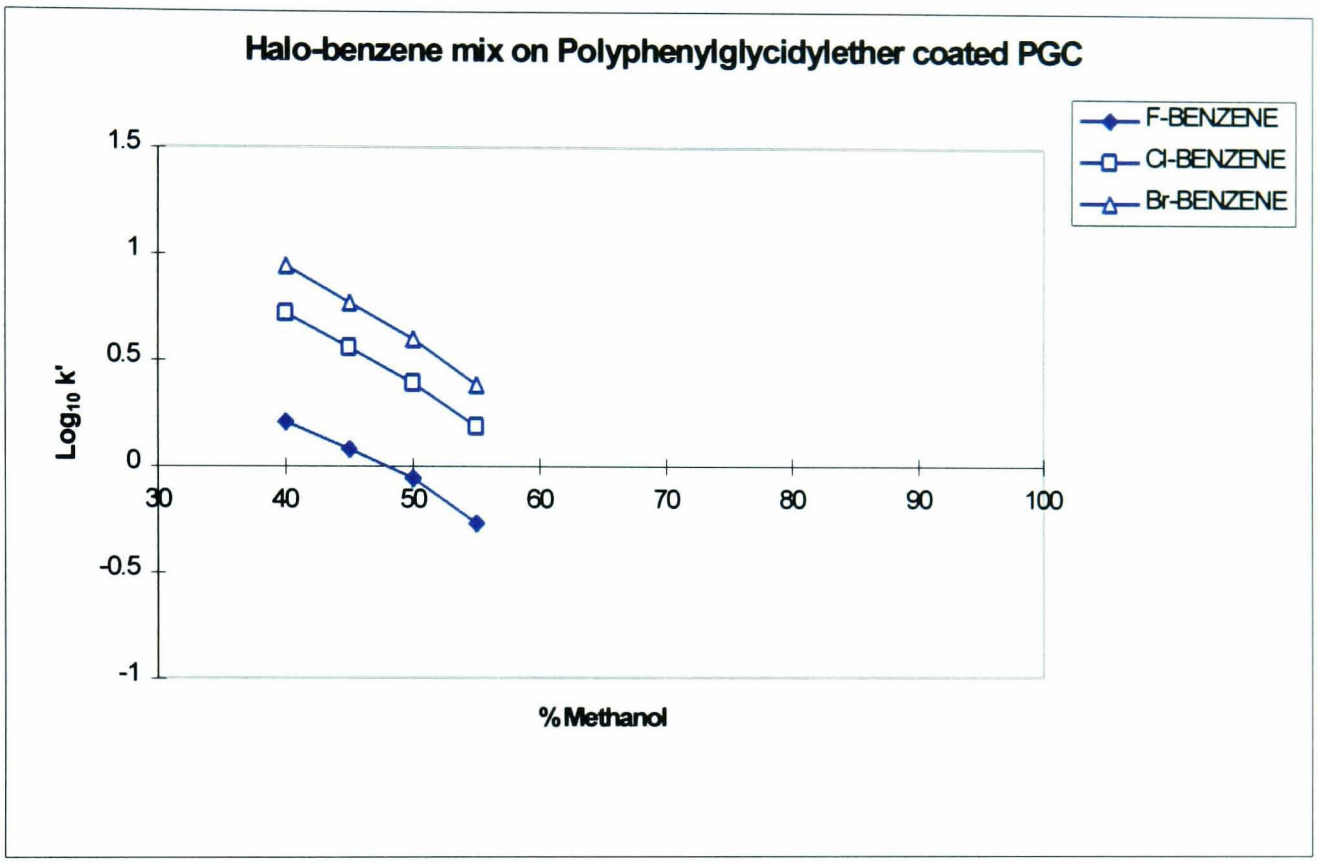

Fig 4.15e Decacyclene coated PGC not tested

Fig 4.15f

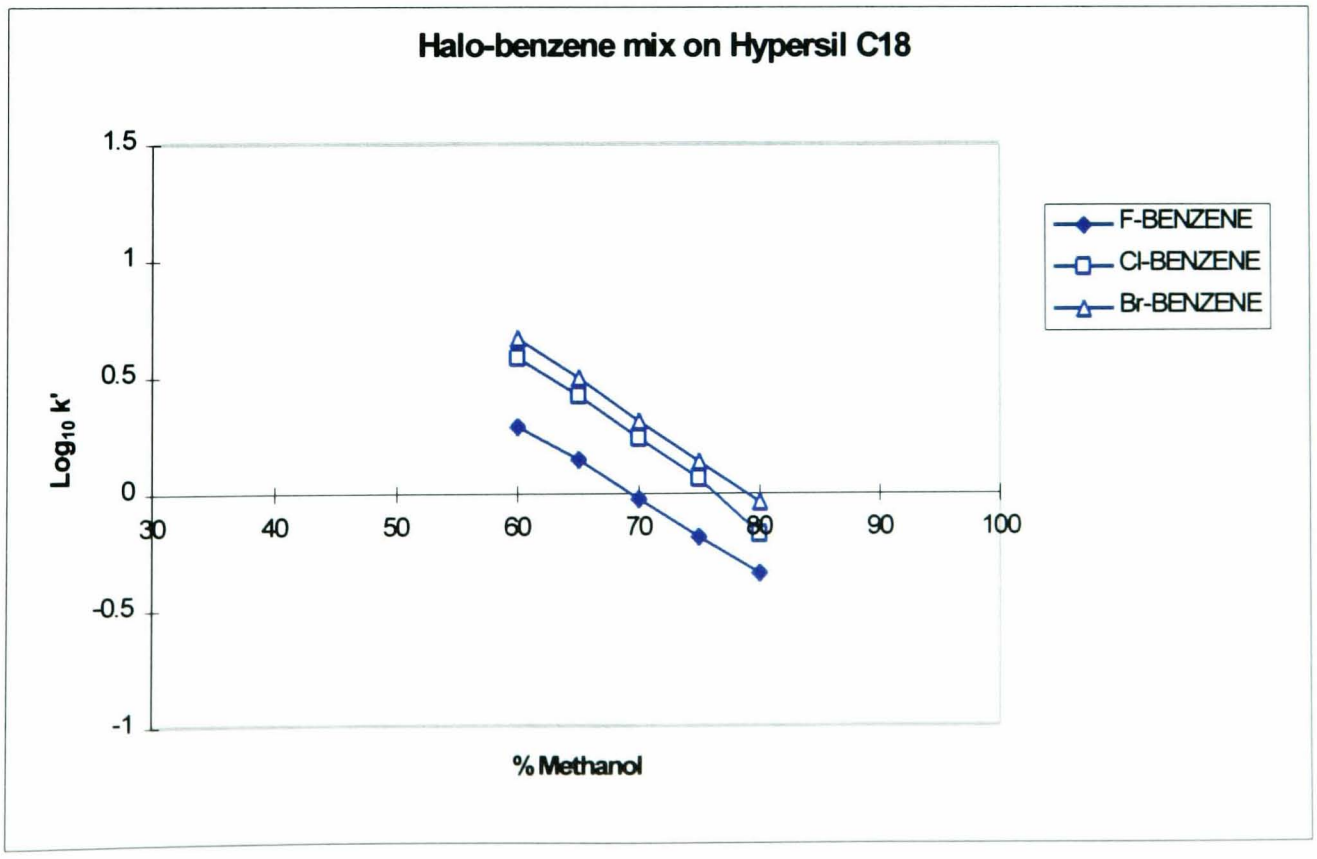

Fig 4.16

Retention of Other Monosubstituted Benzenes in Various Methanol:Water Compositions for PGC Coating Experiments

Fig 4.16a

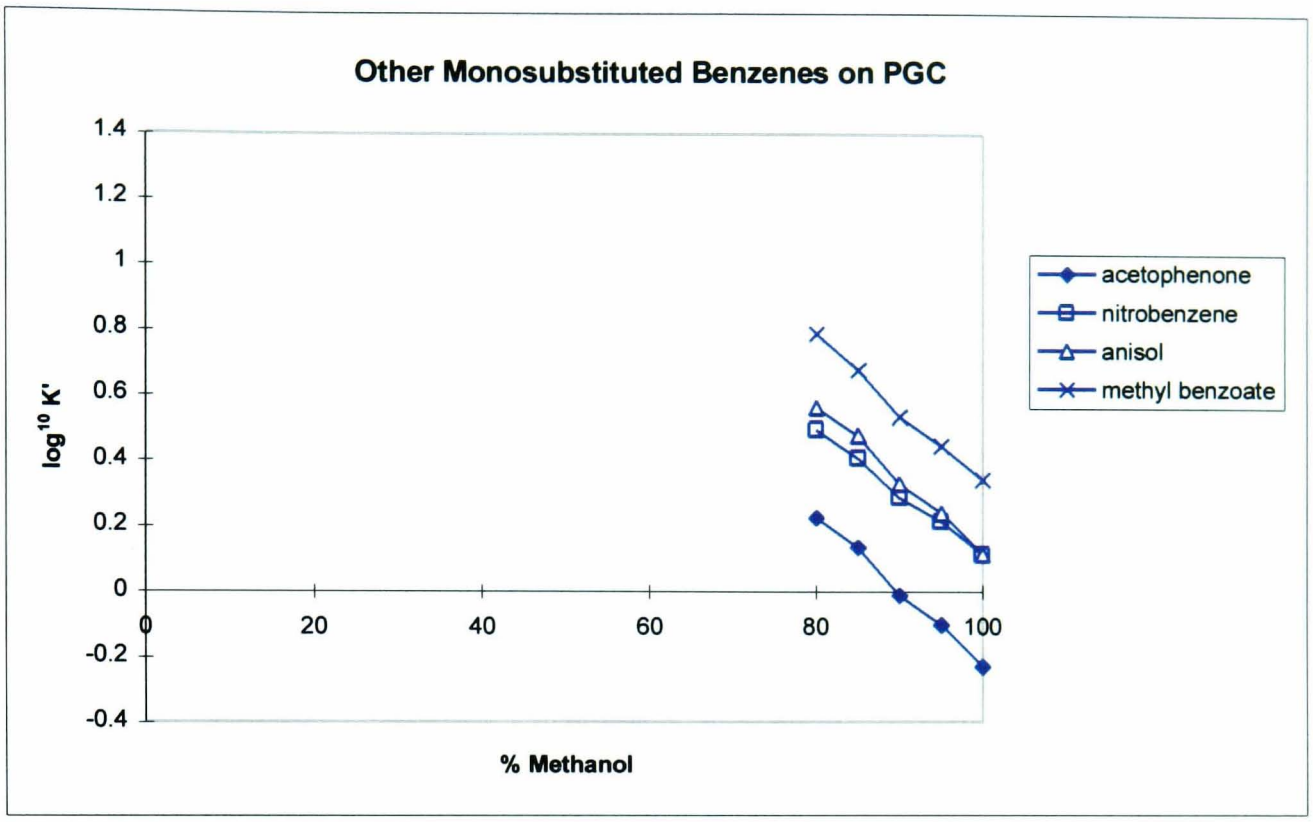

Fig 4.16b - squalane coated PGC not tested

Fig 4.16c

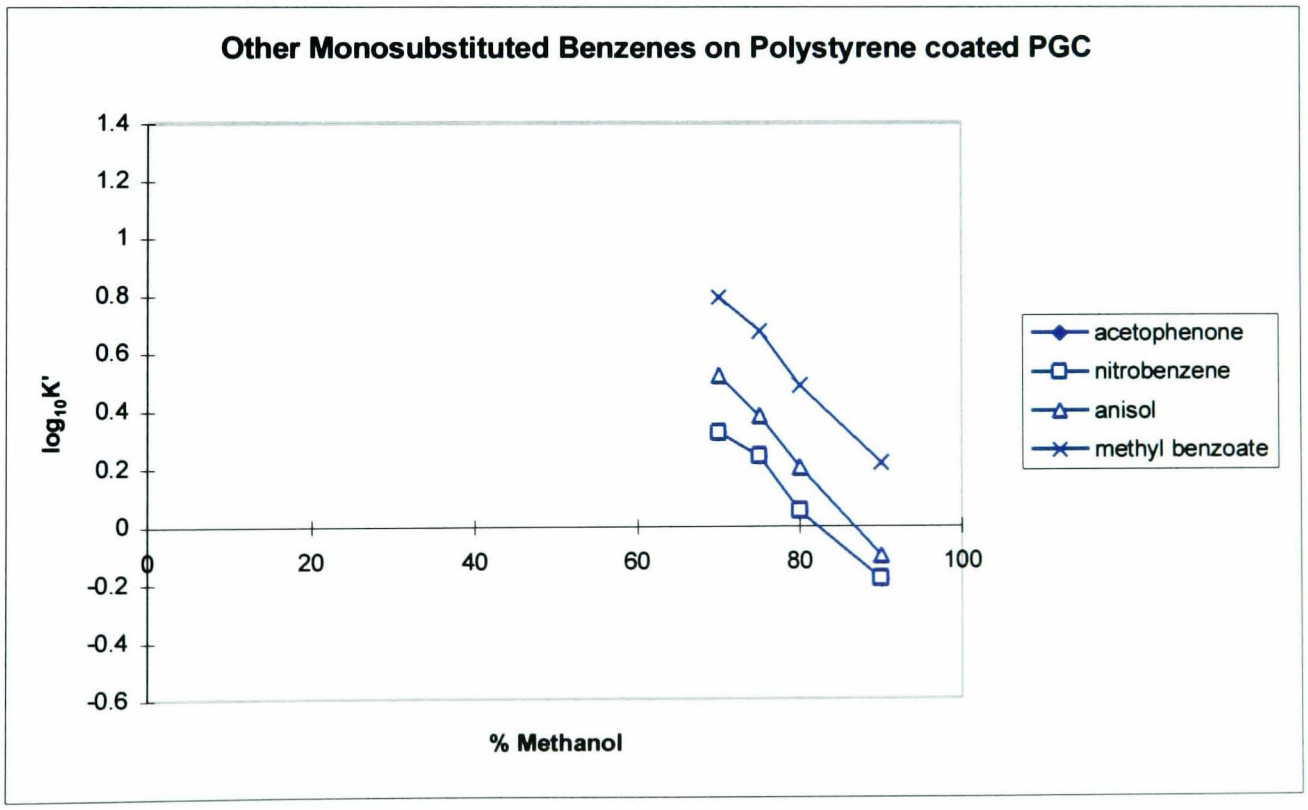

Retention of Other Monosubstituted Benzenes in Various Methanol:Water Compositions for PGC Coating Experiments

Fig 4.16d

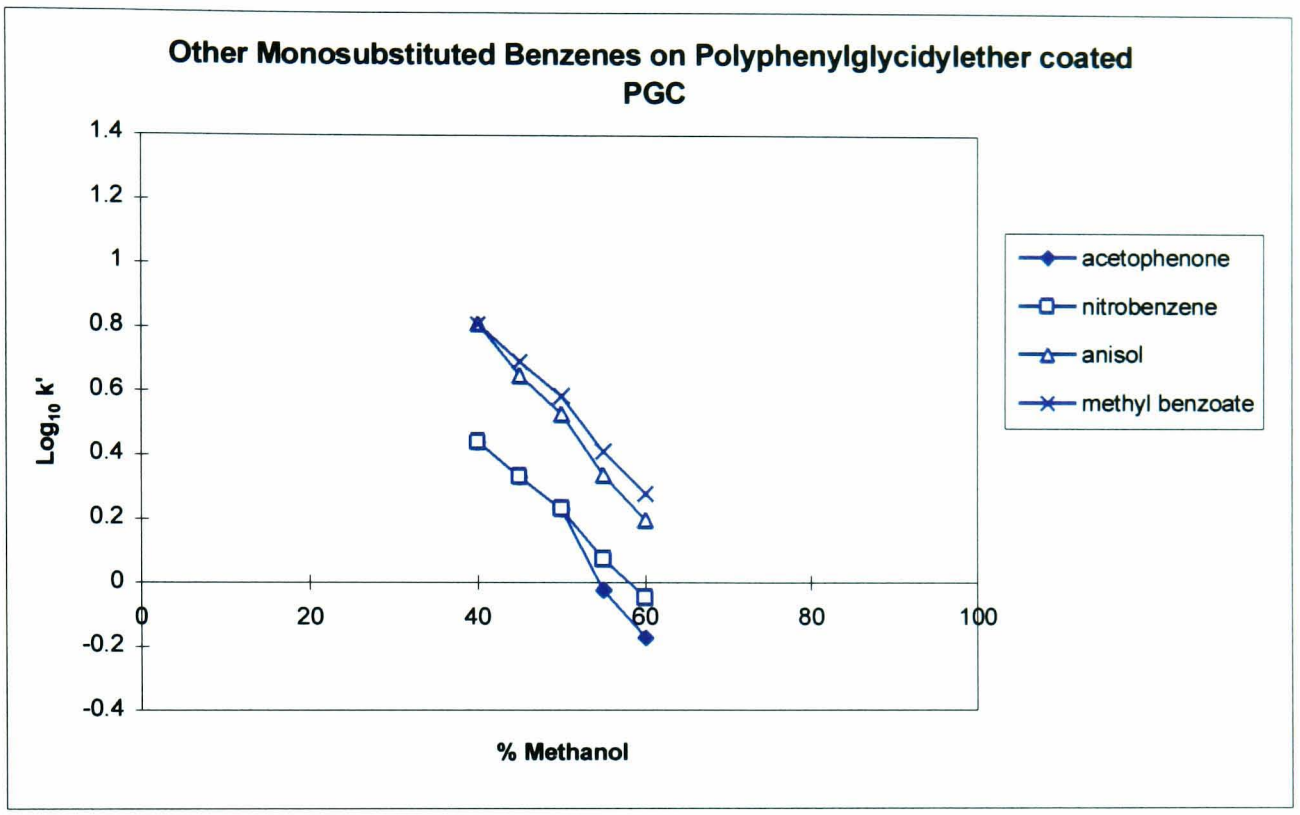

Fig 4.16e

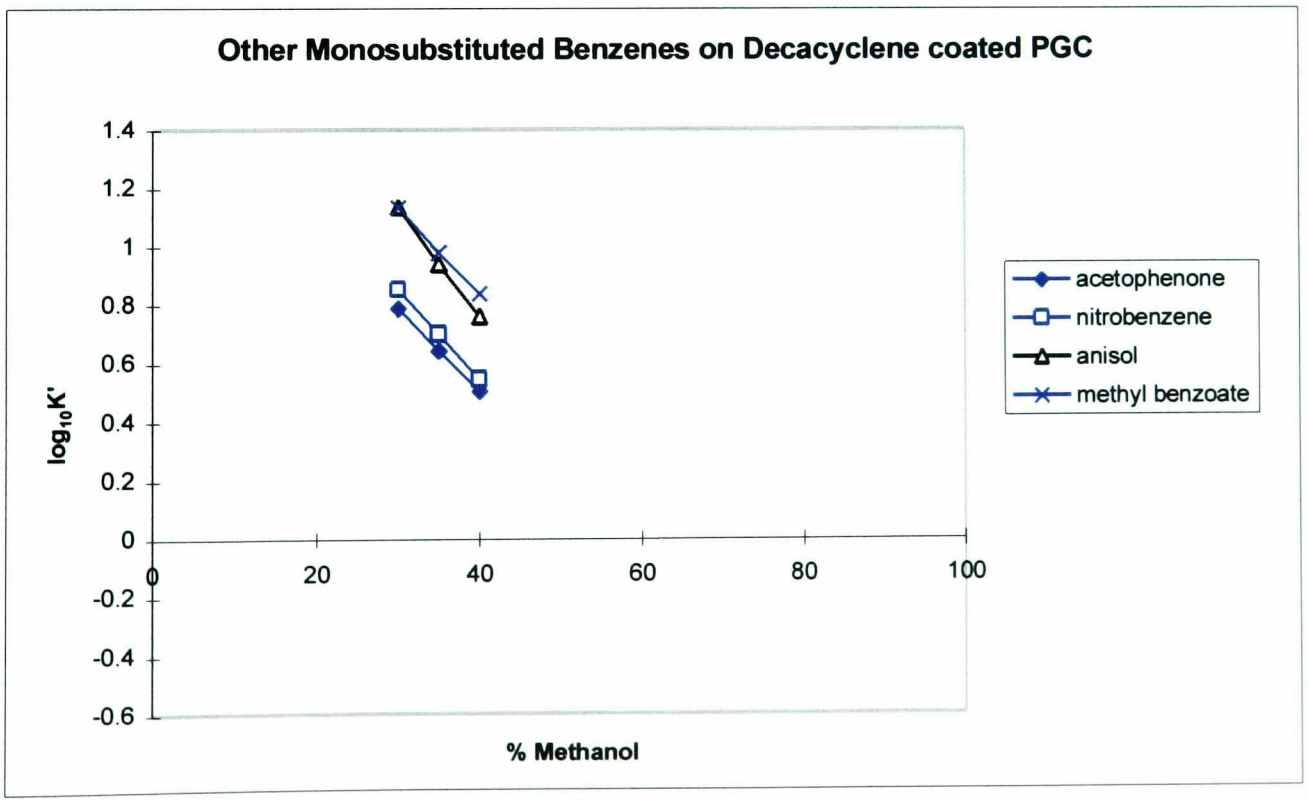

Fig 4.16 continued

Retention of Other Monosubstituted Benzenes in Various Methanol:Water Compositions for PGC Coating Experiments

Fig 4.16f

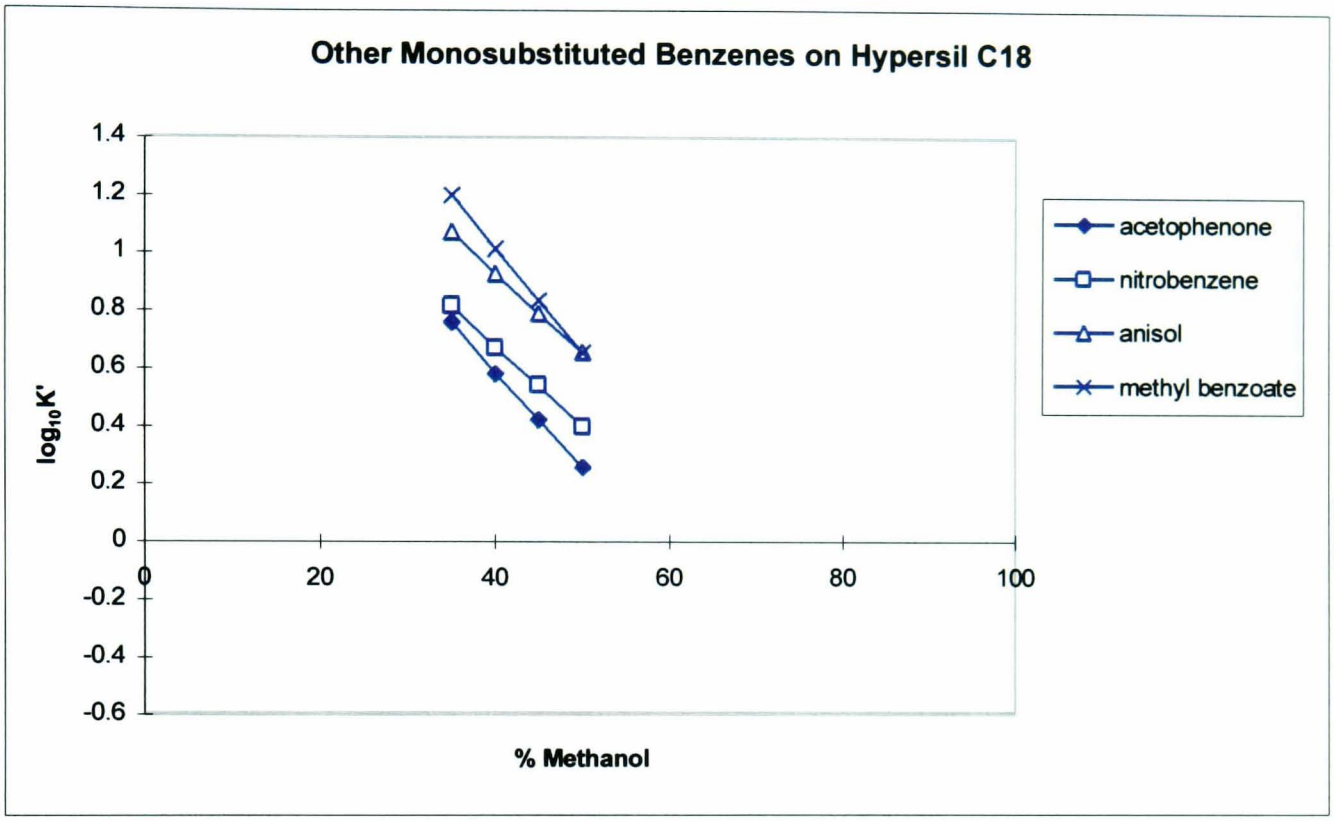

Fig 4.16g

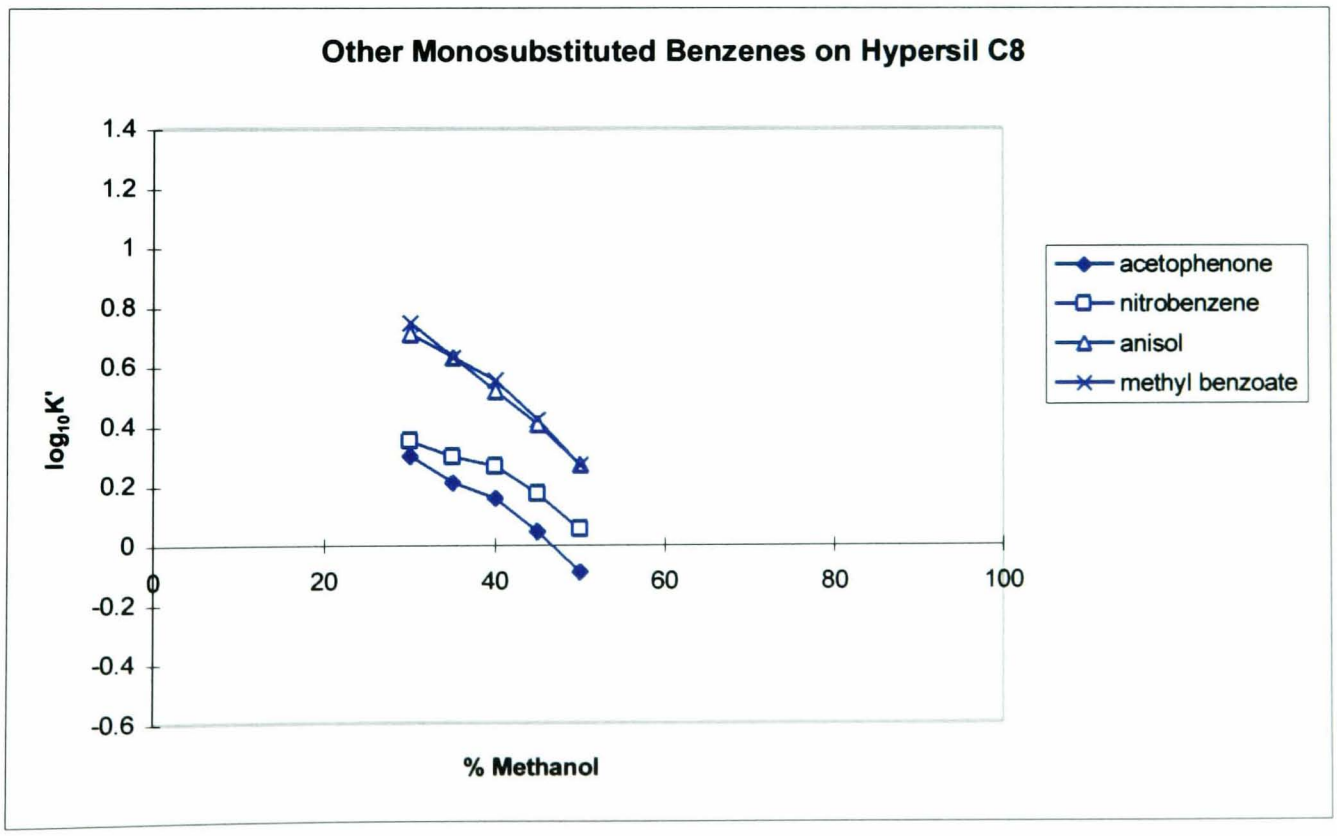

Hypersil C8 and C18 refer to C18 Silica and C8 silica columns purchased form Hypersil

Fig 4.17a

Effect on Chromatographic Retention of Test Mix 1 for Fractional PPGE Coated PGC

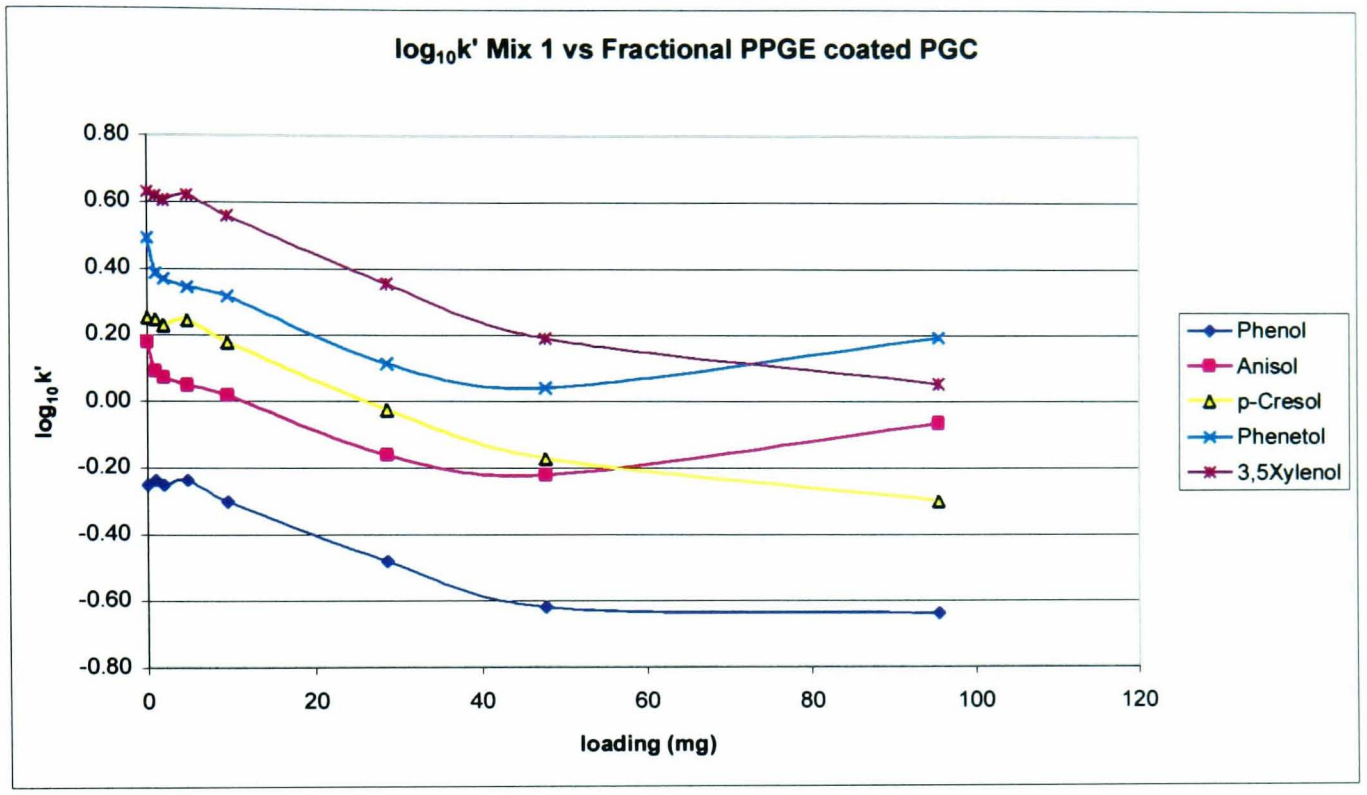

Fig 4.17b

Combination of Breakthrough Loading Data with Evaporative Adsorptive Method

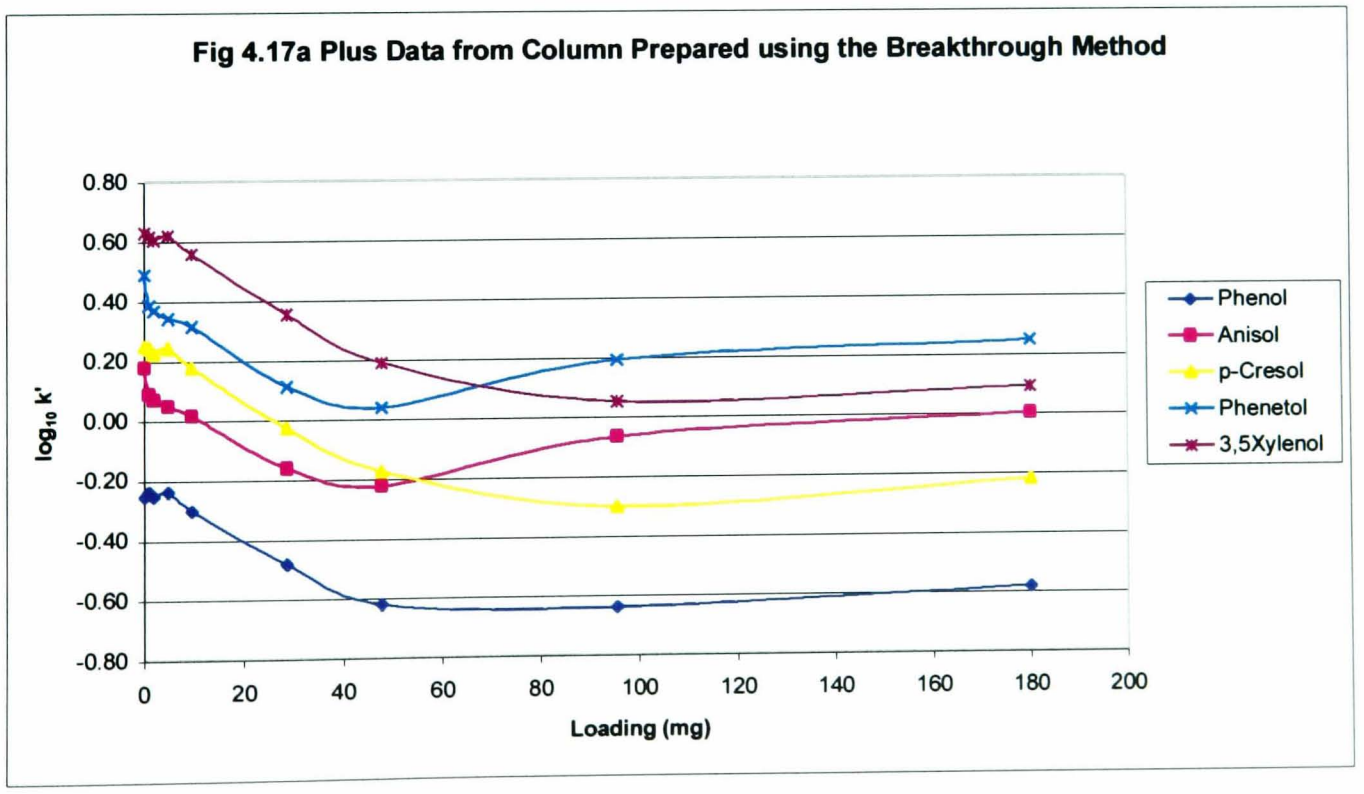

Fig 4.18
Fractional Monolayer Coating with PPGE on PGC and Comparison with Hypersil C18 Selectivity

(a) PGC
mobile phase -95% methanol:water

b) PGC coated with 1mg PPGE
mobile phase -95% methanol:water

c) PGC coated with 100 mg PPGE
mobile phase -60% methanol:water

d) Hypersil C18
mobile phase -60% methanol:water

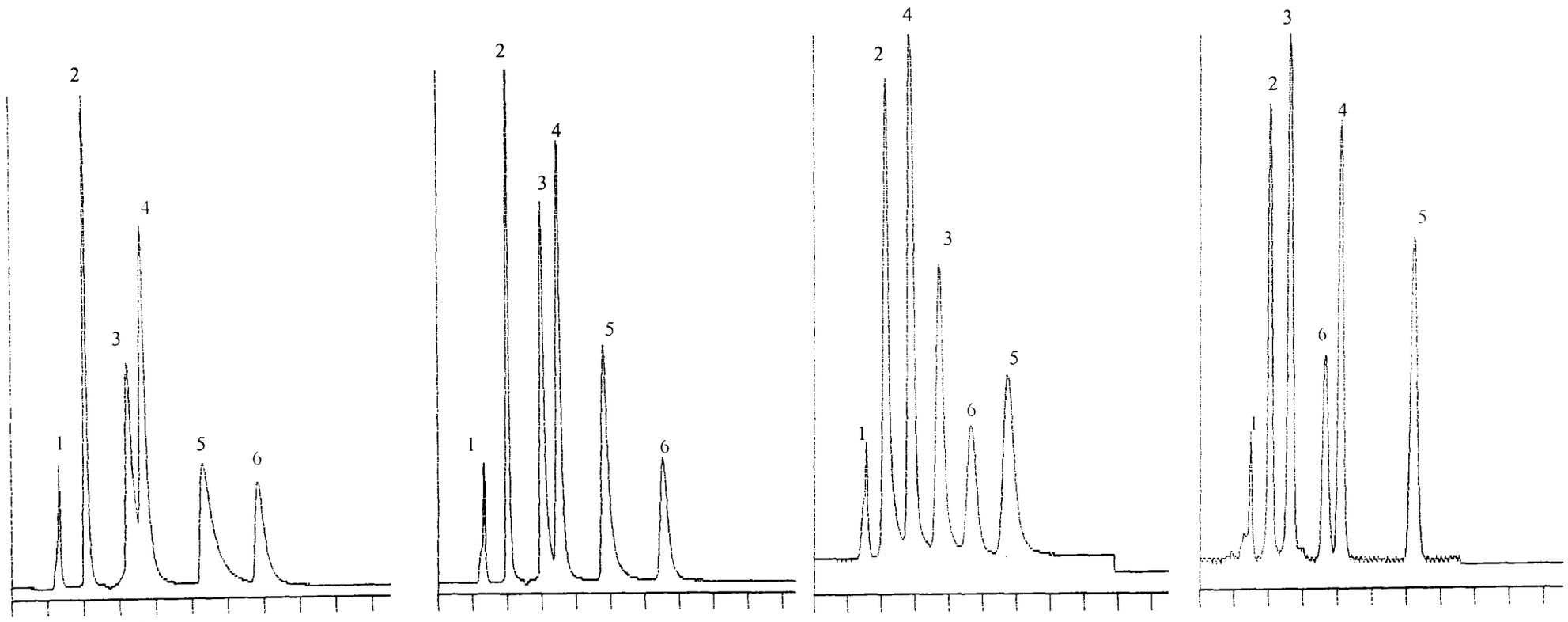

Solutes:
1. Acetone 2. Phenol 3. Anisol 4. Para cresol 5. Phenetol 6. 3,5 Xylenol.

Fig 4.19
Preliminary Coating Experiments with Polyethylene imine and Naphthylsulphonyl-L-Serine

Fig 4.19a PEI Coated PGC

Solutes:
1.Fluoride ion
2.Iodate ion
3.Nitrite ion
4.Bromide ion
5.Nitrate ion

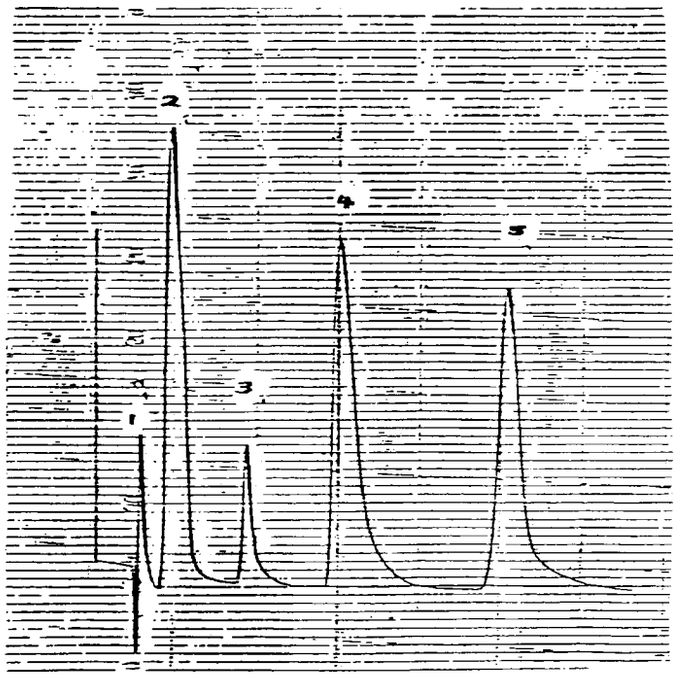

Mobile Phase : 20mM KH_2PO_4
Column : 50mm x 4.6mm
Flow 0.5ml/min
Absorbence: 220nm
chart speed 5mm/min

Fig 4.19b PGC coated with naphthylsulphony L-Serine
The chromatogram shows the separation of D & L Valine enantionmers

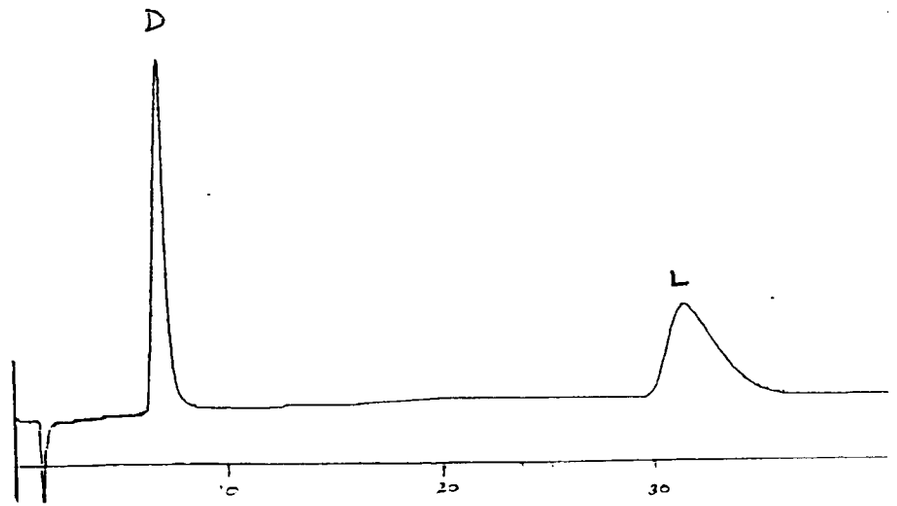

Mobile Phase: 2mM Copper acetate
Column : 50 x 4.6mm
1.0ml/min
Absorbance 210nm

Fig 4.20a

Dynamic Coating of PGC with Pyrene

Analaytes: Dimethylphthalate (DMP)
Phenyl-heptane

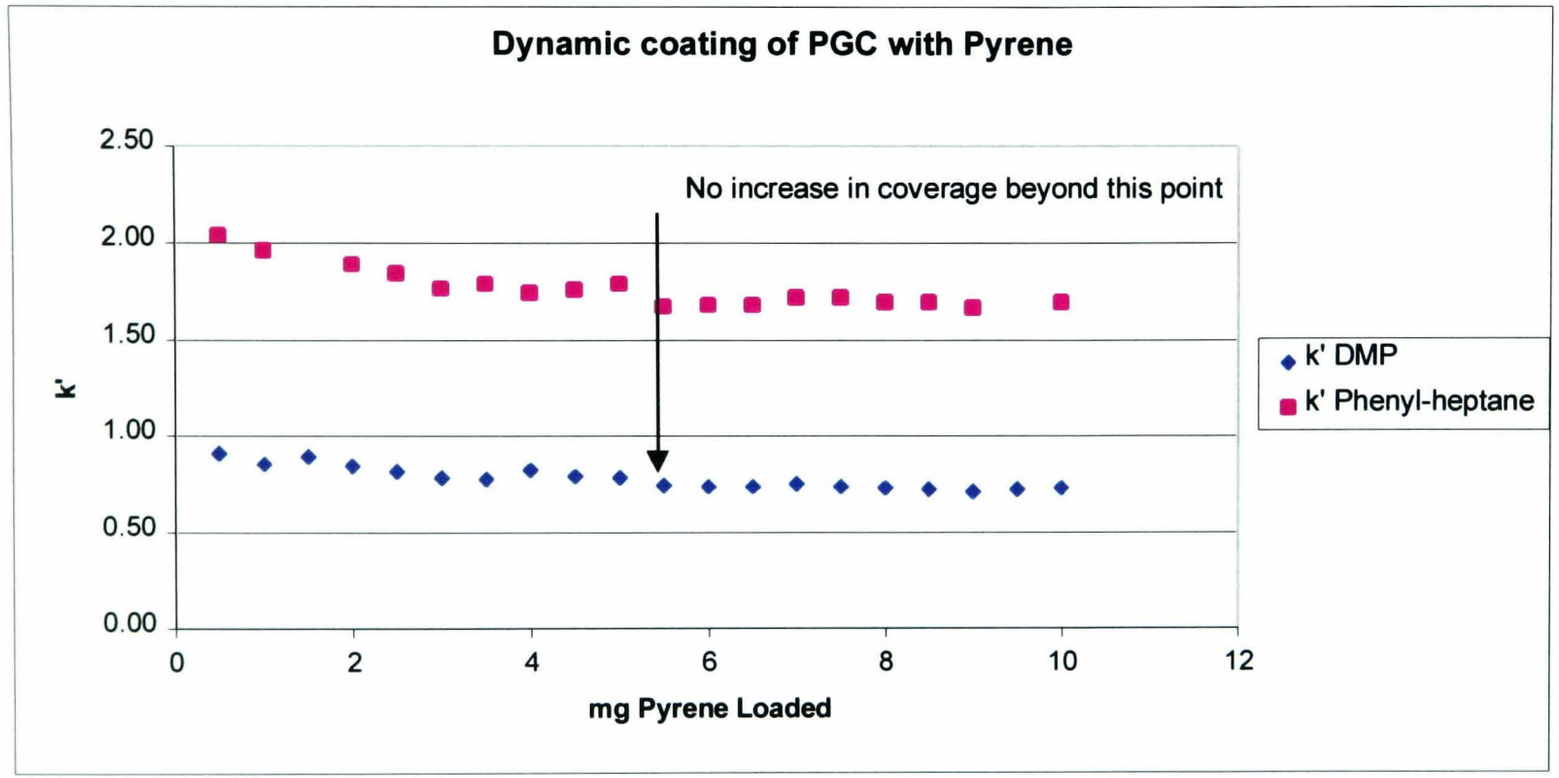

Column : 100 x 4.6mm PGC
Mobile Phase : Ethanol
Flow: 1.0ml/min

Fig 4.20b

Dynamic Coating of PGC with Squalane

Analaytes: Dimethylphthalate (DMP)
Phenyl-heptane

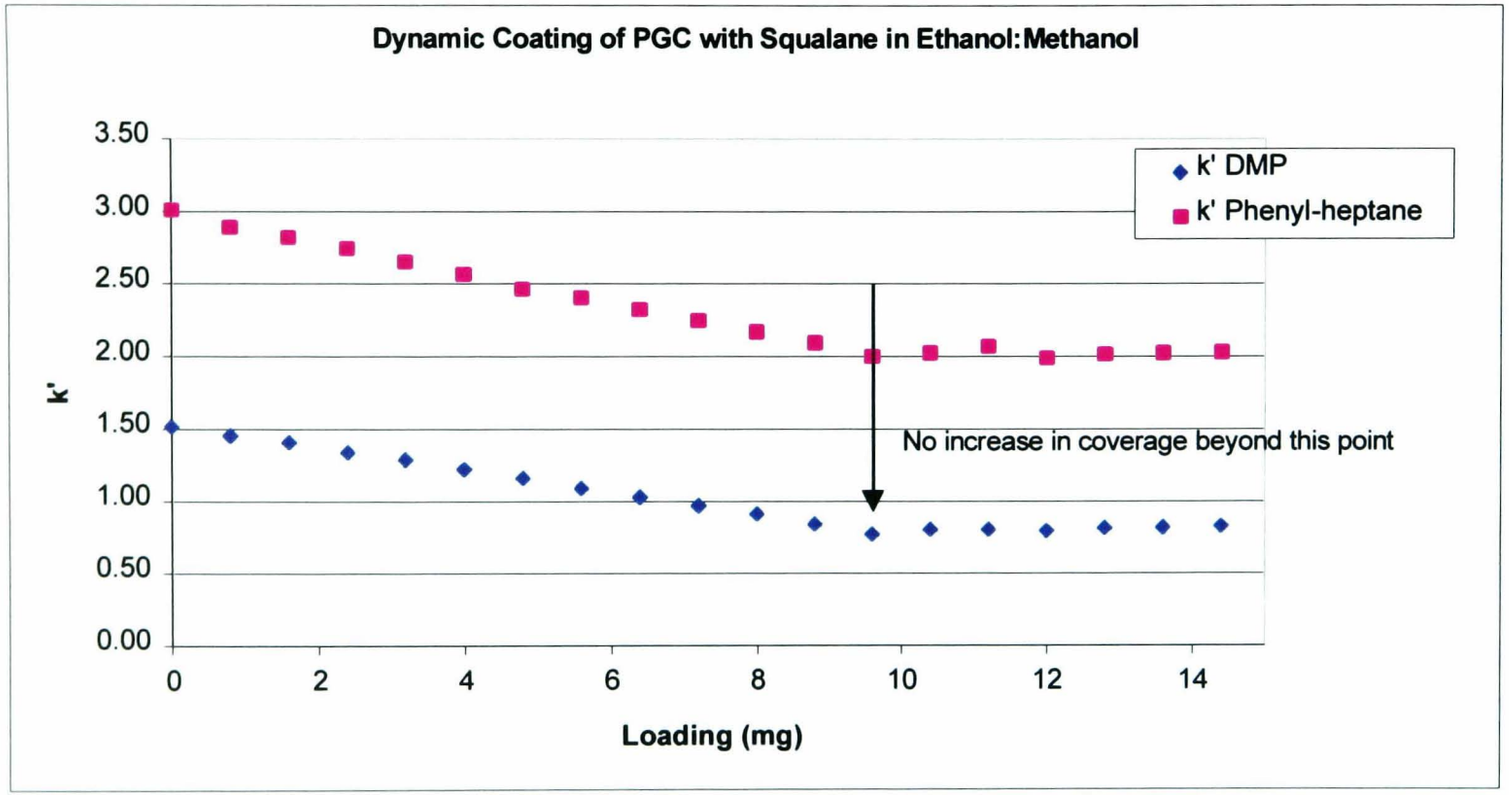

Column : 100 x 4.6mm PGC
Mobile Phase : Ethanol:Methanol (50/50)
Flow: 1.0ml/min

Fig 4.20c

Dynamic coating of PGC with Squalane

Sequential injection 1,25mg/10ul injections

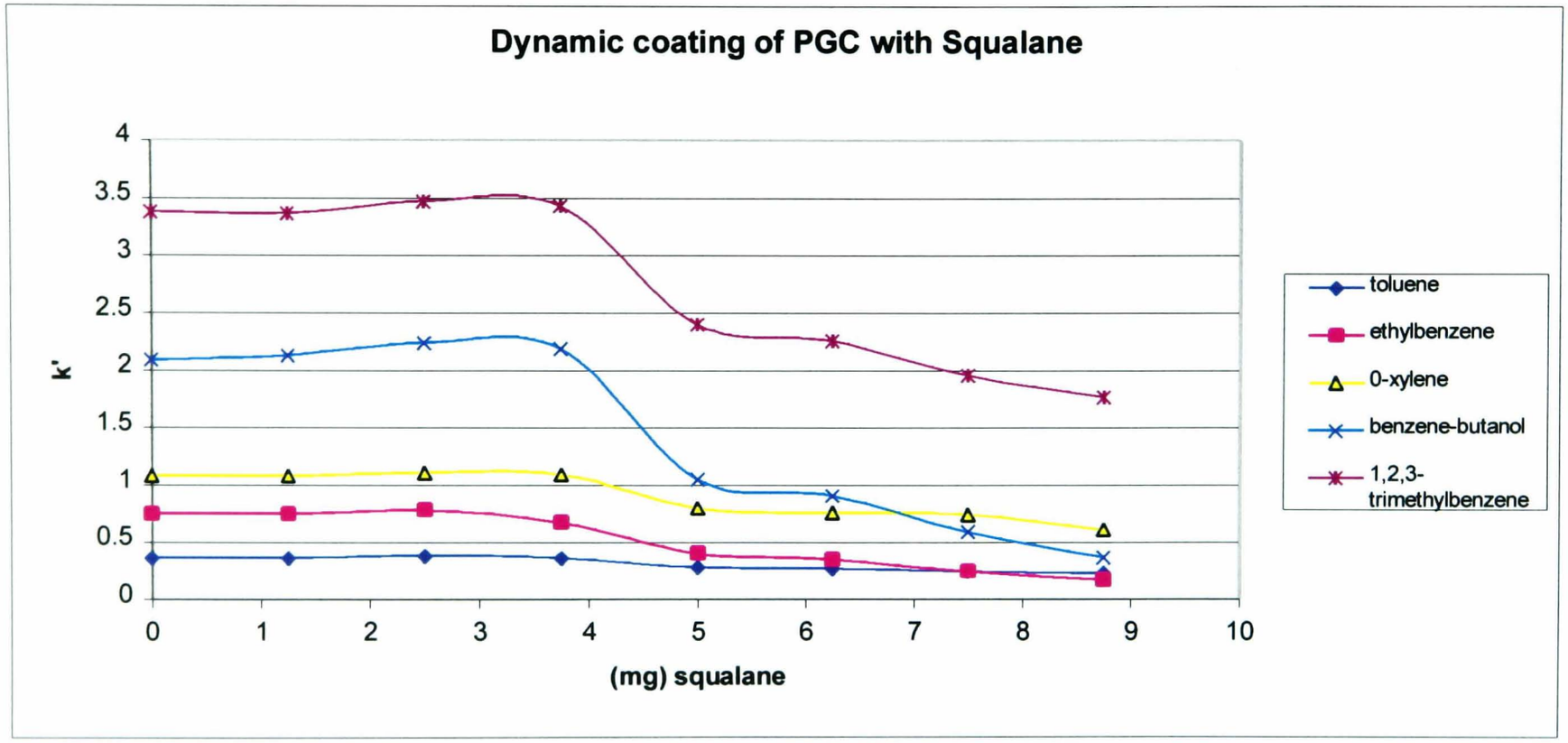

Column 100 x 4.6mm

Mobile Phase : Methanol

Fig4.21a
Thermogravimetric Analysis of Uncoated PGC

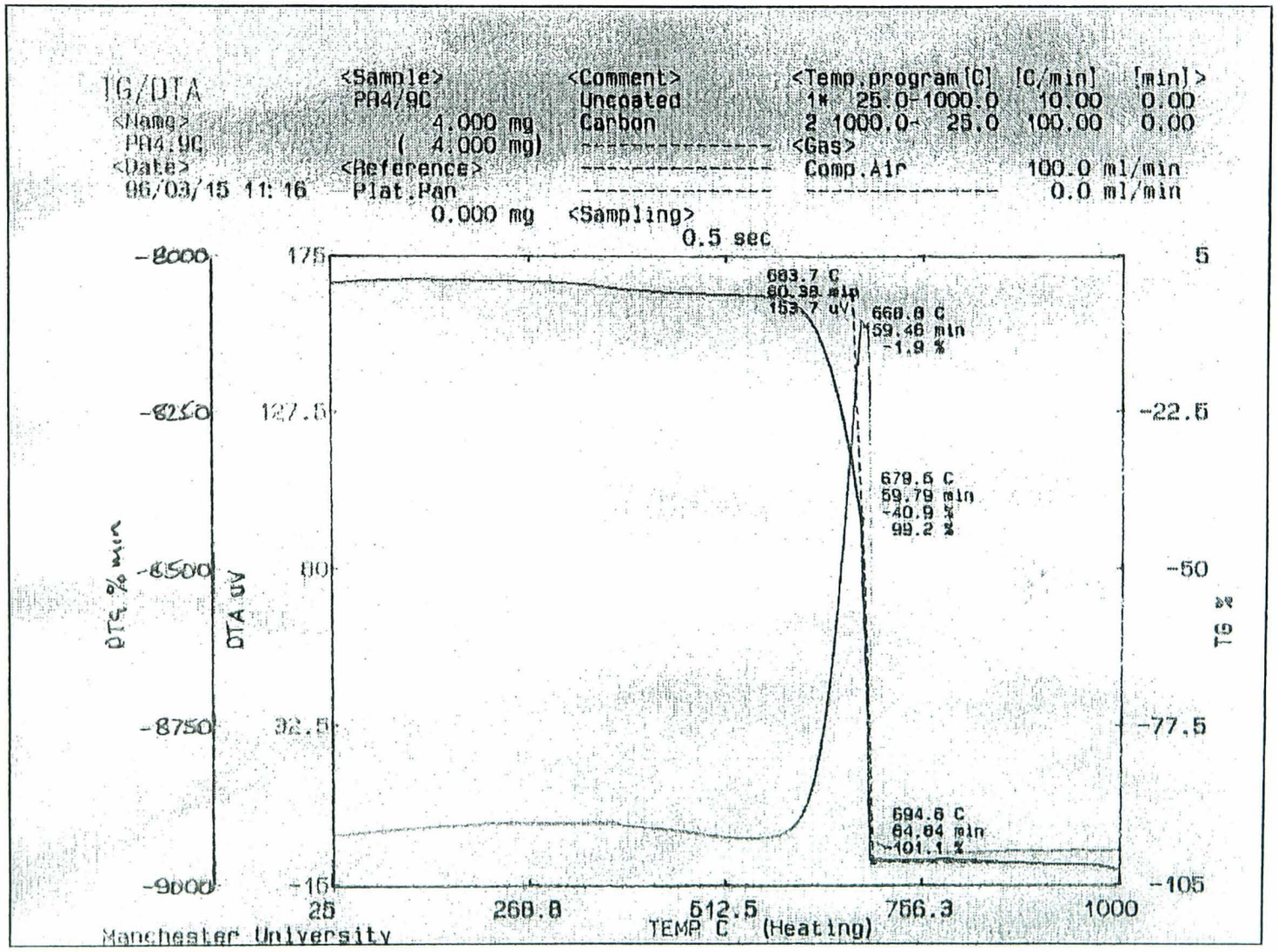

Fig 4.21b,c
Thermogravimetric Analysis for Polystyrene and PPGE

Fig 4.21b (Polystyrene)

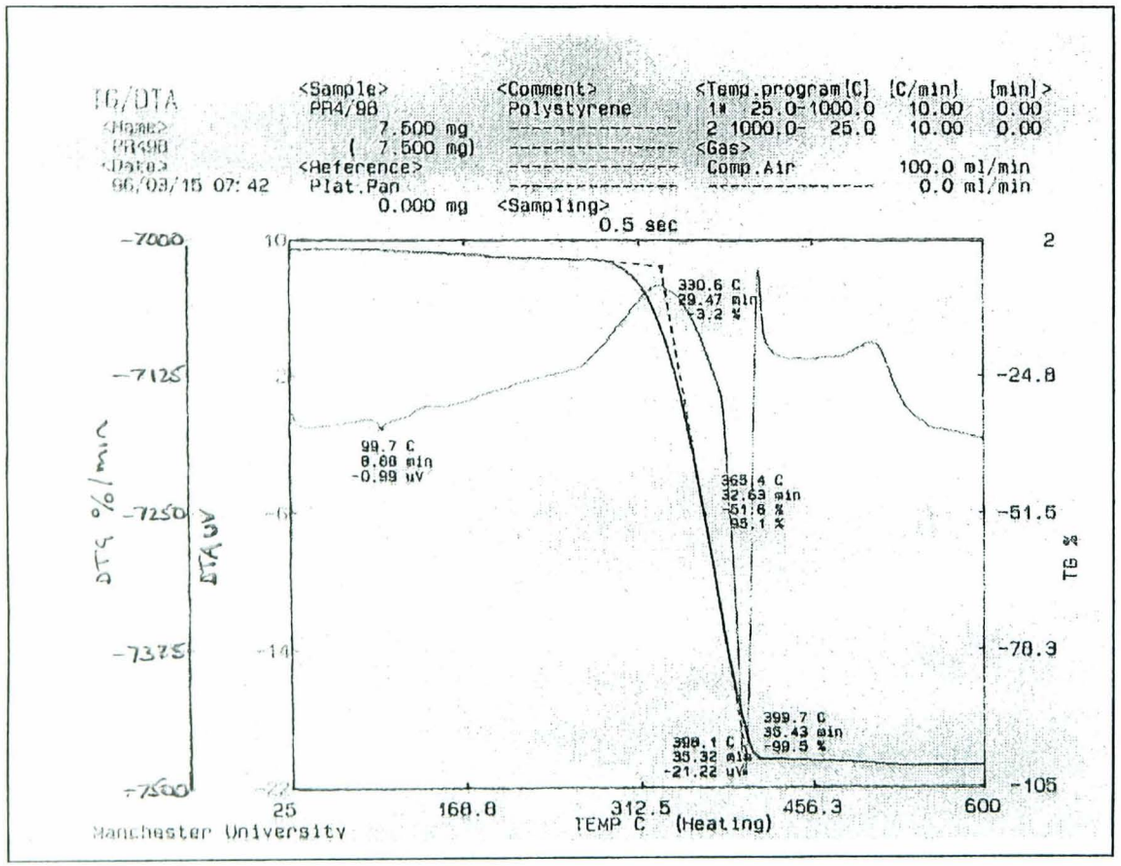

Fig 4.21c (PPGE)

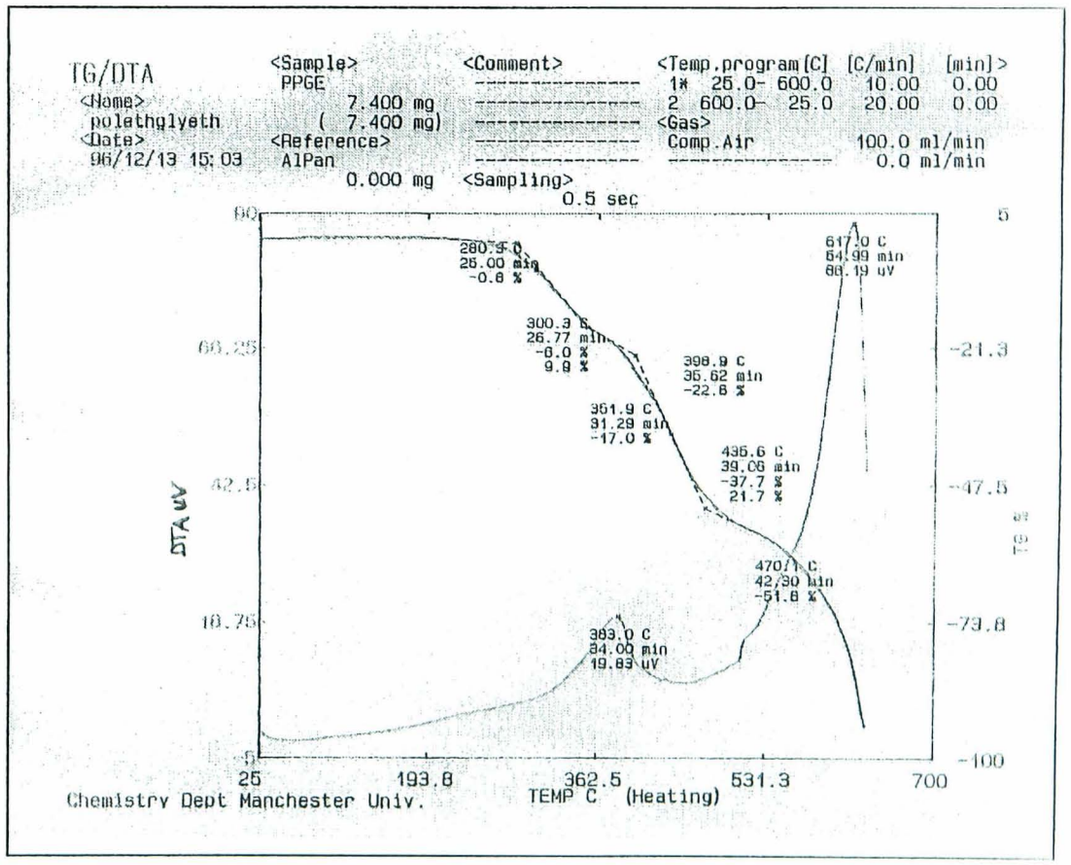

Fig 4.22
Thermogravimetric Analysis for Polystyrene Coated PGC

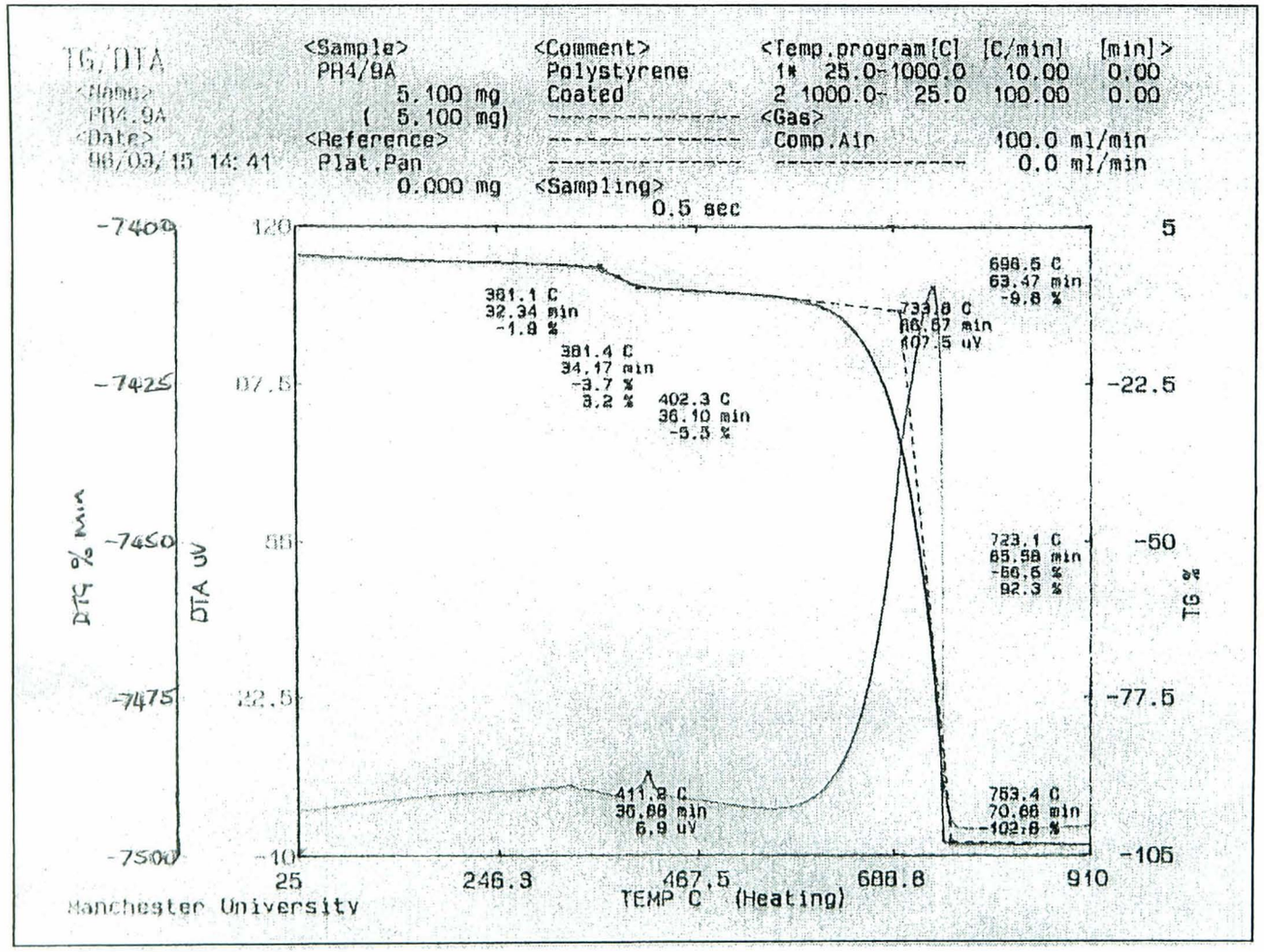

The predicted loading by the breakthrough coating experiment is 28mg/g PGC, while TGA analysis gives 92mg/g PGC. The TGA data and plot of TG % *vs.* temperature is typical of plots normally obtained for the exothermic reaction concerning the combustion of a polymer, *i.e.* a gradual weight loss with temperature increase is observed.

Fig 4.23
Thermogravimetric Analysis of PPGE Coated PGC

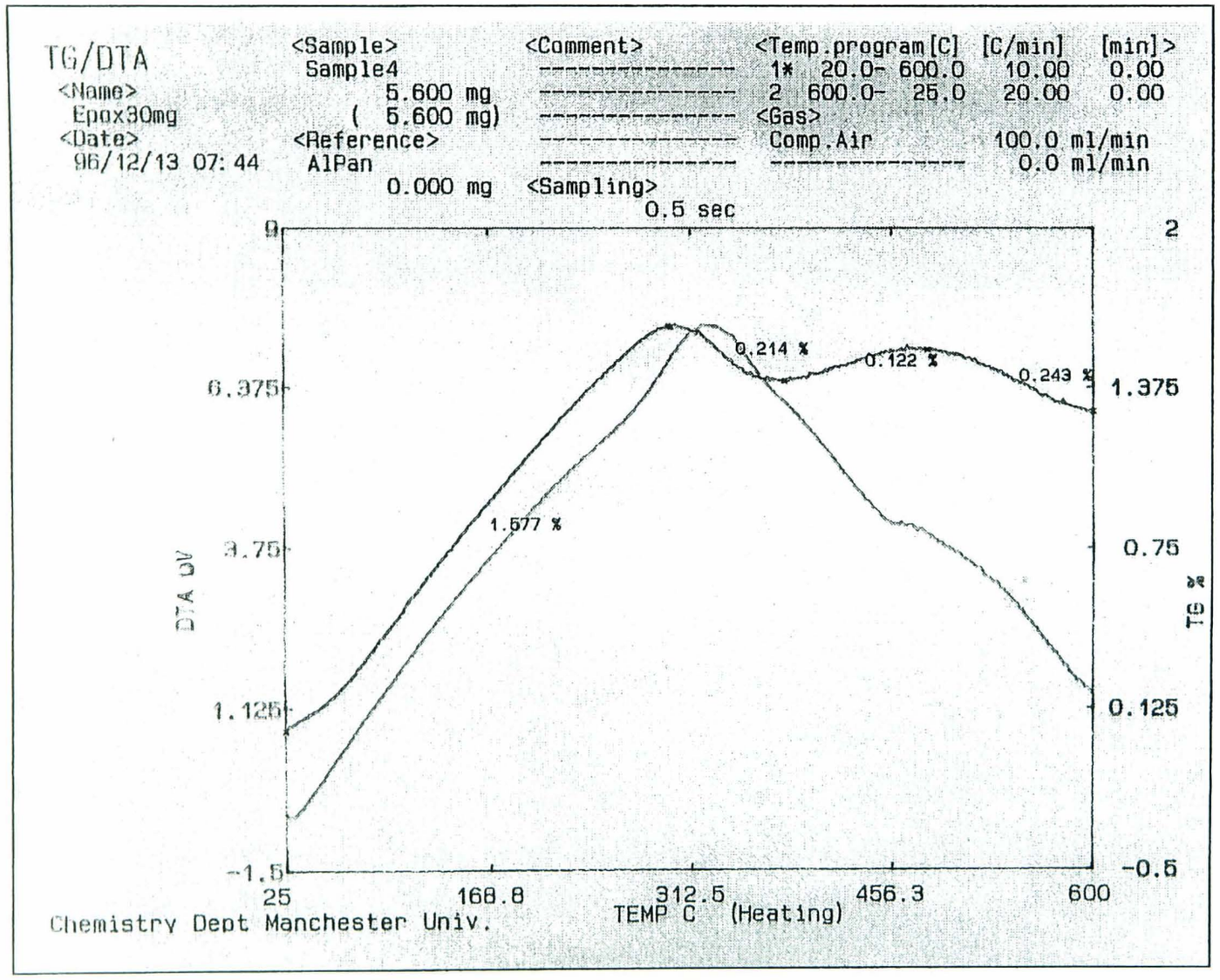

This sample was found to be in good agreement with the loading predicted by the evaporative method, *i.e.* TGA gave 32mg PPGE/g of PGC while the evaporative loading technique predicted 25.5mgPPGE/g of PGC.

Chapter 5 – Quantification of PREG

5.1 Aim of the Chapter

In Chapters 3 and 4 of this Thesis we have shown that the graphite surface plays a significant role in analyte retention. This role is much greater than had originally been expected by those who developed PGC[1]. The fact the graphite surface can interact with both hydrophobic and, of particular interest, hydrophilic analytes, suggests a very unique mechanism of retention on graphite compared to other chromatographic supports. We have called this the Polar Retention Effect on Graphite, or PREG.

In this Chapter we first review the different types of energies associated with molecular interactions likely to occur between the analyte and a support media and an analyte and the solvent. In particular we review attempts to correlate analyte molecular properties with retention behaviour on graphite. Such correlation have proven to be generally unsuccessful in providing a theoretical explanation for PREG. To a large extent this is because there has been no attempt to quantify experimentally the energy associated with PREG. We have therefore developed a procedure that allows for the quantification of PREG.

The second part of this Chapter is therefore concerned with the method developed to quantify PREG, the energies of PREG measured for a range of polar analytes and correlation of this energy with calculated energies of molecular interaction. This, then, provides useful information regarding the types of energies associated with interaction on graphite. It may then be possible to determine the molecular forces associated with PREG.

5.2 Theoretical Background

5.2.1 Molecular Interactions

Intermolecular forces, or forces that can occur between closed-shell molecules, are also called Van der Waals forces, since Van der Waal recognised them as the reason for the non-ideal behaviour of real gases[2]. They can be subdivided into two groups. First are those that are considered to be non-specific, which cannot be completely saturated and which are categorised as comprising directional, inductional and dispersive. Second are those that comprise hydrogen-bonding forces and electron pair donor-acceptor forces. Such forces are categorised as comprising specific directional forces that can be saturated and lead to weakly bonded stoichiometric molecular compounds.

Generally the potential energy (V(r)) of interacting molecules as a function of intermolecular distance r is described by the classical Lennard-Jones equation:

$$V(r) = - a/r^{6} + b/r^{m} \qquad [5.1]$$

where a and b are constants, and the exponent m is significantly greater than 6, usually a value of 9-12 is observed for m experimentally (Figure 5.1).

As is evident from Equation [5.1], at closer distances repulsion forces predominate. Intermolecular attractive interactions are generally of low energy, typically the energy of the Van der Waals bond is lower than 1000-2000 J/mol. At room temperature the thermal energy is about 2500J/mol. This means that Van der Waals interactions between electrically neutral molecules are unable to form stable chemical compounds. Intermolecular forces are therefore usually considered to be weak and to represent attractions between different portions of different molecules, or in some cases within the same molecule.

We now look more closely at the group of molecular interactions with which the Van der Waals interactions have become most closely associated, *i.e.* forces resulting from the electric field generated by the molecules. This type of field depends on whether or not the molecules considered form stable dipoles or their charge distribution is spherically symmetrical. This group of Van der Waals interactions can be sub-divided into three groups: the orientation interactions (Keeson effect), the inductive interactions (Debye effect), and the dispersive interactions (London effect). For very polar molecules the orientation or dipole-dipole interactions are characteristic but generally the effect of orientation interactions is lower than the effect of additive dispersion interactions.

Dipole - Dipole Interactions

Dipole-dipole interactions arise from the attraction of the positive end of one polar molecule for the negative end of another polar molecule (Figure 5.2a). It therefore concerns molecules which posses a permanent dipole moment, μ. In hydrogen chloride (HCl), for example, the relatively positive hydrogen of one HCl molecule is attracted to the relatively negative chlorine of another HCl molecule.

As a result of dipole-dipole interactions, polar molecules are generally held to one another more strongly than are non-polar molecules of comparable molecular weight. This difference in strength of intermolecular forces is reflected in the physical properties of the compounds concerned.

An important feature of dipole-dipole interaction is the tendency of one dipole to align the other into a favourable arrangement. When two dipolar molecules are specifically orientated towards each other the force of attraction is proportional to $1/r^3$ where r is the distance between the dipoles. In normal circumstances the dipoles are essentially randomly averaged and the average energy of interaction of two molecules with permanent dipole moments, μ_1 and μ_2, is then:

$$E_{d\text{-}d} = \frac{2\mu_1^2 \cdot \mu_2^2}{3\, r^6 kT} \frac{1}{4\pi\varepsilon_o\varepsilon_r} \qquad [5.2]$$

where r is distance between the molecules, k is the Boltzmann constant, and T is the absolute temperature. The term $\varepsilon_o = 8.854 \times 10^{-12}$ Fm^{-1} is the electric permittivity of vacuum and ε_r is the relative electric permittivity of the medium. An important point is the dependence of this energy on the inverse sixth power of r, so that the Lennard Jones potential, Figure 5.1, can represent the strength of interaction. $E_{d\text{-}d}$ is also inversely dependent on absolute temperature, reflecting the point that at high temperatures thermal agitation will reduce the mutual orientating effects of the two dipoles. This causes the probability of energetically favoured orientations to decrease, and at very high temperatures all dipole orientations are equally populated and the potential energy of interaction is zero.

Dipole-Induced Dipole Interactions

In 1920 Debye postulated that a polar molecule might induce a dipole moment in a neighbouring non-polar molecule resulting in attraction between the two molecules. Such an induced dipole can also be produced between two polar molecules, that is, molecules already possessing a permanent dipole moment. However, such an induced dipole is relatively small compared to the permanent one.Hence the dipole-induced dipole interaction is weaker than ion-induced dipole interaction. The induced dipole moment always lies in the direction opposite to that of the inducing dipole. Thus, attraction always exists between the two entities, and is independent of temperature. The polarisability, α, is defined as the dipole moment induced in the given molecule by the electric field. Since molecular polarisability is different in different directions, all possible molecular orientations should be considered. For practical purposes, where the electric field of a dipole is of concern one gets:

$$E_{d\text{-}id} = -(1/4\pi\varepsilon_o\varepsilon_r)^2 [1/2(\alpha_1 E_2^2 + \alpha_2 E_1^2)] / \varepsilon r^6 \qquad [5.3]$$

where $\frac{1}{2}\alpha_1 E_2^2$ is the energy of the induced dipole for molecule 1 and $\frac{1}{2}\alpha_2 E_1^2$ is the energy of the induced dipole for molecule 2 when either molecule is place in the electric field of the other (see Figure 5.2b). In fact, because the dipole induces a dipole in the other, only the case of one dipole is relevant. Thus, Equation [5.3] becomes:

$$E_{d\text{-}id} = -2\alpha\mu^2 / (4\pi\varepsilon_o\varepsilon_r)\, r^6 \qquad [5.4]$$

Dispersion Interactions

The origin of intermolecular forces among non-polar species remained a puzzle until F. London developed a quantitative theory based on quantum mechanics. It can be explained by considering the Bhor model of the hydrogen atom. The hydrogen atom has a time-averaged dipole moment of zero because the electron rotates many times during a relatively short period, and the time-averaged centre of gravity of the electron falls on top of the proton. The hydrogen atom, however, has an instantaneous dipole moment since at any given instant the electron and proton are spatially separated. Similarly, molecules with or without permanent dipole moments possess instantaneous dipole moments.

Each molecule "sees" the instantaneous dipole moment of the others (A thus induces an instantaneous dipole in B, and B induces an instantaneous dipole in A). Even although the interaction forces between the instantaneous dipoles of neighbouring molecules averages to zero, London showed that the interaction between the two dipole moments produces attractive forces between non-polar molecules (Figure 5.2c).

The negative end of the dipole will tend to repel electrons, and the positive end will tend to attract them. The dipole thus induces an oppositely oriented dipole in the neighbouring molecule. Although the momentary dipoles and the induced dipoles are constantly changing, the net result is attraction between the two molecules. A feature of these so-called dispersion interactions or charge fluctuations is their additivity. Thus, these forces are associated with all ions and molecules, whether possessing a stable dipole moment or not. Even in atoms and molecules without permanent dipole moments, the continuous electron density fluctuates. At any instant, a small dipole moment can polarise the electron system of neighbouring atoms or molecules. The dipole coupling causes the molecules to synchronise in such a way that mutual attraction result. The dispersive forces are highly sensitive to distance, falling off with at least the sixth power of the distance. An approximate expression for the calculation of the potential energy of dispersion interactions, E_d, is:

$$E_d = - \frac{3\,(I_1 I_2)\,\alpha_1\alpha_2}{4(I_1 + I_2)\,r^6} \cdot \frac{1}{(4\pi\varepsilon_r\varepsilon_o)} \qquad [5.5]$$

where I_1 and I_2 are respective ionisation energies of the interacting molecules 1 and 2, and α_1 and α_2 denote the polarisabilities of the interacting molecules. In the London Equation [5.5] molecular polarisabilities are scalar quantities and the changes in molecular orientation have no effect on E_d. Kaliszan[2] points out that the π-electron systems form a special case due to the anisotropy of electric properties in such systems, as shown in Figure 5.2e. At the same time, in π-electron systems the molecular orientations are especially favoured, and the dispersion interactions are directional to some extent.

The three types of molecular interaction between neutral species, polar or non-polar can be summarised as follows:

Orientational	(dipole-dipole)
Induction	(dipole-induced dipole)
Dispersion	(induced dipole-induced dipole)

Each one falls off the as the sixth power of the intermolecular distance, and the group is often referred to as Van der Waals interactions. Table 5.1 gives relative strengths of these interactions at a fixed r for typical molecules. Except for small molecules with large dipole moments, dispersion forces tend to dominate the other intermolecular forces. Hence, since polarisability increases with size of the molecule, dispersion forces increase with the molar mass.

Hydrogen Bonding Interactions

Hydrogen bonding is an especially strong kind of dipole-dipole attraction, in which a hydrogen atom serves as a bridge between electronegative atoms, holding one by covalent bond the other by purely electrostatic forces (see Figure 5.2d for hydrogen bonding). When hydrogen is attached to a highly electronegative atom, the electron cloud is greatly distorted towards the electronegative atom, exposing the hydrogen nucleus. The strong positive charge of the thinly shielded hydrogen nucleus is strongly attracted by the negative charge of electronegative atom of the second molecule. This attraction has strength of about 20kJ/mol, and is thus much weaker than a covalent bond, which is about 200-400kJ/mol, but considerably stronger than non-specific Van der Waals interactions, which are 1-2 KJ/mol.

Ion-Dipole Interactions

When placed in an ion's electric field, the dipole will orient itself so that the end with the charge opposite to that of the ion will be directed toward the ion, and the other repulsive end will be directed away. The potential energy of an ion dipole interaction, $E_{i\text{-}d}$, is given by the expression:

$$E_{i\text{-}d} = - \frac{z\mu\cos\alpha}{(4\pi\varepsilon_o\varepsilon)r^2} \qquad [5.6]$$

where z is the charge on the ion, r is the distance from the ion to the centre of the dipole and α the dipole angle relative to the line r joining the ion and centre of the dipole, and μ is the dipole moment of the neutral molecule. The higher the relative electric permittivity, ε, of the medium (solvent) the lower the energy of attractive dipole interactions. The electric permittivity of a vacuum is $\varepsilon_o = 8.854 \times 10^{-12}$ Fm^{-1}.

In order to calculate the ion induced dipole interaction energy, we have to take into account the energy cost in inducing a dipole and the energy gain for the dipole field:

$$E_{i\text{-}id} = \alpha z^2 / 2(4\pi\varepsilon_o\varepsilon)\, r^4 \qquad [5.7]$$

The ion induced dipole interactions are half those of ion–dipole (permanent) interactions. The difference arises because in the former case, work has to be done to create a dipole.

5.2.2 Molecular Interactions Which Contribute to Retention in HPLC

The four main factors, which influence retention in HPLC are:

[1] Eluant-analyte interactions (dispersive, dipole-dipole and hydrogen bonding interactions), which occur in the eluant. These discourage retention.

[2] Eluant-analyte repulsion (arising from resistance to the disruption of the structure of hydrogen bonded solvents by non-hydrogen bonding solvents). This repulsion occurs between a hydrophilic eluant and any non-polar segments of the analyte and encourages retention on graphite.

[3] Dispersive interactions of the London type between the support surface and the analyte. These are balanced largely by similar interactions between the support surface and the eluant, which is displaced by the analyte. Their net effect may either encourage or discourage retention, but they may have an important effect on selectivity.

[4] Charge-induced interactions of the analyte with the support. On graphite, these may promote the retention of polar molecules due to PREG. Such interactions are strongest on PGC when the polar groups of the analytes are forced into direct contact with the PGC surface by the stereochemistry of the analyte molecule but are compensated to a greater or lesser extent by polar interactions of the analyte with the eluant. These additional interactions resulting from the substitution of -H by a polar group can then be so strong that they more than compensate for the increased analyte-solvent interactions. When stereochemistry does not allow direct contact of the polar group with the surface, the effect is less strong but still significant. When the support is not graphite, but a silica based reversed phase material such as C18, phenyl or cyanopropyl, these interactions still occur, but via weaker secondary interactions. In the case of C18-silica this secondary interaction is via surface silanols. With the more polar bonded phases, secondary interactions are through interaction with the polar bonded groups (phenyl, or cyanopropyl), in which case charge-induced interactions become increasingly significant.

As the purpose of this study is to investigate the quantification of PREG, we are primarily interested in measuring the charge-induced interactions between an analyte and PGC. From the above discussion, we see that [1] and [2] represent analyte solvent interactions, illustrating how different molecular attractions or repulsive forces can lead to either positive or negative contribution towards retention. It appears that the balance between types [1] and [2] is reasonably well represented by the hydrophobicity parameter, $\log_{10} P$ (octanol/water partition coefficient), which may range from –2 to + 4. Lipid/water partition coefficients play an influential role in many biological processes, and the n-octanol/water partition coefficient is widely accepted as the reference standard. log P has been determined traditionally by the shake flask method. However, practical disadvantages and the limitation to n-octanol/water coefficients have lead researchers to investigate alternative methods for measuring partition coefficients[3]. Reversed phase high performance liquid chromatography has become a popular alternative where log P is fairly well correlated with $\log k_w$ (where $\log k_w$ is the log k' at 100% water) when C18 is employed as the stationary phase. Comparison of log P with a suitable retentive parameter for LC on graphite could therefore be an approach to determine PREG. For any theoretical calculation of PREG we need to isolate the forces associated with it from those associated with dispersive interaction with the graphite surface. Accordingly, we first look more closely at molecular interactions in general, their definition and the energies associated with them.

5.2.3 A Review of Current Thinking on the Mechanism of Retention for Graphite

Since its introduction to the marketplace, the retention mechanism of analytes on PGC has been the subject of considerable scientific research and debate. In 1996 Knox and Ross[4] produced a substantial review of the retention data and correlation of this data with analyte molecular properties. The review gives an in-depth discussion of how this published data fits with currently accepted theories of retention for reversed phase and adsorption chromatography systems and discusses some of the theories put forward so far to explain retention on PGC.

The review notes that there is now unquestionable experimental evidence that graphite shows unusual behaviour for polar analytes (PREG) that cannot be explained by the current theories of retention in chromatographic systems. PREG becomes particularly pronounced when the polar groups are attached to a benzene ring, and presumably with larger aromatic systems. The polar retention effect is in some way related to the charge separation within molecules, and probably involves the ready polarisation of the electronic cloud of graphite. The effect that we have called PREG may be thought of as related to the excess free energy of interaction of an analyte with graphite over and above its interaction energy with a non-polar material, that is:

$$\text{PREG} = RT \log k'_{\text{graphite}} / k'_{\text{non-polar surface}} \qquad [5.8]$$

where the two surfaces would have the same surface area within the packed chromatographic column. These conclusions provided the impetus for our own approach towards understanding PREG. However, before outlining our experimental approach we now recapitulate the arguments given in the above-mentioned review.

5.2.3.1 Current Theories of Retention in Liquid Chromatography

The three main theories of retention in liquid chromatography are those of Horvath *et al*, Martire and Boehm[5] for reversed phase chromatography, and Snyder for adsorption chromatography.

The theory of Horvath is concerned with reversed phase liquid chromatography and is discussed in detail in Chapter 1 of the Thesis. However, when the Horvath theory is applied to retention on graphite,

Gas Phase $A_{gas} + L_{gas} \Rightarrow_{gas} AL_{gas}$

$\Uparrow$ $\Downarrow$

Desolvation Solvation

Solution/Stationary Phase $A_{solv} + \underline{L}_{solv} \Rightarrow_{soln} \underline{AL}_{olv}$

the desolvation of the ligand "L" would be a small part of the graphite surface "G". The desolvation of the ligand ($\Uparrow$) would be the process of removing solvent from the surface of the bare graphite and a corresponding surface of free solvent. Desolvation of A would be represented as it is in the original theory. The formation of AL in the gas phase ($\Rightarrow_{gas}$) would correspond to adsorbing the hydrophobic side of the molecule of A onto this small area of graphite in the gas phase, GA. The solvation of AL ($\Downarrow$) would correspond to wetting the top surface of A adsorbed onto the graphite surface AG ($\Downarrow$). The crucial assumption of the whole theory is that the bond formed between A and L is the result of dispersive interactions. We have already seen that this assumption is incorrect when applied to graphite *i.e.* the bond between A and G because there are additional interactions resulting in PREG. Thus the theory of Horvath *et al* does not provide any insight into PREG.

The theory of Martire and Boehm is also a theory of retention for reversed phase chromatography. It is not discussed in earlier Chapters of this Thesis, so a brief description is presented here along with its application to graphite.

The theory of Martire and Boehm starts from the standpoint of a lattice containing atomic sized cubic cells. A strand of ligand, for example octadecyl or C18, will occupy a number of these cells that are connected together. This number is denoted by r_{ligand}. Likewise, solvent molecules (the theory as presented allows for two eluant species, 1 and 2) occupy r1 and r2 cells. Various energy terms are allowed for bond bending in the hydrocarbon chain, but the crucial energy terms are those for the interactions between segments of the various species. These are called *X* values. The treatment is statistical and provides a rigorous treatment of both the entropy and enthalpy changes for the basic equilibrium $A + L \Leftrightarrow \underline{AL}$. The theory enables various properties of the system to be predicted, such as the degree of solvation of the bonded hydrocarbon chain and the differential partitioning of solvent components into the hydrocarbon layer. Unfortunately, it gives no guidance as to how to

calculate the key energetic parameters, namely the interaction energies between segments, so it likewise gives no lead on the interpretation of PREG.

Snyder regards the process of adsorption of the analyte A as a displacement process of the form:

$$A_{solv} + n\underline{S}_{ads} = \underline{A}_{ads} + nS_{solv} \qquad [5.9]$$

where A is an analyte molecule and S is a solvent molecule. The analyte displaces n solvent molecules from the surface. The free energy change, ΔG, can then be written as:

$$\Delta G = G(S_{solv}) + G(\underline{A}_{ads}) - nG(\underline{S}_{ads}) - G(A_{solv}) \qquad [5.10]$$

The free energies, G, are taken with respect to the isolated (*i.e.* not solvated) species in the gas phase. The free energies of solvated species are evidently similar to those used by Horvath *et al* in their theory. The free energy of adsorbed species would contain a free energy contribution for attachment of one face of the molecule to the adsorbate, and a second contribution for solvation of the side of the molecule in contact with the solvent. The second part of this contribution will cancel part of the total free energy of the fully solvated species, so we only need to consider the free energy of solvation of those parts of A and S which become desolvated when A and S are adsorbed. When Snyder applied this theory to oxide adsorbents he assumed that the solvation free energies, $nF(S_{solv})$ and $F(A_{solv})$, cancelled. This was the crucial assumption of the theory and it was justified only because the major interactions of oxide adsorbents with typical solvents, $F(S_{ads})$, are dominated by the possibility of hydrogen-bond formation between –OH groups in the adsorbents and atoms such as -O-, -N-, -Cl, and so forth, in the solvents. Accordingly, solvents could be effectively organised in the order of their hydrogen bonding capacity and lead to the development of the eluotropic strength parameter of the solvent, ϵ^o. As soon as we apply the theory to a non-polar surface such as graphite or C18, the dominant interaction is no longer that of hydrogen bonding. It is then no longer appropriate to cancel the solvation enthalpies of A and nS. Indeed, they now become key to retention selectivity.

The three theories that are currently accepted for reversed phase and oxide adsorbent liquid chromatography cannot explain the unique retentive properties of graphite. We now therefore review the experimental data and discuss the correlative data of retention behaviour with molecular properties of analytes, gathered so far.

5.2.3.2 Correlation of Retention on Graphite with Measured or Calculated Physical Properties

Nearly all attempts thus far to try to explain the retentive properties of graphite tried to explain log k' in terms of independent physical properties of the analyte. In this way it had been hoped that one could identify one or more key physical parameters that would correlate with retention.

There are two basic approaches to identifying the appropriate physical properties: the single parameter approach and the factor analysis approach. In the former, correlation is sought with a single, hopefully dominant, physical parameter. In the latter, a weighted group of parameters is sought which gives an optimum correlation of the experimental data with independent physical parameters.

Single Parameter Approach – Electronic Parameters

Several researchers have evaluated the (excess) electronic charges on the individual atoms of analyte molecules. These charges are both positive and negative, with the total being zero for a neutral molecule. Various combinations of these have been used in correlation of retention on PGC.

(1) Submolecular parameter

Kaliszan's submolecular polarity parameter[6] is an example of this type of evaluation. It is defined as the sum of the largest excess negative and largest excess positive charge in the molecule.

(2) Local dipole index

The local dipole index is obtained by evaluating the charge difference over the atoms at the ends of each bond in the molecule and adding them together.

(3) Excess charge

Cocquart and Hennion[7] used the excess charge C_n that is defined as:

$$C_n = 1/2\Sigma|q_i| \qquad [5.11]$$

where q_i is the excess charges on the individual atoms. Knox[4] suggested that a more appropriate descriptor than C_n would be the sum of the squares of the charges. This value would reflect the interaction of excess charge on each atom with corresponding features in some kind of induced charged footprint in the graphite surface:

$$S = \Sigma(q_i)^2 \qquad [5.12]$$

(4) Mirror Image charge

Kaliszan[8,9] noted that PGC had properties analogous to metal in that it behaves as a two dimensional conductor, the graphite layers being metallic through the presence of the π-electron cloud. The energy of interaction of a charged body with a conductor is equal to its energy of interaction with its imaginary charge image (of opposite sign) reflected in the surface. The interaction energy, U, of each atom in the analyte molecule with each atom in its image, both being separated by a distance r_{ij}, can be calculated by:

$$U_{ij} = \frac{1}{4\pi\in_o} \cdot \frac{q_i q_j}{r_{ij}} \qquad [5.13]$$

For a molecule comprising three atoms, the total energy of interaction, U, is given by the sum of all nine energy terms in the matrix (see Figure 5.3):

$$U = \sum^{\text{all pairs}} \{1/4\pi\in_o \cdot q_i q_j / r_{ij}\} \qquad [5.14]$$

The diagonal elements of the matrix represent the interaction energies of each atom in the analyte with the atom in its image that is directly below it. Their sum, denoted by U', is given by:

$$U' = \frac{1}{4\pi\in_o} \cdot \Sigma\{\frac{q_i q_j}{r_{ij}}\} \qquad [5.15]$$

where r is the distance between the charges in the molecule and its image. For a flat molecule, such as phenol, positioned parallel to the surface, U' is closely approximated by:

$$U'' = \frac{S}{4\pi\varepsilon_o r} \qquad [5.16]$$

For Equation 5.16 to be true, it is assumed that all r_{ij} are the same and equal to r. Knox points out however that although S and C_u may give a general assessment of the overall charge separation, they cannot represent the interaction energy of a charged body with a perfect linear conductor. This is because the overall interaction energy, U, has to include all nine terms in the matrix and will approach U' only if the distances between the atoms in the molecule and its image, r_{ij}, are much smaller than interatomic distances within the molecule.

In fact, this can never be the case and the full calculation of U must be made for a molecule and its mirror image. U' and U'' will then be expected to be much larger than U.

(5) HOMO

The energies of the highest occupied molecular orbital[2], E_{homo}, and the energy of the lowest occupied molecular orbital, E_{lumo}, of the analyte are two further quantum mechanical parameters which allow for correlation with selectivity (α) on graphite. This type of correlation may well be relevant on graphite because graphite being a conductor can certainly act as a ready donor or acceptor of electrons.

(6) Other Parameters

Other parameters such as the total binding energy, E_T, and various connectivity and structural parameters are also thought to be correlated to PGC's overall capacity to take part in dispersive interactions.

Single Parameter Approach – Hammet-type parameters

A second group of empirical parameters are those related to σ, originally devised by Hammett.[10] The purpose of σ is to quantify the effects of benzene ring substitution on the reaction rate and equilibrium constants of group reactions. These can include reactions (*e.g.* hydrolysis of esters) which involve a reactive centre that is influenced by a substituent, X. The value of σ_x for any substituent X was defined by:

$$\sigma_x = \log K_{a(x)} - \log K_{a(H)} \qquad [5.17]$$

where $K_{a(x)}$ and $K_{a(H)}$ are the rate constants for the test molecule and the molecules with the substituent X, respectively. When the substituent X is an electron-withdrawing group, σ values are positive. When it is an electron-donating group, σ values are negative. The total range of values for σ is from about –1 to +1. The value of σ for any substituent X depends on whether it is in the ortho-, meta- or para-position. The Hammett equation for any rate or equilibrium constant K_x can then be expressed by:

$$\log K_x = \rho\sigma + \log K_H \qquad [5.18]$$

where the constant ρ is characteristic of the process or equilibrium under consideration. Insofar as retention on graphite can be regarded as a reaction or equilibrium, then the Hammett parameters are relevant. Such a contention would be in line with Kaliszan's assertion that a localised polar segment of the molecule was responsible for retention. However, Knox points out that this cannot account for PREG in general. It is likely that the whole electronic distribution of an analyte molecule and its polarisability is relevant and will have to be taken into account.

Conclusions drawn from the various correlation and observations made can be summarised as follows:

Although there was no correlation of log k_w on graphite (k'_w refers to k' for analytes eluted in pure water – extrapolated if necessary) with log P, Coquart[11] demonstrated a significant correlation between log k'_w and the total charge denoted by C_n. Because S correlates very closely with C_n a similar correlation is obtained. Kaliszan also showed good correlation of log k'_w with heat of formation and local dipole index. The evidence suggested that retention is strongly influenced by distribution of molecular charge within the molecule. However plots log k'_w for both alkylbenzenes and phenylalkanols show no correlation with C_n or S. Here C_n and S are independent of chain length while k'_w is highly dependent on chain length. Thus the charge distribution within an analyte is clearly not the whole story to retention on graphite.

No correlation was observed for Kaliszan's polarisability parameter, Δ, when the substituents of the benzene ring were identical (*e.g.* polysubstituted acids or hydroxy acids). The reason for this is that the most polar group, and not the number of such groups, determines the largest charge differences within the molecules of any such series. However, good correlation was observed when the benzene ring substituents were changed, suggesting that where a molecule had a single localised segment, this could be responsible for enhanced retention either directly or through polarisation of the ring.

Correlation of Coquart's log k'_w values with U (Equation [5.15]) proved to be disappointing when compared with calculated values of PREG. The values of U proved to be much too small to account for the additional retentive effects on graphite over those expected for hydrophobic interaction. Calculated values for U were generally below 2kJ/mol whereas RTlog (k'_{RX}) – RT log (k'_{RH}) were up to >10kJ/mol. The term k'_{Rx} refers to the retention of

the analyte when all functionality, *i.e.* oxygen and nitrogen, is replaced by $-CH_2-$ (methylene) groups.

Factor Analysis Approach

Both the Single Parameter and the Factor Analysis approaches start from a listing of the electronic parameters from a range of analytes. However, if no firm theoretical link exists between a physical or computed property and the retention parameter, it may be that a weighted combination of physical properties will provide a better correlation than any single parameter. An examination of the optimum combinations for different classes of analytes may lead to a more detailed understanding of the factors leading to retention. This approach is the "Factor Analysis approach."

Kaliszan[12] applied factor analysis to the log k' values on graphite of benzene derivatives having a range of simple substituents ($-CH_3$, $-COCH_3$, -Cl, $-COOCH_3$, $-NO_2$, $-NH_2$, $-OCH_3$, $-CH_2OH$ and –OH), alkylphenols with alkyl groups having up to four carbon atoms, and pyridine. The chromatography was carried out using hexane as the eluant. Such an eluant would be expected to show little sensitivity to alkyl chain length. The best correlation was found with the submolecular parameter Δ, which suggested that a localised segment of the molecule was responsible for retention rather than the π-orbitals of the benzene ring. They also found that retention on graphite was well correlated with retention on palladium metal spheres, suggesting that graphite behaved like a metal. Unfortunately, Coquart's data shows that correlation with Δ does not hold for benzene derivatives containing more than one functional group.

In a second article, Bassler *et al*[13] analysed data from a similar group of compounds using the principal component method. Again the eluant was hexane. It was observed that molecules of high polarity are much more retained by graphite than those of low polarity. They also observed, that the increase in size and number of the alkyl substituents has less effect on retention than changes in polarity. It was also clear that the position of a substituent in an alkylphenol, for example, can have a very significant effect on its retention, with para-substituents providing the highest retention. The principle component, which provided best correlation with experimental data, was heavily, weighted with molecular size and to a lesser extent those, which related to molecular polarity. This simply reflects either the importance of dispersive interactions or the fact that alkane retention on graphite increases with carbon number. The second principle component was loaded with heat of formation and local dipole index. The evidence is, therefore, that retention on

graphite with hexane eluant is strongly influenced by both molecular size and by the distribution of molecular charge in the analyte.

Forgacs and Cserhati *et al*[14,15,16,17,18] also carried out extensive correlative work using reversed phase conditions on graphite with methanol:water and acetonitrile:water as eluants. The primary experimental measurements demonstrated a linear dependence of log k' on the percentage of organic component in the otherwise aqueous mobile phase. Using multicomponent analysis they found that combinations of electronic parameters gave the best correlation with both log k'_w and the concentration of methanol. They concentrated primarily on correlation with empirical parameters related to Hammet's σ. Then, using stepwise regression analysis they examined the correlation of retention data and physico-chemical parameters for forty-five barbiturates on PGC/Hypercarb using methanol:water eluants. These physico-chemical parameters included: the Hasch-Fujita constant characteristic of hydrophobicity, proton acceptor and proton donor properties, molar refractivity, the Hammett constant σ, the electron withdrawing power of substituents, steric effects of substituents, and the two Swain Lupton electronic Parameters, F and R, which characterise the inductive and resonance effects.

The physical parameter which best correlated with retention was the Swain Lupton electronic parameter F, which characterises the inductive effect. In similar studies of the retention characteristics of phenols on graphite, the authors once again showed an elution order differing from those expected from simple reversed-phase behaviour, with the more polar analytes being more strongly retained than otherwise expected. They concluded that retention was governed mainly by the analyte's steric parameters, electron-withdrawing power, and hydrogen donor capacity of substituents, but not hydrophobicity. This would indicate that polarisation of graphite by analytes was an important factor in their retention.

5.2.4 Theoretical Approach to Our Work – The Equivalent Hydrocarbons

It has been noted that two types of relationships exist for reversed phase materials:

(a) For a homologous series[19] (*e.g.* n-alkylbenzenes, n-alkyl homologues):

$$\log k' = \beta + \alpha n \qquad [5.19]$$

where n = number of C atoms in the carbon chain of the substituted alkane, $R(CH_2)_nH$.

The plots of log k' *vs.* n are usually linear, for some limited range of the alkyl chain length. The reported range of linearity does not exceed six to eight carbon atoms, depending on the other functional groups present in the series. β gives the intercept value, corresponding to the hypothetical retention (log k') for benzene, and α gives the gradient (slope) of the linear relationship.

(b) For a given analyte where organic content of eluant is changed[20]:

$$\log k' = \log k'_w + AC \qquad [5.20]$$

where C is the volume fraction of organic component, *e.g.* methanol or acetonitrile, $\log k'_w$ is the capacity factor for the analyte in pure water, and A is the gradient (slope) for the linear relationship observed when log k' is plotted against C. A, also represents the distribution coefficient. Equation [5.20] is particularly useful since there is often a limited range of mobile phase organic compositions for which linearity of retention can be measured experimentally, due to the solubility of the analyte. Values of log k' are obtained by isocratic elution of the analyte recorded at various methanol:water ratios. It was Pietrogrande *et al*[15] who advocated the method of linear extrapolation from retention data experimentally derived at rather narrow concentration ranges to pure water. $\log k'_w$ values obtained by extrapolation correlate well with log P values. In fact, Equations [5.19] and [5.20] also hold true for the partition of an analyte from any non-polar phase to an aqueous:organic phase e.g methanol:water.

$$\log D = \beta + \alpha n \qquad [5.21]$$

i.e.

$$\log D = \log D'_w + AC \qquad [5.22]$$

The relationship also holds true for graphite[21,22] where in general for relationship (a) described above, the gradient, α, is larger on graphite than for say a non-polar bonded silica such as an C18-silica. For relationship (b) the gradient A on graphite also differs from C18-silica.

The difference in retention behaviour on graphite compared to C18-silica is most apparent with polar compounds. For instance, if the retention of a compound that has a polar substituent is compared to that of a compound without a polar substituent, *e.g.* an alkanol with the corresponding alkane, it is generally found that retention of the parent compound is lowered by polar substitution. This is generally the case for all C18-silica materials, while for graphite the retention is lowered to a lesser extent and indeed sometimes increases. In

other words, when compared to a typical non-polar phase, polar substitution on the analyte enhances retention on graphite. This is the effect which we call PREG. Ultimately, we hope to be able to predict the extent of PREG. But first it is necessary to find a method of quantifying it.

We propose that the best way to quantify PREG will be based on comparing the retention of test polar compounds with those of "equivalent hydrocarbons". The equivalent hydrocarbon is defined as the hydrocarbon obtained by replacing atoms such as O and N, with CH_2 and CH_3 respectively. Thus the hydrocarbon equivalent to phenol, C_6H_5OH, is toluene, $C_6H_5CH_3$, and the hydrocarbon equivalent to nitrobenzene, $C_6H_5NO_2$, is isopropylbenzene, $C_6H_5CH(CH_3)_2$.

To quantify PREG it is proposed that the substituted compound (x) be compared with the equivalent hydrocarbon (HC) in respect to its (1) retention ratio on graphite from typical chromatographic solvents, *i.e.* k' and (2) partition coefficient into a non-polar phase from the same solvent, D. Thus:

$$\text{PREG(1)} = \log (k'_x/k'_{HC})_{\text{graphite}} - \log (D_x/D_{HC})_{\text{non-polar phase}} \qquad [5.23]$$

$$\text{PREG(1)} = \log (k'_x/D_x) - \log (k'_{HC} / D_{HC}) \qquad [5.24]$$

where PREG(1) is PREG given in units of $\log_{10}$.

In order to consider PREG in energy terms we employ PREG(2), which is expressed as follows

$$\text{PREG(2)} = 2.303RT \log_{10} (k'_x/D_x) - 2.303RT \log_{10} - (k'_{HC} / D_{HC}) \qquad [5.25]$$

In free energy terms, we write:

$$\text{PREG} = (\Delta G^{o}_{x(chr)} - \Delta G^{o}_{x(partition)}) - (\Delta G^{o}_{HC(chr)} - \Delta G^{o}_{HC(partition)}) \qquad [5.26]$$

where $\Delta G_{(chr)}$ and $\Delta G_{(partition)}$ are the free energy changes for transfer of an analyte from eluent to graphite and from eluant to a non-polar phase, respectively. The non-polar phase could in principle be either a non-polar chromatographic support or a non-polar liquid. The most obvious choice of the former would be an C18-silica, but this has the disadvantage that such

materials still contain free silanols groups which can prejudice the non-polar nature of the phase especially for polar materials. This can most easily be illustrated by Equation [5.21]. Although this provides a linear relationship for a homologous series of alkylbenzenes, in a C18-silica deviations from linearity are found when the series contains a more polar substituent. The deviations from linearity arise due to differences in shielding of the polar functional group. Tomlinson *et al*[23] illustrate non-linearity for log k' versus carbon number plot for (a) trichloro, (b) dimethoxy and (c) dinitro -substituted alkylbenzoates. There are clearly difficulties in employing reversed phase chromatography as the non-polar phase since it does not strictly behave as such when compounds with polar functionality are present. Their main advantage is the ease of obtaining the data. A non-polar liquid such as hexane or octane would thus be preferable.

There is, of course, a huge amount of data on partition of compounds between water and octanol, the basis of the well-known P-values. The octanol-water system was originally chosen to mimic biological systems and is useful for predicting the uptake of compounds or their partitioning between aqueous bodily fluids (*e.g.* blood) and fatty tissues. Unfortunately, water is not a very useful chromatographic solvent, and octanol with its OH group is not a good candidate for a non-polar phase, which should interact with the analytes by purely dispersive interactions. log P values are not therefore suitable as candidates for D_x in our calculation of PREG by Equation [5.23] to [5.25].
Furthermore, mixed solvents such as methanol:water will be significantly partitioned into octanol so the system cannot be adapted to use solvents other than water. Accordingly, we have used hexane as our candidate for the non-polar phase. Hexane is also readily available in high purity, an important consideration if we wish to be free from impurities which may affect the measurement and validity of our data.

We now examine the thermodynamic situation in more detail. To do this we first consider the thermodynamics of each individual system, that is:

(1) adsorption of the analyte onto graphite (g) from methanol:water (m) *i.e.* m-g

(2) partition of the analyte into hexane (h) from methanol:water (m) *i.e.* m-h

Information from systems (1) and (2) allow us to consider a third system:

(3) adsorption of the analyte onto graphite (g) from hexane (h) *i.e.* h-g

In order to compare the adsorption of the analyte in the graphite system (1) with that of the partition of the analyte in solvent system (2) we have chosen to discuss the process in terms of capacity factors.

In the case of the graphite system (1):

The equilibrium coefficient $K_{m\text{-}g}$ for an analyte between eluant and graphite is expressed as:

$$K_{m\text{-}g} = C_g/C_m \qquad [5.27]$$

If the phase ratio is ϕ_{mg} is defined as:

$$\phi_{m\text{-}g} = A_g/V_m \qquad [5.28a]$$

then the chromatographic capacity ratio is:

$$k'_{m\text{-}g} = q_g/q_m = C_g A_g / C_m V_m \qquad [5.28b]$$

In the case of the hexane system (2):

We define the distribution coefficient, D, for the distribution of the analyte between the eluant and the non-polar solvent (hexane) as:

$$D = C_h/C_m \qquad [5.29]$$

If hexane were a stationary phase, then a phase ratio

$$\phi = V_h/V_m \qquad [5.30]$$

could be defined along with capacity ratio by:

$$k'_{m\text{-}h} = q_h/q_m = C_h/C_m = C_h V_h / V_m C_m \qquad [5.31]$$

where C_h is the concentration of analyte in hexane and C_m is the concentration of analyte in the methanol:water system (polar phase).

We can then describe the equilibrium coefficient for the hexane-graphite system (3) in terms of capacity ratio, so that for the graphite system $k'_{(m\text{-}g)}$:

$$k'_{(m\text{-}g)} = q_g/q_m \qquad [5.32]$$

Thus:

$$k'_{(m\text{-}g)}/k'_{(m\text{-}h)} = C_g A_g/C_m V_m \times C_m V_m/ C_h V_h \qquad [5.33]$$

$$= K_{m\text{-}g}\phi / D_{m\text{-}h}\phi \qquad [5.34]$$

where we assume that the phase ratios are identical and that they cancel. Then:

$$k'_{(h\text{-}g)} = K_m'/D = C_g /C_h \qquad [5.35]$$

One deduces that K_m/D will in fact be equal to the partition ratio value required for the adsorption of the analyte onto graphite from hexane and so should be independent of

composition of the intermediate or working eluant (methanol:water). In reality K_m/D is found to depend upon the intermediate solvent. This means the gradients A in Equation [5.20] are not identical for plots of log k' and log D. To be consistent we have to think in terms of a 3-phase equilibrium, as shown in Figure 5.4, where the hexane becomes saturated with methanol:water (hs), and the methanol:water (ms) becomes saturated with hexane. System (3) then becomes the adsorption of the analyte onto graphite from hexane (hs) saturated with methanol:water. Thus:

$$k'_{(ms\text{-}g)}/k'_{(ms\text{-}hs)} = C_gA_g/C_{ms}V_{ms} \times C_{ms}V_{ms}/C_{hs}V_{hs} \qquad [5.36]$$

Then, ifmethanol (ms) and hexane (hs) are alternative eluants for the same column we assume that the phase volumes are identical and that they cancel:

$$V_{ms} = V_{hs} \qquad \text{so } \phi = 1 \qquad [5.37]$$

We then get:

$$k'_{(ms\text{-}g)}/k'_{(ms\text{-}hs)} = C_gA_g/C_{ms}V_{ms} \times C_{ms}\cancel{V_{ms}}/C_{hs}\cancel{V_{hs}} \qquad [5.38]$$

$$k'_{(hs\text{-}g)} = K_{ms\text{-}g}\,\phi/D \qquad [5.39]$$

If the two liquids are in thermodynamic equilibrium, then, by thermodynamics, the graphite surface in contact with either liquid phase has the same composition with regard to the adsorbed monolayer. This monolayer is likely to be hexane-rich. In practice it may be possible to mimic this surface by using a hydrocarbon coated graphite, (*e.g.* with squalane). However the composition of the surface layer is now shown to depend upon the methanol:water ratio and, consequently, the ratio $k'_{g\text{-}m}/k'_{h\text{-}m}$ is also dependent upon the intermediate eluant. The value $k'_{g\text{-}ms}/k'_{h\text{-}ms}$ now represents the k' value from hexane saturated with the intermediate solvent methanol:water, and depends upon the composition of this intermediate phase. However we show later that the presence of hexane makes little difference to the chromatographic retention i.e. we have carried out experiments with methanol:water compositions containing hexane at 0.1% and higher, and hydrocarbon (squalane) coated graphites.

The consequences of this observation are presented in Section 5.4, where the chromatographic data is discussed in detail.

Since it is not the practice in chromatography to use hexane-saturated eluants we have decided to accept the dependence of K_m/D upon composition and, correspondingly, the dependence of PREG upon composition as an artefact of the method.

The corresponding free energy equations for each system (1), (2) and (3) are then:

$$\Delta G^{\circ}_{g\text{-}m} = - RT \ln C_g/C_m = - RT \ln [k'_{g\text{-}m}(V_m/A_g)] \qquad [5.40]$$

$$\Delta G^{\circ}_{h\text{-}m} = - RT \ln C_h/C_m = - RT \ln D \qquad [5.41]$$

$$\Delta G^{\circ}_{h\text{-}g} = - RT \ln C_g/C_h = - RT\ln [k'_{h\text{-}g} (V_m/A_g)] \qquad [5.42a]$$

Our values of PREG are therefore obtained from Equation [5.25] where the solvent m is methanol:water. We accept that PREG will be dependent on the methanol:water ratio.

5.3 Experimental Approach

5.3.1 Experimental Details

HPLC apparatus was used to measure k' values for all analytes. It was also used as a detector to measure and quantify the concentrations of analyte in either the hexane fraction or the methanol:water fraction for each log D determination. Details for the experimental procedure for the determination of the partition coefficient are given in Table 5.2. The HPLC apparatus was a Hitachi 6000 UV detector, Hitachi 2000 pump, autoinjector, and software system. Solvents were HPLC grade solvents and were mixed by the HPLC system. Columns used were either Hypersil BDS C18-silica or PGC 4.6mm ID of various lengths (50mm, 100mm, or 250mm).

PREG determination

PREG is calculated from:

$$\text{PREG} = \log [k'_x/D]_{\text{analyte}} - \log [k'_{HC}/D]_{\text{hydrocarbobn}} \qquad [5.24]$$

Values for log D and log k' are therefore determined for analytes and equivalent hydrocarbons using the same methanol:water compositions.

5.3.2 Equivalent Hydrocarbons

The equivalent hydrocarbon for an analyte "x" should show any substituents in roughly the same geometric positions as those of the polar functionality present in the test analyte. For example, for phenol the equivalent hydrocarbon would be toluene, while for nitrobenzene the equivalent hydrocarbon would be isopropylbenzene. However in the time which was available it was not possible to obtain $[k'/D]_{HC}$ values for hydrocarbons which strictly fit our description of the "equivalent hydrocarbon." We have therefore chosen two homologous series of hydrocarbons: polymethybenzenes substituted only in the ortho position , and a range of n-alkylbenzenes. We then make the assumption that $[k'/D]_{HC}$ would be similar to that for the true equivalent hydrocarbon, *e.g.* $[k'/D]_{HC}$ isopropylbenzene = $[K_m/D]_{HC}$ n-propylbenzene.

There are therefore two main areas for deviation from the true equivalent hydrocarbon:

[1] Where a polar group such as NO_2 or CO_2H is now replaced by an linear side chain alkylbenzene instead of a branched side chain alkylbenzene. The use of the n-alkylbenzenes then also extends where polar groups of the same functionality are present as di- or tri-substituted isomers in the benzene ring. Thus for dinitrobenzene the true equivalent hydrocarbon (HC) would be 1,3-diisopropylbenzene, where we have used n-phenylhexane.

[2] Where a simple polar analyte with more than one substituent in the benzene ring, *e.g.* 1,3-dihydroxybenzene is now replaced by 1,2-ortho xylene, and not the geometrically correct 1,3-xylene.

It is unlikely that values of D are affected by whether or not the alkylbenzene is branched or linear. In fact, our data has shown that there is no discrimination between the polymethylbenzenes and n-alkylbenzenes of similar carbon number. However, values of k' do show differences and consequently bring into question the accuracy of PREG.

Kriz *et al*[24] compared the retention of a wide range of alkylbenzenes and polymethylbenzenes including the hydrocarbons that we have chosen to use in our study and also some of those which might have been considered as the true equivalent hydrocarbons.

They showed that the retention of alkylbenzenes by graphite is largely affected by whether they are linear or branched. The latter are found to be considerably less retained than the

former. They attribute this to the "ability of the analyte to show a 'good' or 'poor' fit to the graphite surface." For example, where the eluant is 100% methanol:

k' for n-Propylbenzene = 0.67

k' for Isopropylbenzene = 0.35

While for polymethylbenzenes they showed that, in all cases, substitution of a methyl group in the ortho-position shows a higher retention than for substitution in any other geometric position:

k' for o-xylene = 1.26

k' for m-xylene = 1.04

k' for p-xylene = 1.22

where the eluant is again 100% methanol

Consequently, the two equivalent hydrocarbon sets that we used, the n-alkylbenzenes and the polymethylbenzenes, will give the highest values for $[k'/D]_{HC}$. PREG values, if inaccurate in any way, will therefore always be too low rather than too high in value.

In general, however, analytes having a polar group directly attached to the benzene ring might also be expected to show a "good fit" to the surface of the graphite. We can make this assumption on the basis that $-CO_2H$, NO_2, benzene-NH_2 and benzene-OH all show sp^2 hybridisation (*i.e.* a degree of planarity) which may allow them to fit closely to the graphite surface. In this respect they behave much more like the n-alkylbenzenes than the branched alkylbenzenes and possibly also polymethylbenzenes with regard the proximity of each equivalent carbon atom to the graphite surface.

Thus the actual hydrocarbon equivalents chosen are those which appear to offer the best compromise between a close fit to the surface (the highest contribution in terms of dispersive interaction between analyte and graphite, *i.e.* the greatest $[k'/D]_{HC}$) and the exact geometric configuration. A full breakdown of the polar analytes used in our study with their true and actual equivalent hydrocarbon is given in section 5.3.4.

5.3.3 Reproducibility and Accuracy of log D Measurement for Equivalent Hydrocarbons

For meaningful PREG calculations the accuracy of log D measurements was very important. In order to assess the reproducibility of the log D determination the following experiments were carried out.

HPLC was used to determine the quantities of analyte present in both the hexane and the methanol:water fractions of the partitioning mixture. Injection reproducibility for a given analyte was assessed by recording the integrated area under the peak for a series of ten injections with the same injection volume. Table 5.3 shows that the % coefficient of variation for peak area and consequently injection reproducibility was found to be less than or equal to 1%.

Single point partition coefficient (D) and log D determination were assessed by preparing a solution of 20% methanol in water containing a mixture of four of the polymethylbenzenes.

Seven separate samples were made from this solution and partitioned with hexane as described in the method in Table 5.2. The hexane and methanol:water samples were separated after partitioning into 1mL glass vials that were then sealed with screw cap septa in order to prevent evaporation. Two injections into the HPLC system were made for each sample. The integrated areas were then averaged before being used to calculate the partition coefficient (D) and then log D:

$$D = \frac{\text{Peak Area analyte in hexane x volume of methanol:water solution injected}}{\text{Peak Area of the analyte in methanol:water x volume of hexane solution injected}}$$

Normally the volumes of the sample in hexane and methanol:water are equal.

Table 5.4 shows the data for peak areas measured both for the hexane and methanol:water fractions. The percent standard deviation for peak areas is typically 6% with the exception of the peak areas associated with sample 6-CH3, which are much higher, 16%. Accurate integration of the peak area became difficult when the size of the peak became very small. Consequently in the case of 6-CH3 we find very little of the compound actually partitions into the 80% methanol:water phase, the majority partitioning into the hexane phase. Only small peaks are therefore observed for 6-CH3 when the methanol:water fraction is injected into the HPLC system, with the result that the accuracy of the peak area and therefore D and log D are affected.

In subsequent experiments a larger volume was injected or the concentration of the was increased to improve accuracy. In this study however we have decided to omit this data

from determining the overall accuracy of the measurement of D. The calculated values of D and log D are given in Table 5.5. The results are summarised in Table 5.6.

The percent standard deviation for values of D are typically 15% (values for 6-CH_3 are not included based on the points made above). This gives rise to an average deviation in log D of approximately 0.06 log units which is in keeping with those quoted in the literature for log P determination, *i.e.* $\pm$ 0.1[25] log units and $\pm$ 0.04[26] log units.

Temperature Effects on the Accuracy of measurement of D

The effect of temperature on D and log D values were investigated by measuring values of D for a given analyte over a range of methanol:water compositions at three different temperatures(20°C, 25°C and 30°C). Plots of log D *vs.* % methanol:water were then recorded and errors determined. The tabulated results and a plots of log D vs. % methanol for each temperature are given in Table 5.7. A summary of the results is given in Table 5.8.

The results suggest that a deviation in temperature of $\pm$ 5°C causes minimal change in the value of D. In fact, % STDEV values are less than that data presented in Table 5.8. The improvement in accuracy over the earlier experiments is thought to have been due to improvement in general technique. Control of the temperature during the full-scale study is maintained at 25°C to within $\pm$ 1°C and consequently any observed measurement inaccuracy does not arise from temperature deviation.

The variation of D with temperature depends upon the heat transfer of the analyte from the methanol:water mixture to the hexane mixture, and follows the van't Hoff equation:

$$d \log_{10} k'/dT = \Delta H_{(h\text{-}m)} / RT^2 \qquad [5.43]$$

ΔH represents the heat transfer that takes place as the analyte transfers from methanol:water to hexane and visa versa. The gradient (slope) of the plot of $\log_{10}$ D vs. 1/T (Kelvin) (Figure 5.5) allows us to calculate ΔH for each of the methanol:water systems employed. Gradient values and ΔH values are presented in Table 5.9.

As we can see from the data, $\Delta H_{(h\text{-}m)}$ is low and is typical of transfer between two liquids. The change in ΔH with mobile phase composition is also small but, surprisingly, seems to increases as the % methanol is increased.

5.3.4 Experimental Overview

In order to calculate values of PREG for a range of analytes, we employ the following equation:

$$PREG = \log_{10} [k'/D]_{analyte} - \log_{10} (k'/D)_{hydrocarbon} \quad [5.24]$$

Values of log k' and log D for each series of equivalent hydrocarbons using a range of different methanol:water compositions are determined to provide calculated values for $\log_{10} [k'/D]_{HC}$. The same procedure is used to determine $\log_{10} [k'/D]_{analyte}$ for the polar analytes used in our study. From this data we can then calculate values for PREG in units of $\log_{10}$. Finally we convert these values of PREG into units of $KJ \cdot mol^{-1}$ by multiplying by 2.303RT/1000. The location of data relating to each of the analytes studied is summarised in Table 5.10.

(a) Equivalent Hydrocarbons - Determination of $\log_{10} k'_{HC}$, $\log_{10} D_{HC}$ and $\log k'_{HC} / D_{HC}$
(Results are discussed in section 5.4.1.)

In order to provide a useful range of $[k'/D]_{HC}$, we have chosen to measure k' and D values for

alkylbenzenes and polymethyl-substituted benzenes. The alkylbenzenes range from toluene to dodecylbenzene. The polymethylbenzenes range from toluene through

hexamethylbenzene, with all substitutions occurring in the ortho position. Throughout this Chapter, we refer to each individual alkylbenzene and polymethylbenzene in their abbreviated form, as described below:

Alkylbenzenes - Abbreviations used throughout the Chapter

Alkylbenzene	Abbreviation	Alkylbenzene	Abbreviation
Toluene	C1	n-Phenylhexane	C6
Ethyl Benzene	C2	n-Phenylheptane	C7
n-Phenylpropane	C3	n-Phenyloctane	C6
n-Phenylbutane	C4	n-Phenylnonane	C8
n-Phenylpentane	C5	n-Phenyldodoecane	C9

Ortho-substituted methylbenzenes - Abbreviations used throughout the Chapter

Polymethylbenzenes	Abbreviation
Toluene	1-CH_3
o-Xylene	2-CH_3
1,2,3-Trimethylbenzene	3-CH_3
1,2,3,4,5-Pentamethylbenzene	5-CH_3
Hexamethylbenzene	6-CH_3

Extrapolation of Data

In order to calculate PREG for polar analytes it was necessary to determine $\log_{10} k'_{HC}$, $\log_{10} D_{HC}$ and $\log_{10} k'/D_{HC}$ for the equivalent hydrocarbons over a wide range of solvent composition. This was due to the fact that the composition ranges over which similar measurements were made for analytes very often failed to overlap with the range for the equivalent hydrocarbons. This required extrapolation of data where measurements could not be made due to poor solubility, *i.e.* at high aqueous content. Extrapolation is made in accordance with either Equation [5.20] which relates to the linear relationship for change in the log of k' with changing methanol:water composition, or according to Equation [5.22] for extrapolation to gain log D values.

Before extrapolation of data was accepted as means of predicting behaviour in highly aqueous mixtures, trials with several of the small chain alkylbenzenes were made at 60% methanol:water for both log k' and log D determination. Lower chain alkylbenzenes were chosen because they show greater of solubility in the more aqueous mixtures of methanol:water. Linearity was confirmed in each case. Consequently, extrapolation was accepted as a means of determining a much wider range of log $[k'/D]_{HC}$ values than could otherwise have been determined.

In this section we present the results and discuss the data concerning the log k', log D and log $[k'/D]_{HC}$ values for the two sets of equivalent hydrocarbons:

(a) a homologous series of n-alkylbenzenes

(b) a series of polymethylbenzenes

Initially we focus on how values from each system compare when related to Equations [5.20] and [5.22] and what the differences between these two systems tell us about graphite. The discussion is then expanded to consider how the data for each system compares with

that of C18-silica and how values of log k', log D and log $[k'/D]_{HC}$ correlate with log P when Equation [5.19] and [5.21] are considered.

Further consideration is also given to the measurement of k' values on graphite when the methanol:water composition contains quantities of hexane for both n-alkylbenzenes and polymethylbenzene analytes.

(b) Results and observations for log k', log D and log $[k'/D]_x$ for polar analytes

(Results are discusses in section 5.4.2)

We first discuss the data concerning log k', log D and log $[k'/D]_x$ values for;

(1) Hydroxybenzenes
(2) Anilines
(3) Halobenzenes
(4) Other mono-substituted benzenes – acetophenone, nitrobenzene, anisole, methylbenzoate
(5) Carboxylic acid-substituted benzenes

Next we discuss how log k', log D and log [k'/D] were relate to Equations [5.20] and [5.22] for each of the three systems: hexane/methanol:water, graphite/methanol:water, and graphite/hexane. The discussion is then expanded to consider how the data for each set of analyte molecules compare to their retention and selectivity on C18-silica, and how log k'_w and log D_w correlate with log P.

The discussion of the results for the hydroxybenzenes also includes consideration for measurement of k' values on graphite when hexane-saturated methanol:water is employed.

(c) Results and discussion of PREG

(Results are discussed in section 5.4.3)

Table 5.10 gives a summary of all tables showing the location of data for each analyte type. A breakdown of the equivalent hydrocarbons used to calculate PREG are given in Table 5.38b. The values of PREG calculated are given in units of $\log_{10}$ and in units of energy ($Jmol^{-1}$) in Tables 5.39–5.44.

5.4 Results and Discussion, Part 1: Comparison of log k'$_{PGC}$ and log D for the Equivalent Hydrocarbons

5.4.1 Alkylbenzenes

We first consider the case of the alkylbenzenes where linearity is confirmed in accordance with Equations [5.20] and [5.21] for both log k', log D over a range of methanol:water compositions ranging from 80:95% methanol. Data is presented in Table 5.11 and Figures 5.6 and 5.7. This data also includes extrapolated points at 60% methanol:water.

$$\log k'_w = \log k' + AC \qquad [5.20]$$

$$\log D_w = \log D + AC \qquad [5.22]$$

The extrapolated data for log k', log D and log k'/D data is highlighted as shaded text in Table 5.11. The log k'/D data is presented graphically in Figure 5.8. Extrapolation has been used to determine data for several intermediate methanol:water compositions extending to 100% water, for all of the alkylbenzenes. We refer to the value for log k'/D at the 100% water point as log $(k'/D)_w$.

log k' values are also observed to increase with the carbon number ($-CH_2-$). Both observations are in keeping with the literature.[27] Extrapolated values to give retention in pure water (log k'$_w$) show the same order to that given by log P values ($\log_{10}$ octanol:water partition coefficient). A summary appears in Table 5.13.

Partition into hexane, *i.e.* log D, also increases as: a) the aqueous content of the methanol:water composition increases, and b) as the side chain carbon number ($-CH_2-$) of each homologue increases. Extrapolation of the log D data to pure water gives log D_w values which are in good agreement with log P values. Values of gradient A (slope) for log k', log D and log k'/D were determined and are presented in Table 5.12 along with extrapolated values of log k'$_w$ and log D_w.

In general, values of A calculated from log D data are higher than from log k' values suggesting that for these compounds at least there is greater selectivity offered by the hexane methanol:water system. The values of A calculated from log k'/D illustrate the

discrepancy between the values of k' and D, where A becomes increasingly positive as the side chain carbon number increases (Figure 5.8). It was shown earlier that:

$$\log k'/D = \log k'_h$$

Linearity is also observed for plots of log k' and log D *vs.* n, in accordance with Equations [5.19] and [5.21] for each methanol;water composition and is in keeping with literature.

$$\log k' = \beta + \alpha n \qquad [5.19]$$

$$\log D = \beta + \alpha n \qquad [5.21]$$

Plots of log k', log D and log k'/D *vs.* n ($-CH_2-$) are given in Figures 5.9, 5.10 and 5.11. In each case the methanol:water composition was found to significantly alter the value of the gradient (α). The variation of α with composition was much more pronounced for the log D data (see change ratio given in Table 5.13) suggesting that there is an additional analyte-PGC interaction which some how compensates for this solvent effect, *i.e.* interactions on PGC are not purely via dispersive interactions. The (α) and (β) values for Equations [5.19] and [5.21] are also given in Table 5.13 and are presented graphically in Figure 5.12.
A comparative plot of log P, k'_w and D_w *vs.* n (see Figure 5.13) where n is the side chain carbon, number illustrates the similarity of the gradient (α) for log P and log D_w data, while that for the log k'_w on graphite is much reduced.

Values of β represent the extrapolated data for the n = 0 point at the log k' or log D axis and thus represents a hypothetical value for benzene for each of the two systems. For log D, β is more sensitive to changes in the methanol:water composition than log k'/D values. In fact, very little if any selectivity would be predicted by using hexane as the eluant. This is confirmed by the very low rank ratio for the log k'/D data.

The effect of methanol:water composition on α and β values is most significant for log D values. It is important to remember that log k'/D should equal log k'_h and therefore be independent of methanol:water composition. At first it was thought possible that, because the hexane system is saturated with methanol:water, it may have been more susceptible to changes in the methanol:water composition than the graphite system where no such saturation occurs.
The basis of our experimental approach is that the two systems behave the same whether or not the hexane is saturated with methanol:water. In light of the results and discussion

relating to Table 5.13, several experiments were carried out to determine if k' measurement of alkylbenzenes were significantly altered when methanol:water compositions with varying quantities of hexane were employed.

The alkylbenzenes used in this part of the study were restricted to n ($-CH_2-$) = 2, 3, 4, 5, and 6. The experiment involved running each alkylbenzene chromatographically in four different methanol:water mixtures containing 0.1% hexane (Table 5.14, Figures 5.14). Only very minor differences in retention were observed when compared to retention of the same compounds in methanol:water mobile phase without hexane present. When the log k' values were extrapolated to give log k'_w, the α and β values were again found to have altered very little; α was found to be 0.64 compared to 0.65 while β was 1.25 compared to 1.2. This suggested that the presence of hexane in the mobile phase causes only minor differences in retention behaviour.

The only conclusion that can be reached is that log k'_h values would depend quite strongly upon whether pure hexane or hexane saturated with methanol:water was used. Regrettably, experiments with hexane as eluant (or hexane saturated with methanol:water) were not carried out. The k'/D values are the equivalent values for retention in hexane and are also very low, well below unity (see Figure 5.11). Direct measurement of log k'_h would not therefore have been feasible in practice. This implies that saturation of hexane with methanol:water has a large effect on retention, since saturation of methanol:water with hexane has very little effect. In other words, methanol must be quite strongly adsorbed onto the graphite surface (as might water) from the solvent. This may be another indication of PREG. It would be interesting to measure this by an peak disturbance method or isotopic labelling.

A further experiment employing the same alkylbenzenes was carried out using 95% methanol in water. The percent hexane was then increased from 0% to 0.2%, 0.5%, 1% and 3%, the data is given alongside Figure 5.15 and Table 5.14b. Very little change in retention was once again observed for any of the hexane/methanol:water compositions. The negligible effect of 3% hexane suggests that, quite contrary to general belief, hexane is very little adsorbed out of methanol by graphite.

The results confirmed our hypothesis that the two systems (graphite/methanol:water and hexane/methanol:water) were comparable and that the calculation of PREG according to Equation [5.24] is allowable. Further observations which support the hypothesis are also

made for polymethybenzenes and the hydroxybenzenes. The results are discussed in greater detail later in the Chapter.

From the above discussion it follows that the differences in slope (α) and intercept (β) between the two systems (graphite and hexane) must be due to the properties of the graphite itself. Consequently, the ratio of log k'/D is also be affected by solvent composition, and ultimately PREG itself.

Comparison of log k'$_{PGC}$ and log D for the polymethylbenzenes

The log k' and log D and log k'/D data is given in Table 5.15. We obtain good linear relationships for both log k' and log D when plotted against methanol:water composition in accordance with Equations [5.20] and [5.22].

Figure 5.16 shows the linear plots of log k' *vs.* % methanol:water for each polymethylbenzene. Retention is observed to increase as the aqueous content of the mobile phase is increased. Also for any given mobile phase composition retention increases as the number of methyl substitutions is increased (-CH_3). Both observations are in keeping with the literature[28].

Figures 5.17 shows the linear plots of log D *vs.* % methanol:water. Once again retention is observed to increase as the aqueous content of the mobile phase increases. For any given methanol:water composition, retention is also observed to increase as the number of methyl substituents, n (-CH_3), is increased.

Extrapolation of the data to obtain values of log k'$_w$ and log D$_w$ for pure water show log D$_w$ values to be in good agreement with log P values (log_{10} octanol: water partition coefficient). However, log k'$_w$ values are greater than log P values only once we reach the third methyl substitution.

Plots of log k'/D *vs.* methanol: water composition are presented in Figures 5.18. They show that there is a small positive contribution towards retention on PGC, which becomes slightly more apparent as the mobile phase becomes increasingly high in organic content, although this is only a very gradual trend.

Table 5.16 illustrates values of gradient A calculated from Equations [5.20] and [5.22], from which extrapolated values of log k', log D and log k'/D were determined. Plots of log D or log k' *vs.* % methanol:water composition show a progressive increase in the gradient (A) as the number of methyl substituents on the benzene ring is increased. The increase in gradient A values for log D become significantly greater than those of log k', the greater the number of methyl substituents.

Values of A for log D are generally higher than for log k', suggesting, as for the alkylbenzenes, that for these compounds the solvent has the potential to play a greater role in determining the overall retention. That is, partition of the analyte into hexane is more sensitive to the methanol:water composition than is adsorption onto graphite. Graphite appears to dampen the effect of the change in solvent composition.

Good linearity is also observed for both log k' and log D when plotted against n ($-CH_3$) in accordance with Equations [5.19] and [5.21]:

$$\log k' = \beta + \alpha n \qquad [5.19]$$

$$\log D = \beta + \alpha n \qquad [5.21]$$

A summary of the values determined for α and β are given in Table 5.17. In each case, the gradient, α, was found to alter with methanol:water composition. See Figures 5.19a-c for the comparison for log D and log k' and Figure 5.20 for the observed change in log k'/D with change in methanol:water composition. Interestingly α values for log D were found to be the same as for the corresponding n ($-CH_2$) for the alkylbenzenes. (The same observation was not made for retention on graphite where we see clear differentiation between the two sets of compounds. We will return to discuss this in more detail later in the Chapter.)

In this instance α represents the selectivity difference for $(-CH_3)_n$ and $(-CH_3)_{n+1}$. A much steeper gradient, α, is observed for log k'_{PGC} than for log D in any given solvent composition, illustrating that graphite shows significantly more selectivity towards these compounds than that of the hexane system. This observation is illustrated in Figure 5.21, where α for the log k'/D data is seen to approach zero, suggesting that in hexane very little selectivity of these analytes would exist, which is similar to what had been observed for the alkylbenzenes. For these compounds however, values of α calculated from log k'_w are noted to be significantly higher than those calculated for log P values.

Both log k' and log D values of β are significantly affected by methanol:water composition. In general β is seen to increase with increase in aqueous content of the methanol:water mixture. The hexane system appears to be significantly more affected by this than the graphite system, as shown by the column in Table 5.17 headed 'Rank'.

The comparative plots of log k' and log D *vs.* n (CH_3) seen in Figures 5.22a-b, highlight the differences in the value of α for the two systems. In order to confirm that the saturated hexane system was not in some way affecting the results compared to that of the straight methanol:water system on graphite, several of the polymethylbenzene were run chromatographically in methanol:water compositions containing 0.1% hexane. Data is summarised in Table 5.18 and Figure 5.23. No change in retention was observed when compared to the solvent systems without hexane. Extrapolated values to pure water gave values of $\alpha = 0.80$ and $\beta = 1.30$, both of which were in good agreement with the pure methanol:water systems which gave 0.81 and 1.17, respectively. This once again indicated that observed differences between the hexane system and graphite system were not due to the hexane-saturated solvent systems, but primarily to differences between the properties of hexane and graphite.

Expanded Discussion to Include Comparison of Retention of Both the Polymethylbenzenes and n-Alkylbenzenes.

We now expand our discussion of these results to include a comparison of the two systems, graphite and hexane, to that of Hypersil C18-silica, which represents a typical reversed phase chromatographic system. To do this we compare results using a methanol:water composition which is common to all three systems, *i.e.* 95 % methanol in water. The data for Hypersil C18-silica has been presented previously in Chapter 4 of this Thesis.

The comparison is centred mainly on how each of the three systems behave in accordance with Equations [5.19] and [5.21]. Values of log k' and α and β are summarised in Table 5.19.

In Table 5.19, n represents the number of methylene substituents ($-CH_2-$) or methyl substituents ($-CH_3$). The value for α_2 is calculated from ($\alpha_1 CH_3$ less $\alpha_1 CH_2$).

The hexane and C18-silica systems show low values for α_2 compared to that of graphite, and are essentially unable to differentiate between the two types of compound when n has the same value. A comparative plot of log k'_{C18}, D and k'_{PGC}, *vs.* n, where n is either (CH_3) or

($-CH_2-$), highlights the points made regarding α_1 and α_2 (see Figure 5.24). In general the hexane system quite closely mimics the C18-silica system, while the graphite system shows quite different behaviour and is much more selective in its ability to differentiate between these two sets of compounds. In Figure 5.25, the comparison is extended to include log P. log P has a steeper slope than that of the log D or the log k' on C18-silica. But like these two systems it is essentially unable to differentiate between the two types of analytes. One possible reason for the change in slope may be the presence of the hydroxyl group on the octanol which may allow for interactions other than purely dispersive interactions, *e.g.* dipole interactions. This confirms our reason for choosing hexane for our experimental study, where no interactions other than dispersive interaction are allowed. Partition into octanol thus has some of the features of retention by PGC, but not the distinction between the $-CH_2-$ and $-CH_3$ series.

Both the hexane and C18-silica systems discriminate between compounds solely on the differences in their hydrophobic properties, *i.e.* interaction between analyte and stationary phase is based on dispersive interactions. The similarity in α values for both the hexane system and C18-silica system support this view and suggest that a different and/or additional mechanism of interaction takes place between the analytes and the surface of graphite. According to Kriz *et al*[29] this difference is as a result of slightly different fit of the two homologue types to the graphite surface.

Another less obvious observation is that if we plot the gradient α of log k' or log D against methanol:water compositions for each set of analytes, the value of the gradient α changes to quite different extents for each methanol:water composition, see Table 5.20. The figures in bold type given in the final row of Table 5.20 represent the percentage difference in the gradient observed for retention of the analytes in 95% to 60% methanol in water. The data is presented graphically in Figure 5.26.

As can be seen, the change in α is consistently much higher for the hexane system. Equation [5.35] rules out any contributory effect from methanol:water-saturated hexane since it assumes the phase ratio for each system is the same. Following through with this argument then we must consider that graphite itself plays a role in this observation. Equation [5.39] however considers the possibility of saturated solvent systems in which the phase ratios are not the same, that is no such saturation of the graphite can occur. Although we have investigated the effect of increasing concentrations of hexane on the log k' behaviour of the hydrocarbons on graphite, we did not consider the effect of hexane

saturated with methanol:water. Again, due to very low k' values on PGC, no experimental method would have been feasible. However it is quite possible that changes in the degree of saturation of hexane due to different methanol:water compositions may well explain the observation shown in Figure 5.26 and also Figure 5.22.

Literature Support for Observations Made on Non-Polar Analytes.

The experimental data obtained in this study for the retention of alkylbenzenes and polymethylbenzenes compare well with literature values. Where Mockel[30] found $\alpha_{CH2} = 0.25$ in 100% methanol, we found $\alpha_{CH2} = 0.23$. Where Tanaka[31] reports a value for α_{CH2} of 0.31 in 80% methanol in water, we report $\alpha_{CH2} = 0.29$.

In the comparison of CH_2 selectivity, α (gradient for the plot of log k' vs n), is observed to increased as the methanol content is reduced for both PGC and hexane. The gradients of the two plots are not equivalent and it is apparent that the selectivity in hexane falls of at a slightly faster rate than on PGC, so much so that at 100% methanol, selectivity on PGC (α=0.23) is more than three times that of hexane (α=0.08). We note that Mockel[32] reports α_{CH2}=0.08 for C18-silica at 100% methanol while Tanaka[33] reports α_{CH2}=0.18 for C18-silica at 80% methanol in water. Our own results with hexane give values for α_{CH2} between 0.18 and 0.21at these two compositions. log D values therefore relate very well to selectivity on C18-silica much as may have been expected from Horvath's theory discussed earlier, where the mechanism of retention is thought to rely solely on dispersive interactions.

Chromatographic analysis of polymethylbenzenes by Kriz *et al* produced values for α_{CH3} which also compare well with our results (0.42 *vs.* our results of 0.46 in 100% methanol). However we note that the values for α (gradient for the plot of log k' vs n) are significantly less affected by solvent composition for these compounds compared to the alkylbenzenes.

5.4.2 Polar Analytes

Hydroxybenzenes

The experimental data for log k', log D values and log k'/D are given in Table 5.21. Plots of log k', log D, log k'/D *vs.* % methanol:water are given in Figures 5.27 to 5.29. Plots of log k' and log D *vs.* methanol:water composition gave good linearity according to Equations [5.20] and [5.22]. However, considerable differences were observed between the two sets of data. These differences are outlined below:

a) log D became progressively lower as the polarity of the analyte was increased. Extrapolated values are in good agreement with log P. However the order of elution on graphite is completely the reverse to that which is predicted by log D or log P, *i.e.*:

$\log k'_{PGC}$	1,3,5-trihydroxybenzene > 1,3-dihydroxybenzene > phenol
log D	phenol > 1,3-dihydroxybenzene > 1,3,5-trihydroxybenzene
log P	phenol > 1,3-dihydroxybenzene > 1,3,5-trihydroxybenzene
$\log k'_{C18}$	phenol (Table 5.22) >> 1,3-dihydroxybenzene ≈ 1,3,5-trihydroxybenzene

b) For log D, the gradient of the plot was found to be positive for 1,3-dihydroxybenzene and 1,3,5-trihydroxybenzene. As the polarity of the analyte increases it has a greater affinity for the methanol:water than the hexane.

c) For graphite, the gradient of the plot was found to remain negative. Despite the increasing attraction of the more polar analytes for the aqueous phase, retention on graphite was observed to increase as the aqueous content of the mobile phase was increased. The data is summarised in Table 5.23.

The data is in keeping with published data by Hennion and Cocquart[34] and confirms the polar retention effect on graphite (PREG). Significant retention of these polar compounds is achieved on graphite. Consequently, plots of log k'/D *vs.* methanol:water show negative gradients and closely resemble those plots of retention on graphite rather than the log D system (Figure 5.29). The polar retention effect on graphite is thus sufficiently large to overcome any solvent interactions that might take place. Interactions between polar compounds and aqueous solvents via hydrogen bonding are usually much stronger in comparison to dispersive interactions, as in the case of C18-silica where 1,3-

dihydroxybenzene and 1,3,5-dihydroxybenzene cannot be retained in highly aqueous mixtures (see Table 5.22).

In order to investigate our hypothesis that the saturated hexane system behaves in the same way as the graphite/methanol:water system, the hydroxybenzenes were run chromatographically in several 0.1% hexane in methanol:water compositions (see Table 5.24 and Figure 5.30). The results are summarised in Table (5.25-26)

The order of elution was not affected by the presence of hexane, although retention values for 1,3-dihydroxybenzene and 1,3,5-dihydroxybenzene are reduced to a greater extent than for phenol. Only minor differences in gradient A are observed and consequently changes in extrapolated values of log k'_w are also observed.

The results were in keeping with earlier results with squalane coated PGC (see Table 5.27) where once again PREG could not be masked, only partially reduced. It appears that adsorption of a hydrocarbon can mask PREG to some extent, but not entirely.

Substituted Anilines

The experimental data for log k' and log D values and log k'/D are given in Table 5.28. Figures for plots of log k', log D, log k'/D *vs.* % methanol:water are given in Figures 5.31 to 5.33. log k' *vs.* % methanol:water shows the same elution order as the log D plot and both show good linearity.

The order of elution is:

log k'_{PGC} 1,4-phenylenediamine > 1,3-phenylenediamine < 1,2-phenylenediamine < aniline

log D 1,2-phenylenediamine > 1,4-phenylenediamine < 1,3-phenylenediamine < aniline

log k'_{C18} phenylenediamine isomers not retained < aniline (Table 5.29)

These results were not in agreement with those of Coquart and Hennion[35] who show the reverse order of retention to ours for these analytes on PGC. After repeating the chromatographic measurements we have assumed our results to be correct and have calculated log k'/D in the usual way (see Table 5.28 and Figure 5.33). This plot shows the gradient A to be near zero for each of the analytes. Retention is still significantly greater than obtained for Hypersil C18-silica suggesting that there is still some contribution from

PREG. We return to discuss this further in our discussion of PREG later in the Chapter. The results are summarised in Table 5.30.

The di-substituted anilines have higher log $(k'/D)_w$ than aniline (Table 5.28), so PREG is again demonstrated.

Values of log D_w and log $k'_{w\text{-}C18}$ are in good agreement with log P values. The log $k'_{w\text{-}PGC}$ values appear to be much less affected by the increased polarity of the isomeric positions of the phenylenediamines.

Other Mono-Substituted Benzenes: Acetophenone, Nitrobenzene, Anisole, Methylbenzoate

The experimental data for log k' and log D values and log k'/D are given in Table 5.31. Figures for plots of log k', log D, and log k'/D *vs.* % methanol:water are given in Figures 5.34 to 5.36. Plots of log k' and log D show good linearity, in accordance with Equation [5.20] and [5.22]. Gradient A values for graphite (log k' values) for acetophenone, anisole and methybenzoate are identical with a significant negative gradient observed for nitrobenzene. When the data is extrapolated to give values of log k'_w, this change in gradient for nitrobenzene has the effect of reversing the elution order for anisole and nitrobenzene, when in fact good resolution in the reverse order is observed the higher the methanol content of the mobile phase. The change in slope suggests a slightly different mechanism of interaction for nitrobenzene on graphite. A similar observation is made for the retention of methybenzoate on Hypersil C18-silica (Table 5.32). However, in this instance there is no change in elution order when the data is extrapolated. The data is summarised in Table 5.33.

The extrapolated data to give log D_w for anisole and nitrobenzene is quite different to that of log P, suggesting perhaps that the log P may not be an accurate descriptor of hydrophobic behaviour for these compounds, due to interactions other than dispersive interactions between the octanol-hydroxyl group and the analyte.. When compared to log k'_{PGC} values the hexane system appears to be much less able to discriminate between these two compounds based on dispersive interaction. This suggests that PREG plays a contributing role in the retention of both anisole (an aromatic ether) and nitrobenzene. We discuss these observations further in our discussion of PREG later in the Chapter.

Relative retention order is:

log k'_{PGC} acetophenone < nitrobenzene < anisole < methylbenzoate

log D anisole < nitrobenzene < acetophenone < methylbenzoate

log k'_{C18} acetophenone < nitrobenzene < anisole < methylbenzoate

However the order of retention on graphite is similar in this instance to that observed for C18-silica. However log D_w values appear to be suspiciously low when compared with log P values.

The plot of log k'/D *vs.* % methanol:water (Table 5.31, Figure 5.36), shows a positive contribution towards retention on graphite for nitrobenzene and anisole when the aqueous content of the mobile phase is increased, while acetophenone and methylbenzoate show a positive contribution towards retention when the aqueous content of the mobile phase is reduced.

Halobenzenes

The experimental data for log k' and log D values and log k'/D are given in Table 5.34. Figures for plots of log k', log D, and log k'/D *vs.* % methanol:water are given in Figures 5.37 to 5.39. Plots for log k'_{PGC} and log D *vs.* % methanol:water show fluorobenzene to have the lowest affinity for both PGC or hexane (lower k' and D values) compared to the chloro- and bromo-benzenes. PGC retains these halobenzenes in the same order as log P so that the bromobenzene is retained slightly more strongly than the chlorobenzene. This is most easily observed when the data is extrapolated to give log k'_w and log D_w values. In the hexane system, differentiation between fluorobenzene and chlorobenzene is more difficult but the increased value for bromobenzene is in good agreement with both C18-silica (Table 5.35) and graphite.

The data is summarised in Table 5.36.

Gradient A values for log k' and log D plots *vs.* % methanol:water were similar, suggesting that PREG only plays a small role in the retention of these analytes on graphite.

The plot of log k'/D *vs.* % methanol:water (Figure 5.39), supports this view showing a zero gradient for each of the analytes. Consequently very little contribution from PREG is expected. We do see a slightly positive gradient suggesting an increased contribution from graphite, but this time it is when the composition of the mobile phase becomes less aqueous. In this respect these analytes behave in a similar manner to the polymethylbenzenes, *i.e.*

non-polar analytes with functionality directly attached to the benzene ring. We consider this observation further later in the Chapter when we discuss PREG.

Benzene Carboxylic Acids

The experimental data for log k', log D values and log k'/D are given in Table 5.37. Figures for plots of log k', log D and log k'/D *vs.* % methanol, water are given in Figures 5.40 to 5.42. Plots of log k' and log D show reasonable linearity in accordance with Equation [5.20] and [5.22]. Gradient values A for log D are positive for the more polar compounds 1,2-dicarboxybenzene acid and 1,2,4-tricarboxybenzene acid. The gradient values for graphite appear to be largely unaffected by the number of
–COOH groups present. However the order of elution predicted by log k'_w is the reverse to that predicted by either log D_w or log P. In this respect these compounds behave in a similar manor to the hydroxybenzenes. The data is summarised in Table 5.38.
The plot of log k'/D *vs.* % methanol:water in Figure 5.42 also shows a negative gradient suggesting that PREG plays a significant role in the retention of these compounds.

5.4.3 Experimental Results for PREG

In this section we discuss the results for PREG. For each set of data referring to the different analyte types PREG values are given in log units to the base ten and in units of free energy, kJ mol^{-1}.
For several of the analyte groups the value of PREG is observed to change considerably with the solvent composition. These groups are the, hydroxybenzenes, benzene carboxylic acids, and the group of analytes which we have called "other monosubstituted benzenes." Plots of PREG *vs.* % methanol:water for each set of analytes are given in Figures 5.43 to 5.57. We express this relationship as retention over and above that which might have been expected if the interactions were purely dispersive interactions. In order to calculate the free energy we have calculated the retention behaviour, k'/D or k'_{h}, of each analyte in hexane. This removes the possibility of interactions between the solvent and the polar analyte other than dispersive interactions, that might interfere with our measurement of PREG. We then subtract from this value any dispersive interactions between the analyte and the graphite surface. We do this by measuring the retention behaviour, k'/D_{HC} , for an "equivalent hydrocarbon" in hexane:
PREG is then given by:

$$PREG = \log [k'/D]_{analyte} - \log [k'/D]_{Hydrocarbon} \quad [5.42b]$$

Following Equation [5.42b] and using the extrapolated data, *i.e.* $\log k'_w$ and $\log D_w$, it is possible to calculate PREG all analytes in 100% water. This provides a useful data point which not only allows us to compare PREG for each of the analytes in the same solvent conditions but also at the point where PREG is largest. In general values of PREG are highest when the methanol concentration is lowest. We refer to values of PREG calculated for retention of analytes in pure water as $PREG_w$. We first however discuss the relationship of PREG for each set of analytes with the methanol:water composition.

Equivalent hydrocarbons:Polymethylbenzenes and n-Alkylbenzenes

As pointed out in section 5.3.1 for the polymethylbenzenes and n-alkylbenzenes to have been truly equivalent hydrocarbons, $\log [k'/D]_{HC1} - \log [k'/D]_{HC2} = 0$ PREG. This a clearly not the case since PREG values of between 5 and 10 kJ/mol are observed for the polymethylbenzenes (see Table 5.39 and Figure 5.43).

There is thus a PREG for going from the alkylbenzene to the corresponding methylbenzene and a further contribution going from, say, toluene to phenol. It is the latter which we have tried to measure for the phenols and amines, *etc.*

There appears to be a genuine contribution to retention on graphite from PREG. It appears to be additive as subsequent methyl groups are substituted to the ortho-position.

However our real interest is in showing that various groups contribute to PREG and the idea of using the polymethylbenzenes as the equivalent hydrocarbons still holds. But we now recognise that there may also be additional contributions to PREG.

Hydroxybenzenes

PREG data for the hydroxybenzenes is given in Table 5.40. Figure 5.44 shows that for the di- and tri-substituted hydroxybenzenes there is a considerable increase in PREG as the composition of methanol:water becomes more aqueous. PREG also increases as the number of hydroxyl substituent groups increases. The PREG values for phenol are apparently not affected by changes in the methanol:water composition and values are in general are much lower than that obtained for the di- and tri-substituted hydroxybenzenes.

Anilines

PREG data for the anilines is given in Table 5.41. Figure 5.45 shows that once again the di-substituted anilines have considerably higher values of PREG than aniline and are also influenced by the composition of methanol:water. PREG values increase very slightly as the aqueous content is increased. Aniline itself is relatively unchanged by changes to the methanol:water composition.

Other Mono-Substituted Benzenes

PREG data for the other mono-substituted benzenes is given in Table 5.42. Figure 5.46 shows that all of the mono-substituted benzenes are affected by increasing aqueous content. PREG values are highest for nitrobenzene and anisole, while the results for acetophenone and methylbenzoate are very similar to one another. These observations are in keeping with the earlier discussion for the values of k'/D. Values for these mono-substituted benzenes are lower than those of the di- and tri-substituted benzenes already discussed.

Halobenzenes

PREG data for the halobenzenes is given Table 5.43. In general, values are lower than the other polar analytes investigated in this study. Figure 5.47 shows an increase in PREG for chlorobenzene and bromobenzene as the aqueous content is increased. For fluorobenzene, a negative PREG value is observed which becomes less negative and finally positive as the solvent composition becomes less aqueous. This suggests that the influence of PREG exceeds that of any dispersive interactions shown by the equivalent hydrocarbon (toluene) only in highly aqueous eluants. In this case there appears to be less contribution to retention by PREG than there is for the equivalent hydrocarbon (toluene).

Benzene-carboxylic acids

PREG data for the benzene carboxylic acids is given in Table 5.44. Figure 5.48 shows that retention of all of the analytes, including the benzoic acid (mono-substituted), increase significantly as the aqueous content increases. As with the hydroxybenzenes PREG also increases substantially as the number of substituents (carboxylic acid groups) increases.

5.5 Results and Discussion, Part 2: PREG

5.5.1 Correlation and Discussion of $PREG_{(w)}$

The values obtained for $PREG_{(w)}$ up to 41KJ mol^{-1} suggest that that the energy involved is much higher than the molecular interactions (dispersive, dipole-dipole, *etc.*) which are usually considered to be responsible for chromatographic interactions. The energies associated with these types of interactions are typically less than 2KJ mol^{-1}. Hydrogen bonding interactions cannot occur with graphite. Consequently in trying to correlate the values of $PREG_w$ with energies associated with molecular interactions we have concentrated on energies of interaction, which are significantly higher than those interactions usually responsible for chromatographic retention.

We therefore consider:

a) How the energy values associated with PREG correlate to the heats of formation for each group of analytes.

b) How the energies associated with PREG correlate to the energy of a charge approaching a flat metal surface, *i.e.* a conductor. Values of U'' (the sum of all energies of interaction) have been calculated according to Equation [5.16].

c) How the energy associated with PREG correlates with the potential energy of the charge induced dipole of a polar analyte at the graphite surface.

5.5.2 Correlation with latent heat of formation (ΔH_f)

Table 5.45 shows the heat of formation measured for each analyte. The data was acquired from the MOPAC information program, courtesy of Tropos, Ltd. The energies associated with the heat of formation concern those forces which are responsible for holding the molecules together and are considerably higher than the forces observed for PREG (see Figure 5.49). There is a trend with the high negative values of ΔH_f giving highest PREG. Low values of ΔH_f indicate strong binding and probably high polarity and so correlation may be realistic.

5.5.3 Correlation with U''

Calculations of U'' are based on the simple model that the molecule is adsorbed from a vacuum for which the dielectric constant is unity. U'' is then given as;

$$U'' = \frac{S}{4\pi\varepsilon_0 r} \qquad [5.16]$$

where it is assumed that all r_{ij} are the same and equal to r (as they would be for a planar molecule parallel to the surface).

The case of a charge approaching a metal surface is generally covered in terms of an "image charge," that is, an image of the approaching charge in the surface of the metal. According to this model the image charges are equal but opposite to the approaching charge, and can be thought of as positioned at the same distance inside as the metal the molecule is from its surface.

A working example illustrating the method to calculate S (charge distribution) and U'' is given in Table 5.46. However, this is not correct U for image charge theory as no cross terms are included. When the molecule is adsorbed from a liquid, allowance should be made for the fact that lines of force emerging above the horizontal will be strongly affected by the solvent. A proper allowance for the affect of solvent is difficult. As a first allowance for the testing of this model as an explanation of PREG, it has been assumed that Equation [5.13] applies without modification.

$$U_{ij} = \frac{1}{4\pi\in_o} \cdot \frac{q_i q_j}{r_{ij}} \qquad [5.13]$$

The analyte data calculated for U'' is given in Table 5.45. A plot of U'' *vs.* $PREG_w$ is shown in Figure 5.50. Here we observe that values for U'' are typically 2 to 3 times the value of $PREG_w$, but correlation is generally poor.

Graphite, however, misinterprets the model since the true model applies to an infinitely thin conducting sheet that is a plane of constant potential. This means that all the lines of go through the surface normal to it. In its turn this means that if we reflect these lines of force in the surface, we get an exact mirror image in the surface with the lines of force normal to the surface on both sides. Exactly the same pattern of lines of force would be present if the metallic surface were replaced by a mirror image of the original charge. Thus the forces experienced by the original molecule with respect to the surface will be exactly the same as the forces experienced by the original molecule with its mirror image (the conducting surface now being removed). The difficulty of linking PREG with U'', as pointed out by Knox[36] is that the difference in distance between the points of charge and the surface of the graphite must be less than the distances between the atoms in the molecule itself. In reality this is not the case. The distance between the charged molecule and image is likely to be about 7Å, whereas the distances between charges within the molecule would be

approximately 1-4 Å. There is then considerable cancelling out of the charge when cross terms in the energy matrix for U are allowed for. The only explanation is that there is a polarisation effect where the surface of the graphite surface is polarised to give a type of electron transfer to the charged parts of the analyte. The idea can be likened to the formation of a charged footprint such as the ferrocene compounds, where polarisation of the benzene occurs. We therefore consider the possibility of the analyte behaving as a charge inducing a dipole perpendicular to the surface of the graphite.

5.5.4 Correlation of PREG with the potential energy of the analyte charge/ induced dipole in the graphite surface

When a molecule is placed in an electric field it is distorted because of the forces that act on the electrons and nuclei. The extent to which distortion occurs is determined by the molecule's polarisability. In our work this refers to the polarisability of the graphite and the electric field is that associated with the charge on the polar analyte approaching the graphite surface. A high polarisability indicates that a large distortion can be caused by even a moderate field (we use 1.5 x 10^{-24}cm^3 for graphite[37,38]). As an analyte approaches the surface of graphite its charge centre induces a dipole immediately beneath it, with the axis of the dipole perpendicular to the carbon surface. A schematic representation of a single charge approaching the graphite surface is given in Figure 5.51. The potential energy for this charge induced dipole at separation r (we have used 3.5Å, distance between graphite planes) is given by the equation:

$$E_{i\text{-}id} = \alpha z^2 / 2(4\pi\varepsilon_o\varepsilon)\, r^4 \qquad [5.7]$$

where and α is the polarisability of graphite and z is the charge.

If we follow the implications of this simple equation, then one would expect that the contribution to the energy of adsorption would be related to the sum of the squares of the local charges (S), and not to the sum of the positive or negative charges (Cn). Cn was the parameter employed by Hennion and Coquart in their correlation of polar analytes on graphite. Equation [5.7] then becomes:

$$U_{cind} = \alpha S / 2(4\pi\varepsilon_o\varepsilon)\, r^4 \qquad [5.44]$$

Accordingly we have used this form of Equation [5.44] to calculate values of U_{cind} presented in Table 5.45. A worked example of the calculation is given in Table 5.48 .

In general the data is in reasonable agreement with $PREG_w(2)$ values (Figure 5.52) where we observe energy levels of similar magnitude. Replotting the points for PREG(2) values at 50% methanol in water where extrapolation of data was not required, shows only a marginal improvement in correlation (Figure 5.52b). We continue our discussion on the basis of values of PREG in pure water. The relationship is not perfect but when given closer inspection by labelling the points in their analyte family groupings, the correlation improves still further (see Figure 5.53).

If we accept this correlation, then the retention of polar analytes, their dependence on mobile phase composition and the selective retention based on geometric configuration can all be explained. We therefore review once again the observations made for PREG for the different groups of analytes.

5.5.5 Consequences of different shape and alignment of analytes at the Graphite Surface

The image of the induced dipole might therefore be expected to have the hypothetical appearance of a three dimensional contour map. The intensity of the peaks and troughs would be generally determined by the distribution of the charge in the analyte, the size of the charge and the distance (r) of the charge from the graphite surface. The effect of the position and alignment of the analyte at the PGC surface will therefore directly influence the magnitude of potential energy associated with the charge-induced dipole, and ultimately the retention of a polar analytes at the graphite surface.

In our calculation of U_{cind} we assume that each atom in the analyte is equidistant (r) from the graphite surface. In reality, for the following reasons this is unlikely to be the case:

a) Some atoms are larger than others and will cause the analyte molecule to be tilted at the surface. This will cause some of the atoms in the molecule responsible for charge induced dipole interaction to be nearer to or farther away from the surface than other atoms.

b) Steric interaction of adjoining groups, such as geometric isomers, may cause a similar effect as above.

c) Interaction of the lipophillic (hydrophobic) part of the analyte with the graphite may be so strong that the polar functionality is directed away from the surface. On the other hand, because of PREG polar groups may be attracted to the surface.
d) Bond angles associated with particular functionality may also prevent the molecule from lying flat on the surface.

Consequently, analytes might be expected to correlate most closely with U_{cind} when they lie flat on the surface (good fit), since this orientation allows for the smallest value of r, thus maximising the potential energy of the induced dipole.

As an example, a flat molecule like 1,3,5-trihydroxybenzene would be positioned parallel to the plane of the graphite (PGC) surface. The distance r between each atom of the analyte with the surface of the PGC would be very similar *i.e.* $r_1 = r_2 = r_3 = r_4$ *etc.* The potential energy of the induced charge image in the surface of the PGC would be at a maximum as shown in Figure 5.54a. When a molecule cannot lie flat on the surface, r_1, r_2, r_3 *etc.* are not longer equal. Consequently the potential energy of the induced charge image in the graphite surface is less than that which might have been expected for a distribution of charge at 180° to the surface. An example of <u>this</u> type is given in Figure 5.54b, where the approaching molecule is 1,2,4-tricarboxybenzene. A move away from the surface of one C-C bond length (1.54Å) would result in a drop in energy of approximately 50KJ mol^{-1}. This suggests that the charge image created in the surface of the graphite is particularly sensitive to changes in proximity of the approaching molecule's charge centre from the surface (r). The potential energy of the charge induced dipole and intensity of the charge image then become significantly weaker as the value of r increases.

Clearly, distribution of charge and the distance between the charge centre and the graphite surface both have a major role in determining retention of polar analytes on graphite.

5.5.6 Review of the PREG data for different analytes based on correlation with U_{cind}

Figure 5.57 shows the relationship between PREG and U_{ind} for the specific groups of analytes.

The points for the hydroxybenzenes lie nearly along a straight line and offer the best correlation between PREG and U_{cind}, suggesting that each analyte molecule lies flat against the surface of the graphite.

The points for the benzene carboxylic acids show a steeper increase in U_{cind} relative to the increase in PREG. This means that although PREG is observed to increase on PGC as the number of polar substituents are increased, the increase is not as large as predicted by U_{cind}. In this case we can assume that as the number of substituents increases the molecule finds it increasingly difficult to lie completely flat against the surface of the PGC. The distance 'r' is now no longer the same for each atom. The potential energy (adsorption energy) of the charge induced dipole is then reduced.

PREG values for the phenylenediamines are about 50% to 75% of the values predicted by U_{cind}. The correlation is not quite as good as the hydroxybenzenes but is still reasonable, following at least the same order as PREG. The PREG value for aniline is very low. This suggests that aniline may not lie flat at the PGC surface, the amino group perhaps pointing away from the surface. In such circumstances, the charge image in the surface associated with the amino group is very small or disappears completely.

Correlation of U_{cind} with the other mono-substituted benzenes is somewhat unclear. PREG (2) values are observed to be significantly lower for methylbenzoate than U_{cind} and consequently do not correlate well. Anisole and nitrobenzene appear to have PREG (2) values greater than U_{cind} differing by a factor of 2. While the values for acetophenone correlate very well indeed. The range of observations outlined here may be due in part to the nature of the equivalent hydrocarbons employed.

5.5.7 The Role of the Solvent Composition

U_{cind} values are also based on the simple model that shows the molecule is adsorbed from water, for which the relative permittivity is unity. Based on the correlation with U_{cind} we

might expect that a change in composition may well influence the relative permittivity of the solvent, *i.e.* it is no longer unity and that a change in U_{cind} or PREG results. We do in fact observe a change in the magnitude of PREG as the methanol:water composition changes. The relative permittivity may influence retention on graphite in two ways: (1) it may change the charge distribution within the analyte due to solvation, or (2) it may cause changes to the polarised state of the graphite surface, *i.e.* the value of α may alter as the ε_r changes. Clearly, considerably more work may be required to determine the full role of the solvent and how it influences retention on PGC.

Final conclusions

In the following paragraphs we review the consequences of the observations made in chapter 5 for data determined in earlier chapters of the thesis. This is followed by concluding remarks concerning: a new hypothesis for retention of compounds on PGC, our choice in a range of equivalent hydrocarbons used to measure PREG and recommendations with final suggestions for future research.

5.5.8 PREG and Surface Tension – Chapter 3

In Chapter 3 we compared retention on graphite with calculated values of k'_{ST}. These values had correlated well with C18-silica and log P, but had shown very little correlation with retention on graphite for compounds of increasing polarity. The k'_{ST} values are, of course, calculated on the basis of molecular interaction between the solvent and the analyte. In this Chapter we have shown that the energy associated with PREG is that associated with a charge inducing a dipole in the graphite surface. The energies which relate to this interaction are between 5 to 25-times greater than those associated with analyte-solvent interaction. Consequently we are now able to explain the lack of any correlation for compounds of increasing polarity with k'_{ST}.

5.5.9 PREG and Coated PGC - Chapter 4

In Chapter 4 we observed the effect on the retention of polar compounds on graphite coated with various molecules, either polymeric molecules such as polystyrene, polyphenylglycidylether (PPGE), or discrete molecules such as decacyclene and squalane.

The PPGE-coated graphite was the only one that did not revert to typical graphite retention behaviour when the mobile phase was at highest aqueous composition. In this Chapter we show that the energy associated with PREG is greatest when the solvent has a high aqueous content. Under these conditions the forces associated with the retention of polar molecules are so great that it is likely that they displace the relatively non-polar polymeric molecules such as polystyrene or the discrete non-polar molecules, squalane or decacyclene. These molecules are adsorbed primarily via dispersive interactions and there is little contribution to retention by charge induced dipole interactions. The behaviour of the PPGE-coated graphite in resisting a return to retention behaviour similar to graphite, even at high water composition is now understandable. This molecule has significant polar character as well as hydrophobic character and therefore is held tightly to the surface of the graphite by the additional strong charge induced dipole forces associated with PREG. As a consequence PPGE would be much more difficult to displace from the surface by a polar analyte such as 1,3,5-trihydroxybenzene. Interaction therefore takes place between the analyte and the PGGE and not the graphite. This results in a retention order for the hydroxybenzenes that is the same as that of C18-silica, *i.e.* phenol > 1,3-dihydroxybenzene > 1,3,5-dihydroxybenzene.

5.6 Mechanism of retention on graphite

In this Chapter we have concerned ourselves with the energy of interaction of an analyte with the surface of graphite over and above that which might be expected for purely dispersive forces (PREG). We have given a hypothesis for the properties of the graphite surface that allow this kind of interaction to take place. We now therefore consider the overall retention of a molecule at the graphite surface. The total free energy, ΔG_{TOT}, associated with interaction of an analyte at the surface can now be given by:

$$\Delta G_{tot} = \Delta G_1 + \Delta G_2 + \Delta G_3 + \Delta G_4 \qquad [5.45]$$

where ΔG_1 = free energy associated with dispersive interactions between a hydrophobic functionality of an analyte molecule and the graphite surface, ΔG_2 = energy associated with dispersive interactions between the polar functionality of an analyte molecule and the graphite surface, ΔG_3 = energy associated with the electrostatic interactions of the analyte and the electrostatic properties of the graphite surface (PREG), and ΔG_4 = energy associated with analyte solvent interactions. ΔG_4 is small compared to ΔG_1, ΔG_2 and ΔG_3.

ΔG_1 and ΔG_2 are concerned with Lennard Jones type interactions. They prefer molecular orientations that bring as many atoms of the analyte molecule close to the graphite surface as possible without allowing repulsive forces to take over. ΔG_3 accounts for the charge induced dipole interactions associated with PREG. These interactions prefer to have the charge centre as close to the substrate as possible. Clearly, on occasions there may be competition between the two different types of interactions particularly when the adsorbed molecule is not flat. Alternatively they may combine to give considerably stronger energy of adsorption.

Furthermore, the results suggest that when alignment of the analyte at the surface is favourable the contributions from various polar functional groups (PF1, PF2, PF3 *etc.*) are additive. The total free energy contribution made by PREG can be thought of as:

$$\Delta G_{PREG} = \sum \Delta G_{PF1} + \Delta G_{PF2} + \Delta G_{PF3} \ldots \textit{ etc.} \qquad [5.46]$$

The values of each ΔG_{PF} will of course depend on substituted position of the functional group *i.e.* 1,2-phenylenediamine will make a different contribution than 1,4-phenylenediamine, due to the shift in charge distribution (S) in accordance with Equation [5.44].

5.7 Equivalent Hydrocarbon Hypothesis

The quantification of PREG using the equivalent hydrocarbon hypothesis has proven to be successful in helping to establish a mechanism by which we can start to understand the polar retention effect on graphite and ultimately complete retention on graphite. Its use will clearly be of benefit to those who wish to expand the research into PREG. Our choice of "actual equivalent hydrocarbons" has proven to be useful for simple analytes such as those used in this study. Here, it is important to maintain as close a value of "r" as possible for the equivalent hydrocarbon to that of the analyte even if this means a slight deviation from the true equivalent hydrocarbon. We have shown that the data produced in this study to be of sufficient quality to allow correlative work to be carried out.

5.8 Conclusion

We have successfully obtained a measure of the energies involved with PREG. The magnitudes of these energies correlate closely with the potential energy a charge approaching a polarisable surface U_{cind}.

The charge distribution (S) associated with each analyte is shown to play an important role in determining the magnitude of U_{cind} and consequently correlation with chromatographic behaviour.

The degree to which PREG plays a role in retention on graphite is largely influenced by the structural properties of the analyte and its ability to lie flat against the surface (or give a good fit to it) that allow it to interact with the polarisable surface of graphite. The greater the distance the analytes charge centre is from the surface, the lower the energy of interaction, and the lower the value of PREG.

The analyte's electronic properties responsible for interaction with the PGC, may also be affected by the electric permittivity of the solvent, as may be the polarised state of the graphite surface. In general, electronic interactions (PREG) with PGC are seen to increase as the percent aqueous in the mobile phase increases.

Further substantiation of our hypothesis should now be possible by expanding the study to include a much broader range of analytes, and perhaps comparing the behaviour with compounds such as ferrocene. In the ferrocene molecule, the charge induced dipole interactions with benzene may already be quantified in the literature.
It may now also prove possible to study the hypothetical retention of analytes on graphite by using molecular modelling software. This might help explain our results which have shown that changes in analyte orientation and charge distribution at the graphite surface play an important role in determining the value of PREG.

Chapter 5 References

[1] Knox, J. H. and Gilbert, M. T., UK Patent, 2 035 282, 1078.
[2] Kaliszan, R., *Quantitative-Structure – Chromatographic Retention Relationships*, Chemical Analysis Vol 93, Wiley Interscience (1987)

[3] Hanfa Zou *et al.*, J. Liquid Chromatography, 16(16), 3443 (1993)
[4] Knox, J. H, and Ross, P., Advances in Chromatography, Vol 37, 3A, (1997)
[5] Martire,D.E., and Boehm, R. E., *J. Phys. Chem.*, 87: 1045 (1983)
[6] Kaliszan, R., *Quantitative-Structure – Chromatographic Retention Relationships*, Chemical Analysis Vol 93, Wiley Interscience (1987)
[7] Coquart, F.,Ph.D Thesis, ESPCI Paris (1993)
[8] Kalsiszan, R, Osmialowski K, .Bassler B. J, and Hartwick, R. A, J. Chromatogr., 499, 333 (1990)
[9] Bassler, B. J., Kalszan, R., and Hartwick, R. A, J. Chromatogr., 461, 139 (1989)
[10].Hammett, L. P, Chem. Rev, 17, 125 (1935)
[11] See reference 7
[12] Kaliszan, R *Quantitative-Structure – Chromatographic Retention Relationships*, Chemical Analysis,Vol 93, Wiley Interscience
[13] Bassler, B .J., Kaliszan, R., and Hartwick, R., J. Chromatogr., 461, 139 (1989)
[14] Forgacs, E. and Cserhati, T., J. Pharm.Biomed.Anal., 10, 861 (1992)
[15] Forgacs, E. and Cserhati, T., and Valko K., J. Chromatogr., 592, 75-83 (1992)
[16] Forgacs, E. and Cserhati, T., J. Chromatogr.,600, 43 (1992)
[17] Forgacs E. and Cserhati T., J. Chromatographia, 33, 356 (1992)
[18] Forgacs, E., Valko, K., Cserhati T., and Magyar K., J. Chromatogr., 631, 207 (1993)
[19] Koopmans, R. E. and Rekker, R. F., J. Chromatogr., 285, 267 (1984)
[20] Pietrogrande, M.C. *et al*, J. Liquid.Chromatog., 8, 1711 (1985)
[21] Kriz, J., Adamcova, E., Knox J. H., and Hora J., J. Chromatogr., 663, 151 (1995)
[22] Hennion, M.-C.and Coquart, V., J. Chromatogr., 642, 211 (1993)
[23] Tomlinson, E., Poppe, H., and Kraak, Int. J. Pharm., 7, 225 (1981)
[24] See reference 21
[25] Cheung, A. P.and Kenny, D., J. Chromatogr., 506, 110 (1990)
[26] Ford, H., Jr., Merski, C., Kelly, J., J. Liquid Chromatogr., 14(18), 336-3386 (1991)
[27] Kalsizan, R., *Quantitative-Structure – Chromatographic Retention Relationships*, Chemical Analysis,Vol 93, Wiley Interscience
[28] See reference 21
[29] See reference 21
[30] Mockel, H. J., Braedikow, A, Melzer, H., and Aced, G., J.Liq. Chromatogr., 14, 2477 (1991)
[31] Tanaka, N., Tanigawa, T., Kimata, K, Hosoya, K and Araki, T., J. Chromatogr., 549, 29 (1991)
[32] Mockel, H. J., Braedikow, A, Melzer, H., and Aced, G., J. Liq. Chromatogr., 14, 2477 (1991)
[33] Tanaka, N., Tanigawa, T., Kimata, K, Hosoya, K and Araki, T., J.Chromatogr., 549, 29 (1991)
[34] Cocqart, V.and Hennion, M.-C., J. Chromatogr., 600, 195 (1992)
[35] See reference 7
[36] See reference 4
[37] Hammond, W. R.,.Mahanti, S. D, Surface Science, 234, 308-314 (1990)
[38] Purcell E. M., Electricity and Magnetism, McGraw-Hill, New York (1965)

Table 5.1[1]

Relative Strengths of van der Waals Interactions

Species	Orientation	Induction	Dispersion
Ne-Ne	0	0	4
CH_4-CH_4	0	0	102
HCl-HCl	11	6	106
HBr-HBr	3	4	182
NH_3-NH_3	38	10	63
H_20- H_2O	96	10	33

[1] G.K.Vemulapalli, Physical Chemistry, Prentice and Hall International Editions.

Fig 5.2

Experimental Shake Flask Method for log D Determination.

10ml sealable flasks, 100ul syringe, spatula, HPLC Grade Hexane, HPLC Grade Water and HPLC Grade Methanol. 100ml syringe , top pan four figure balance. Hittachi Oven. 2ml sealable sample vials.

Method

1 Dissolve X(g) of analyte in 10ml hexane* - so that the concentration is between 10-20mg/ml

2 Transfer 2(g) of solution(1) to a 10ml sealable flask ,

3 Add 2(g) of methanol:water

4 Seal the flask

5 Shake the flask for 30seconds by hand

6 Place the flask in a thermostated oven at 25°C and leave for 15mins

7 Remove flask and shake for a further 30 seconds and replace in the oven for 15mins

8 Remove from the oven

9 Transfer approx. 2ml aqueous layer (lower) to a 2ml sample vial (a)

10 Transfer approx. 2ml hexane layer (upper layer) to a second 2ml sample vial (b)

11 Repeat (1) to (10) with at least four different methanol water mixtures for each analyte

12 Analyse each sample by HPLC** - mobile phase 100% methanol, injection volume 50ul from a 100ul injection loop

13 Measure the area under the peak for (a) the methanol:water sample (b) the hexane sample – where the area under the peak represents the quantity of analyte present.

14 D is calculated for area(a)/area(b), the ratio of peak areas.

*Note where solubility of the analyte was poor in hexane the reverse procedure was followed, i.e., the sample dissolved in 10ml methanol:water mixture, (2g) transferred to 10ml sealable flask and a further 2g hexane added.

**HPLC Method

The samples were run in pure methanol, since the presence of water would have caused hexane to become retained on the column due to the poor solubility in water. This would have caused increased back pressure and non reproducible chromatography. Samples were run using a short 50 x 4.6mm PGC column for most non polar compounds and a 100 x 4.6mm PGC column for the polar compounds where increased retention was required

Table 5.3
Injection / Peak Area Reproducibility

	C6	C7	C8	C9
20H-1	437713	646539	720052	563501
20H-1	434124	642574	710205	556876
20H-1	432385	632992	703085	550669
20H-2	426303	630097	695168	546726
20H-2	435434	645807	717789	559907
20H-2	430937	636153	711555	557000
20H-3	433966	641524	711517	555694
20H-3	425352	634475	711546	559067
20H-3	426115	632732	710019	558320
20H-4	425770	631904	703928	554708
20H-4	422535	627426	708048	557689
20H-5	428864	629899	701350	550471
20H-5	431176	638755	717348	562646
20H-5	428858	631755	709575	568885

sum	6019532	8902632	9931185	7802159
average	429967	635902	709370	557297
std	4440	6145	6798	5713
RSD %	1.03	0.97	0.96	1.03

Where 20 represents the % water used in the methanol:water sample
H represents the hexane fraction
Then numbers 1-5 represent the sample numbers and repeat injections
C6 to C9 are alkylbenzene homologues

Table 5.4
Sample Peak Area Reproducibility Study Employing the Polymethylbenzenes

H=Hexane	Inj	1CH3	3CH3	5CH3	6CH3	M=Methanol	Inj	1CH3	3CH3	5CH3	6CH3
H-Fraction	1	456922	399901	286545	180508	M-Fraction	1	2428	101040	29811	11484
H-Fraction	1	434000	404162	284665	182159	M-Fraction	1	2400	102558	28471	8085
H-Fraction	2	322212	483530	270995	164499	M-Fraction	2	2254	92404	30307	12021
H-Fraction	2	499189	546410	302932	184519	M-Fraction	2	2579	130055	32943	11212
H-Fraction	3	428226	521727	288646	192282	M-Fraction	3	2286	97224	30808	14333
H-Fraction	3	400000	520000	280000	190000	M-Fraction	3	2681	139840	30205	12742
H-Fraction	4	465671	538349	295897	185612	M-Fraction	4	1835	86496	20240	6487
H-Fraction	4	499189	546410	302932	184519	M-Fraction	4	2376	90764	28600	7620
H-Fraction	5	352695	479087	280787	167203	M-Fraction	5	2234	95505	30843	8037
H-Fraction	5	448547	497318	291167	182254	M-Fraction	5	2356	134766	31277	15438
H-Fraction	6	449842	519944	297620	180852	M-Fraction	6	2185	113290	27977	12817
H-Fraction	6	467326	397578	297447	186836	M-Fraction	6	2258	118677	29324	9349
H-Fraction	7	522098	515517	296400	185640	M-Fraction	7	2258	127358	28346	14337
H-Fraction	7	467326	397578	297447	186836	M-Fraction	7	2258	128038	28154	7897
STDEV		36849	48046	6630	6091	STDEV		132	12663	2416	2011
SUM		3106622	3383756	2036740	1276860	SUM		16194	779008	203653	75930
MEAN		517770	563959	339457	212810	MEAN		2699	129835	33942	12655
% STDEV		7	9	2	3	% STDEV		5	10	7	16

Table 5.5
Reproducibility Trials for log D employing the Polymethylbenzenes

	PARTITION RATIO (D)					PARTITION RATIO LOG D			
	1-CH3	3-CH3	5-CH3	6-CH3		1-CH3	3-CH3	5-CH3	6-CH3
Sample 1	2.84	4.38	15.29	45.53	Sample 1	0.45	0.64	1.18	1.66
Sample 2	2.61	3.69	12.99	35.35	Sample 2	0.42	0.57	1.11	1.55
Sample 3	2.57	3.49	13.57	30.59	Sample 3	0.41	0.54	1.13	1.49
Sample 4	3.53	5.44	19.76	68.40	Sample 4	0.55	0.74	1.30	1.84
Sample 5	2.69	3.48	12.90	34.13	Sample 5	0.43	0.54	1.11	1.53
Sample 6	3.18	3.95	16.01	41.38	Sample 6	0.50	0.60	1.20	1.62
Sample 7	3.37	3.87	17.51	44.50	Sample 7	0.53	0.59	1.24	1.65

Table 5.6
Summary for Table 5.5

SUM	1350.45	28.31	108.02	299.88	SUM	3.29	4.21	8.28	11.33
MEAN	192.92	4.04	15.43	42.84	MEAN	0.47	0.60	1.18	1.62
STDEV	25.16	0.69	2.56	12.56	AVDEV	0.05	0.05	0.06	0.08
% StDEV	13.04	17.04	16.57	29.33					

The % Standard deviation for 'D' is approximately 15% when the results for analyte 6-CH3 are excluded.

6-CH3 is excluded on the basis that accurate determination of peak areas at very low concentrations became

very difficult. Consequently concentrations in later experiments were increased in order to allow for

more accurate measurements to be made. The average deviation log D is then on average approximately + or - 0.06 log units

Table 5.7
Data Showing the Effect of Temperature on the Partition Coefficient (D) Employing Phenyloctane as the Analyte

TEMP 20C	%METHANOL[2]	Sample[3]	M-Fraction[3]	200μL[4]	20μL[4]	H-Fraction[6]	20UμL[7]	D[8]
	95	1	M-Fraction	96539	9653.9	H-Fraction	150507	15.59
	95	1	M-Fraction	100878	10087.8	H-Fraction	145330	14.41
	90	2	M-Fraction	39506	3950.6	H-Fraction	145363	36.80
	90	2	M-Fraction	38269	3826.9	H-Fraction	142353	37.20
	87	3	M-Fraction	18521	1852.1	H-Fraction	142291	76.83
	87	3	M-Fraction	21065	2106.5	H-Fraction	144169	68.44
	83	4	M-Fraction	10393	1039.3	H-Fraction	142321	136.94
	83	4	M-Fraction	8962	896.2	H-Fraction	142922	159.48
TEMP 25C	%METHANOL	Sample	M-Fraction[3]	200UL[4]	20UL[4]	H-Fraction[6]	20UL[7]	D[8]
	95	1	M-Fraction	99490	9949	H-Fraction	145202	14.59
	95	1	M-Fraction	96978	9697.8	H-Fraction	144315	14.88
	90	2	M-Fraction	39390	3939	H-Fraction	142214	36.10
	90	2	M-Fraction	41488	4148.8	H-Fraction	141803	34.18
	87	3	M-Fraction	20111	2011.1	H-Fraction	138762	69.00
	87	3	M-Fraction	23075	2307.5	H-Fraction	138328	59.95
	83	4	M-Fraction	12440	1244	H-Fraction	148328	119.23
	83	4	M-Fraction	11432	1143.2	H-Fraction	148328	129.75

Table 5.7 continued.....

[2] % Methanol used to make up the methanol:water composition, [2] each sample injected twice[3] methanol fraction [4] Peak areas for Injection volume 200μl in hexane
[5] Peak area normalised to 20ul injection size [6]Hexane fraction [7]Peak areas for 20μl injection of hexane fraction [8]Partition coefficient (D)

Table 5.7 continued

TEMP 30C	%METHANOL	Sample	M-Fraction[3]	200UL[4]	20UL[4]	H-Fraction[6]	20UL[7]	D[8]
	95	1	M-Fraction	102939	10293.9	H-Fraction	149413	14.51
	95	1	M-Fraction	105327	10532.7	H-Fraction	144789	13.75
	90	2	M-Fraction	42918	4291.8	H-Fraction	144427	33.65
	90	2	M-Fraction	40195	4019.5	H-Fraction	144865	36.04
	87	3	M-Fraction	20687	2068.7	H-Fraction	140472	67.90
	87	3	M-Fraction	22772	2277.2	H-Fraction	142840	62.73
	83	4	M-Fraction	9399	939.9	H-Fraction	139491	148.41
	83	4	M-Fraction	12044	1204.4	H-Fraction	139748	116.03

Table 5.8

Summary Table Showing Statistical Data for Table 5.7

Temperature °C	Mean log D at 95% MeOH	Mean log D at 90% MeOH	Mean log D at 87% MeOH	Mean log D at 83% MeOH
20	15.00	37.00	72.63	148.21
25	14.74	35.14	64.47	124.49
30	14.13	34.85	65.31	132.22
mean	14.62	35.66	67.47	134.97
STDEV	0.45	1.17	4.49	12.10
% STDEV	3.05	3.27	6.65	8.96

Table 5.9
van't Hoff Plots for the Determination of ΔH for n-Phenyloctane

Temperature	1/T(K)	Mean log D at 95% MeOH	Mean log D at 90% MeOH	Mean log D at 87% MeOH	Mean log D at 83% MeOH
20	3.41E-03	1.18	1.57	1.86	2.17
25	3.36E-03	1.17	1.55	1.81	2.10
30	3.30E-03	1.15	1.54	1.82	2.12
Gradient		229.78	230	409	440
ΔH/ kJmol^{-1}		1.9	2.0	3.5	3.7

Table 5.10
References for Tables of Results Data and Figures

Tables for log k' log D and log k'/D data

	alkylbenzenes (1)	Ortho-xylenes (2)	comparative study of (1)& (2)	Hydroxybenzenes	Anilines	Other	Halobenzenes	Benzene carboxilic acids
log k', log D, log k'/D	5.11	5.15	-	5.21	5.28	5.31	5.34	5.37
Summary table re equations	5.12	5.16	5.19	5.22	5.29	5.32	5.35	5.38
Summary table re equations	5.13	5.17	5.20	5.23	5.30	5.33	5.36	
	5.14	5.18		5.24				
				5.26				
				5.27				

Tables for PREG Data

Figures alkylbenzenes	Figures Ortho-xylenes	Figures Hydroxybenzenes	Figures Anilines	Figures Halobenzenes	Figures Other	Figures Benzene carboxylic acids
	5.39	5.41	5.40	5.42	5.43	5.44

Table 5.11

log k', log D and log k'/D Data for n-Alkylbenzenes on PGC

Log k' Data Alkylbenzenes

	log k'	log k'	log k'	log k'	log k'	log k'	log k'	A'	log k'_w
% Methanol	60	70	75	80	85	90	95		
C1	0.63	0.33	0.18	0.01	-0.12	-0.24	-0.36	-0.03	2.34
C2	0.72	0.4	0.26	0.04	-0.08	-0.24	-0.36	-0.03	2.64
C3	1.08	0.7	0.52	0.31	0.15	-0.01	-0.16	-0.04	3.21
C4	1.45	1	0.81	0.57	0.4	0.21	0.04	-0.04	3.82
C5	1.88	1.41	1.18	0.91	0.72	0.51	0.32	-0.05	4.58
C6	2.25	1.75	1.5	1.21	1	0.76	0.55	-0.05	5.22
C7	2.65	2.1	1.82	1.51	1.28	1.02	0.87	-0.05	5.89
C8	3.04	2.45	2.15	1.81	1.56	1.27	1.14	-0.06	6.58
C9	3.43	2.82	2.48	2.11	1.84	1.53	1.43	-0.06	7.3
C10	3.82	3.16	2.8	2.41	2.12	1.79	1.7	-0.07	7.93

Log D Alkylbenzenes

	Log D	Log D	Log D	Log D	Log D	A'	log D_w
% Methanol	60	83	87	90	95		
C1	1.15	0.41	0.32	0.16	0.07	-0.03	3.13
C2	2.23	1.14	0.95	0.75	0.49	-0.05	5.19
C3	2.34	1.28	1.06	0.86	0.64	-0.05	5.3
C4	2.78	1.46	1.18	0.93	0.65	-0.06	6.48
C5	3.17	1.63	1.41	1.14	0.81	-0.07	7.23
C6	3.42	1.81	1.6	1.34	0.96	-0.07	7.58
C7	3.61	1.96	1.7	1.42	1.06	-0.07	7.99
C8	3.92	2.1	1.82	1.55	1.17	-0.08	8.66
C9	4.18	2.3	2.03	1.73	1.33	-0.08	9.08
C10	4.96	2.55	2.22	1.86	1.38	-0.10	11.16

Shaded areas represent extrapolated data

Table ..... continued

Table 5.11 Continued

Log k'/D data Alkylbenzenes

	log k'/D	log k'/D	log k'/D	log k'/D	log k'/D	log k'/D	log k'/D	log k'/D	log k'/D	log k'/D	log k'/D	A	$(k'/D)_w$
% MeOH	10	20	30	40	50	60	70	80	85	90	95		
C1	-0.62	-0.6	-0.58	-0.6	-0.54	-0.53	-0.48	-0.47	-0.48	-0.43	-0.5	0.00	-0.79
C2	-2.22	-2.08	-1.94	-1.79	-1.65	-1.50	-1.39	-1.25	-1.14	-0.98	-0.83	0.01	-2.55
C3	-1.75	-1.66	-1.56	-1.46	-1.36	-1.26	-1.22	-1.12	-1.01	-0.87	-0.80	0.01	-2.09
C4	-2.17	-2.01	-1.84	-1.67	-1.50	-1.34	-1.26	-1.09	-0.92	-0.71	-0.61	0.01	-2.66
C5	-2.26	-2.07	-1.88	-1.69	-1.49	-1.30	-1.11	-0.92	-0.82	-0.63	-0.48	0.02	-2.65
C6	-2.02	-1.85	-1.68	-1.51	-1.34	-1.17	-0.98	-0.81	-0.74	-0.57	-0.41	0.02	-2.36
C7	-1.75	-1.59	-1.43	-1.28	-1.12	-0.96	-0.82	-0.67	-0.57	-0.41	-0.20	0.02	-2.10
C8	-1.82	-1.63	-1.44	-1.25	-1.07	-0.88	-0.71	-0.52	-0.41	-0.27	-0.03	0.02	-2.08
C9	-1.55	-1.39	-1.23	-1.07	-0.91	-0.75	-0.59	-0.43	-0.35	-0.20	0.11	0.02	-1.78
C10	-2.78	-2.45	-2.12	-1.79	-1.46	-1.14	-0.78	-0.45	-0.31	-0.04	0.33	0.03	-3.23

Shaded areas represent extrapolated data according to equations [5.19],[5.20],[5.21],[5.22]

Table 5.12

Comparison of log k'_w, log D_w Alkylbenzenes Data in Pure Water Calculated from Equations [5.20],[5.22] with MOPAC log P

	% MeOH	C1	C2	C3	C4	C5	C6	C7	C8	C9	C10
log k_w	0	2.34	2.64	3.21	3.82	4.58	5.22	5.59	6.58	7.3	7.93
log D_w	0	2.38	5.19	5.3	6.48	7.23	7.58	7.99	8.66	9.08	11.16
log P	0	2.11	3.17	3.7	4.23	4.76	5.29	5.82	-	-	-

Table 5.13

Summary of α and β Values for the Alkylbenzenes Calculated using Equations [5.19] [5.21] from log k' and log D data

α and β	95% MeOH	90% MeOH	85% MeOH	80% MeOH	60% MeOH	0% Methanol	Rank 60/95
α for log k'	0.26	0.25	0.28	0.30	0.39	0.65	0.13
α for log D	0.11	0.14	0.17	0.20	0.35	0.56	0.24
α log k'/D	0.15	0.12	0.10	0.1	0.05	-0.09	-0.1
α for log P	-	-	-	-	-	0.53	-
β for log k'	-1.0	-0.8	-0.7	-0.6	-0.1	1.2	0.9
β for log D	0.2	0.4	0.7	0.9	1.4	4.2	1.2
β log k'/D	-1.2	-1.2	-1.3	-1.4	-1.5	-2	-0.8
β for log P	-	-	-	-	-	2	-

Table 5.14

Log k' Data for n-Alkylbenzenes in Methanol:Water (95:5) Eluent with 0.1% Hexane

	log k' data					
	Log k'	Log k'	Log k'	Log k'	A'	log k'_w
	70	80	90	95		
C2	0.40	0.07	-0.20	-0.33	-0.03	2.48
C3	0.70	0.32	0.01	-0.14	-0.03	3.11
C4	1.00	0.58	0.23	0.06	-0.04	3.70
C5	1.38	0.92	0.52	0.33	-0.04	4.39
C6	1.72	1.21	0.77	0.55	-0.05	5.06

Table 5.15

log k', log D and log k'/D Data for Polymethylbenzenes on PGC

Log k' data for Polymethylbenzenes

	log k'	log k'	log k'	log k'	log k'	log k'	A'	log k'w
% Methanol	60	70	80	85	90	95		
1-CH3	0.51	0.26	0.01	-0.12	-0.24	-0.36	-0.02	2.01
2-CH3	1.18	0.86	0.54	0.39	0.24	0.10	-0.03	2.99
3-CH3	1.75	1.42	1.10	0.93	0.76	0.61	-0.03	3.70
5-CH3	2.98	2.58	2.18	1.97	1.75	1.57	-0.04	5.40
6-CH3	3.60	3.16	2.73	2.49	2.25	2.06	-0.04	6.25

Log D data for Polymethylbenzenes

	Log D	Log D	Log D	Log D	Log D	Log D	Log D	Log D	A'	log Dw
% Methanol	60	70	80	83	85	87	90	95		
1-CH3	1.15	0.85	0.54	0.41	0.38	0.32	0.16	0.07	-0.03	2.94
2-CH3	1.75	1.44	1.03	0.88	0.79	0.67	0.53	0.27	-0.03	3.85
3-CH3	2.03	1.61	1.18	1.05	0.96	0.91	0.79	0.55	-0.04	4.38
5-CH3	2.89	2.32	1.75	1.55	1.44	1.35	1.18	0.89	-0.05	6.09
6-CH3	3.07	2.50	1.93	1.73	1.66	1.54	1.37	1.14	-0.05	6.30

Log k'/D data for Polymethylbenzenes

	Logk'/D	Logk'/D	Logk'/D	Logk'/D	Logk'/D	Logk'/D	Logk'/D	Logk'/D	Logk'/D	A	Log $(k'/D)_w$
% methanol	20	40	50	60	70	80	85	90	95		
1-CH3	-0.60	-0.58	-0.56	-0.54	-0.53	-0.48	-0.47	-0.48	-0.43	0.00	-0.79
2-CH3	-0.75	-0.66	-0.64	-0.57	-0.57	-0.49	-0.40	-0.30	-0.17	0.01	-1.07
3-CH3	-0.76	-0.53	-0.53	-0.30	-0.20	-0.10	-0.04	-0.03	0.06	0.01	-0.88
5-CH3	-0.57	-0.24	-0.24	0.10	0.27	0.44	0.53	0.53	0.69	0.01	-0.96
6-CH3	0.14	0.34	0.34	0.55	0.69	0.81	0.83	0.85	0.92	0.01	-0.21

Table 5.16

Summary Data for the Polymethylbenzenes - Extrapolated From Values of log k', log D and log k'/D.

	% MeOH	CH3-1	CH3-2	CH£-3	CH3-5	CH3-6
Gradient 'A'						
log k'	95 -60	-0.02	-0.03	-0.03	-0.04	-0.04
log D	95 -60	-0.03	-0.04	-0.04	-0.06	-0.06
log k'/D	95 -0	0.01	0.01	0.01	0.02	0.01
Intercept						
log k'_w	0	2.01	2.99	3.70	5.40	6.25
log D_w	0	2.94	3.85	4.38	6.09	6.3
log P	0	2.64	3.09	3.54	4.44	4.84

Table 5.17

Summary Data for Polymethylbenzenes, α and β Calculated from log k' and log D Data.

α and β	95% MeOH	90% MeOH	85% MeOH	80% MeOH	60% MeOH	0% MeOH	Rank 60/95
α for log k'	0.48	0.50	0.52	0.54	0.62	0.81	0.14
α for log D	0.20	0.19	0.23	0.25	0.35	0.61	0.15
α log k'/D	0.29	0.29	0.29	0.31	0.28	0.21	-0.01
α for log P	-	-	-	-	-	0.44	-
β for log k'	-0.8	-0.7	-0.6	-0.5	-0.1	1.17	0.7
β for log D	-0.1	0.2	0.3	0.5	1.1	3.04	1.2
β log k'/D	-0.7	-0.9	-0.9	-1.1	-1.3	-1.7	-0.6
β for log P	-	-	-	-	-	2.24	-

Table 5.18

Log k' Data for Polymethylbenzenes in Methanol :Water Eluent with 0.1% Hexane

Log k' data Polymethylbenzenes

	Log k'	Log k'	Log k'	Log k'	A'	log k'_w
	70	80	90	95		
CH3-1	0.29	0.02	-0.23	-0.37	-0.03	2.10
CH3-2	0.85	0.53	0.25	0.10	-0.03	2.93
CH3-3	1.42	1.07	0.77	0.60	-0.03	3.71

Table 5.19

Comparison Data for log k'_{PGC}, log D and log k'_{C18} for n-Alkylbenzenes and Polymethylbenzenes Eluent 95% Methanol:Water

		[1]n = 1 log	n = 2 log	n = 3 log	n = 5 log	n = 6 log	[2]α_1 = log k'(n+1)/n	[3]$\Delta\alpha = \alpha_1 CH_3 - \alpha_1 CH_2$
Log k'_{ODS}	where 'n' is -CH2-	-0.44	-0.31	-0.17	0.10	0.23	0.13	
Log k'_{ODS}	where 'n' is –CH3	-0.44	-0.25	-0.09	0.23	0.37	0.14	
log k'_{ODS}	CH_3 less CH_2	0	0.06	0.08	0.13	0.14		0.01
Log D	where 'n' is -CH2-	0.07	0.49	0.64	0.83	0.96	0.15	
Log D	where 'n' is –CH3	07	0.27	0.55	0.89	1.14	0.18	
Log D	CH_3 less CH_2	0	-0.22	-0.09	-0.08	-0.18		0.03
log P	where 'n' is -CH2-	2.11	3.17	3.7	4.23	4.76	0.53	
log P	where 'n' is -CH3	2.64	3.09	3.54	4.44	4.84	0.4	
log P	CH_3 less CH_2	0.53	-0.08	-0.16	0.21	0.08		-0.13
log k'_{PGC}	where 'n' is -CH2-	-0.36	-0.36	-0.16	0.32	0.55	0.15	
Log k'_{PGC}	where 'n' is -CH3	-0.36	0.1	0.61	1.57	2.07	0.41	
Log k'_{PGC}	CH_3 less CH_2	0	0.46	0.77	1.25	1.52		0.26
log k'/D	where 'n' is -CH2-	-0.43	-0.85	-0.80	-0.49	-0.41	0.08	
log k'/D	where 'n' is -CH3	-0.43	-0.17	0.06	0.69	0.92	0.23	
log k'/D	CH_3 less CH_2	0.06	0.76	0.86	1.17	1.33		0.16

[1] n is the number of (-CH_2-) groups or (-CH_3) groups in the homologue , [2] α^1 is the homologue selectivity
[3] $\Delta\alpha$ is the difference between the two homologue selectivities

Table 5.20

Summary of Gradient (α) for n-Alkylbenzenes and Polymethylbenzenes at Different Methanol:Water Compositions

Methanol	Gradient log k' $_{PGC}$ (CH_3)	Gradient log D (CH_3)	Gradient log k' $_{PGC}$ (CH_2)	Gradient log D (CH_2)
95	0.49	0.22	0.28	0.12
90	0.50	0.21	0.36	0.15
87		0.22		
85	0.53	0.22	0.29	0.19
83		0.21		
80	0.55	0.23	0.31	0.20
75			0.33	
70	0.58	0.27	0.36	
60	0.60	0.33	0.40	0.36
	22%	**50%**	**42%**	**200%**

Table 5.21

log k', log D and log k'/D data for Hydroxybenzenes on PGC

Log k' data Hydroxybenzenes

	Log k'	Log k'	Log k'	Log k'	Log k'	A'	log k'_w
% Methanol	20	30	40	50	60		
Phenol	1.42	1.01	0.69	0.45	0.18	-0.03	1.83
1,3-Hydroxybenzene	1.80	1.20	0.88	0.64	0.34	-0.03	2.07
1.3.5-Hydroxybenzene	2.35	1.94	1.66	1.35	0.99	-0.03	2.88

Log D data Hydroxybenzenes

	Log D	Log D	Log D	Log D	A'	log D_w
% Methanol	20	40	50	60		
Phenol	-0.096	-0.25	-0.403	-0.67	-0.01	0.19
1,3-Hydroxybenzene	-2.497	-2.3	-2.227	-2.11	0.01	-2.69
1.3.5-Hydroxybenzene	-3.325	-3.2	-3.161	-3.09	0.01	-3.44

Log k'/D Hydroxybenzenes

	Logk'/D	Logk'/D	Logk'/D	Logk'/D	A	log $(k'/D)_w$
% Methanol	20	40	50	60		
Phenol	1.52	1.26	1.09	1.12	-0.01	1.64
1,3-Hydroxybenzene	4.30	3.50	3.11	2.75	-0.04	4.76
1.3.5-Hydroxybenzene	5.68	5.14	4.82	4.43	-0.03	6.32

Table 5.22

log k' Data Hydroxybenzenes on Hypersil BDS C18 Silica

log k' data Hydroxybenzenes on C18

	log k'	lok k'	log k'	log k'	log k'	'A'	log k'w
	5	10	15	20	30		
Phenol	0.79	0.72	0.61	0.53	0.33	-0.02	0.92
1,3-dihydroxybenzene	0.21	0.07	-0.10	-0.20	-0.46	-0.03	0.34
1,3,5-trihydroxybenzene	x	x	x	x	x	x	x

Table 5.23

Summary of data for Hydroxybenzenes

	% MeOH	Phenol	1,3-dihydroxybenzene	1,3,5-trihydroxybenzene
Gradient 'A'				
log k'PGC	20 - 60	-0.03	-0.04	-0.03
log D	20 - 60	-0.01	0.01	0.01
log k'C18	5 -30	-0.02	-0.03	-
log k'D	20 – 60	-0.01	-0.04	-0.03
Intercept "k'$_w$"				
log k'$_{w\text{-PGC}}$	0	2.05	2.53	3.03
log D$_w$	0	0.19	-2.69	-3.44
log $_{kw\ C18}$	0	0.89	0.23	-
log P	0	1.47	0.81	0.14

Table 5.24

Log k' Data for Hydroxybenzenes in Methanol :Water Eluent with 0.1% Hexane

Log k' data Hydroxybenzenes in 0.1% hexane methanol :water eluent

	Log k'	Log k'	Log k'	Log k'	'A'	log k'_w
	20	30	50	60		
Phenol	1.05	0.94	0.40	0.15	-0.02	1.95
1,3-dihydroxybenzene	1.26	1.01	0.44	0.24	-0.03	2.28
1.3.5-trihydroxybenzene	1.58	1.25	0.77	0.43	-0.03	2.73

Table (5.25-26)

Comparison of Results for Methanol:Water Compositions with Hexane and Non Hexane Methanol:Water Compositions for Hydroxybenzenes

	Phenol	1,3-dihydroxybenzene	1,3,5-dihydroxybenzene
log k'_w	2.05	2.53	3.03
log k'_w - hexane	1.95	2.28	2.73
Gradient 'A'	-0.03	-0.04	-0.03
Gradient 'A' - hexane	-0.03	-0.03	-0.03

Where 'hexane ' refers to mobile phase , methanol:water containing with 0.1% hexane.

Table 5.27

Log k' Data for Hydroxybenzenes on Squalane Coated PGC

Log k' data

	log k'	lok k'	log k'	log k'	log k'	A'	log k'w
% Methanol	5	10	15	20	30		
Phenol	0.86	0.79	0.67	0.54	0.24	-0.02	1.84
1,3-dihydroxybenzene	1.05	0.78	0.56	0.35	-0.07	-0.04	2.85
1.3.5-trihydroxybenzene	1.43	1.13	0.83	0.56	-0.15	-0.06	3.96

Table 5.28

log k', log D and log k'/D Data for Anilines on PGC

Log k' data for Anilines

	log k'	log k'	log k'	log k'	A'	$\log k'_w$
%Methanol	40	50	60	70		
Aniline	0.35	0.14	-0.09	-0.27	-0.02	1.19
1,2-Phenylenediamine	0.26	0.07	-0.10	-0.25	-0.02	0.94
1,3-Phenylenediamine	-0.13	-0.32	-0.48	-0.59	-0.02	0.49
1,4-Phenylenediamine	-0.08	-0.27	-0.38	-0.50	-0.01	0.48

Log D data for Anilines

	Log D	Log D	Log D	Log D	Log D	A'	$\log D_w$
%Methanol	30	40	50	60	70		
Aniline	0.44	0.24	0.02	-0.18	-0.35	-0.02	1.06
1,2-Phenylenediamine	-1.67	-1.76	-2.09	-2.15	-2.22	-0.02	-0.70
1,3-Phenylenediamine	-3.04	-3.18	-3.26	-3.42	-3.74	-0.01	-2.28
1,4-Phenylenediamine	-1.94	-2.03	-2.00	-2.08	-2.08	-0.005	-1.67

Log k'/D data for Anilines

	Logk'/D	Logk'/D	Logk'/D	Logk'/D	A	$\log (k'/D)_w$
%Methanol	40	50	60	70		
Aniline	-0.09	-0.10	-0.11	-0.10	0.000	0.13
1,2-Phenylenediamine	1.93	1.83	1.99	1.90	-0.001	0.70
1,3-Phenylenediamine	2.91	2.86	2.77	2.83	-0.003	2.28
1,4-Phenylenediamine	1.87	1.76	1.61	1.59	-0.009	1.67

Table 5.29

Log k' Data for Anilines on Hypersil BDS C18 Silica

Log k' data for Anilines on BDS C18

	log k'	log k'	log k'	log k'	A'	log k'_w
%Methanol	30	35	40	45		
Aniline	0.11	0.01	-0.11	-0.20	-0.02	0.71
1,2-Phenylenediamine	-	-	-	-	-	-
1,3-Phenylenediamine	-	-	-	-	-	-
1,4-Phenylenediamine	-0.61	-0.67	-0.70	-	-0.01	-0.22

Table 5.30

Summary of Results for the Anilines

	% MeOH	Aniline	1,2-Phenylenediamine	1,3-Phenylenediamine	1,4-Phenylenediamine
Gradient 'A'					
log k'_{PGC}	40 -70	-0.02	-0.02	-0.02	-0.01
log D		-0.02	-0.02	-0.01	-0.005
log k'C18		-0.02	-	-	-
Intercept					
log $k'_{w\text{-}PGC}$	0	1.19	0.94	0.49	0.48
log D_w	0	1.06	-0.70	-2.28	-1.67
log $k_{w\ C18}$	0	0.71	-	-	-
log P	0	0.9	0.15	-	-

Where (-) refers to elution of the analyte at the solvent front. In the case of log P, (-) represents values approaching zero.

Table 5.31

log k', log D and log k'/D Data for Other Mono-Substituted Benzenes on PGC

Log k' data for Other Mono substituted Benzenes

	Log k'	Log k'	Log k'	Log k'	Log k'	Log k'	Log k'	Log k'	A'	log k'_w
% Methanol	30	50	70	80	85	90	95	100		
acetophenone	1.37	0.91	0.46	0.23	0.14	-0.01	-0.10	-0.23	-0.02	2.06
nitrobenzene	1.45	1.07	0.69	0.50	0.41	0.29	0.21	0.11	-0.02	2.03
anisole	1.69	1.24	0.79	0.56	0.48	0.33	0.24	0.11	-0.02	2.37
methyl benzoate	1.91	1.46	1.01	0.79	0.68	0.54	0.45	0.34	-0.02	2.59

Log D data for Other Mono Substituted benzenes

	Log D	Log D	Log D	Log D	Log D		A'	log D_w
% Methanol	30	40	50	70	90			
acetophenone	1.71	1.38	1.00	0.12	-0.52		-0.04	2.91
nitrobenzene	0.33			-0.02	-0.39		-0.01	0.59
anisole	0.05	-0.05	-0.30	-0.66	-0.92		-0.02	0.58
methyl benzoate	2.03	1.83	1.43	0.57	0.02		-0.04	3.13

Log k'/D for Other Mono Substituted benzenes

	Logk'/D	Logk'/D	Logk'/D	Logk'/D		A	log $(k'/D)_w$
% Methanol	30	50	70	90			
acetophenone	-0.34	-0.47	-0.55	0.11		0.01	-0.85
nitrobenzene	1.12	1.07	0.69	0.52		-0.01	1.43
anisole	1.64	1.28	1.09	1.22		-0.01	1.79
methyl benzoate	-0.13	-0.37	-0.42	0.22		0.01	-0.54

Table 5.32

Log k' Data for Other Mono-Substituted Benzenes on Hypersil BDS C18 Silica

	Log k'	Log k'	Log k'	Log k'	A'	log k'_w
% Methanol	35	40	45	50		
acetophenone	0.76	0.58	0.42	0.26	-0.03	1.94
nitrobenzene	0.82	0.67	0.54	0.40	-0.03	1.79
anisole	1.07	0.93	0.79	0.66	-0.03	2.05
methyl benzoate	1.20	1.02	0.84	0.66	-0.04	2.47

Table 5.33

Summary Table of Data for Other Mono Substituted Benzenes

	% MeOH	Acetophenone	Nitrobenzene	Anisole	Methylbenzoate
Gradient A'					
log k'PGC	30 - 90	-0.023	-0.019	-0.023	-0.023
log D	40 - 90	-0.04	-0.01	-0.02	-0.02
log k'C18	35 - 50	-0.03	-0.03	-0.03	-0.04
log k'/D	40 - 90	0.01	-0.01	-0.01	0.01
Intercept					
log $k'_{w\text{-}PGC}$	0	2.06	2.03	2.37	2.59
log D_w	0	2.91	0.59	0.58	3.13
log $_{k'w\ C18}$	0	1.94	1.79	2.05	2.47
log P	0	1.58	1.88	2.06	2.11

Table 5.34

log k', log D and log k'/D Data for Halobenzenes on PGC

Log k' data Halobenzenes

	Log k'	Log k'	Log k'	Log k'	Log k'	Log k'	Log k'	Log k'	A'	log k'_w
%Methanol	40	50	60	80	85	90	95	100		
Fluorobenzene	0.81	0.54	0.27	-0.27	-0.40	-0.55	-0.67	-0.77	-0.03	1.90
Chlorobenzene	1.34	1.05	0.77	0.20	0.06	-0.09	-0.22	-0.31	-0.03	2.48
Bromobenzene	1.53	1.24	0.94	0.36	0.21	0.07	-0.08	-0.17	-0.03	2.70

Log D data Halobenzenes

	Log D	Log D	Log D	Log D					A'	log D_w
%Methanol	40	50	60	90						
Fluorobenzene	2.23	1.91	1.25	0.05					-0.044	3.97
Chlorobenzene	2.49	2.11	1.78	0.71					-0.036	3.92
Bromobenzene	2.72	2.19	1.81	0.64					-0.04	4.39

Log k'/D for the Halobenzenes

	Log k'/D	Log k'/D	Log k'/D	Log k'/D	A	Log $(k'/D)_w$
%Methanol	40	50	60	90		
Fluorobenzene	-1.42	-1.37	-0.98	-0.32	0.02	-2.08
Chlorobenzene	-1.15	-1.06	-1.01	-0.50	0.01	-1.43
Bromobenzene	-1.19	-0.95	-0.86	-0.28	0.02	-1.69

Table 5.35

Log k' Data for Halobenzenes on Hypersil BDS C18 Silica

	Log k'	Log k'	Log k'	Log k'	Log k'	A'	log k'_w
%Methanol	60	65	70	75	80		
Fluorobenzene	0.29	0.15	-0.03	-0.19	-0.34	-0.03	1.55
Chlorobenzene	0.58	0.42	0.23	0.06	-0.18	-0.04	2.10
Bromobenzene	0.67	0.50	0.31	0.14	-0.04	-0.04	2.07

Table 5.36

Summary Table for the Halobenzenes

Summary table	% MeOH	Fluorobenzene	Chlorobenzene	Bromobenzene
Gradient 'A'				
log k'_{PGC}	40 - 100	-0.03	-0.03	-0.03
log D	40 – 90	- 0.04	- 0.04	-0.04
log k'_{C18}	60 – 80	- 0.03	- 0.04	- 0.04
log k'/D		-0.02	0.01	0.02
Intercept				
log $k'_{w\text{-}PGC}$	0	1.9	2.48	2.7
log D_w	0	3.97	3.92	4.39
log $k'_{w\ C18}$	0	1.55	2.10	3.01
log P	0	2.28	2.86	2.07

Table 5.37

log k', log D and log k'/D Data for Benzene Carboxylic Acids

Log k' data for Benzene Carboxylic Acids

% Methanol	60	70	80	85	90	95	A'	log k_w
benzoic acid	0.52	0.33	0.12	0.02	0.05	-0.19	-0.02	1.72
1,2 di-benzoic acid	0.60	0.43	0.28	0.20	0.12	0.05	-0.02	1.56
1,2,4-tri-benzoic acid	1.94	1.73	1.57	1.47	1.51	1.29	-0.02	3.07

Log D data for Benzene Carboxylic Acids

	Log D	Log D	Log D	Log D	A'	log D_w
% Methanol	80	85	90	95		
benzoic acid	0.32	0.21	0.13	-0.28	0.02	-1.79
1,2 di-benzoic acid	2.24	2.23	3.17	1.93	0.00	-2.31
1,2,4-tri-benzoic acid	3.20	3.10	3.08	2.73	0.01	-2.61

Log k'/D data for Benzene Carboxylic Acids

	Logk'/D	Logk'/D	Logk'/D	Logk'/D	'A'	log $(k'/D)_w$
% Methanol	80	85	90	95		
benzoic acid	0.32	0.21	0.13	-0.28	-0.04	3.51
1,2 di-benzoic acid	2.24	2.23	3.17	1.93	-0.02	3.86
1,2,4-tri-benzoic acid	3.20	3.10	3.08	2.73	-0.03	5.68

Table 5.38

Summary Data for Benzene Carboxylic Acids

	% MeOH	Benzoic acid	Phthalic Acid	Iso-phthalic acid
Gradient "A"				
log k'PGC	60 -90	-0.02	-0.02	-0.02
log D	5 -20	-0.02	-0.004	-0.01
log k'C18	15 - 30	-0.03	-0.04	-0.03
log k'/D	5 - 20	-0.04	-0.02	-0.03
Intercept				
$\log k'_{w\text{-}PGC}$	0	1.72	1.56	3.07
$\log D_w$	0	0.20	-1.87	-1.39
$\log k'_{w\ C18}$	0	1.66	1.21	1.26
$\log (k' D)_w$	0	3.51	3.86	5.68
log P	0	1.88	0.73	0.56

Table 5.39

PREG Data in Log Units to the Base 10 for Ortho substituted Xylenes

	Mol wt	[1]Eq-C	PREG	PREG	PREG	PREG	PREG	PREG	PREG	PREG	PREG	PREGw
%Methanol			20	40	50	60	70	80	85	90	95	0
1-CH3	92.1	C1	0.00	-0.02	-0.02	-0.02	-0.04	-0.02	0.01	-0.05	0.09	0.00
2-CH3	106.2	C2	1.33	1.13	1.01	0.93	0.82	0.76	0.74	0.68	0.66	1.48
3-CH3	120.2	C3	0.90	0.93	0.83	0.96	1.02	1.02	0.97	0.84	0.87	1.21
5-CH3	148.2	C5	1.50	1.16	0.96	1.00	0.91	0.81	0.78	0.60	0.55	1.69
6-CH3	162.3	C6	1.98	1.85	1.68	1.72	1.67	1.63	1.57	1.43	1.33	2.15

[1] Eq-C is the equivalent hydrocarbon

PREG Data in Log Units Joules Per Mole for Methyl Substituted Ortho Xylenes

	PREG	PREG	PREG	PREG	PREG	PREG	PREG	PREG	PREG	PREGw
	J/mol	J/mol	J/mol	J/mol	J/mol	J/mol	J/mol	J/mol	J/mol	J/mol
%Methanol	20	40	50	60	70	80	85	90	95	
1-CH3	0	-105	-104.6	-104.6	-234	-105	77.2	-293	505	0
2-CH3	7581	6440	5745	5300	4687	4337	4231	3895	3753	8409
3-CH3	5107	5291	4729	5475	5826	5810	5548	4811	4936	6900
5-CH3	8541	6590	5492	5703	5175	4623	4436	3443	3110	9629
6-CH3	11292	10547	9577	9801	9526	9273	8937	8130	7582	12274

Table 5.40

PREG Data in Log Units to the Base 10 for the Hydroxybenzenes

	Mol wt	[1]Eq-C	PREG	PREG	PREG	PREG	PREGw
% Methanol			20	40	50	60	
Phenol	94.1	1-CH3	2.12	1.84	1.66	1.67	2.43
1,3-hydroxybenzene	110.1	2-CH3	5.04	4.16	3.75	3.32	5.83
1.3.5-hydroxybenzene	126.1	3-CH3	6.44	5.66	5.35	4.73	7.20

[1] Eq-C is the equivalent hydrocarbon

PREG Data in Log Units Joules Per Mole for the Hydroxybenzenes

	PREG J/mol	PREG J/mol	PREG J/mol	PREG J/mol	PREGw J/mol
% Methanol	20	40	50	60	
Phenol	12073	10491	9436	9501	13854
1,3-hydroxybenzene	28732	23719	21352	18935	33215
1.3.5-hydroxybenzene	36668	32264	30460	26963	41010

Table 5.41

PREG Data in Log Units to the Base 10 for the Anilines

	Mol wt	Eq-C	PREG	PREG	PREG	PREG	PREGw
%Methanol			40	50	60	70	
aniline	93	1-CH3	0.49	0.47	0.43	0.43	-0.27
1,2-Phenylenediamine	108	2-CH3	2.59	2.47	2.56	2.47	1.77
1,3-Phenylenediamine	108	2-CH3	3.57	3.50	3.35	3.40	3.35
1,4-Phenylenediamine	108	3-CH3	2.53	2.40	2.19	2.16	4.22

PREG Data in Log Units Joules Per Mole for the Anilines

	PREG J/mol	PREG J/mol	PREG J/mol	PREG J/mol	PREGw J/mol
%Methanol	40	50	60	70	
aniline	2798	2658	2471	2450	-1542
1,2-Phenylenediamine	14736	14042	14606	14087	10081
1,3-Phenylenediamine	20355	19923	19056	19376	19082
1,4-Phenylenediamine	14396	13650	12454	12289	24017

Table 5.42

PREG Data in Log Units to the Base 10 for Other Mono Substituted Benzenes

	Mol wt	[1]Eq-C	PREG	PREG	PREG	PREG	PREGw
% Methanol			30	50	70	90	
acetophenone	120.2	C3	1.21	0.99	0.81	1.37	1.70
nitrobenzene	123.1	C3	2.68	2.43	1.91	1.39	3.52
anisole	108.1	C2	3.57	2.93	2.49	2.20	4.34
methyl benzoate	136.2	C4	1.71	1.14	0.84	0.93	2.12

[1] Eq-C is the equivalent hydrocarbon

PREG Data in Log Units Joules Per Mole for the Other Mono Substituted Benzenes

	PREG J/mol	PREG J/mol	PREG J/mol	PREG J/mol	PREGw J/mol
% Methanol	30	50	70	90	
acetophenone	9073	6707	4837	6212	9700
nitrobenzene	15238	13821	10876	7913	20071
anisole	20356	16699	14161	12544	24710
methyl benzoate	9738	6471	4799	5298	12076

Table 5.43

PREG Data in Log Units to the Base 10 for the Halobenzenes

	Mol wt	[1]Eq-C	PREG	PREG	PREG	PREG	PREGw
%Methanol			40	50	60	90	
Fluorobenzene	96.1	C1	-0.86	-0.82	-0.45	0.11	-1.29
Chlorobenzene	112.6	C2	0.64	0.59	0.50	0.48	1.12
Bromobenzene	157.0	C6	0.31	0.38	0.30	0.29	0.67

[1] Eq-C is the equivalent hydrocarbon

PREG Data in Log Units Joules Per Mole for the Halobenzenes

	PREG	PREG	PREG	PREG	PREGw
	J/mol	J/mol	J/mol	J/mol	J/mol
%Methanol	40	50	60	90	
Fluorobenzene	-4884	-4687	-2566	619.4	-7338
Chlorobenzene	3647	3341	2835	2722	6365
Bromobenzene	1794	2185	1731	1666	3839

Table 5.44

PREG Data in Log Units to the Base 10 for Benzene Carboxylic Acids

	Mol wt	[1]Eq-C	PREG	PREG	PREG	PREG	PREGw
% Methanol			80	85	90	95	PREG
benzoic acid	122.1	C3	1.44	1.22	1.00	0.52	5.60
1,2-benzene dicarboxylic acid	166.1	C6	3.05	2.97	2.64	2.34	6.22
1,2,4-benzene tricarboxylic acid	210.1	C9	3.63	3.45	3.28	2.63	7.46

[1] Eq-C is the equivalent hydrocarbon

PREG Data in Log Units Joules Per Mole for Benzene Carboxylic Acids

	PREG J/mol	PREG J/mol	PREG J/mol	PREG J/mol	PREGw J/mol
% Methanol	80	85	90	95	
benzoic acid	8203	6973	5680	2961	31907
1,2-benzene dicarboxylic acid	17385	16914	21318	13344	35455
1,2,4-benzene tricarboxylic acid	20702	19658	18693	14969	42476

Table 5.45

Correlation of PREG

	[1]$PREG_w$ kJ/mol	[2]$PREG_{50}$	[3]Cn	[4]S	U" kJ/mol	U" /PREG	Heat of Formation	Ucind kJ/mol	Ratio PREG/Ucind
Toluene	0.0	0.0	0.39	0.04	8.70	0.00	16.51	3.04	-
0-Xylene	8.4	5.7	0.41	0.04	8.30	0.99	11.61	2.92	0.35
1,2,3 polymethylbenzene	6.9	4.8	0.44	0.04	8.00	1.16	7.96	2.79	0.40
1,2,3,4,5 polymethylbenzene	9.6	5.5	0.48	0.04	7.30	0.76	1.36	2.54	0.26
1,2,3,4,5,6 polymethylbenzene	12.2	9.6	0.50	0.03	6.90	0.57	2.34	2.42	0.20
Phenol	13.8	9.4	0.60	0.21	42.60	3.09	-19.57	14.89	1.08
1,3-dihydroxybenzene	33	21.3	0.84	0.39	76.60	2.32	-61.91	26.81	0.81
1,3,5-trihydroxybenzene	41	30.5	1.09	0.56	111.40	2.72	-103.65	38.96	0.95
Flourobenzenes	-11	-4.6	0.44	0.09	17.74	-1.60	-23.27	6.2	-0.56
Bromobenzene	3.8	3.3	0.33	0.04	7.53	1.98	27.36	2.6	0.69
Chlorobenzene	6.4	2.2	0.35	0.04	8.53	1.34	16.23	3.0	0.47
Acetophenone	9.7	6.7	0.58	0.15	29.80	3.46	-10.45	10.4	1.07
Anisole	24.7	16.7	0.53	0.17	33.60	1.21	-12.44	11.8	0.48
Nitrobenzene	20.1	13.8	0.52	0.09	18.4	2.97	36.68	6.4	0.32
Methylbenzoate	12.1	6.5	0.86	0.30	59.60	5.68	-54.99	20.9	1.73
Benzoic acid	31.9	16.4	0.87	0.35	68.50	2.15	-62.43	23.98	0.75
Phthalic acid	35.5	23.8	1.39	0.65	129.30	3.65	-141.92	45.22	1.28
1,2,4-Benzene tricarboxilic acid	42.5	28.7	1.89	0.95	188.90	4.45	-220.74	66.08	1.56
Aniline	-1.5	2.7	0.82	0.32	64.30	-42.87		22.51	-15.01
1,2-Phenylenediamine	10	14.2	1.07	0.38	75.30	7.53	Data not	26.34	2.63
1,3-Phenylenediamine	19	19.9	1.21	0.47	93.10	4.90	available	32.58	1.71
1,4-Phenylenediamine	24	13.6	1.21	0.47	93.10	3.88		32.58	1.36

[1]PREGw values are PREG in pure water

[2]$PREG_{50}$ values of PREG in 50% methanol:water

[3]Cn is the electon energy excess in units of electronic 'charge'

[4]S is the electronic charge distribution in units of 'charge sqaured'

Table 5.46

Calculation of Correlation Parameters C_n and S

A worked example is given below for the calculation of Cn (electron energy excess) and S (the charge distribution) for 1,3 dihydroxyphenol,

where $Cn = (\sum q_i)^2$

and where $S = \sum (q_i)^2$

For each equation q_i is the atomic charge. Analyte atomic charge data were obtained from a MOPAC information program and was kindly forwarded to us from TRIPOS Associates Ltd.

The molecular structure for 1,3 hydroxyphenol is given below

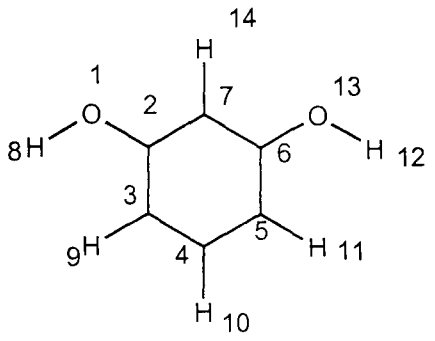

Atomic Charges for 1,3 dihydroxyphenol

Atom	Atomic Charge	[Atomic Charge]^2	Atom	Atomic Charge	[Atomic Charge]^2
1 O1	-0.3597	0.12938	8 H1	0.2173	0.04722
2 C2	0.075	0.00563	9 H2	0.2173	0.04722
3 C3	-0.0318	0.00101	10 H3	0.0643	0.00413
4 C4	-0.0569	0.00324	11 H4	0.0619	0.00383
5 C5	-0.0318	0.00101	12 H5	0.0643	0.00413
6 C6	0.075	0.00563	13 O19	-0.3597	0.12938
7 C7	-0.0022	4.8E-06	14 H7	0.0669	0.00448

[Atomic Charge]^2 is the square of the atomic charge and is required in order to calculate S.

Where

$C_n = 1/2\sum |q_i|$ for 1,3 dihydroxyphenol is 0.48 in units of charge, where 1 unit of charge the charge on a single proton ($e = 1.602 \times 10^{-19}$ C).

$S = \sum (q_i)^2$ for 1,3 dihydroxyphenol is 0.386 in units of charge squared.

C_n values are included to allow comparison with those values obtained by Coquart and Hennion. In general the results are in good agreement but those obtained by Coquart being slightly higher.

i.e for Phenol we get C_n as 0.60, Coquart gets 0.58

1,3 di-hydroxyphenol we get C_n as 0.84, Coquart gets 0.94

1,3,5 tri-hydroxyphenol we get C_n as 1.09, Coquart gets 1.32

The differences may be explained by the fact that different MOPAC information programs our results representing the most recent software package.

Table 5.47

Calculation of Correlation Parameter U''

U'' is calculated according to the equation ,

$$U'' = S/4\pi\varepsilon_o r \qquad [5.15]$$

Where S is the sum of the squares for atomic charge on the analyte and $4\pi\varepsilon_o$ is the electrostatic energy, r is the distance between the molecule and the surface of the metal.

A worked example is given below for the calculation of U'' for 1,3 dihydroxyphenol, the molecular structure for this compound is given below

$S = \sum(q_i)^2$ for 1,3 dihydroxyphenol $S = 0.386$ in units of charge squared.

$4\pi\varepsilon_o = 8.854 \times 10^{-12}$m

$r = 7 \times 10^{-10}$m

The formula applies when the units of charge are coulombs and the units of distance of meters. We therefore are arrive at

$$U'' = S/4\pi\varepsilon_o r$$

$$= \frac{0.386 \times 1.602 \times 10^{-19} \times 1.602 \times 10^{-19}\ \text{J}}{4 \times 3.142 \times 8.854 \times 10^{-12}\text{m} \times 7 \times 10^{-10}\text{m}} \quad \text{Units of Joules per molecule}$$

$$= 1.273 \times 10^{-19} \times 6.022 \times 10^{23} \quad \text{Units of J per mol}$$

$$= 76645 \text{ J per mol}$$

$$U'' = 76.6 \text{ kJ per mol}$$

Where S is now given in SI units of charge i.e 1.602×10^{-19} is the unit of charge and 8.854×10^{-12}m is the electric permittivity in a vacuum (ε_o). r is the distance of the molecule from the surface. We have chosen a value of 7×10^{-10}m which represents approximately twice the distance between graphite layers (i.e.3.35Å)

We then use Avagadro's number to give us U'' in units of Joules per mol.

The values of U'' presented in table 5.45 are all calculated on the same basis as the example just given.

Table 5.48

Calculation of Correlation Parameter U_{cind}

U_{cind} is the potential energy of a charge inducing a dipole in the surface of the graphite. It is calculated according to the equation ,

$$U_{cind} = \alpha.S /4\pi\varepsilon_o 2r^4 \qquad = \alpha U'' / 2r^3$$

Where $4\pi\varepsilon_o$ the electrostatic unit for energy and S is the charge distribution analyte, α is the polarasability constant for the medium which in this case is graphite $1.5 \times 10^{-10} cm^3$, r is the distance between the analyte charge and the surface of the graphite.

A worked example is given below for the calculation of U_{cind} for 1,3 dihydroxyphenol. where

S	0.386 in units of charge squared
$4\pi\varepsilon_o$	$8.854 \times 10^{-12} m$
r	$3.5 \times 10^{-10} m$
α	$1.5 \times 10^{-30} m^3$ (in SI Units)

Where S is now given in SI units of charge i.e 1.602×10^{-19} is the unit of charge and $8.854 \times 10^{-12} m$ is the electric permittivity in a vacuum (ε_o). r is the distance of the molecule from the graphite surface. We have used a value of $3.5 \times 10^{-10} m$ which represents approximately the distance between graphite layers (i.e.3.35Å)

The formula applies when the units of charge are coulombs and the units of distance of meters. We therefore are arrive at

$$U_{cind} = \alpha S/4\pi\varepsilon_o r$$

$$= \frac{1.5 \times 10^{-30} \times 0.386 \times 1.602 \times 10^{-19} \times 1.602 \times 10^{-19} /}{4 \times 3.142 \times 8.854 \times 10^{-12} m \times 2 \times (3.5 \times 10^{-10} m)^4}$$

$$= 4.453 \times 10^{-21} \text{ J/molecule}$$

$$= 4.453 \times 6.022 \times 10^{23} \text{ J/mol}$$

$$= 26{,}815 \text{ J/mol}$$

$$U_{cind} = 26.815 \text{ kJ/mol}$$

Where Avagadro's number is $6.022 \times 10^{23} mol^{-1}$

The values of U_{cind} presented in table 5.45 are all calculated on the same basis as the example just given.

Fig 5.1
Lennard Jones Potential

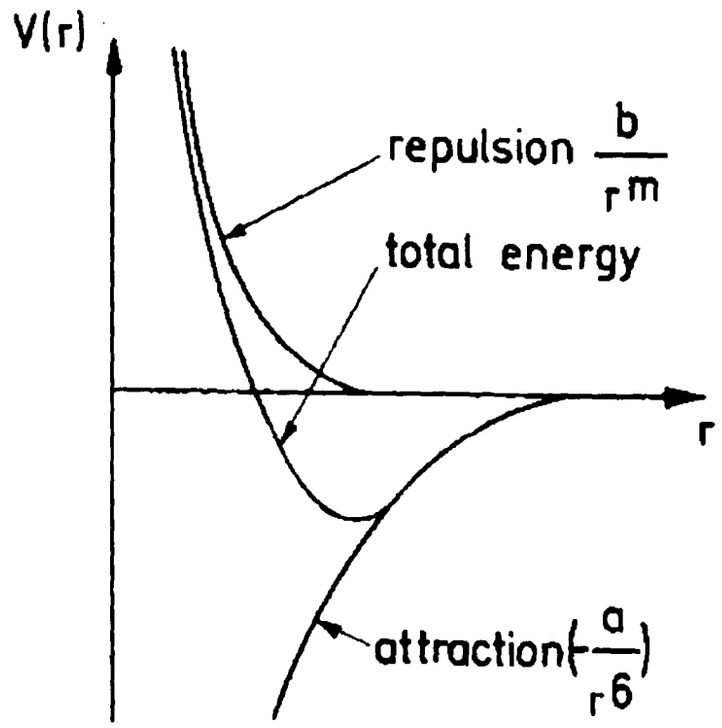

- potential energy of intermolecular interactions as a function of distance

Fig 5.2
Types of Intermolecular Forces

Ion dipolee preferred orientation

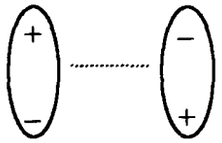

Dipole-Dipole preferred orientation

(a) • Orientation interactions
- ~Ion -dipole
- Dipole-dipole

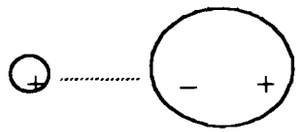

Ion /Induced dipolee preferred orientation

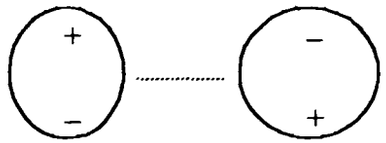

Dipole /Induced dipole preferred orientation

(b) • Polar-nonpolar interactions
- Ion-induced dipole
- Dipole-induced dipole

Induced dipole - induced dipole

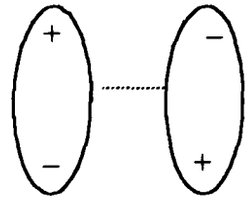

(c) • Nonpolar interactions
- Induced dipole - induced dipole

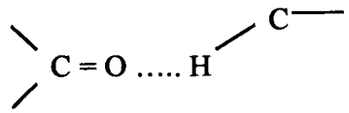

Hydrogen bonding

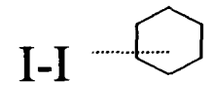

Donar-acceptor

(d)
(e) • Specific interactions
- Hydrogen bonding
- Donar-acceptor interaction

Fig 5.3
PGC as a Chromatographic Conductor

Lines of force between charged particle and its imaginary image in the surface

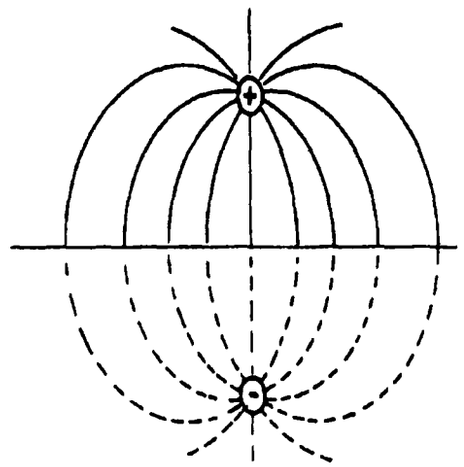

Interaction of a three charge body with its oppositely charged image; lines represent interactions which have to be taken account in determining total energy of interaction

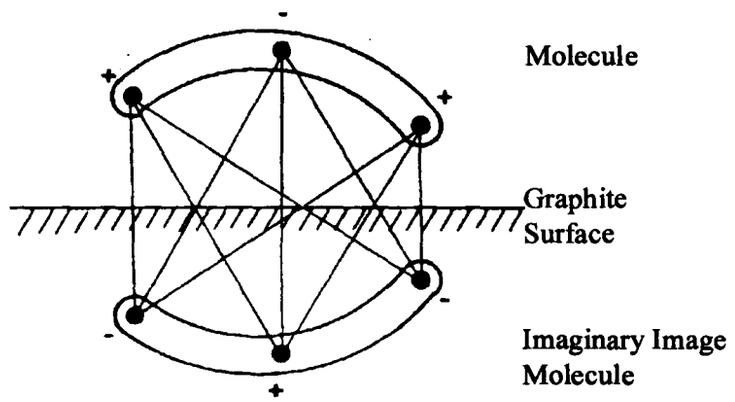

Right:
Matrix of Interaction Energy Terms for the interaction of a charge with its image in the Graphite Surface.

Analyte atom	Coordinates of analyte atom			Interatom energies		
1	x_1	y_1	z_1	U_{11}	U_{12}	U_{13}
2	x_2	y_2	z_2	U_{21}	U_{22}	U_{23}
3	x_3	y_3	z_3	U_{31}	U_{32}	U_{33}

Fig. 5.4
Schematic Representation for the Determination of $k'_{(g\text{-}hs)}$

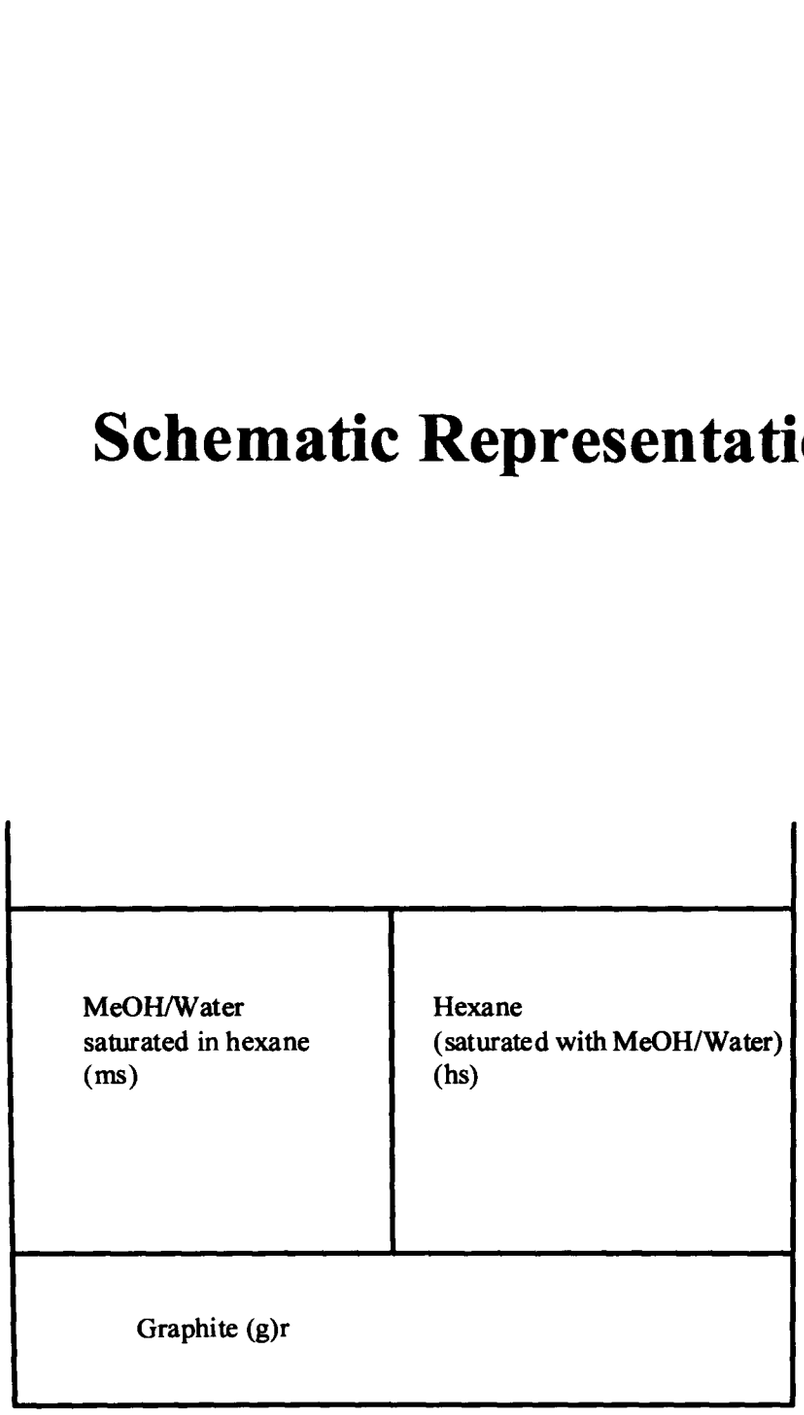

$k'_{g\text{-}ms} = C_g.A_g / C_{ms}.V_{ms} = K_{g\text{-}ms} \cdot \phi_{g\text{-}ms}$

$k'_{g\text{-}hs} = Cg.Ag / Chs.Vhs = K_{g\text{-}hs}.\ \phi_{g\text{-}hs}$

$k'_{hs\text{-}ms} = C_{ms}.\ V_{ms} / C_{hs}.V_{hs} = D_{hs\text{-}ms} \cdot \phi$

Here

$k'_{g\text{-}hs} = K_{g\text{-}ms} \cdot D_{hs\text{-}ms} \cdot \phi_{hs\text{-}ms}$

when ms and hs are alternative eluents for the same column $V_{ms} = V_{hs}$ so $\phi_{hs\text{-}ms} = 1$

when $k'_{g\text{-}hs} = K_{g\text{-}ms} \cdot D_{hs\text{-}ms}$

Fig 5.5

van't Hoff Plot of log D vs 1/T

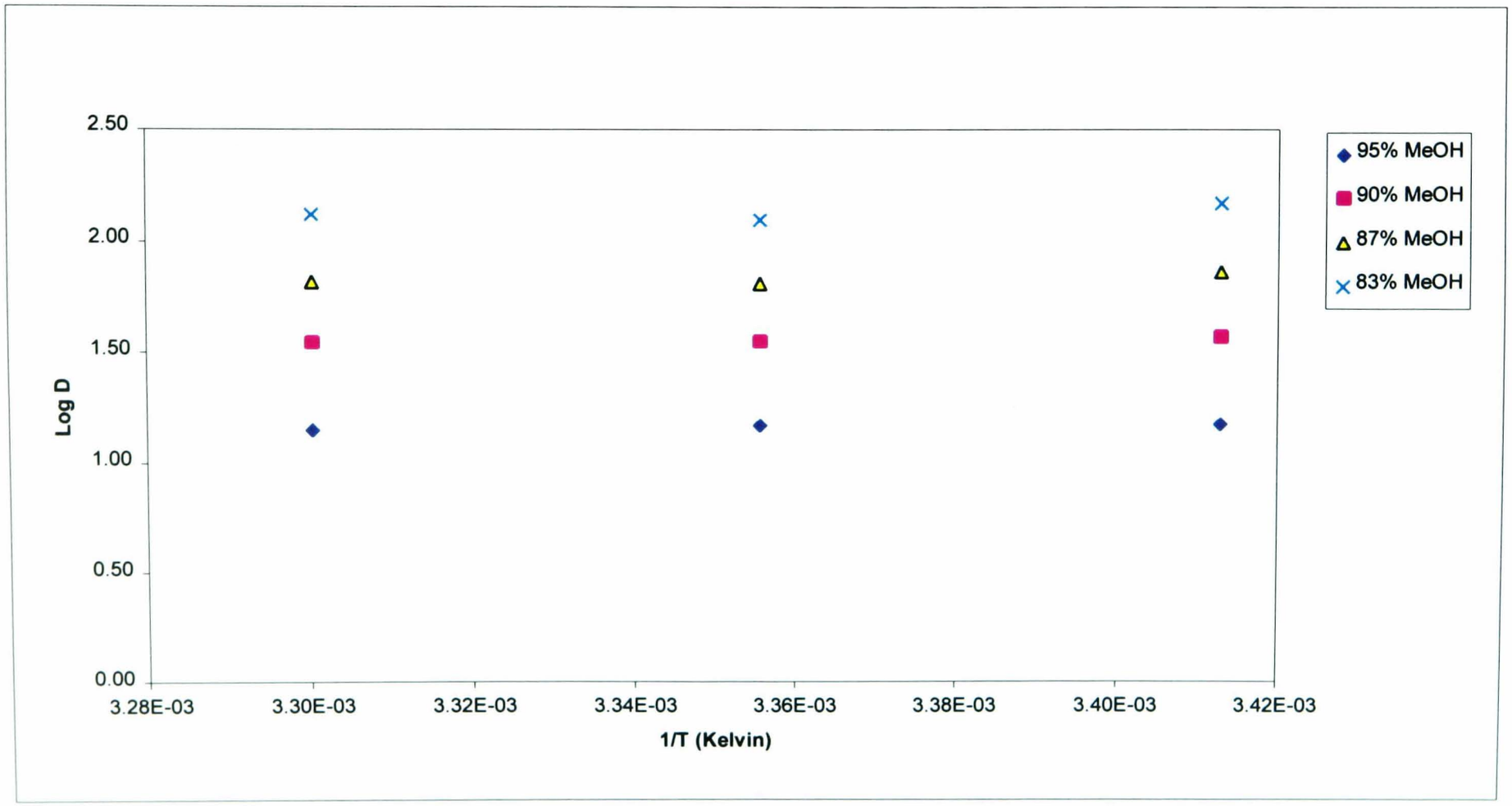

Fig 5.6

Plot of log k' Alkylbenzenes vs % Methanol:Water

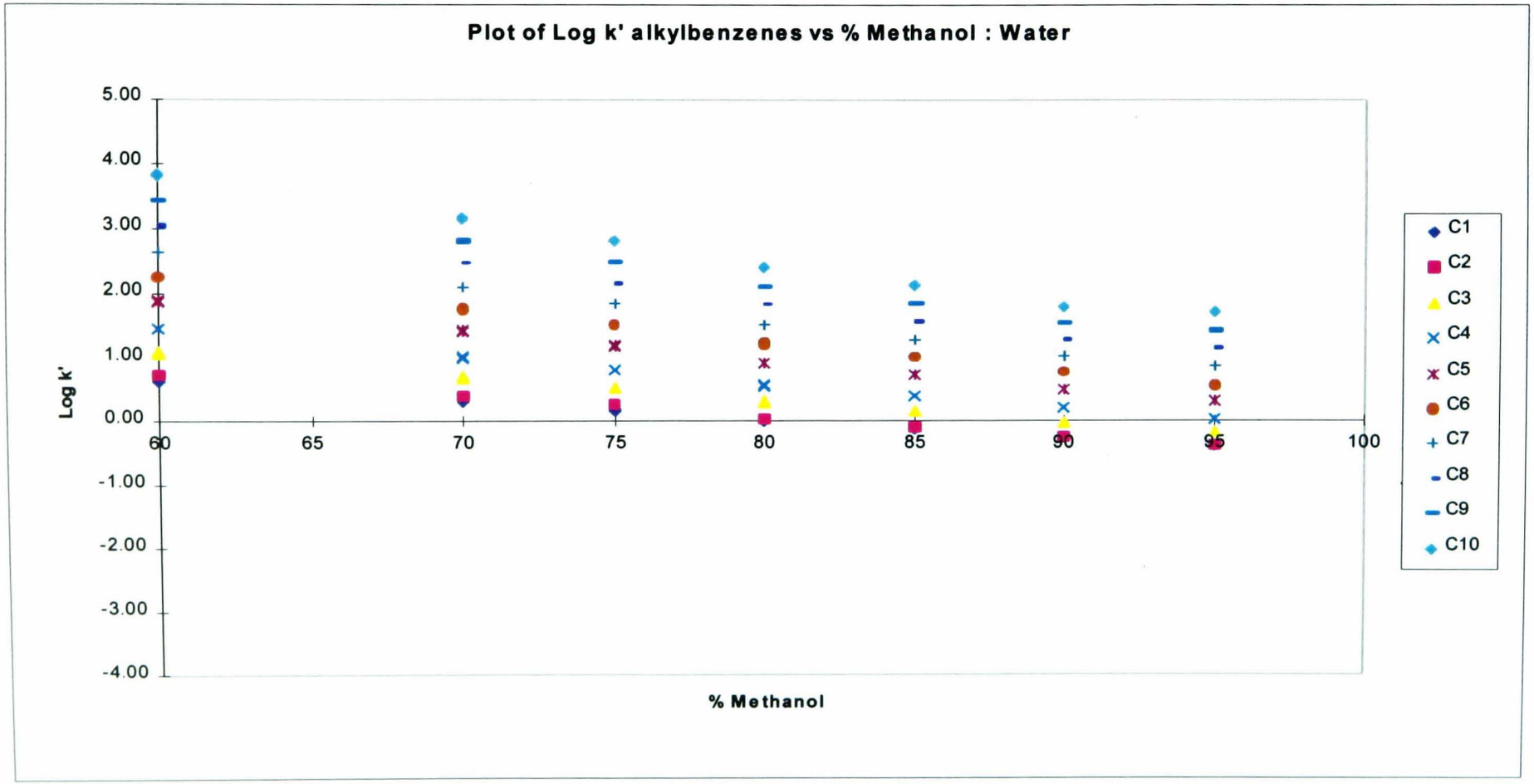

Fig 5.7

Plot of log D vs % Methanol:Water for the Alkylbenzenes Plus Confirmation of Extrapolated Data at 60% Methanol:Water

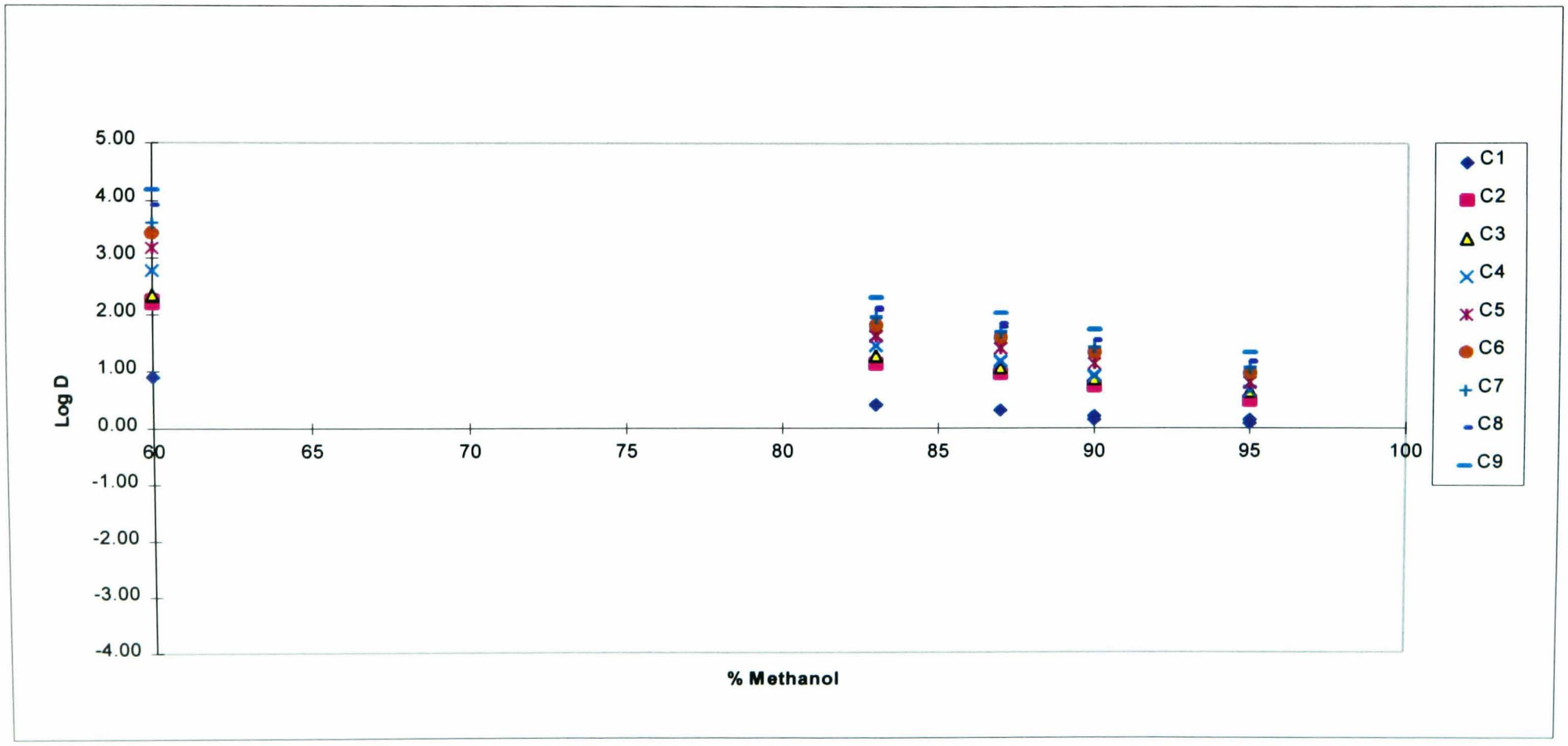

Fig 5.8

Plot of log k'/D vs % Methanol:Water for the Homologous Series of Alkylbenzenes

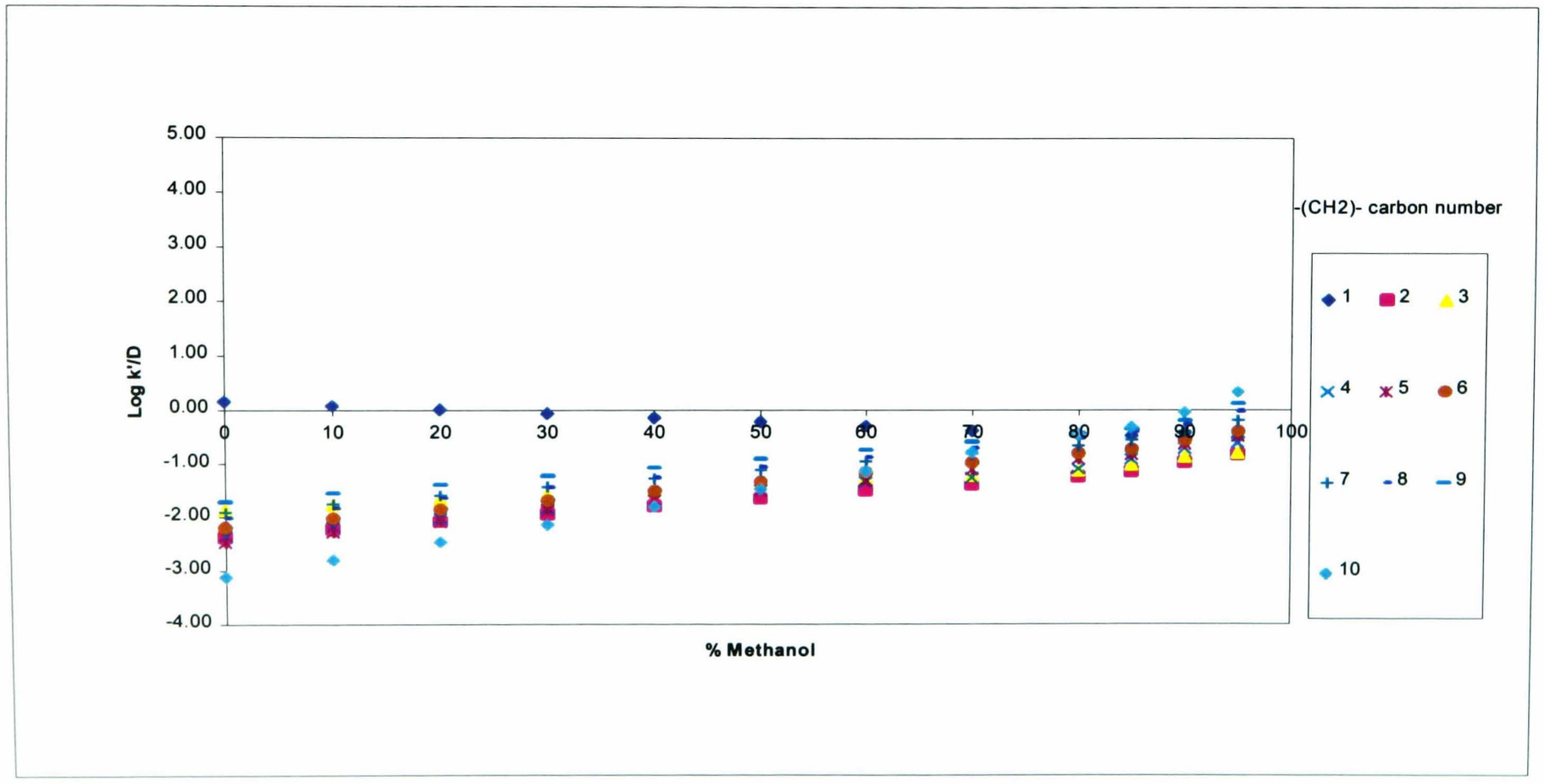

Fig 5.9

Plot of log k' Alkylbenzenes vs Side Chain Carbon Number (n) for Different Methanol:Water Compositions

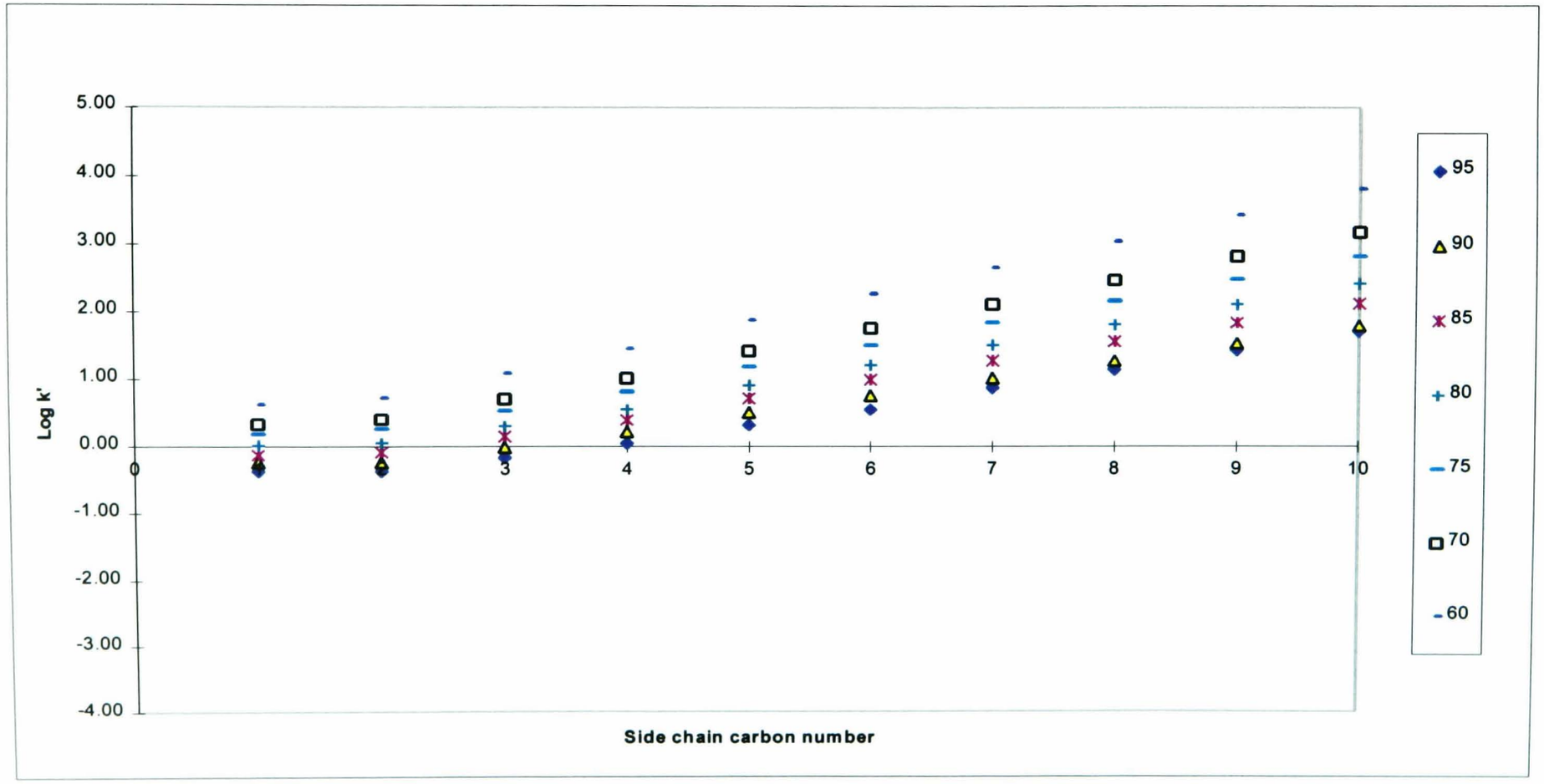

Fig 5.10

Plot of log D Alkylbenzene vs Side Chain Carbon Number (n) for Different Methanol:Water Compositions

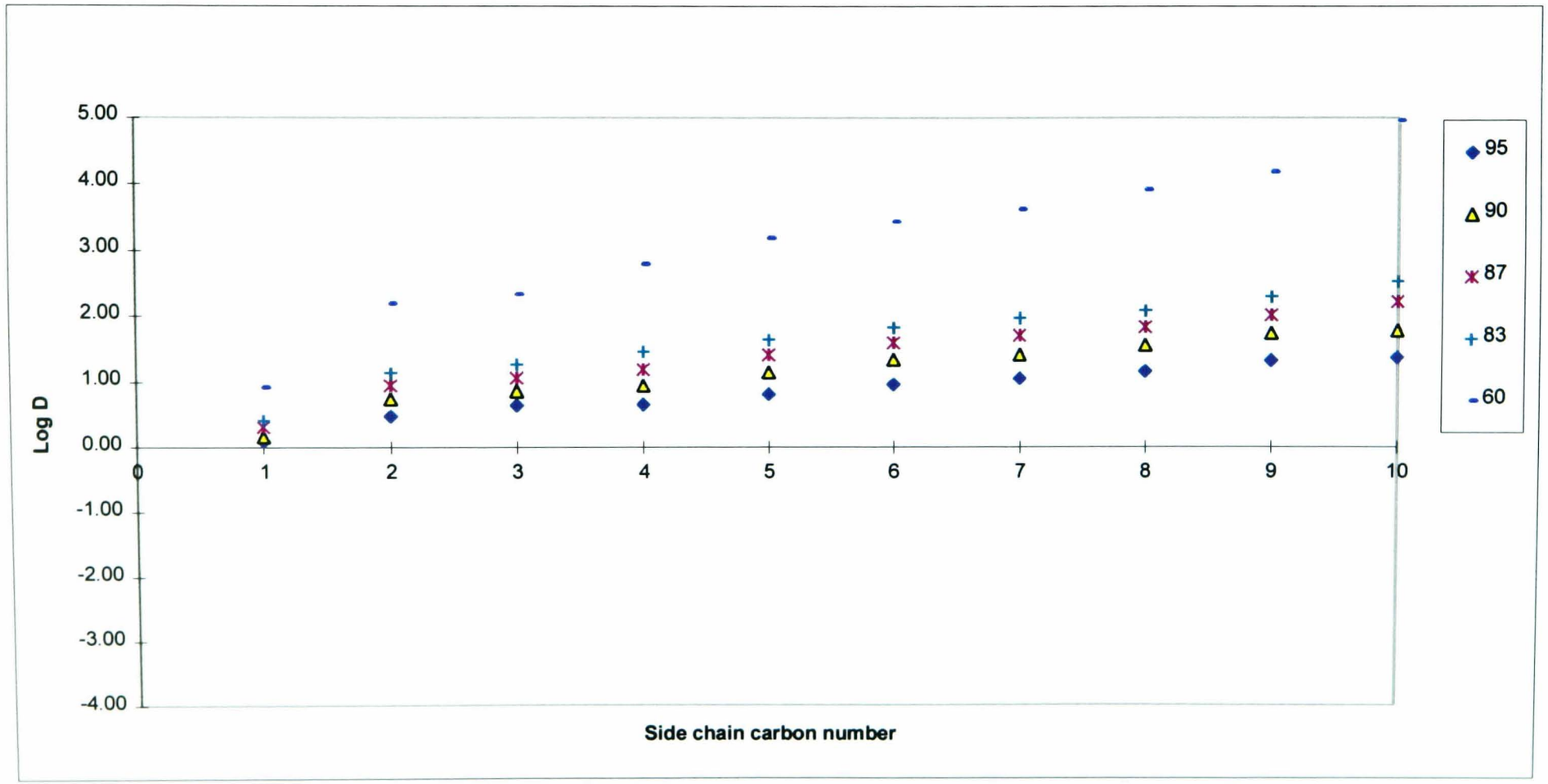

Fig 5.11

Plot of log k'/D vs Side Chain Carbon Number (n) for the Alkylbenzenes for Different Methanol:Water Compositions

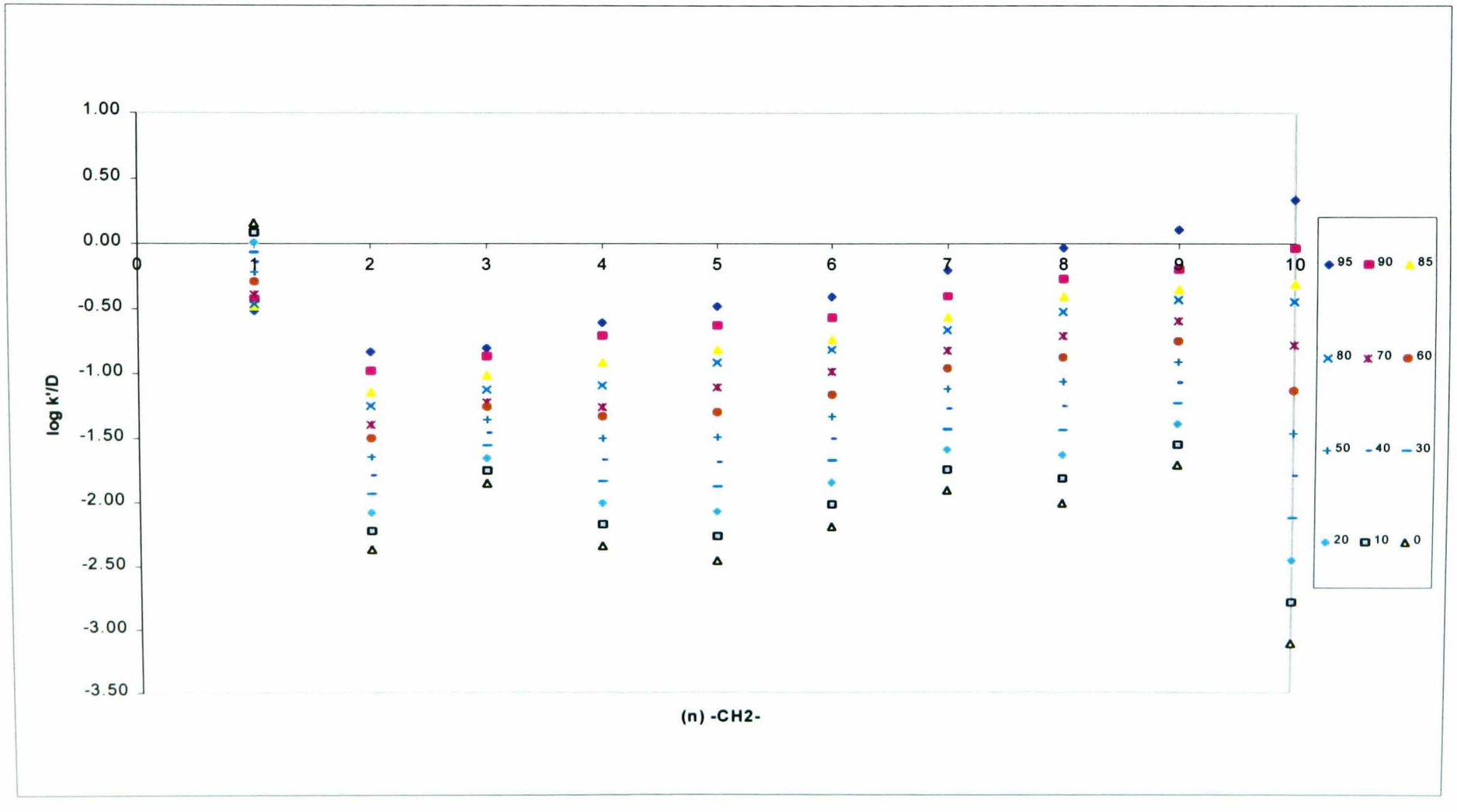

Fig 5.12

Plot of Homologue Selectivity (α) vs Side Chain Carbon Number for the Alkylbenzenes

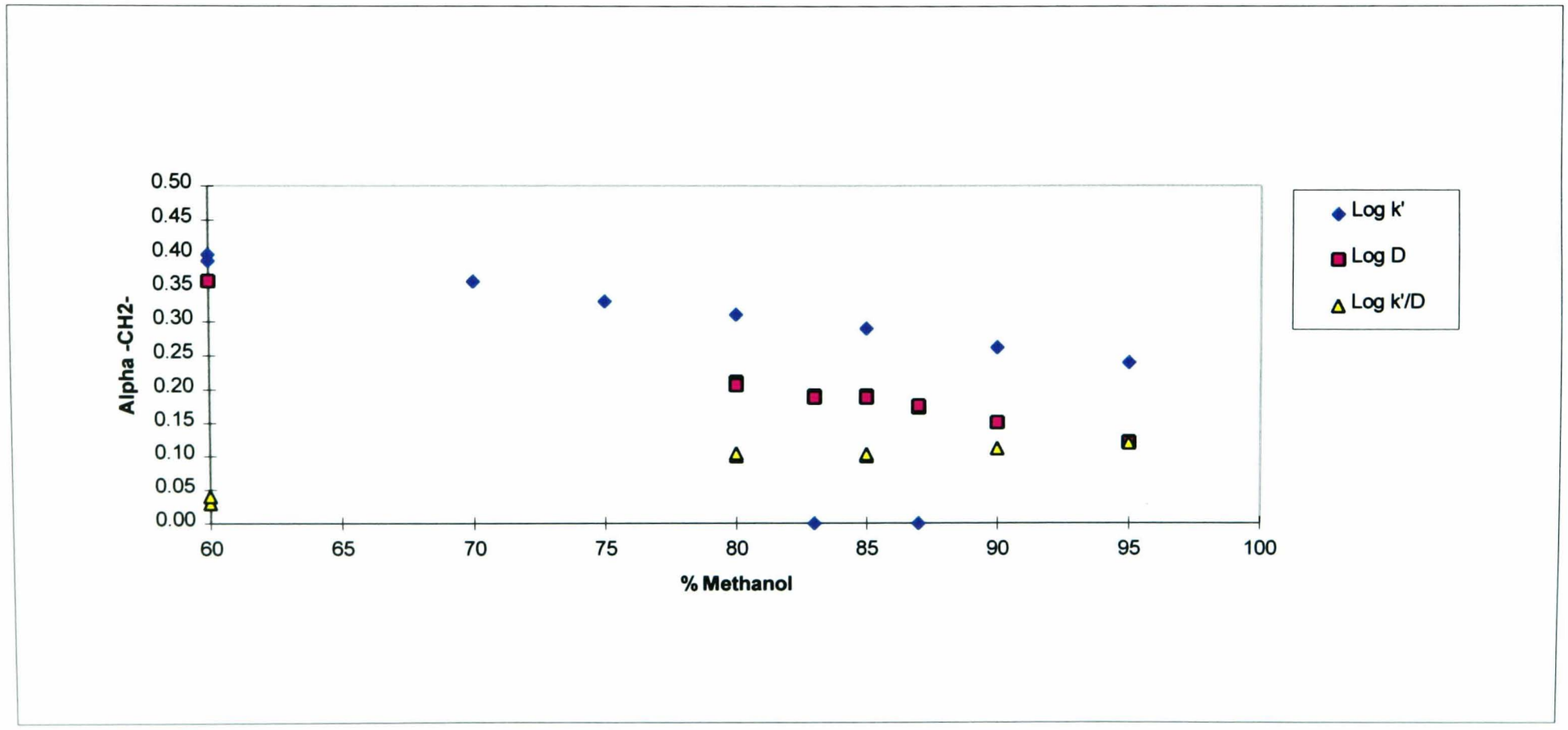

Fig 5.13

Plot of log k'_{PGC} , log D & log P vs $(CH_2)n$

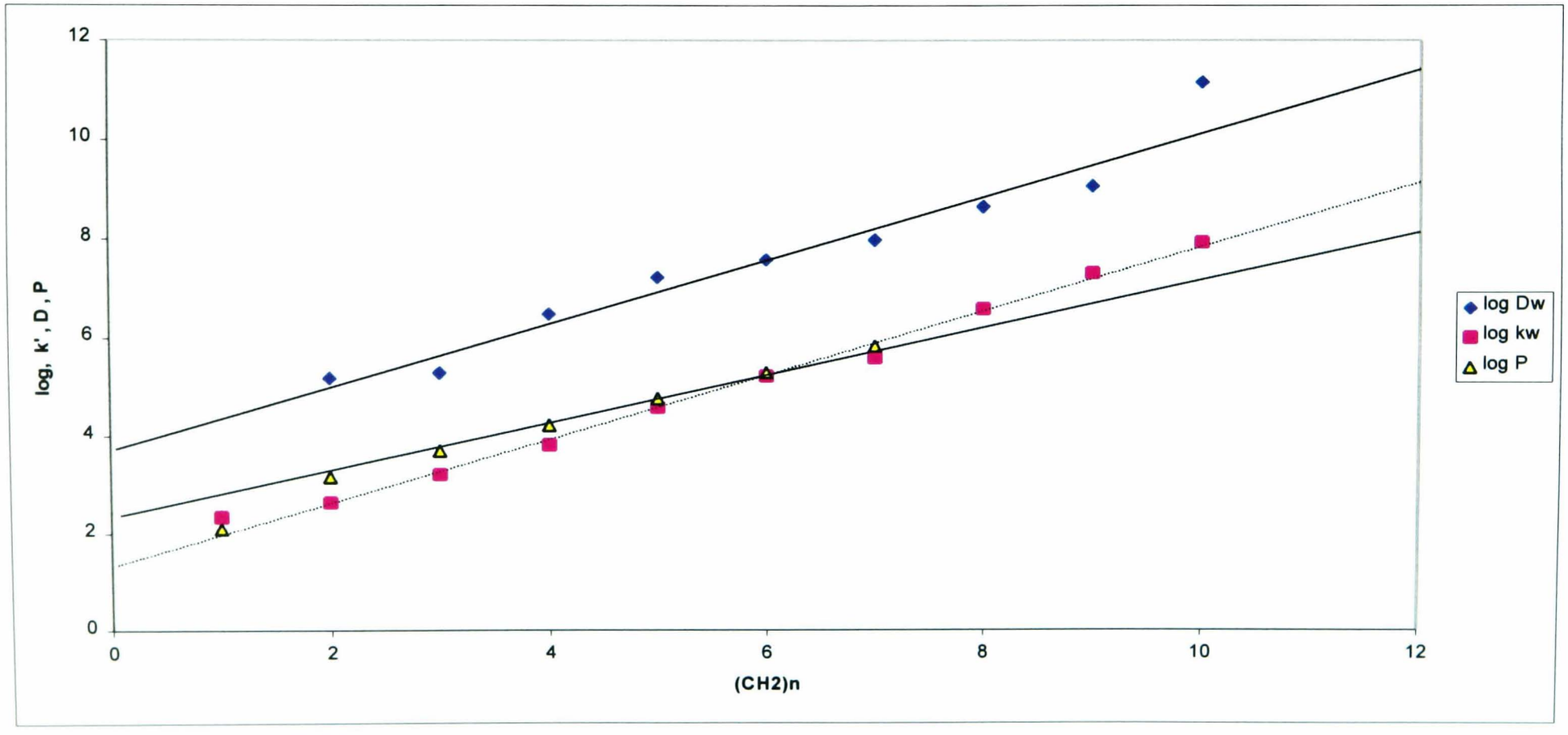

Fig 5.14

Comparative Plots of log k' vs Methanol:Water and Methanol:Water with Hexane

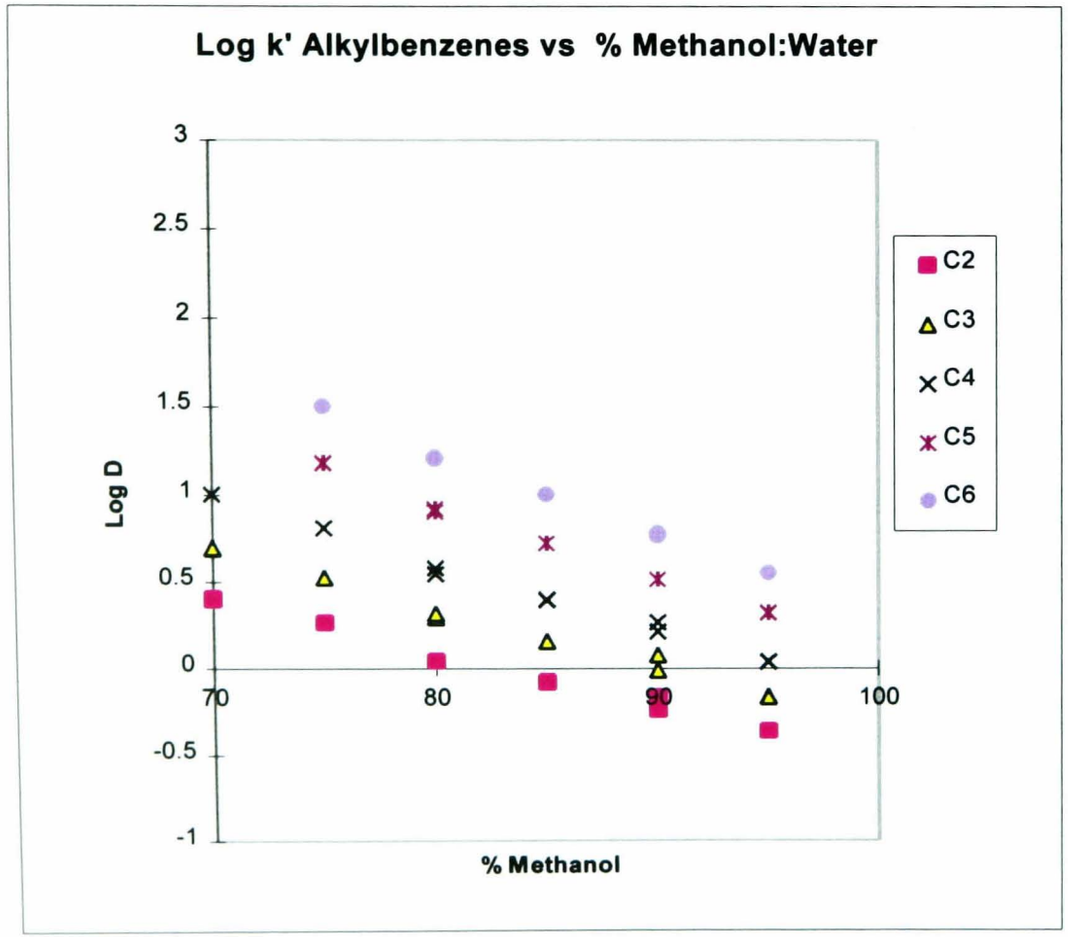

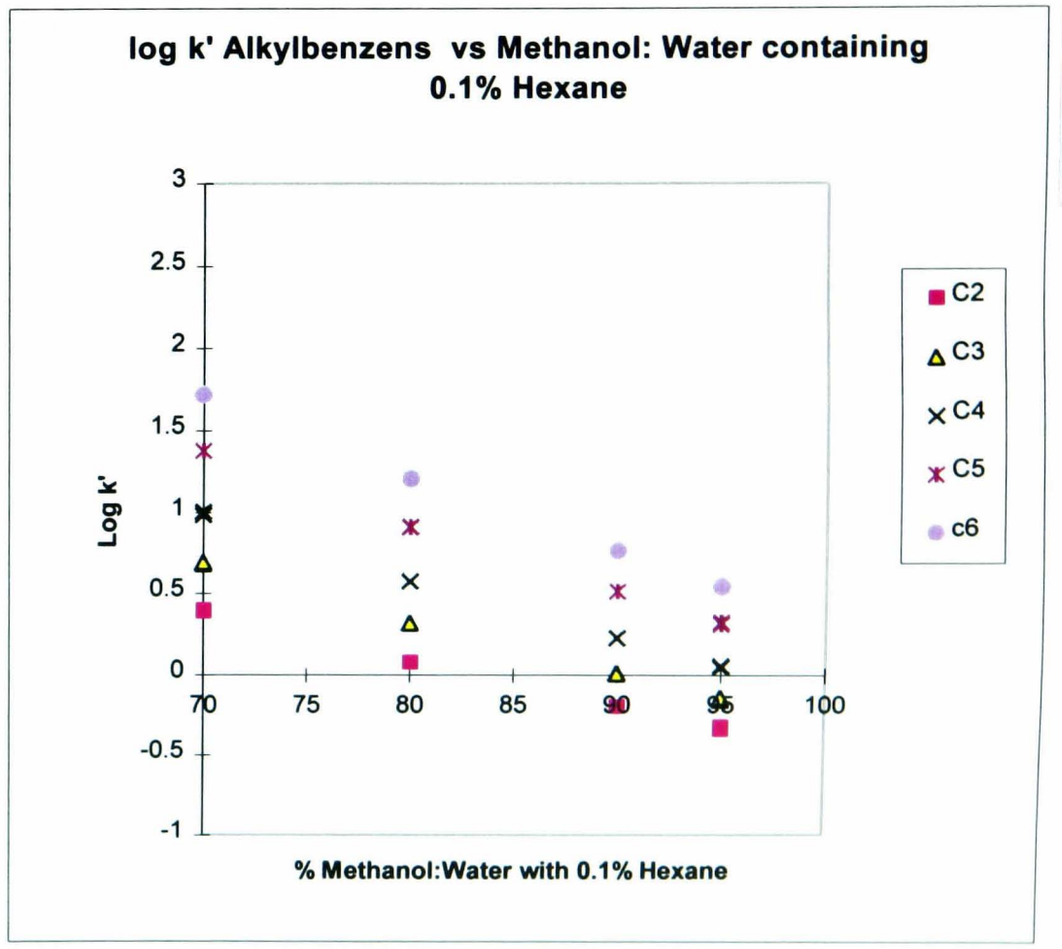

Fig 5.15

Plot of log k' vs % Hexane in 95% Methanol:Water

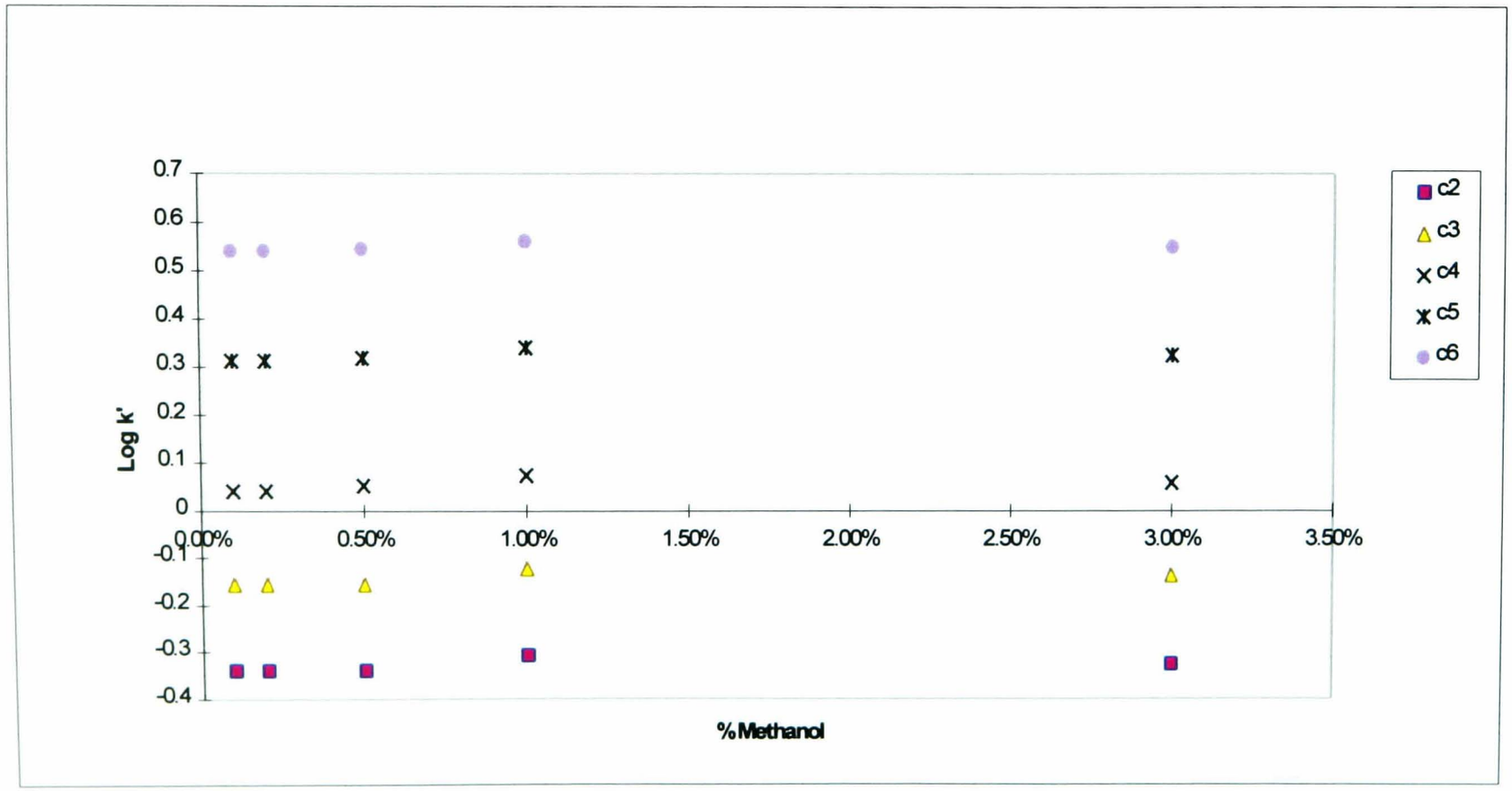

Fig 5.16

Plot of log k' vs % Methanol: Water for the Methyl Substituted Ortho-Xylenes

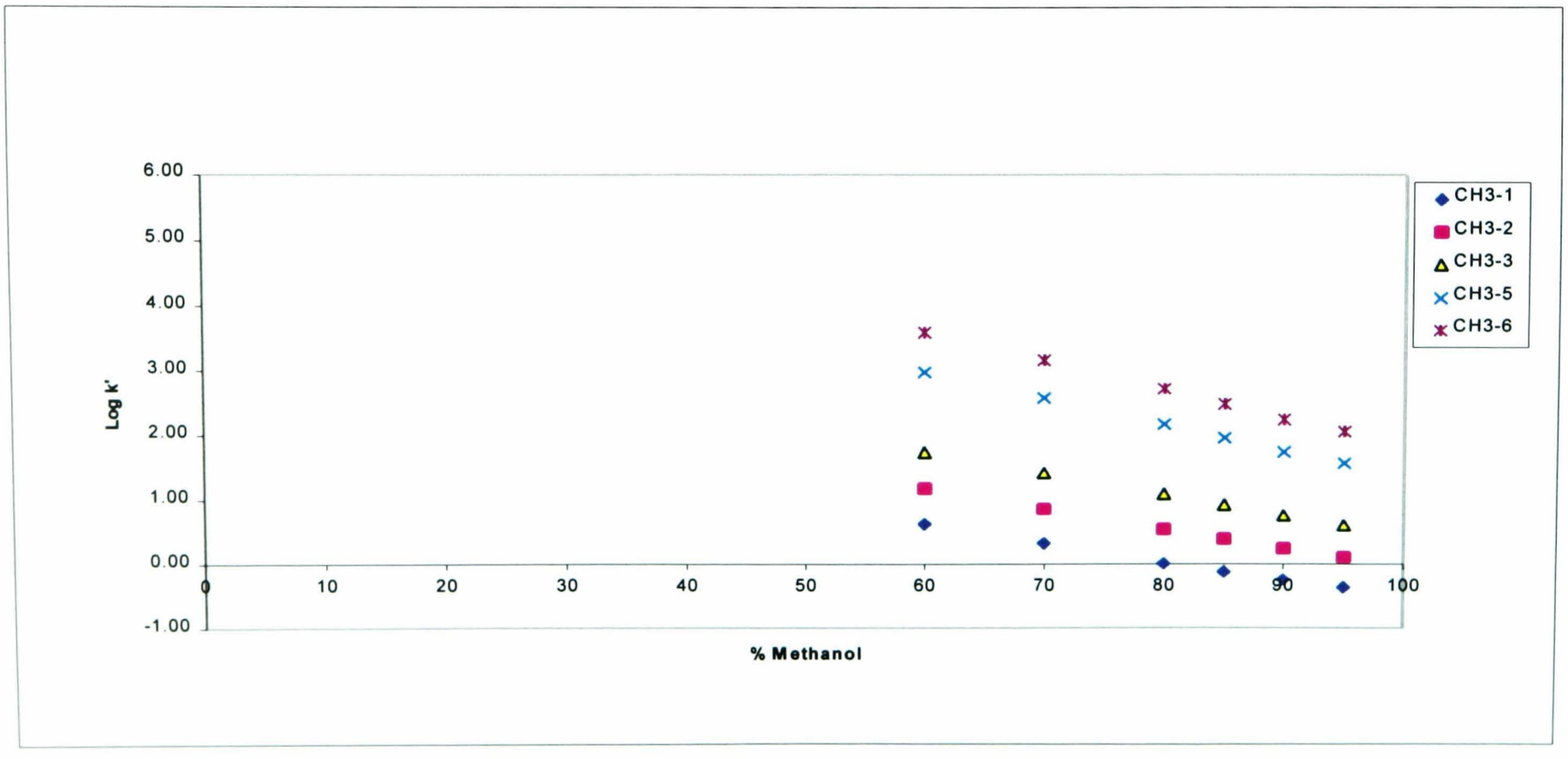

Fig 5.17

Plot of log D vs % Methanol: Water for the Methyl Substituted Ortho-Xylenes

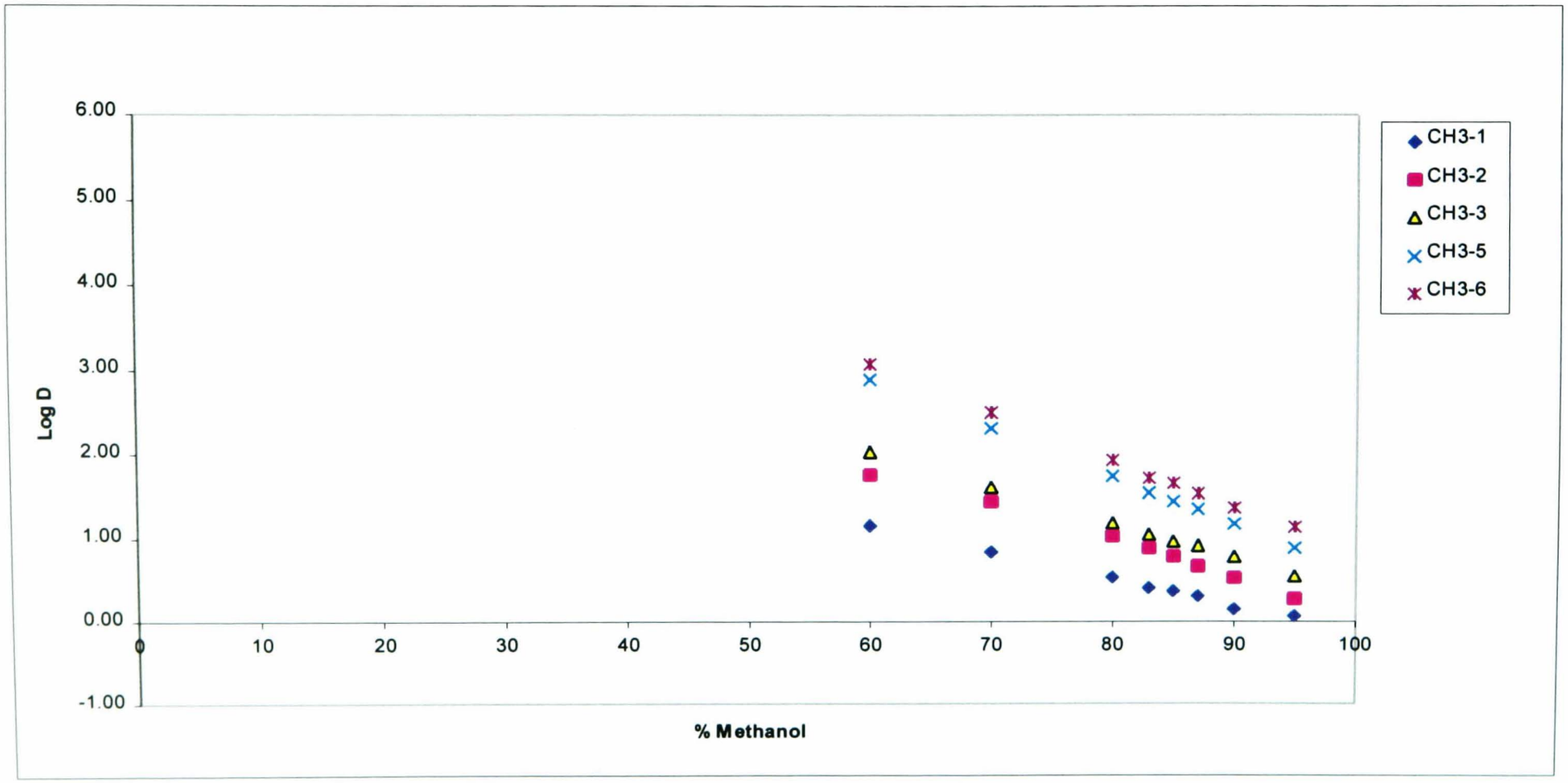

Fig 5.18

Plot of log k'/D vs % Methanol: Water for the Polymethylbenzenes

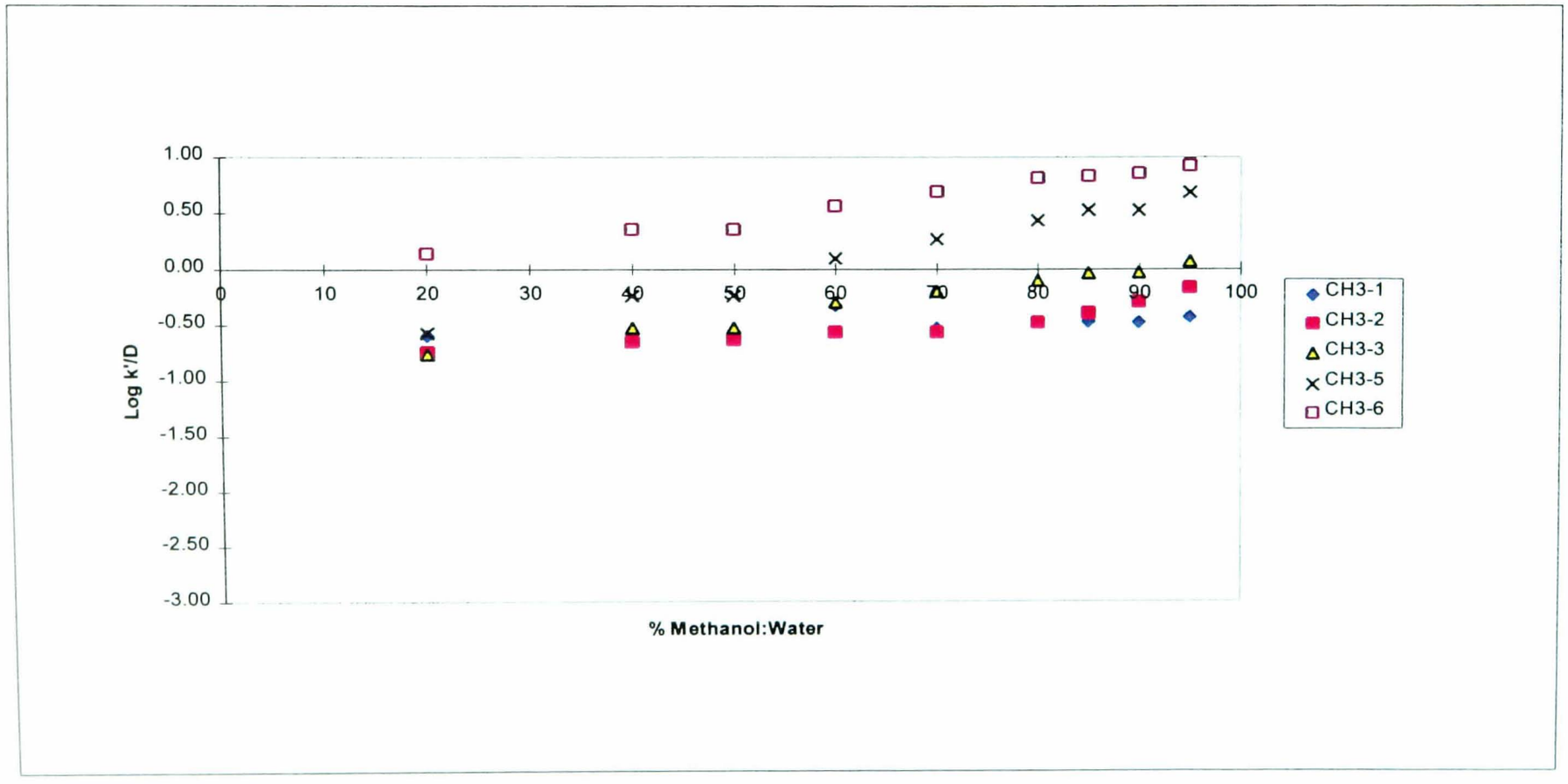

Fig 5.19a

Plot of log D , log k' vs the Number of Methyl Substituents (n) for the Polymethylbenzenes in 60% Methanol:Water

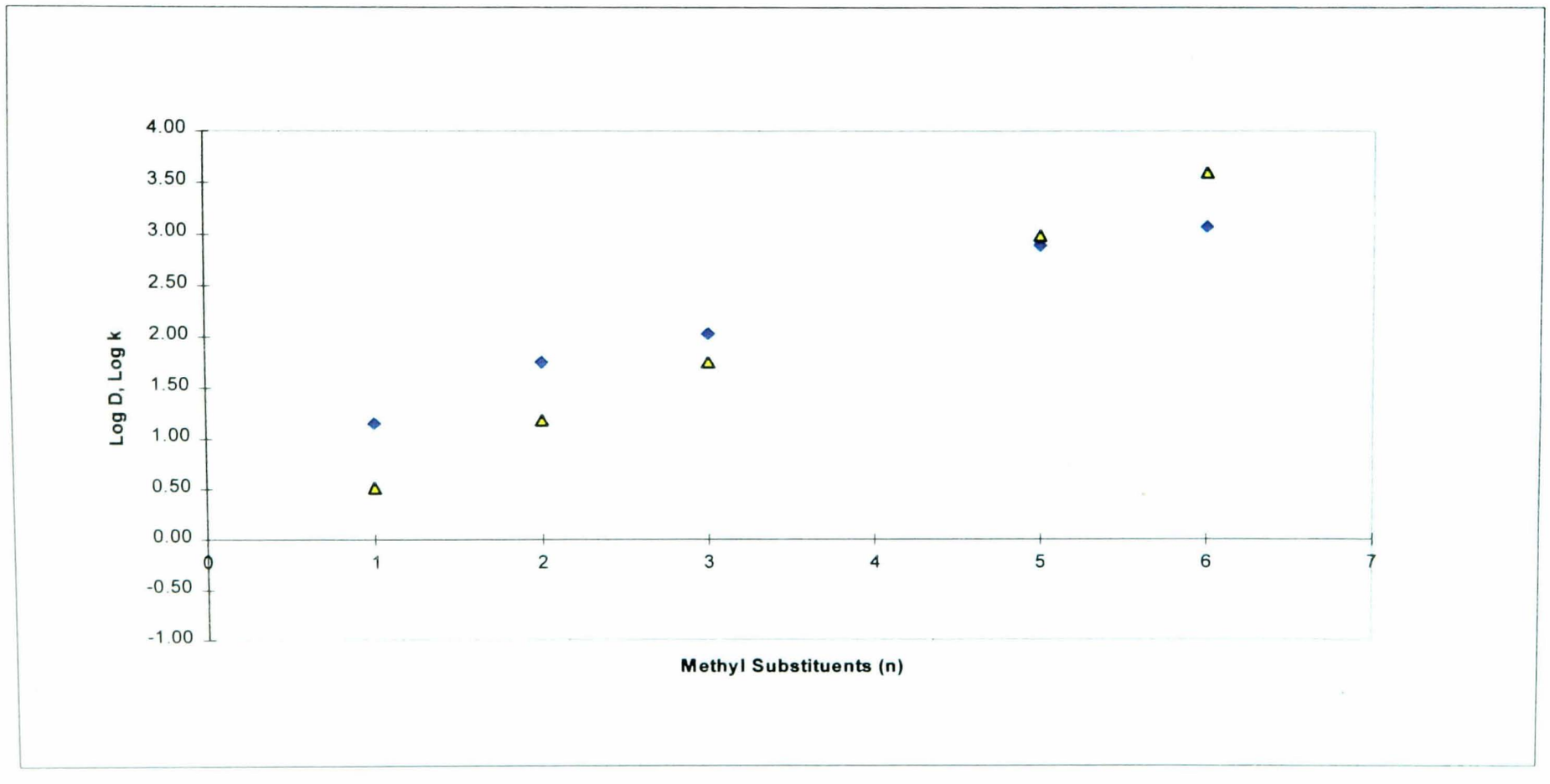

Diamonds - log D
Triangles – log k'

Fig 5.19b

Plot of log D , log k' vs the Number of Methyl Substituents (n) for the Polymethylbenzenes in 80% Methanol:Water

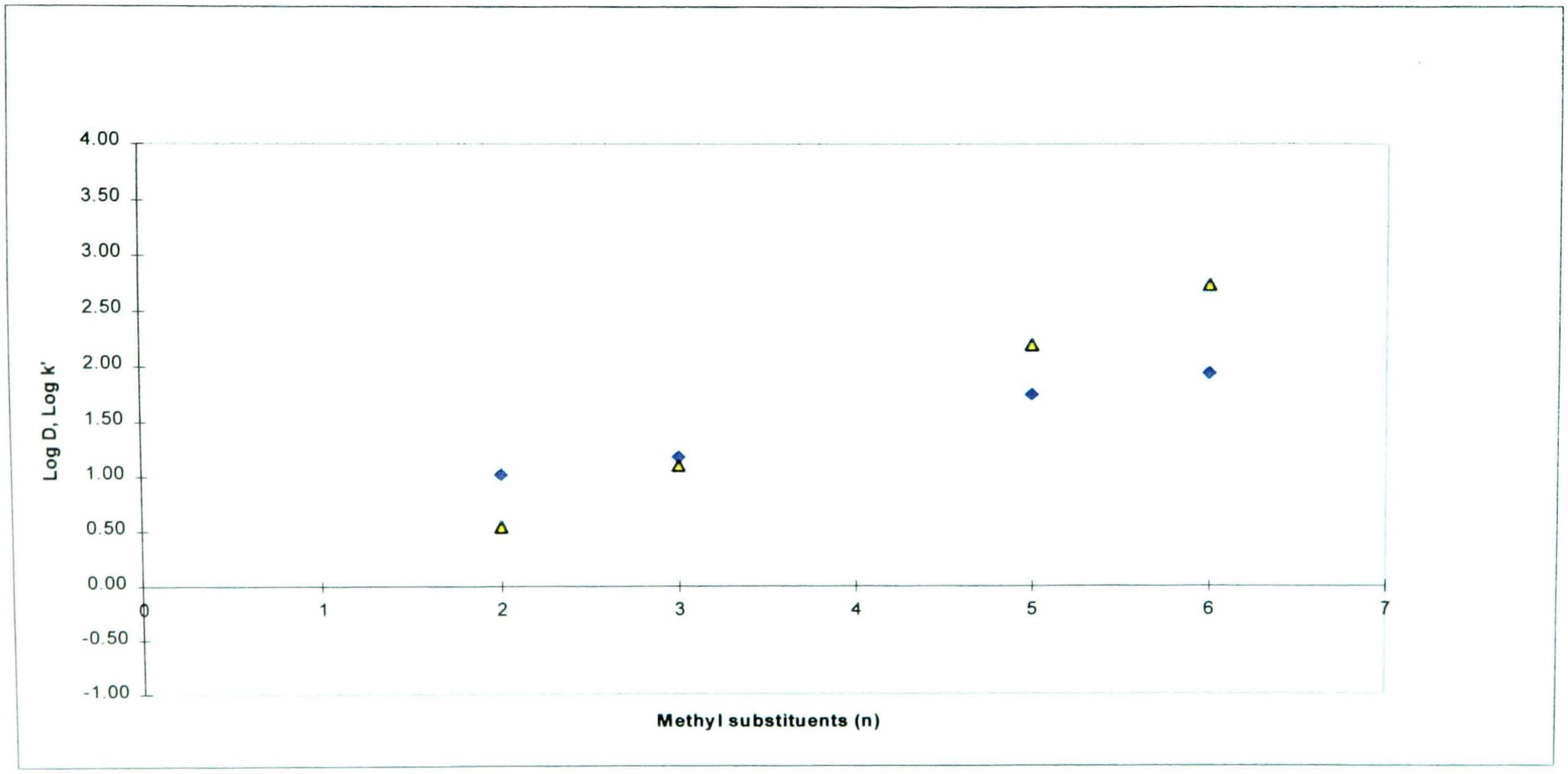

Diamonds - log D
Triangles – log k'

Fig 5.19c

Plot of log D , log k' vs the Number of Methyl Substituents for the Polymethylbenzenes in 90% Methanol:Water

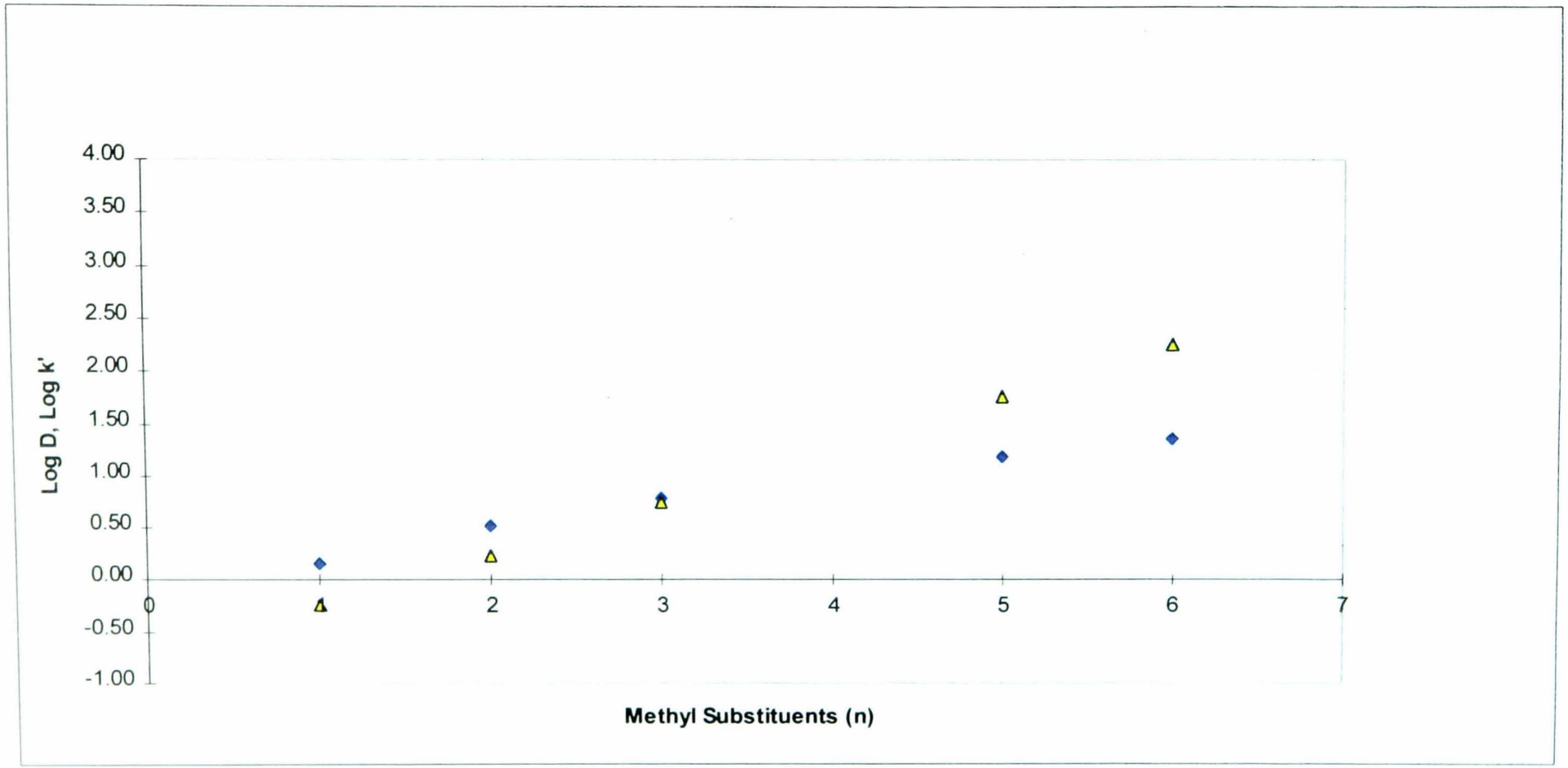

Diamonds - log D
Triangles – log k'

Fig 5.20

Plot of log k'/D vs $(CH_3)n$ for the Polymethylbenzenes

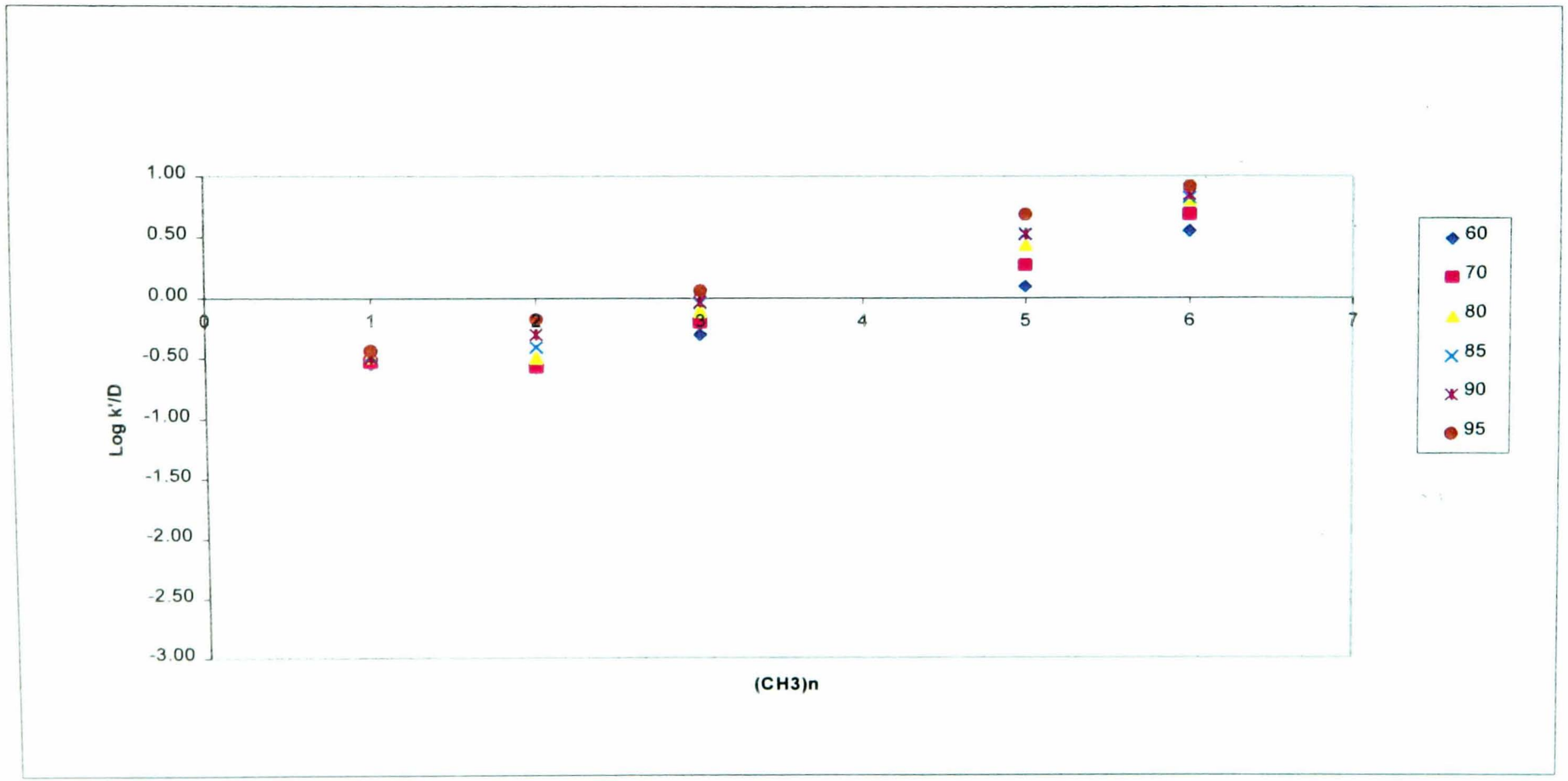

Fig 5.21

Comparison of Selectivity (α) for PGC and Hexane vs Methanol:Water Composition for the Polymethylbenzenes

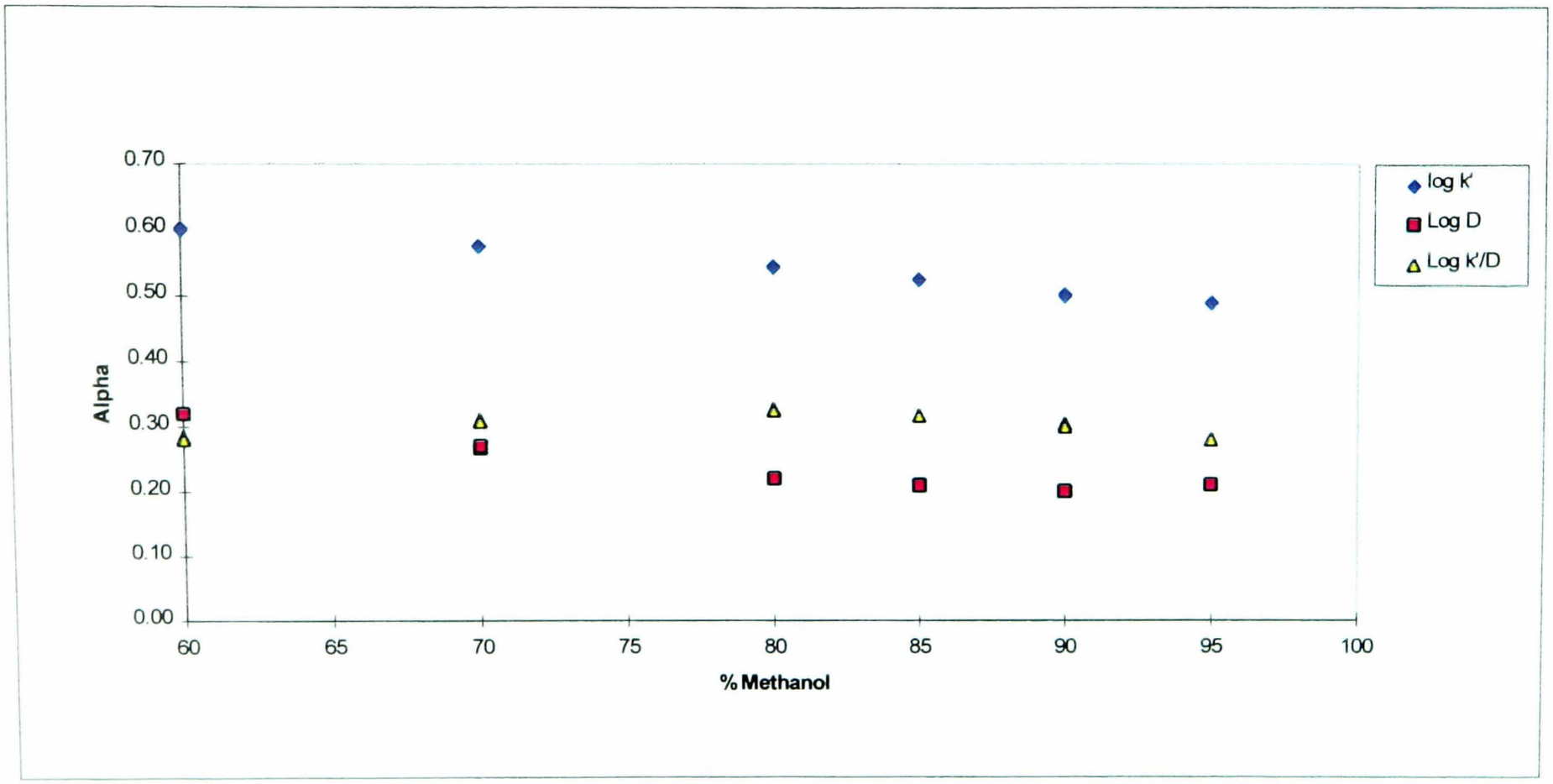

Fig 5.22

Log D , Log k' vs $(-CH_3)n$ for the Polymethylbenzenes at 90% and 60 % Methanol:Water

(a)

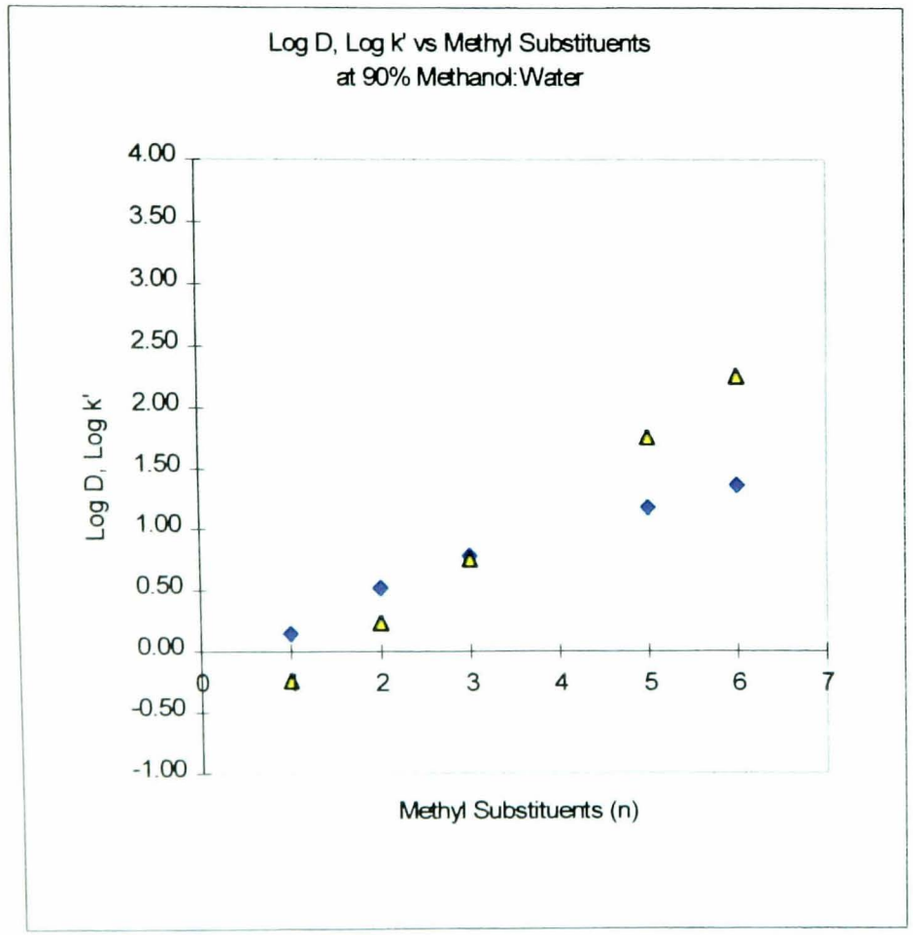

(b)

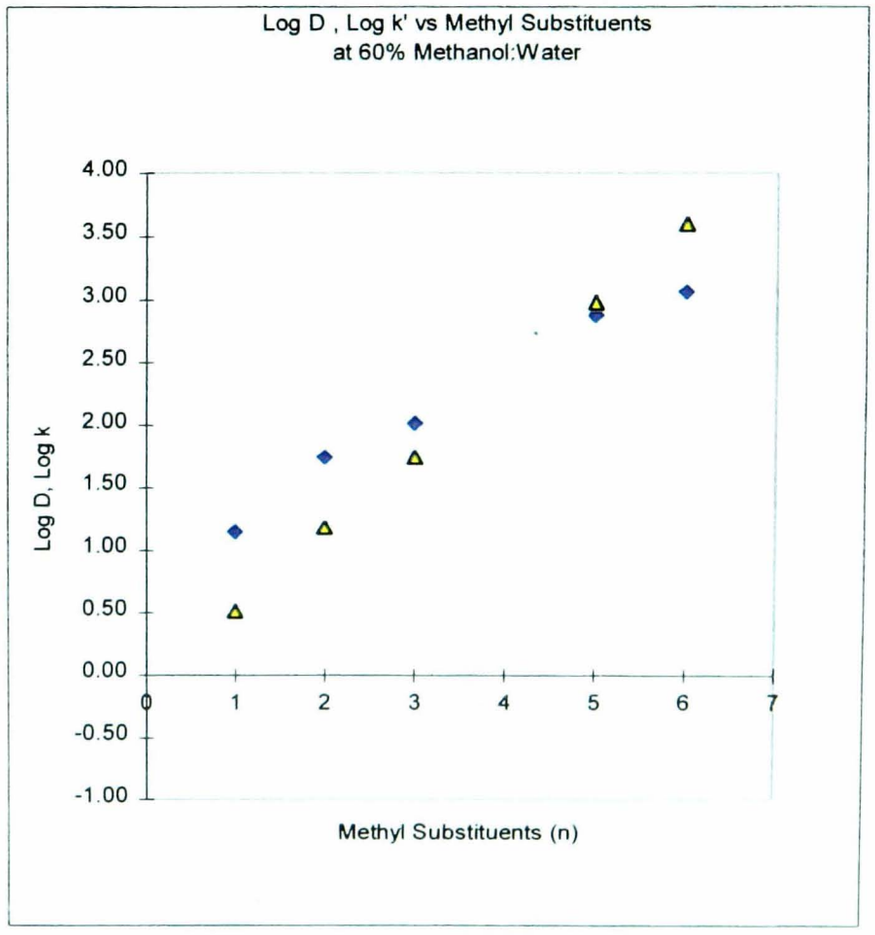

Fig 5.23

Comparison of Retention Behaviour for the Polymethylbenzenes in Both Methanol:Water and Methanol:Water with hexane

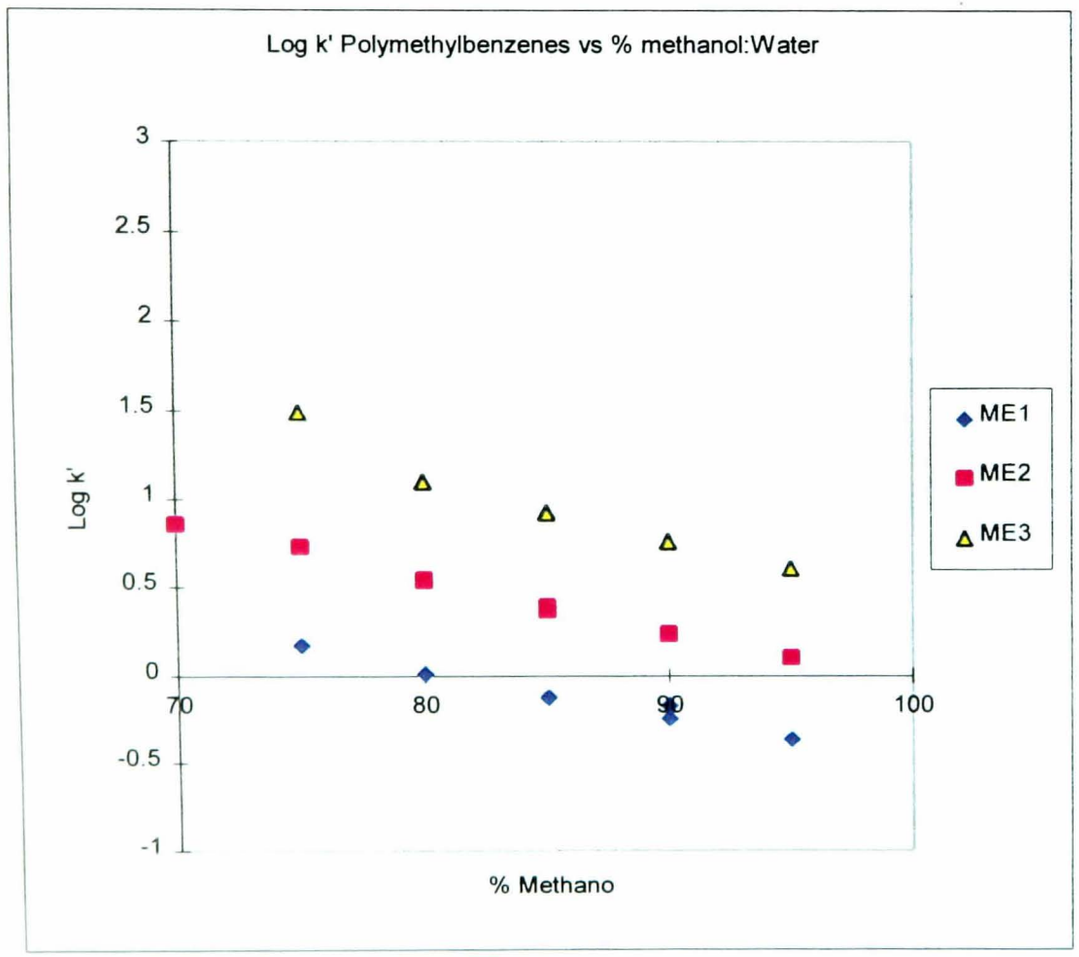

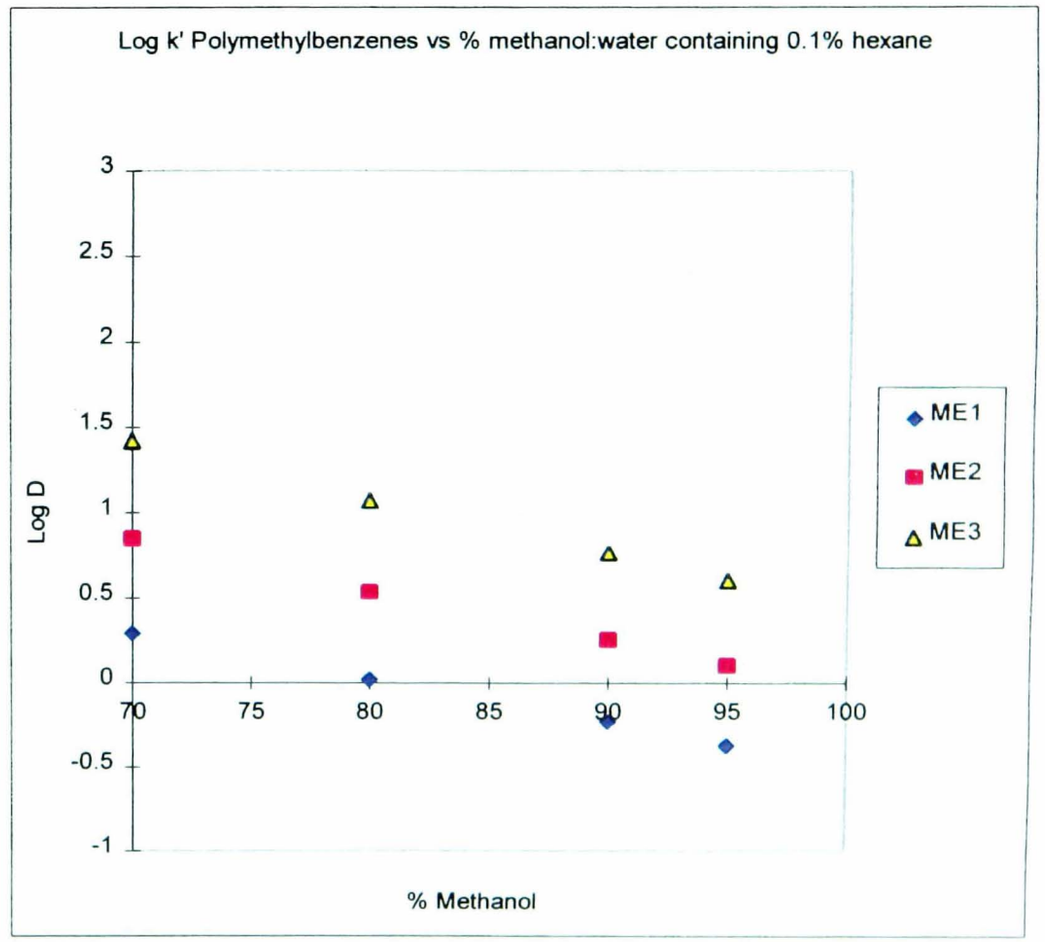

Fig 5.24

Summary Chart Showing a Plot of log k'PGC , log D and log k'C18 vs Homologue Carbon Number - $(CH_2)n$ and $(CH_3)n$

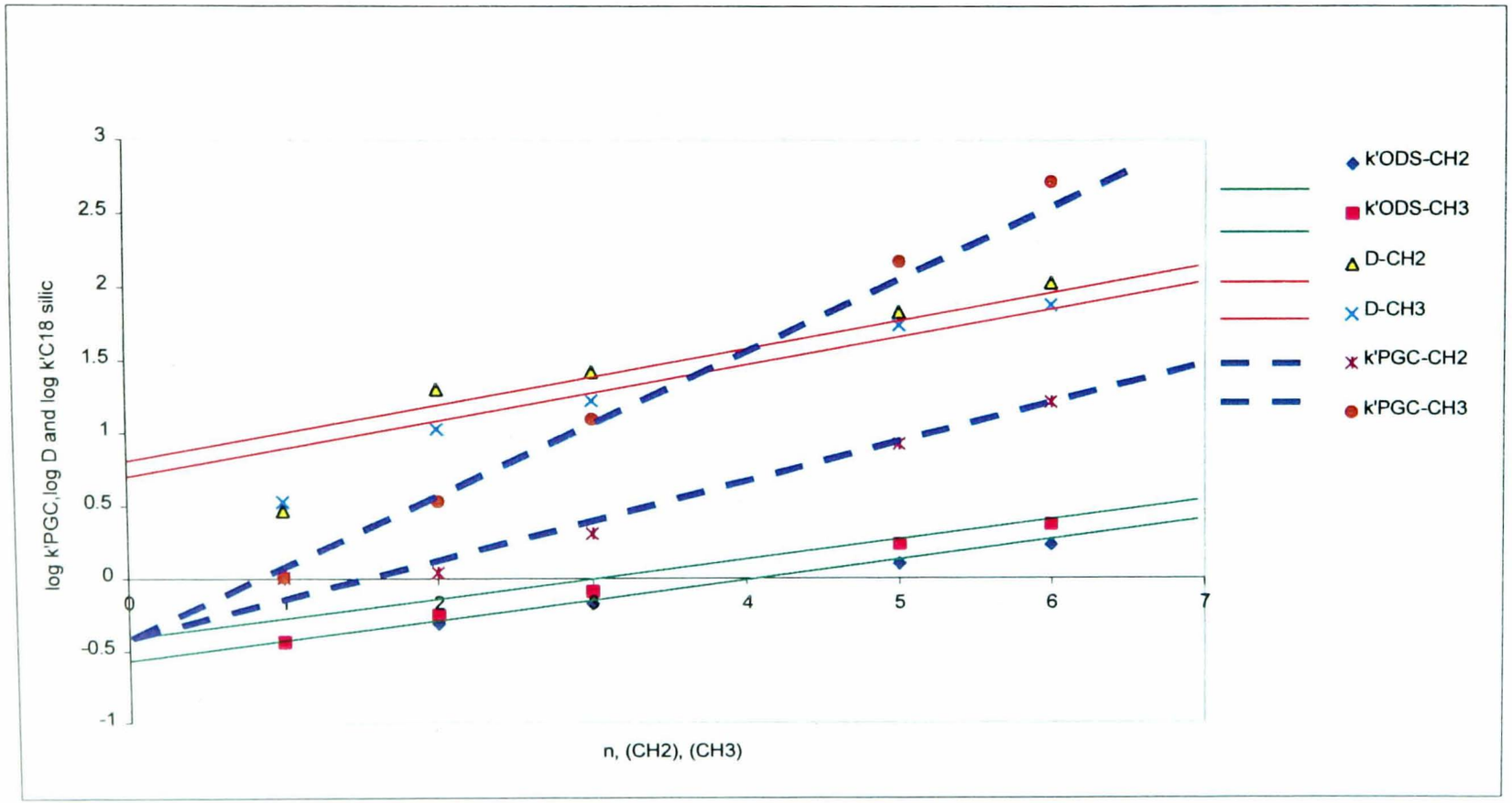

Fig 5.25

Summary Chart Showing log k'PGC, log D, log k'C18 and log P vs Homologue Carbon Number -(CH_2)n and (CH_3)n

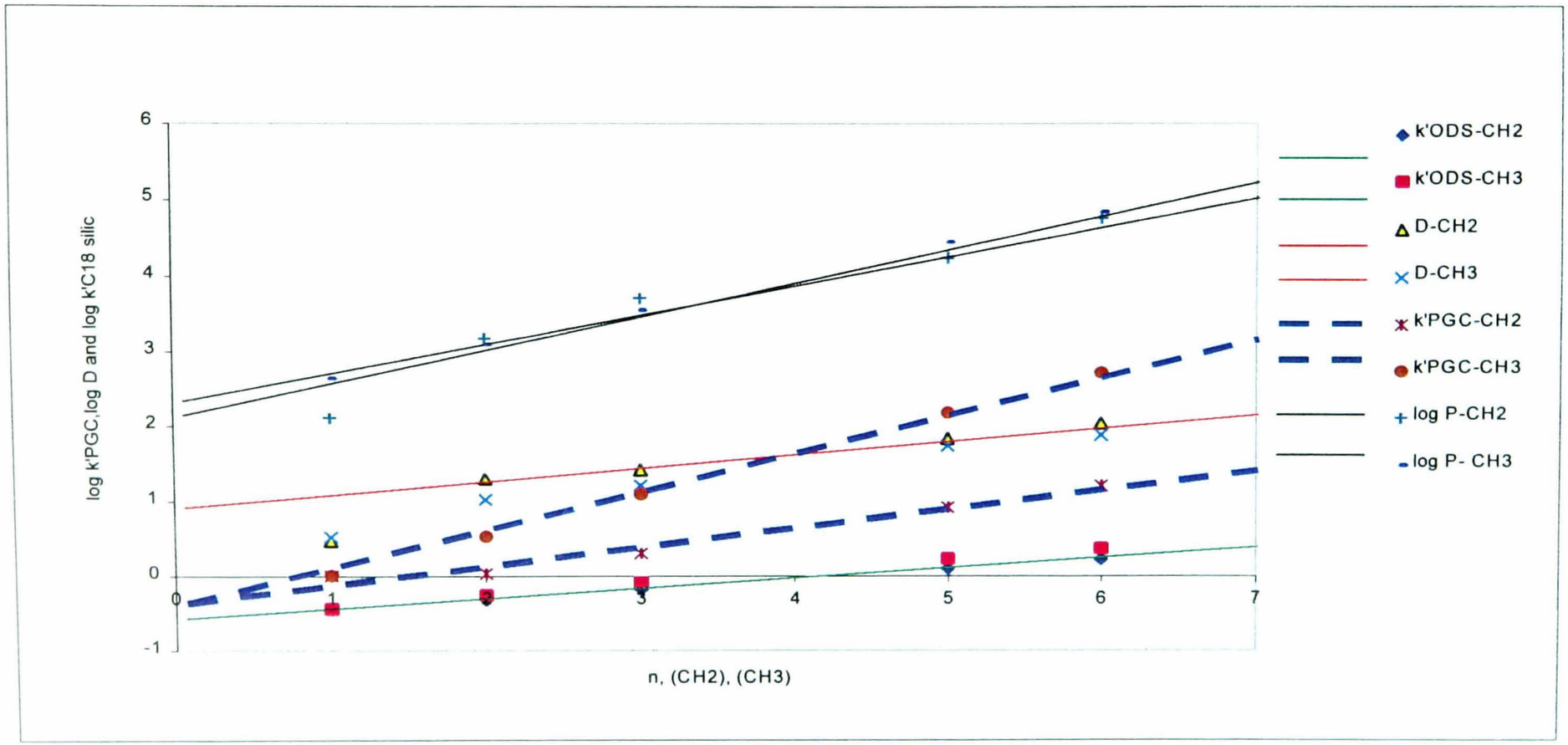

Fig 5.26

Comparison of Selectivity for Equivalent Hydrocarbons, Alkylbenzenes and Polymethylbenzenes on PGC and in Hexane

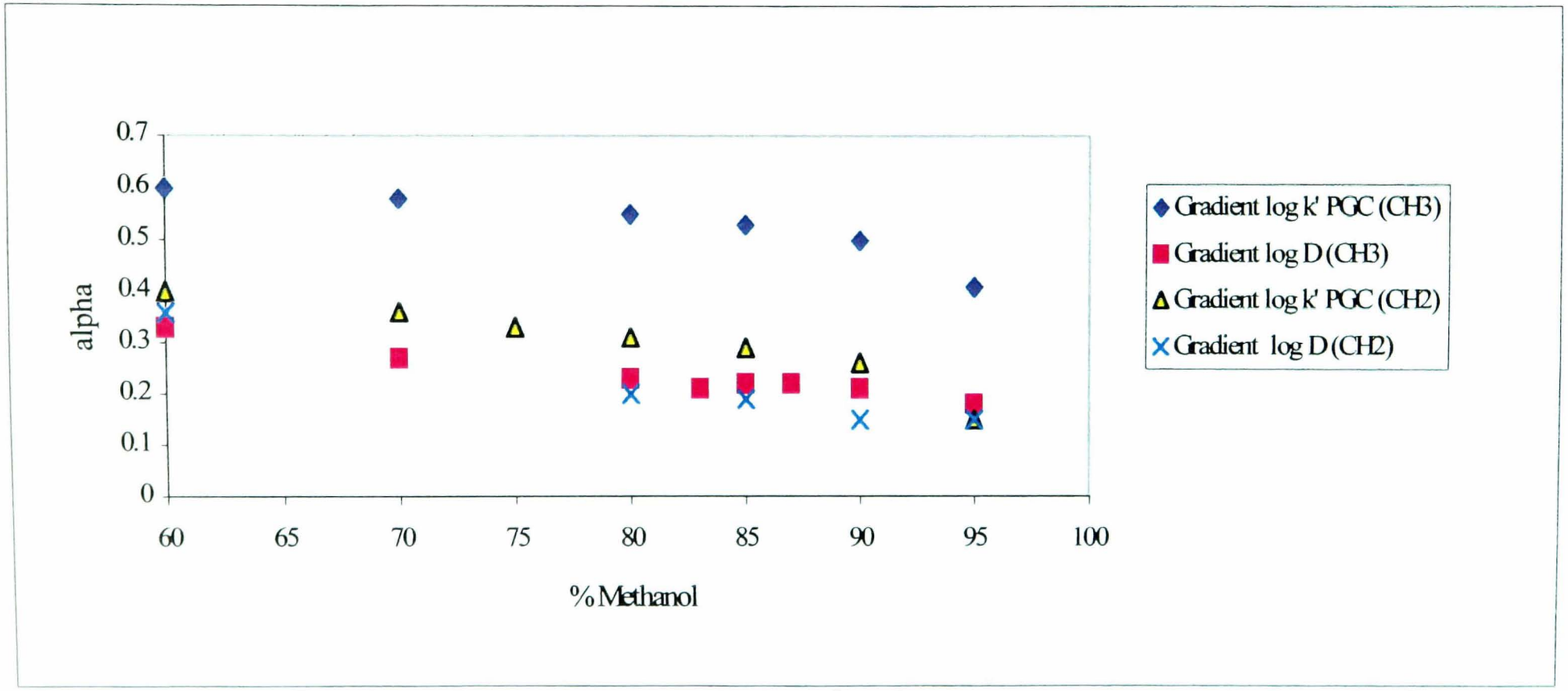

Fig 5.27

Plot of log k' Hydroxybenzenes vs % Methanol :Water

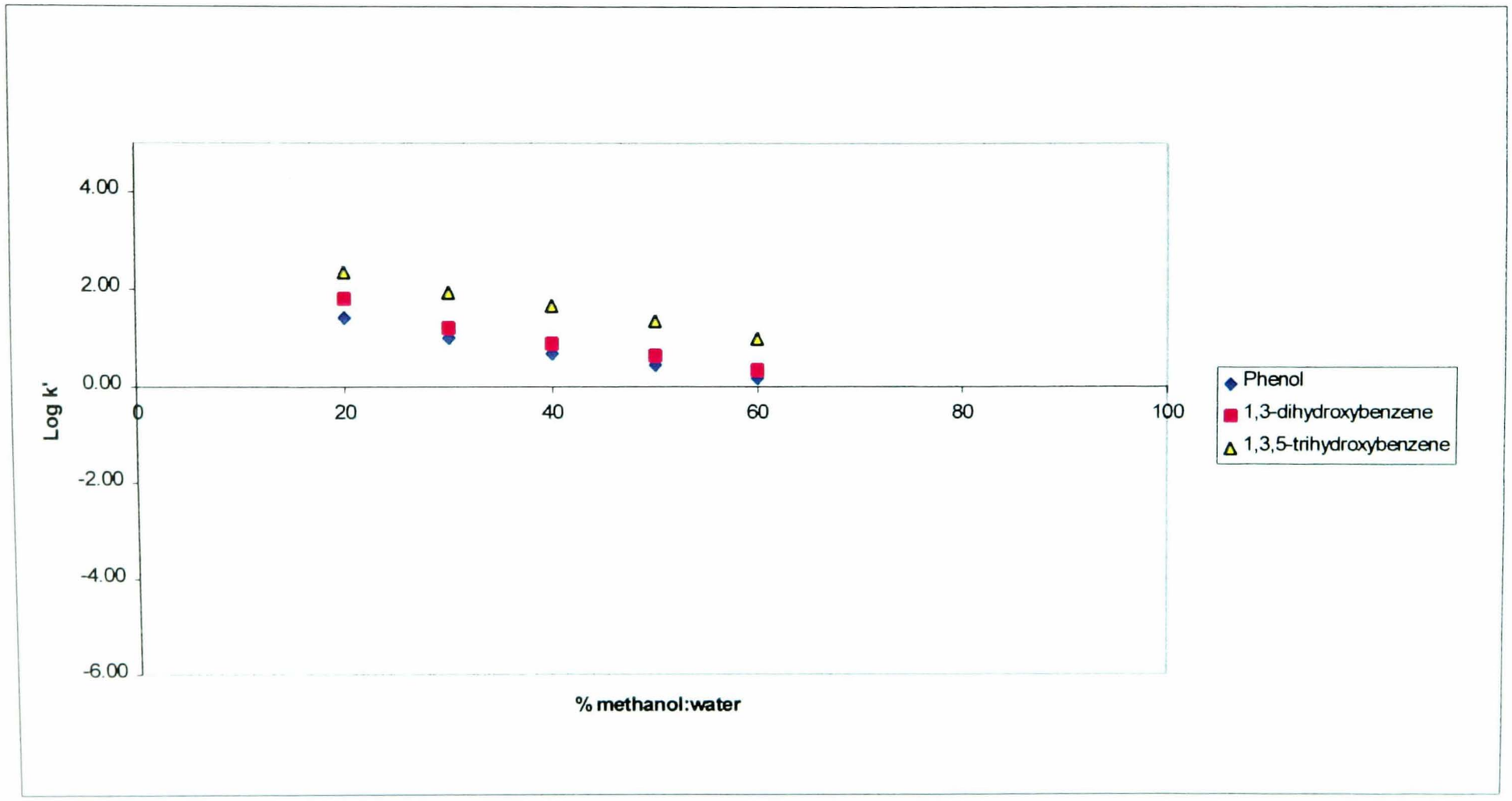

Fig 5.28

Plot of log D Hydroxybenzenes vs % Methanol:Water

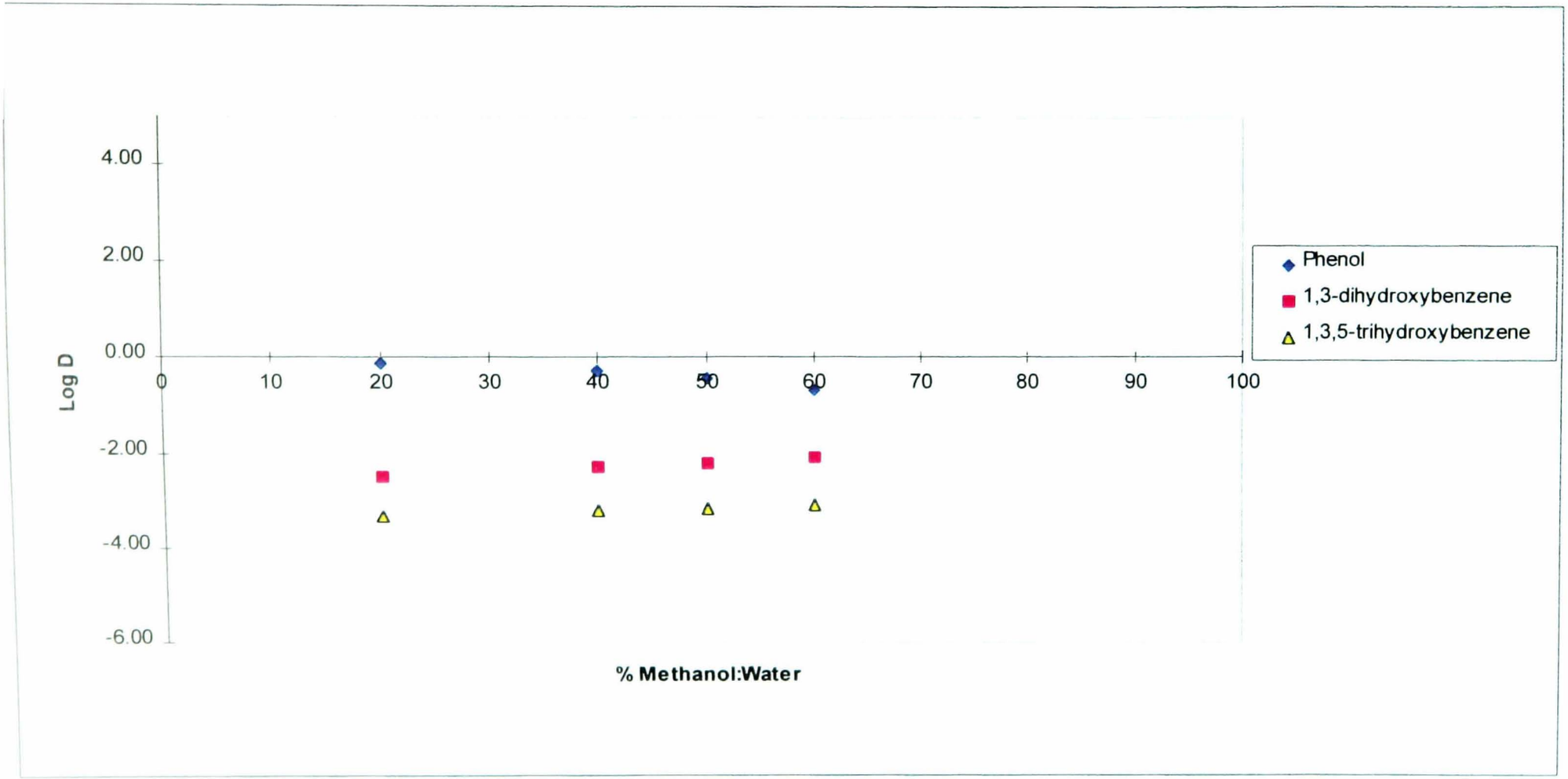

Fig 5.29

Plot of Log k'/D Hydroxybenzenes vs % Methanol:Water

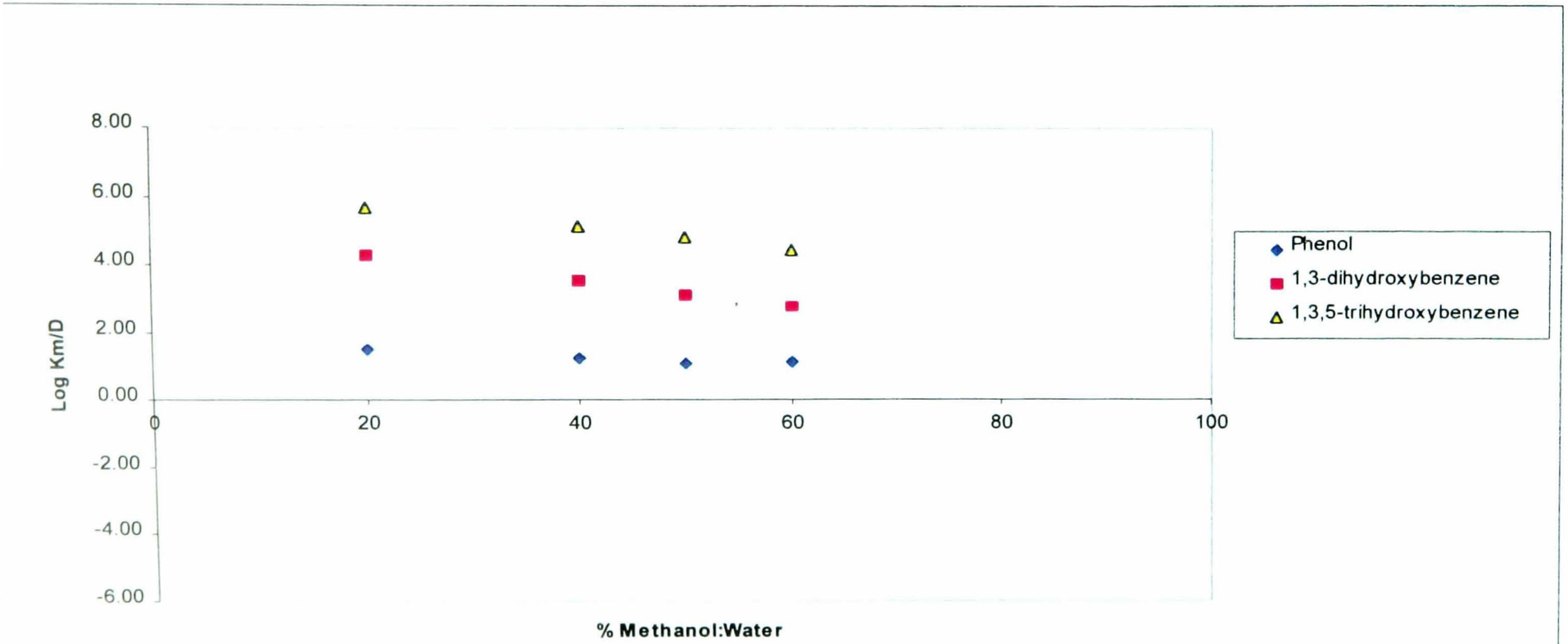

Fig 5.30

Comparison of Retention Behaviour of the Hydroxybenzenes in Both Methanol:Water Compositions and Methanol:Water Compositions with Hexane

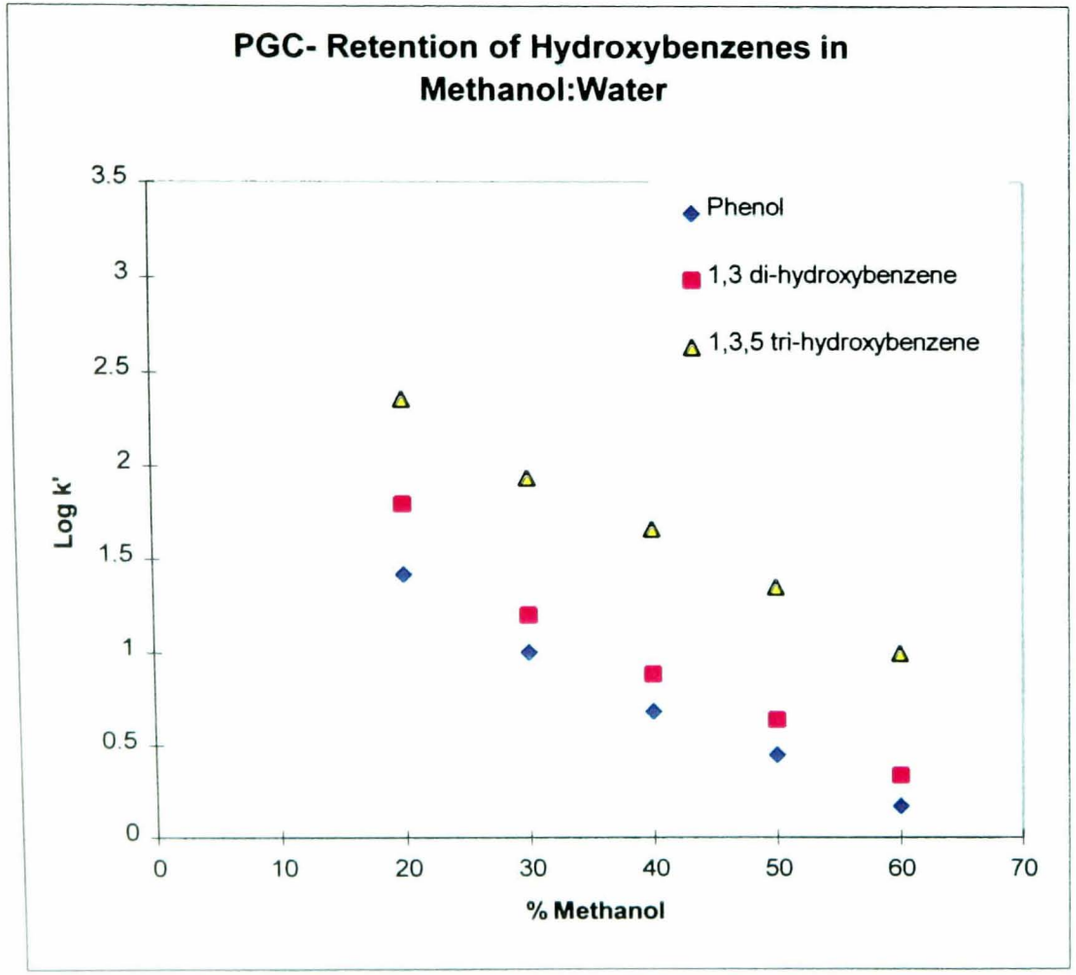

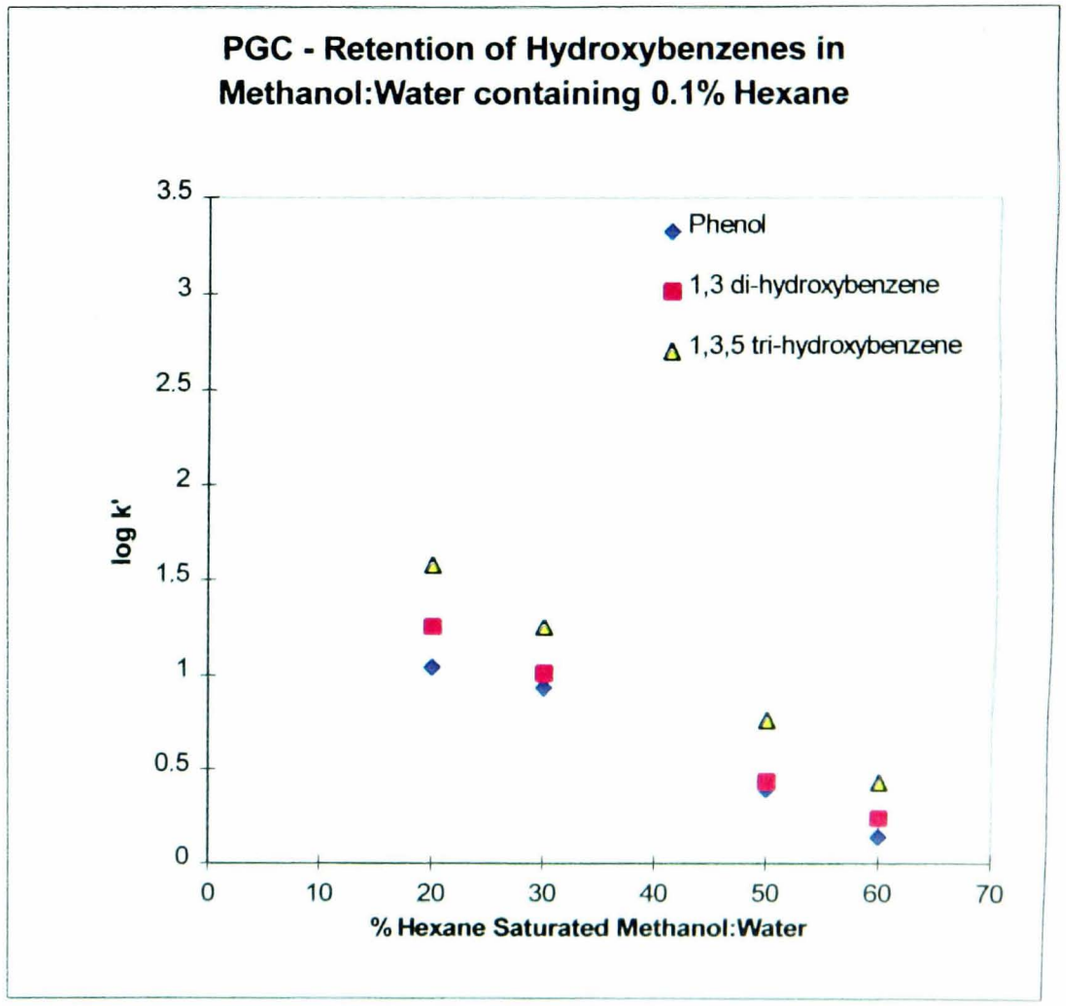

Fig 5.31

Plot of Log k' Anilines vs % Methanol:Water

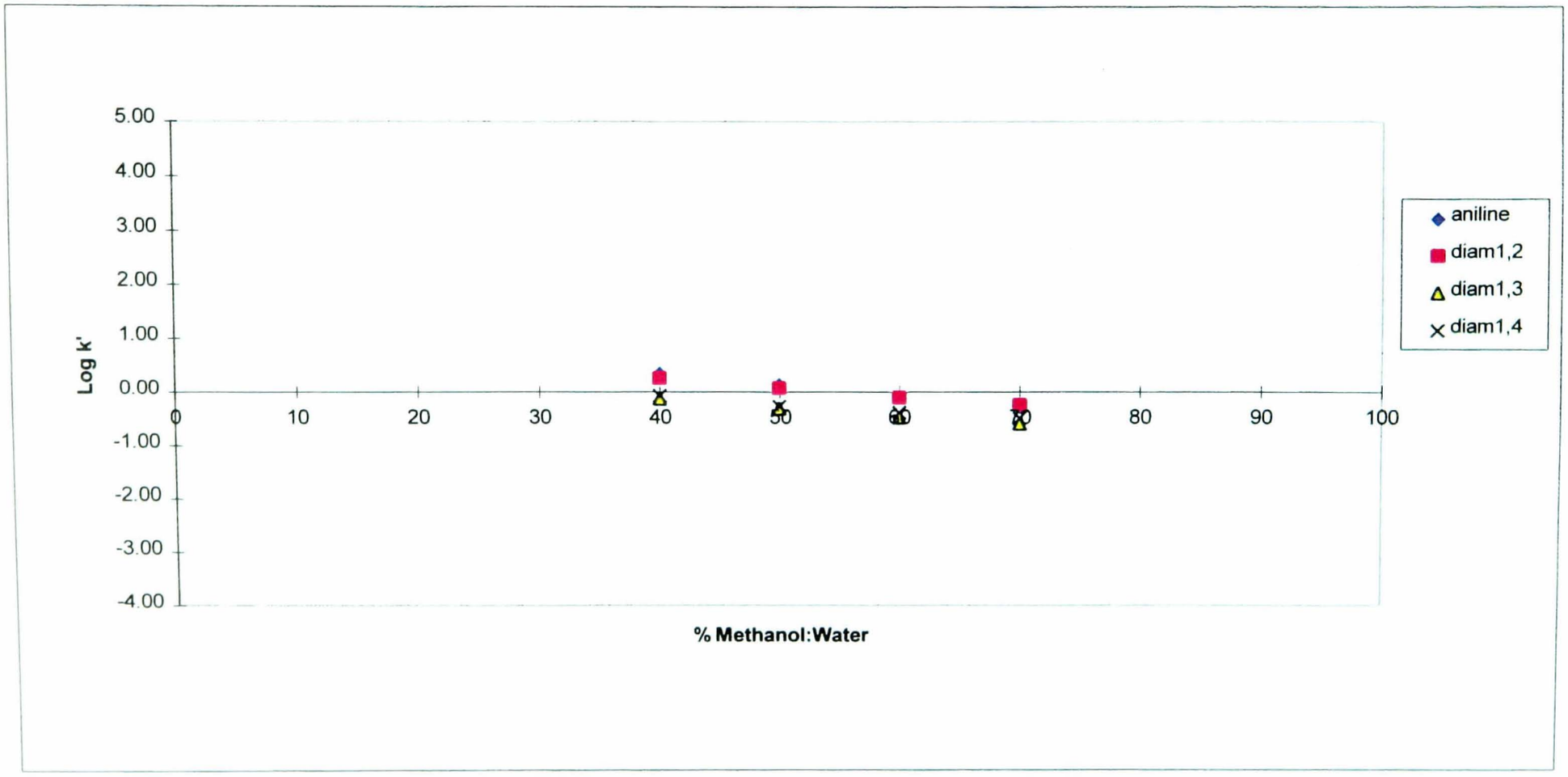

'diam' is used as the abbreviation for phenylenediamine

Fig 5.32

Plot of log D Anilines vs % Methanol:Water

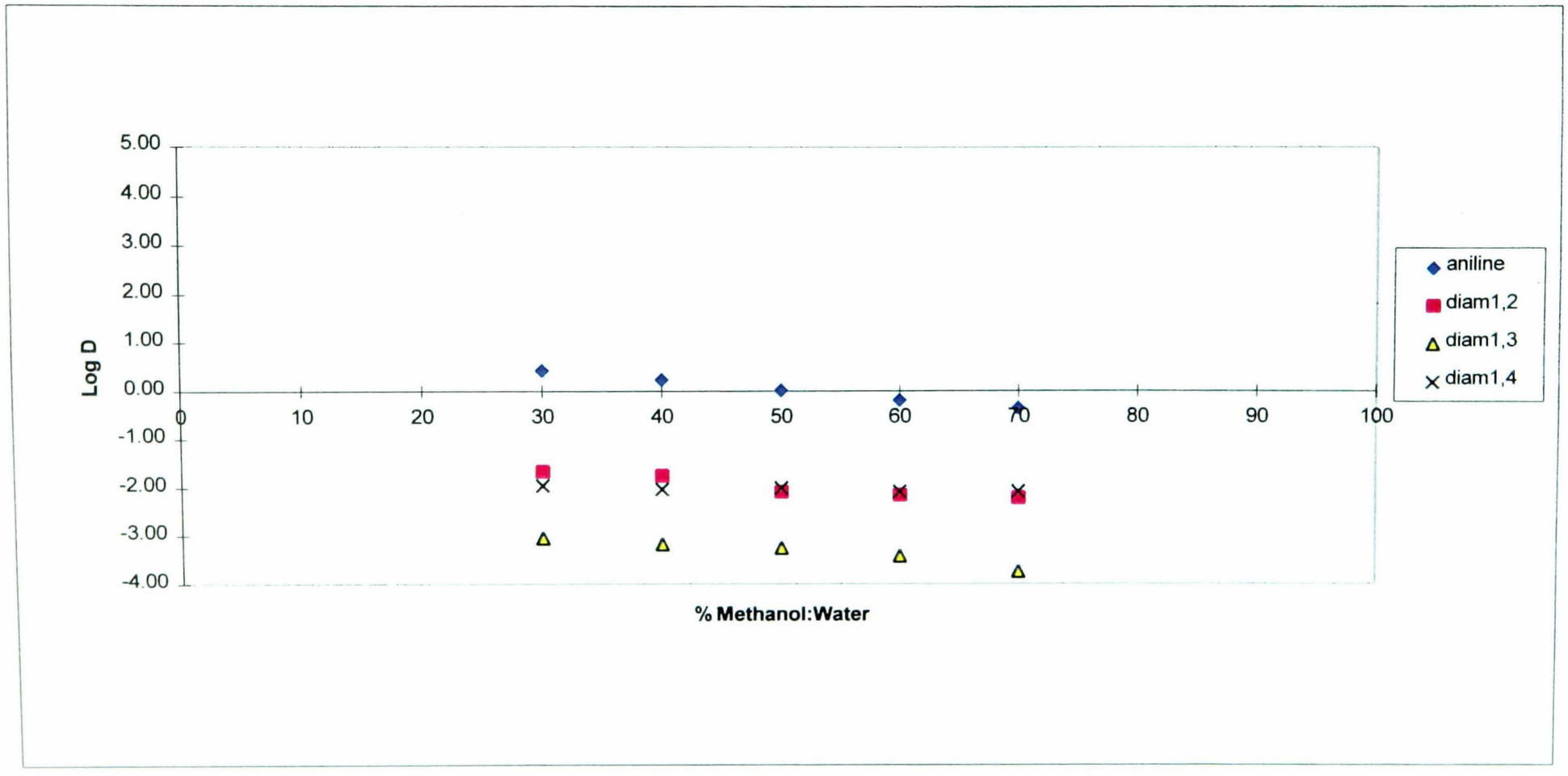

'diam' is used as the abbreviation for phenylenediamine

Fig 5.33

Plot of log k'/D Anilines vs % Methanol:Water

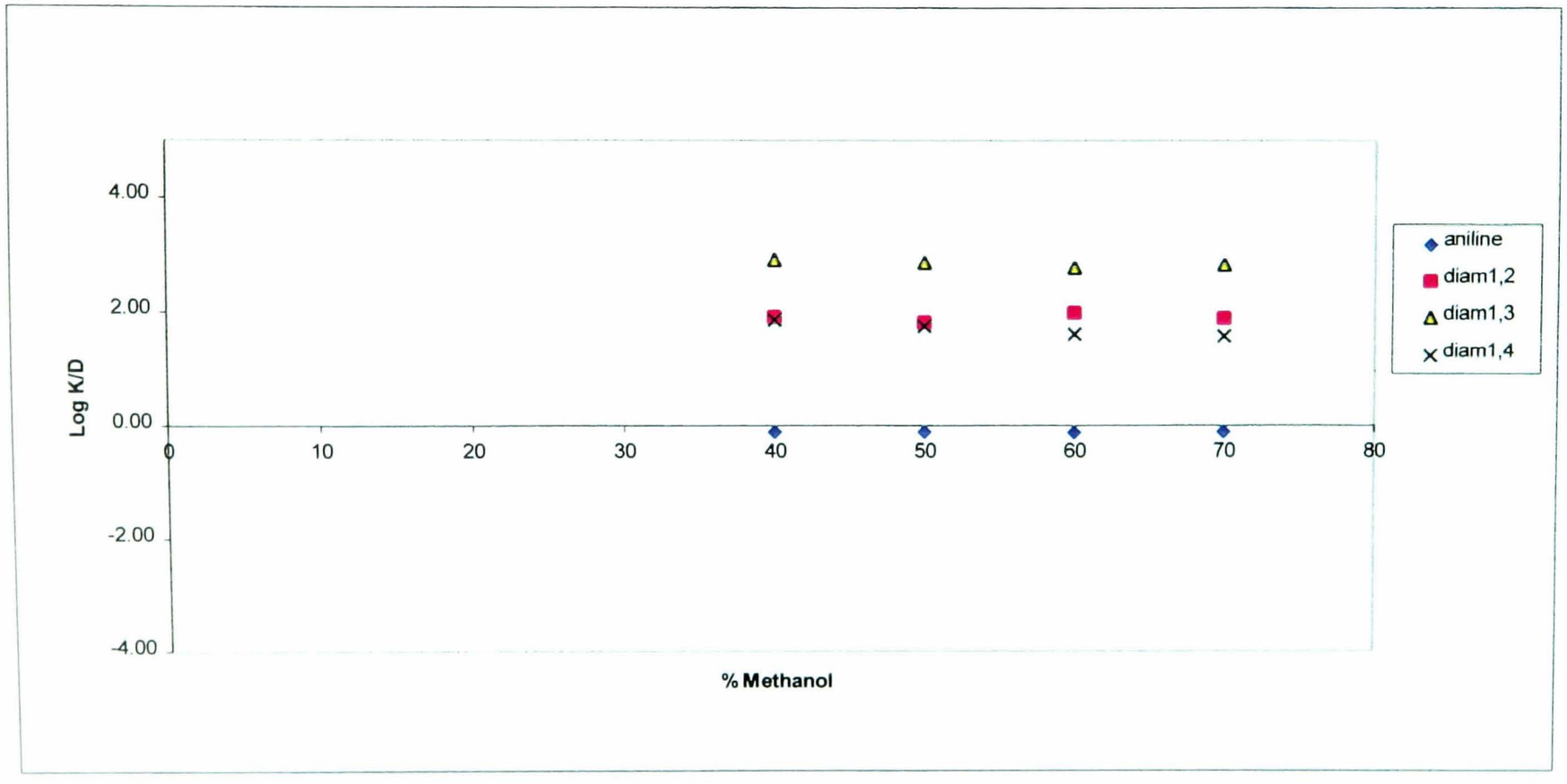

'diam' is used as the abbreviation for phenylenediamine

Fig 5.34

Plot of log k' vs % Methanol:Water for Other Mono-Substituted Benzenes

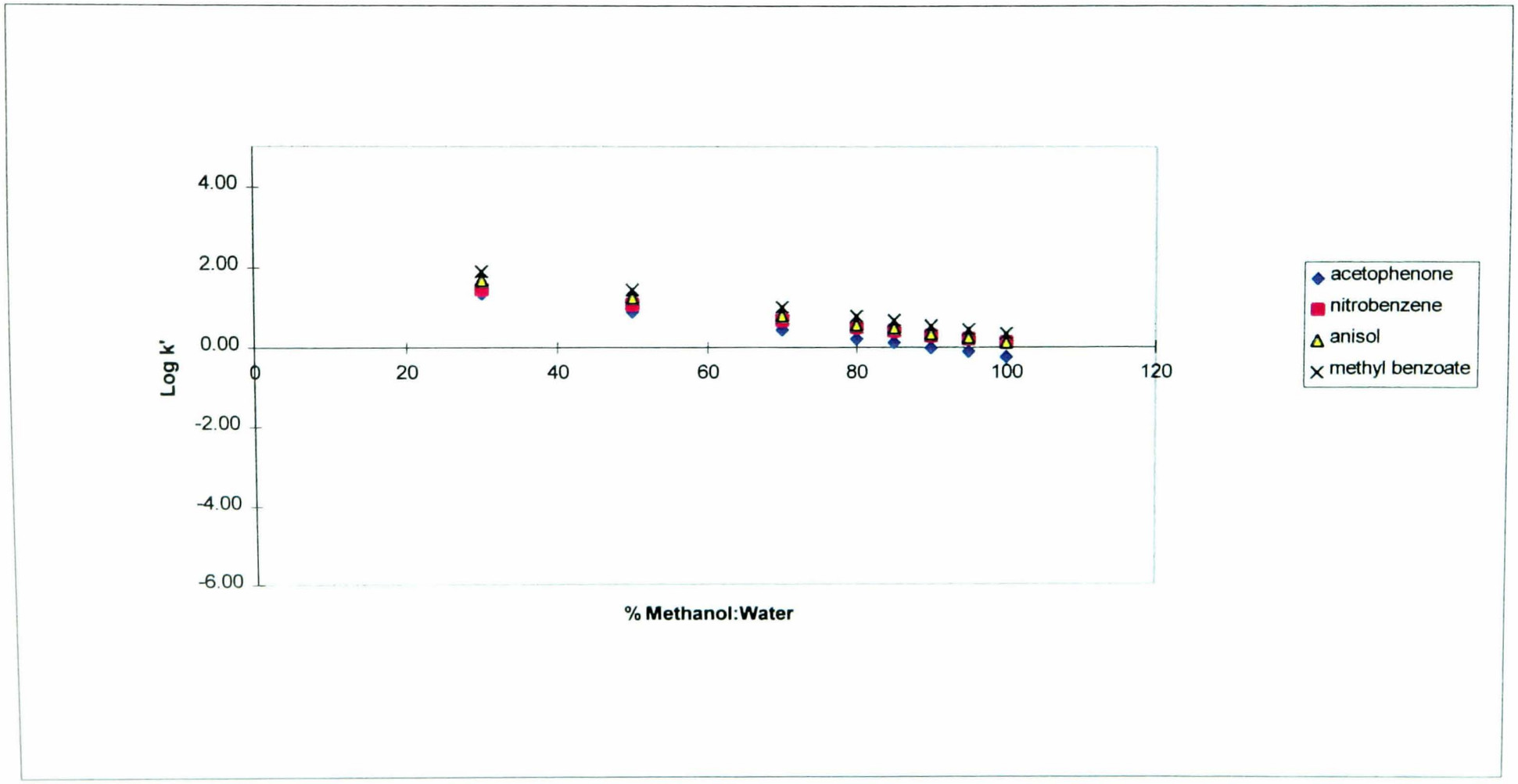

Fig 5.35

Plot of log D vs % Methanol:Water for Other Mono-Substituted Benzenes

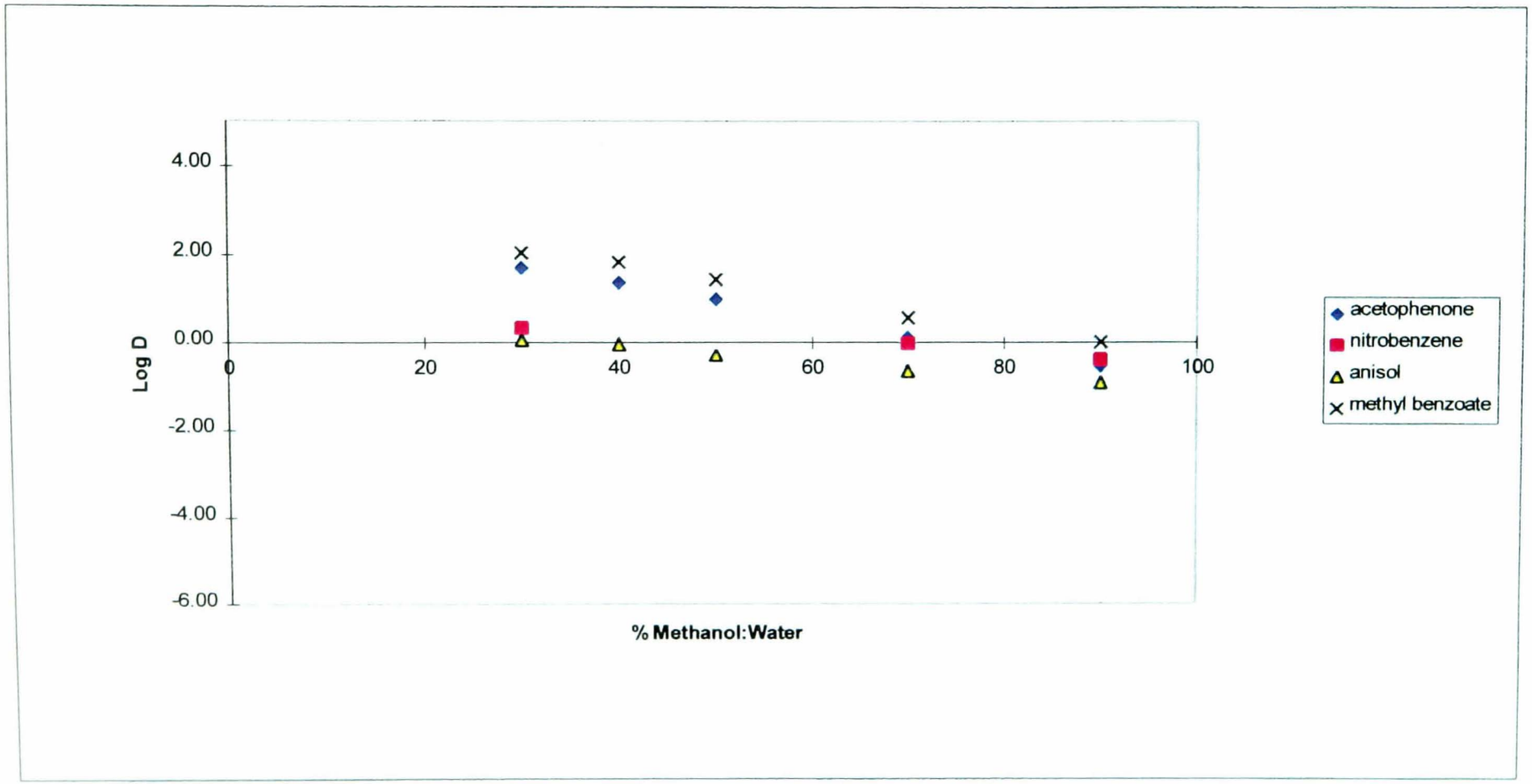

Fig 5.36

Plot of log k'/D vs % Methanol:Water for Other Mono-Substituted Benzenes

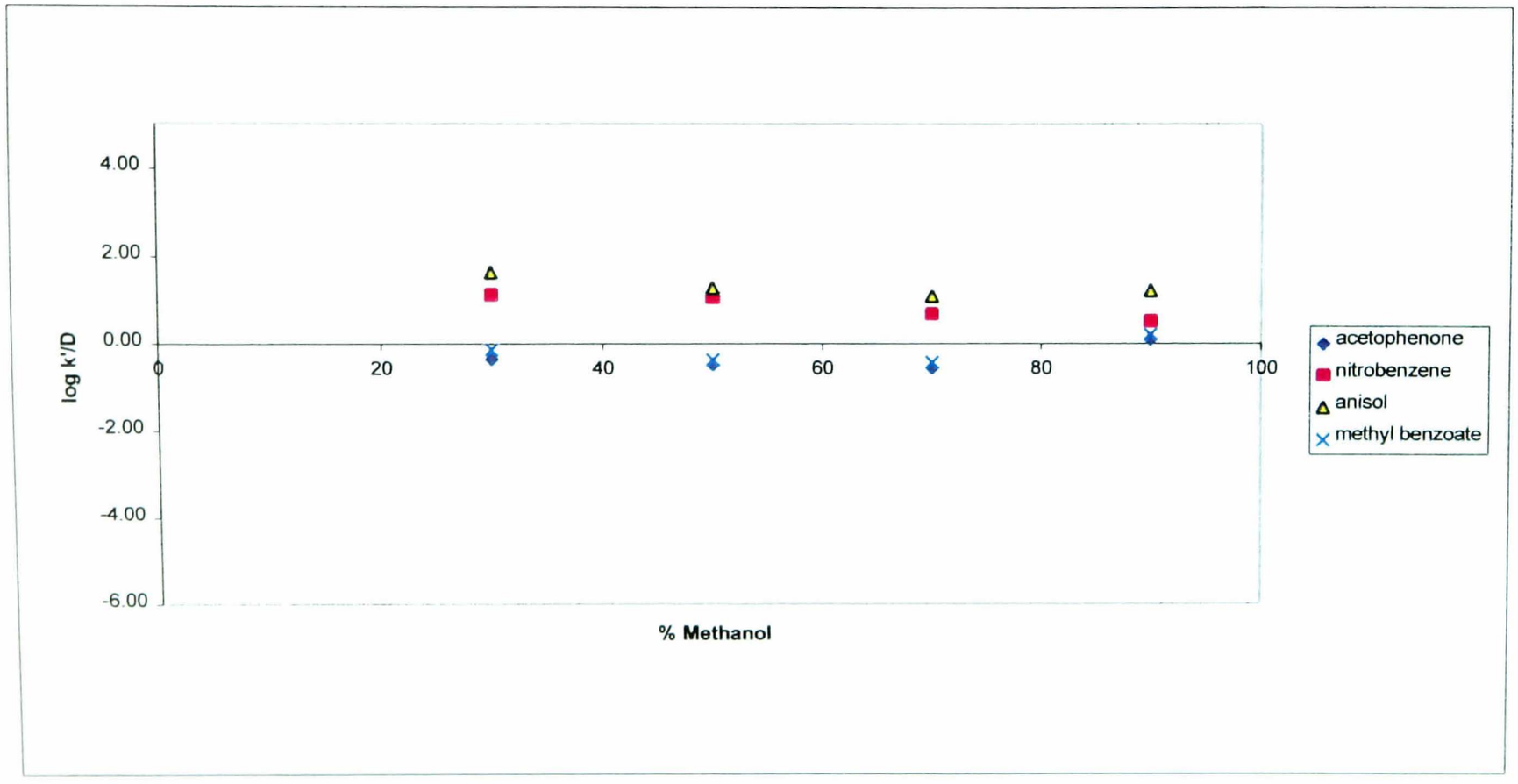

Fig 5.37

Plot of log k' Halobenzenes vs % Methanol:Water

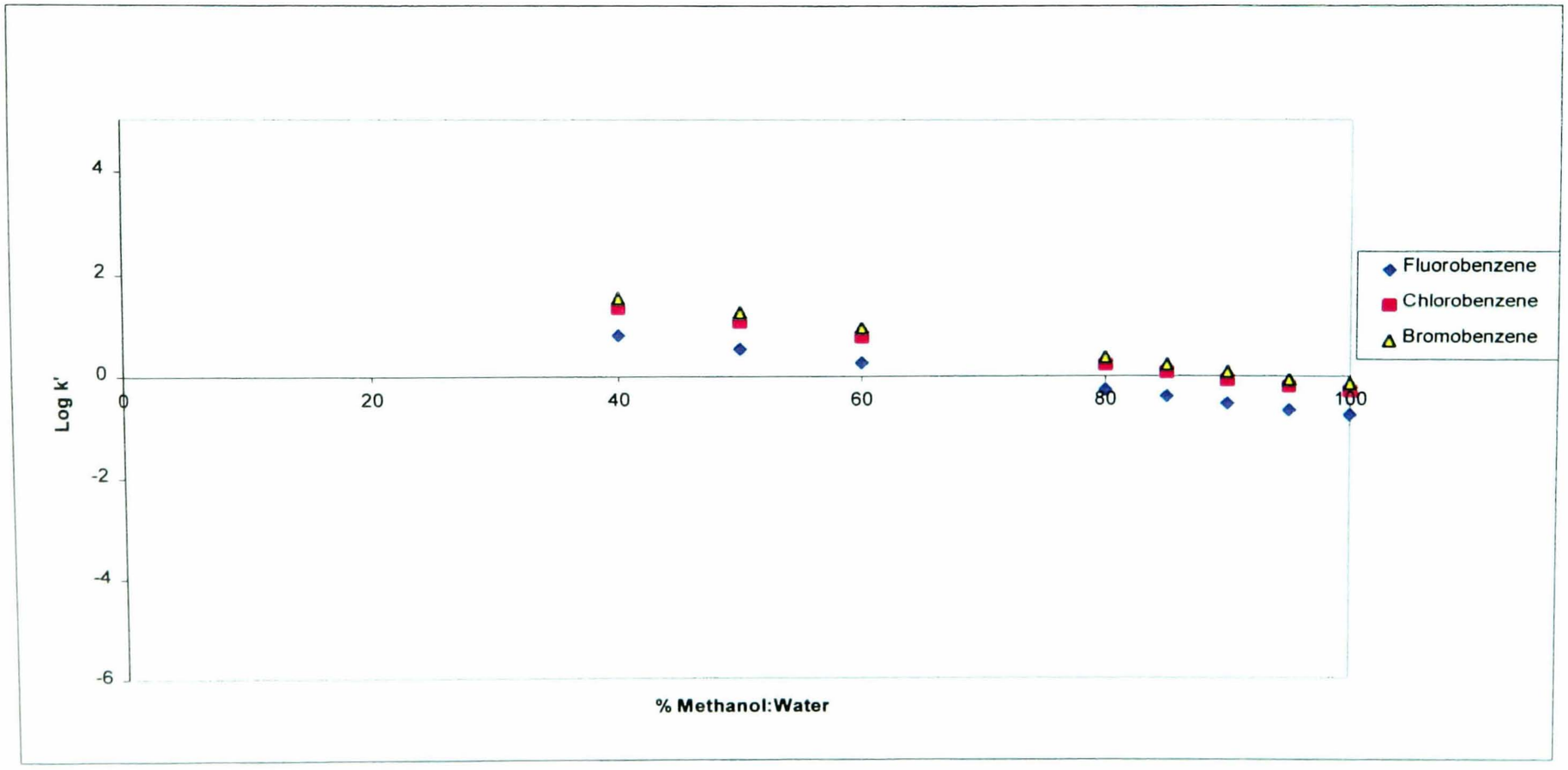

Fig 5.38a

Plot of log D Halobenzenes vs % Methanol:Water

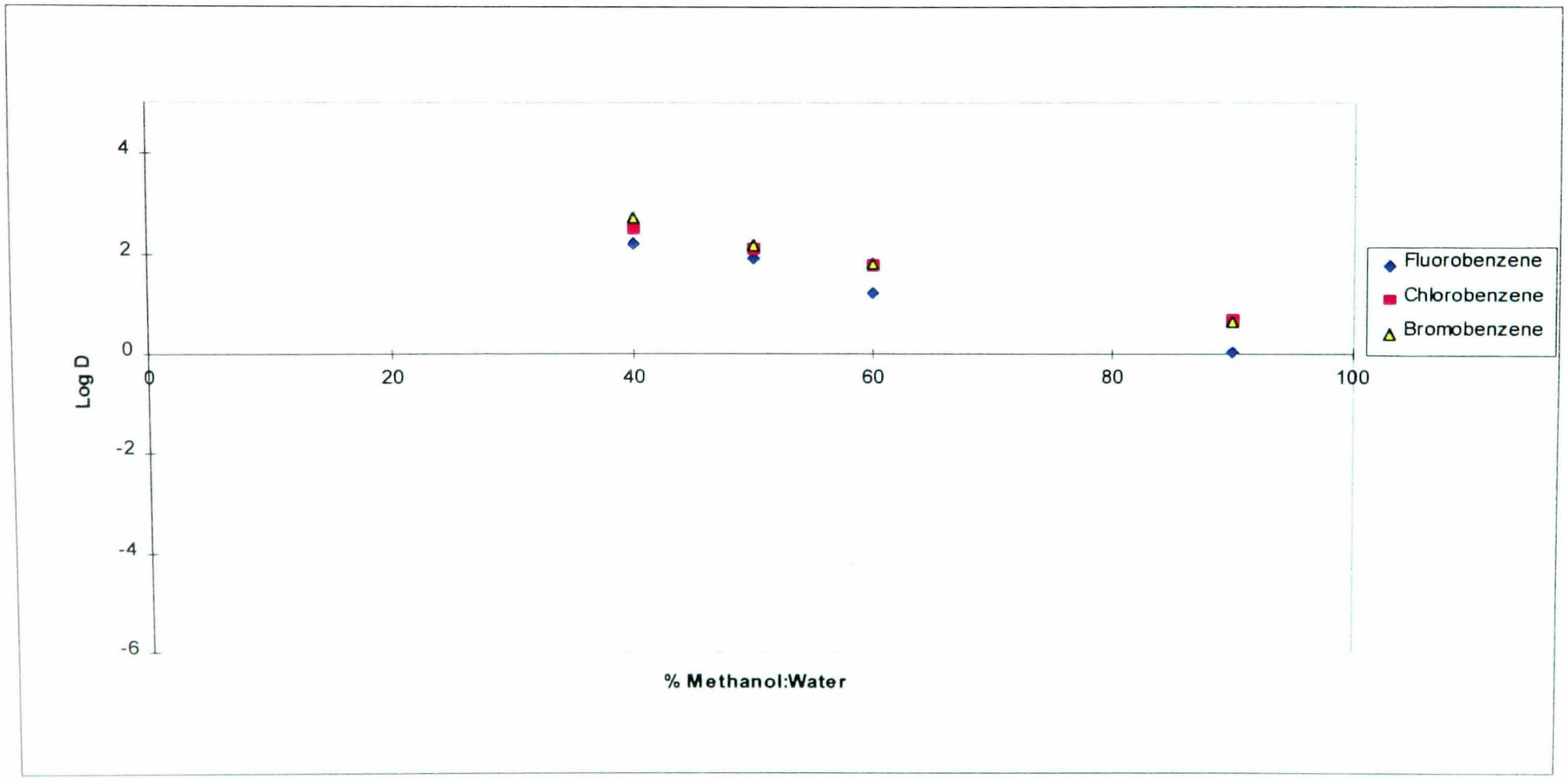

Table 5.38b
Equivalent Hydrocarbons

	Analyte	True Equivalent Hydrocarbon	Actual Equivalent Hydrocarbon
Phenol	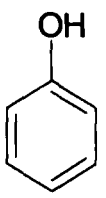	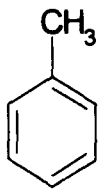	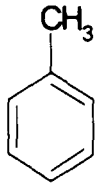
1,3 dihydroxyphenol	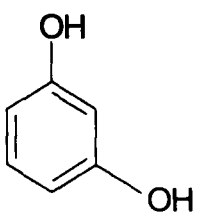	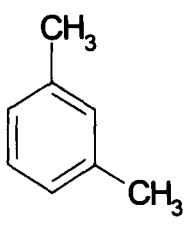	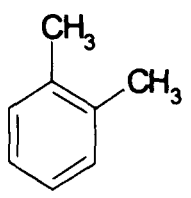
1,3,5 trihydroxyphenol	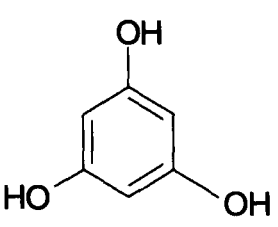	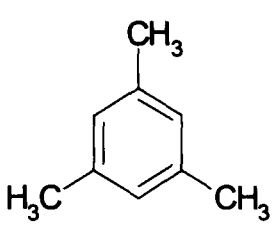	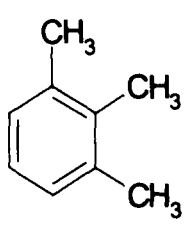
Aniline	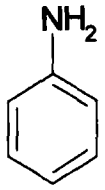	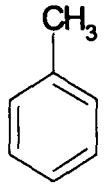	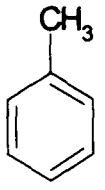
1,2 Phenylenediamine	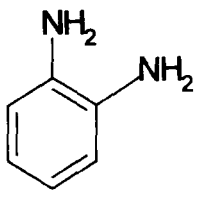	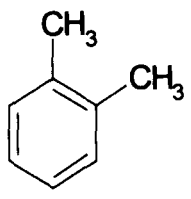	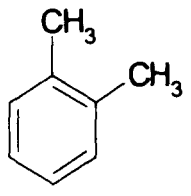
1,3 Phenylenediamine	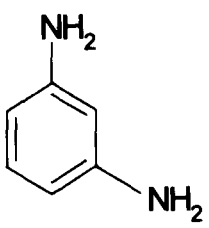	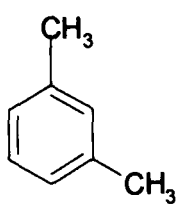	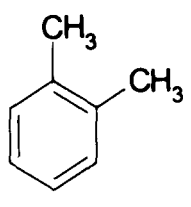
1,4 Phenylenediamine	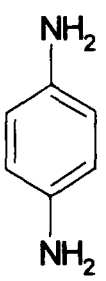	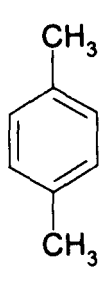	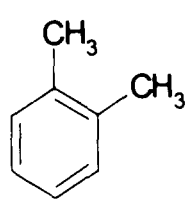

Table 5.38b
Equivalent Hydrocarbons ...Continued

	Analyte	True Equivalent Hydrocarbon	Actual Equivalent Hydrocarbon
Benzoic Acid	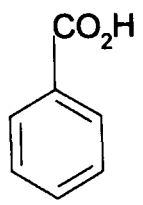	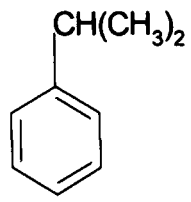	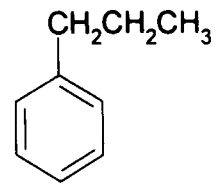
1,2-carboxybenzene	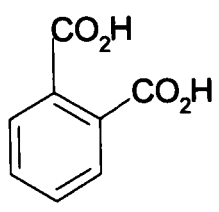	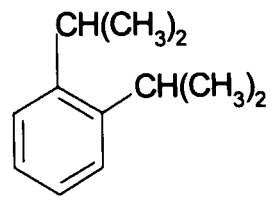	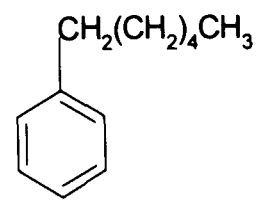
1,2,4-Carboxybenzenei	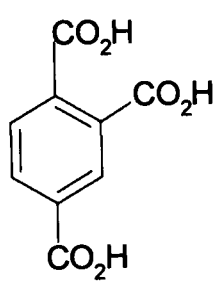	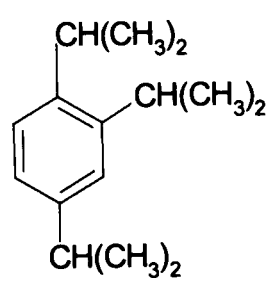	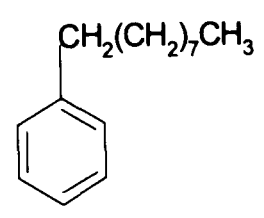

Fig 5.39

Plot of log k'/D Halobenzenes vs % Methanol:Water

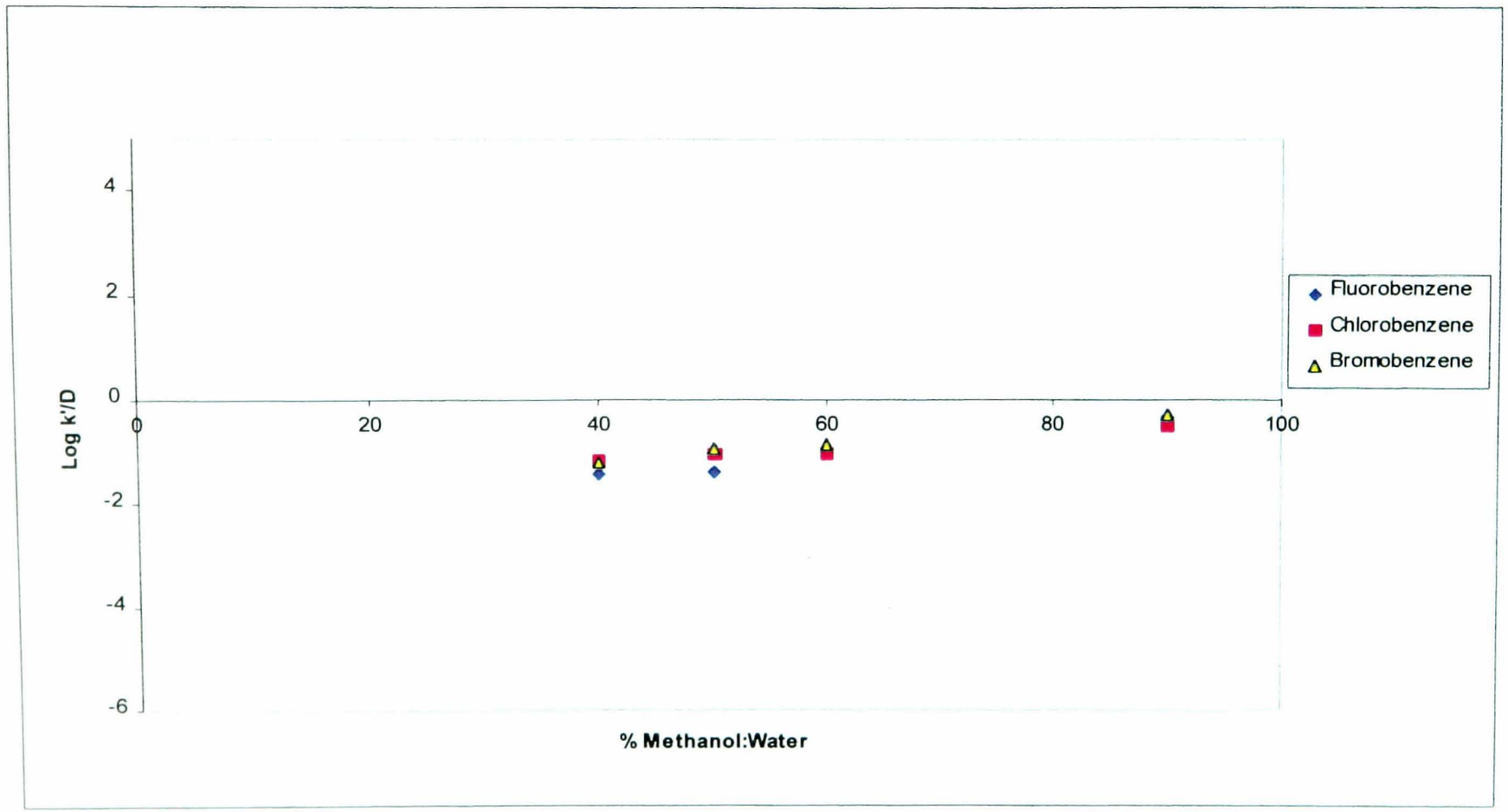

Fig 5.40

Plot of log k' for Benzen e Carboxylic Acids vs % Methanol:Water

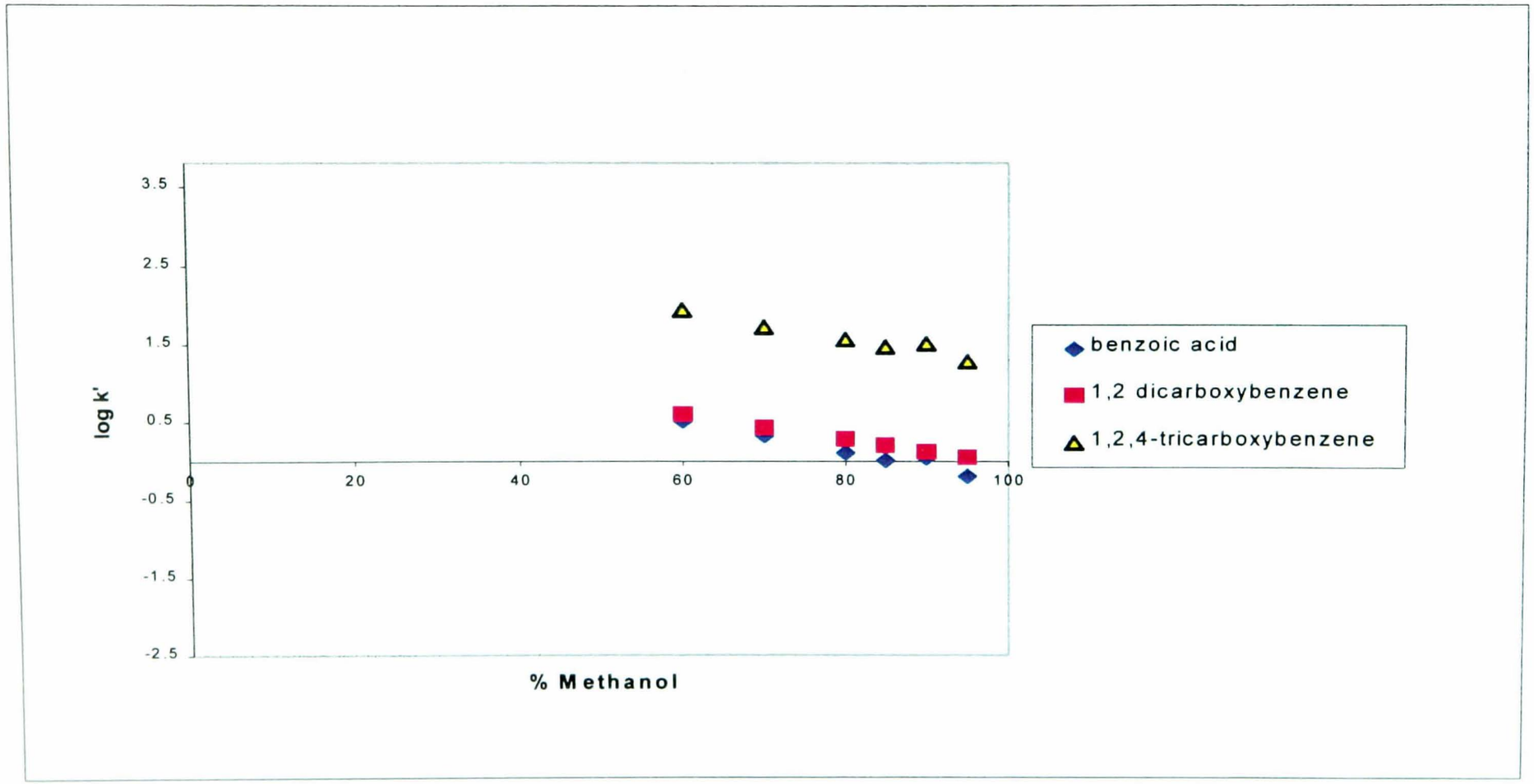

Fig 5.41
Plot of log D for Benzene Carboxylic Acids vs % Methanol:Water

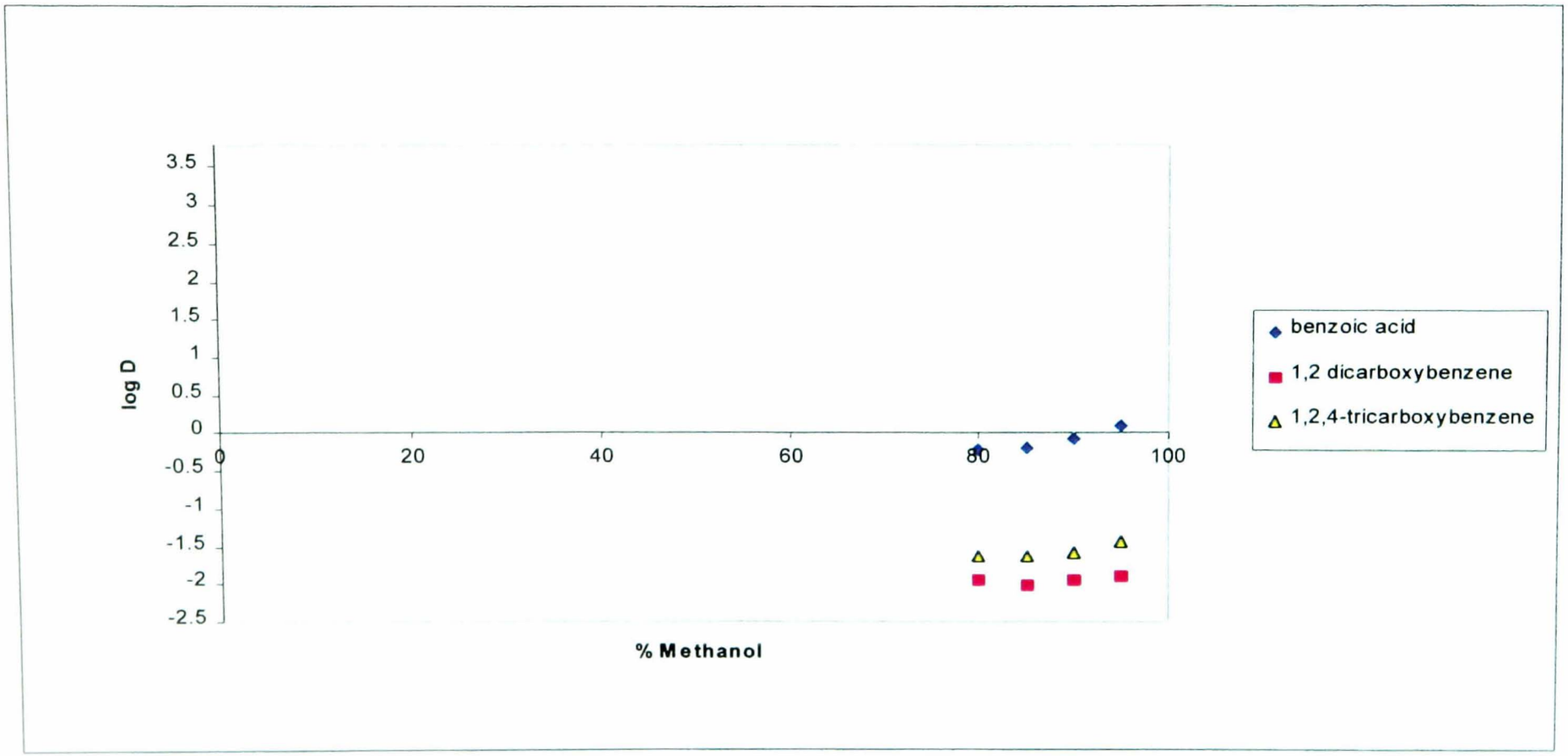

Fig 5.42
Plot of log k'/D Benzen e Carboxylic Acids vs % Methanol:Water

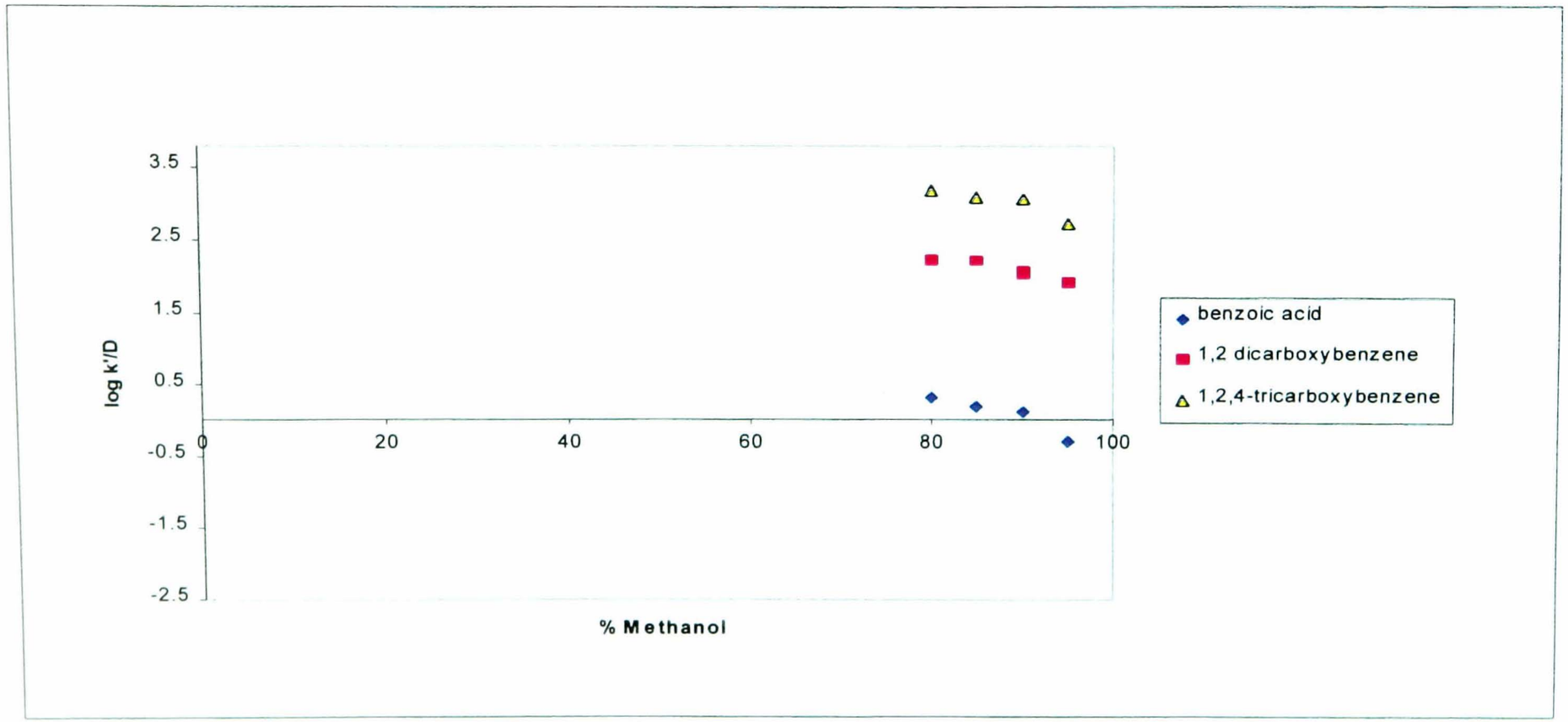

Figs 5.43

Plot of PREG(1) for the Polymethylbenzenes vs % Methanol:Water

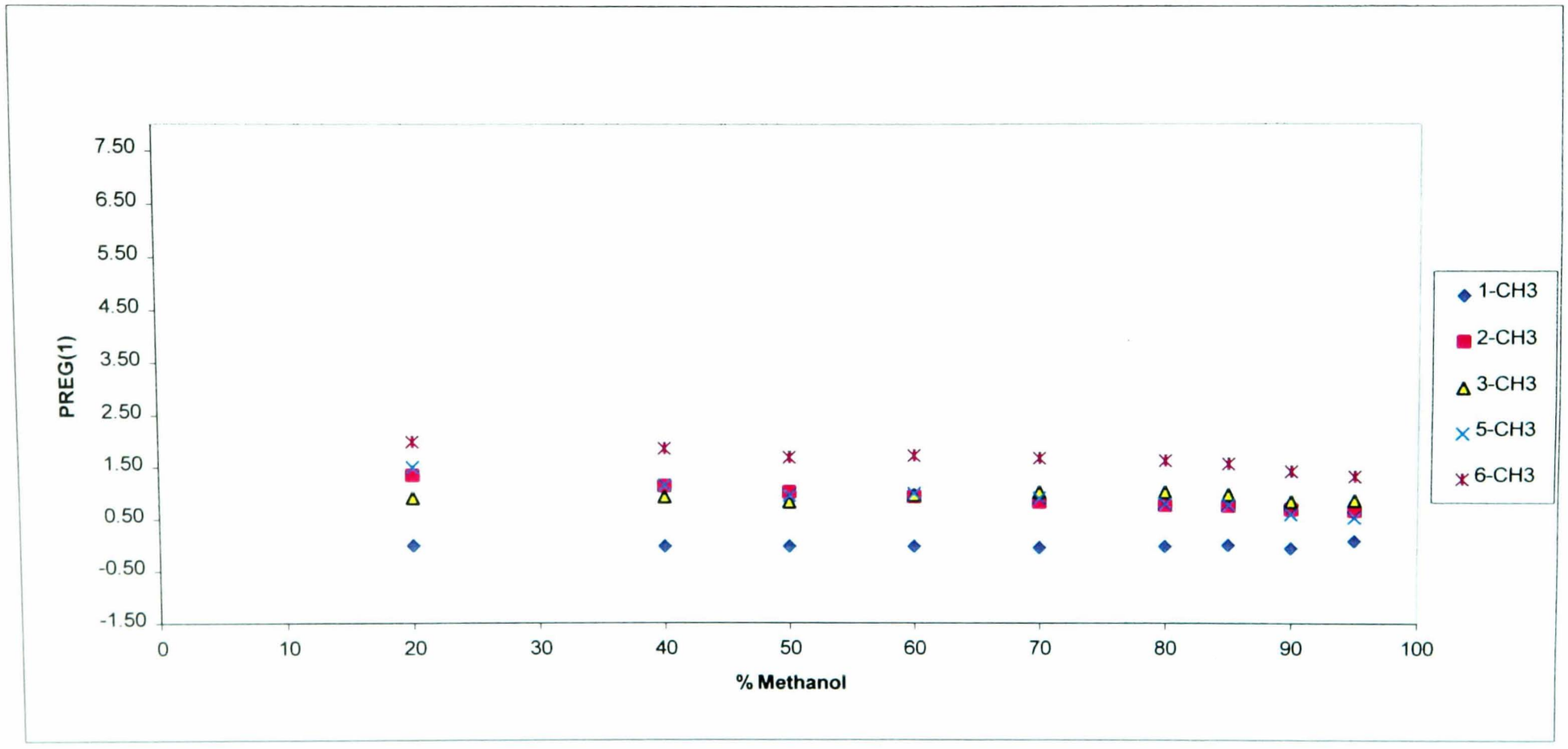

Figs 5.44

Plot of PREG(1) vs %Methanol:Water Composition for the Hydroxybenzenes

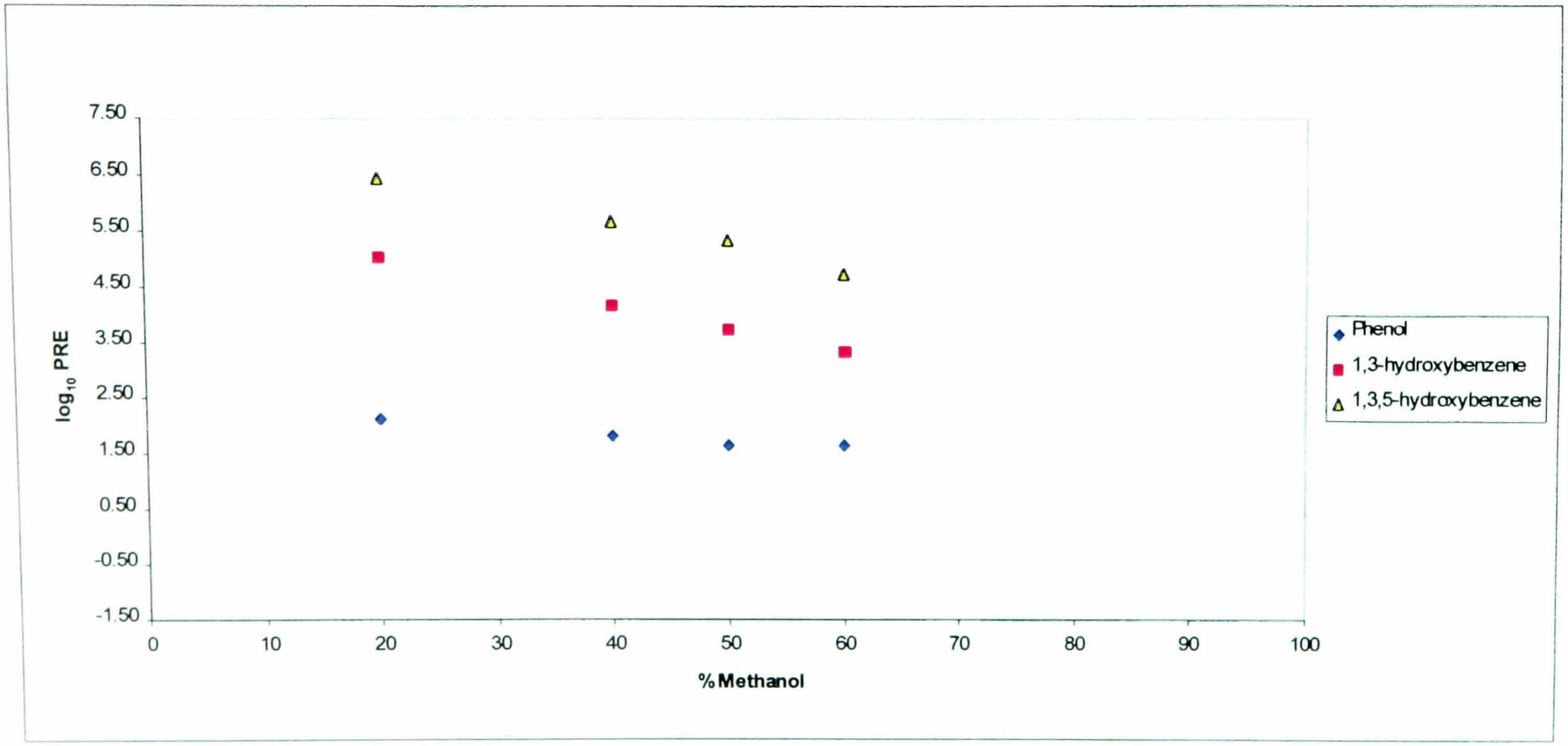

Figs 5.45

Plot of PREG(1) vs % Methanol:Water Composition for the Anilines

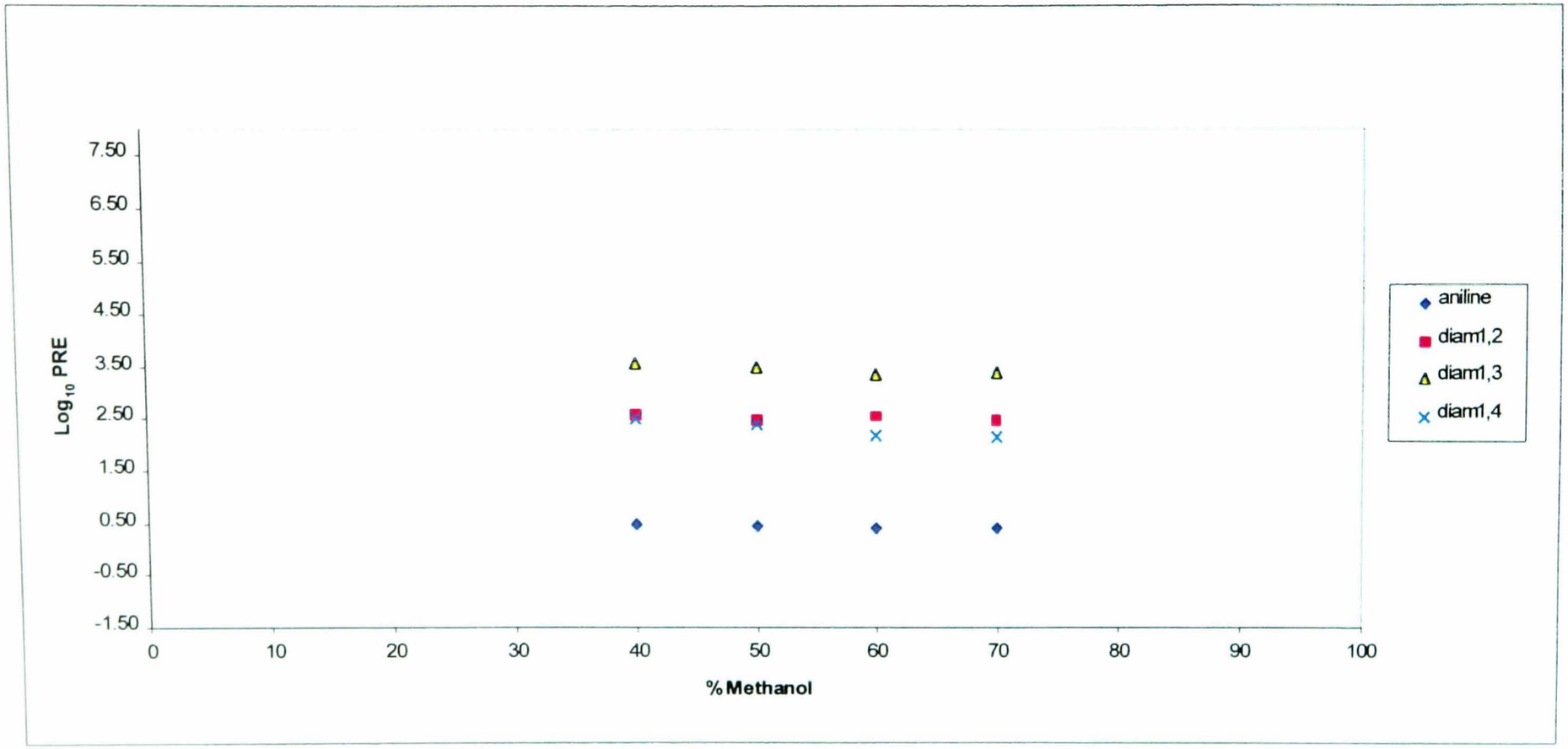

Fig 5.46

Plot of PREG(1) vs % Methanol:Water Composition for Other Mono Substituted Benezenes

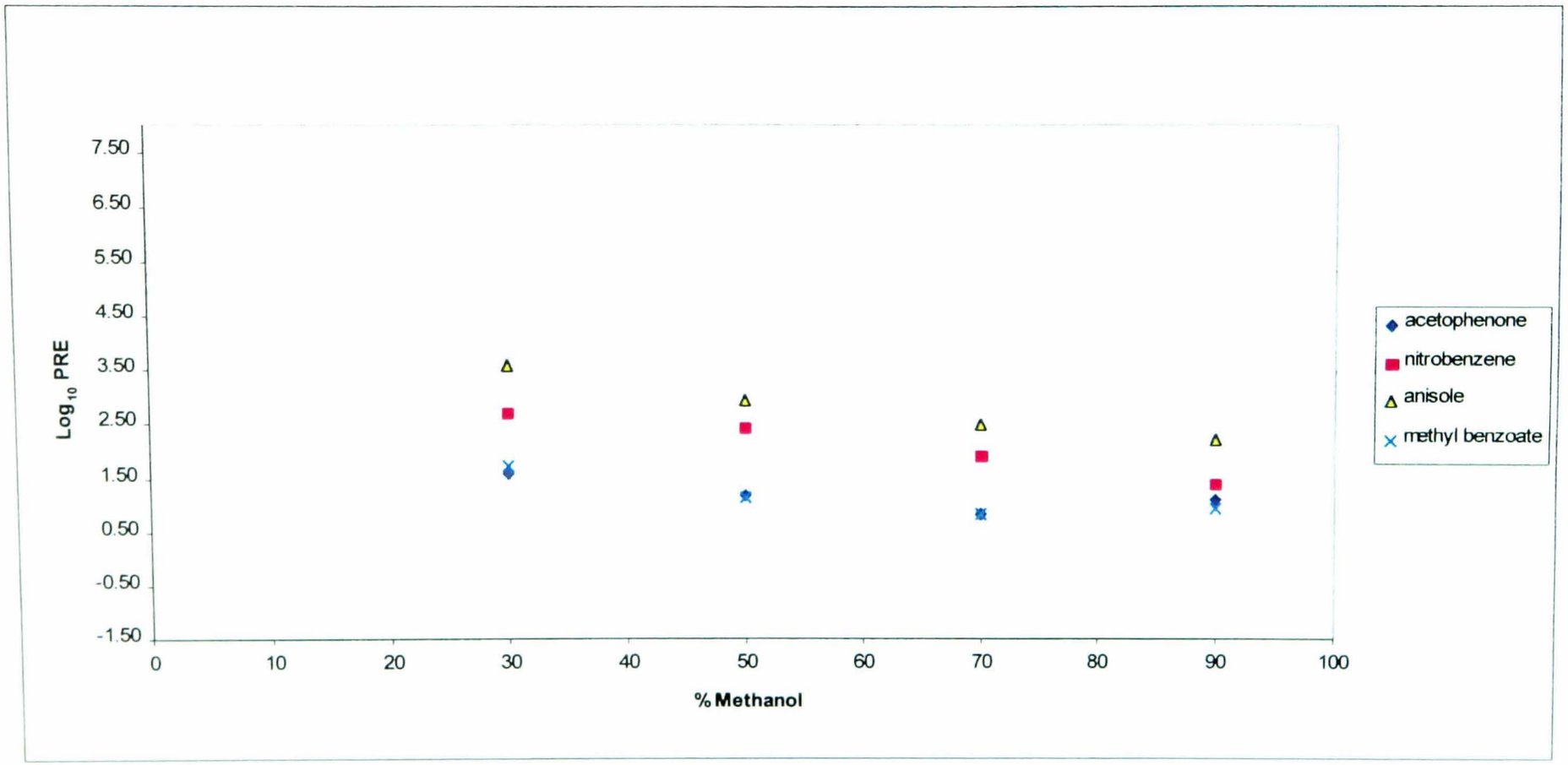

Figs 5.47

Plot of PREG(1) vs % Methanol:Water for the Halobenzenes

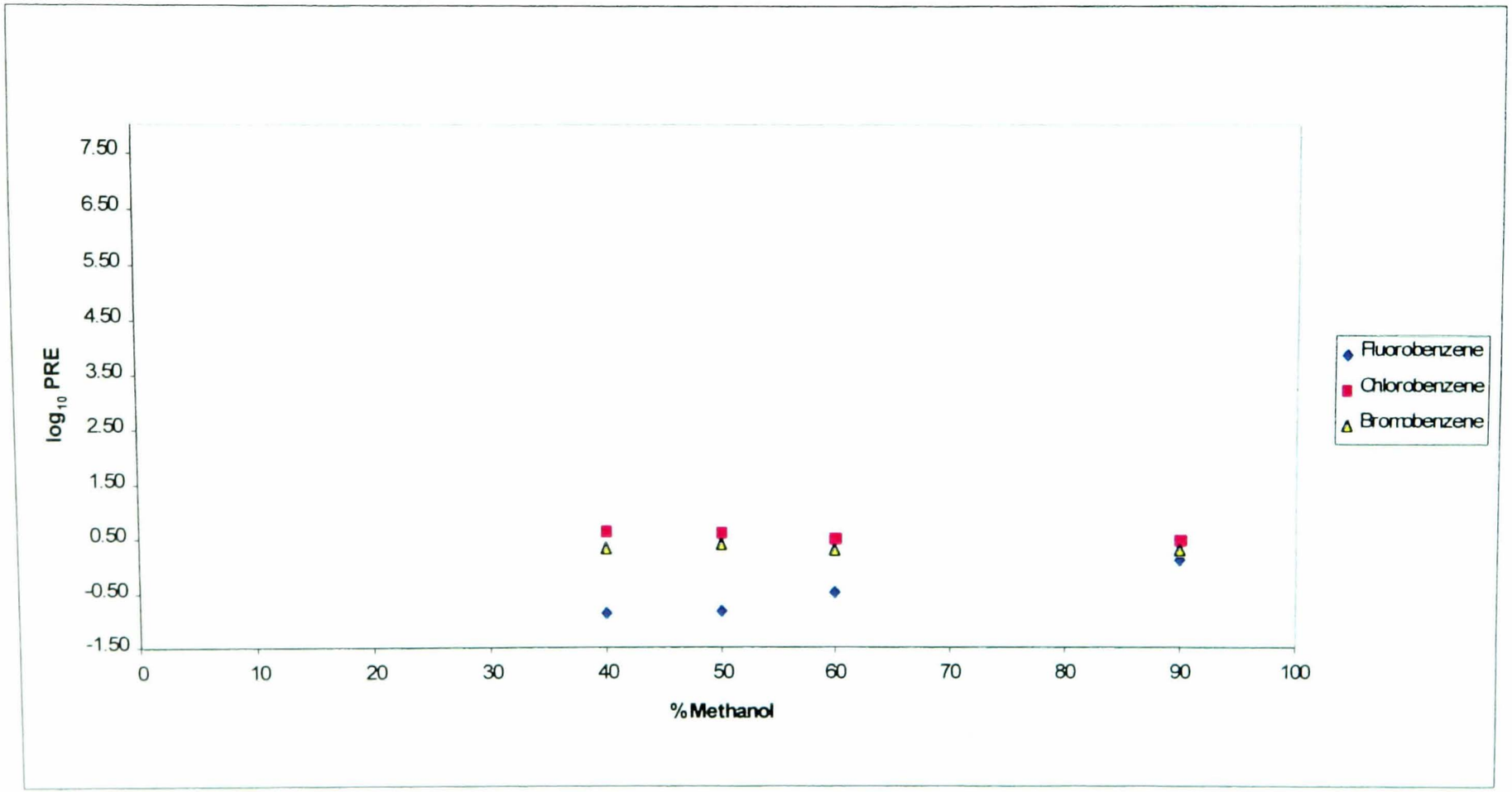

Figs 5.48

Plot of PREG(1) vs % Methanol:Water for the Benzene Carboxyilic Acids

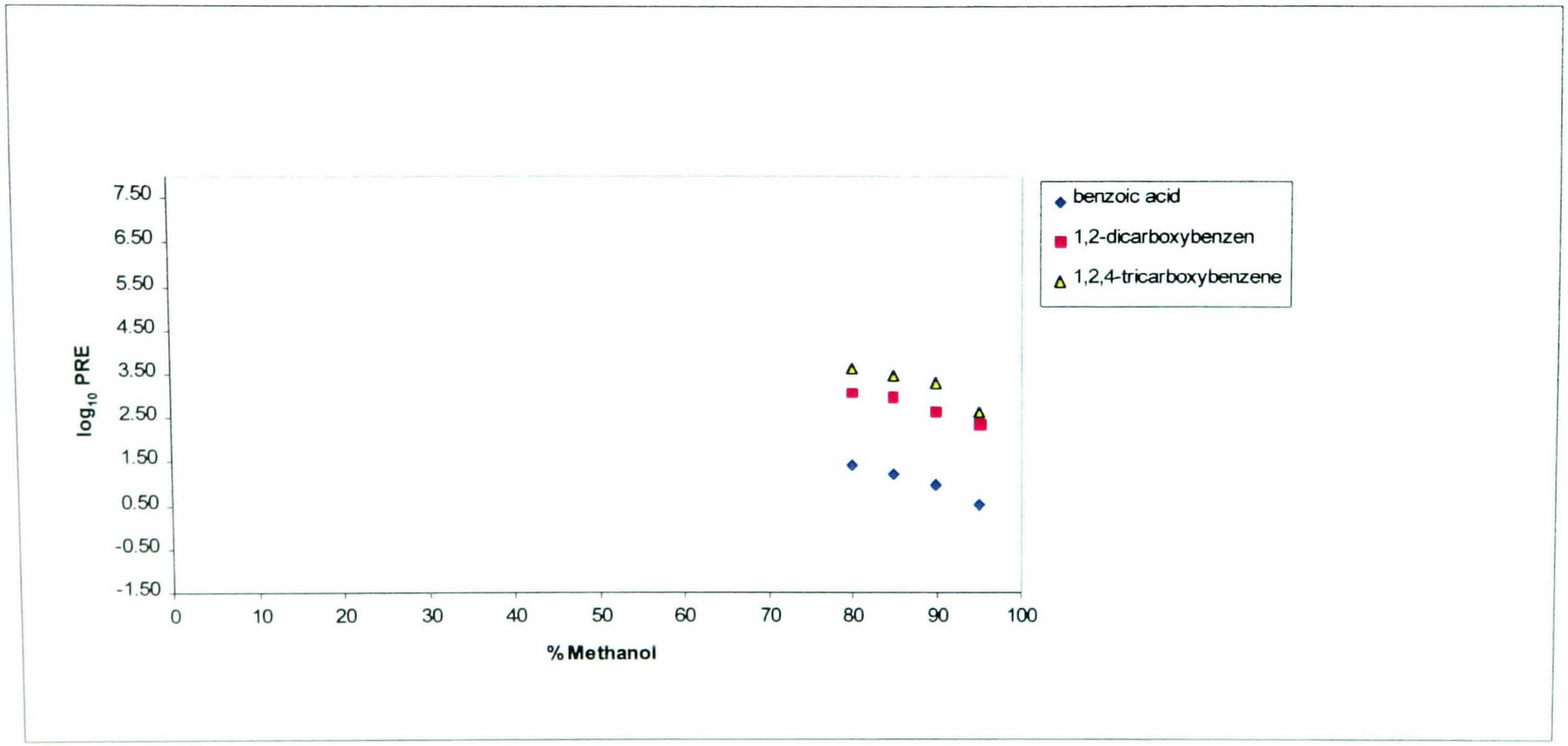

Fig 5.49
General Overview of Relationship Between Analyte Heat of Formation and PREG(2) in Units of kJ/mol

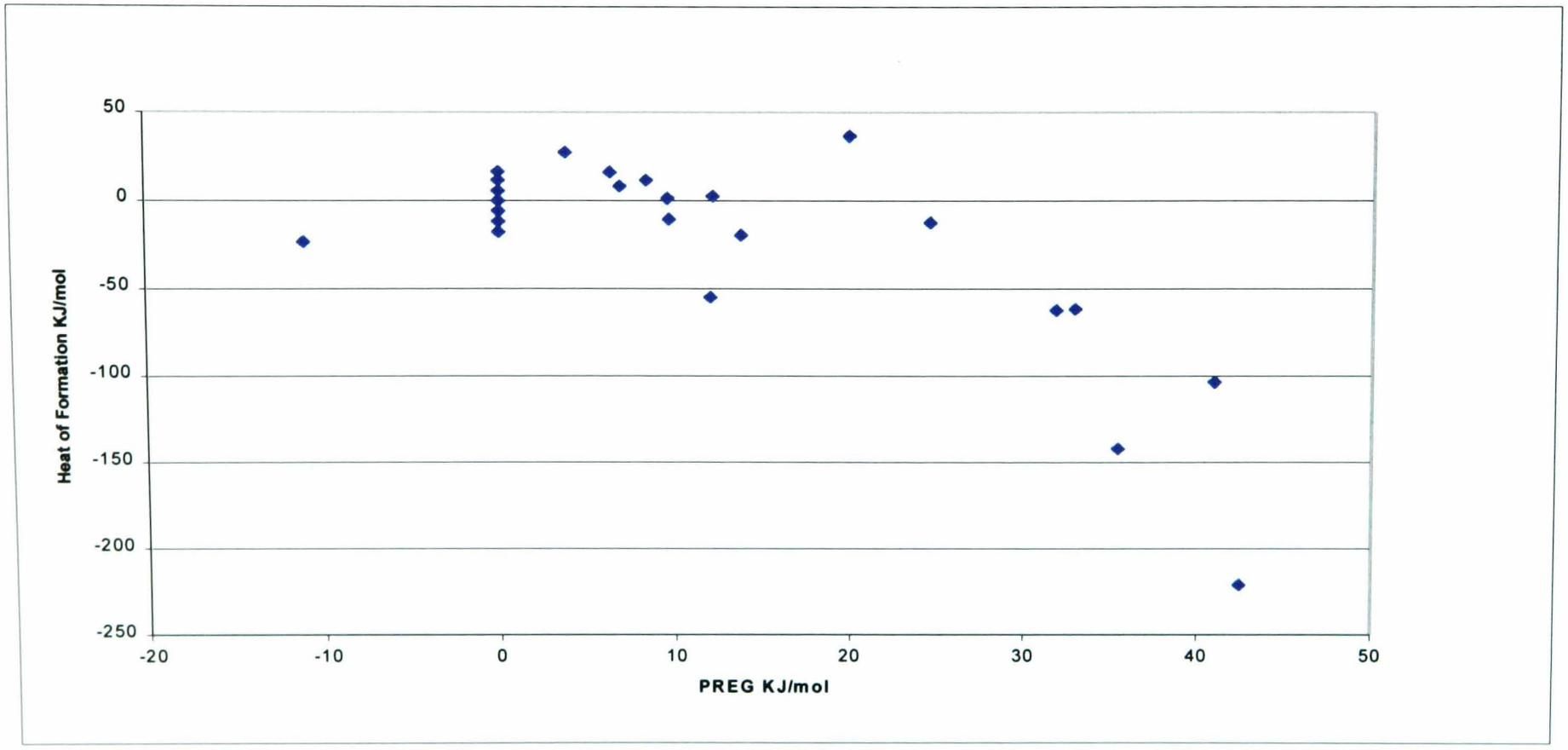

Fig 5.50
General Overview of Relationship between U'' and PREG(2) in units of kJ/mol

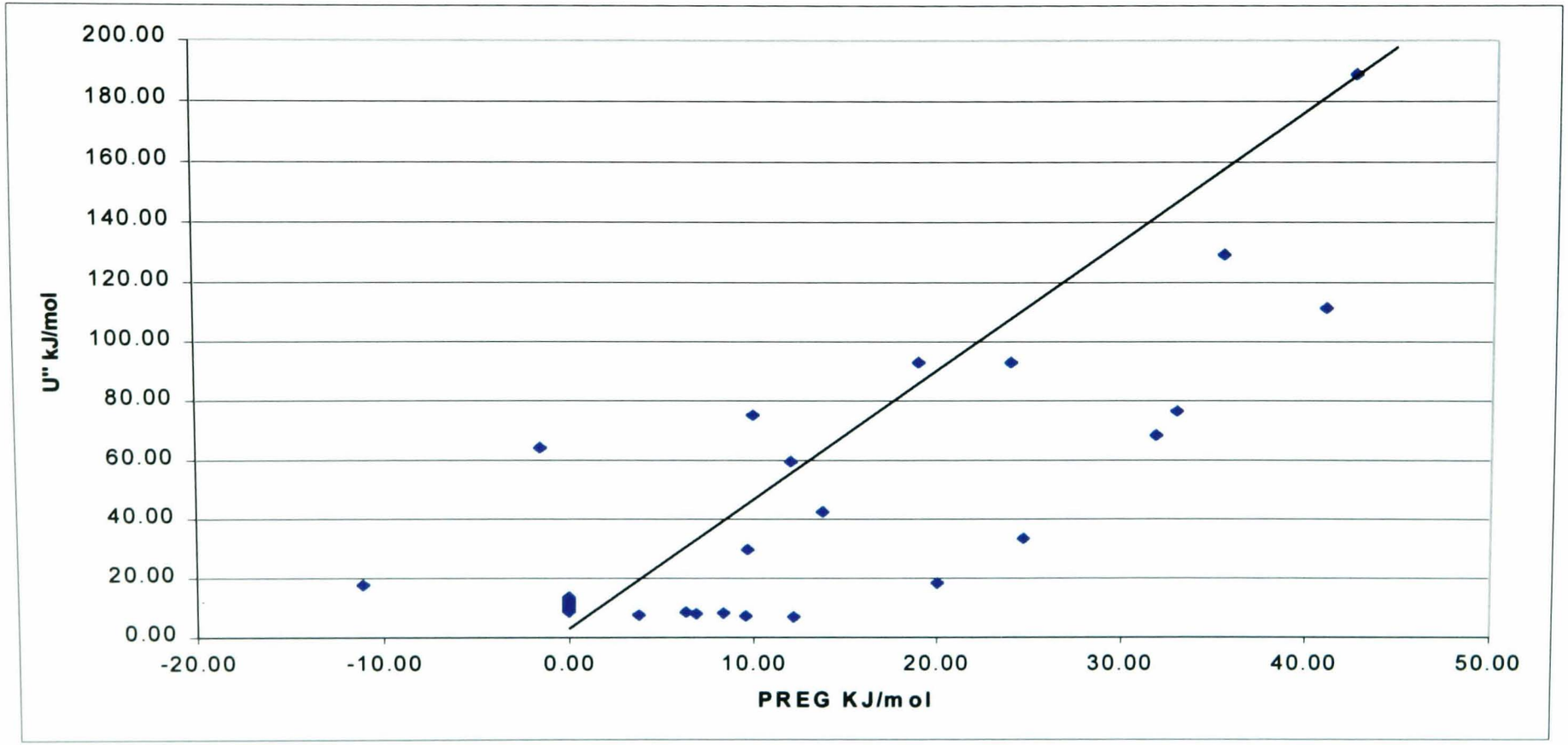

Gradient approx 4.5

Fig 5.51
Schematic Representation of a Point Charge Approaching the Graphite Surface

(a) A positive charge approaching the graphite surface

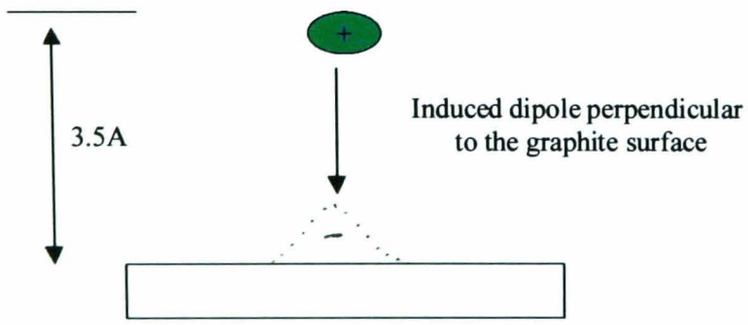

Electrons in the polarizable surface of graphite attracted towards posive charge

(b) A negative charge approaching the graphite surface

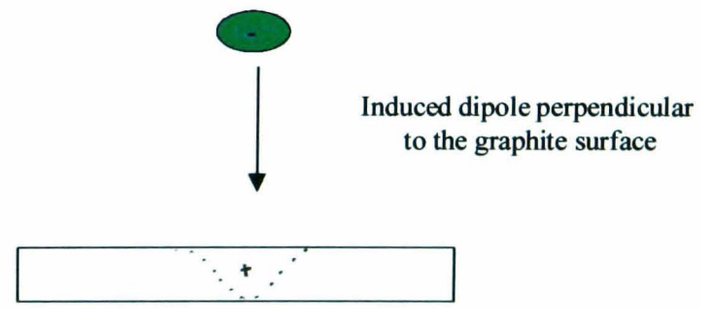

Electrons in the polarizable surface of graphite repelled away from a negative charge

Fig 5.52a
General Overview of Relationship between U_{cind} and $PREG_W(2)$ in units of kJ/mol

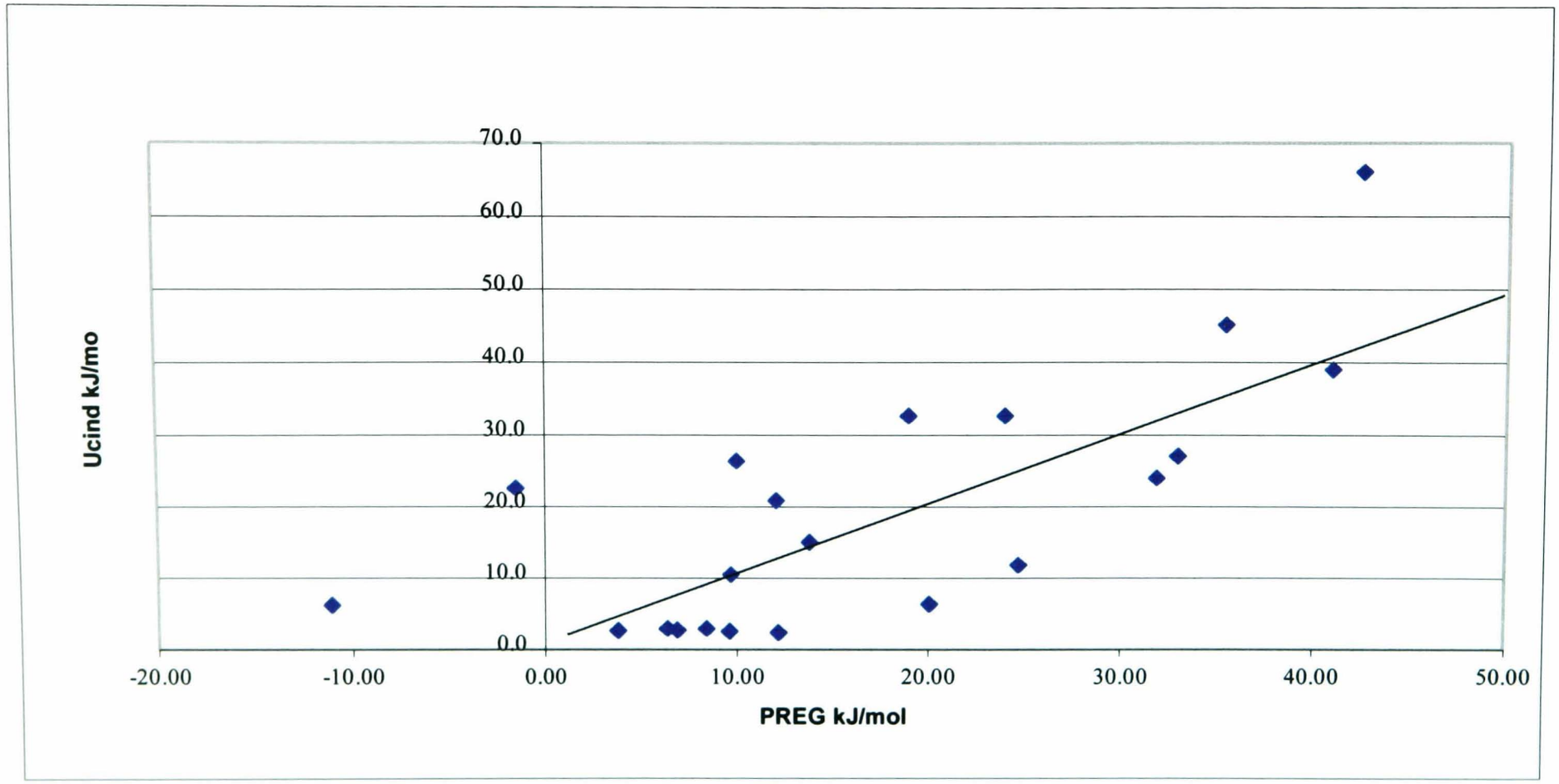

Fig 5.52b

Plot of U_{cind} $PREG_{50}(2)$ Calculated at 50% Methanol:Water Eluent Composition

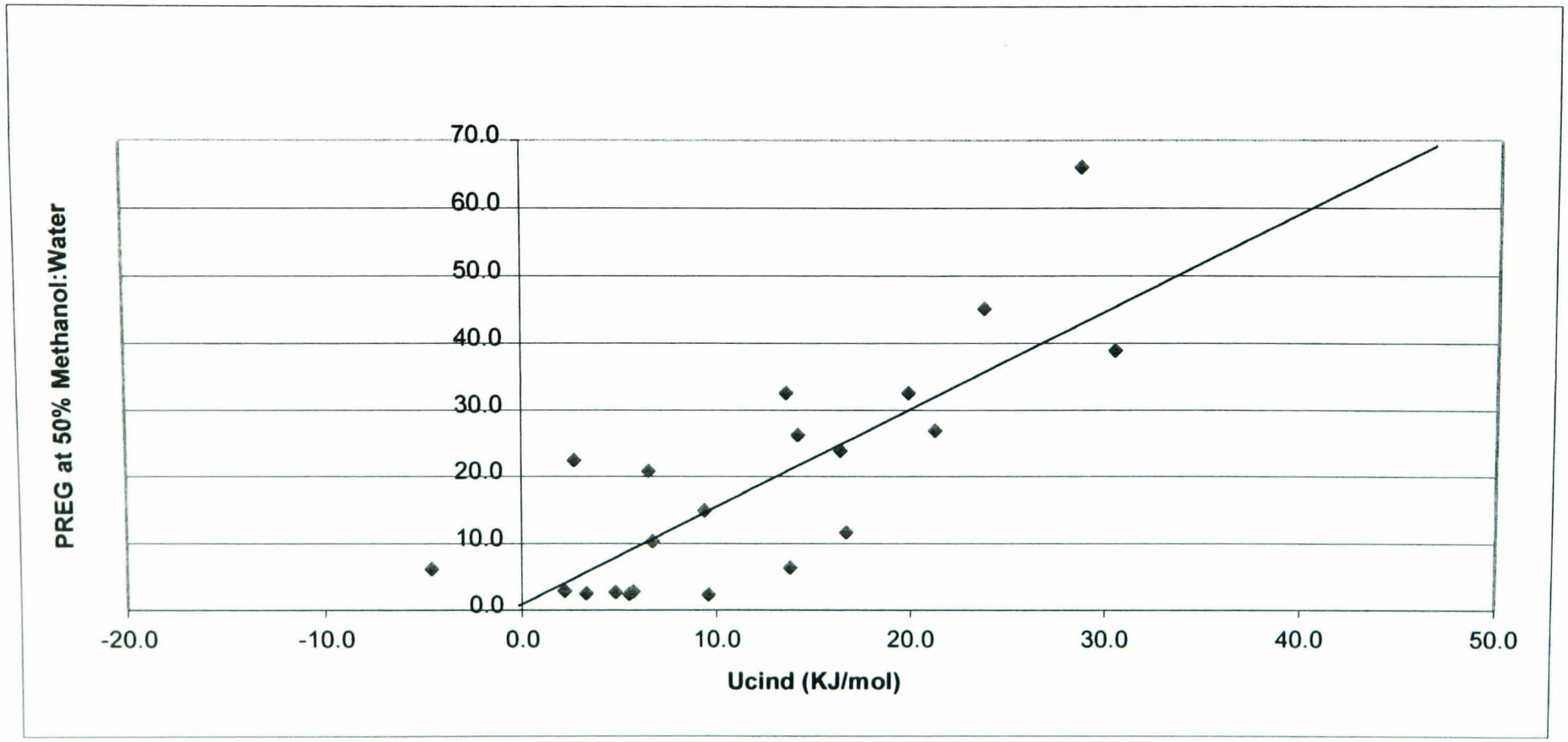

Fig 5.53
Specific Analyte Relationship Between U_{cind} and $PREG_w(2)$ in Units of kJ/mol

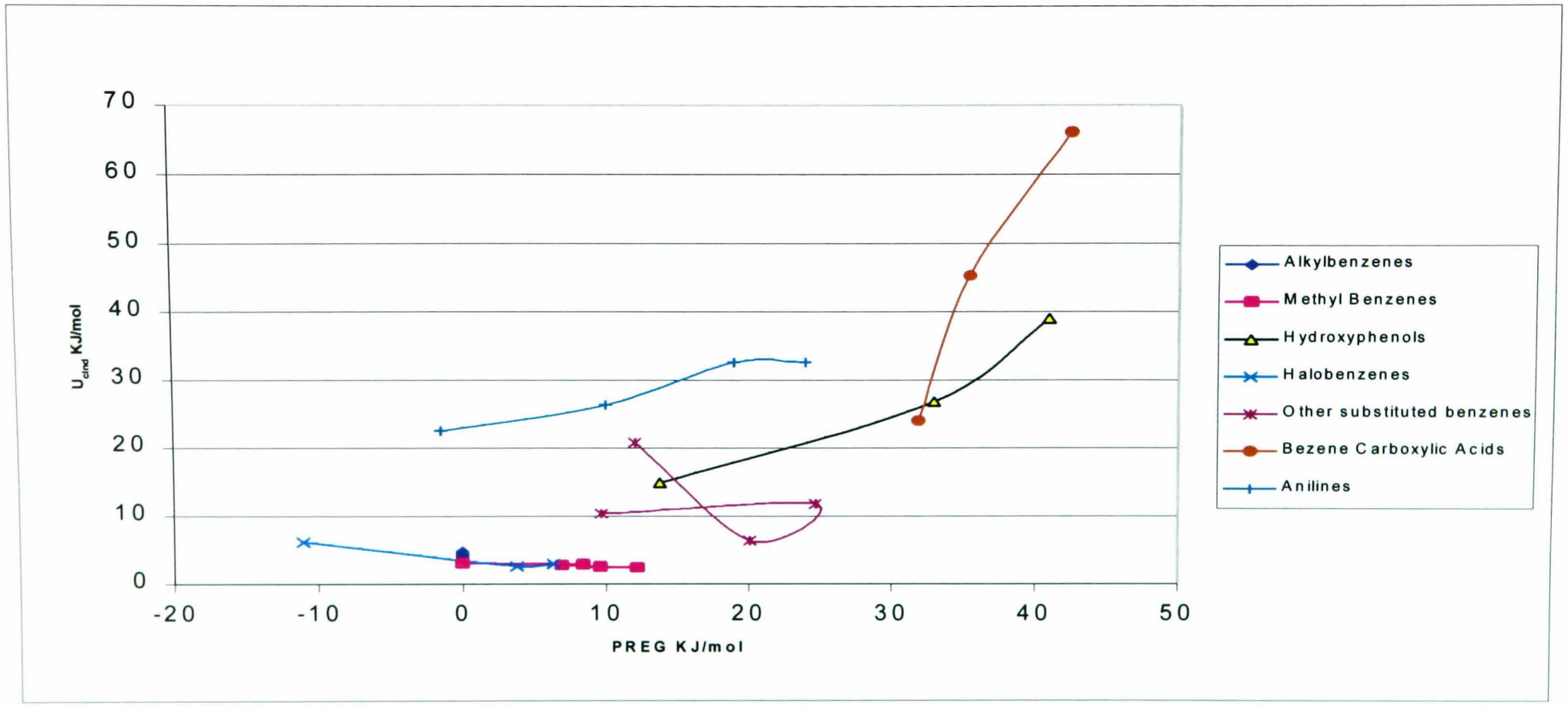

Fig 5.54

Analyte Charge Distribution Image and Alignment at the Surface of Graphite

Fig 5.54a

Example a) A schematic representation of 1,3,5 tri-hydroxybenzene
r1 = r2 = r3 =r4

All hydroxyl groups and benzene parallel to the surface pore of graphite. The analyte then induces a dipole in the surface of the graphite which perpendicular to the surface. In this maximum dipole inducement is possible and the energy of adsorption greatest.

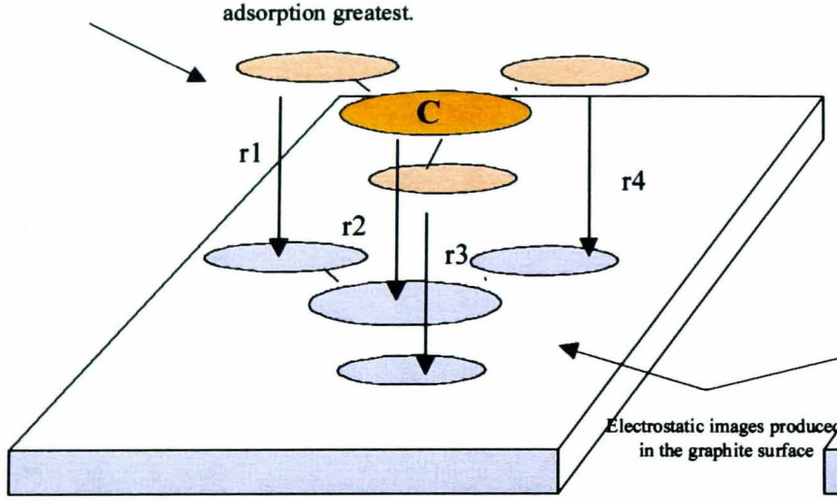

Fig 5.54b

Example b) schematic representation of Benzene -tri-carboxylicacid
r1 < r2 < r3 < r4

Carboxylic acid group perpendicular to the plane of graphite
In this case steric restrictions cause atoms in the molecule to lie in a non planar arrangement, consequently charge centres lie at different distances from the graphite surface and the energy of adsorption associated with the induced dipole is reduced from the possible maximum.

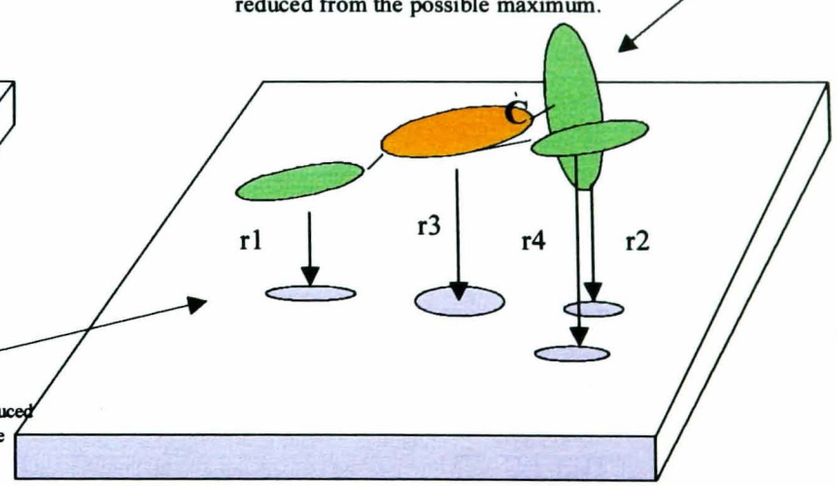

Electrostatic images produced in the graphite surface

'C' represents the expected position for the overall centre of charge for each molecule

Appendix (a) to Thesis

List of Tables

Chapter 1 List of Tables

Chapter 2 List of Tables

Chapter 3 List of Tables

Table Titles for Chapter 4

Chapter 5 List of Tables

Appendix (b) to Thesis

List of Figures

List of Figures for Chapter 2

List of Figures for Chapter 3

List of Figures for Chapter 4

List of Figures for Chapter 5